MARTIN MARIETTA ENERGY SYSTEMS LIBRARIES
3 4456 0049754 9

ORNL-2654
Reactors-Power
TID-4500 (14th ed.)

Cy. 9

HOMOGENEOUS REACTOR PROJECT

QUARTERLY PROGRESS REPORT

FOR PERIOD ENDING OCTOBER 31, 1958

[redacted]

OAK RIDGE NATIONAL LABORATORY
operated by
UNION CARBIDE CORPORATION
for the
U.S. ATOMIC ENERGY COMMISSION

CENTRAL RESEARCH LIBRARY
DOCUMENT COLLECTION
LIBRARY LOAN COPY
DO NOT TRANSFER TO ANOTHER PERSON
If you wish someone else to see this document, send in name with document and the library will arrange a loan.

Printed in USA Price $4.00 Available from the

Office of Technical Services
U. S. Department of Commerce
Washington 25, D. C.

LEGAL NOTICE

This report was prepared as an account of Government sponsored work. Neither the United States, nor the Commission, nor any person acting on behalf of the Commission:

A. Makes any warranty or representation, express or implied, with respect to the accuracy, completeness, or usefulness of the information contained in this report, or that the use of any information, apparatus, method, or process disclosed in this report may not infringe privately owned rights; or

B. Assumes any liabilities with respect to the use of, or for damages resulting from the use of any information, apparatus, method, or process disclosed in this report.

As used in the above, "person acting on behalf of the Commission" includes any employee or contractor of the Commission to the extent that such employee or contractor prepares, handles or distributes, or provides access to, any information pursuant to his employment or contract with the Commission.

ORNL-2654
Reactors-Power
TID-4500 (14th ed.)

Contract No. W-7405-eng-26

HOMOGENEOUS REACTOR PROJECT

QUARTERLY PROGRESS REPORT

for Period Ending October 31, 1958

Project Director – R. B. Briggs
Associate Director – C. E. Winters

Homogeneous Reactor Test – S. E. Beall
Reactor Design, Research, and Analysis – R. N. Lyon
Engineering Development – R. N. Lyon
Reactor Materials Research – E. G. Bohlmann
Chemical Engineering Development – D. E. Ferguson
Supporting Chemical Research – H. F. McDuffie
Analytical Chemistry – M. T. Kelley

DATE ISSUED

FEB 9 – 1959

OAK RIDGE NATIONAL LABORATORY
Oak Ridge, Tennessee
operated by
UNION CARBIDE CORPORATION
for the
U. S. ATOMIC ENERGY COMMISSION

MARTIN MARIETTA ENERGY SYSTEMS LIBRARIES
3 4456 0049754 9

HRP QUARTERLY PROGRESS REPORT

SUMMARY

PART I. HOMOGENEOUS REACTOR TEST

1. HRT Operations

Reactor power run 17 was made to obtain additional information on the loss of uranium vs power and on power excursions. The run was highly successful from the standpoint of mechanical performance. In 1074 hr (2500 Mwhr) of continuous operation, it was established that the reversible uranium loss is linear with power to at least 3.5 Mw, amounting to approximately 540 g of U^{235} per megawatt, and that the loss is not significantly affected by temperature within the 240–290°C limits explored. Much of the missing uranium appears to collect on the metal surfaces of the core tank and contributes to the core reactivity. This evidence is reinforced by the examination of the core interior and by metallurgical samples which indicated that some metal surfaces had been heated above 1000°C, presumably as a result of uranium collection and the consequent nuclear heating.

Chemically, the reversible, power-dependent uranium (and other cation) losses appear to result from hydrolytic precipitation, as a solid or liquid phase. On two occasions the sulfuric acid concentration was increased and appeared to reduce the uranium loss.

The additional acid also reduced the frequency of power excursions, although they were still observed whenever the power-dependent loss of uranium was more than 0.5 kg. On one occasion a power excursion from 3.5 to 25 Mw occurred in a period of about 10 sec; this was much larger and endured longer than any previous surge.

Operational procedures were revised and additional instrumentation was provided to permit continued study of the uranium-loss and power-excursion phenomena without abnormal safety hazards.

2. Remote Operations and Development

Following run 17, the core access flange was removed and the corrosion-specimen assembly was transferred to the storage pool. It was noted that 22 of the original 48 specimens were missing from the holder. The missing samples were later found inside the core vessel.

The radiation level in the core was measured at over 1000 r/min.

The thickness of the core wall, which had been measured in July 1957, was measured again in September 1958 with an ultrasonic device; the core wall was found to have lost 43 mils.

The hole in the core tank was first viewed from the blanket side with a folding-arm tilt-mirror periscope. The hole is on the south side of the core at the intersection of the 30- and 90-deg cones.

A 2-in.-dia hole was cut in the center of the upper six diffuser screens to permit viewing of the hole from the core side. Four of the six pieces of screen were recovered in the cutter.

Six corrosion specimens were recovered by use of a special retriever mounted below a tilt-mirror periscope. This operation was seriously hampered, however, because the top two diffuser screens had become detached from the core wall. Recovery operations are being continued with the retriever and other grappling tools.

3. HRT Processing Plant

Chemical compositions of solids removed by the hydroclone in run 17 varied markedly from those of the previous run; furthermore, the solids removal rates and the weight of solids collected approximately doubled in run 17. Zirconium oxide was the major corrosion-product constituent collected, increasing from 7% in run 16 to 47% in run 17. Over 180 g of uranium solids were separated by the chemical plant, but only about 10 g of copper and 1 g of nickel were removed as solid phase.

Material balances on selected insoluble fission products reveal that only a few per cent of these isotopes have been collected in the underflow pot; however, the reactor fuel solution contained less than 0.5% of these isotopes at the end of run 17. Based on rare-earth activity analyses, two isotopes – Y^{91} and Nd^{147} – show a significant concentration by the chemical plant. Concentrations reached the lower levels of detection

by spectrographic method, but the quantitative data available are limited at the present time.

An equation was developed to correlate the rate and magnitude of fission-product heating and the reactor power history with solids collected in the underflow pot. The equation should prove useful in observing day-to-day trends in solids removal and in ascertaining when the underflow receiver should be drained.

A fire occurred in charcoal bed A and burned for five days without detection after a large quantity of deuterium escaped to the beds at the beginning of run 17. A resulting release of short-lived krypton and xenon activities necessitated the routing of the off-gas to a spare bed for several days. Subsequent tests showed that no more than 2% of the charcoal in bed A had been consumed; the bed was placed back on stream for the final 28 days of the run without further difficulties.

Transfer of the nickel-contaminated fuel batch from run 13 to a solvent-extraction facility for uranium decontamination was accomplished, with gadolinium being used as a soluble poison for criticality control. The associated D_2O was recovered by boiling from the waste evaporator prior to the transfer.

4. HRT Reactor Analysis

Power "excursions" and "oscillations" observed during HRT operations were analyzed. "Excursions" are associated with relative power changes greater than 7%; "oscillations" are associated with "normal" power fluctuations of 1 to 3%. These two types of fluctuations appear to be instigated by different reactivity-addition mechanisms. Only a few excursions were identified at core powers less than 1.0 Mw; above that power, excursions occurred with a frequency that increased with the power level. The frequency of power-fall excursions had little correlation with power level and was much lower than that of power-rise excursions. The frequency of excursions appeared to decrease after sulfuric acid had been added to the fuel fluid. In run 17 there were four excursions in which the power increased more than 100%; the largest percentage power increase in run 16 was 50%, while in run 14 the corresponding value was 20%. There was no evidence that the relative-power rise during an excursion was a function of the time between any two excursions. Averaged over a period of time, the frequency of excursions was between 1 and 2 per hour; as a function of magnitude of the excursion, the average frequency became less as the magnitude increased.

There appear to be two classes of power excursions; in one the reactivity rises rather smoothly with time and reaches a peak in 2 to 4 sec. The reactivity then falls, but it rises again after 5 or 6 sec. This behavior would result if uranium were effectively added to the core region and followed the over-all movement of the fluid. In the second class of excursions, the reactivity rises to a peak value and stays near this value for about 10 sec; generally, a second peak is not observed.

The frequency of the "normal" power oscillations remained fairly constant throughout periods of steady reactor operation; about 13 oscillations occurred per minute at a reactor power of 3.5 Mw. The frequency of these oscillations appeared to increase slightly with increasing power level. Lowering the fluid flow rate, the reactor pressure, or the fuel feed rate did not influence the oscillation frequency.

The reactivity associated with movement of U^{235} from one reactor position to another was calculated. If 1 g of U^{235} were moved from outside the reactor to a position of average importance in the core region, it would add about 0.023% Δk_e. Movement of a stainless steel corrosion sample from the center of the core to the top screen would add about 0.013% Δk_e. The associated power fluctuation would be about 2% of the initial power. The introduction of a 10-liter void in the center of the core would reduce reactivity by about 2% Δk_e.

Some calculations were made of the reactivity effect associated with movement of 3 liters of "cold" reactor fluid; this fluid was assumed to be at a temperature of either 275 or 265°C, with the reactor temperature being 280°C. Movement of this 3-liter volume from the top of the reactor core to the center added 0.012% Δk_e when the associated fluid temperature was 275°C.

A study was made of the HRT time behavior following a reactivity addition to the reactor system; the time-delay characteristics associated with the external system were considered. Based on results obtained, the "normal" power oscillations which were observed during HRT operation do not appear to be a natural property of the circulating system.

Calculations were performed to determine the effect that uranium deposited on the core-tank

wall would have on the critical fuel concentration (no change in critical temperature). With small, uniformly deposited amounts of uranium, 1 g of U^{235} on the core wall is equivalent to 3 or 4 g distributed throughout the circulating system; if large amounts are deposited (~1 kg of U^{235}), 1 g on the core wall is equivalent to about 1 g in solution.

The effect that the core corrosion-sample assembly had upon the thermal-flux distribution in the HRT was calculated. Although the assembly caused the thermal flux along the reactor axis to be lower than that existing when the assembly was not present, the fraction of reactor power generated in the core with the assembly present was virtually the same as the fraction generated without it.

Nuclear characteristics of the HRT were calculated on the basis of operation with different core and blanket temperatures. Power density at the core wall was only slightly affected by changing the blanket-fluid temperature from 280 to 200°C, with the core fluid remaining at 280°C.

5. HRT Design

Comparative cost estimates are being obtained for two concepts of a replacement pressure vessel for the HRT. In one concept a bolted vessel closure is utilized to permit removal of the core.

Design work was completed for the following items:

1. a thimble which will allow fast-neutron flux monitors to be inserted in the vicinity of the pressure vessel;
2. a specimen holder for use in corrosion tests of condenser tubing in the turbine condenser;
3. a core-solution purge tube, with an extension to the chemical plant, for installation in the HRT in an attempt to remove solids or heavy-phase uranyl sulfate if they are present in the core screen area during operation;
4. a tool for use in remote cleaning of the grooves of ring-joint flanges in the HRT;
5. a device for collecting samples of loose scale and solids from the HRT core during shutdown periods.

6. HRT Component Development

Prototype HRT circulating pumps and feed pumps continued to operate in endurance tests without failures.

The effect of changes in the diffuser screens of the HRT core was investigated in a flow model. An optimum location for a sample probe to serve as an intake to the HRT chemical plant was found to be at the intersection of the core wall and the top diffuser screen.

Tests of a proposed re-entrant replacement core indicated that wall temperatures could be maintained within 5.5°F of the fluid temperature if no uranium is present on the wall. Tests of a model with a vaned annular inlet and a polar outlet are being continued in an effort to devise a configuration which will have stable flow characteristics and from which solids can be readily removed.

The HRT mockup, containing a titanium letdown heat exchanger and titanium pressurizer and feed heater, was operated for 1726 hr on 0.045 *m* UO_2SO_4, 0.025 *m* H_2SO_4, and 0.035 *m* $CuSO_4$. The operation was at 1500 psi and 280°C, with boiling fuel serving as a source of steam for pressurization. The generalized corrosion rate was 0.73 mpy for the first 700 hr and 1.3 mpy for the remaining time. The reason for the change in rate has not been discovered. The stainless-steel-to-titanium transmission joints have shown no visible corrosion.

The two fuel-feed-pump heads have operated 6,936 hr and 11,128 hr, respectively, since the last diaphragm failure. The titanium letdown heat exchanger has been operated for 4350 hr without trouble, and the titanium-to-stainless-steel joints have remained tight during this time.

7. HRT Controls and Instrumentation

A system for indicating control-valve stem position was developed for the reactor letdown valve. The system utilizes standard modular elements and only three vacuum tubes.

The experimental ⅛-in.-dia-port letdown valve with a lower stem guide was installed on the HRT mockup loop; it has since operated satisfactorily for 1776 hr.

A blanket-system dump valve, which was removed from the reactor after power operation, was decontaminated and repaired and was then returned to the reactor spare-part inventory.

As a result of operating experience, revisions were made to the reactor control circuitry to prevent a signal of high stack radioactivity from isolating the instrument cubicles. Power-monitor lights were installed in the main control room for each a-c and d-c control bus.

PART II. REACTOR DESIGN, RESEARCH, AND ANALYSIS

8. HRE-4 Design

Preliminary design studies were completed for HRE-4, a small single-region slurry reactor. One feature of the system is the use of a high-pressure dump tank, which also serves as the system steam pressurizer. An acid-egg type of transfer tank is used for transfer of slurry in the high-pressure system. An inverted-L tube shape was selected for the heat exchanger, on the assumption that such a design would minimize slurry plugging and caking problems. Steam generated in the shell of the heat exchanger is condensed in an air-cooled coil. A 600-gpm canned-motor pump circulates the slurry. The off-gas system is similar to that installed in the HRT.

ORNL Building 7503 will have to be heightened to accommodate a reactor of the size contemplated. Additional shielding will be required around the existing containment vessel.

9. Research and Analysis

Parameter studies of the nuclear characteristics of single-region slurry reactors were extended to include moderator mixtures of light and heavy water. Reactor diameters between 4 and 5 ft were considered, with the average moderator temperature being 280°C; diameters of 1.5, 2, and 2.5 ft were assumed at operating temperatures of 200°C and less. At a thorium concentration of 200 g/liter, a 4-ft reactor containing water of 95% D_2O content had the same critical fuel concentration as a 4.5-ft reactor containing 99.8% D_2O. At 200°C, the reactor diameter had to be greater than 1.5 ft for critical-mass ratios (ratio of U^{235}/Th) less than 0.10. For moderator mixtures less than about 50 mole % D_2O, the minimum critical-mass ratio occurred at thorium concentrations greater than about 1000 g/liter. At 80% D_2O content, the minimum critical-mass ratio occurred at thorium concentrations between 400 and 600 g/liter.

Reactivity effects associated with slurry settling were calculated for 2- and 2.5-ft-dia one-region reactors operating at 20, 100, and 200°C. Initial slurry concentrations ranged from 100 to 500 g of Th per liter, and the moderator (D_2O-H_2O mixtures) contained either 25, 50, or 75% D_2O. The peak value of reactivity encountered as the slurry settles decreased as the reactor size decreased, as the D_2O fraction in the moderator increased, and as the reactor temperature increased.

The nuclear characteristics of reflected slurry reactors were obtained; core diameters of 1, 1.5, 2, and 2.5 ft were considered; slurry concentrations ranged from 200 to 600 g of Th per liter; average temperatures considered were 20, 100, and 200°C. The moderators in the core and the reflectors were various mixtures of H_2O and D_2O. With core thorium concentrations between 200 and 400 g/liter in 2- and 2.5-ft-dia cores, the lowest critical-mass ratio occurred when the water contained 60 to 80% D_2O. Except when the moderator was about 100% D_2O, almost all the 2.5-ft-dia cores had critical-mass ratios below 0.10. Dumping the reflector of these reactors caused the reactors to become subcritical. The reactivity worth of the reflector increased with decreasing core diameter. With an initial reactor temperature of 100°C and with a stainless steel core wall $\frac{3}{8}$ in. thick, the reflector of a 1-ft-dia core was worth about 22% Δk_e, while that of a 2-ft-dia core was worth about 7% Δk_e.

Reactivity changes associated with slurry settling in the core were calculated for moderator-reflected reactors; the reactivity characteristics were about the same as those associated with slurry settling in single-region reactors, except that for the "equivalent" systems the core diameter of the reflected reactor was smaller than that of the bare reactor.

Conditions were examined under which storage of thoria-water slurries would be "eversafe." The maximum "eversafe" diameter was about 9 in. for an infinite H_2O-reflected cylinder containing ThO_2-H_2O slurries having U/Th mass ratios less than 0.10; approximately 4 in. was the corresponding maximum thickness of an infinite slab having an infinite H_2O reflector. If 1-in.-dia boron rods were placed in a large volume of this slurry, the rod pitch would have to be 2.5 in. or less in order to ensure "eversafe" conditions.

Pressure and thermal stresses in bare spherical reactors were calculated for reactors operating at 2000 psi and 280°C and having diameters from 3 to $4\frac{1}{2}$ ft, thorium concentrations from 0 to 400 g of Th per liter, and either H_2O or D_2O as the moderator. It was assumed that the power density was the same in all systems and equal to that in a $4\frac{1}{2}$-ft-dia reactor operating at 5 Mw (3.7 kw/liter). Reducing the core diameter reduced the minimum stresses. Increasing the thorium

slurry concentration decreased the wall heat-generation rate and the thermal stresses. For stainless steel vessels, stresses were below the maximum permissible level for thorium concentration greater than 200 g/liter.

The age of fission neutrons in D_2O-H_2O mixtures was correlated in terms of an age-diffusion model. For 99.8% D_2O, the age to indium-resonance energy was 109 cm^2, with the Gaussian age contributing 51.8 cm^2.

A number of machine programs were written; one calculates the reactivity changes associated with slurry settling in one-region aqueous-thoria reactors. The harmonics method for calculating reactor criticality was programmed; criticality is based on the vanishing of a determinant of the seventh order. A program was written which calculates thermal-disadvantage factors for a lattice of rods in an infinite fuel region. Another program calculates the reactivity addition which will produce a known power-time relation for one-region reactors.

Two-group nuclear constants have been prepared for thoria-H_2O-D_2O slurries for temperatures of 20, 100, and 200°C.

Pressure-drop data obtained for flow of non-Newtonian ThO_2-H_2O slurries through tubes 0.124, 0.318, and 1.030 in. in inside diameter have been analysed. The friction factors associated with the nonlaminar-flow data were correlated in terms of the Reynolds number, provided that the viscosity was replaced by the coefficient of rigidity. The friction factors for the laminar-flow data agreed with those predicted on the basis of the associated Hedstrom and Reynolds numbers, with the data obtained with the 0.124-in. tube being used as a norm.

Several 30-gpm loop runs were completed in which thoria caking factors were investigated. Autoclaving the thoria from batch LO-20 for 36 hr at 300°C and in the presence of 800 ppm H_2SO_4 did not prevent cake formation in a subsequent loop run. Pretreatment of batch LO-20 thoria by use of the Waring Blendor resulted in a slurry which did not cake in subsequent loop runs. This change in caking behavior appears to be associated with the change in particle-size distribution.

PART III. ENGINEERING DEVELOPMENT

10. Development of Fuel- and Slurry-System Components

The high-pressure natural-circulation recombiner appeared to operate well at 1500 psi pressure in preliminary runs. Syracuse University reported a lower reaction limit of 29% for $D_2 + \frac{1}{2}O_2$ in D_2O in a 0.434-in.-dia tube at 300°C.

A Belleville spring gasket, with wire sealing inserts, was developed to produce a leak-free thermal-barrier joint in the Reliance 6000-gpm pump. Electrical insulation for the pump motor was demonstrated to be operable after 1.2×10^9 rad dosage.

The 300A loop pressurizer was modified to eliminate gas entrainment, which caused pump failures. Conversion of the 400A-2 pump to the 200Z slurry pump was completed; construction of its loop is 65% complete. A Koppers floating-bushing rotary shaft seal was shown to virtually eliminate mixing; a search is being made for a suitable material of construction.

Performance tests of the three-stage remote-drive oxygen compressor are scheduled for the first week of November at the vendor's factory. The hydraulic parts of the Roth single-stage turbine pump were observed to be in excellent condition after 3370 hr of fuel-solution service.

A high-pressure slurry feed pump, a duplex unit consisting of a diaphragm head with remote check values and a single-contour head with close-coupled check values, was operated successfully for 1400 hr. The only subassemblies which deteriorated appreciably during this test were the tungsten carbide ball check valves.

The solution valve test loop has been reworked to promote the circulation of solids, so that future tests can be more severe. Promising results were obtained with tungsten-carbide-trimmed hand valves and with capillaries in slurry throttling tests.

A titanium lining of a small heat exchanger was found to contain several cracks introduced during fabrication. A seven-tube horizontal tube bundle was operated in thoria slurries containing 200 to 1000 g of ThO_2 per liter without plugging or any other difficulties.

A dimensionless correlation was developed to permit prediction of surface heat transfer coefficients in re-entrant cores. Flow tests of a cone-bottom core model proposed for slurry application were conducted in an effort to optimize the geometry.

The feasibility of suspending slurry settled beds by use of an externally heated conical bottom was demonstrated. Particle size and electrolyte environment were shown to be key variables in determining slurry settled-bed density and mobility.

11. Development of Reactor Slurry Systems

Four slurry circulation runs were completed during the past quarter, three in the 200-gpm loop and one in a 100-gpm loop. Run 200A-15, to determine the circulation and degradation characteristics of 1600°C-fired thoria, was terminated after 3822 hr of circulation at 300°C and 2000 psig. The addition of uranium trioxide and of molybdenum oxide substantially reduced the yield stress and the coefficient of rigidity. Attack rates remained generally low throughout the run. The titanium scroll liner was in good condition, in contrast to high attack on a stainless steel liner under similar conditions. There was evidence that a small amount of uranium and molybdenum was in solution during the run. A piece of black, crystalline material was found lodged in the pump impeller. The material, primarily uranium, molybdenum, and chromium, had apparently come from the pressurizer.

In runs 200A-16 and -17, spheres from 16 to 25 μ in diameter were produced for fluidized-bed studies.

The 100-gpm run (in loop S) was a control for comparison with a run with undigested 800°C-fired thoria. No cakes or films were observed when the loop was opened. Spheres formed early in the run but disappeared with time.

Thoria microspheres were fluidized at 285°C for 264 hr at a void fraction from 0.70 to 0.72. The measured attrition rate was estimated to be 0.26 wt % per day, although photomicrographs indicate that the spheres retained their integrity throughout the run.

A statistical analysis of all the data taken in the five 300-SM loop blanket runs during the last two years showed that vertical and radial concentration gradients existed in the blanket. The titanium and the Zircaloy-2 impellers showed about one-tenth the attack rate of stainless steel.

Fabrication of the 30-in.-dia high-pressure vessel for core and blanket circulation studies is proceeding on schedule. The dump tank for the revised 300-SM loop is ready for shipment; most of the other components are on hand. Plans to install gamma absorption equipment on the new pressure vessel have been delayed, and slurry distribution within the pressure vessel will be determined by sampling.

Model studies of slurry flow in reactor core vessels were started in order to obtain slurry distribution data for establishing scaling relationships. A 6-in. Lucite vessel is being used, and a similar 15-in. model is being designed.

Experiments were performed on adapting a commercial gamma density meter for use in continuously monitoring slurry samples to be withdrawn from the 30-in. high-pressure vessel. The precision achieved was better than that required for the high-pressure distribution studies, and response to density changes was practically instantaneous.

12. Instrument and Valve Development

General-purpose sampling valves for high-pressure solution service were obtained which are designed with a bellows stem seal and replaceable plugs and seats. The valve may be manually actuated or is easily converted for use with a reversible-action all-metal pneumatic actuator.

The control-valve actuating system which utilized 500-psi water as the hydraulic fluid suffered an actuating-cylinder failure after 86,715 test cycles.

To facilitate the removal of pneumatically actuated reactor control valves, a remotely disconnectable coupling for the air supply and exhaust lines was designed. The coupling force is supplied by air pressure acting on a bellows-lever mechanism.

Chromium carbide was found to be unsatisfactory as a valve trim material for thorium oxide slurries at high temperature. A Zircaloy plug and seat and a type 17-4 PH stainless steel plug-guide were operative after 800 hr in the same valve.

A special adapter using a metal-to-metal conical pressure seal was designed which allows greater flexibility in the application of heated-thermocouple-probe liquid-level sensors and metal-sheathed thermocouples.

An experimental flush-diaphragm differential-pressure transmitter to avoid line plugging in

slurry applications and based on an ORNL conceptual design is now being fabricated by The Foxboro Company.

A liquid-level alarm transmitter which develops a signal-producing motion from differential expansions was tested on a high-pressure test loop. The expansion of the measuring tube is caused by the difference in heat loss from the liquid- and vapor-filled sections of the tube.

A capacitance-type liquid-level measuring system for high-pressure applications was tested and found to be pressure-sensitive. A short-term hysteresis error due to water adhering to the electrodes and insulators was also noted.

PART IV. REACTOR MATERIALS RESEARCH

13. Solution Corrosion

A simulated HRT fuel solution was unstable when passed through a heated Zircaloy-2 bypass section installed on a titanium loop. Losses of uranyl, cupric, and nickel sulfates were observed when the temperature of the solution emerging from the bypass was as low as 290°C. The solution was completely stable, however, when circulated isothermally at 320°C. Experiments are in progress to determine whether a second liquid or solid phase formed on the hot pipe wall.

The 0.04 *m* UO_2SO_4 solutions containing 0.025 *m* D_2SO_4 and 0.03 *m* $CuSO_4$ in heavy water were not completely stable at 300°C when either 0.04 *m* Na_2SO_4 or 0.04 *m* K_2SO_4 was added to the solution. In both cases about 30% of the copper was lost from solution. Magnesium sulfate was the only alkali or alkaline-earth sulfate which, when added to the uranyl sulfate solution containing this amount of acid, gave a stable solution less corrosive than the uranyl sulfate solution.

The rate at which chromium(III) is oxidized to chromium(VI) in a ruthenium-containing uranyl sulfate solution was measured at 225, 250, and 275°C. At 300°C the rate was too fast to be measured with the existing equipment.

The effect of cold work and heat treatment on type 347 stainless steel was investigated. The effect of cold work was not discernible. Treatment at 1950°F for 1 hr followed by a water quench produced a more corrosion-resistant condition than was present in the as-received alloy.

Tests run in chloride-containing water at 200°C showed that both phosphate and fluoride ions partially inhibited stress-corrosion cracking of type 347 stainless steel but neither was completely effective.

Type 347 stainless steel is highly subject to stress-corrosion cracking when exposed to 0.04 *m* UO_2SO_4–0.02 *m* H_2SO_4–0.005 *m* $CuSO_4$ solutions containing chloride ions at atmospheric boiling temperature. Recent tests have shown that the uranyl ion enhances the effectiveness of the chloride ion in producing cracking. Other tests have shown that the concentration of uranyl sulfate is also important; cracks occurred when the solution contained 0.04 and 0.20 *m* UO_2SO_4 and 50 ppm chloride, but no cracking was observed in either more dilute or more concentrated solutions.

In chloride- and oxygen-containing water at 300°C, all wrought type 347 stainless steel U-bend specimens cracked in 500 hr or less whether the surface had been electropolished or pickled or had been left covered with a heavy oxide scale. Cracking also occurred even when the specimens were annealed after having been stressed. Pretreatment in high-temperature dilute chromate solutions did not prevent cracking. However, pretreatment in 100°C uranyl sulfate solutions appears to give some protection against cracking on subsequent exposure of type 347 stainless steel to high-temperature chloride-containing water.

Cast (as opposed to wrought) type 347 stainless steel specimens have shown no susceptibility to cracking in either boiling 42% magnesium chloride or high-temperature chloride-containing water. Also, type 347 stainless steel and Zircaloy-2 U-bend specimens have not cracked during exposure to oxygenated thoria slurries containing 100 ppm chloride at 300°C.

Tests were run with a Luminol solution to determine the applicability of chemiluminescence as a means of providing illumination for detection of defects in unlighted vessels. With the proper concentration of reagents, the glow of the solution persists for more than an hour.

Corrosion tests with type CD4MCu stainless steel and Multimet showed both materials to be more resistant (but not completely immune) to stress-corrosion cracking than type 347 stainless steel. In high-temperature uranyl sulfate solutions CD4MCu is as resistant to corrosion as type 347 stainless steel; Multimet is only slightly less resistant. Both materials should be suitable for certain reactor applications.

14. Slurry Corrosion

The 0.4-in. hydroclones, which had effectively removed slurry from pump loops in previous tests, would not remove slurry from the loops during runs BS-23 and ES-5. It was necessary to modify the hydroclone system by the addition of a return line from the top of the underflow pot to the loop to provide continuous hydroclone underflow. With this continuous forced underflow the 0.4-in. hydroclone operates effectively.

Dynamic-corrosion data and operating observations are reported for two 100A pump loop tests utilizing slurries of 1600°C-calcined thoria. In one test, thoria of 2.4-μ average particle size was circulated at 280°C at an average concentration of 445 g of Th per kg of D_2O for 485 hr in an oxygen atmosphere and for 478 hr in a deuterium atmosphere. The generalized attack rate of the austenitic stainless steel system was 0.9 mpy during operation with oxygen and 6 mpy with deuterium in the system. No attack was noted on the circulating pump, fabricated of titanium. The corrosion rate of the system was not detectably affected by the addition of ~0.01 m MoO_3, a proposed recombination catalyst. Slurry pH values ranged from 2.3 to 5.7 with oxygen in the system and from 3.6 to 8.6 with deuterium. At room temperature the handling characteristics of the slurry were shown to be markedly affected by the addition of 0.03 m MoO_3.

The second run was a materials evaluation test made with an oxygenated slurry of ThO_2, 0.9-μ average particle size, at 280°C at an average concentration of 277 g of Th per kg of water. Over the velocity range 16 to 25 fps, attack rates generally less than 1 mpy were observed for specimens of austenitic, ferritic, and martensitic stainless steels; Incoloy; and Nionel. At 38 to 50 fps attack rates of Incoloy and Nionel were threefold higher than those of the stainless steel alloys (for type 347 stainless steel: 0.6–1.5 mpy at 38 fps, 0.9–1.9 mpy at 50 fps). Attack of Inconel was four to five times higher than that of the stainless alloys at all velocities studied. Attack of alloy steels (Croloys) containing varying percentages of chromium was found to diminish with increasing chromium content.

Oxygenated aqueous slurries of thoria prepared by the new draft-tube precipitation method were circulated in toroids for 100 hr at 280°C, 26 fps, and at concentrations of 1500 g of Th per kg of H_2O. There were normal substantial differences in the response of the various metals. A significant difference between thoria preparations was also noted. An attempt to correlate attack rates with original particle size was not conclusive.

Aqueous slurries of 1600°C-calcined thoria microcubes were circulated at concentrations of 250, 1000, and 1500 g of Th per kg of H_2O at 26 fps and 280°C in 100-hr tests. Seven tests were conducted with an oxygen atmosphere; one test was conducted in hydrogen. There was a normal difference in the response of the various metals. A difference in thoria preparations was noted, as well as an effect of concentration. The attack under hydrogen atmosphere was much more severe on all materials.

Distinct types of attack on type 347 stainless steel pin specimens and toroid rings were observed.

One HB-6 type rocking-autoclave experiment, L6Z-127S, containing a thorium-uranium oxide slurry in D_2O was assembled and is now in operation in beam hole HB-6 of the LITR to obtain radiation-corrosion data and radiolytic-gas recombination data. Molybdenum trioxide was added to the slurry to catalyze the recombination of radiolytic gas.

In rocking-autoclave experiment L6Z-126S, an over-all corrosion rate of 2 mpy at an average fission energy of 1.2 w/ml and a maximum fission energy of 6 w/ml was observed for a Zircaloy-2 autoclave containing thoria-urania slurry in D_2O and a deuterium atmosphere at 280°C. This rate was based on time at high temperature after pretreatment. The slurry, with a concentration of 980 g of Th per kg of D_2O, contained 0.04 m MoO_3 added as a recombination catalyst. The thoria contained 5% coprecipitated enriched uranium based on thorium. The autoclave was operated at elevated temperature for 144 hr prior to any irradiation and for 169 hr at temperature in hole HB-6

of the LITR. After 22 hr of smooth operation at 6 w/ml, a number of sharp pressure surges and subsequent drops were experienced, requiring the autoclave to be moved to a retracted position. The pressure effects appear to have been due to an increased rate of gas production by the slurry. During the early smooth inserted operation, values of G_{D_2} of 0.016 and 0.005 molecule of D_2 per 100 ev were observed, while after this time, five observations ranged from 0.10 to 0.16. No abrupt changes in catalyst activity were associated with the onset of the pressure surges; however, the values, averaging 0.1 mole of D_2 per liter per hour (100 psi radiolytic D_2), became more irregular as the run continued.

A test model of an in-pile slurry toroid rotator has demonstrated satisfactory mechanical reliability in a 1500-hr, 1000-rpm, out-of-pile test at room temperature. Further test and development work on the in-pile toroid rotator has now been suspended in favor of work on other projects.

Two test runs with thorium oxide slurry were made on the 5-gpm in-pile type slurry loop, L-4-24S. A sintered-metal filter with a 3-μ mean pore size was used to remove slurry from the pressurizer feed stream to prevent the accumulation of slurry in the horizontal pressurizer. The loop was operated for approximately 300 hr with thorium oxide slurries at concentrations up to 500 g of Th per kg of H_2O and temperatures up to 250°C. The operation was entirely satisfactory, with no apparent plugging of the filter and no accumulation of slurry in the pressurizer.

15. Radiation Corrosion

In-pile loop experiment L-2-21 was completed and is reported. This was an all-stainless-steel loop with principal specimens of Zircaloy-2, various alloys of zirconium submitted by the Metallurgy Section, type 347 stainless steel, and Ti-110AT. The loop operated in-pile at 280°C with three different charges of solution, each solution of about the same initial composition: 0.17 *M* UO_2SO_4, 0.04 *M* H_2SO_4, and 0.022–0.015 *M* $CuSO_4$ in D_2O.

The over-all corrosion rates in the loop, as determined from oxygen data, were greater with each of the three solution charges than rates found in previous 280°C experiments with solutions of other initial compositions: 0.17 *M* UO_2SO_4, 0.025–0.03 *M* H_2SO_4, and 0.015 *M* $CuSO_4$ in H_2O. The over-all rates with the second and third charge were much greater than those observed in previous 280°C experiments.

The results of examination and measurement of specimens and components from the loop indicate that most of the corrosion shown by the oxygen data occurred in the stainless steel in the loop core. Localized corrosion of stainless steel was detected in several out-of-core locations, and apparently there was more of this type of attack than in the prior 280°C experiments. It is estimated, however, that the total amount of metal oxidized out-of-core was less than 20% of the total amount of stainless steel oxidized during the in-pile operation. Maximum rates of greater than 500 mpy in the core probably prevailed when the over-all rate from oxygen data was at the maximum of 30 mpy.

A comparison of the stainless steel corrosion behavior in L-2-21 with that in previous 250°C loop experiments containing 0.04 *M* H_2SO_4 (0.17 *M* UO_2SO_4 and 0.03 *M* $CuSO_4$ in H_2O) reveals that the high rates in L-2-21 were probably a result of the use of 0.04 *M* H_2SO_4 concentration. On the basis of the results to date, it is suggested that a pronounced adverse effect on steel corrosion is obtained in 0.17 *M* UO_2SO_4 solutions containing excess H_2SO_4 at concentrations greater than a critical value of 0.03 *M*. Little is known about any critical acid concentration in solutions of uranium concentration other than 0.17 *M*. It is noted, however, that stainless steel corrosion in experiment L-2-17, which employed 0.025 *M* excess H_2SO_4 in 0.04 *M* UO_2SO_4 solution in H_2O at 300°C, was not considered excessive in comparison with that in the prior 280°C experiments mentioned above.

The results for the Zircaloy-2 specimens in L-2-21 fall near the line which has been drawn through the data from the previous loops L-2-19 (0.17 *M* UO_2SO_4, 0.02 *M* $CuSO_4$, 0.2 *M* Li_2SO_4, 0.1 *M* H_2SO_4 in H_2O at 280°C) and L-2-14 (0.17 *M* UO_2SO_4, 0.15 *M* $CuSO_4$, 0.4 *M* H_2SO_4 in H_2O at 280°C). This line is considered to be the probable relationship between corrosion rate and fission power density in solution in the absence of any contribution of fission power at the Zircaloy-2 surface from uranium sorbed on the surface. The uranium adsorption on Zircaloy-2 core specimens in L-2-21 was small and consistent with the position of the data near the line mentioned above. No explanation is apparent for the low uranium absorption on Zircaloy-2.

The mockup of the ORR in-pile loop was operated for more than 100 hr to determine its reliability and control under simulated in-pile conditions. Operation and control were excellent under heat-load transients of up to 14 kw. In one uninterrupted run, the loop was operated at 280°C for 700 hr with an HRT-type fuel solution containing 0.04 *M* UO_2SO_4, 0.025 *M* D_2SO_4, and 0.01 *M* $CuSO_4$ in D_2O. The over-all stainless steel corrosion rate was less than 0.5 mpy, based on nickel and oxygen data.

Specimens exposed in the blanket region of the HRT during runs 13 and 14 were examined and weighed in the as-removed condition. A portion of one specimen each of Zircaloy-2 core-tank material, type 347 stainless steel, and Ti-A40 were submitted for scale analyses. Uranium was not detected on either the steel or Zircaloy-2 specimens, but an amount equivalent to 2 $\mu g/cm^2$ was reported for the Ti-A40 specimen. The appearance and the results of weight measurements for the blanket specimens indicate that the attack was in no case appreciably different from that which would have occurred in the absence of radiation.

A new, freshly machined, type 347 stainless steel flange with an attached type 347 stainless steel specimen was installed in the HRT following run 14 and was removed for examination following run 16. As received from the reactor, all surfaces of this assembly which had been exposed to solution were covered with an off-white-colored scale. This scale was easily dislodged, and, when it was flaked off, a rust-red deposit was revealed next to the metal. The results of scale analyses indicated that part of each scale was comprised of the oxides of stainless steel constituents and part of zirconium (average zirconium 10 wt %). Uranium in the concentration range 0.3 to 5 wt % was also reported. The average weight of scale on the stainless steel specimen was 6 mg/cm^2. The metal lost by the specimen was 0.3 mg/cm^2. These results indicate that appreciable quantities of oxides were transported by the solution during run 16. However, the amount of zirconium oxide found is no more than expected with a moderate corrosion rate for the Zircaloy-2 core tank during run 16.

Five in-pile rocking-autoclave experiments – four HB-5 type and one HB-6 type – were assembled and were operated in the LITR during the quarter to obtain radiation-corrosion data. Results from one of the autoclaves, which employed a solution 0.17 *M* UO_2SO_4 and 0.04 *M* $CuSO_4$ in D_2O and operated above the two-liquid-phase separation temperature (285°C), are discussed. The corrosion rate as indicated by oxygen consumption vs temperature over a temperature range above and below the two-phase separation temperature was similar to that in previous experiments with one-phase solution. Postirradiation examination showed no visual evidence of preferential attack on specimens or bomb walls. A loose pin which lay on the bottom of the bomb during exposure and probably contacted a heavy phase showed a weight loss per unit area similar to that of the other specimens, which probably did not contact the heavy phase. Radiolytic-gas pressures at temperatures above the probable temperature of two-liquid-phase separation were in most cases abnormally high as compared with the radiolytic pressures at the lower temperatures. This behavior probably resulted from a change in the uranium and copper distribution in the two phases from that in the single-phase solution.

The data from a recent exposure of type 347 stainless steel specimens in a Zircaloy-2 system at 280°C are compared with similar previous experiments. The recent test employed a very low copper concentration (0.002 *M*) which resulted in a high radiolytic-gas pressure (average 653 psi). An anomalous pressure maximum somewhat similar to a previously reported phenomenon was observed. The type 347 stainless steel corrosion rate observed agrees well with data obtained in similar autoclave systems with low radiolytic-gas pressure (50 psi); no effect of radiolytic-gas pressure on the steel corrosion rate is apparent in the various results. There is also no evidence of any difference in radiation corrosion between solutions with initial H_2SO_4 concentrations of 0.03 *M* and those with 0.06 *M*.

Several series of batch adsorption experiments were carried out in a study of the adsorption of uranium from UO_2SO_4 solution on hydrous zirconium oxide at elevated temperatures. Exposures were made in ampoules of Pyrex glass heated to the desired temperature and then cooled to room temperature before the oxide and the solution were separated for analysis. The hydrous oxide was prepared from zirconium sulfate and was air-dried at 100°C. A measurement of the surface area of the as-prepared material showed 220 m^2/g. Adsorption temperatures of 25, 150, 100, 250°C were

employed. In general, the adsorption of uranium per gram of oxide increased with increasing temperature to 150°C. However, the adsorption per gram of oxide at 250°C was less than at 100°C. There is evidence that the decrease in adsorption in going from 150 to 250°C is associated with a decrease in surface area of the hydrous oxide during the high-temperature exposure.

Several adsorption tests were made at 150 and 250°C with UO_2SO_4 solutions containing additives of 0.2 *M* Li_2SO_4 and 0.1 *M* H_2SO_4. In general, the adsorption per gram of hydrous oxide from these solutions was less than that from solutions without the high concentrations of additive.

16. Metallurgy

Zircaloy-2 stock was fabricated to ten experimental and two commercial fabrication schedules, including some cross-rolling, asthe first portion of a study of the effects of fabrication variables on the mechanical anisotropy of plate material. Tensile specimens were broken from all schedules at room temperature and 300°C. The standard tensile values showed so little variation that the effects of the fabrication variables could not be determined. An analysis of the cross sections of fractured round tensile specimens has shown that the cross section is elliptical wherever plastic flow has occurred, with the major axis of the ellipse in the direction normal to the rolling plane. The effects of the fabrication variables can be separated by such analyses, and on this basis it has been shown that none of the experimental schedules produce material appreciably superior in isotropy or properties to the schedule now used for fabricating HRP stock.

The alpha/alpha-plus-beta temperature of normal Zircaloy-2 containing 40 to 50 ppm H_2 was found to be 815°C by resistometric measurements at temperature, in agreement with the prior metallographic determination of 815°C. The alpha/alpha-plus-beta temperature for material vacuum annealed to less than 5 ppm H_2 was raised to 832°C. The beta/alpha-plus-beta temperature for both materials was found to be 985°C. The resistance of Zircaloy-2 approximately doubles in heating from room temperature to 700°C, rises little after that, but decreases rapidly as beta phase is formed.

A study of chemical machining and chemical pickling baths for Zircaloy-2 showed that the rate of metal removal is a function of both HF and HNO_3 content; that the HNO_3 content controls pitting and, when sufficiently high, produces smoothing of the surface; and that in a bath containing 2% HF, a minimum rate of attack occurs at a content of 5% HNO_3.

Determination of the H/D ratio and the total hydrogen contents of zirconium-alloy specimens exposed to D_2O–uranyl sulfate fuel solutions in in-pile loops and to D_2O in the HRT blanket region indicated that no deuterium was picked up during radiation corrosion of the specimens; the deuterium, 3 to 6 ppm D, found in the in-line loop specimens was probably due to absorption or entrapment in the rather heavy oxide film found on the specimens.

Preplaced root inserts were suitable for obtaining flush weld reinforcement in small titanium pipe. Air welds made with inserts were found to have higher hardnesses than similar welds made with hand-fed wire, but the hardnesses were acceptably low.

Filler wire which sparks when used for welding titanium or zirconium has been found to give poor weld quality. The microstructure of this type of wire contained inclusions and had generally distributed porosity. Most of the wire which gave acceptable welds also exhibited porosity, but it was centrally located.

In zirconium welds properly made in air some nitrogen and oxygen pickup during welding leads to poor corrosion resistance, but the contamination has been found to be confined primarily to the top layer of the weld metal. Removal by etching of 0.005-in. of metal gives a surface equal to dry-box welds in resistance to hot-water corrosion.

Air-welding methods developed for Zircaloy-2 were found to be suitable for zirconium–15% niobium alloy. Multipass welds were made on the 15% niobium alloy without causing any appreciable hardening of either weld or base metal.

Measurements of the attenuation of ultrasound in stainless steel weld metal were made as part of a study of the use of ultrasonics for nondestructive testing of welded structures. Welds in stainless steels have so far shown very high attenuation characteristics, making satisfactory examination with ultrasound impossible. Attenuation of ultrasonic energy in Zircaloy-2 base metal has been found to follow the fourth power of frequency in the low-megacycle range. This is characteristic of particulate or Rayleigh scattering. Measurements on carbon and stainless steel base metals

showed that an additional factor is involved in their attenuation of ultrasound.

Resonance measurements at a single location on the HRT core have shown a change in wall thickness from 0.315 in. to 0.278 in. This change occurred during runs 15, 16, and 17. Equipment is being assembled to permit measurements at other locations on the core.

Attempts were made to determine the limiting conditions for the ignition of Zircaloy-2 samples in oxygen atmospheres, but it has not yet been possible to obtain reproducible data. Over a variation in oxygen pressure range of almost 1000 psi, some samples will ignite and others will not. In a dynamic test, ignition occurred at pressures as low as 50 psi oxygen.

The radiation-induced transition-temperature increase in high-purity iron and iron–0.1% carbon alloys was found to be much less than in steels. Thus the high sensitivity of steels to radiation effects is not an inherent property of the carbon-containing body-centered-cubic iron lattice. The ductile behavior of irradiated steels, as evidenced by uniform elongation and the shape of the stress-strain curve, is strongly dependent on microstructure. The notch impact properties of Zircaloy-2 weld metal were not appreciably affected by irradiation.

PART V. CHEMICAL ENGINEERING DEVELOPMENT

17. Uranyl Sulfate Fuel Processing

Exposure of iodate-containing solutions simulating HRT fuel solutions to Co^{60} irradiation at intensities ranging up to 23 w per kg of H_2O did not affect the equilibrium valence distribution of iodine between the elemental and iodate states. Losses of iodine from simulated fuel solutions to the rubber closures used in the HRT sampling operation were as large as 85% of the iodine initially present after 24-hr irradiation at an intensity of 23 w/liter. Loss of iodine from similar solutions at 270°C to corrosion-product solids was about 50% of the iodine initially present, but exchange of iodine between solution and solids is sufficiently rapid to establish equilibrium in 5 min.

A hydroclone attached to a corrosion test loop removed 10% of the solids produced by corrosion of carbon-steel pins placed in the loop as a source of corrosion-product solids. The effect of changing the hydroclone feed take-off position is being evaluated.

18. Gaseous Fission-Product Disposal

Combustion products resulting from burning of charcoal under HRT conditions have been shown to contain CO_2 and are in agreement with the observations of gas composition observed at the HRT during abnormal behavior of the charcoal beds. A decrease of krypton holdup time of 50% was observed when CO_2 was substituted for oxygen as the sweep gas carrying krypton through a charcoal bed. Recombination of hydrogen and oxygen on HRT charcoal was not observed under a variety of flow conditions in the absence of radiation.

19. Equipment Decontamination

The development of improved methods for the decontamination of the HRT is being attempted. Primary emphasis has been placed on use of chromous sulfate, with parallel investigations of other reagents such as those of Turco Products, Inc.

20. Thorium Oxide Slurry Development

Two heavy-water slurries of 1000°C-fired thorium–5% natural uranium were irradiated in the LITR at 300°C, one under an atmosphere of air and the other under D_2. No radiolytic-gas pressure was observed in either experiment at 300°C. Similar slurries irradiated and recovered, along with an out-of-pile test slurry, showed high corrosion-product pickup indicative of a highly abrasive oxide. In other slurry irradiations in the ORNL Graphite Reactor, initial gas production rates at 200°C in heavy-water slurries of thorium–2.8% uranium oxide containing enriched uranium were $4.8–4.9 \times 10^{-4}$ mole of D_2 per hour per liter as

opposed to 3.3×10^{-4} mole of H_2 per hour per liter in the light-water system.

A 1600°C-fired oxide irradiated in a settled condition for 3235 hr contained dark sandlike particles. Refluxing the irradiated oxide for 30 min in 4 *N* HNO_3 solubilized 36% of the U^{233}, 40% of the protactinium, 0.2% of the thorium, and 40% of the gross beta and gamma activities.

In out-of-pile gas recombination studies a slurry of 1600°C-fired oxide containing 0.008 *m* MoO_3 pumped at 280°C under an O_2 atmosphere showed an induction period for catalytic activity under that for $H_2 + \frac{1}{2}O_2$ atmospheres, the length of the induction period increasing with increased pumping time. Substitution of a D_2 atmosphere for the O_2 in the high-temperature loop eliminated the induction period. Both MoO_3 (0.03 *m*) and PdO (1000 ppm Pd, based on thorium) gave acceptable recombination rates in slurries of mixed oxide (U/Th = 0.05) prepared from the coprecipitated oxalates (1000°C firing). The MoO_3, however, was not an effective catalyst in a similar slurry prepared from the simple oxide mixtures. A slurry of the mixed oxide prepared from the coprecipitated oxalates containing Fe_2O_3 (2080 ppm Fe, based on total oxide) did not give satisfactory recombination activity.

An investigation was made of the changes occurring in the thorium oxalates and its oxide product as a function of the oxalate digestion time and temperature. Properties investigated were particle size, chemical nature of the surface, x-ray crystallite size, surface area, and caking tendencies of slurries of the oxide product. Digestion reduced the number of large particles in the fired oxide and virtually eliminated the caking propensity, as indicated by a zero cake resuspension index. The addition of certain bi- and polydentate organic compounds, principally amines, to the oxalate precipitate system caused freshly precipitated thorium oxalate to grow on digestion into square-faced, more or less cubic, particles whose characteristics were essentially retained in the oxide product.

Mixed thorium-uranium oxides were prepared by direct denitration of methanol solutions of TNT and UNH in reflected flames. The initial product particle size, surface area, and chemical composition were within the range considered of interest for mixed slurries.

Two methods of adding uranium to the thorium oxide in the production of engineering quantities of mixed oxide for fuel slurry studies were studied: one, the coprecipitation of the thorium-uranous oxalates and their subsequent decomposition and, the other, the precipitation of the uranium onto a 650°C-fired thorium oxide from ammonium uranyl carbonate solution and subsequent firing to incorporate the uranium in the solid. Particle-size control was achieved in the former method by controlling the precipitation temperature and reagent concentration. The mixed oxide from the latter method retained the particulate properties of the thorium oxide used. Leaching studies with nitric acid showed that a 4-hr firing at 1000°C incorporated the bulk of the uranium in the solid and also showed a fairly homogeneous distribution of uranium in the 1000°C-fired product.

About 2900 lb of thorium oxide fired at 800 and 1600°C was prepared for slurry engineering study. Mixed-oxide products prepared for engineering study were 300 lb with a U/Th ratio of 0.005 and 40 lb containing 0.08 U/Th.

21. In-Pile Slurry Loop

Testing at Westinghouse of the in-pile mockup loop has been delayed a minimum of six weeks by failure of the Graphitar thrust bearing of the Westinghouse model A-13 Cl pump and rupture of a bellows seal on a modified Aminco valve. The Graphitar bearings will be replaced with aluminum oxide bearings and journals, and the balancing holes in the impeller will be replaced with balancing vanes. A slurry demonstration run is tentatively planned for January 1, 1959.

Since the revised loop will be tested at Westinghouse, the ORNL installation will continue with minor delay. Completion is scheduled for about May 1, 1959, with auxiliary equipment to be installed by March 1.

Cylindrical hydroclones tested at ORNL were slightly less efficient than conical hydroclones, but are expected to eliminate plugging of the underflow pot caused by slurries that tend to cake. Apparent efficiencies were higher for intermediate than for low or high ThO_2 slurry concentrations.

A cascade of two (0.4- and 0.25-in.-dia) hydroclones tested for clarification of slurries of 240–400 g of Th per kg of H_2O was more efficient than a three-stage cascade (0.8-, 0.4-, and 0.25-in.-dia). Feed-to-final-overflow concentrations were 6–61 and 1.3–18, respectively. For slurries of

800 g of Th per kg of H_2O, the two-stage ratios decreased to ~2.

PART VI. SUPPORTING CHEMICAL RESEARCH

22. Reactions in Aqueous Solutions

Studies of the homogeneous catalysis of the hydrogen-oxygen reaction by dissolved copper salts in aqueous solutions at elevated temperatures were extended to lower temperatures with improved temperature control. The effects of acidity, copper concentration, and temperature were determined at 175 and 200°C. Increasing the acidity lowered the reaction rate at a given hydrogen pressure. Substitution of dissolved hexavalent chromium for oxygen gas did not affect the reaction rate.

Experiments were performed to test various hypotheses advanced as possible explanations of the reactions causing the disappearance of uranium and copper from the HRT fuel solution during run 17-A and previous runs. The results of these experiments suggested that neither peroxide precipitation nor partial reduction could account for the simultaneous disappearance of both uranium and copper. The available information appeared to support the hypothesis of hydrolytic phase instability.

PART VII. ANALYTICAL CHEMISTRY

23. Analytical Chemistry

A method was devised for the determination of uranium in low concentrations of tin, with a coefficient of variation of about 3%. A coulometric stripping technique was utilized as a means of determining microgram quantities of chloride in solutions of uranyl sulfate. From 1 to 10 μg of chloride in a final volume of 10 ml can be measured by the method, with a coefficient of variation of about 15%. A rapid, sensitive method was developed for the extraction and subsequent flame-photometric determination of microgram quantities of iron in uranyl sulfate solutions containing copper or in 0.5 *M* $CuSO_4$, 1 *M* H_3PO_4, 1 *M* H_2SO_4, or 1 *M* HF solutions. Iron in the range of 2 to 10 μg/ml in uranyl sulfate or the other solutions can be measured, with a coefficient of variation of 2%.

CONTENTS

SUMMARY iii

PART I. HOMOGENEOUS REACTOR TEST

1. HRT OPERATIONS 3
   1.1 Reactor Operations 3
   1.2 Experimental Analysis 4
   1.3 Solution Chemistry and Corrosion 6
   1.4 Conclusions 7
2. REMOTE OPERATIONS AND DEVELOPMENT 8
   2.1 Preliminary Investigation Following Run 17 8
   2.2 Observation of the Hole in the Core Tank 8
   2.3 Screen-Sample Cutting 9
   2.4 Corrosion-Sample Recovery 9
   2.5 External Light Source and Telescope 9
   2.6 Television Camera and Manipulator 13
3. HRT PROCESSING PLANT 14
   3.1 Performance of the Hydroclone System 14
      3.1.1 Corrosion-Product Removal Data 14
      3.1.2 Concentration of Uranium, Copper, and Nickel 14
      3.1.3 Fission-Product Removal Data 15
      3.1.4 Calculated Solids Accumulation in the Underflow Pot from Fission-Product Heating Data 15
      3.1.5 Equipment Performance 16
   3.2 Auxiliary Processing Systems 16
      3.2.1 Iodine Behavior in Run 17 16
      3.2.2 Charcoal-Bed Status 17
      3.2.3 Waste System 18
      3.2.4 Removal of Initial Fuel Batch from Fuel Storage Tanks 18
4. HRT REACTOR ANALYSIS 19
   4.1 Power Excursions in the HRT 19
      4.1.1 Frequency of Excursions 19
      4.1.2 Magnitude of Excursions 21
      4.1.3 Analyses of Excursions 21
   4.2 Small Power Oscillations in the HRT 24
   4.3 Reactivity Changes Associated with Various Events 25
      4.3.1 Reactivity Associated with Uranium Movement 25
      4.3.2 Reactivity Associated with Movement of Core Corrosion Specimen 26
      4.3.3 Reactivity Associated with Void Formation 26
      4.3.4 Estimated Power and Reactivity Fluctuations Due to "Cold-Fluid" Motion 27
      4.3.5 Effect of Fuel Circulation upon Time Behavior of Reactor Power 27

4.4 Effect of HRT Changes upon Critical Conditions 28
4.4.1 Effect of Uranium Deposition on Critical Fuel Concentration 28
4.4.2 Effect of Introduction of Corrosion-Sample Assembly upon Thermal-Flux Distribution 29
4.4.3 Operation of HRT with Different Core and Blanket Temperatures 29

5. HRT DESIGN 31
5.1 Temperature Distribution in Existing Reactor Vessel 31
5.2 Replacement Pressure Vessel 31
5.3 Thimble for Flux Monitors 31
5.4 Condenser Stress-Corrosion Specimens 31
5.5 Solution Purge Tube in Core 31
5.6 Maintenance and Inspection 34
5.6.1 Flange-Groove Spray Device 34
5.6.2 Collector for Radioactive Solids 35

6. HRT COMPONENT DEVELOPMENT 36
6.1 Pumps 36
6.2 HRT Core Studies 36
6.2.1 Modifications in Present Geometry 36
6.2.2 HRT Replacement Core 36
6.3 HRT Mockup 38
6.3.1 Operation 38

7. HRT CONTROLS AND INSTRUMENTATION 40
7.1 Component and System Testing 40
7.1.1 System for Indicating Control-Valve Stem Position 40
7.2 Component Development 40
7.2.1 Letdown Valves 40
7.3 Maintenance and Modifications 41
7.3.1 Blanket Dump Valve 41
7.3.2 Control-Circuit Revisions 41

PART II. REACTOR DESIGN, RESEARCH, AND ANALYSIS

8. HRE-4 DESIGN 45
8.1 HRE-4 Preliminary Design 45
8.1.1 Design Data 45
8.1.2 Flowsheet 45
8.1.3 Operation 45
8.1.4 Heat Removal System 47
8.1.5 Circulation Pump 48
8.1.6 Dump Tank 48
8.1.7 Transfer System 48
8.1.8 HRE-4 Off-Gas System 49
8.1.9 Reactor Shielding 49
8.1.10 Conceptual Layouts 50

9. RESEARCH AND ANALYSIS 53
9.1 Nuclear Characteristics of Single-Region Slurry Reactors 53
9.1.1 Criticality Parameters and Reactivity Coefficients 53
9.1.2 Reactivity Changes Associated with Slurry Settling 57
9.2 Nuclear Characteristics of Reflected Slurry Reactors 58
9.2.1 Critical-Mass Ratios 58
9.2.2 Reactivity Control Associated with Dumping the Reflector 61
9.2.3 Reactivity Changes Associated with Slurry Settling 62
9.3 Criticality Considerations in the Design of Slurry Dump Tanks 62
9.4 Stress Analysis of Vessels for Small Single-Region Slurry Reactors 64
9.5 Age of Fission Neutrons in D_2O-H_2O Mixtures 66
9.6 Machine Programming 67
9.7 Nuclear Constants 68
9.8 Flow Properties of Thoria-Water Slurries 68
9.8.1 Friction-Factor Measurements 68
9.8.2 Critical Reynolds Number 71
9.9 Physical Properties of Thoria-Water Slurries 73
9.9.1 Influence of Surface-Active Agents on Slurry Behavior 73
9.9.2 Thoria Caking Studies 73

PART III. ENGINEERING DEVELOPMENT

10. DEVELOPMENT OF FUEL- AND SLURRY-SYSTEM COMPONENTS 81
10.1 Recombiner and Pressurizer Development 81
10.1.1 High-Pressure Recombiner Loop 81
10.1.2 Syracuse Contract 81
10.1.3 Solubility of Oxygen and Hydrogen in Fuel Solution 81
10.2 Centrifugal Pumps 81
10.2.1 20-cfm Allis-Chalmers Blower 81
10.2.2 Reliance 6000-gpm Pump 81
10.2.3 300A Slurry Pump and Loop 82
10.2.4 200Z Loop and Pump 82
10.2.5 320A SBM Pump 82
10.2.6 Slurry-Bearing Test Program 82
10.2.7 Shaft Seals 82
10.2.8 Impeller-Velocity Study 83
10.3 Oxygen Compressors 83
10.3.1 Turbine Pump 83
10.3.2 Slurry Feed Pumps 83
10.4 Valve Trim 85
10.4.1 Dump-Valve Trim for Solutions 85
10.4.2 Slurry Hand Valves 85
10.4.3 Slurry Letdown Valves 85
10.5 Titanium Program 86
10.6 Slurry Heat Exchanger Flow Tests 86

10.7 Core Hydrodynamics 87
10.7.1 HRE-3 Re-entrant Core Model 87
10.7.2 Single-Region Slurry Core 87
10.8 Slurry Dump Tanks and Evaporators 87
10.9 Properties of Settled Beds 87
11. DEVELOPMENT OF REACTOR SLURRY SYSTEMS 89
11.1 Circulating-Slurry Behavior 89
11.1.1 200-gpm Loop Operation 89
11.1.2 Circulating Test in S-Loop (100 gpm) 95
11.1.3 Fluidized-Bed Test in T-Loop (100 gpm) 95
11.2 Blanket System Development 99
11.2.1 System Performance Data 99
11.2.2 Conversion of 300-SM Loop to High-Pressure Operation 99
11.2.3 Pressure-Vessel Model Studies 99
11.2.4 Development of Gamma-Transmission Density Measurements 100
12. INSTRUMENT AND VALVE DEVELOPMENT 102
12.1 Instrument Development 102
12.1.1 Flush-Diaphragm Differential-Pressure Transmitter 102
12.1.2 Heated Thermocouple-Probe Liquid-Level Sensor 102
12.1.3 Liquid-Level Alarm Transmitter 102
12.1.4 Capacitance-Type Liquid-Level Measuring System 104
12.2 Valve Development 104
12.2.1 Solution Sampling Valve 104
12.2.2 Valve Actuators 109
12.2.3 Remotely Actuable Air-Line Disconnect 109
12.2.4 Slurry Service Valves 111

PART IV. REACTOR MATERIALS RESEARCH

13. SOLUTION CORROSION 115
13.1 Dynamic Solution Corrosion 115
13.1.1 Instability of Dilute Uranyl Sulfate Solutions in a Heated Bypass Section 115
13.1.2 Stability of Dilute Uranyl Sulfate Solutions Containing Alkali or Alkaline-Earth Sulfates 116
13.1.3 Oxidation of Chromium(III) in Uranyl Sulfate Solutions in the Presence of Ruthenium 117
13.1.4 Effect of Cold Work and Heat Treatment on the Corrosion of Type 347 Stainless Steel 117
13.1.5 Stress-Corrosion Cracking of Stainless Steel in Water at 200°C; Effects of Fluoride and Phosphate Ions 118
13.2 Laboratory Corrosion Studies 119
13.2.1 Stress-Corrosion Cracking in Uranyl Sulfate Solution 119
13.2.2 Stress-Corrosion Cracking in Chloride-Containing Water 120
13.2.3 Stress-Corrosion Cracking in Oxygenated Thorium Oxide Slurry 121
13.2.4 Chemiluminescent Solution for Detection of HRT Core-Tank Defect 121
13.2.5 Miscellaneous Corrosion Tests 122

14. SLURRY CORROSION 124
14.1 Pump Loops 124
14.1.1 Loop Engineering: Hydroclone for Slurry Removal 125
14.1.2 Introduction to Pump Loop Tests 125
14.1.3 Circulation of ThO_2-D_2O Slurry in Oxygen and Deuterium Atmospheres 125
14.1.4 Materials Evaluation Tests 126
14.2 Toroids 128
14.2.1 Introduction 128
14.2.2 Tests with Slurries of Thoria Prepared by the Draft-Tube Method 128
14.2.3 Tests with Slurries of Thoria Microcubes 129
14.2.4 Examination of a Severe Impingement and Eddy Erosion Attack 129
14.3 In-Pile Autoclave Slurry Corrosion Tests 133
14.3.1 Development, Construction, and Operation 133
14.3.2 Introduction to Autoclave Experiments 133
14.3.3 Abnormal Pressure Behavior 133
14.3.4 Recombination of Radiolytic Gases 135
14.3.5 Effects of Time and Radiation on Generalized Corrosion Rates 137
14.3.6 Examination of Irradiated Thoria and Pin Corrosion Specimens 139
14.4 In-Pile Slurry Toroid 140
14.4.1 Engineering Development 140
14.5 In-Pile Slurry Loop 140
14.5.1 Loop Development 140
15. RADIATION CORROSION 142
15.1 In-Pile Loops 142
15.1.1 General Description of In-Pile Loop Experiment L-2-21 142
15.1.2 Results of Qualitative Inspection and Metallographic Examination of Loop L-2-21 148
15.1.3 Analysis of Data from Loop L-2-21 152
15.1.4 Development and Construction 164
15.2 In-Pile Rocking-Autoclave Tests – LITR 166
15.2.1 Development, Construction, and Operation 166
15.2.2 Results and Discussion 166
15.3 Corrosion Specimen Exposed in the HRT Blanket Region During Runs 13 and 14 177
15.4 Examination of Core Access Flange, Attached Specimen, and Scales Removed from the HRT After Run 16 178
15.5 Supporting Radiation-Corrosion Studies 179
16. METALLURGY 184
16.1 Physical Metallurgy 184
16.1.1 Zircaloy-2 Fabrication Study 184
16.1.2 Morphology of Zircaloy-2 186
16.1.3 Chemical Machining and Pickling Study of Zirconium-Base Alloys 187
16.1.4 Electroless Nickel Plating on Zirconium Alloys and Oxide 187
16.1.5 Zirconium-Hydrogen Study 187
16.1.6 Zirconium-Alloy Development 188
16.2 Welding Development 189
16.2.1 Titanium 189
16.2.2 Zircaloy-2 189

16.3 Nondestructive Testing Development 190
16.3.1 Ultrasonic Attenuation 190
16.3.2 Resonance Measurements of the Zircaloy-2 Core Shell 191
16.3.3 Combustion of Titanium and Zirconium 191
16.4 Effects of Radiation on Structural Metals and Alloys 192
16.4.1 Equipment and Facilities 192
16.4.2 Impact Tests 192
16.4.3 Tensile Tests 192

PART V. CHEMICAL ENGINEERING DEVELOPMENT

17. URANYL SULFATE FUEL PROCESSING 197
17.1 Iodine Chemistry 197
17.1.1 Laboratory Experiments 197
17.1.2 HRT Operating Experience 197
17.2 Solids Behavior 198
17.3 Alternate Core Processing Development 198
18. GASEOUS FISSION-PRODUCT DISPOSAL 199
18.1 Abnormal Behavior of HRT Charcoal Beds During Run 17 199
19. EQUIPMENT DECONTAMINATION 201
19.1 HRT Decontamination Studies 201
20. THORIUM OXIDE SLURRY DEVELOPMENT 202
20.1 Slurry Irradiation Studies 202
20.1.1 Slurry Irradiations in the LITR 202
20.1.2 Postirradiation Examinations 202
20.1.3 In-Pile Gas Production and Recombination Studies 203
20.1.4 Equipment Development 204
20.2 Gas Recombination Studies 204
20.2.1 High-Temperature Loop Experiments 204
20.2.2 Catalysis in Thorium-Uranium Oxide Slurries 205
20.3 Thorium Oxide Preparation Development 207
20.3.1 Thorium Oxalate Precipitation 207
20.3.2 Preparation of Cubic Particles 207
20.3.3 Flame Denitration Studies 209
20.3.4 Fluidized-Bed Denitration Studies 211
20.4 Thorium-Uranium Oxide 211
20.4.1 Coprecipitation 212
20.4.2 Adsorption 213
20.5 Thorium Oxide Production 214
21. IN-PILE SLURRY LOOP 215
21.1 Westinghouse Status 215
21.2 ORNL Status 215

21.3 Equipment Development 220
21.3.1 Hydroclone Collection of ThO_2 Slurry 220
21.3.2 Hydroclone Purge-Water Preparation 221

PART VI. SUPPORTING CHEMICAL RESEARCH

22. REACTIONS IN AQUEOUS SOLUTIONS 225
22.1 Homogeneous Catalysis of the Hydrogen-Oxygen Reaction in Aqueous Solutions 225
22.2 Chemical Studies Relating to HRT Run 17-A 226

PART VII. ANALYTICAL CHEMISTRY

23. ANALYTICAL CHEMISTRY 231
23.1 Determination of Uranium in Tin 231
23.2 Determination of Chloride in Uranyl Sulfate Solutions 231
23.3 Determination of Iron in Uranyl Sulfate and Other Solutions 231
ORGANIZATION CHART 233

Part I

HOMOGENEOUS REACTOR TEST

S. E. Beall

1. HRT OPERATIONS

S. E. Beall P. N. Haubenreich J. W. Hill, Jr.
H. F. Bauman D. F. Frech D. M. Richardson
N. C. Bradley R. H. Guymon J. A. Russell
J. R. Buchanan R. J. Harvey D. Scott, Jr.
S. R. Buxton J. Hirota[1] J. E. Sutherland
J. R. Engel J. O. Kolb W. Terry
J. D. Flynn K. W. West

As reported in the previous progress report, several questions remained outstanding after run 16 power operation with the hole in the core tank. First, it appeared that uranium was being lost from the fuel solution as the reactor power was increased. Second, on several occasions unexplained brief power excursions occurred. Third, the amount of corrosion-product solids removed by the chemical processing plant was low by comparison with the amount of solids thought to be in the reactor system. The purpose of run 17 was to explore these three problems, as well as to expose arrays of corrosion samples which had been installed in the core and blanket regions during the three-week shutdown which followed run 16.

1.1 REACTOR OPERATIONS

Run 17 was begun on July 31, with heavy water circulating in both fuel and blanket systems at 1750 psig and 270°C. These and other operating conditions were to be similar to those used for run 16, with a core fuel concentration of 6 g of U^{235} per kg of D_2O, approximately three times the blanket fuel concentration. In order to maintain these conditions with the poison associated with the new corrosion specimens, it was necessary to increase the fuel charge by the addition of 1.3 kg of U^{235}. In the course of the startup, critical experiments were performed to determine the concentrations of fuel required for criticality at several core temperatures (see Sec. 1.2).

In all previous runs the solution temperatures within the core had to be estimated, because no thermocouples were present. The corrosion-specimen assembly installed for run 17 contained three thermocouples and afforded an opportunity to explore core solution temperatures. Temperatures were observed as the reactor was operated first at heat-loss power, then at 1 and 2 Mw.

After the reactor had been at 2 Mw for 4 hr, the fuel-dump-tank pressure, which had been rising gradually, suddenly dropped to atmospheric pressure. At the same time the off-gas meter started indicating a vacuum in the charcoal-bed exit, and no off-gas flow was indicated for a period of 4 hr. The significance of this event did not become apparent until several days later when the off-gas activity rose. Investigations showed that the sudden pressure reduction was caused by recombination of radiolytic gas throughout the low-pressure system and must have ignited carbon in one of the two adsorption beds, which burned slowly and released some of the adsorbed radioactivity. This incident is reported more fully in Sec. 3.2.2. The release of activity was stopped quickly by routing the off-gas into a spare adsorption bed.

The thermocouple temperatures behaved reasonably during the first 100 hr. On the fifth day, however, after the power level had reached 3.0 Mw, the lowest of the three core thermocouples, which had been reading only 3°C above the solution outlet temperature suddenly indicated an emf equivalent to 1250°C. By reducing the reactor power, it was found that the indicated temperature varied with reactor power and returned to normal at zero power. For the next 24 hr while the reactor power was gradually raised to 4 Mw, the temperature indication was very erratic, and the first thermocouple was assumed to have failed. The second thermocouple failed in a similar fashion the next day, but the third thermocouple, located near the core outlet, continued to indicate normally until the end of the run. Its maximum temperature was approximately 14°C above the core outlet temperature when the reactor was at 3.5 Mw.

Small power excursions had been observed from time to time during operation at lower power, but at 3 to 4 Mw they appeared to be much more frequent (see Secs. 4.1 and 4.2). Furthermore, the uranium

[1]Japanese Atomic Energy Research Institute.

inventory as determined from the reactor critical temperature was in wide disagreement with the reactor inventory determined from uranium analyses (see Sec. 1.3). On August 10, the fuel-inventory problem was studied as the reactor power was reduced to 0.5 Mw for several hours and then was quickly raised to 3.5 Mw; the fuel solution was sampled immediately after the 3.5-Mw level was attained and again 2 hr later. The results of these samples showed that a uranium loss of approximately 1500 g had occurred in the 2 hr between sampling and provided additional proof that the uranium loss was power-dependent. Furthermore, the fact that the reactor temperature did not indicate a significant loss of reactivity suggested that the missing uranium was accumulated in the core where it could contribute to the reactivity. The uranium inventory decreased further when the reactor power was raised in steps to 5 Mw, although the frequency and magnitude of the power excursions did not appear to increase.

The possibility of an acid deficiency in the fuel solution was explored on August 21 by increasing the acidity of the solution approximately 15%. The acid addition appeared to reduce the uranium loss, although it was several days before this could be conclusively shown from the accumulated sample analyses. The relationship of lost uranium to power was again demonstrated by reducing the reactor power to 0.5 Mw. When the reactor was returned to the 3.5-Mw level, it was found that the uranium loss occurred within the first hour.

At this time it was discovered that a small amount of kerosene was leaking from the refrigeration system into the shield. Because this could create an explosion hazard, the reactor power level was reduced for 36 hr while the kerosene vapors were purged from the container with nitrogen gas. The nitrogen atmosphere was maintained for the remainder of the run and will be maintained in future runs.

On August 28, in a study of the effects of flow on the uranium loss and power excursions, the fuel circulating pump was run in reverse, causing the fuel circulating rate to be reduced from its normal 450 gpm to approximately 130 gpm. The reduction in flow rate did not result in any apparent reduction in uranium loss but appeared to increase the frequency of excursions.

It was next decided to undertake a systematic study of the relationship between temperature, power, and uranium loss from the circulating liquid. Throughout the next 12 days the reactor operation was continued at temperatures from 240 to 290°C and at power levels from 0.1 to 3.5 Mw. No clear relationship between temperature and uranium loss could be determined, although the variation with power was established in detail (see Sec. 1.2). There was no apparent relationship between the frequency or magnitude of power excursions with temperature, but an unusual excursion occurred on August 30. The reactor had been steady at 3.5 Mw and an average temperature of 245°C for 20 hr when the power increased rapidly to 25 Mw. This excursion involved a total of 2.1% Δk_e, introduced over the relatively long period of 10 sec. The power level was immediately reduced to zero and held there for 36 hr. It was then increased to 1.8 Mw and held at that level for the next 36 hr, but no excursions were experienced. When the reactor power was raised again to 3.5 Mw, operation remained normal, and the temperature-power study was continued.

On September 10, another acid addition was made to increase the free acid of the fuel solution by approximately 12.5%. After two days the reactor pressure was gradually reduced from the normal 1750 psig to 1250 psig. Neither of these experiments produced observable changes in the inventory and power-excursion behavior, although the beneficial effect of the acid was not to be recognized until the complete chemical data were available (see Sec. 1.3).

Run 17, the longest continuous run to date, was concluded on September 12, after accumulating 1074 hr during which 2526 Mwhr of thermal power was generated. The reactor was shut down so that the mass of data collected during the 43 days of operation could be studied in detail, and to allow another examination of the internal parts of the reactor (see Chap. 2). Except for the minor mechanical difficulties already mentioned, equipment performance was trouble-free and completely satisfactory, as had been the experience in previous runs.

1.2 EXPERIMENTAL ANALYSIS

Solution behavior during run 17 was studied by computing from sample results the total amount of uranium out of circulation and the net effectiveness (from a reactivity standpoint) of the noncirculating uranium.

The total amount of uranium in the reactor system is known from records of all additions and withdrawals, including removal through the chemical plant and burnup. The amount of uranium present can also be calculated from sample analyses and the indicated weights (or volumes) of solution. During run 17, as in earlier runs, the amount of circulating uranium, as calculated from the uranium concentration in samples, was considerably less than the total mass known to be in the system. The amount of *noncirculating* uranium, or the difference between the amount based on inventory records and the amount apparently in circulation, was found to depend on reactor power, as shown in Fig. 1.1. There appeared to be no significant correlation of noncirculating uranium with temperature. The amount missing at zero power is about the same fraction of the total inventory as appeared to be missing during earlier operation at zero power, including depleted-uranium runs and the initial critical experiments.

During run 17, the reactor was critical at low power at a number of different temperatures. Sample results taken under these conditions were used to establish the relation between critical concentrations and temperature. Figure 1.2 shows results

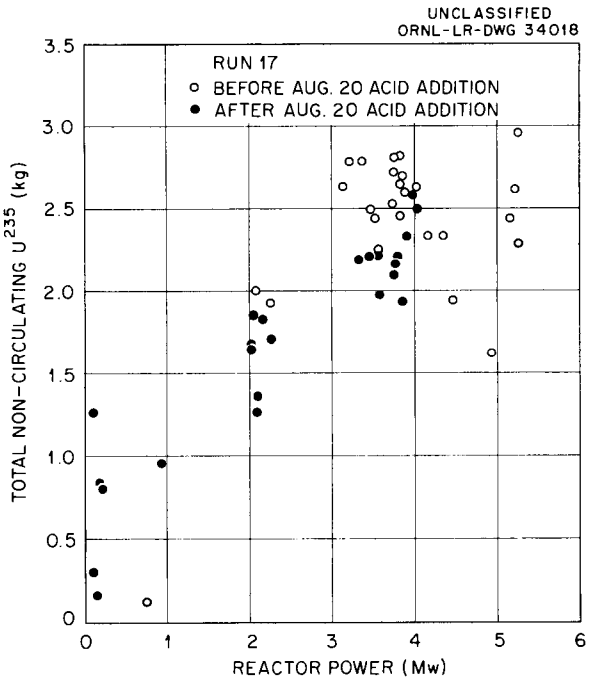

Fig. 1.1. Total Mass of Noncirculating U^{235} vs Reactor Power During Run 17.

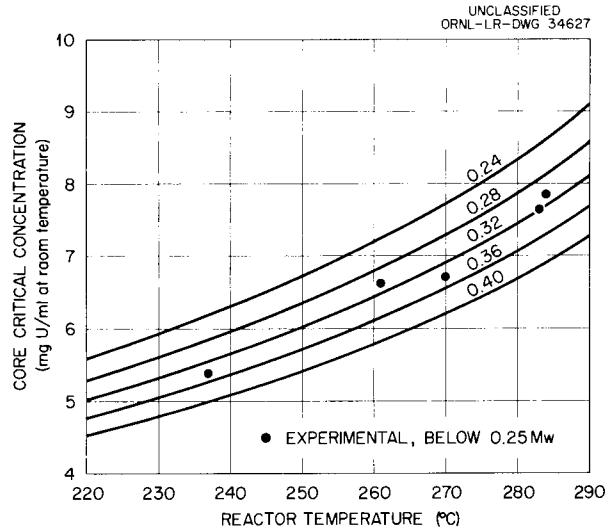

Fig. 1.2. Core Critical Concentration vs Reactor Temperature with Ratio of Blanket Core Concentration as a Parameter. Corrosion assemblies were present in the core and blanket.

of fuel high-pressure samples taken when the reactor power was 0.25 Mw or less. Individual blanket samples taken during run 17 indicated concentrations between 0.25 and 0.40 of the core concentrations, with an average (based on uranium, sulfate, and copper results) of 0.32. The curves shown on Fig. 1.2 were obtained by adjusting results of critical calculations to give agreement with the low-power sample analyses.

Any time the reactor is operating at power, it is possible to estimate the ratio of concentrations in the core and blanket from the observed ratio of power produced in the core to that in the blanket. With this concentration ratio and the critical temperature, Fig. 1.2 can be used to estimate concentrations in both regions. Concentrations obtained in this way are "effective" values, which are greater than the concentration of circulating material if there is any noncirculating material contributing to the reaction. The magnitude of the effective increase in concentration is determined by the product of the mass of effective noncirculating uranium and its average specific importance as compared with the average specific importance of circulating uranium. The mass and the average specific importance cannot be measured separately. Some indication of the magnitude of the effect of noncirculating uranium during run 17 was obtained by calculating the amount of noncirculating uranium

with an arbitrarily assumed importance which could account for the difference between the effective and the circulating concentrations. Figure 1.3 shows results of some of these calculations. These results are based on the assumption that noncirculating uranium contributing to power in the core was at a

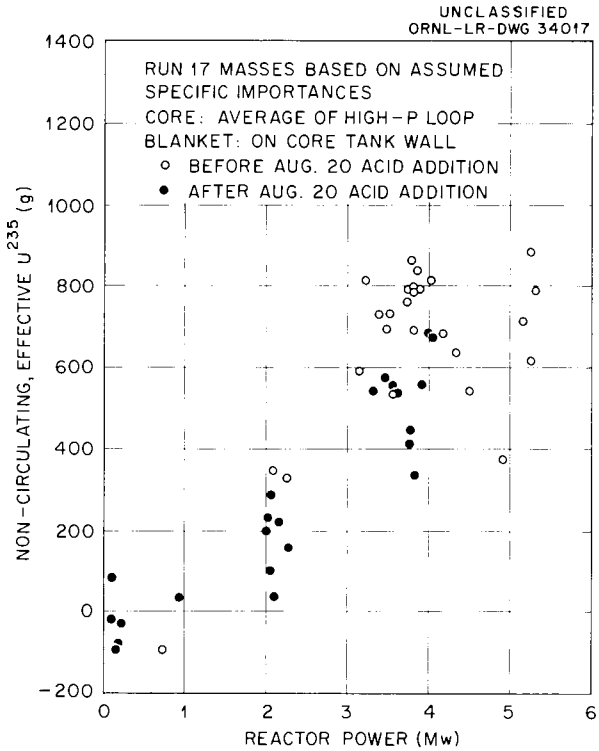

Fig. 1.3. Mass of Noncirculating Effective U^{235} vs Reactor Power During Run 17.

position of importance equal to the average importance of uranium circulating in the fuel high-pressure system. (Uranium in the screen region of the core inlet near the intersection of the conical sections has about this importance.) In this analysis, noncirculating uranium contributing to blanket power was assumed to be on the spherical part of the core tank.

1.3 SOLUTION CHEMISTRY AND CORROSION

In addition to the proportional loss of uranium with reactor power as mentioned in Sec. 1.2, the fuel-solution analyses also established that the loss of metal cations was accompanied by an increase in free sulfuric acid relative to total sulfate and suggest that the loss of cations is by hydrolysis.

The data from 62 samples of core solution are plotted in Fig. 1.4 as the mole fraction metal cation (of the total metal cations analyzed) vs total nuclear power. This graph shows that the relative amounts of U, Cu, and Ni remained constant at all power levels and therefore that the material missing from solution contained the same proportions of U, Cu, and Ni. The change of inventory with time can also be observed; the uranium points from runs 17-B and 17-C were lower and the nickel points were higher than the average. The decreasing uranium inventory was consistent with nuclear burnup and chemical-plant removals. The increasing nickel inventory was consistent with an average corrosion rate of 1 mpy for the type 347 stainless steel in the core and blanket high-pressure systems.

Two indications that the power-dependent loss of solute was in part at least the result of low free-acid inventory were noted in run 17: First, the loss of circulating uranium plotted in Fig. 1.3 appeared to reach a limit at 3.5 to 4.0 Mw total power, and plots of the increase in free acid with power showed similar indications of leveling-off. Second, the loss of metal cations from solution was less, at a given power level, following each of two additions of sulfuric acid to the reactor (runs 17-B and 17-C). An interpretation of these effects is that metal cations were lost from solution as partial hydrolysis products until the free acid reached a level sufficient for fuel-solution stability. The analysis of run 17 samples, based on inventory and solution data, indicated that the ratios of solute to free acid required for fuel-solution stability were UO_2SO_4/H_2SO_4 0.5, $CuSO_4/H_2SO_4 = 1.0$, and $NiSO_4/H_2SO_4 = 1.0$ and that the precipitated inventory was composed of $2UO_3 \cdot SO_3$, $3CuO \cdot SO_3$, and $NiO \cdot SO_3$. The solution data of run 16-C were consistent with this model, since the calculated stable fraction of metal inventory in solution (for which there was adequate free acid according to this model) also reached, but did not exceed, unity with increasing power.

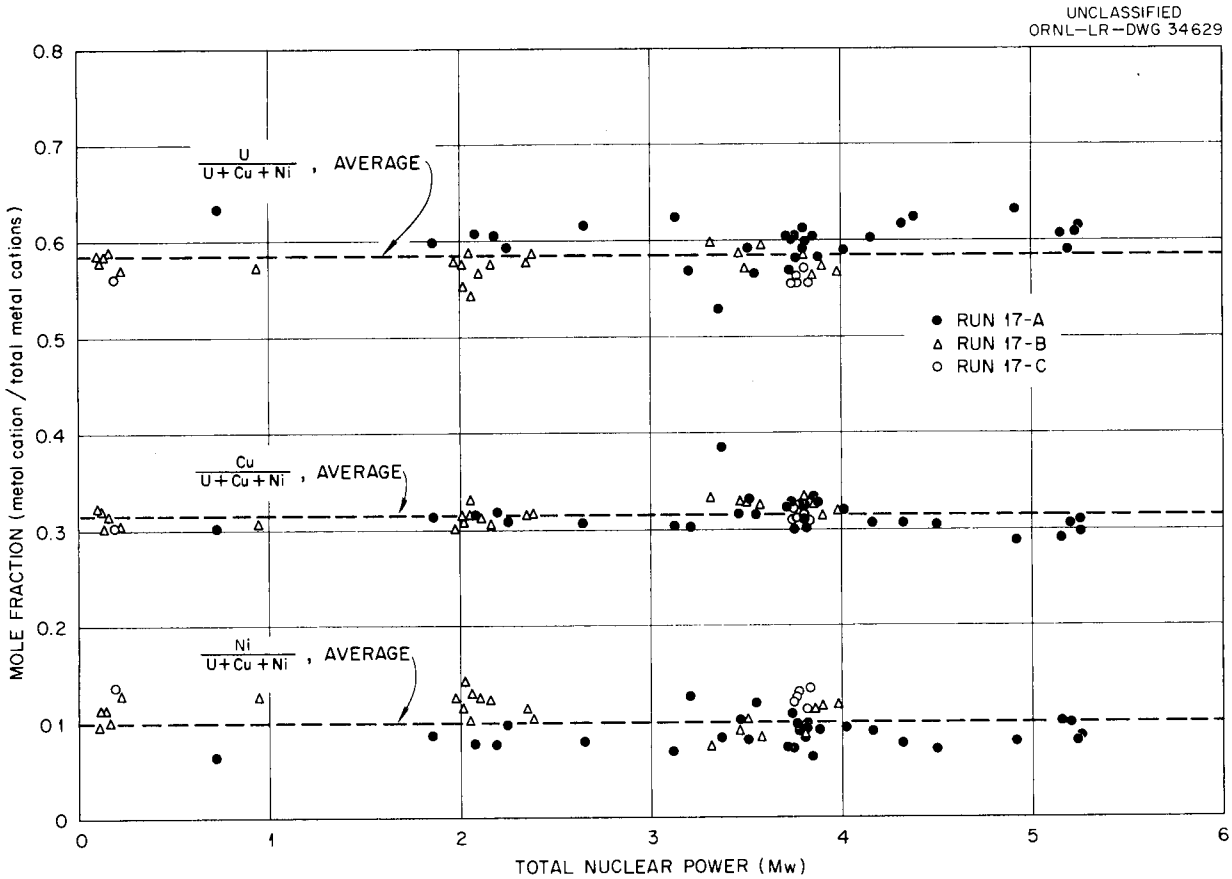

Fig. 1.4. Core Solution Data for Run 17.

1.4 CONCLUSIONS

As discussed in the foregoing sections, it is concluded that uranium separates reversibly from the fuel solution in a manner which is related to the composition of the fuel and to the reactor power. From the criticality data, it appears that much of the separated uranium collects on the metal surfaces of the core tank, presumably because they are at high temperature. After the fuel solution has lost a kilogram or more of uranium, power excursions occur that can be attributed to shifting of the material in the core or to redissolution with resulting changes in reactivity. If enough uranium collects in one place on a metal surface in the core, the nuclear heating causes the temperature to rise uncontrollably, and the metal melts. Examination of the interior of the core with periscopes (Chap. 2) and metallographic examination of the corrosion specimens and pieces removed from the perforated plates in the core inlet indicate that some of the metal has been heated to temperatures above 1000°C. There is reason to believe that the hole in the core tank and the severe corrosion of the perforated plates in the core inlet resulted from overheating.

2. REMOTE OPERATIONS AND DEVELOPMENT

S. E. Beall W. R. Gall I. Spiewak

H. F. Bauman
R. Blumberg
N. C. Bradley
J. R. Buchanan
C. W. Collins
J. S. Culver
J. D. Flynn
D. F. Frech
R. J. Harvey
J. W. Hill, Jr.
E. C. Hise
P. P. Holz
J. E. Jones
M. I. Lundin
R. L. Moore
J. L. Redford
J. N. Robinson
R. C. Roller
D. Scott
F. C. Zapp

Run 17 was terminated for the purposes of removing the exposed corrosion specimens and of examining the interior of the core and pressure vessel, including the hole in the wall of the core tank.

2.1 PRELIMINARY INVESTIGATION FOLLOWING RUN 17

After the reactor was rinsed with condensate, the core access flange was opened and the corrosion-specimen assembly was moved to the hot storage pool. The radiation level in the air approximately 4 ft below the core specimen holder was 400 r/hr. The crane operator was behind temporary shielding during the transfers.

On September 17, approximately 100 hr after shutdown, radiation measurements were made inside the core vessel with a Victoreen Instrument Company roentgen rate meter, which has a full-scale reading of 1000 r/min. The meter went off-scale[1] in the core outlet pipe, nearly 3 ft above the core vessel.

During the period September 18–21, a tilting-mirror periscope was used for viewing the interior of the core vessel. The inner surface of the upper hemisphere had a uniform light-gray-to-metallic color and appeared as it had before power operations were started. However, the top diffuser screen and the core wall near the top screen were deeply attacked, and at several locations small portions of the screen webbing had corroded away. Several corrosion specimens were seen to be lying on the top screen. When the corrosion-sample assembly was examined in the hot storage pool, it was seen that 22 of the 48 specimens had become detached from the holder.

On September 28, all the missing corrosion specimens were located and their positions on the top diffuser screen were "mapped," by use of a tilting-mirror periscope.

[1] K. W. West, "Radiation Level Measurements in HRT Core Vessel," memorandum to S. E. Beall, Sept. 23, 1958.

After the blanket access flange was opened and the blanket corrosion assembly was moved to the hot storage pool, a core-vessel thickness measurement was made at the equator of the vessel by means of an ultrasonic probe.[2] The observed thickness, 0.278 in., was 0.043 in. less than that measured in July 1957, in the same location.

2.2 OBSERVATION OF THE HOLE IN THE CORE TANK

Prior testing in the core flow model had disclosed that gas bubbles rise vertically through the screen system. Accordingly, on September 19, oxygen was metered into the blanket vessel with the condensate level in the core just above the top screen. The hole was indicated to be about 15 deg west of south at the elevation of the intersection of the 60- and 90-deg cones. A tilting-mirror periscope was used to view the escaping bubbles, which were illuminated by two screen-enclosed drop lights.

A refined model of the remotely operated mirror devices used during the two previous shutdowns was installed in the blanket region at the position indicated by the bubble test, and the hole which had been in the core vessel since April 4 was clearly visible. It was estimated to be very nearly round and between 1 and 2 in. in diameter. Future study of the photographs, one of which is reproduced in Fig. 2.1, should reveal its exact dimensions. Its location coincided with the elevation previously determined by pumping condensate through the hole.[3]

The entire outside surfaces of the 30- and 90-deg cones of the core vessel, normally out of view, were

[2] J. K. White, "Resonance Measurement of Zircaloy-2 Core Shell of the HRT," memorandum to G. M. Adamson, Sept. 25, 1958.

[3] R. Van Winkle and R. H. Guymon, *A Review of the Data and Observations Taken for the Purpose of Locating and Estimating the Size of the Hole in the Core*, ORNL CF-58-6-112 (June 13, 1958).

Fig. 2.1. Photograph of Hole in HRT Core Tank as Seen in Viewing Mirror (View from Blanket Side).

examined by use of the remote mirror. There was only one hole. The nearer half of the core exterior was also observed in detail; the appearance of all surfaces was essentially the same as it had been before runs 14 and 16.

The device used to view the hole is shown in Fig. 2.2 in the extended position with its lamp cage hanging down from the extreme end of the arm. A 200-w projection lamp enclosed in wire mesh, with metal reflector, provided the light; a spare lamp was included. A fused-silica window was mounted at the bottom of the square envelope to protect the periscope from contamination.

2.3 SCREEN-SAMPLE CUTTING

It was decided, after the hole in the core tank had been viewed from the blanket side, to cut 2-in. samples from the center of the top six diffuser screens. This would permit viewing of the diffuser system and the inside of the hole in the core tank.

A hole cutter had been designed to cut and remove 1-in.-dia samples from the edge of the top screen. A new tool was built, eliminating the folding arms required for the offset and increasing the size of the cutter. The tool-steel cutting head is shown in Fig. 2.3 with several test specimens retained on the pilot by a spring clip. As each screen is cut, the piece is forced up into the hollow cutter and retained by the spring. The long pilot was intended to ensure insertion in the aligned center holes of the diffuser screens.

Holes 2 in. in diameter were cut in the top six screens on October 2. When the cutter was removed to the hot storage pool, it was found that the cutter pilot had broken, which allowed two of the screen specimens and the tip of the pilot to remain in the core.

By use of a tilting-mirror periscope with a 6-v bulb, detailed observations were made of the inner wall of the core down to the seventh screen from the top. The hole was clearly visible. (A composite view of the hole from the interior of the tank is shown in Fig. 2.4.) As a result of these observations and tests with a lifting hook, it was established that the first, second, and fifth screens are not attached to the core and that all but 2 of the 22 corrosion specimens had fallen below the top screen during the cutting operations.

2.4 CORROSION-SAMPLE RECOVERY

A retrieving tool, shown in Fig. 2.5, was developed for transferring the specimens from the top screen to a bucket mounted at the central channel. This tool contains remotely operated jaws built into a standard tilt-mirror periscope, which permits viewing while specimens are being retrieved. The two specimens on the top screen were recovered. Then, after the two loose top screens were moved to a standing position out of the way, four samples were recovered from the third screen. Recovery operations for the remaining specimens and other objects are still in progress.

2.5 EXTERNAL LIGHT SOURCE AND TELESCOPE

An external light source and telescope, Fig. 2.6, has proved very useful in observing the area in the center of the screens while auxiliary manipulating and viewing devices are being inserted in the core tank. Since the apparatus does not occupy the core opening, anything can be inserted which does not seriously obstruct the line of sight or beam of light. The device consists of a 45-deg Stellite mirror and a 20-power telescope that looks down the core

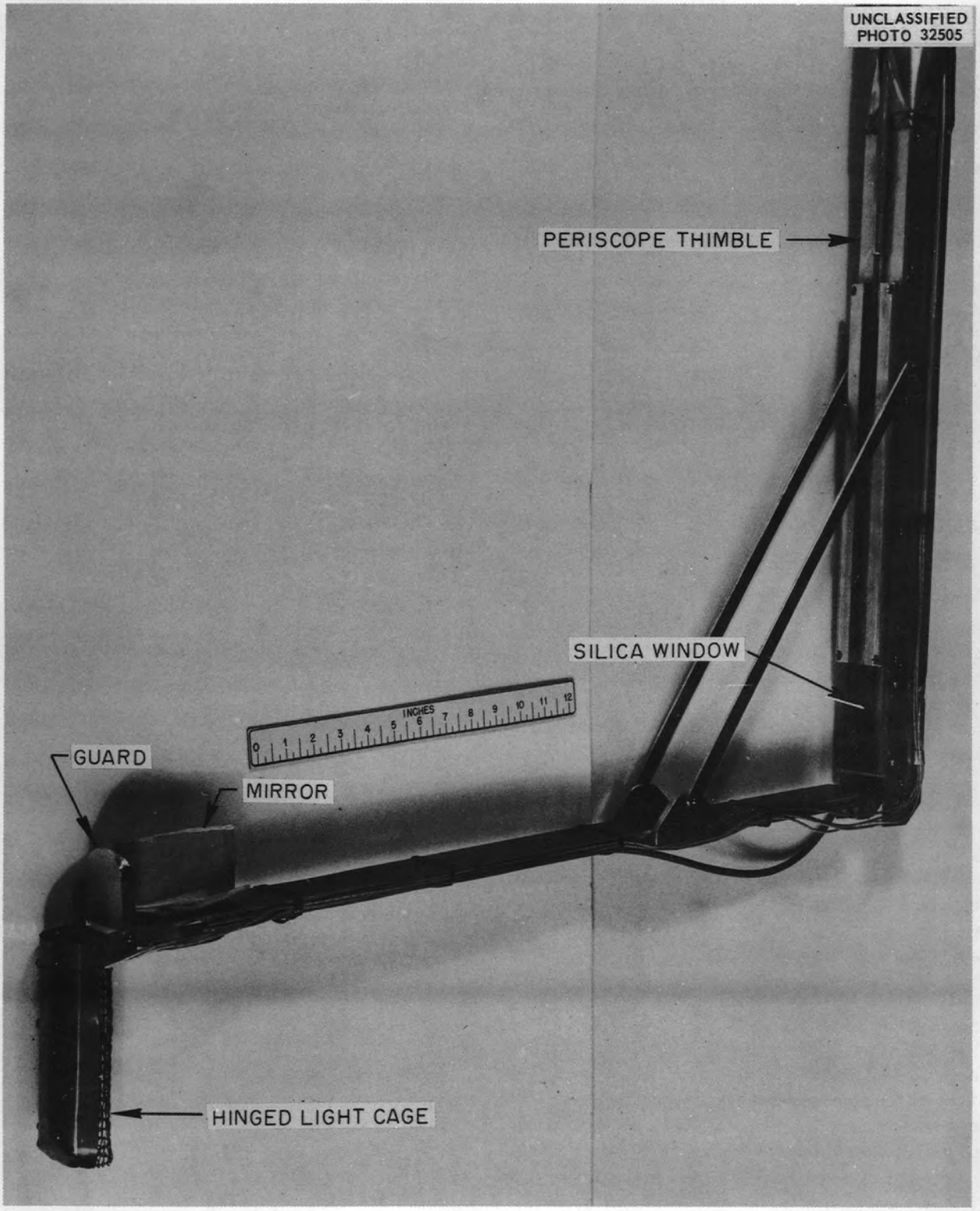

Fig. 2.2. Folding-Arm Viewing Device.

UNCLASSIFIED
PHOTO 32599

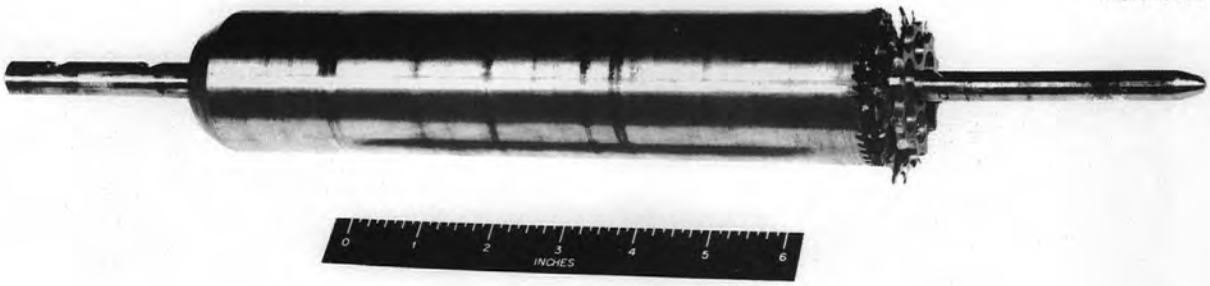

Fig. 2.3. Two-inch Cutting Head with Samples in Position.

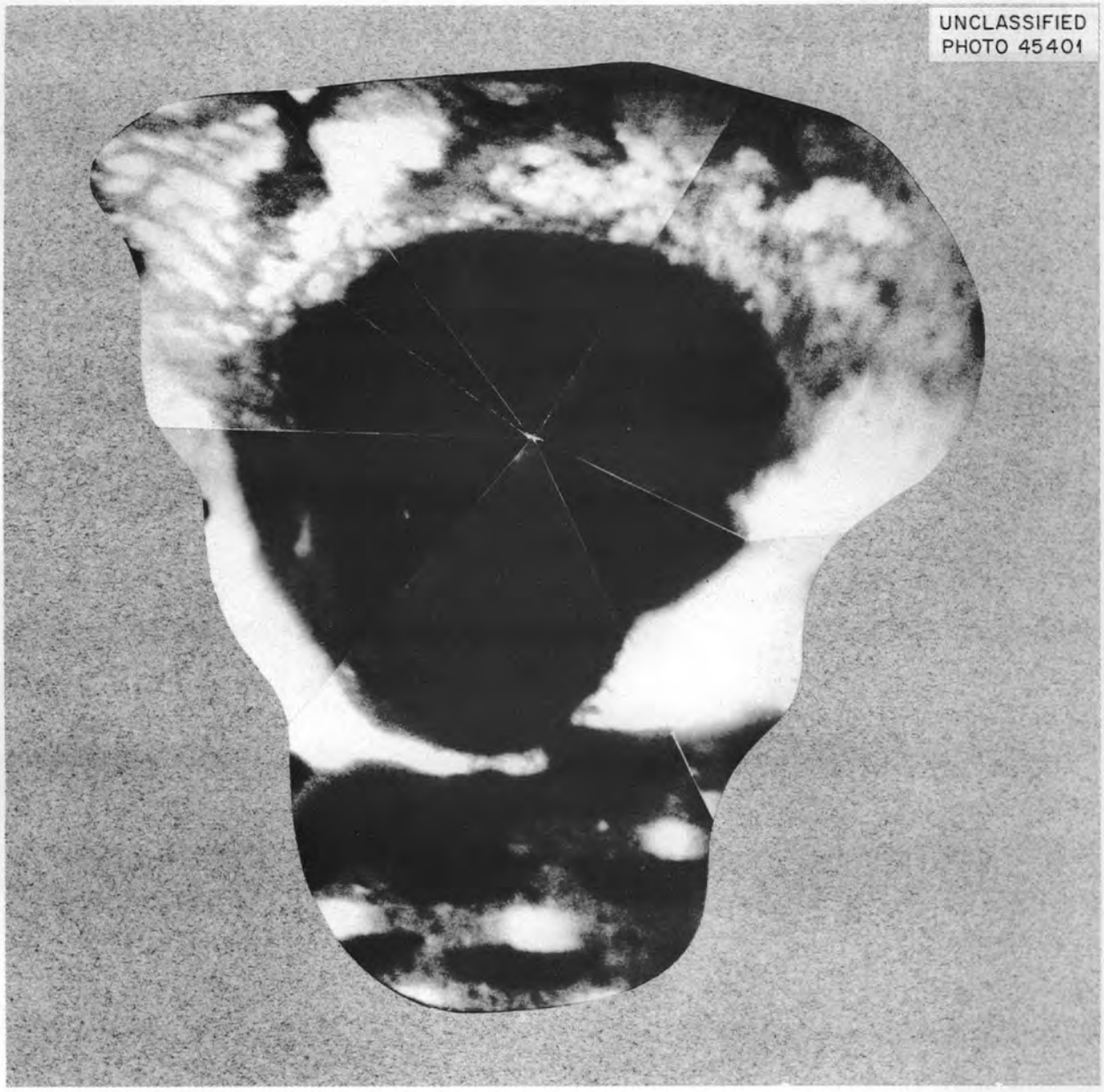

Fig. 2.4. Composite Photograph of Hole in HRT Core Tank (View from Inside the Tank).

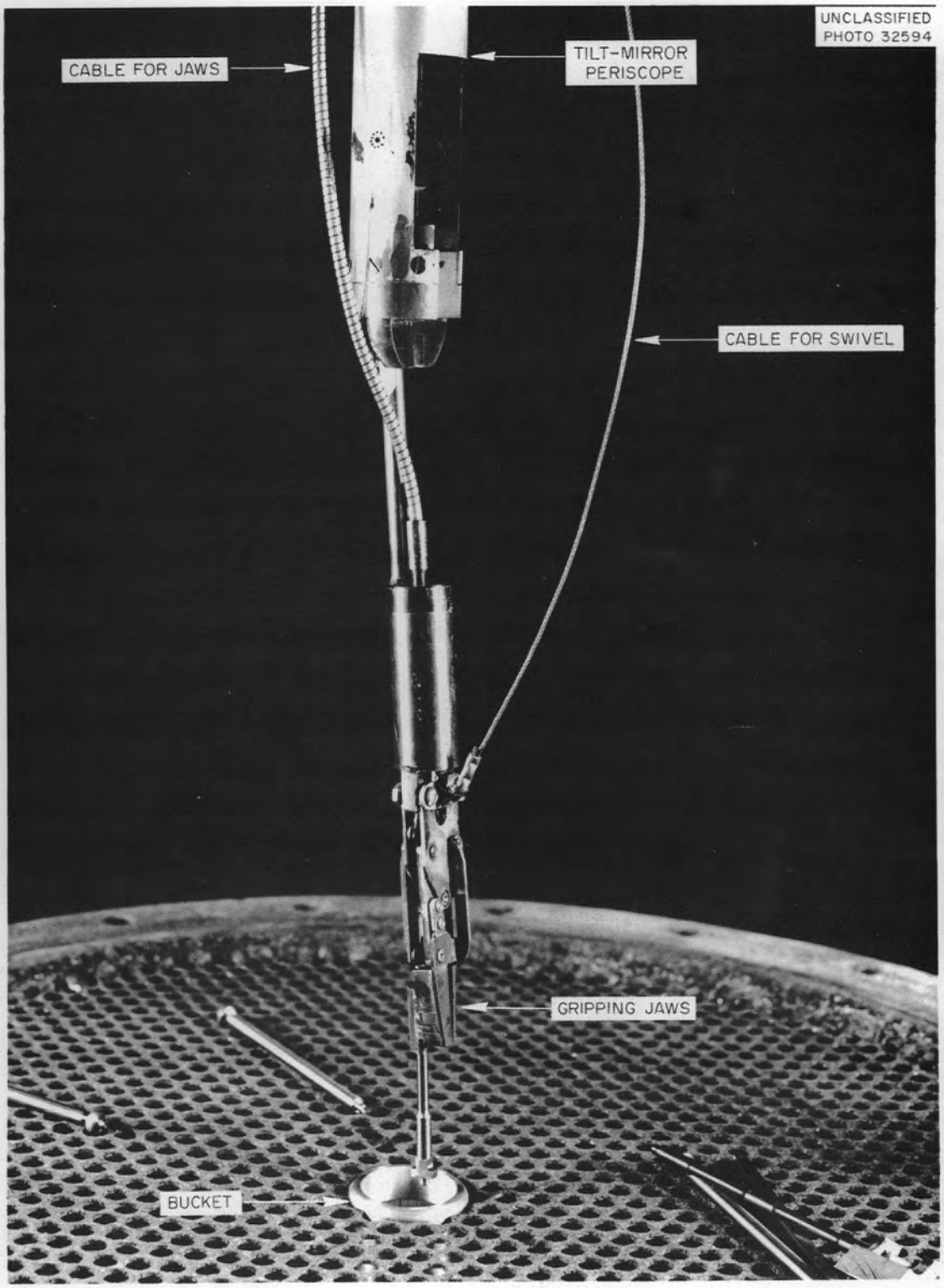

Fig. 2.5. Sample Retriever Shown Depositing Specimen in Bucket.

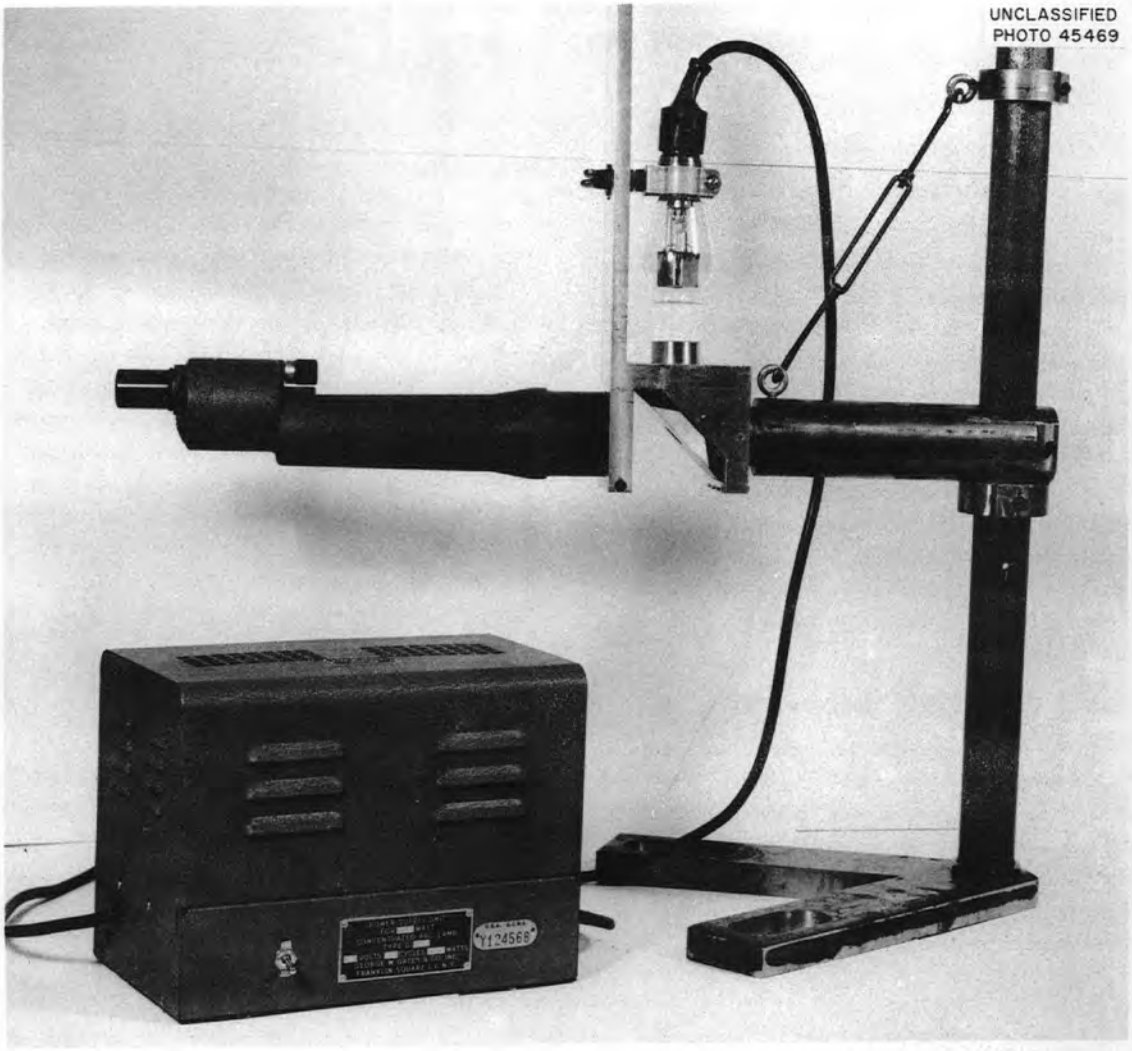

Fig. 2.6. External Light Source and Telescope.

opening. Light is supplied by a zirconium oxide arc light and a collimating lens, which directs a high-intensity beam of light through a hole in the center of the mirror. Due to the large objective lens, the observer does not see the hole in the mirror.

A number of simple tools mounted on long $\frac{3}{8}$-in. rods or tubes have been tested for use with the telescope. These are being used at the reactor to supplement the retrieving tool in the recovery of lost objects.

2.6 TELEVISION CAMERA AND MANIPULATOR

Development of the television camera and manipulator for viewing the outside of the HRT core[4] was completed, and a successful demonstration was conducted in a full-scale mockup of the core and pressure vessel. A new light source with a spare bulb and improved cooling was built and tested. The fatigue life of the stainless steel tubing, used to operate the hydraulic manipulator, was found to be limited to several reactor insertions, and since the manipulator had been tested several times in the mockup, its tubing was replaced. However, the camera was not used at the reactor following run 17, because of the adequacy of the other, simpler, viewing devices.

[4] I. Spiewak *et al.*, *HRP Prog. Rep. for Quarters Ending April 30 and July 31, 1958*, ORNL-2561, p 35.

3. HRT PROCESSING PLANT

W. D. Burch

R. H. Winget O. O. Yarbro

3.1 PERFORMANCE OF THE HYDROCLONE SYSTEM

The chemical plant hydroclone loop was operated continuously during HRT run 17 except for the downtime required to drain and rinse the underflow receiver between three scheduled runs. Operating time for the three runs totaled 829 hr, and operating conditions were held essentially constant. Hydroclone flow rates varied from 1.22 to 1.38 gpm, the underflow-pot temperature was maintained constant at 290°C throughout most of the runs, and the solution heater was operated to maintain an arbitrary maximum heater wall temperature of 305°C. Summaries for these runs are being prepared.

3.1.1 Corrosion-Product Removal Data

The chemical composition of corrosion-product solids removed by the hydroclone in run 17 varied markedly from the composition in the previous run. Zirconium oxide became the predominant corrosion product, increasing from an average of 7% of the total in run 16 to about 47% in run 17. The only apparent significant difference between runs 16 and 17 was the presence of the corrosion specimens and holder in the reactor core in run 17. Total reactor integrated power and operating time were approximately equal in the two runs. Data for the last period of run 16 and the three operating periods of run 17 are listed in Table 3.1, along with data from runs 16-1 and 16-2, which have been reported previously.[1] Included in the table also are pertinent operating variables and calculated removal rates for corrosion-product solids.

Titanium found in the underflow pot for the first time in run 17 is assumed to have resulted from corrosion of the core specimen holder.

3.1.2 Concentration of Uranium, Copper, and Nickel

Another marked difference in the solids concentrated by the hydroclone in run 17 is the greatly increased uranium content. Approximately 90 g was accumulated in each of the first two runs

[1] W. D. Burch *et al.*, *HRP Prog. Rep. for Quarters Ending April 30 and July 31, 1958*, ORNL-2561, p 19.

Table 3.1. Corrosion-Product Solids Removed

	Chemical Plant Run No.					
	16-1	16-2	16-3	17-4	17-5	17-6
Operating time, hr	120	310	339	290	439	101
Integrated power, Mwhr	0	224	1235	710	1126	152
Total corrosion products removed, g	150	99	115	530	145	51
Average removal rate, g/hr	1.25	0.32	0.34	1.83	0.33	0.50
Chemical composition, %						
Fe	52	48	56	22	19	19
Cr	5	5	5	4	4	4
Ni		3	0	0	0.3	0
Zr	11	8	6	45	49	48
Ti	0	0	0	0.2	1	0.8
Ag	0	0	0	0	0.1	0.2

(17-4 and 17-5) above that in solution at reactor concentrations. For reasons not understood, the amount concentrated in run 17-6 was less, averaging about the same as in run 16. The exact quantities of uranium removed are listed in Table 3.2, along with values for copper and nickel to show the behavior of these elements. The quantity of excess material was calculated by subtracting the amount of the particular element in solution in reactor samples from the total found in the dissolver after the normal acid dissolution at the end of each run. Unfortunately, in the case of copper and nickel, the amount in solution is such a large fraction of the total that the calculated excess quantity may be in error.

3.1.3 Fission-Product Removal Data

(*a*) **Material Balances.** – Activity analyses of important fission products are made routinely on samples removed from the reactor high-pressure system and from the dissolver. Material balances of a selected group have been calculated from results of these samples and from the reactor power history and are presented in Table 3.3.

Two facts of interest should be noted concerning the very insoluble fission products, such as zirconium, tellurium, and ruthenium. First, the removal rate is proportional to the removal rate of corrosion-product solids, and secondly, although a large fraction of the total accountable material has been collected by the hydroclone, this amount is only a few per cent of the total generated. From these facts, it may be inferred that the insoluble fission products are predominantly associated with corrosion-product solids, and, as evident from other data, the hydroclone has removed only a small fraction of the total corrosion products formed to date. For instance, a uniform attack of 40 mils on the entire core tank (see Sec. 2.1) would remove over 20 kg of zirconium, but only 338 g has been collected by the hydroclone.

Cesium is the only fission product analyzed which appears to be completely soluble; strontium is the only other one which is soluble to a large degree.

(*b*) **Concentration of Rare Earths.** – Radiochemical analyses of circulating-fuel and underflow-pot samples have indicated that Y^{91} and Nd^{147} began to disappear from the reactor circulating system near the end of run 16 or the beginning of run 17. Chemical-plant concentration factors were unity in run 16 but averaged 8.0 and 3.5, respectively, for Y^{91} and Nd^{147} in runs 17-4 and 17-5. The fraction of Y^{91} and Nd^{147} activity which could be accounted for in reactor and chemical-plant samples dropped from approximately 100% in run 16 to about 40% in run 17-6. Sensitive spectrographic analyses for the rare-earth fission products have only recently been developed. Results available on one reactor low-pressure sample taken at the end of run 17 accounted for 72% of the yttrium expected in the reactor system.

3.1.4 Calculated Solids Accumulation in the Underflow Pot from Fission-Product Heating Data

The postulate that all insoluble fission products are associated uniformly with corrosion products makes it possible to use the fission-product heating to estimate the quantity of corrosion products

Table 3.2. Uranium, Copper, and Nickel Removed by the Chemical Plant

	Chemical Plant Run No.					
	16-1	16-2	16-3	17-4	17-5	17-6
Total uranium, g	20.7	47.9	65.1	173.3	147.7	73.9
Excess uranium, g	2.1	0.8	11.6	92.3	95.1	12.6
Total copper, g	4.7	5.9	8.8	14.5	11.9	5.9
Excess copper, g	0.5	0.0	0.0	3.6	4.3	0
Total nickel, g	2.2	3.5	1.6	3.1	3.1	2.7
Excess nickel, g	0.2	2.4	0.0	0.4	0.4	0

Table 3.3. Fission-Product Material Balances

Run No.	Zr^{95}	Ru^{103}	Te^{132}	I^{131}	Sr^{89}	Cs^{137}
			Activity Calculated from Reactor Power History, curies			
16-2	1.0×10^4	8.3×10^3	3.3×10^4	1.5×10^4	8.6×10^3	68
16-3	4.0×10^4	3.6×10^4	1.5×10^5	7.4×10^4	3.3×10^4	230
17-4	4.1×10^4	3.1×10^4	9.2×10^4	4.3×10^4	3.3×10^4	310
17-5	6.0×10^4	4.6×10^4	1.1×10^5	6.6×10^4	4.9×10^4	460
17-6	6.5×10^4	4.7×10^4	6.0×10^4	5.2×10^4	5.1×10^4	500
			% of Calculated Activity Removed by Chemical Plant			
16-2	0.51	0.55	0.12	0.02	0.23	0.54
16-3	0.26	0.19	0.04	0.06	0.39	0.63
17-4	3.5	0.04	2.3	0.01	0.65	1.3
17-5	0.65	0.47	0.46	0.004	0.60	1.0
17-6	0.22	0.13	0.14	0.002	0.39	0.83
			% of Calculated Activity Circulating in Reactor			
16-2	0.20	0.14	0.66	3.1	49	99
16-3	0.24	0.09	0.14	2.5	59	87
17-4	0.10	0.13	0.50	1.4	40	120
17-5	0.04	0.02	0.19	0.30	46	110
17-6	0.03	0.03	0.30	0.27	40	93

accumulated in the underflow pot. With data from runs 17-5 and 17-6 a preliminary equation was developed to relate the rate of solids accumulation to the rate of increase in, and the magnitude of, fission-product heating and to the reactor power history.

By use of this equation and fission-product heating data from run 17-4, obtained by heat balances around the underflow pot, the integrated accumulation during this run was calculated and is plotted in Fig. 3.1. Also included is the observed fission-product heating. The agreement between calculated and observed solids was unexpectedly good in this instance.

3.1.5 Equipment Performance

Performance of all equipment was excellent. The high-pressure system has operated for 1800 hr at temperature since the start of radioactive operation. There were some minor difficulties with auxiliary equipment outside the cell, but there was no lost operating time or unscheduled shutdowns.

3.2 AUXILIARY PROCESSING SYSTEMS

3.2.1 Iodine Behavior in Run 17

Radiochemical analyses of the amount of iodine in the HRT during run 17 indicated rapid removal of iodine from the circulating system, while I^{133}/I^{131} ratio determinations indicated a much slower removal. The apparent age of iodine during the latter part of run 16 was 19 hr in the core and 32 hr in the blanket. The discrepancy between the analytical and age measurements may be explained by assuming that 90% of the iodine in the core was held out of solution by solids but was free to exchange with iodine in solution at reactor temperature (see Sec. 17.1.2).

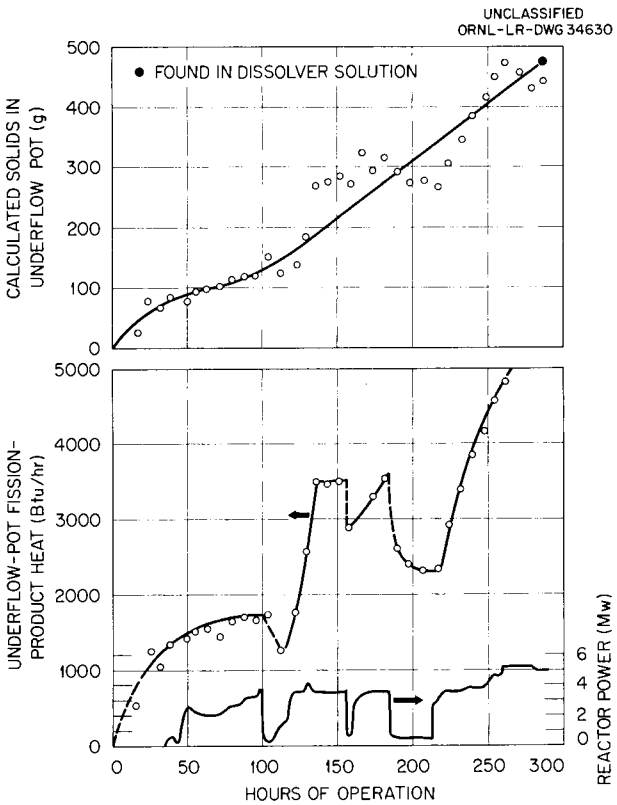

Fig. 3.1. Solids Accumulation and Fission-Product Heating in Run 17-4.

3.2.2 Charcoal-Bed Status

(*a*) **Ignition Incident in Bed A.** – Routine performance of the charcoal adsorber beds was interrupted by an incident at the beginning of run 17 which resulted in the release of short-lived activity from bed A. Subsequent observations revealed that the bed had been ignited, but damage to the bed appears minor.

During the initial hours of run 17 malfunction of the recombiners permitted deuterium gas to enter the charcoal beds. Shortly after a massive recombination occurred throughout the low-pressure vapor system, high temperatures were noted at the beginning of the 6-in. sections of both beds A and B. These temperatures returned to normal within a short time. Approximately five days later, during which time the exit gas flow rate was very erratic, a burst of gaseous activity was released from bed A. The reactor off-gas was then routed through beds B and C for eight days, at which time bed B was closed off and bed A was opened.

Chemical analyses of the effluent from bed A showed high concentrations of CO_2, which increased to a maximum value of 45% and then decreased in a period of ten days to less than 1%. A total of 6000 liters of CO_2 was eluted from the bed, indicating that no more than 10 lb, or 2%, of the total charcoal in the bed was consumed. Since normal oxygen holdup on each bed is only 2000 liters, it is possible that the bed was burning throughout most of the five-day period, the combustion being supported by oxygen vented to the bed continuously from the reactor. Isolation of the bed stopped the supply of oxygen and prevented further burning.

Samples taken from bed A immediately following the activity release were analyzed by use of a single-channel gamma spectrometer, which indicated the presence of Kr^{85m} (4.36 h), Kr^{85} (10.27 y), Kr^{88} (2.77 h), Xe^{131m} (12 d), and Xe^{133} (5.27 d). Samples from beds B and C taken during this same period indicated the presence of Kr^{85}, Xe^{131m}, and Xe^{133}. At the flow rate of 2.5 liters/min through the beds it was expected that the long-lived isotopes would be present in the effluent gas stream in the concentrations found.[2]

During the 10-day period when CO_2 was being eluted from bed A, Kr^{85m} was noted in exit gas samples. This short-lived isotope should not pass through when the bed is operating in a normal fashion; after the CO_2 was eluted, it was no longer detected. The interference of CO_2 with the holdup of fission gases has since been demonstrated in the laboratory (see Sec. 18.1) and accounts for the observed behavior.

Semiquantitative values for the amount of activity released into the off-gas stack indicate that the maximum rate of activity discharge throughout the run ranged from 5 to 15 curies per day; the allowable discharge rate is approximately 80 curies per day.[2] A detailed report of this incident is in preparation.

(*b*) **Design of Replacement Beds.** – As a result of the damage to bed A, additional adsorber-bed capacity is being designed for possible installation at the HRT. This additional capacity will be equivalent to two of the present beds and is designed to be installed north of, and in parallel with,

[2] R. E. Adams and W. E. Browning, *Fission Gas Holdup Tests on HRT Charcoal Beds*, ORNL CF-58-4-14 (April 2, 1958).

the existing beds. The inlet tie-in will be made in the valve pit preceding the present beds; the outlet tie-in will be downstream. The new bed will be installed vertically to eliminate the channeling which may result from settling of charcoal in horizontal beds and will consist of 30-ft lengths of ½-, 1-, 2-, and 6-in. pipe mounted in a 24-in. well about 35 ft deep. A 4 × 4 × 3 ft box above the well, for inlet and outlet flanges and thermocouple connections, will be covered with 10 ft of earth for shielding. The bed will be water-cooled in the same manner as the existing beds.

Thermocouples spaced at frequent intervals in the center of the various pipe sections will aid in the detection of hot spots before the bed can be damaged seriously.

3.2.3 Waste System

Ten to twenty curies of activity were discharged to the waste retention pond following maintenance operations in the reactor cell after run 16. This activity was discharged by draining the pond after a decay period had reduced the level to 2–4 curies. Tests in the laboratory on pond samples showed that the activity present, predominantly Ba^{140} and La^{140}, could be effectively precipitated by the coagulation and settling of a precipitate resulting from the addition of trisodium phosphate to give a concentration of about 0.002 *M* in the basin. After about two-thirds of the water had been drained, tests demonstrated decontamination factors of 5, as compared with factors of 100 in the laboratory tests.

Fifty curies of activity, accumulated in 9600 gal of solution in the high-level waste tank, were concentrated in the waste evaporator to a volume of 50 gal for ultimate disposal in the plant high-level waste system.

On several occasions gaseous activity has been released to the stack during sampling operations. After run 17, a 2-ft^3 charcoal bed was installed in the vent line from the sampler housings so that future releases can be adsorbed and allowed to decay on the bed.

3.2.4 Removal of Initial Fuel Batch from Fuel Storage Tanks

The initial HRT fuel charge (from run 13) was transferred to the fuel storage tanks when high corrosion rates resulted in excessive buildup of nickel in solution. The 6-kg charge of uranyl sulfate was processed during the quarter. A total of 379 lb of D_2O was recovered from an estimated inventory of 410 lb. The concentrated uranium was transferred to the solvent extraction facility in the Thorex Pilot Plant in a 33-gal shielded carrier, with gadolinium being used as a soluble poison for criticality control. A discrepancy of 800 g between recovered uranium and book inventory is assumed to have resulted either from holdup in the transfer piping or as a part of corrosion-product solids[3] in the reactor. A report was issued describing the details of the fuel transfer and D_2O recovery steps.[4]

---

[3] G. H. Jenks, A. R. Olsen, and W. C. Yee, *Examinations of Specimens and Scales Taken from the HRT Following Runs 13 and 14*, ORNL CF-58-9-37 (Sept. 11, 1958).

[4] R. H. Winget, *Transfer of Initial Fuel from the HRT and Recovery of the Associated Heavy Water*, ORNL CF-58-10-44 (Oct. 3, 1958).

4. HRT REACTOR ANALYSIS

P. R. Kasten

R. Chalkley
S. Jaye
T. H. Mauney
C. W. Nestor, Jr.
M. P. Lietzke
M. W. Rosenthal
M. Tobias

4.1 POWER EXCURSIONS IN THE HRT

Statistical data on the occurrence of power excursions in HRT runs 13, 14, 16, and 17 were obtained by examination of various recorder charts. All excursions in run 13 could be accounted for by changes in reactor operation; in runs 14, 16, and 17, however, many instances of a rapid increase or decrease in fission power for which there was no apparent explanation were registered by the Log N recorder (RR-160). That the indicated excursions were actually changes in fission rate was confirmed by changes in other variables which are functions of reactor power. Of these, the liquid level in the core pressurizer and the output signal of the core corrosion-sample thermocouple X-7 (when present) were generally the most sensitive to power changes.

Excursions in which the power changed by less than 5% of the initial value are difficult to identify because of the frequent, small fluctuations which normally occur. Hence, only the occurrence of excursions larger than 5% were noted, and only those larger than 7% were included in most treatments of the data.

4.1.1 Frequency of Excursions

During runs 14, 16, and 17 there were more than 800 positive excursions in which the power rose over 7% and more than 70 negative excursions in which it fell over 7%. The frequency of occurrence of positive power excursions larger than 7% of normal power is plotted in Fig. 4.1 as a function of the power level in the core region.

Only a few excursions were identified at core powers less than 1 Mw. However, at core powers above 1 Mw the positive excursions occurred with a frequency that increased with the power level. The frequency at a given core power was lowest in run 14 (in this run, fission power was generated in the core region only). In run 17 the corresponding power-excursion frequencies were slightly higher than in run 16. (Run 14 was terminated by development of the hole in the core vessel. In runs 16 and 17 about 40% of the total fission power was generated in the blanket. There was a corrosion sample assembly in the core during run 17; it was not present in run 16.)

The frequency of occurrence of negative excursions in which the power decreased more than 7% is plotted in Fig. 4.2 vs reactor power. The frequency was much lower than that for positive excursions; there appears to be little correlation with power level. There were no events during run 14 in which the power decreased as much as 7%, although there appear to have been several smaller negative excursions. Negative excursions were more frequent in run 17 than in run 16.

During run 17 there was an addition of 3.44 moles of sulfuric acid on August 20, and a further addition of 5.02 moles on September 10. These additions divide the run into three periods, identified in chronological sequence as 17-A, 17-B, and 17-C. The frequency data for the various portions of run

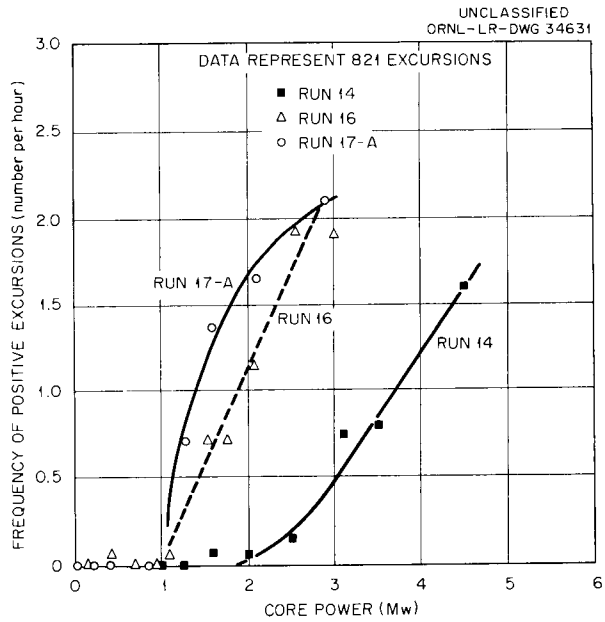

Fig. 4.1. Effect of Power Level on Frequency of Positive Excursions Exceeding 7% of Normal Power Level.

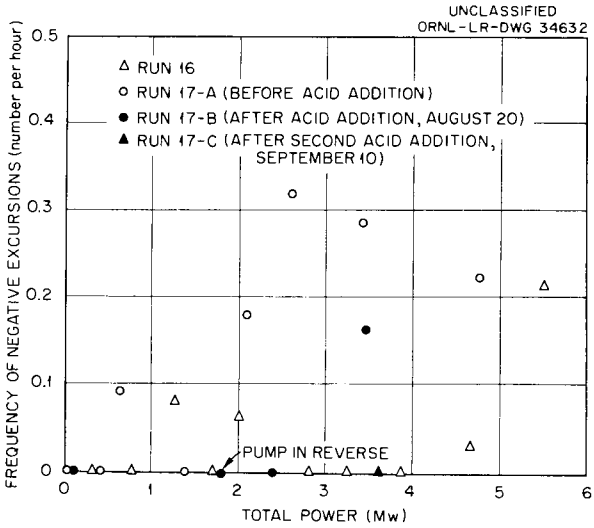

Fig. 4.2. Effect of Power Level on Frequency of Negative Excursions Exceeding 7% of Normal Power Level.

17 were therefore considered separately. Figure 4.3 plots the excursion frequency vs total power for these separate periods of reactor operation. The average core temperature during most of run 17 was near 270°C; the data in Fig. 4.3 are for the periods at that temperature.

There was a period of about 2 hr on August 28 when the core flow was reduced to about 40% of normal (the pump was operated in reverse). With the normal core circulation rate there were no positive excursions in run 17 at total powers less than 1.8 Mw. However, at the lowered flow rate an excursion occurred at 1.4 Mw; the average frequency at levels between 1.4 and 1.9 Mw (based on just 2 hr of operation) was higher than that at 4.8 Mw with normal flow.

The average frequency of excursions in run 17-A as a function of total power is indicated in Fig. 4.3 by the curve; the average frequency in run 17-B was below the corresponding value of run 17-A, while the one average-frequency point obtained for run 17-C was below the corresponding value of run 17-B. The acid additions thus appear to have resulted in a decrease in the frequency of power excursions larger than 7% of normal power. The frequency of negative excursions was lower in run 17-B than in 17-A, and there were no negative excursions after the second acid addition. There were no negative excursions during the short period of reduced flow.

During run 17-B the reactor was operated at average core temperatures between 243 and 272°C, with the total power generally near either 1.9 or 3.6 Mw. The positive-excursion data during this run are plotted in Fig. 4.4 as a function of arithmetic-average core temperature. As shown, at the 1.9-Mw power level, no significant effect of temperature was observed. The frequency during the periods at 3.6 Mw was somewhat higher at 270 than at 250°C (however, as pointed out in the next section, three of the largest excursions which have occurred happened during a 22-hr period at 250°C

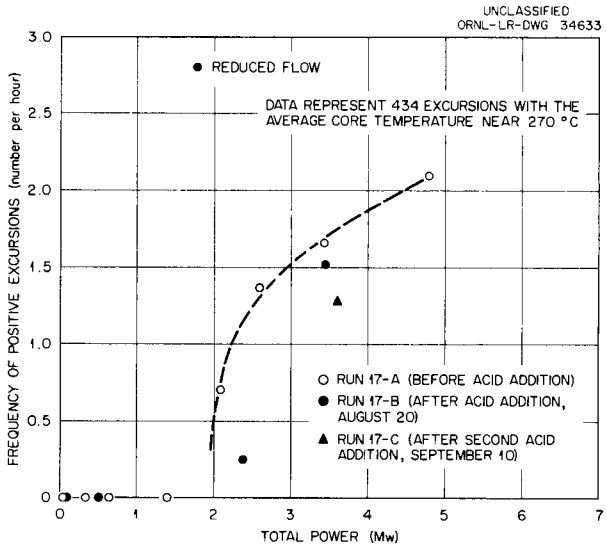

Fig. 4.3. Effect of Power Level on Frequency of Positive Excursions Exceeding 7% of Normal Power in Run 17.

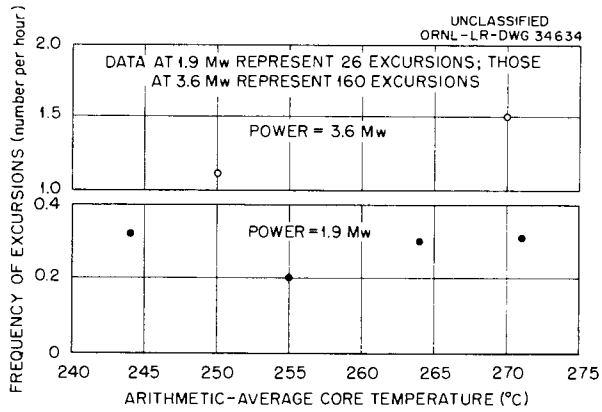

Fig. 4.4. Effect of Core Temperature on Frequency of Positive Excursions Exceeding 7% of Normal Power in Run 17-B.

and 3.6 Mw). Since the frequency of occurrence was low at 1.9 Mw, the data in Fig. 4.4 for that power represent only 26 excursions; the data at 3.6 Mw represent 136 excursions at 270°C but only 24 at 250°C.

Although the *average* frequency of excursions over large periods correlates well with the power level, the time between events is not at all regular. For example, at one power level in which the average time between events was 36 min, the individual spacings ranged from less than 1 min to 141 min. During many periods of operation the excursions occurred relatively frequently for a short time and then at relatively much longer time intervals.

4.1.2 Magnitude of Excursions

The power increase associated with the largest excursions during runs 14, 16, and 17 are listed in Table 4.1. In run 17 there were four excursions in which the power increased more than 100%. One occurred with the power at 2.4 Mw at a time when the temperature had just been increased from about 245 to 260°C. The other three all occurred in a 22-hr period of operation in run 17-B, following a reduction in critical temperature from 270 to about 250°C; the power during this period was near 3.6 Mw (during this interval the frequency of excursions was only 1.1 per hour, which is less than the average frequency during run 17 at a power level of 3.6 Mw). This period was terminated by the surge in which the power rose 575% (from 3.7 to 25 Mw). There were no excursions approaching this magnitude during a later 10-hr period in which the reactor was operated at 3.6 Mw and 250°C.

Table 4.1. Relative Magnitude of Maximum Power Excursions

Run No.	Largest Positive Excursion		Largest Negative Excursion	
	Initial Power (Mw)	Power Increase (%)	Initial Power (Mw)	Power Increase (%)
14	2.5	20	2.0	3
16	5.4	50	5.0	15
17	3.5	575	2.6	17

The data were examined for a relationship between the size of an excursion and the time from the preceding excursion. There was no evidence that $\Delta P/P$ was a function of the time from the previous event.

Plotting the relative number of excursions as a function of their magnitude reveals that the frequency of occurrence generally became less as the magnitude increased. A histogram of the relative frequency of positive excursions vs the percentage change in power is presented in Fig. 4.5 for runs 14, 16, and 17-A. Each bar represents the events over a size range of three percentage points, and frequencies are given in terms of the number per 100 positive excursions.

All the data in Fig. 4.5 were taken from RR-160, the Log N recorder on the reactor instrument panel. Since excursions in which the power increased less than 5% are difficult to identify, it is possible that some of the excursions near 5% in size were overlooked; therefore it is not certain that the frequency of occurrence at a power increase of 6% in run 17-A, was actually less than the frequency associated with a power increase of 9%.

The normalized frequency distribution of negative excursions as a function of $\Delta P/P$ has the same general appearance as the distribution shown in Fig. 4.5, except that the frequency decreased more rapidly with increasing excursion size.

4.1.3 Analyses of Excursions

A computer program which estimates the time variation of the reactivity associated with a power excursion was prepared for the IBM-704. For the input the power-time relation is represented by a large number (up to 500) of straight-line segments. The instantaneous core temperature and the delayed-neutron precursor concentration are computed from the power-time relationship by the computer routine. These results are then used to estimate the reactivity required to produce the observed power-time behavior. The equation used to compute the reactivity (Δ) is:

$$(1)\quad -\left(\frac{\Delta-\beta}{l}\right)\frac{P}{P_0} = -\frac{d(P/P_0)}{dt} + \frac{1}{l}\left(\frac{\partial k_e}{\partial T}\right)_c \Delta T_c \left(\frac{P}{P_0}\right) + \sum_{i=1}^{5} \lambda_i C_i \ ,$$

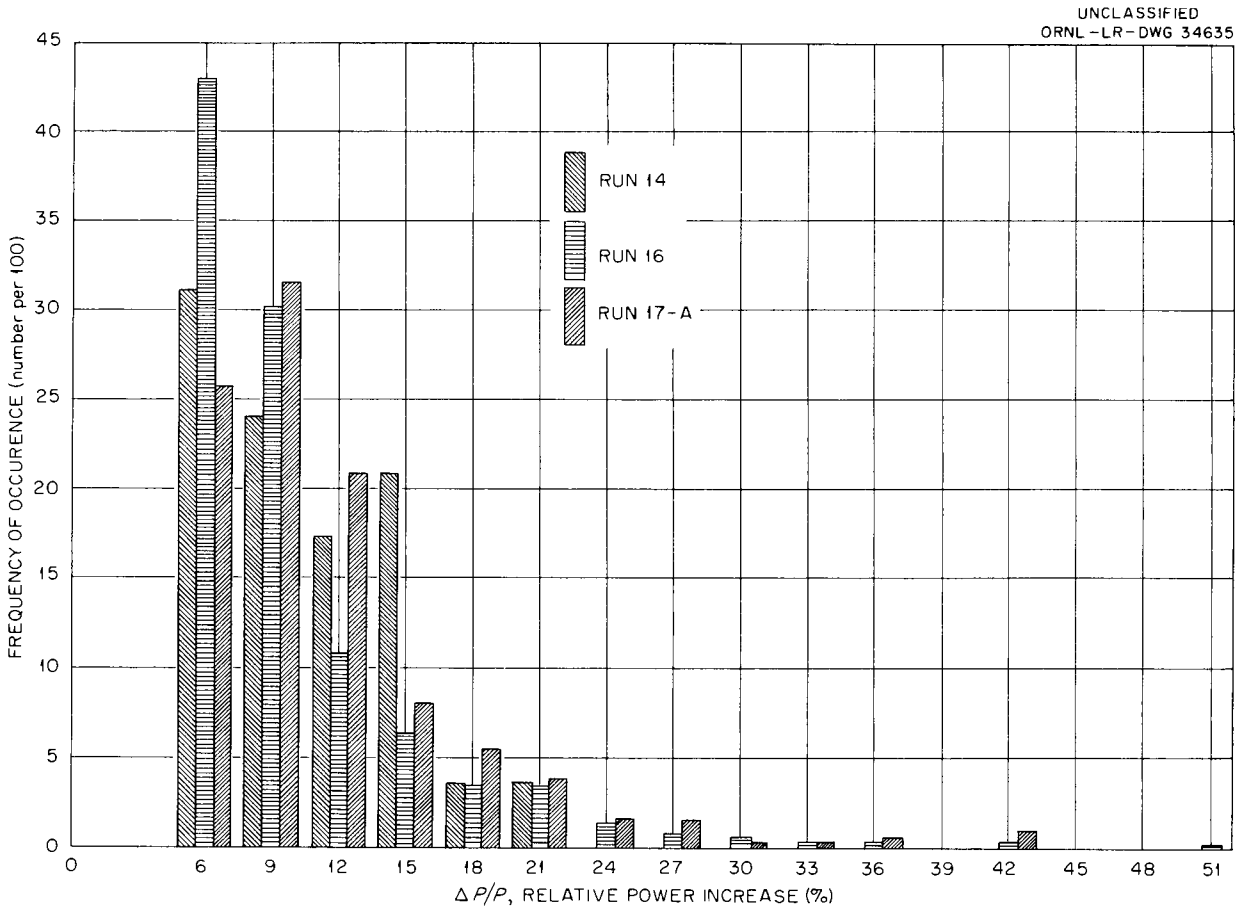

Fig. 4.5. Relative Frequency of Positive Excursions as a Function of Relative-Power Increase (Frequencies Are Normalized to 100 Excursions Exceeding 5% of Normal Power).

where

C_i = latent "power" associated with the ith group of delayed neutrons,

$(\partial k_e/\partial T)_c$ = temperature coefficient of reactivity of the core,

l = effective neutron lifetime,

P/P_0 = ratio of instantaneous to initial power,

t = time,

ΔT_c = change in the effective core temperature, assuming inlet fluid temperature is constant,

β = effective fraction of neutrons which are delayed,

Δ = total reactivity addition at specified time,

λ_i = decay constant of the ith group of delayed neutrons.

The reactivity obtained from Eq. 1 is that which is associated with effects other than those produced by changes in delayed-neutron concentration and core temperature.

Power-time relations for a number of excursions during run 17 were taken from the linear power trace on the Sanborn high-speed recorder and analyzed by use of the program described above. Two types of positive excursions are illustrated in Figs. 4.6 and 4.7; a negative excursion is shown in Fig. 4.8. The ratio of instantaneous to initial power and the estimated reactivity are plotted vs time.

Figure 4.6 is representative of a class of excursions in which the reactivity rises rather smoothly with time and reaches a peak in 2 to 4 sec. It then falls from the peak until interrupted by a second, smaller rise, after which it falls again, perhaps going through other peaks of decreasing size. In this type of excursion the time between the first maximum and the beginning of the second rise was

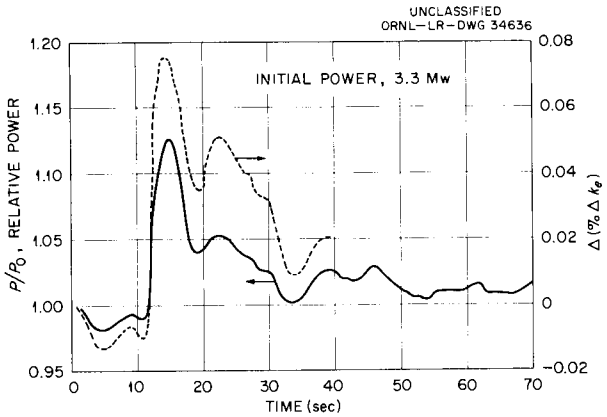

Fig. 4.6. Relative Power and Reactivity Associated with an HRT Power Excursion on August 15, 1958.

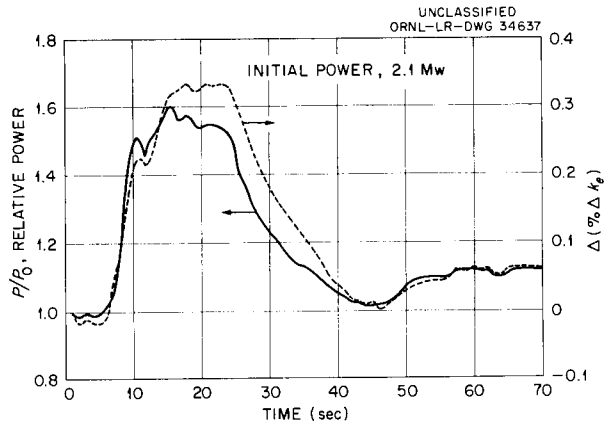

Fig. 4.7. Relative Power and Reactivity Associated with an HRT Power Excursion on September 8, 1958.

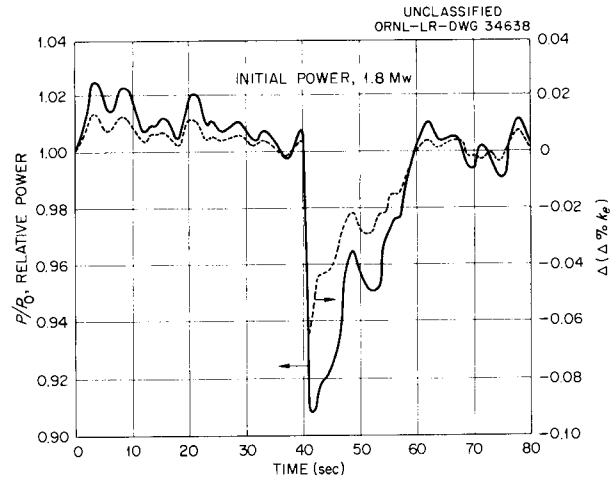

Fig. 4.8. Relative Power and Reactivity vs Time for a Negative Power Excursion on September 6, 1958.

between 5 and 6 sec, except during the period with the pump in reverse, when the time was between 12 and 14 sec. This type of reactivity behavior would result if uranium moved from a position of lesser to one of greater importance in the core, then was carried out of the core, and finally reentered after passage through the external core circuit. The time required for fuel solution to pass from the exit of the core to the inlet is about 6 sec with normal flow and 15 sec with the pump reversed. If this is actually the mechanism of reactivity addition in this type of excursion, then part of the flow through the core must be at higher-than-average velocities to account for the short core residence time (2 to 4 sec in this case, compared with the normal average of 10 sec).

The peak reactivity addition in Fig. 4.6 is near 0.08%. This value is equivalent to 2.5 g of U^{235} moving from outside the core to its center, or 8 g moving from the upper screen to the core center.

The excursion plotted in Fig. 4.7 is representative of a class in which the reactivity rises rapidly to a level near which it stays for perhaps 10 sec. It may then fall to a low value without displaying a second peak. This type of excursion could have occurred if precipitated uranium moved into a region of greater importance, circulated there for a period, and then returned to a region of low importance.

The peak reactivity addition computed for a number of positive excursions in run 17 is shown in Fig. 4.9 vs the maximum increase in power during the excursion. The amounts of uranium which would produce the estimated reactivity additions if moved

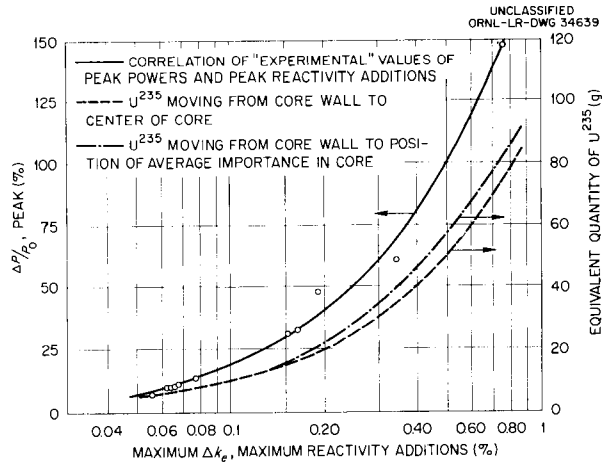

Fig. 4.9. Maximum Relative-Power Increase and Equivalent U^{235} Addition vs Calculated Peak Reactivity Addition.

from the core wall to the center of the core or to the position of average importance in the core are also shown.

For the negative excursions in run 17 the most striking feature was the rapidity with which the power and reactivity decreased, as illustrated in Fig. 4.8. Only a few negative excursions have been analyzed, but from the power traces it is clear that reactivity was removed from the system in about 1 sec and that the rate of removal was interrupted sharply at the end of this period. Such behavior would be observed if uranium-bearing material in the reactor fell to a position of less importance.

In at least five excursions in run 17 the power rose rapidly and then fell quickly to a value below the initial power level. Figure 4.10 illustrates one of these excursions, as seen on the linear power trace of the Sanborn recorder. This type of event would occur if uranium fell from the upper part of the core to the screen area.

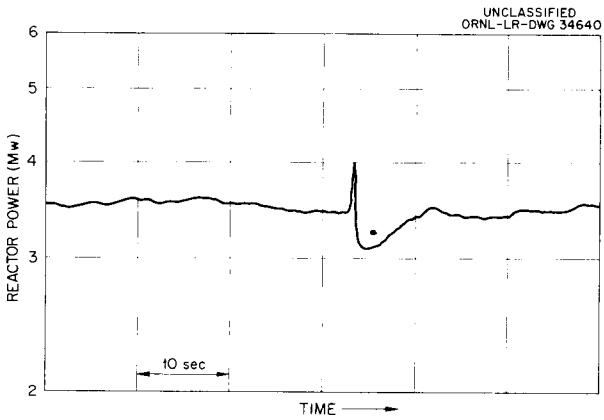

Fig. 4.10. Sanborn-Recorder Trace of Log-Power Showing Negative Excursion Preceded by Sharp Positive Rise in Power.

4.2 SMALL POWER OSCILLATIONS IN THE HRT

The relative reactor power in the HRT is measured in terms of the electrical current generated in a compensated ion chamber; when registered on a high-speed recorder, this current (and thus the reactor power) is seen to undergo continuous variation with time. An example of the power oscillations is shown in Fig. 4.11. That the indicated fluctuations actually represent changes in power was confirmed by the reading of the pressurizer level, which oscillated in phase with the power reading when the

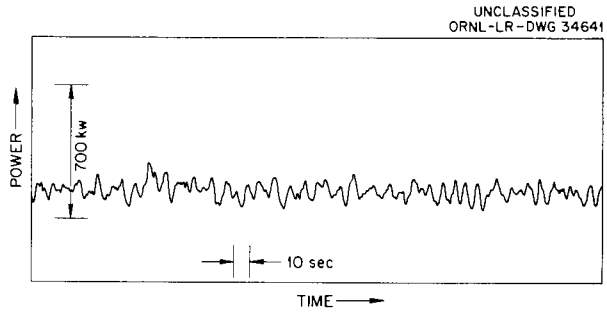

Fig. 4.11. Sanborn-Recorder Trace of Reactor Power Showing "Normal" Oscillations (Average Power Level Is 3.6 Mw).

letdown-valve position was controlled manually. Further confirmation was obtained by the output of the core corrosion-sample thermocouple (designated X-7), which fluctuated with the same frequency as the power trace; however, changes in the heat storage and heat-transfer rate (associated with the thermocouple), which accompany changes in the thermocouple temperature, beclouded the phase relationship.

The frequency of the oscillation was fairly constant throughout periods of steady operation at constant power (frequency was based on average values obtained during 200-sec intervals). For example, the extreme values of the "200-sec-average" frequency obtained in 20 averages over a 9-hr period were 11.1 and 15.6 peaks per minute, and the standard deviation was 11%. However, the frequency does appear to be a function of the core power.

On August 28, the reactor was operated for 2 hr with the core circulation rate 40% of normal (the pump was run in reverse). At the end of this period the flow rate was returned to its normal value, and the power was increased in steps from 1.0 to 3.2 Mw during the following 4 hr. The "200-sec-average" frequency was obtained for a number of intervals; Fig. 4.12*a* illustrates the increase in frequency with increasing power level and also shows that reducing the flow did not result in any significant change in frequency relative to the frequency obtained with normal fluid flow. (With the flow 40% of normal the temperature rise across the core was about $2\frac{1}{2}$ times as great as with normal flow.) The frequency of oscillations at powers near zero was uncertain because the absolute magnitude became too small to be detected on the recorder.

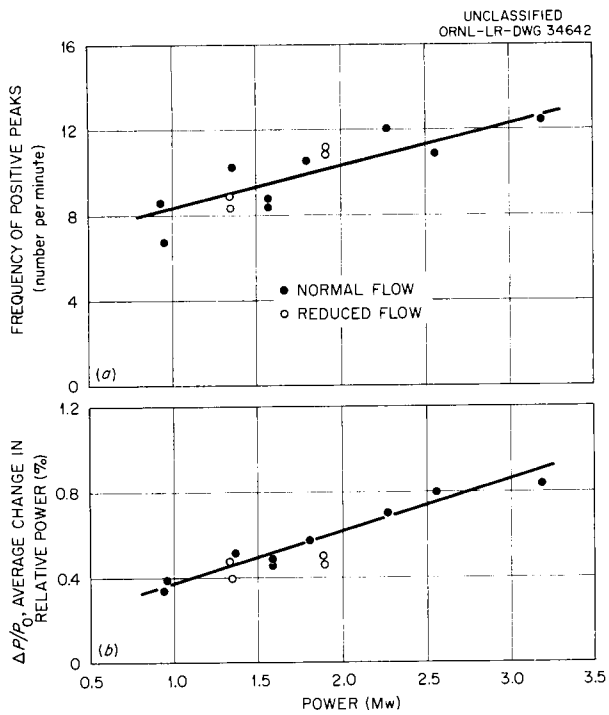

Fig. 4.12. Frequency and Size of "Normal" Power Oscillation vs Power Level with Core Circulating Pump Running Forward and Reversed (August 28, 1958).

The power oscillations do not appear to be associated with the feed of fuel to the core; there was no change in the oscillation frequency when the feed rate was reduced to zero. Neither did the oscillations appear to result from changes in the letdown-valve position, since the frequency remained the same when the valve was manually controlled. The frequency also did not change throughout a period in which the core pressure was reduced in steps from 1750 psig to about 1200 psi (this latter pressure was near that at which gas bubbles should appear). The blanket flow rate was not changed, and so its effect on power fluctuations was not studied.

(*a*) Size of Oscillations. – The "regular" oscillations were small, the peaks generally being less than 3% above or below the average power. The average size of the peaks, $\Delta P/P_0$ (based on measurements during 200-sec periods), was found to be a function of the power level, increasing with increasing power; this is shown in Fig. 4.12*b*.

The data in Fig. 4.12*b* cover the period in which the pump was reversed. At the reduced flow rate the magnitude of the power peaks does not appear to be significantly different from that observed under normal-flow conditions.

The reactivity associated with the observed power change is quite small. The power curve during one period of reactor operation at 3.4 Mw was analyzed by use of the routine described in Sec. 4.1.3. During that period the reactivity additions associated with the "regular" power oscillations were less than 0.02% Δk_e.

(*b*) Differences between "Oscillation" and "Excursions." – Extrapolation of the data given in Fig. 4.5 concerning the relative frequency of excursions as a function of the associated power increase suggests that the frequency increases to a high value as $\Delta P/P$ becomes small; under these circumstances the power "excursions" might appear to be less frequent occurrences of the same phenomenon observed during "regular" power oscillations. However, there are other characteristics associated with the data which argue against this conclusion. First, the occurrence of excursions in run 17 ceased when the power was reduced to below about 2 Mw (see Fig. 4.1), whereas the frequency of the "regular" oscillations (see Fig. 4.12*a*) was still high at 1 Mw and appears to extrapolate to a finite value at zero power. Also, if both phenomena had the same basis and if the frequency-vs-relative-power change is a statistical function (as it appears to be), then the "normal" oscillation frequency should decrease in the same proportion as the "excursion" frequency. This is not the case. It therefore appears that "excursions" and "oscillations" are caused by different phenomena.

4.3 REACTIVITY CHANGES ASSOCIATED WITH VARIOUS EVENTS

4.3.1 Reactivity Associated with Uranium Movement

The reactivity associated with the introduction of a small quantity of U^{235} at various positions in the HRT has been estimated on the basis of perturbation theory. The fluxes and adjoint fluxes needed in the computation were obtained from the standard two-group, two-region, spherical-reactor code for the Oracle. The adjoint fluxes were calculated by interchanging the coefficient of the slow flux in the fast-flux equation with the coefficient of the fast flux in the slow-flux equation.

Figure 4.13 shows the reactivity per unit mass of U^{235} as a function of distance from the center of

the core for a temperature of 280°C and a ratio of blanket fuel concentration to core fuel concentration of 0.4. Table 4.2 gives the reactivity addition resulting from the introduction of 1 g of U^{235} at various positions. The reactivity associated with movement of 1 g of uranium from one position in the reactor to another can be obtained from Fig. 4.13 or Table 4.2 by taking the difference between the reactivity values at the specified positions. For example, movement of 1 g from the core wall to the center of the core would add 0.018% Δk_e.

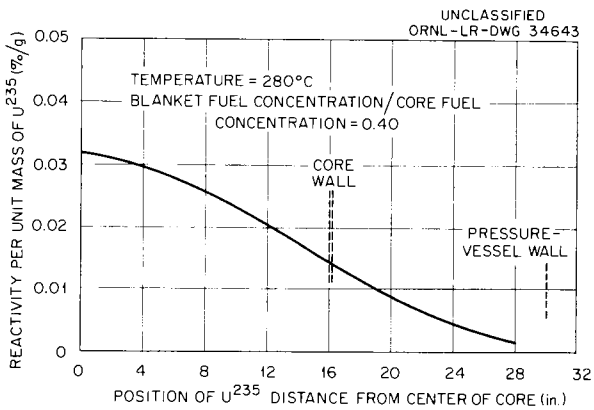

Fig. 4.13. Reactivity Addition Associated with Introduction of 1 g of U^{235} as a Function of Position.

Table 4.2. Reactivity Addition Associated with Moving 1 g of U^{235} from Outside the Reactor to Specified Locations

Additions of 1 g of U^{235} to Following Locations	Associated Reactivity Addition (% Δk_e)
Center of core	0.032
Core-vessel wall	0.014
Uniformly distributed in core	0.023
Uniformly distributed in core circulating system	0.013
Pressure-vessel wall	0.0014
Uniformly distributed in the high-pressure system	0.0080

4.3.2 Reactivity Associated with Movement of Core Corrosion Specimen

The reactivity added by a *clean* corrosion specimen falling from the core corrosion-specimen holder to the surface of the top screen has been estimated on the basis of perturbation theory. The reactivity addition is due to the difference in nuclear importance associated with the two positions and also includes that due to the effective movement of fuel solution. Movement of a stainless steel specimen from the center of the core to the screen would add 0.013% Δk_e, but a Zircaloy sample would add only 0.0007% Δk_e. If the stainless steel specimen moved rapidly, it would cause a power surge in which the ratio of maximum power to initial power would be about 1.02.

If uranium were adhering to the surface of the corrosion sample, fall of the sample could cause a negative excursion, with its magnitude dependent on the quantity of uranium involved.

4.3.3 Reactivity Associated with Void Formation

The effect of the presence of a void region in the HRT was studied with a one-dimensional, two-group diffusion code. The core, blanket, and void were treated as concentric spherical annular regions. The void was a shell of 10- or 20-liter volume with inside radius of 0, 5, 10, 15, 20, and 25 cm; (the radius of a 10-liter sphere is 13.36 cm; that of a 20-liter sphere is 16.84 cm). The void was treated as a diffusion region having a high diffusion constant (D = 1000 cm), with no absorption or slowing-down cross section. The reactor temperature was 280°C, and the blanket-to-core uranium ratio was 0.4. The results are given in Fig. 4.14, which shows

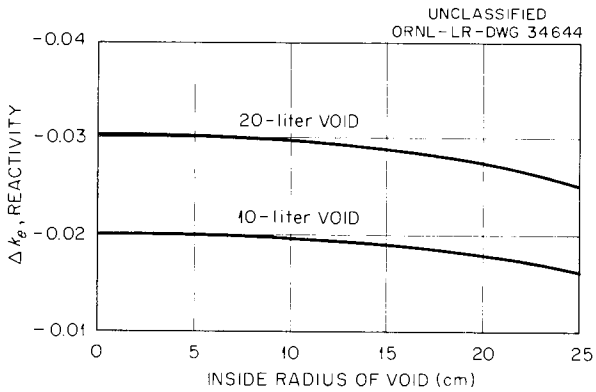

Fig. 4.14. Reactivity Decrement Due to Annular Spherical Void in HRT as a Function of Distance of Void from Core Center.

the relation between the reactivity reduction and the inside radius of the void. A 10-liter void at the center is seen to correspond to a reduction in reactivity of 0.02 Δk_e; as the void is moved out from the center, the reactivity reduction decreases slowly.

4.3.4 Estimated Power and Reactivity Fluctuations Due to "Cold-Fluid" Motion

Some studies were made concerning power fluctuations which could result from convective fluid flow. A two-dimensional, group-diffusion code (PDQ) was used to determine the reactivity addition associated with the introduction of a small volume of relatively cold (thermally) fluid within the reactor core. This small volume was 1% of the volume of the reactor and had cylindrical geometry. The reactivity (Δk_e) of the reactor was calculated as a function of the position of the small, "cold" volume. The Δk_e's were calculated on the assumption that the reactor was at 280°C, while the small volume was assumed to be at either 265 or 275°C. The Δk_e associated with movement of this small volume from the edge to the center of the reactor core was 0.012% Δk_e for 275°C and 0.025% Δk_e for 265°C.

The power responses due to the above reactivity additions were calculated on the assumption that reactivity increased linearly with time up to its maximum value and then decreased linearly to the initial value; the total time interval was taken as either 9 or 18 sec. The initial reactor power was assumed to be 3.5 Mw. The power fluctuations obtained are plotted in Fig. 4.15. They are of the same magnitude as the "regular" power fluctuations which have been observed in the reactor itself.

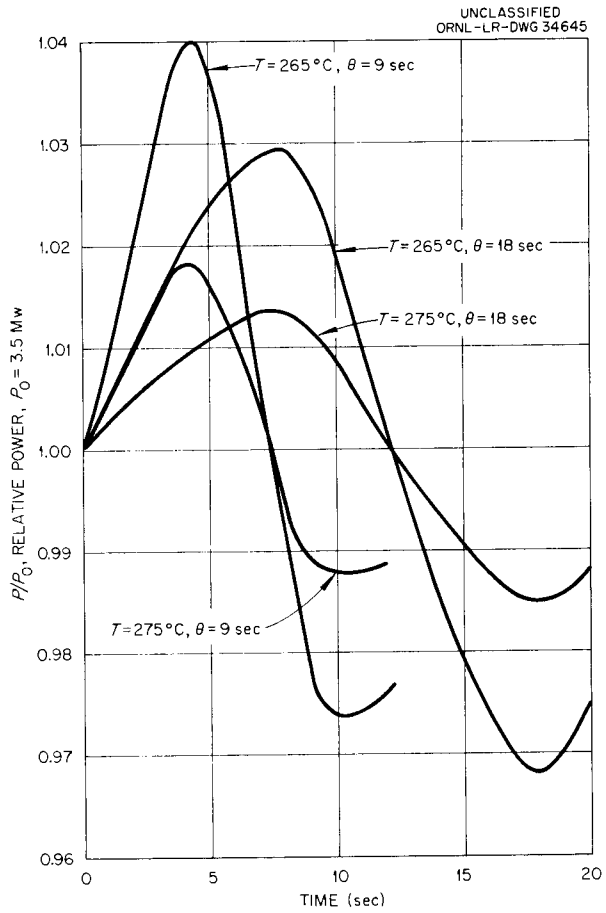

Fig. 4.15. Relative Power as a Function of Time in HRT-Type Reactor. Power fluctuations are those produced by a 3-liter cylinder of fuel solution moving along the core axis; initial reactor temperature, 280°C; small cylinder initially at temperature T; the value of θ is the time for small cylinder to move across the core.

4.3.5 Effect of Fuel Circulation upon Time Behavior of Reactor Power

With the use of the ORNL electronic-analog computer, a study has been initiated of the time behavior of power and temperatures in the HRT following reactivity additions. The object of these studies is to determine whether the small, "regular" power fluctuations which are observed during HRT operation are a natural property of the circulating systems. The nonlinear difference-differential equations employed include five delayed-neutron groups and the time-delay characteristics of the core and blanket circulating systems. It was assumed that the ratio of blanket-to-core power was always constant. The fluid on the shell side of the heat exchangers was assumed to have a constant temperature, and the over-all heat transfer coefficients of the heat exchangers were also assumed to be constant. The mean core and blanket temperatures are assumed to be arbitrary averages of the core-inlet and -outlet temperatures, so that all types of flow conditions ranging from complete mixing to slug flow may be considered. Some initial results have been obtained for step reactivity additions ranging from 0.5% to 2% Δk_e at an initial reactor power of 5 Mw. The power traces obtained so far show none of the oscillatory behavior such as has been observed during HRT operation; rather stable behavior is observed. The power excursion which follows the reactivity addition is rapidly damped and does not undergo oscillations due to fluid circulation effects.

4.4 EFFECT OF HRT CHANGES UPON CRITICAL CONDITIONS

4.4.1 Effect of Uranium Deposition on Critical Fuel Concentration

The presence of noncirculating uranium in the HRT core reduces the concentration in the fuel solution required for criticality (at a given temperature). The amount of deposited uranium which will account for a given decrease in concentration depends on its location. Three positions at which uranium might accumulate are the core-vessel surface, the pressure-vessel surface, and the screens in the entrance to the core region.

The effects of U^{235} being distributed uniformly on either the core vessel or the pressure vessel were investigated by use of WANDA, a two-group, multiregion, spherical-reactor code. In Fig. 4.16 the ratio of the critical concentration with uranium on the core-vessel wall to the critical concentration with no deposited uranium is given as a function of the quantity of uranium on the wall. Figure 4.17 gives the amount of uranium which must be removed from the fuel solution in the high-pressure system to maintain the critical temperature at 280°C, as a function of the quantity of uranium on the core vessel; curves are given for core concentrations (based on no deposited fuel) of 4, 5, and 6 g of U^{235} per liter. The figures indicate that as a thin deposit, 1 g of uranium on the core vessel is worth 3 to 4 g in the circulating system; as the deposit becomes heavier, 1 g on the vessel becomes more nearly equivalent to 1 g in solution. This reduced effectiveness is largely due to a strong flux depression for heavy deposits. Thus the effectiveness per gram would be reduced if a quantity of uranium accumulated on small areas instead of uniformly on the core vessel.

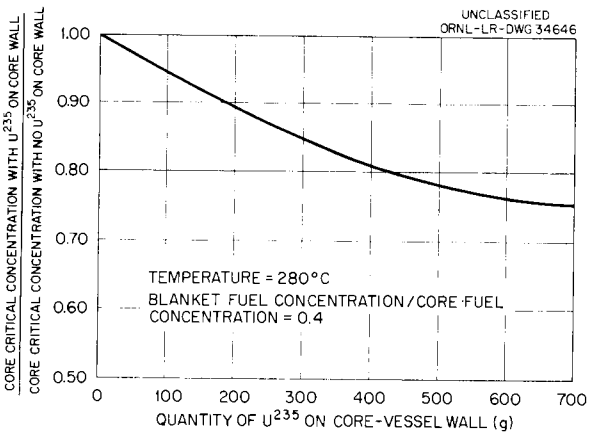

Fig. 4.16. Relative Change in HRT Critical Con-Centration vs Amount of U^{235} on Core Wall.

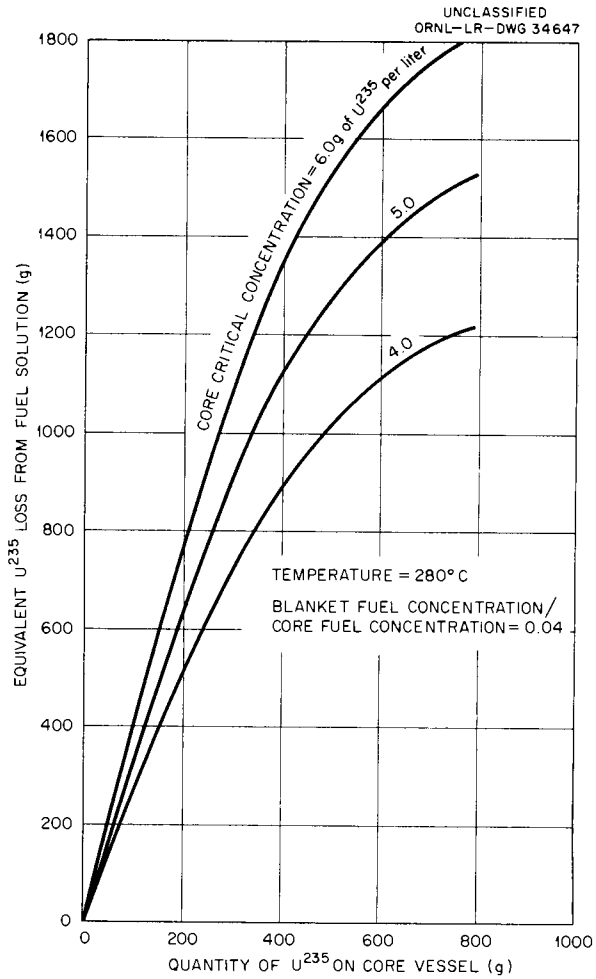

Fig. 4.17. Effect Which U^{235} Deposited on Core Wall Has on the Amount of U^{235} Which Can Be Removed from the High-Pressure System Without Changing the Critical Temperature.

Because of the low nuclear importance of the pressure-vessel wall, transfer of a quantity of uranium from the circulating system to the pressure-vessel wall would result in a decrease in critical temperature. An accumulation of 1 kg of U^{235} on the pressure vessel would be equivalent to less than one-eighth that much spread uniformly throughout the high-pressure circulating solution; deposition of 1 kg would result in a critical-temperature decrease of about 50°C.

The effect of uranium depositing on the screens was investigated with a two-group, two-space-variable reactor code (CURE). One kilogram of U^{235} was distributed in a 2.98-liter torus located at the intersection of the 60- and 90-deg inlet cones. The results indicate that approximately an equal amount of fuel could be removed from the circulating system with no change in critical temperature.

4.4.2 Effect of Introduction of Corrosion-Sample Assembly upon Thermal-Flux Distribution

The core corrosion-sample assembly was represented by a cylindrical region, 2 in. in diameter, composed of a homogeneous mixture of 80 vol % fuel solution and 20 vol % sample-holder materials. The product of the volume and cross section of the equivalent cylinder was the same as that of the actual assembly. The computations were performed by means of a two-group, two-dimensional program (CURE).

Figure 4.18 shows the thermal-flux distribution, normalized to unity at its maximum value, with and without the presence of the sample assembly. Although the assembly causes a depression in the thermal flux at the center of the reactor, its presence decreased the fraction of total power produced in the core by less than 1%.

4.4.3 Operation of HRT with Different Core and Blanket Temperatures

A parameter study was made of some of the characteristics the HRT would have if the core and blanket were operated at different temperatures. Critical concentrations, fluxes, and power densities were computed with a two-group, two-region routine for the Oracle. Core temperatures of 250 and 280°C were studied; blanket temperatures ranged from 200 to 280°C. The ratio of fuel concentration in the blanket to that in the core was varied. The fuel was U^{235}, and the moderator was 99.8% D_2O.

The effects of operation with different temperature combinations on the critical concentration and fraction power generated in the core are shown in Fig. 4.19. The critical concentrations in the core are normalized to values associated with operation of core and blanket at 280°C. It should be noted

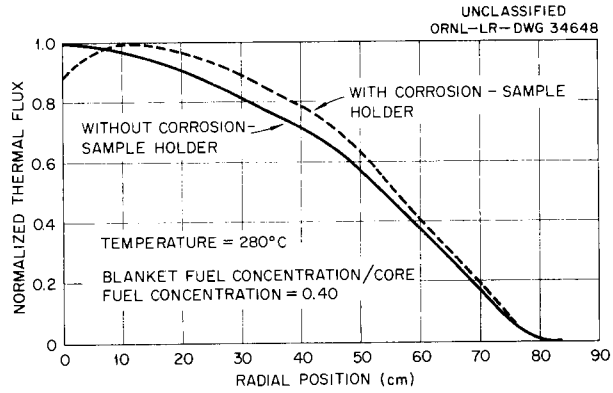

Fig. 4.18. Thermal-Flux Distribution vs Radial Position Measured in a Horizontal Plane Passing Through the Center of the HRT Core.

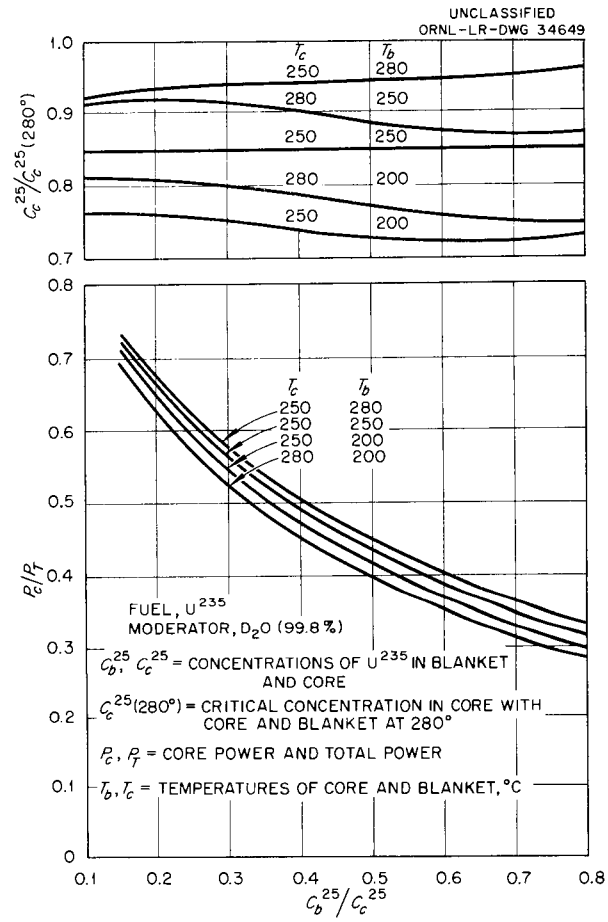

Fig. 4.19. Normalized Core Critical Concentration and Fraction of Total Power Generated in Core vs Ratio of Fuel Concentration in Blanket to That in Core.

that the power distribution applies only to the fission energy which is absorbed near the point of fissioning. No allowance is made for the distribution of energy deposited by prompt, decay, and capture gamma rays.

The power density in the fuel solution at the inner surface of the core tank was affected very little by the temperature distribution (for the same total power). However, the flux at the core-tank wall increased by about 30% when the core temperature was lowered from 280 to 250°C in combination with lowering of the blanket temperature from 280 to 200°C. This flux change was a consequence of the reduced critical concentration.

5. HRT DESIGN

W. R. Gall M. I. Lundin J. R. McWherter

R. E. Aven C. W. Collins J. N. Robinson
C. A. Burchsted E. H. Gift R. E. Schappel
R. H. Chapman H. A. McLain C. L. Segaser
C. J. Claffey G. H. Owen F. C. Zapp
R. C. Robertson

5.1 TEMPERATURE DISTRIBUTION IN EXISTING REACTOR VESSEL

Data from HRT run 16, which had been used to estimate the inside surface temperature[1,2] of the pressure vessel, were further analyzed to estimate the actual heat-transfer film coefficient between this surface and the blanket solution.

A heat-transfer film coefficient at this surface was estimated by comparing the heat flux at the inside surface of the pressure vessel with the temperature drop across the blanket solution film, which would be required to force compliance with the theoretical equations. A rough correlation[2] between this film coefficient and the temperature drop across the film indicates that heat is being transferred principally by natural convection.

5.2 REPLACEMENT PRESSURE VESSEL

Conceptual design studies of the replacement pressure-vessel assembly and its installation are continuing. In addition to the concept previously shown,[1] a vessel concept having a bolted ring-joint closure to permit removal of the core tank (see Fig. 5.1) was prepared. Comparative cost estimates are being obtained for the two concepts from the Newport News Shipbuilding & Dry Dock Co.

5.3 THIMBLE FOR FLUX MONITORS

In order to permit measurements of the fast-neutron flux in the vicinity of the HRT pressure vessel, a thimble was designed in which specimens can be inserted for activation analyses. This device (Fig. 5.2) can be permanently installed through a roof plug into the rear of the blanket corrosion-specimen holder. The activated specimens can be utilized to maintain a cumulative record of the flux dosage being received by the reactor vessel.

5.4 CONDENSER STRESS-CORROSION SPECIMENS

A stress-corrosion assembly for testing condenser tubing was designed and will be exposed in the turbine condenser. The array includes three stressed tube specimens and a tube-to-tube-sheet joint sample (Fig. 5.3).

5.5 SOLUTION PURGE TUBE IN CORE

A purge tube was designed to remove a continuous stream of solution from the HRT core, so that the solution and its solids content during operation can be studied. This tube, as shown in Fig. 5.4, will be inserted into the core through the sample access port and will extend through the upper neck of the vessel down to the top screen. The tube has a swivel joint located in the upper neck of the core to permit location of the tube inlet at the outer edge of the top screen. Zircaloy-2 ($\frac{3}{8}$-in. sched-40 pipe) was chosen to be the construction material for the portion of the tube located within the vessel.

The purge tube will be connected to an extension of the chemical processing line (line 167) so that the chemical plant equipment can be used to collect any solid material removed by the tube.

Fluid-flow analyses show that the fluid velocity in the purge tube will be about 2.3 fps. Assuming a particle density of 5 g/cc, this velocity will allow pickup of spheroids up to 0.008 in. in diameter, according to Stokes' law.

Heat-transfer studies show that the 2.3-fps flow velocity should prevent overheating of the purge tube when the reactor is operating at 5 Mw total power (3 Mw core power). If there is no flow, the total reactor power must be less than 0.5 Mw in order to prevent overheating. In these calculations it was assumed that the outlet temperature of the reactor solution is 280°C and that boiling may occur

[1] W. R. Gall *et al.*, *HRP Prog. Rep. for Quarters Ending April 30 and July 31, 1958*, ORNL-2561, p 57.

[2] R. E. Aven, *HRT Pressure Vessel Temperatures During Operation – An Evaluation Using Data from Run 16*, ORNL CF-58-7-35 (July 7, 1958)

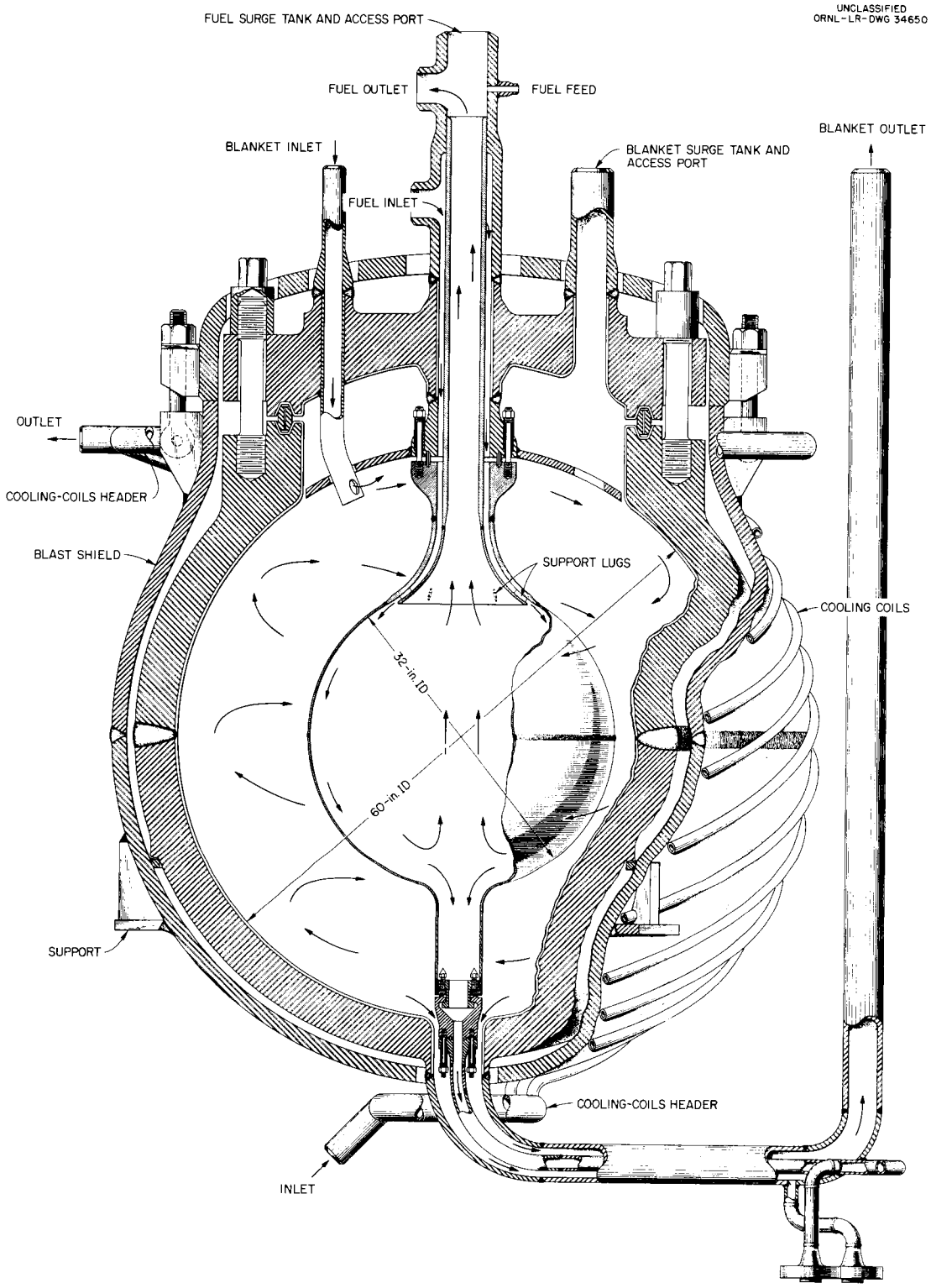

Fig. 5.1. Proposed HRT Replacement Pressure Vessel.

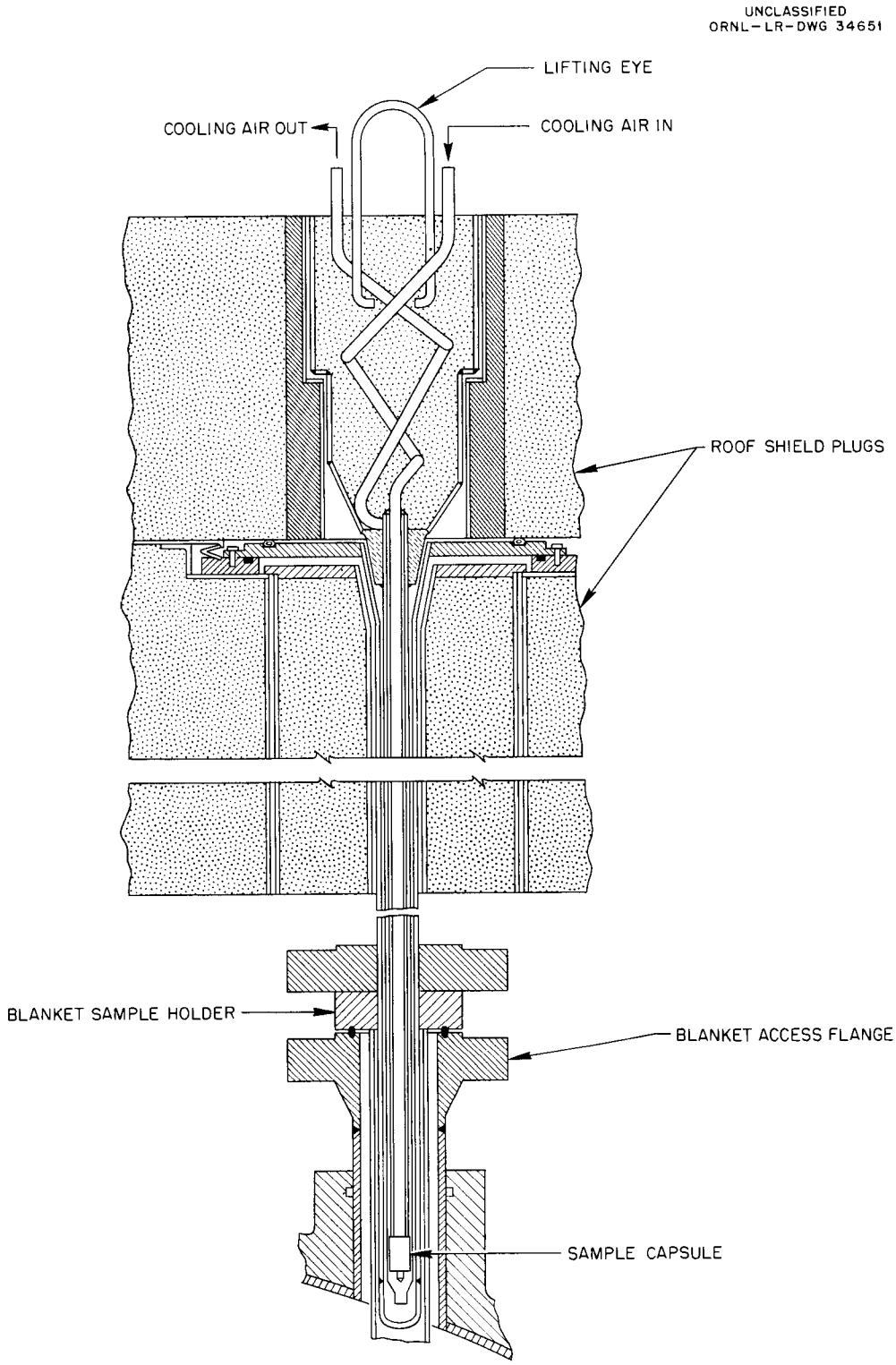

Fig. 5.2. Thimble for Flux Monitors.

above 290°C. Heating in the fluid outside the purge tube was assumed to be approximated by a stagnant layer of fluid of k/h thickness (k is the solution thermal conductivity; h is the heat-transfer coefficient). The possibility of a buildup or deposit of uranium on the tube was not accounted for, and effects due to the additional amount of metal required at the swivel joint were excluded from the calculations.

5.6 MAINTENANCE AND INSPECTION

5.6.1 Flange-Groove Spray Device

A tool was designed for use in cleaning of the grooves of ring-joint flanges in the HRT. Cleaning is accomplished by the use of a stop-plug and a spray-ring apparatus as shown in Fig. 5.5. The flange grooves can be sprayed with water and/or air as desired.

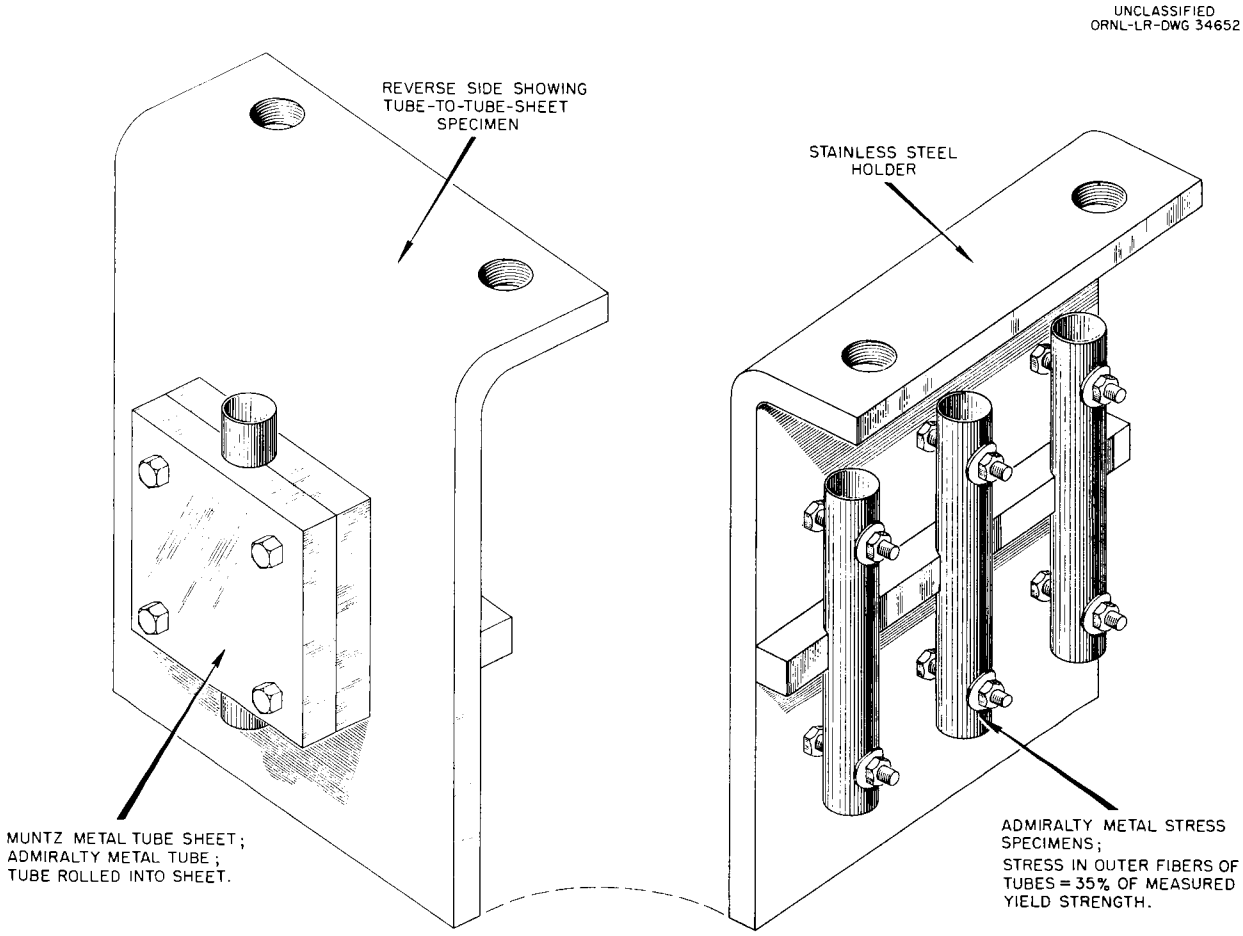

Fig. 5.3. Condenser Stress-Corrosion Assembly.

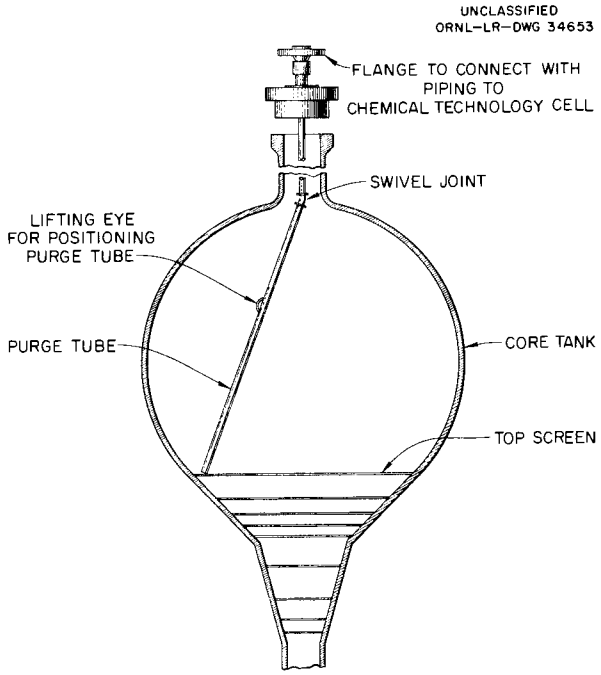

Fig. 5.4. Solution Purge Tube in Core.

5.6.2 Collector for Radioactive Solids

A preliminary design was completed of a collector for removing samples of loose scale and other solids from the screens of the HRT core during shutdown periods. An air-jet exhauster with discharge into the building stack provides the necessary suction. Samples will be collected on filter paper backed up by two porous stainless steel filters in a special holder. The filters will be integrally shielded so that they can be easily removed from the sampling system. Additional backup filters are utilized to reduce particulate activity in the air discharge stream. This device can be fitted into the existing sample-handling shield for transfer to an examination facility.

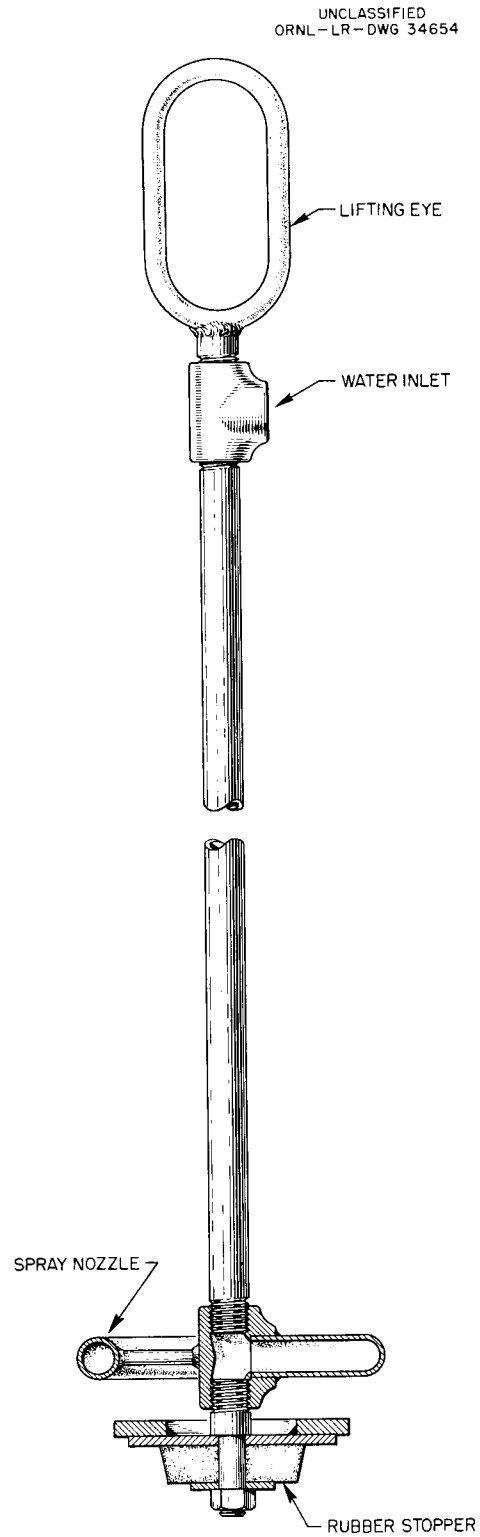

Fig. 5.5. Flange-Groove Spray Device.

6. HRT COMPONENT DEVELOPMENT

I. Spiewak

R. Blumberg
D. M. Eissenberg
C. H. Gabbard
E. C. Hise
C. G. Lawson
J. E. Mott
J. C. Moyers
R. P. Wichner

6.1 PUMPS

Since circulating pumps and feed pumps have performed well in the HRT, no further changes in these items are contemplated. Some development pumps are being operated to provide additional information on the life expectancy of the reactor equipment. The prototype 400A-1 development pump has circulated 0.04 *m* uranyl sulfate solution for 4550 hr in the HRT mockup without difficulty. Prototype fuel feed pumps continued to operate without failure up to a total of 12,500 hr. Two purge pumps in an accelerated life test have operated the equivalent of 15,000 hr.

6.2 HRT CORE STUDIES

6.2.1 Modifications in Present Geometry

The full-scale carbon-steel flow model of the HRT was operated to determine the effect on flow distribution of cutting 2-in. samples from the center of the top six diffuser screens. A central jet, extending to the top outlet line, was observed. Upward flow velocities were reduced in the remainder of the core, although velocities near the core-tank wall were not greatly affected.

A perforated-plate plug assembly was inserted in the hole formed by the removal of the samples. This assembly effectively replaced the screen samples of the first, third, and fifth screens, counting from the top. The flow pattern observed was the same as before the screen samples were cut.

The welds joining the top and the fifth perforated plates to the tank wall were cut to allow a study of their behavior in a flowing stream; corresponding screens were known to be loose in the reactor. The weight of the top plate was observed to be great enough to stabilize it in the flow stream. However, the fifth screen was lifted by the stream and held against the fourth; approximately 5 lb of weight added to the fifth screen stabilized it.

Runs were made to select an optimum location for a sample probe which would serve as an intake for the HRT chemical plant in hopes that information could be obtained to explain the core instability. When the probe was located in the central channel formed by the 2-in. holes cut in the screens, the only solids collected were those which managed to fall from above. When it was located near the intersection of the top screen and the core wall, foreign materials were readily removed from the vicinity. These materials included a heavy liquid (perchloroethylene), a granulated solid (sand), and a flocculated solid (lead oxide).

A general observation made in these tests was that small changes in the screen system could introduce marked perturbations in the flow. It is expected, therefore, that the reactor flow distribution now differs considerably from the original distribution and that it will vary from time to time, depending on the positions and physical condition of the screens.

6.2.2 HRT Replacement Core

In the selection of a core configuration for a replacement reactor vessel for the HRT, attempts are being made to eliminate the hydrodynamic difficulties experienced in the present HRT core. Screening criteria to reject undesirable flow situations are that solids must be removed readily, a stable flow pattern must be achieved, and high wall shear stress must be provided to promote wall cooling and cleanliness. Two models are being given close considerations: one with a polar inlet and an annular outlet and the other with a vaned annular inlet and a polar outlet.

The polar-inlet core satisfies the screening criteria. Heat-transfer measurements were made at two wall positions of a 32-in.-dia core model with hot and cold water.[1] These data were generalized with similar data on the HRE-3 core model, and the generalization was used to develop the core-side heat-transfer coefficient distribution of a 32-in.-dia

[1] J. E. Mott, *Hydrodynamic and Heat Transfer Tests of a Full Scale Reentrant Core*, ORNL CF-58-8-54 (Aug. 8, 1958).

vessel with a 400-gpm flow at 280°C. The predicted coefficients and wall temperatures as a function of position at 5 Mw are plotted in Fig. 6.1.

The predicted wall temperatures are quite close to the fluid temperature. However, the key assumption on which this prediction depends is that the amount of uranium located on the core wall is consistent with in-pile loop experience, that is, that the wall is free of scale. It is doubtful that this is the case in the present HRT core. Other assumptions in the temperature prediction are: no cooling from the blanket side, metal heat generation of 3 w/cc, and fluid-film heat generation of 17 w/cc. Any cooling from the blanket side would decrease the wall temperature, whereas a uranium precipitate on the core side would increase the temperature rise. These effects are being considered further.

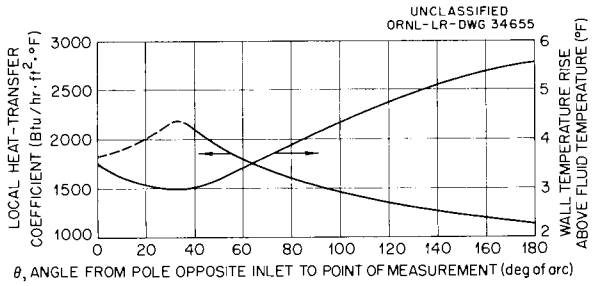

Fig. 6.1. Local Heat Transfer Coefficient and Temperature Rise of Wall for Polar-Entry–Concentric-Outlet HRT Replacement-Type Vessel at 5 Mw.

The annular-inlet type of vessel currently being tested is shown in Fig. 6.2. The main fluid outlet is at the top pole, with provision to remove about 10% at the bottom pole. Vanes are provided at the inlet to impart any desired degree of rotation to the fluid entering the core.

Wall heat-transfer coefficients were measured by means of o specially made instrument mounted flush against the core wall, as shown in Fig. 6.3. A known heating rate is applied to the Electrofilm coating on the back surface of the aluminum parallelpiped containing the thermocouple. From the known fluid temperature and the temperature at the internal thermocouple, the average heat-transfer coefficient along the length of the meter is calculated. This is related to wall shear stress by an expression derived by Ludwerg,[2] which assumes that the thermal

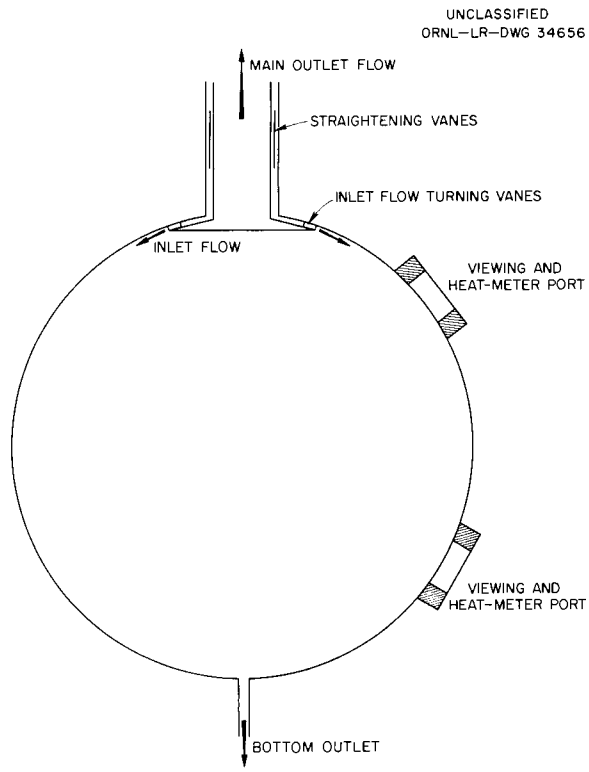

Fig. 6.2. Mockup of HRT Replacement-Type Core with an Annular Inlet.

boundary layer does not extend beyond the hydrodynamic laminar sublayer. Calculated results obtained with 45- and 10-deg rotational vanes at the inlet annulus are summarized in Table 6.1. Heat-meter positions in the top and bottom hemisphere are located at polar angles of 52 and 120 deg, respectively.

For comparison, the wall shear stress at the 10-fps slot in corrosion-coupon holders in in-pile loops is approximately 0.5 lb/ft^2, while at the 0.8-fps position (in the annulus) the wall shear is estimated to be 0.008 lb/ft^2.

To satisfy the solids-removal criterion in this type of core vessel, there must be a bottom outlet flow of about 10%. At an inlet-flow turning angle of 45 deg, the centrifugal force on solids was observed to collect them at the core wall at a point 10 deg from the bottom pole, where they formed a rotating ring.

[2]H. Ludwieg, *Instrument for Measuring the Wall Shearing Stress of Turbulent Boundary Layers*, NACA-TM-1284 (May 1950).

UNCLASSIFIED
ORNL-LR-DWG 34657

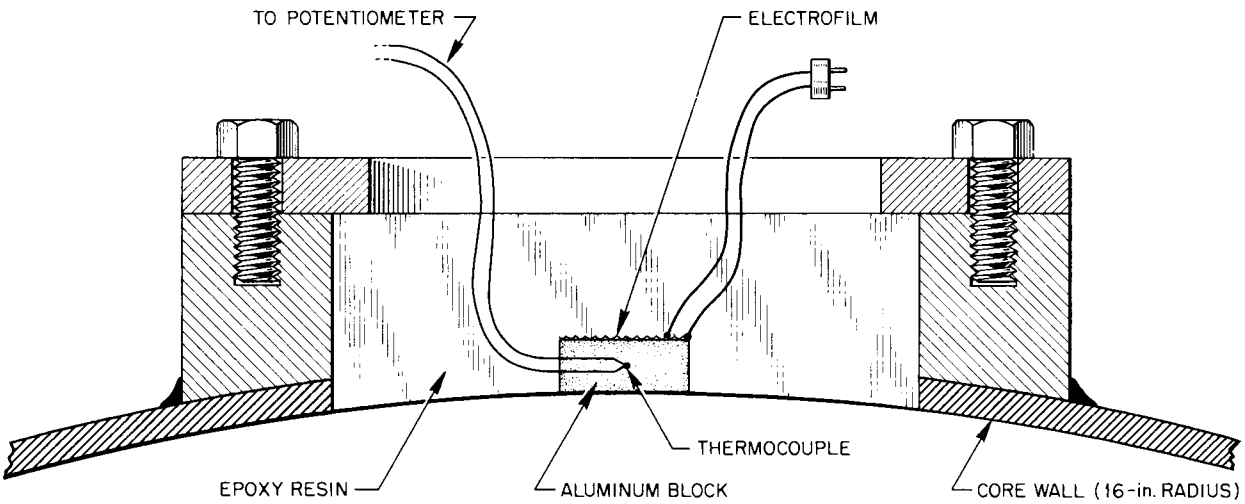

Fig. 6.3. Heat Meter in Position at Port Hole.

Table 6.1. Wall Conditions in Annular-Inlet Core at 300 gpm, Room Temperature

Inlet-Vane Turning Angle (deg)	Heat Transfer Coefficient ($Btu/hr \cdot ft^2 \cdot {}^\circ F$)		Wall Shear Stress (lb/ft^2)		Estimated Velocity at Wall (fps)	
	Top Hemisphere	Bottom Hemisphere	Top Hemisphere	Bottom Hemisphere	Top Hemisphere	Bottom Hemisphere
45	2710	1750	1.25	0.70	14	8.7
10	1460	980	0.41	0.10	7.3	4.9

A bottom outlet flow of 10% did not remove the solids in this case.

Although the annular-inlet system has an advantage in that the fluid boundary layer at the wall is close to the inlet temperature, the boundary becomes unstable near the bottom pole at low vane angles. At high vane angles, solids removal is difficult. Further work is planned with this configuration.

6.3 HRT MOCKUP

R. B. Korsmeyer

P. H. Harley D. E. Willis

6.3.1 Operation

The HRT mockup, containing a titanium letdown heat exchanger and titanium pressurizer and feed heater, was operated for 1726 hr during the past quarter. Operation was at 1500 psi and 280°C with a fuel composition of 0.045 *m* UO_2SO_4, 0.025 *m* H_2SO_4, and 0.035 *m* $CuSO_4$.

The main objective of the run was to evaluate the use of boiling fuel solution in a titanium heat exchanger[3] as a steam supply for pressurizing the system. No difficulties were encountered with the pressurizer operation. However, the maximum fuel temperature (315°C) was about 15°C lower than the temperature at which the second liquid phase forms, according to sample analyses.

A letdown valve with a $\frac{1}{8}$-in. port, a level-controlled feed rate with a manually adjusted letdown

[3] R. B. Korsmeyer, P. H. Harley, and D. E. Willis, *HRP Prog. Rep. for Quarters Ending April 30 and July 31, 1958*, ORNL-2561, p 36.

rate, and a stainless steel rotameter in the purge-pump suction were also evaluated. All gave trouble-free operation. The letdown valve has remained leak-tight when shut with a 1500-psi pressure differential; it passes a flow of 1 gpm when 70% open.

The chemical stability of the fuel solution during the run was better than in previous runs. This can be attributed to the elimination of the purge flow to the pressurizer, which was known to cause precipitation.[4]

The generalized corrosion rate during the first 700 hr of the run was 0.73 mpy based on the increase of nickel in solution. However, for the last 1000 hr the corrosion rate increased to 1.3 mpy. At present, the increase cannot be explained. An examination of the stainless-steel-to-titanium transition flanges showed no visible corrosion, and analysis of the pressurizer vapors did not indicate a corrosive environment.

The 400-gpm canned-rotor circulating pump has been in operation for 4477 hr since the last inspection. A possible shaft-seal leak has been indicated by high uranium concentrations (1.5 g/liter) in the motor end of the pump.

The north fuel-feed-pump head has operated for 6936 hr and the south head for 11,128 hr since the last diaphragm failure. The south-head diaphragm is 21-mil, $\frac{1}{4}$-hard stainless steel with a 40-mesh screen filter. The north head, a later design, has a 31-mil diaphragm and a 100-mesh screen filter. The purge pump has operated for 7431 hr since the last failure. The titanium letdown heat exchanger has operated for 4350 hr without trouble; the titanium-to-stainless-steel transition flanges have remained leak-tight during this time.

[4] *Ibid.*, p 38.

7. HRT CONTROLS AND INSTRUMENTATION

D. S. Toomb

A. M. Billings R. L. Moore
J. R. Brown J. A. Russell
K. W. West

7.1 COMPONENT AND SYSTEM TESTING

7.1.1 System for Indicating Control-Valve Stem Position

A system for indicating control-valve stem position was developed and was installed on the reactor fuel letdown valve and on the HRT mockup letdown valve for testing. The linear variable-differential transformer previously described[1] is used for a transmitting element. A simple electropneumatic transducer system for the 60-cps signals from the differential transformer was developed around standard modular elements. The system, shown in Fig. 7.1, employs three vacuum tubes in the controller and is used to derive a pneumatic signal proportional to the valve position for alarm and indication or record. Performance tests indicate a linearity of ½%, no change in output signal with supply pressure changes from 15½ to 25 psi, and freedom from zero drift with electric supply changes from 95 to 125 v.

7.2 COMPONENT DEVELOPMENT

7.2.1 Letdown Valves

The fuel letdown valve[2] (serial No. R-21) which was installed in the HRT on May 1 has performed satisfactorily to date. Total operating time for this valve is now 2075 hr.

The experimental ⅛-in.-dia-port letdown valve[3] with a lower stem guide was installed on the HRT mockup loop; it has since operated satisfactorily for 1776 hr. Very good control of the pressurizer level was achieved by this valve, which is slowly cycled between 70 and 72% of the full-open position by the automatic liquid-level controller on the pressurizer.

[1] D. S. Toomb *et al.*, *HRP Quar. Prog. Rep. Jan. 31, 1958*, ORNL-2493, p 18.

[2] D. S. Toomb *et al.*, *HRP Prog. Rep. for Quarters Ending April 30 and July 31, 1958*, ORNL-2561, p 49.

[3] *Ibid.*, p 50.

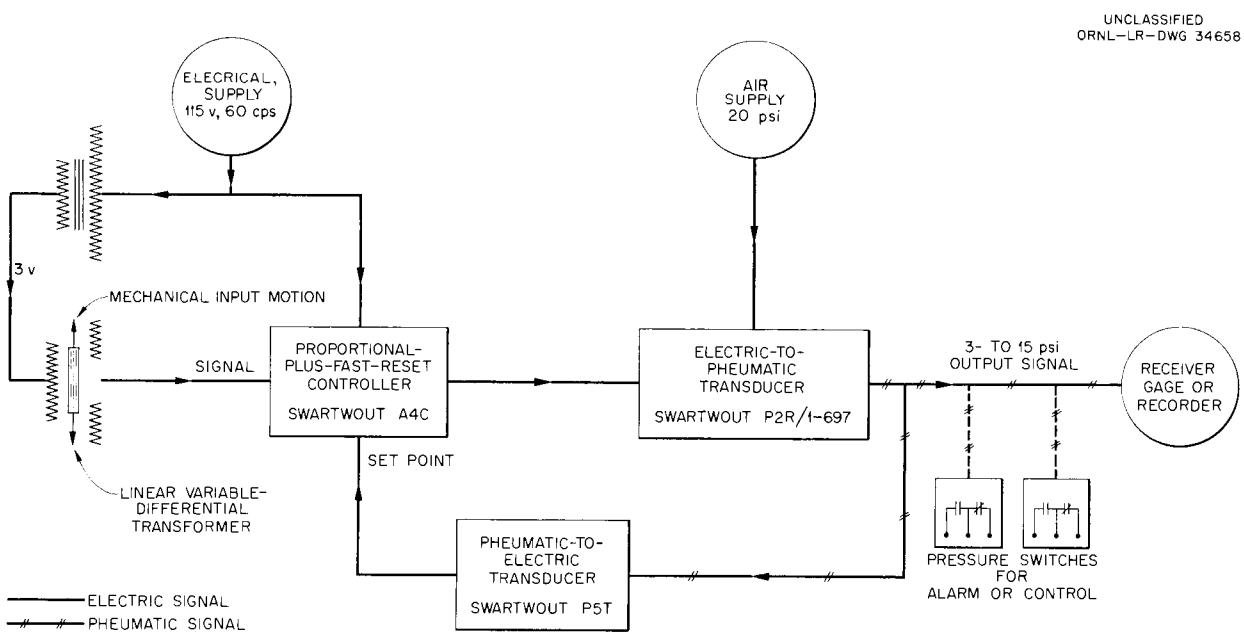

Fig. 7.1. Block Diagram of Electropneumatic Transducer System for Indicating Control-Valve Stem Position.

7.3 MAINTENANCE AND MODIFICATIONS

7.3.1 Blanket Dump Valve

The blanket-system emergency drain valve[4] (serial No. K-71), which was removed from the reactor after power operation, was decontaminated sufficiently to permit repairs in a "hot" shop. The valve was disassembled by the use of extension-handle tools and was seal-welded with the aid of an exhaust fan which removed contaminated vapors. The repaired valve was then returned to the reactor spare-part inventory.

7.3.2 Control-Circuit Revisions

As a result of operating experience, several revisions were made to the reactor control circuits. The circuits were revised to prevent a signal of high stack radioactivity from isolating the instrument cubicles and thereby causing erratic pneumatic signals because of air accumulation in the cubicles. The cubicles will be isolated by block valves in case of detection of activity in the oxygen injection system or of high activity in the cell air.

Power-monitor lights were installed in the main control room for each a-c and d-c control bus. A bus failure will extinguish a lamp and thereby provide easy identification of the failed circuit.

A new control panel was installed near the waste handling system to centralize the control of this facility.

---

[4] *Ibid.*, p 53.

Part II

REACTOR DESIGN, RESEARCH, AND ANALYSIS

R. N. Lyon

8. HRE-4 DESIGN

W. R. Gall M. I. Lundin J. R. McWherter
J. C. Bolger N. Hilvety
R. H. Chapman H. A. McLain
E. H. Gift R. C. Robertson
L. A. Haack D. W. Vroom

8.1 HRE-4 PRELIMINARY DESIGN

Design studies on HRE-4, a small single-region slurry reactor, were completed and are to be described in detail in a forthcoming report.[1] These studies, mentioned in a previous progress report,[2] are summarized in the following subsections.

8.1.1 Design Data

Some of the design bases for HRE-4 are given in Table 8.1.

Table 8.1. Some Preliminary Design Bases for HRE-4

Slurry fuel	ThO_2 with enriched UO_2 in D_2O
U^{235}/Th ratio	0.08
Slurry concentration	231 g of Th per kg of D_2O
Design power level	5 Mw (thermal)
Operating temperature	275°C (average)
Operating pressure	1500 psia
Circulation rate	600 gpm
Core inside diameter	4.5 ft
Core volume	1520 liters

8.1.2 Flowsheet

The proposed flowsheet is shown in Fig. 8.1. Slurry flow is upward through the core vessel and downward through the heat exchanger. A second pump is shown in phantom. This pump would be added to the system if additional flow is required in the core vessel. The system is pressurized by boiling the slurry continuously in the high-pressure dump tank. A standpipe at the high point in the loop is connected by two open lines to the dump tank. The lower line provides a path for slurry overflow from the loop. The upper line assures pressure equalization, which permits the vapor volume in the dump tank to serve as a surge volume for the reactor.

A dump valve is located in the drain line between the low point in the loop and the dump tank. Since some slurry particles may be left behind after a dump, provisions are made for rinsing the loop with D_2O from the condensate storage tank. The D_2O in this tank is maintained at or near the loop operating temperature.

Transfer of slurry from the dump tank to the loop is accomplished by use of an acid-egg type of transfer tank. By allowing steam to condense in the transfer tank, the pressure is reduced sufficiently to permit slurry to be forced into this tank from the dump tank.

A homogeneous internal catalyst is used to recombine radiolytic gas formed in the reactor, and a high-pressure catalytic recombiner is used in the vapor line to the condensate production system to minimize radiolytic-gas concentration in the high-pressure condenser.

The low-pressure off-gas system is similar to the HRT off-gas system, with an iodine removal bed, recombiner, condenser, secondary recombiner, cold traps, charcoal beds, and filters ahead of the stack.

8.1.3 Operation

For startup of the reactor, the circulating system is first filled with D_2O and heated to above the normal operating temperature. Slurry is then slowly added to the main loop by transfer from the dump tank until the desired concentration is reached. The temperature is then lowered until criticality occurs.

During normal operation of the reactor, D_2O added to the circulating loop as purge water tends to increase the system volume. The operating level will be maintained constant either by overflow from the standpipe to the dump tank or by evaporation in the standpipe, the latter being

[1] J. R. McWherter *et al.*, *Design Studies for HRE-4 Feasibility Report*, ORNL CF-58-11-9 (to be issued).

[2] W. R. Gall *et al.*, *HRP Prog. Rep. for Quarters Ending April 30 and July 31, 1958*, ORNL-2561, p 63.

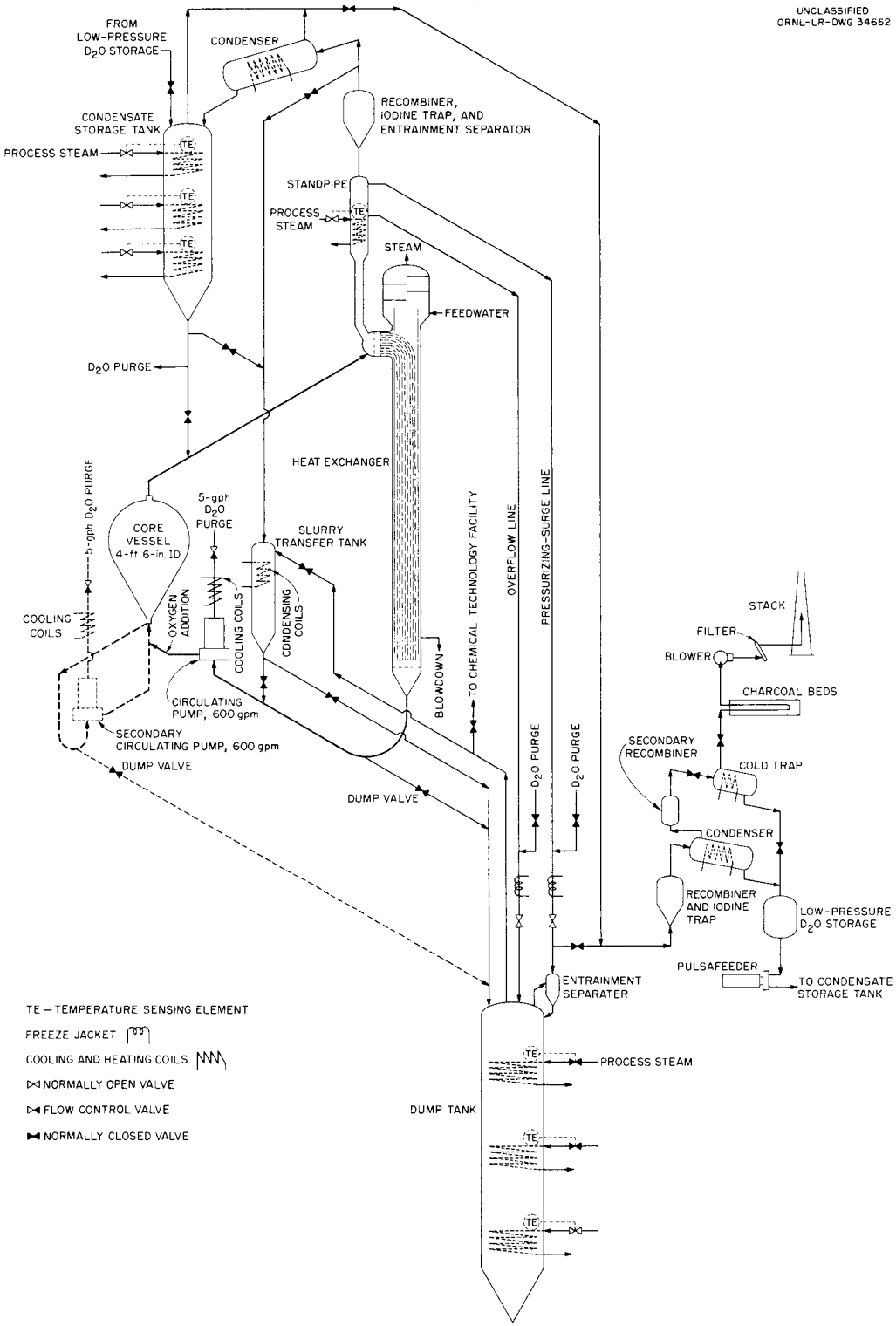

Fig. 8.1. Proposed HRE-4 Flowsheet.

employed if slurry tends to overflow in appreciable amounts.

A normal shutdown is conducted by first stopping the steam flow from the heat exchanger, which causes the power to decrease to the heat-loss amount, and then gradually decreasing the slurry concentration. The reactor is maintained at a subcritical temperature by adding heat through condensing steam on the shell side of the main heat exchanger. Dilution and circulation continue until essentially all the slurry has been rinsed from the system and transferred to the dump tank.

In an emergency, the reactor will be made subcritical by draining the contents of the main loop to the high-pressure dump tank.

During normal shutdowns the slurry is stored in the high-pressure dump tank. Provision is made, however, for transferring the slurry to the chemical technology facilities when necessary.

8.1.4 Heat Removal System

The reactor heat is dissipated to the atmosphere. This is done by generating steam in the main heat exchanger at pressures varying from 326 psia at 5-Mw reactor power to about 1100 psia at zero power, and condensing the steam at about 20 psig in an air-cooled coil. A 30-hp high-head feed-water pump of about 40-gpm maximum capacity is required. Water level in the heat exchanger is regulated by changing the feed-water flow rate. Auxiliary equipment includes a deaerating feed-water heater, blowdown system, make-up, sampling, and chemical treatment system.

To decrease the possibility of activity getting outside the biological shielding, steam leaving the main heat exchanger is delayed approximately 10 sec in a 100-ft^3-holdup volume inside the shield. In case of a slurry leak into the steam system, this delay would allow a stop valve in the steam line and a valve in the feed-water line to close upon signal of high radiation.

The design concept for the main heat exchanger is shown in Fig. 8.2. Some of the design data are given in Table 8.2. The inverted-L exchanger operates with slurry in turbulent flow in the tubes and with water boiling in the shell. Slurry enters the exchanger near the top, flows downward through the tubes, and leaves through the conical header at the bottom. These locations of inlet and outlet facilitate a compact plant layout. Feed water is introduced at the top of the unit and flows down an annular passage between a shroud and the shell. A mixture of steam and water travels upward along the tubes and is separated in the section at the top of the exchanger. A blowdown line is provided near the bottom of the shell.

The standpipe, which is necessary for venting and pressurizing and for taking care of surges and overflow, is located for convenience on the heat exchanger inlet header but is not an integral part of the exchanger.

Use of the L-shaped tubes was based on the assumption that such a design would minimize slurry plugging and caking problems.

A slurry velocity of 10 fps was selected in order to obtain a Reynolds number above the transition region between laminar-to-turbulent flow. For a fixed flow rate, reactor power, and tube diameter, the length of tubes increases with velocity. As

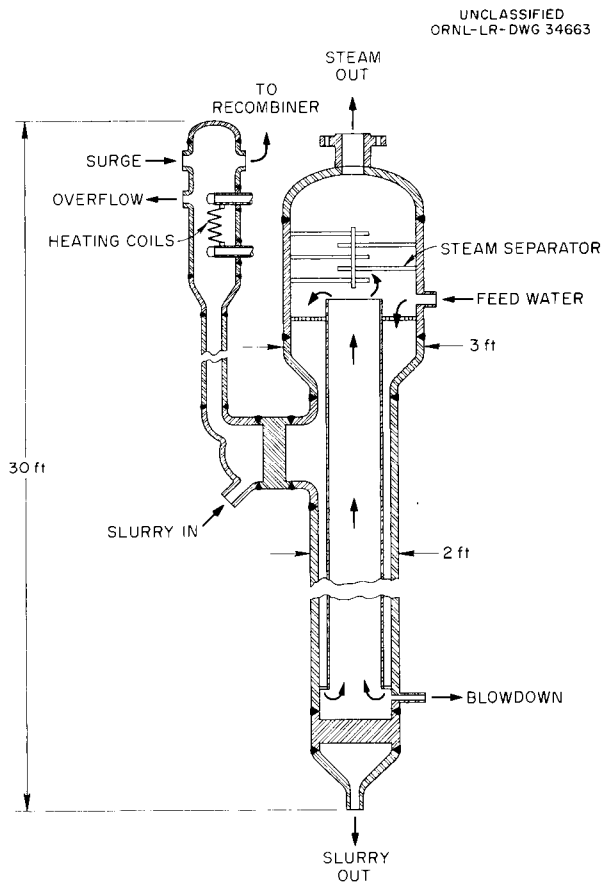

Fig. 8.2. HRE-4 Main Heat Exchanger.

Table 8.2. Design Data for HRE-4 Main Heat Exchanger

Power level	5 Mw
Tube size	$\frac{5}{8}$-in. OD (0.083-in. wall)
Tube shape	Inverted L
Slurry velocity	10 fps
Slurry flow rate	600 gpm
Slurry shear stress	0.025 lb/ft^2
Slurry viscosity	2.42 lb/hr·ft^2
Heat transfer coefficient (tubes dirty)	420 Btu/hr·ft^2·°F
Area	407 ft^2
Temperature difference	100°F
Number of tubes	114
Length of tubes (effective)	21.5 ft
Over-all pressure drop	23 ft fluid

height is at a premium in the containment vessel, velocities greater than 10 fps were not considered.

A nominal tube size of $\frac{5}{8}$ in. was chosen because smaller tubes would increase the probability of drainage problems and larger tubes would increase the tube length.

Poison rods are included in the shell to minimize the possibility of the unit being critical in the event the slurry becomes mixed with light water in the shell.

8.1.5 Circulation Pump

A 600-gpm canned-motor circulating pump has been chosen for circulating slurry through the core and heat exchanger. The head requirement for this pump has been estimated at about 100 ft of slurry.[3] A 35-hp 1800-rpm pump currently on order for development work appears to be of a type well suited to HRE-4 use. The conditions of flow rate and head could probably be met by modifying this pump on the hydraulic end to obtain the particular characteristics needed. The estimated purge-water flow rate for the rear end of the pump is 5 gph. The motor electrical input for the pump is 60 cycle, 3 phase, 440 v.

[3]E. H. Gift, "HRE-4 High Pressure System Pressure Drop," memorandum to W. R. Gall, Aug. 12, 1958.

8.1.6 Dump Tank

The high-pressure dump tank will be a multipurpose unit serving as a subcritical storage tank, a surge volume, and a pressurizer. It must be designed for a pressure of 2000 psi and must accommodate about 6500 liters, including 2000 liters of slurry from the main circulating loop, about 500 liters of slurry heel in the tank, about 3000 liters of rinse water, and a freeboard volume of about 1000 liters to reduce carry-over of possible foam. The dump tank will have a conical bottom, be about 4 ft in inside diameter and 25 ft in over-all height, and have a wall thickness of about 4 in. To minimize the possibility of criticality occurring, even with light water as the carrier and with an infinite light-water reflector, a large number of boron-containing poison tubes 2 in. in outside diameter have been placed in the tank.

The heating surface will consist of 12 coils of 50 ft of 1-in.-OD tubing each, located in the tank. Assuming a log mean temperature difference of 40°F, based on 2000-psia saturated steam as the heating medium, and an over-all heat transfer coefficient of 150 Btu/hr·ft^2·°F, this surface would have a capacity sufficient to make up heat losses from the system (about 1×10^5 Btu/hr), to evaporate about 1 gpm of pump purge water (2×10^5 Btu/hr), and either to heat the dump tank and its contents from room temperature to operating temperature (569°F) in about 12 hr or to fill the rinse tank in about 2 hr (at a rate of 4 gpm) by condensation of steam generated in the dump tank.

8.1.7 Transfer System

Although an acid-egg transfer tank is shown on the flowsheet, it is realized that a transfer pump could be used for moving the slurry from the dump tank. In addition to transferring slurry, a transfer pump could be used to help provide mixing in the storage tank. Should a jet prove feasible, it might be possible to motivate a jet with a small transfer pump so that the pump could be located higher in the cell to facilitate maintenance. If through-the-wall disconnects can be provided and freeze jackets can be employed in conjunction with blocking valves on each side of the pump, it is possible that location of the pump near the bottom of the cell would not be impractical. This system was not selected, because of the unknown useful life expectancy of the pump and the difficulty in replacing such a unit.

8.1.8 HRE-4 Off-Gas System

During normal reactor operation the high-pressure condenser is vented to the off-gas system to prevent buildup of noncondensable gases in the condenser. In case of emergency the high-pressure dump tank may be vented directly to the off-gas system to provide a means of rapid reduction of pressure in the high-pressure system. This latter case determines the required capacity for the off-gas system.

The gas concentrations and partial pressures existing in the reactor at 5 Mw have been calculated.[4] Some of the assumptions made are as follows: deuterium partial pressure of 100 psi at the core outlet, first-order recombination-rate activation energy of 16,000 cal/mole, deuterium and oxygen solubilities in slurry the same as in D_2O.

Based on these assumptions, a recombination rate at 280°C of 0.6 mole of D_2 per hour per liter of slurry is required for 5-Mw operation. The partial pressures existing throughout the system during operation at 5 Mw and with an excess-oxygen partial pressure of 100 psi at the core outlet are shown in Fig. 8.3. The total amount of noncondensable gases in the high-pressure system is estimated at 100 moles. Part of this, 59 moles, is radiolytic gas; the remainder is excess oxygen. Based on the predicted temperatures and volumes of the high-pressure system, the equilibrium conditions after an instantaneous adiabatic dump to the high-pressure dump tank are estimated as 936 psia and 279°C. Of the 936-psia total pressure, 926 psi is D_2O vapor and 10 psi is noncondensable-gas pressure. Assuming that the high-pressure system will be vented at a rate which, if continuous, would remove all the noncondensable gases within 15 min, the flow rates of each of the components in the vapor phase would be: oxygen, 130.1 g/min; deuterium, 10.5 g/min; D_2O vapor, 11,922.1 g/min.

Since the total mass flow into the beds will be less than the maximum encountered in the HRT, the two recombiners and the iodine trap have tentatively been sized as equal to those presently installed in the HRT.

[4]E. H. Gift, "Vapor Pressures and Recombination Rate in HRE-4," HRP-58-381, Sept. 2, 1958.

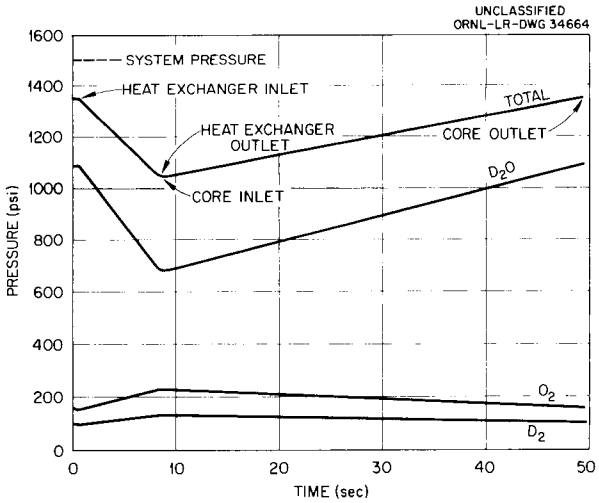

Fig. 8.3. Vapor Pressures in the HRE-4.

8.1.9 Reactor Shielding

The feasibility of utilizing the existing Building 7503 for HRE-4 is being investigated. The high-pressure equipment would be located in the existing containment vessel. A rough estimate has been made of the HRE-4 shielding requirements to indicate the feasibility of this plan from the standpoint of the shielding modifications that may be required. Below the first-floor level the existing shielding consists of the 2-in.-thick steel wall of the inner containment vessel, an annular space of 3 ft between this inner vessel and an outer ½-in.-thick steel vessel, and 1.5 ft of ordinary concrete around the outer vessel. Above the first-floor level there is a minimum of about 5 ft between the inner and outer vessels, and no additional concrete.

The shielding requirements for HRE-4 have been estimated[5] on the basis of 5-Mw reactor power and on a Laboratory tolerance dose rate of 2.5 mrem/hr. It is assumed that borated water will be used in the annular space between the inner and outer vessels. Since the HRE-4 is a single-region unreflected type of reactor, the number of neutrons escaping from the core is quite high. Consequently, in order to reduce the shielding requirements to reasonable values, it is further assumed that a heavy shield will be placed around the reactor-core pressure vessel inside the containment vessel, this shield to be 1 ft thick and to

[5]N. Hilvety, "HRE-4 Biological Shielding," HRP-58-372, Aug. 26, 1958.

consist of 40% lead and 60% borated water. On the basis of the above assumptions, the existing ART cell would require modification by adding $2\frac{1}{2}$ ft of barytes concrete around the outer tank above the first-floor level and about 2 ft of barytes concrete around the concrete shielding below the first-floor level.

8.1.10 Conceptual Layouts

It has been concluded from preliminary layouts that the reactor system as presently contemplated cannot be placed in the existing containment vessel in Building 7503 without considerable modifications of the building to provide additional height. Figures 8.4 and 8.5 show a plan view and an elevation, respectively, of one concept of how the existing facility might be modified to install the reactor equipment. All the required building modifications are not shown; for example, the overhead crane must be raised in order to service the reactor containment vessel.

Because of space requirements and the depths involved for maintenance, it was concluded that it would be impractical to locate the drain tank and its auxiliaries inside the existing containment vessel. These components are therefore shown in a separate containment vessel (12 ft in diameter by 45 ft high), which is connected to the larger containment vessel (24 ft in diameter by 50 ft high) by two 4-ft-dia pipe tunnels. The tunnels also provide sufficient passageway for vapor expansion in the event of a reactor system rupture.

The philosophy on which the equipment layouts are based may be summarized as follows:

1. A vertical, easily drained, heat exchanger will be used in the belief that vertical tubes are less likely to plug than horizontal tubes.
2. Straight-through up-flow will be utilized in the reactor core vessel.
3. Vertical and 45-deg inclined pipe runs will be used where feasible to enhance drainage.
4. Space will be left to add an additional circulating pump if it is found to be desirable or necessary.
5. The existing ART containment vessel will be used.
6. Maintenance access to the system will be from above.

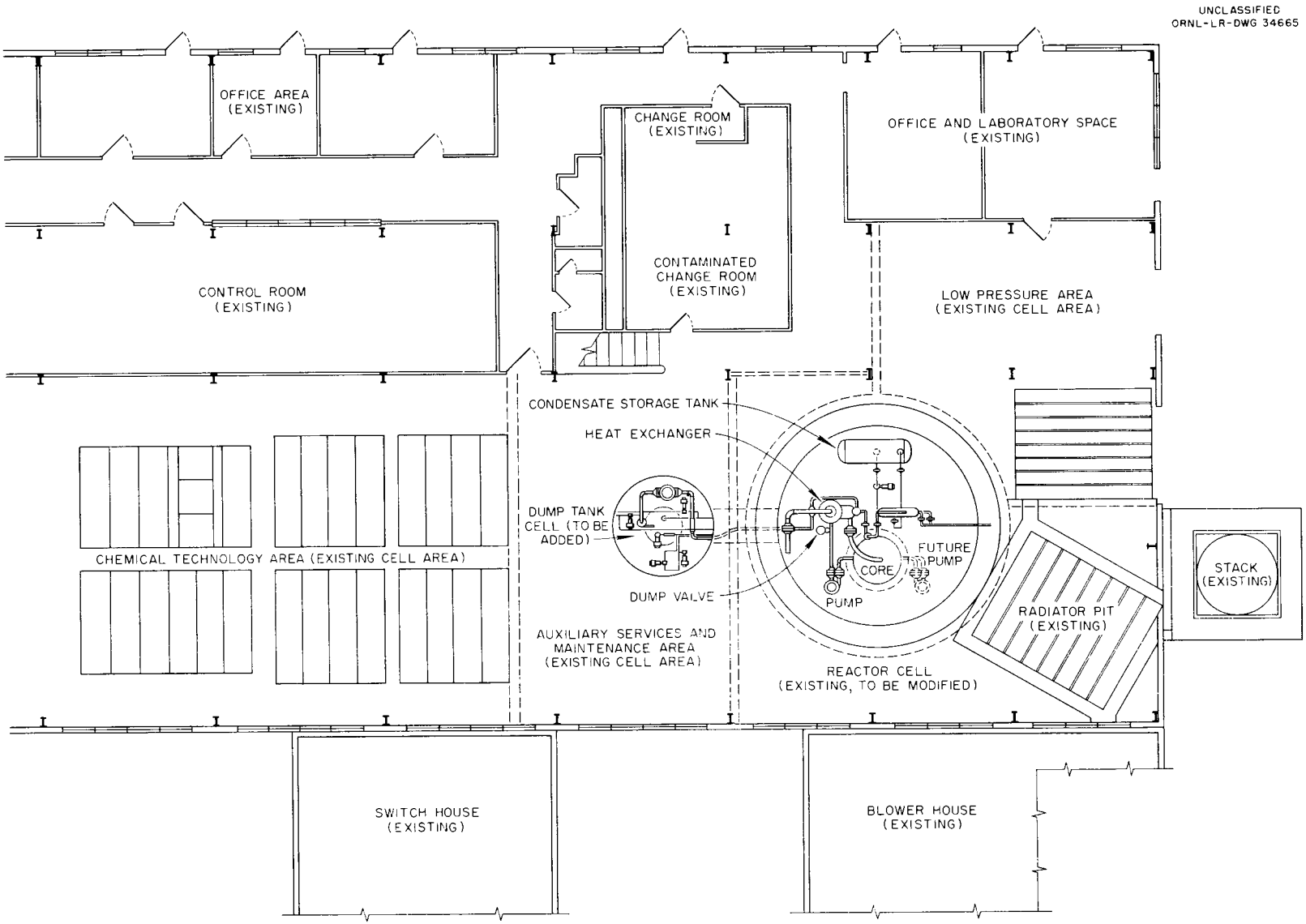

Fig. 8.4. HRE-4 Building and Cell Layout, Plan.

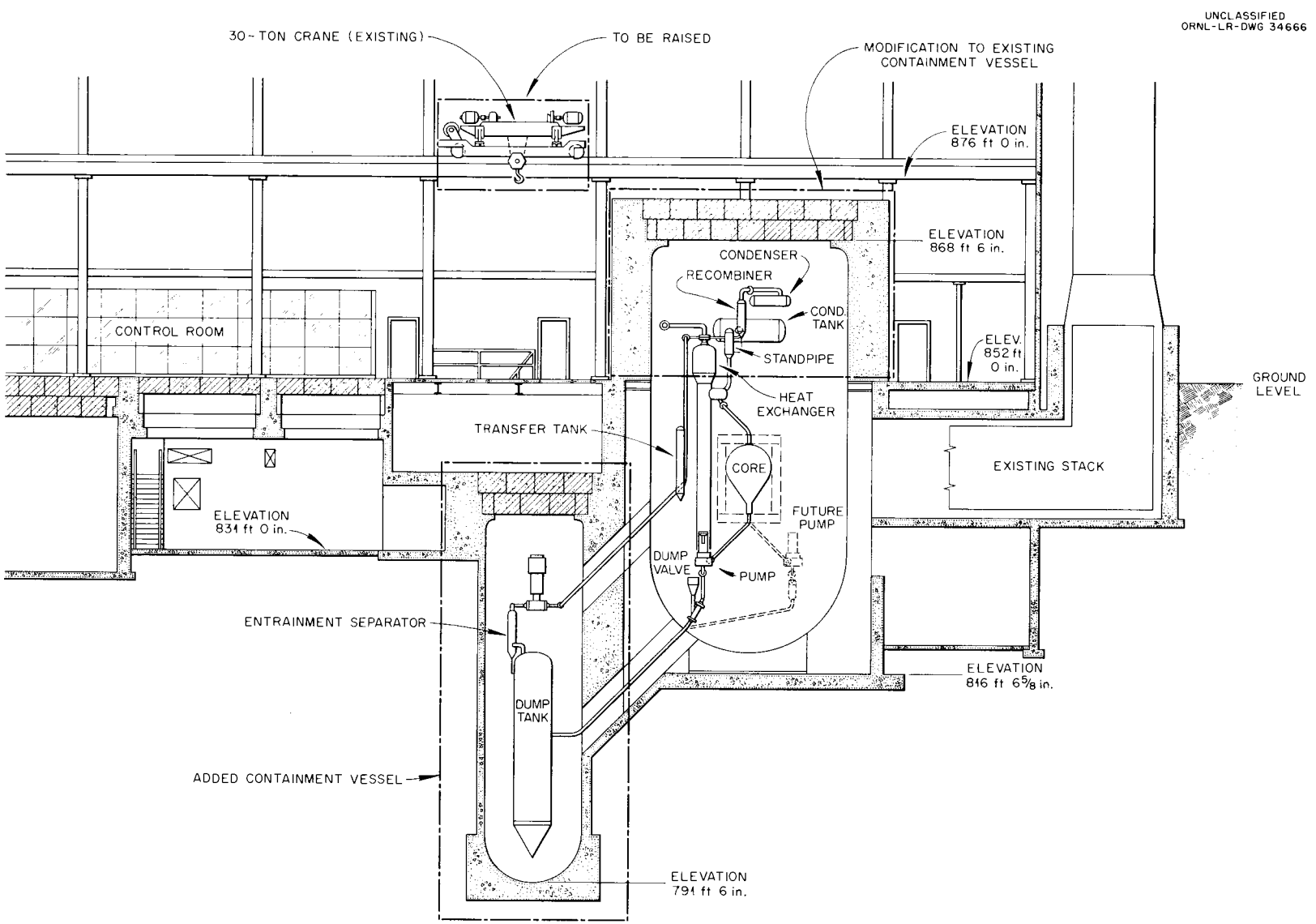

Fig. 8.5. HRE-4 Building and Cell Layout, Elevation.

9. RESEARCH AND ANALYSIS

P. R. Kasten

L. L. Bennett
R. Chalkley
R. D. Cheverton
H. C. Claiborne
T. B. Fowler
S. Jaye
M. P. Lietzke
T. H. Mauney
C. S. Morgan
C. W. Nestor
B. E. Prince
M. W. Rosenthal
D. G. Thomas
M. Tobias

9.1 NUCLEAR CHARACTERISTICS OF SINGLE-REGION SLURRY REACTORS

9.1.1 Criticality Parameters and Reactivity Coefficients

Studies of the nuclear characteristics of single-region slurry reactors were extended to include moderator mixtures of light and heavy water. The analytical method used is discussed elsewhere;[1] neutron ages in mixtures of D_2O and H_2O were obtained from the experiments of Wade.[2] Examination was made of two areas of reactor design parameters:

A. sphere diameters between 4 and 5 ft; temperature, 280°C; D_2O-H_2O mixtures from zero to 99.8% D_2O;
B. sphere diameters less than 3 ft; temperatures less then 200°C; D_2O-H_2O mixtures up to 80% D_2O.

The critical-mass ratios (g of U^{235} per g of Th) determined for part A are presented in Figs. 9.1 and 9.2 for 4- and 4.5-ft-dia reactors, respectively. In part A, a diameter increment of 6 in. (reflector savings of 3 in.) was assumed to account for the presence of the pressure vessel. For example, Fig. 9.1 shows the characteristics of a 4.5-ft-dia bare sphere, or approximately a 4-ft-ID vessel-enclosed reactor.

The principal effect associated with the addition of light water is a reduction in the fast-neutron leakage. Thus reactors of different size can have the same neutron leakage if the moderator compositions are different. Under these circumstances the uranium-to-thorium ratio will be approximately independent of size, and so will the temperature coefficients and neutron lifetimes. For example, near a thorium concentration of 200 g/liter, these parameters will be approximately the same for a 4-ft reactor with 95% D_2O as for a 4.5-ft reactor with 99.8% D_2O.

The results of the calculations for part B are presented in Figs. 9.3 through 9.8. In these cases, the pressure-vessel-diameter savings were assumed to be 4 in. (Because of the thinner pressure-vessel wall associated with smaller-diameter vessels, the reflector savings assumed in part B were less than in part A.) Figures 9.3 and 9.4 give the critical-mass ratios as a function of thorium concentration in 2- and 2.5-ft-dia reactors, respectively. In 1.5-ft-dia reactors, it was found that most of the critical-mass ratios were above 0.10. Figures 9.5 and 9.6 are plots of the critical temperatures in the 2- and 2.5-ft-dia reactors as a function of thorium concentration. Each curve is for a fixed mass ratio of U^{235} to thorium.

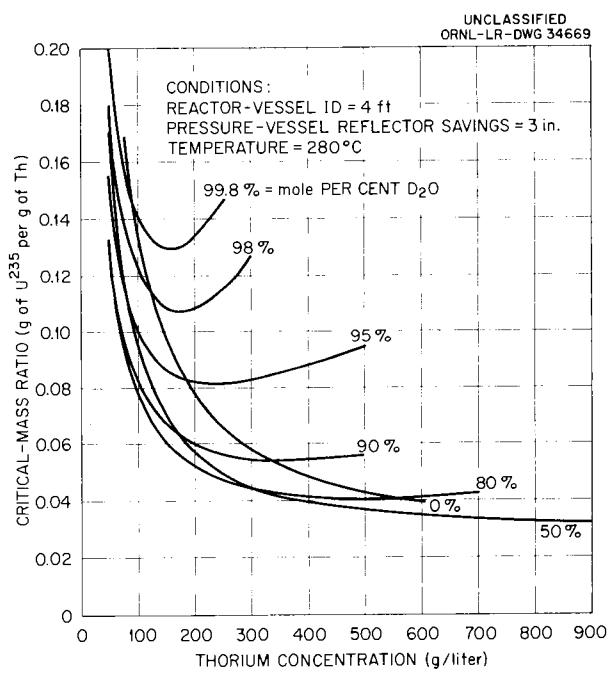

Fig. 9.1. Critical-Mass Ratio vs Thorium Concentration in 4-ft-dia Slurry Reactors with D_2O-H_2O Mixtures.

[1] B. E. Prince and M. W. Rosenthal, *Survey of the Static Nuclear Characteristics of Small, One-Region Slurry Reactors*, ORNL CF-58-7-76 (July 28, 1958).

[2] J. W. Wade, *Nuclear Sci. and Eng.* 4, 12 (1958).

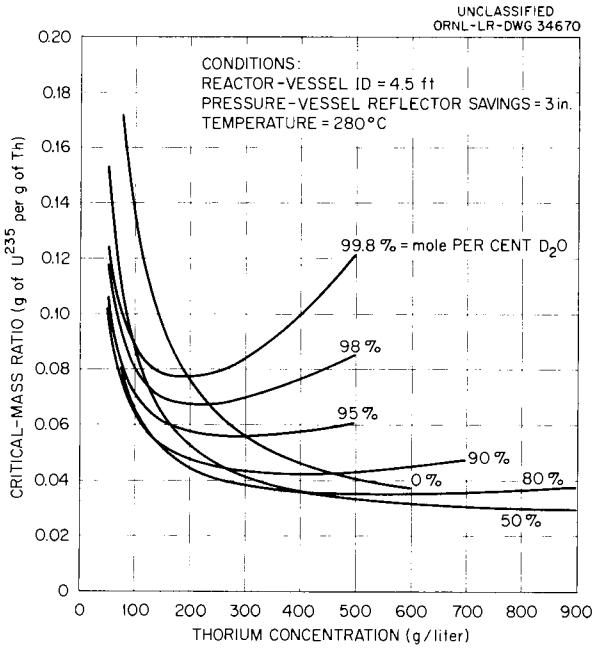

Fig. 9.2. Critical-Mass Ratio vs Thorium Concentration in 4.5-ft-dia Slurry Reactors with D_2O-H_2O Mixtures.

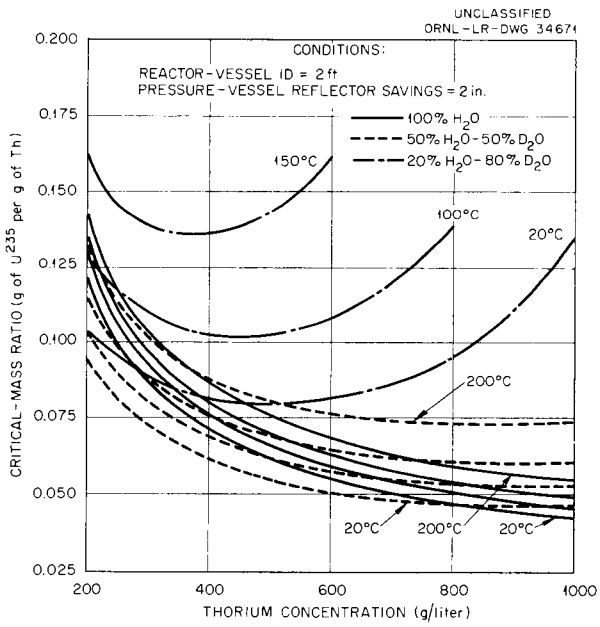

Fig. 9.3. Critical-Mass Ratio vs Thorium Concentration in 2-ft-dia Slurry Reactors.

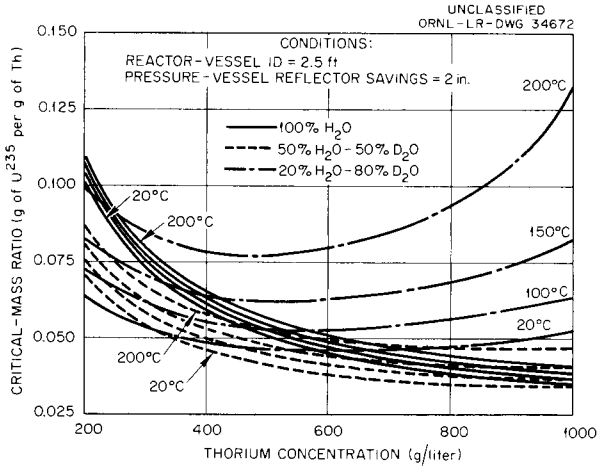

Fig. 9.4. Critical-Mass Ratio vs Thorium Concentration in 2.5-ft-dia Slurry Reactors.

For reactors considered in part B, reactivity coefficients were computed. Tables 9.1 and 9.2 list the values obtained for the temperature and void coefficients of reactivity; the values given are for the extremes of the thorium concentration range studied. The change in reactivity associated with density changes is based on constant fuel-to-moderator ratios. For thorium concentrations between those listed in Tables 9.1 and 9.2, the coefficients decreased nearly linearly with increasing concentration.

An indication of the reactivity added (or removed) when the slurry concentration is changed from the critical condition can be obtained from Figs. 9.7 and 9.8. The concentration coefficient of reactivity applies to uniform, small changes in thorium concentration, at constant temperature and constant ratio of uranium to thorium. As an example, from Fig. 9.4, a 2.5-ft reactor, moderated with a mixture of 80% D_2O and 20% H_2O, is just critical at 200°C with about 400 g of Th per liter and about 0.08 g of U^{235} per g of Th. If a change in concentration is made which is equivalent to a uniform increase of 20 g of Th per liter throughout the reactor, Fig. 9.8 indicates that the reactivity added is:

$$\Delta k_e \cong +(0.14 \times 10^{-3})\,(20) \cong +0.3\% \ .$$

From Table 9.2, the temperature coefficient for the above reactor is about -1.1×10^{-3}/°C. Then, if

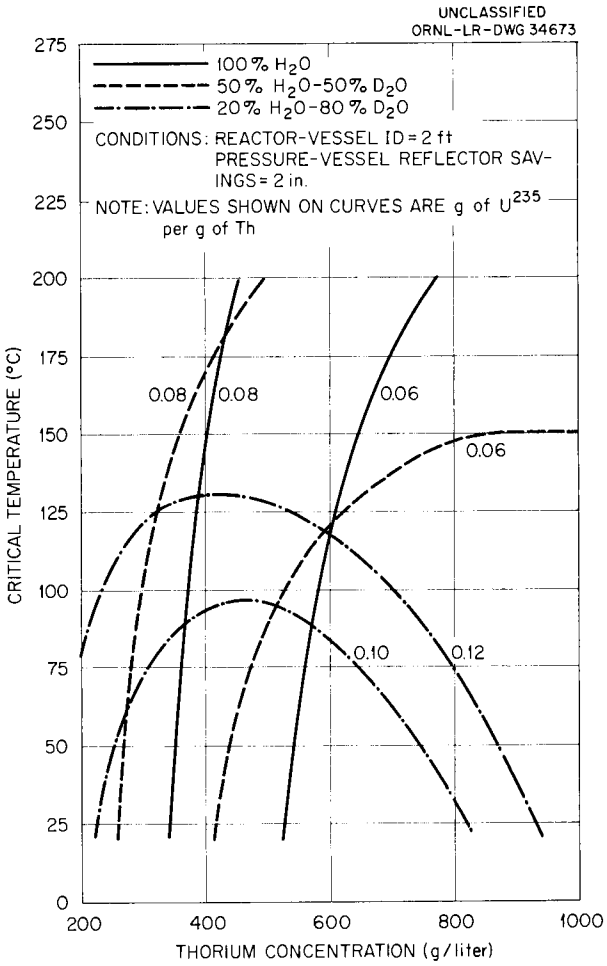

Fig. 9.5. Critical Temperature vs Thorium Concentration in 2-ft-dia Reactors for Various Ratios of U^{235} to Thorium.

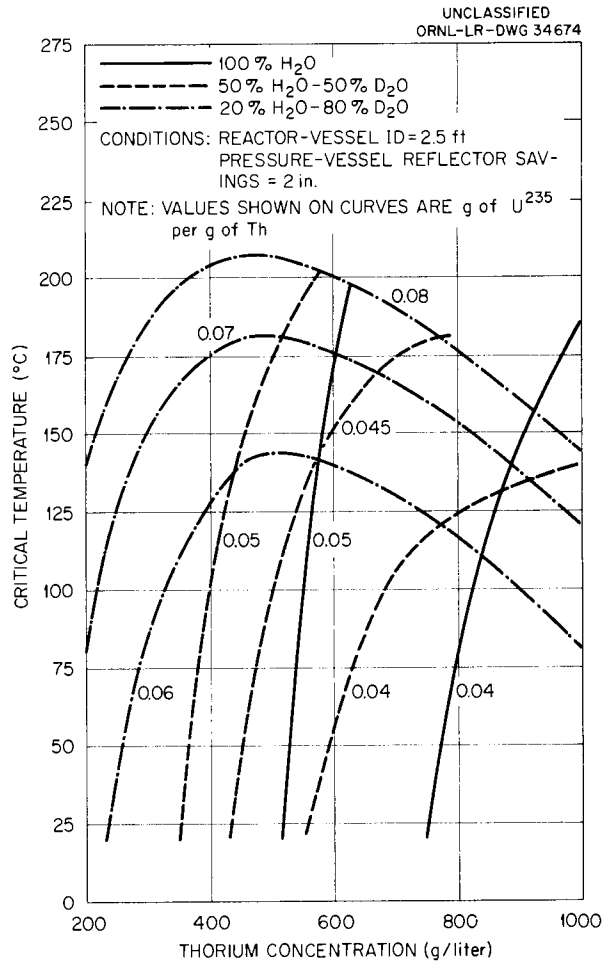

Fig. 9.6. Critical Temperature vs Thorium Concentration in 2.5-ft-dia Reactors for Various Ratios of U^{235} to Thorium.

Table 9.1. Temperature and Uniform-Void Coefficients of Reactivity in a 2-ft-dia Reactor

Temperature (°C)	Mole % H_2O	Temperature Coefficient (Δk_e/°C)		Uniform-Void Coefficient [Δk_e/(void volume/core volume)]	
		200 g of Th per liter	1000 g of Th per liter	200 g of Th per liter	1000 g of Th per liter
		$\times 10^{-3}$	$\times 10^{-3}$		
20	0	−0.21	−0.18	−0.45	−0.43
	50	−0.33	−0.24	−0.58	−0.53
	80	−0.47	−0.25	−0.80	−0.67
200	0	−0.86	−0.79	−0.58	−0.55
	50	−1.44	−0.97	−0.74	−0.67
	80	−1.36		−0.91	

the addition of 0.3% Δk_e were made slowly, the approximate temperature rise would be about 3°C. From Table 9.2, the uniform-void coefficient for this circumstance is about −0.75 Δk_e/(void volume/core volume). The amount of voids which would compensate 0.3% Δk_e would therefore be about 0.4% of the core volume.

Some of the more important characteristics of the reactors studied in part B may be summarized as follows: For moderator mixtures less than 50 mole % D_2O in H_2O, the minimum critical-mass ratio occurred at thorium concentrations greater than about 1000 g/liter. At larger per cents of D_2O, the value of the minimum critical-mass ratio increased,

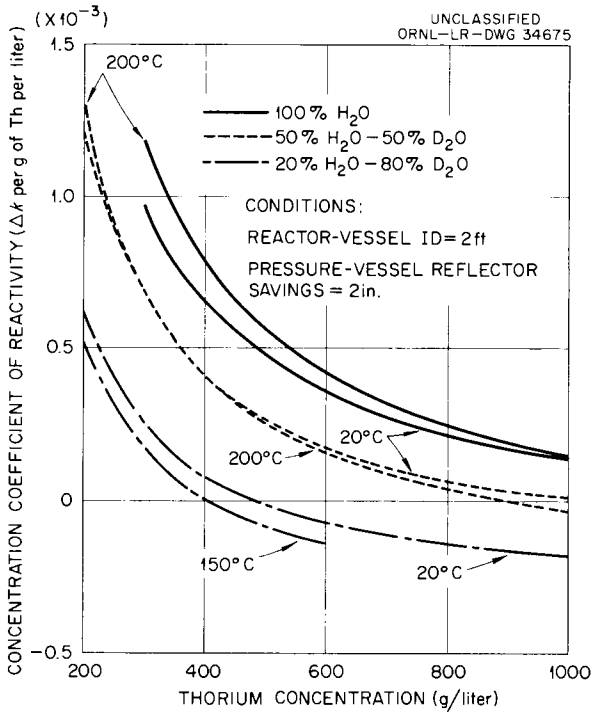

Fig. 9.7. Thorium Concentration Coefficient of Reactivity in 2-ft-dia Reactors at Constant Ratio of U^{235} to Thorium.

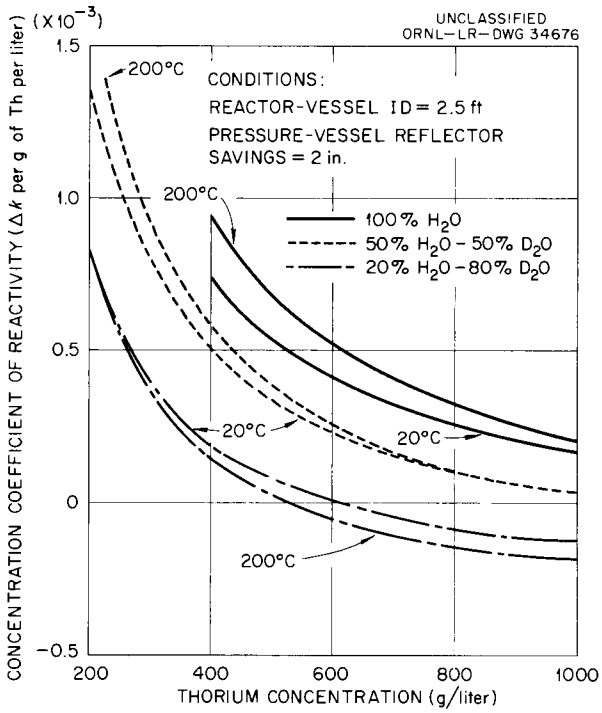

Fig. 9.8. Thorium Concentration Coefficient of Reactivity in 2.5-ft-dia Reactors at Constant Ratio of U^{235} to Thorium.

Table 9.2. Temperature and Uniform-Void Coefficients of Reactivity in a 2.5-ft-dia Reactor

Temperature (°C)	Mole % H_2O	Temperature Coefficient (Δk_e/°C)		Uniform-Void Coefficient [Δk_e/(void volume/core volume)]	
		200 g of Th per liter	1000 g of Th per liter	200 g of Th per liter	1000 g of Th per liter
		$\times 10^{-3}$	$\times 10^{-3}$		
20	0	−0.15	−0.13	−0.33	−0.31
	50	−0.26	−0.18	−0.44	−0.40
	80	−0.43	−0.23	−0.64	−0.53
200	0	−0.65	−0.59	−0.43	−0.41
	50	−0.91	−0.77	−0.58	−0.52
	80	−1.25	−0.88	−0.79	−0.63

and this minimum occurred at smaller thorium concentrations (e.g., 400 to 600 g of Th per liter at 80% D_2O).

9.1.2 Reactivity Changes Associated with Slurry Settling

The change in reactivity, Δk_e, which occurs on settling of ThO_2-$U^{235}O_3$ in a small one-region reactor has been investigated by use of an IBM-704 routine (see Sec. 9.6). In the model used, the core was represented by a "square" cylinder having the same buckling as the sphere size of interest. The settled solids were assumed to be uniformly dispersed in the bottom region of the reactor, with a region of pure moderator in the upper region (note illustration in Fig. 9.9). The inventory of the vessel remained constant.

Calculations were performed for core vessels corresponding to spheres with diameters of 2 and 2½ ft, temperatures of 20, 100, and 200°C, initial slurry concentrations ranging from 100 to 500 g of Th per liter, and moderators (D_2O-H_2O mixtures) containing 25, 50, and 75% D_2O. In all cases the reactor was made critical on the basis of a uniform slurry concentration throughout the entire vessel.

The results obtained for a temperature of 100°C are presented in Figs. 9.9 and 9.10; these are representative of results obtained at other temperatures. As shown, the peak value of reactivity encountered as the slurry settles decreased as the size decreased and as the fraction of D_2O in the moderator increased. Other results showed that the peak value of reactivity encountered decreases with increasing reactor temperature.

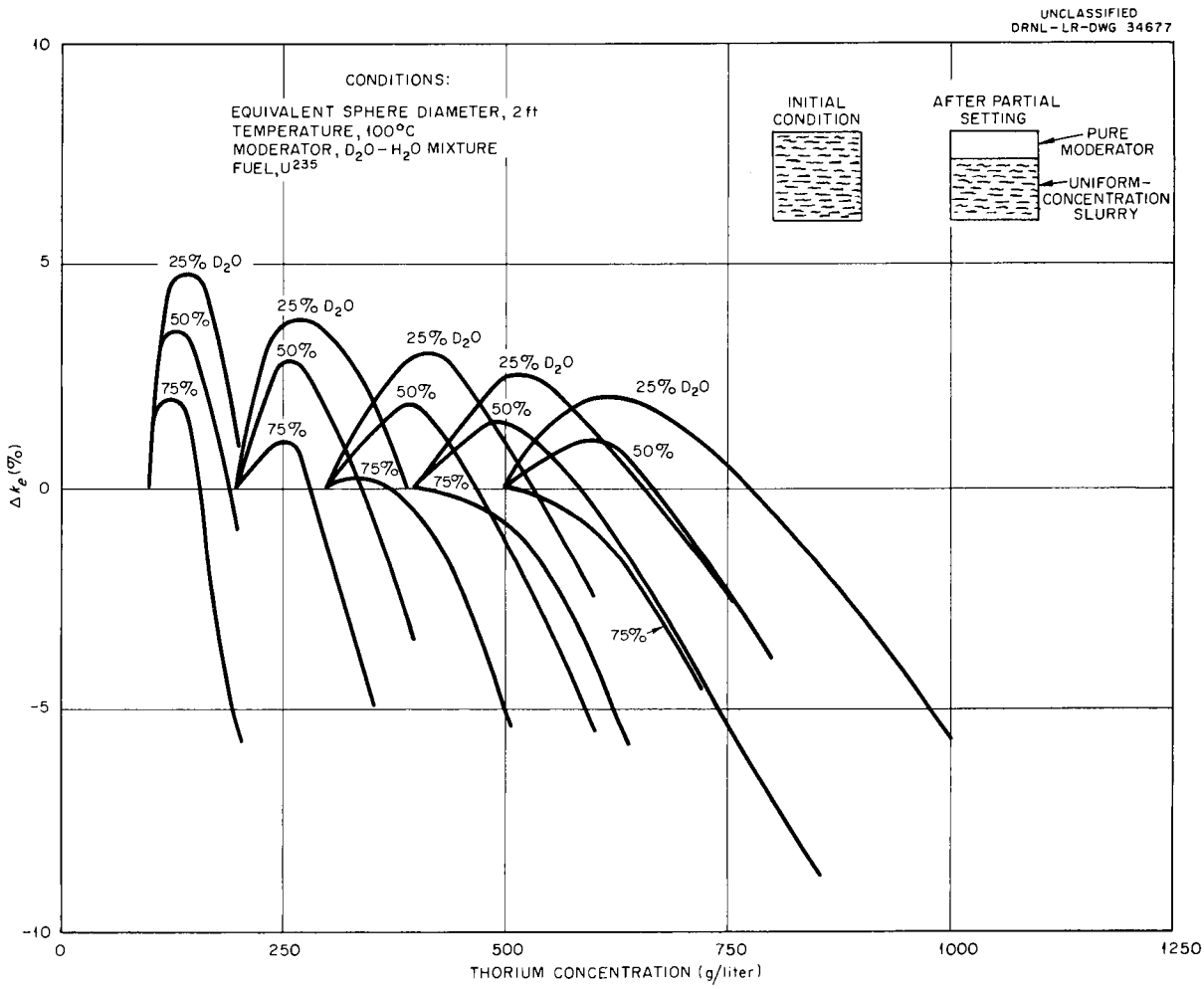

Fig. 9.9. Change in Reactivity on Settling of Slurry in Bare 2-ft-dia Reactors.

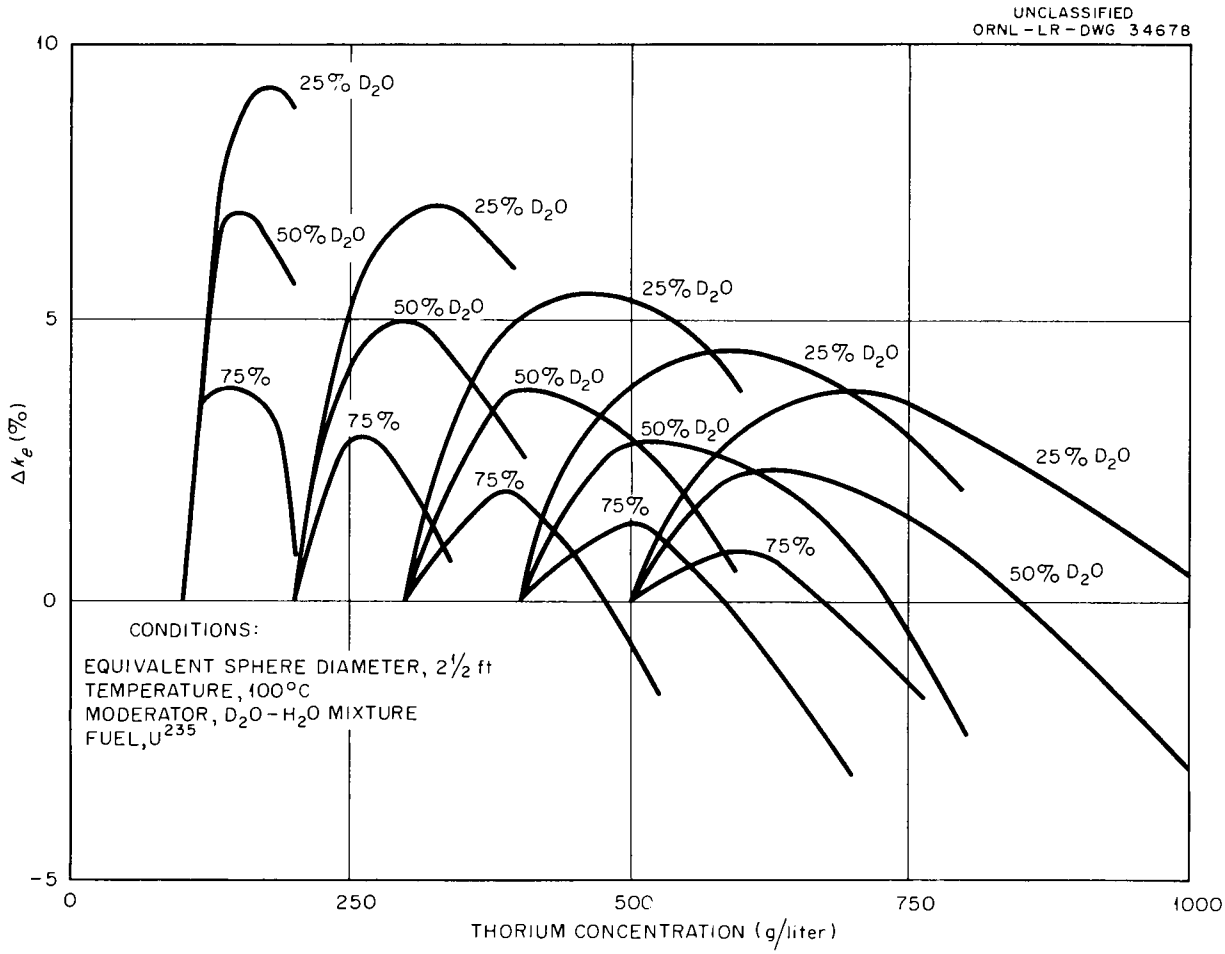

Fig. 9.10. Change in Reactivity on Settling of Slurry in Bare 2.5-ft-dia Reactors.

As settling occurs, there is an increase in neutron resonance captures and in fast-neutron leakage; however, thermal leakage decreases and thermal utilization becomes larger. The first two changes tend to remove reactivity, whereas the last two add reactivity. Increasing the reactor size, decreasing the temperature, and increasing the H_2O concentration all have the effect of decreasing the importance of those terms which remove reactivity and thus lead to the higher reactivity peaks obtained. Making changes in the design and operating conditions which reduce or eliminate the reactivity peaks generally have the effect of increasing the ratio of uranium to thorium required for criticality.

9.2 NUCLEAR CHARACTERISTICS OF REFLECTED SLURRY REACTORS

9.2.1 Critical-Mass Ratios

The ratio of U^{235} to thorium required for criticality has been computed for a number of small slurry cores surrounded by aqueous reflectors. The calculations were performed with a two-group model, by use of a two-region Oracle routine for spherical reactors which allows for absorptions in the core vessel; while useful for survey purposes, the results have the accuracy limitations associated with that model. Cores with diameters of 1, 1½, 2, and 2½ ft were treated; temperatures considered were 20, 100, and

200°C; slurry concentration ranged from 200 to 600 g of Th per liter. The moderators in the core and reflector were mixtures of D_2O and H_2O, and their concentrations were varied from 0 to 99.8% D_2O. The reflector was generally of such thickness that the outside diameter of the reflector region was 5 ft. In some cases, however, the thickness of the reflector was treated as a parameter. The reflector and moderator had the same composition in most cases, but some computations were made with different compositions. All the reactors analyzed had a $^3/_{16}$-in.-thick stainless steel core vessel.

(a) Effect of Moderator Composition. – The effect of moderator and reflector composition on the critical-mass ratio is shown in Fig. 9.11 for various core sizes and thorium concentrations at 200°C. Since H_2O is a good neutron absorber as well as a moderator, its partial replacement with D_2O lowers the critical-mass ratio. However, at high D_2O concentrations the less-effective moderation due to the presence of the D_2O causes the critical-mass ratio to increase with increasing D_2O concentration. With 200 g of Th per liter in 2- and 2½-ft-dia cores, the lowest critical-mass ratio occurred between 60 and 80% D_2O (both at 100 and 200°C); the minima were between 55 and 70% D_2O at 400 g of Th per liter.

(b) Effect of Thorium Concentration. – The change in critical-mass ratio with thorium concentration is illustrated in Figs. 9.12 and 9.13. The minimum critical-mass ratios for these reactors occurred at thorium concentrations above 600 g/liter when the D_2O content was less than 75%. With essentially pure D_2O the minima occurred between 200 and 300 g of Th per liter. As the D_2O concentration is increased from 75 to 99.8%, the shapes of

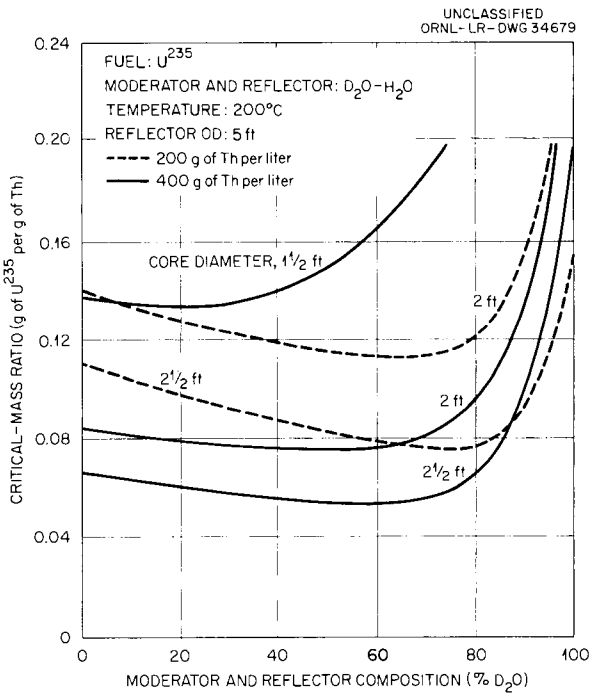

Fig. 9.11. Effect of Moderator and Reflector Composition on Critical-Mass Ratio for Reflected Slurry Reactors.

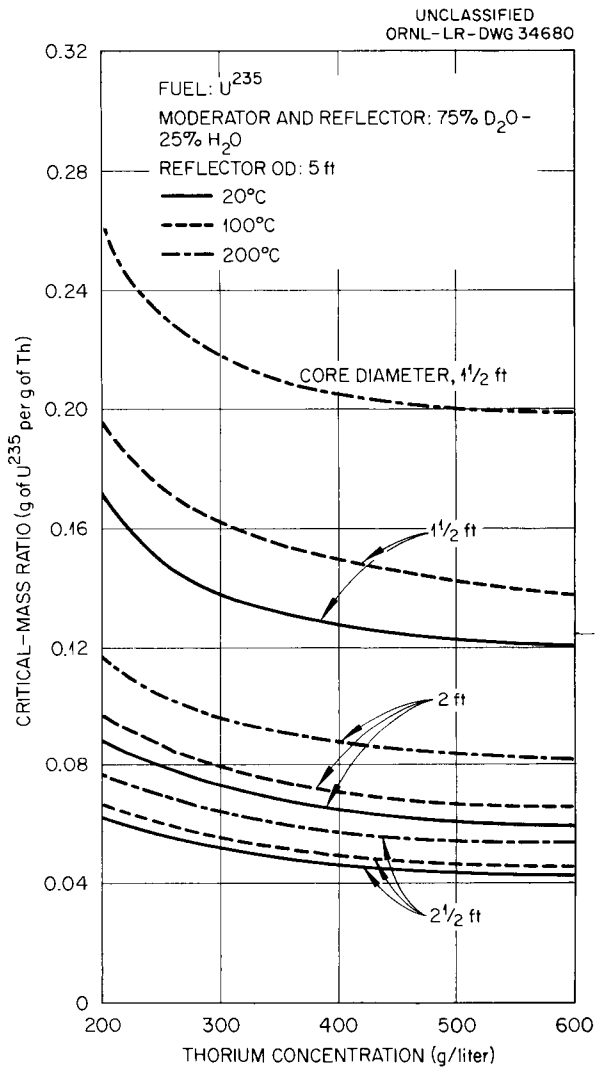

Fig. 9.12. Critical-Mass Ratio vs Thorium Concentration for Reflected Slurry Reactors. Moderator and reflector, 75% D_2O–25% H_2O.

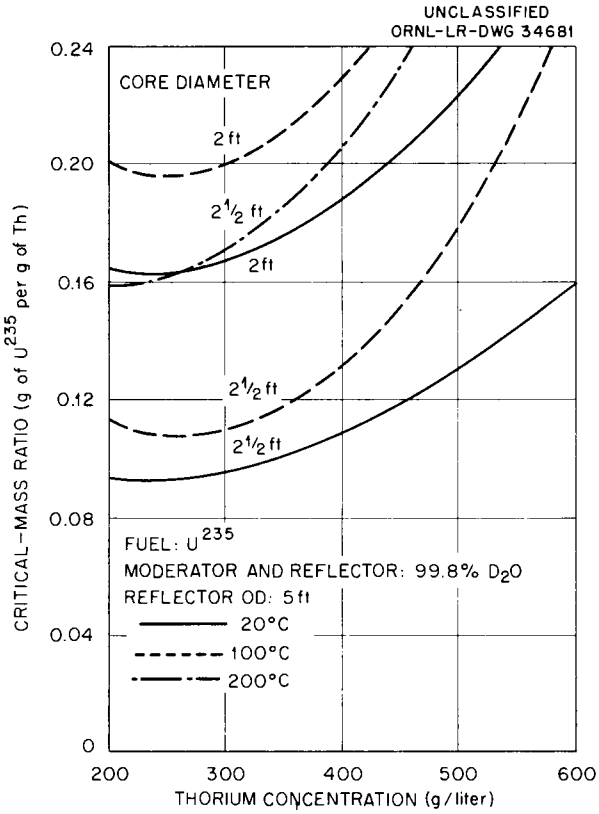

Fig. 9.13. Critical-Mass Ratio vs Thorium Concentration for Reflected Slurry Reactors. Moderator and reflector, 99.8% D_2O.

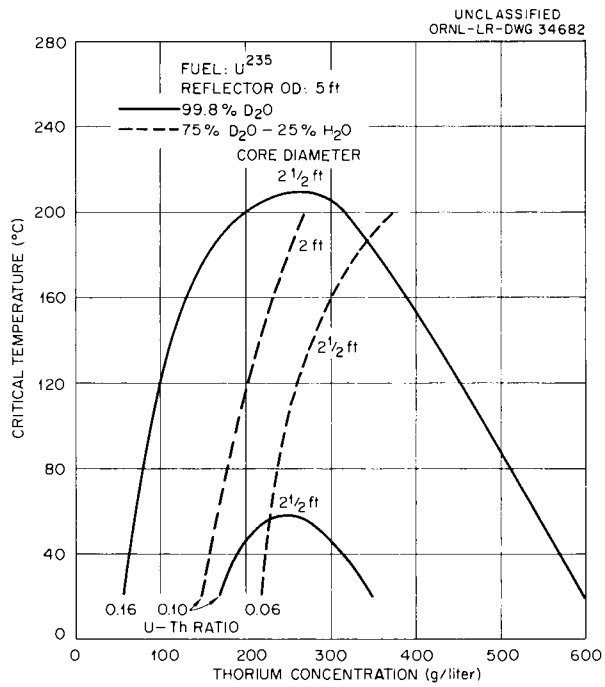

Fig. 9.14. Critical Temperature vs Thorium Concentration for Fixed Ratios of Uranium to Thorium in Reflected Slurry Reactors.

the curves given in Fig. 9.12 shift progressively toward those in Fig. 9.13.

(c) Effect of Core Size. – The critical-mass ratio with 1½-ft-dia cores was generally found to exceed 0.10. Only at 20°C and with thorium concentrations greater than 400 g/liter did this ratio fall below 0.10.

Except when the moderator was about 100% D_2O, almost all the 2½-ft cores had critical-mass ratios below 0.10.

(e) Effect of Temperature. – Reactors having high D_2O concentrations exhibit larger changes in critical-mass ratio with temperature (at a specified thorium concentration) than those with more H_2O. This is another consequence of the H_2O being a poison as well as a moderator. At higher temperatures (corresponding to a reduced moderator density) the lower H_2O absorption cross section partially offsets the increased neutron leakage.

Some examples of the change in critical temperature with thorium concentration for fixed uranium-to-thorium ratios are shown in Fig. 9.14. Reactors of the sizes treated containing 75% or less D_2O required thorium concentrations greater than 600 g/liter before a temperature maximum occurred. The reactors moderated and reflected with pure D_2O exhibited maxima at thorium concentrations around 250 g/liter, but required high uranium-to-thorium ratios for criticality.

(f) Effect of Reflector Thickness. – The change in critical-mass ratio with reflector thickness was investigated for a reflector containing 99.8% D_2O. Two core sizes and two core thorium concentrations were considered; the core moderator was assumed to contain 75% D_2O. The results are shown in Fig. 9.15. The critical-mass ratio increased only slightly as the thickness was reduced from 4 ft to 1 ft; however, with further reduction in thickness the critical-mass ratio began to increase appreciably. The reflector thickness at which the critical-mass ratio would begin to change sharply would be less if the reflector contained H_2O. In these computations there was no allowance for neutron reflection by the pressure vessel.

(g) Effect of Reflector Composition. – The effect of reflector composition on the critical-mass ratio was investigated for 2- and 2½-ft cores with a moderator containing 75% D_2O. The reflectors were

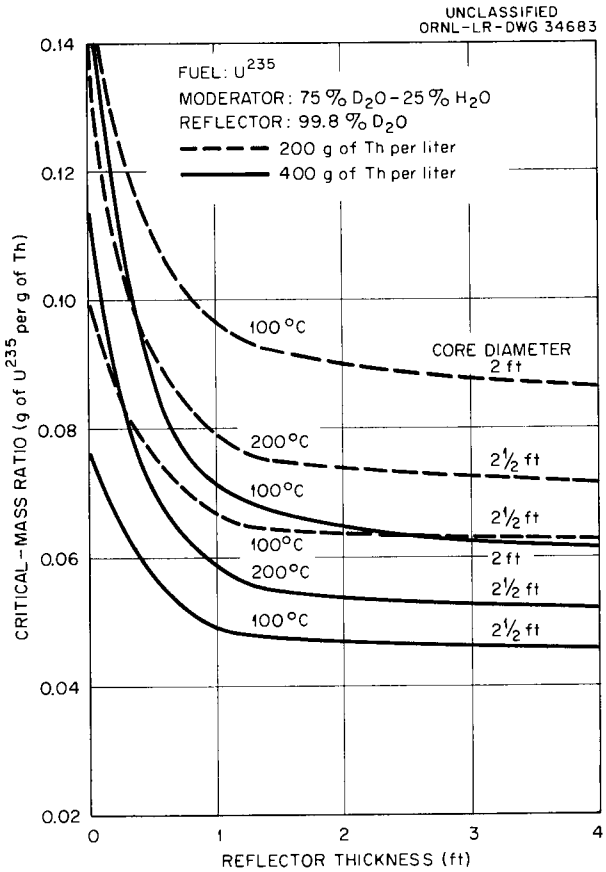

Fig. 9.15. Effect of Reflector Thickness on Critical-Mass Ratio of Reflected Slurry Reactors.

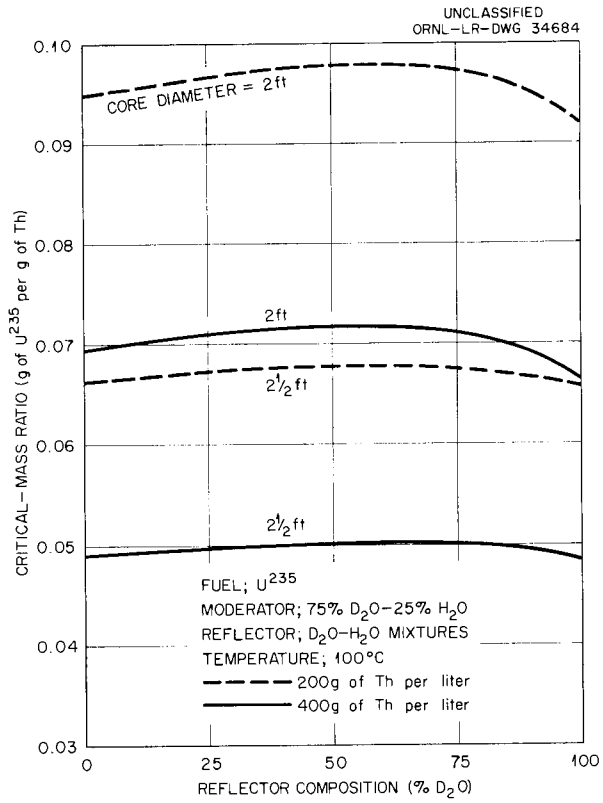

Fig. 9.16. Effect of Reflector Composition on Critical-Mass Ratio of Reflected Slurry Reactors.

$1\frac{1}{2}$-ft thick for the smaller cores and $1\frac{1}{4}$-ft thick for the larger. The results, shown in Fig. 9.16, indicate that for these reactors there is little change in critical-mass ratio with reflector composition ranging from pure D_2O to pure H_2O. There would be a greater effect of composition, however, if the reflectors were relatively thin.

9.2.2 Reactivity Control Associated with Dumping the Reflector

The amount of reactivity which would be removed from an initially critical reactor by discharging the reflector has been estimated by use of WANDA, a two-group multiregion routine for the IBM-704. Spherical cores 2 and $2\frac{1}{2}$ ft in diameter containing either 200 or 400 g of Th per liter were studied. The reflector and the core moderator were water containing 75% D_2O; the temperature of both regions was 100°C; for most cases the core vessel was $\frac{3}{16}$-in.-thick stainless steel. The critical-mass ratio was determined for a reflector thickness of 1 ft. Then, with the same core thorium concentration and the same ratio of uranium to thorium, the effective multiplication factor was computed for various reflector thicknesses. The results are plotted in Fig. 9.17. For the cases studied, about 18% Δk_e would be removed by dumping the reflector of the 2-ft-core reactor, and about 12% Δk_e for the $2\frac{1}{2}$-ft core. For these reactors, there would be almost as much reactivity change associated with dumping a $\frac{1}{2}$-ft-thick reflector as there would be with dumping a 1-ft-thick reflector; the amount of liquid to be dumped would be less than half as much.

In these computations, no allowance has been made for neutron reflection by the pressure vessel. A steel vessel would actually provide some reflection after the liquid was dumped. The effect would be most detrimental to reactivity control of reactors having thin reflectors and thick steel vessels. While this problem has not yet been

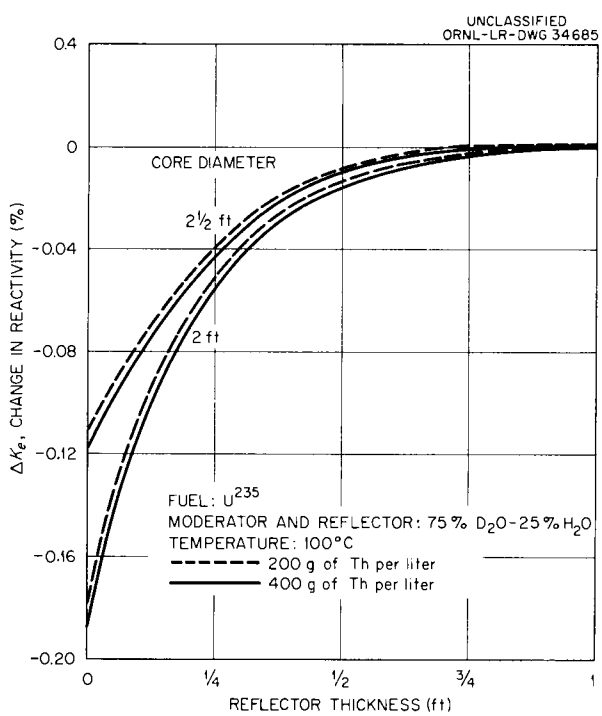

Fig. 9.17. Change in Reactivity with Reflector Thickness.

treated quantitatively, it does not appear to be important for small cores and reasonable reflector thicknesses.

The reduction of reflector effectiveness caused by the presence of a stainless steel core vessel was briefly examined; this was done by computing the Δk_e associated with dumping the reflector with and without the presence of a core tank. One- and two-foot-diameter H_2O cores containing 200 g of Th per liter were treated, and the changes in reactivity on removing a 6-in. reflector were estimated. For the 1-ft core, 33% Δk_e was removed upon reflector dumping with a core vessel of zero thickness, and 22% when there was a ⅜-in.-thick shell. The values were 10% and 7% for the 2-ft-dia cores. Thus in these cases about one-third of the control was lost when the core shell was a relatively thick stainless steel vessel.

9.2.3 Reactivity Changes Associated with Slurry Settling

The changes in multiplication factor which occur on settling of slurry have been estimated for a 2-ft-dia core with a 1-ft-thick reflector. The core moderator and reflector were 75% D_2O–25% H_2O, and the temperature was 100°C. Initial thorium concentrations of 300, 400, and 500 g/liter were treated.

The reactor was represented by a finite cylinder surrounded by a reflector of the same shape, with the initial core size selected to give about the same critical-mass ratio as required for a reflected 2-ft-dia sphere. Settling was assumed to occur in such a manner that the concentration of the slurry region increased *uniformly*, with the core inventory remaining constant (note illustration in Fig. 9.18). Instead of the region of pure moderator (from which the thoria had settled) forming at the top of the core as in the single-region cases (see Sec. 9.1.2), half of this moderator region was assumed to be formed at the top of the core and half at the bottom. Since

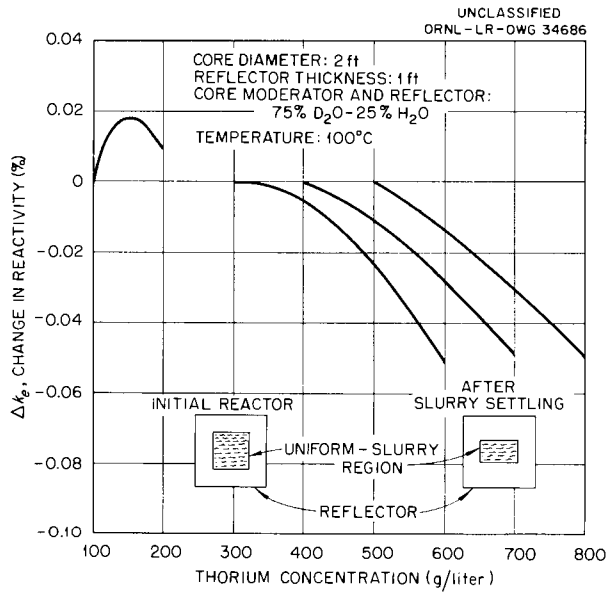

Fig. 9.18. Changes in Reactivity on Uniform Settling of Slurry in Reflected Reactors.

the moderator and reflector were of the same composition, the "settled" reactor could be treated as a symmetrical two-region system. This permitted the computation of the multiplication constant by means of M. L. Nelson's two-group Oracle routine for reflected cylinders. The results of the computations are shown in Fig. 9.18, in which the change in reactivity is plotted versus the thorium concentration of the settled region.

9.3 CRITICALITY CONSIDERATIONS IN THE DESIGN OF SLURRY DUMP TANKS

Conditions were examined under which storage of thoria-water slurries would be "eversafe," assuming

possible addition of light water to the slurry. In this study, the critical thicknesses of infinite slabs and the critical radii of infinitely long cylinders (each with infinite H_2O reflectors) were calculated for slurries with fixed ratios of U^{235} to thorium. Ratios of 0.10 and 0.15 were chosen since these values are reasonable upper limits in reactors of interest.

Figure 9.19 gives the critical thicknesses and diameters as a function of thorium concentration up to 1500 g of Th per liter. The regions below the curves correspond to "eversafe" conditions for the concentrations shown.

The minimum spacings of arrays of control planes and of control rods in an infinite slurry medium were also calculated. In the former case, the planes were considered as thin regions (infinite in their lateral dimensions) which absorb 100% of incident thermal neutrons and transmit all neutrons above thermal energies. Use was made of a two-group diffusion model, with boundary conditions on the neutron currents. The computational results are given in Fig. 9.20, where the critical spacing of the planes is plotted vs thorium concentration; "eversafe" geometry is associated with the region below the appropriate curve.

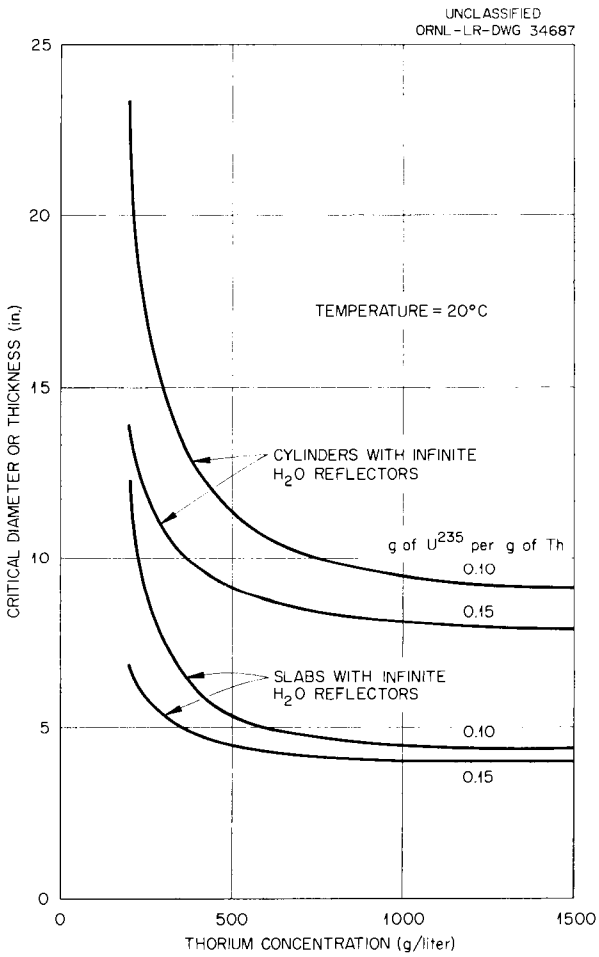

Fig. 9.19. Critical Size of Infinite Cylinders and Slabs of ThO_2-H_2O Slurry with Fixed Uranium-to-Thorium Ratios.

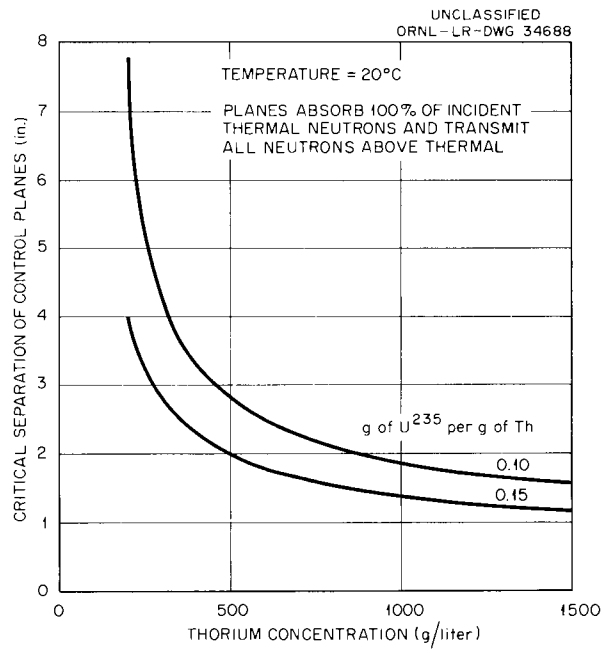

Fig. 9.20. Critical Spacing of an Infinite Array of Control Planes in ThO_2-H_2O Slurries with Fixed Ratios of U^{235}/Th.

The critical condition for a control-rod array in an infinite slurry medium was calculated by use of a cell diffusion model. The effective homogeneous poisoning of a rod was computed in terms of the product of the thermal utilization and thorium resonance escape probability (f_p) in the associated cell. The mathematical model is discussed in reference 3. A program was written for the IBM-704 to evaluate the product f_p as a function of slurry concentration, uranium-to-thorium ratio, rod blackness, and rod diameter and pitch. The value of η^{-1} was taken as the "eversafe" upper limit for f_p in an infinite medium.

[3] P. Greebler, *Nuclear Sci. and Eng.* 3, 445–55 (1958).

Numerical results for the rod-array calculation are presented in Fig. 9.21, where it is assumed that the rods have the neutron absorption characteristics of natural boron. The rod pitch assigned is that of a square array; equivalence of other configurations may be obtained by equating the ratios of slurry volume to control-rod volume, for the same rod diameter.

In all the above calculations, the large reduction in permissible control-rod spacing with increasing thorium concentration (at fixed ratio of fuel to thorium) results from the increased neutron thermal utilization and the reduced diffusion length in the slurry.

The most important characteristics shown in Figs. 9.19 through 9.21 may be summarized as follows:

1. The maximum "eversafe" diameter is about 9 in. for infinite H_2O-reflected cylinders containing ThO_2-H_2O slurries having uranium-to-thorium ratios less than 0.10; approximately 4 in. is the corresponding maximum thickness of an infinite slab with an infinite H_2O reflector.
2. For the same slurry conditions, approximately $1\frac{1}{2}$ in. is the maximum separation of control planes which absorb 100% of incident thermal neutrons and transmit all neutrons above thermal energies.
3. In order for a control-rod array in an infinite light-water-moderated slurry to ensure subcriticality at all thorium concentrations, approximate limitations are as follows: rod pitch (center to center) should be 2.5 in. or less for a 1-in.-dia boron control rod in slurry containing 0.10 g of U^{235} per g of Th; rod pitch should be 3.7 in. or less for a 2-in.-dia boron control rod in slurry containing 0.10 g of U^{235} per g of Th.

The addition of heavy water to the slurry in amounts up to 50% D_2O tends to increase the permissible rod pitch; however, the increase is small.

9.4 STRESS ANALYSIS OF VESSELS FOR SMALL SINGLE-REGION SLURRY REACTORS

The initial concept of the HRE-4 considered bare spherical reactors ranging from 3 to 4.5 ft in diameter and operating at 280°C. In order to evaluate the limitations imposed upon reactor design by stresses in the pressure-vessel wall, an analysis was made[4] to determine what effect reactor conditions would have on heat generation rates in the vessel wall. Two types of vessel construction were considered: (1) carbon-steel base material clad with type 347 stainless steel and (2) type 347 stainless steel with no cladding. The cladding thickness was selected as 0.20 in. Wall thickness was varied from 1 to 3 in. Other parameters considered are listed in Table 9.3.

Table 9.3. Reactor Parameters Considered in Stress Analysis

Inside Diameter of Sphere (ft)	Moderator	Thorium Concentration (g of Th per liter)
3	H_2O	0, 200, 400
$3\frac{1}{2}$	H_2O	0, 200, 400
4	D_2O	0, 200, 400
$4\frac{1}{2}$	D_2O	0, 200, 400

The heat generation rates in the vessel wall were calculated for each reactor considered; from these rates the temperature distribution and maximum thermal stress were obtained. Figure 9.22 gives the maximum stress (pressure plus thermal) as a function of vessel wall thickness; the conditions considered are as follows:

1. average power densities equal,
2. power in $4\frac{1}{2}$-ft-dia reactor = 5 Mw,
3. internal pressure = 2000 psi,
4. maximum stresses are at inside surface of vessel wall,
5. no heat removed from outside surface of pressure vessel,
6. thorium concentration = 0.

Reducing the vessel diameter reduced the stresses; this reduction in stress is due primarily to a reduction in heat generation within the wall, even though the average power density is the same in each case.

[4] R. D. Cheverton, *Preliminary Report on Heat Generation and Stresses in Wall of Spherical HRE-4 Pressure Vessel*, ORNL CF-58-11-1 (to be published).

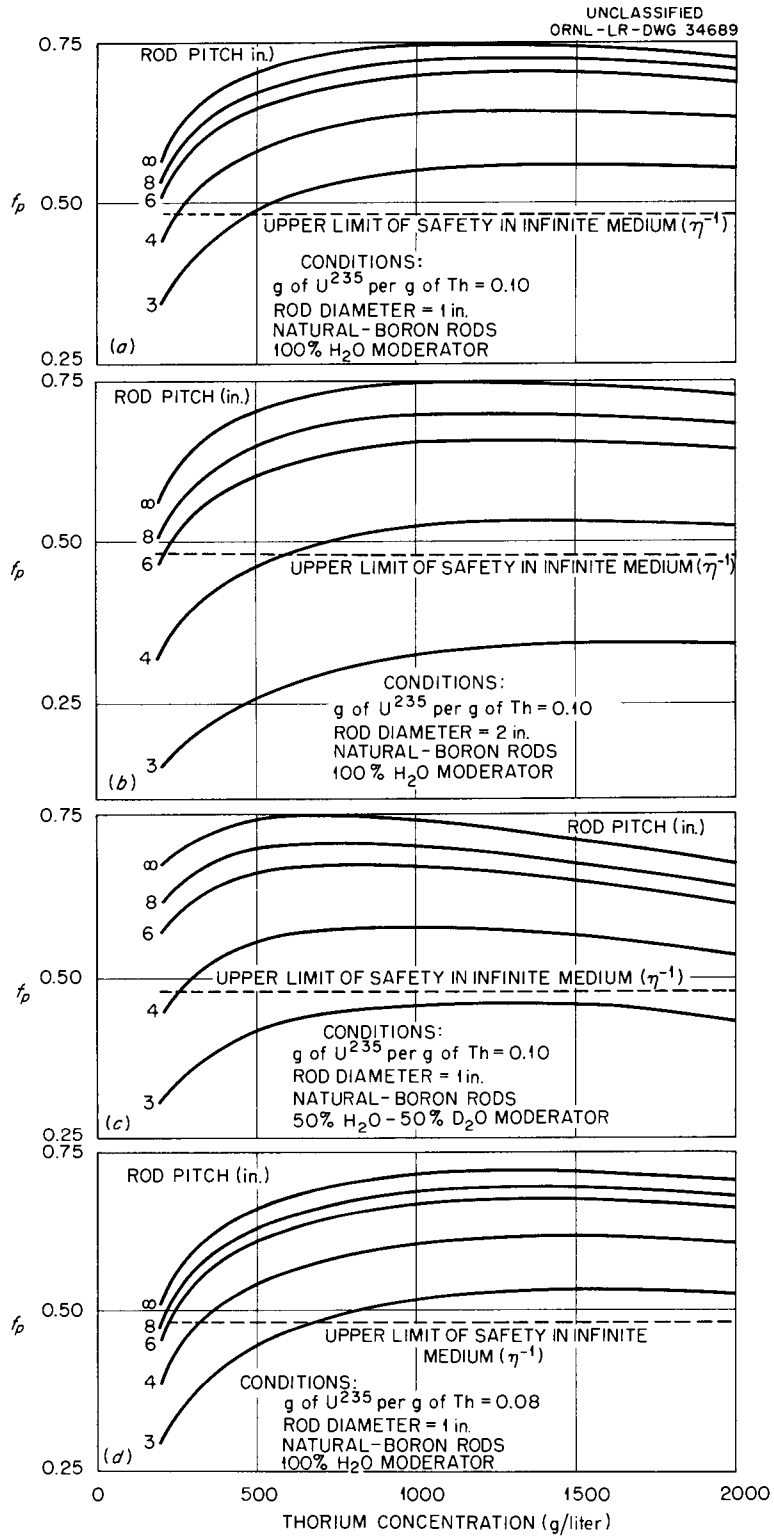

Fig. 9.21. Product of Thermal Utilization and Thorium Resonance Escape Probability in an Infinite Array of Cylindrical Control Rods, Surrounded by ThO_2-H_2O-D_2O Slurry.

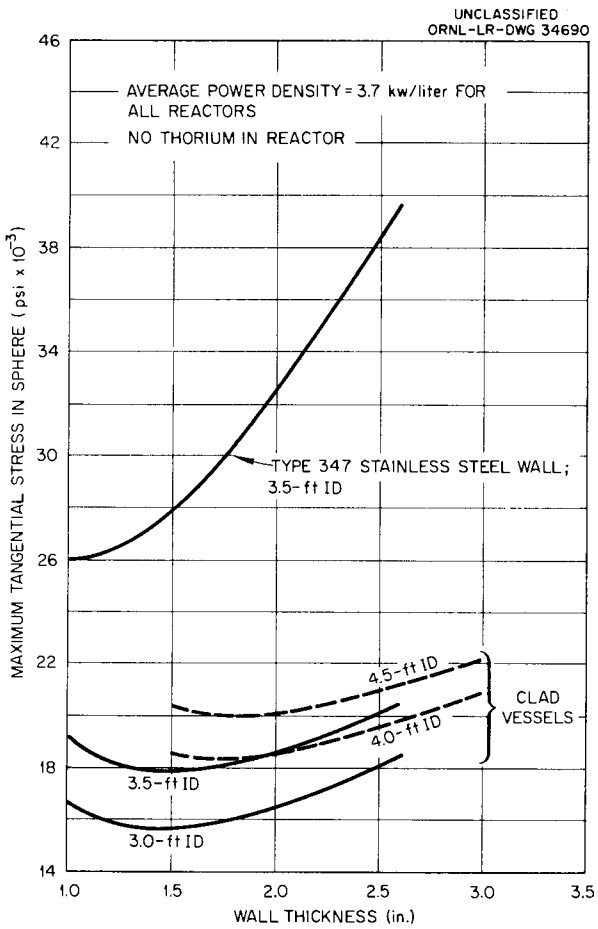

Fig. 9.22. Sum of Pressure Plus Thermal Stresses vs Wall Thickness for Spherical Vessels.

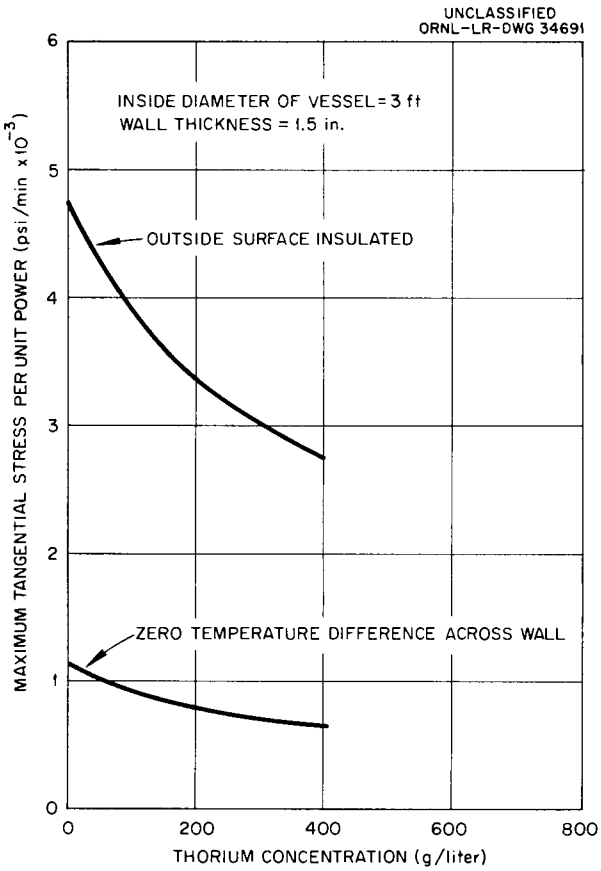

Fig. 9.23. Maximum Thermal Stress vs Thorium Concentration in Clad Spherical Vessel.

The thermal stresses in a stainless steel vessel are about three times those in a nonclad carbon-steel vessel; this is also nearly true for a clad vessel if the tangential stress at the inside surface of the stainless steel vessel is compared with the tangential stress in the carbon-steel base material at the clad-base interface. This latter stress was less than that in the cladding for the cases considered.

Increasing the thorium slurry concentration decreased the heat generation and the thermal stresses in the vessel wall. A further reduction in stresses can be obtained by reducing the temperature drop across the wall, minimum stresses being obtained when the temperatures on the inner and outer wall surfaces are nearly equal. These effects are illustrated in Fig. 9.23, which shows the effect of thorium concentration on thermal stress when the outside wall of the pressure vessel is either insulated or kept at the same temperature as that of the inside surface.

If the reactor is not truly spherical but has a conical region intersecting a spherical region, the wall thickness at the intersection of these regions must be about twice that associated with a spherical reactor. For this situation the thermal stresses will be greater than those in a simple sphere.

9.5 AGE OF FISSION NEUTRONS IN D_2O-H_2O MIXTURES

By use of the Nordheim-Cashwell relation[5] which correlates detector activity by an age-diffusion model, the values obtained by Wade[6] for ages in

[5] E. D. Cashwell, CP-2601, p 39 (April 4, 1945) (classified).

[6] J. W. Wade, *Neutron Ages in Mixtures of Light and Heavy Water*, DP-163 (June 1956); *Nuclear Sci. and Eng.* 4, 12 (1958).

mixtures of light and heavy water have been broken up into Gaussian and diffusion ages. The results are given in Table 9.4.

The age-diffusion correlation fits Wade's data surprisingly well over a wide range of mixtures as shown in Fig. 9.24 for the 99.8, 48.6, and 0 mole % D_2O cases. The results are useful in reactor calculation procedures such as the harmonics method, where an arbitrary slowing-down kernel may be used.

Table 9.4. Ages to Indium Resonance of Mixtures of Light and Heavy Water Broken Up into Gaussian and Diffusion Ages

% D_2O	Diffusion Age (cm^2)	Gaussian Age (cm^2)	Total Age (cm^2)
99.8	57.2	51.8	109
99.0	57.6	49.4	107
98.4	64.4	41.6	106
95.3	55.0	38.0	93
94.0	47.6	38.4	86
91.8	37.4	40.6	78
48.6	28.9	9.7	39
0	26.5	4.5	31

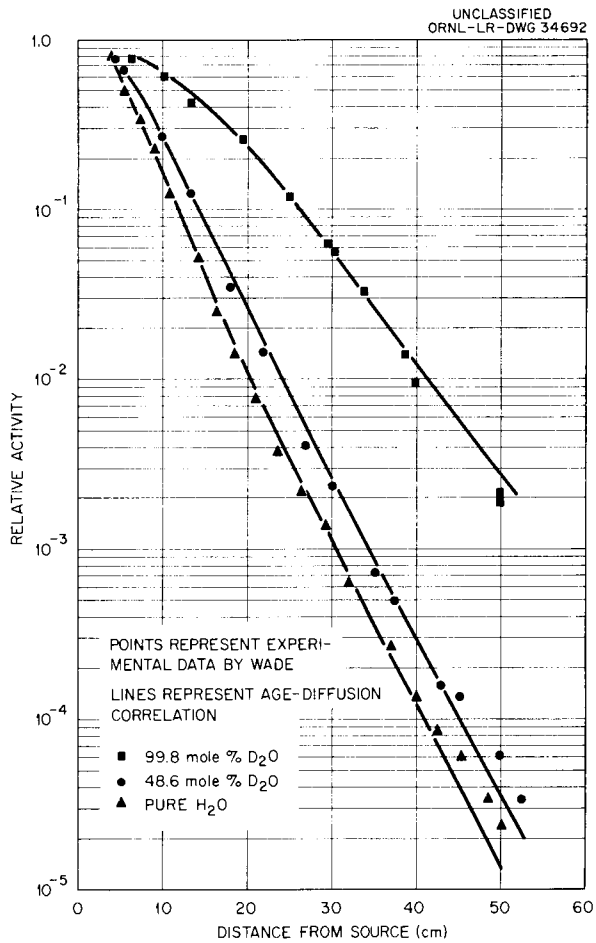

Fig. 9.24. Indium Foil Activity vs Distance from Source in D_2O-H_2O Mixtures as Correlated by Use of an Age-Diffusion Model.

9.6 MACHINE PROGRAMMING

A machine code for the IBM-704 has been written for calculation of reactivity additions associated with slurry settling in a one-region aqueous-slurry reactor. A two-group model is employed in which account is taken of resonance capture and fission in the fuel material, in addition to resonance capture in the fertile material. Initially the critical fuel concentration is calculated for the full, unsettled bare reactor; subsequently the effective multiplication constant is computed for specified heights of the settled region, assuming that the settled material is uniformly distributed in the lower region and that the upper region consists of pure moderator. The mass of fuel and fertile material in the reactor is assumed to be constant.

The harmonics method[7] for calculating the critical fuel concentration in a spherical reactor has as its critical condition the vanishing of a certain infinite-order determinant. This infinite-order-determinant condition has been approximated by requiring the vanishing of certain lower-order subdeterminants located in the upper-left portion of the infinite array. Because of computational difficulty the finite-order subdeterminants considered previously have usually been of the second degree. A program has now been written for the IBM-704 in which the approximating determinant is of the seventh order. The program essentially computes the fuel concentration that would fulfill the second-order determinant condition and then uses this result as a first guess in the iterative solution of the third-degree determinant equation. This procedure is followed for subsequent odd-order determinants.

[7] M. C. Edlund and P. M. Wood, *Physics of the Homogeneous Reactor Test – Statics*, ORNL-1780 (Aug. 27, 1954).

A program has been written for the IBM-704 which calculates thermal disadvantage factors for a lattice of control rods in an infinite fuel region; parameters considered are rod diameter, rod spacing, and rod blackness. Also, a program has been written for single-region reactors which calculates the reactivity-time relation required to produce a known power-time relation. The program is given a series of times and associated powers from which it computes the series of straight-line segments which approximate the power curve. This relation is then used to calculate the associated reactivity. A bare-reactor survey calculation has been programmed for the IBM-704 in which resonance fissions are considered; effective resonance integrals are assumed to be a function of fuel concentration. In addition to critical fuel concentration, reactivity coefficients and conversion ratios are also obtained. This is a permutating-type program which will consider all possible combinations of a set of input parameters.

9.7 NUCLEAR CONSTANTS

Two-group nuclear constants have been prepared for mixtures of light and heavy water and for light water–heavy water–thorium oxide slurries; temperatures considered were 20, 100, and 200°C; the mole fraction of D_2O was assumed to be 0, 0.25, 0.50, 0.75, and 1.0; thorium concentration was varied from 0 to 1200 g/liter. These constants are calculated on the basis of the following correlations:

1. diffusion coefficients,

$$D_i(G) = \frac{D_i(0)}{1 + A_i G} \quad \begin{cases} i = 1 \text{ for fast group} \\ i = 2 \text{ for slow group} \end{cases}$$

2. fertile-material absorption cross section,

$$\Sigma_{02}(G) = S_{02} G \ ,$$

3. effective moderator absorption cross section,

$$\Sigma_M(G) = \Sigma_M(0)\ (1 - S_M G) \ ,$$

4. Fermi age,

$$\tau_M(G) = \tau_M(0)\ (1 + a_1 G + A_2 G^2) \ ,$$

5. resonance escape probabilities for fertile material,

$$p_{02} = \frac{1 + c_1 G}{1 + c_2 G + c_3 G^2} \ ,$$

and for fuel material,

$$p_F = \exp \frac{-A_F G_F}{1 - B_M G} \ ,$$

where

$a_1, a_2, A_F, A_i, B_M, c_1, c_2, c_3, S_M, S_{02}$ are dimensional constants given in Table 9.5;

$D_i(0)$ is the diffusion coefficient for ith group, based on zero thorium concentration;

G is the concentration of fertile material, g/liter;

G_F is the concentration of fuel material, g/liter;

$\Sigma_M(0)$ is the macroscopic absorption cross section of pure moderator;

$\tau_M(0)$ is the Fermi age of pure moderator.

Constants for the first three correlations are derivable from the densities and cross sections of the materials involved; constants for the last two were obtained from data from other calculations.[8,9]

Table 9.5 lists the parameter values to be used in the above correlations for several temperatures.

9.8 FLOW PROPERTIES OF THORIA-WATER SLURRIES

9.8.1 Friction-Factor Measurements

Pressure-drop flow data for some non-Newtonian thoria-water slurries have been interpreted in terms of a Fanning friction factor and a Reynolds number. For a given slurry, friction factors calculated from nonlaminar-flow data obtained with tubes 0.124, 0.318, and 1.030 in. in inside diameter were a single-valued function of the Reynolds number, provided that the coefficient of viscosity was replaced by the coefficient of rigidity. Laminar-flow data obtained with the 0.318- and 1.030-in.-ID tubes gave friction factors which agreed with those predicted on the basis of the associated Hedstrom and Reynolds numbers, with the 0.124-in.-tube data being used as a norm.

Plots of friction factor vs Reynolds numbers indicated two distinctive types of behavior in the laminar-nonlaminar transition region. For some slurries the flow data gave friction factors in the

[8] T. B. Fowler and M. Tobias, *Two-Group Constants for Aqueous Homogeneous Reactor Calculations*, ORNL CF-58-1-79 (Jan. 22, 1958).

[9] L. Dresner, *The Effective Resonance Integrals of U^{238} and Th^{232}*, ORNL CF-55-9-73 (Oct. 5, 1955).

Table 9.5. Typical Nuclear Constants for ThO_2-U^{235}-H_2O Slurries

	Temperature (°C)		
	20	100	200
	Thoria-Water Slurry		
$D_1(0)$, cm	0.586	0.609	0.673
$D_2(0)$, cm	0.160	0.177	0.218
$\Sigma_M(0)$, cm^{-1}	0.0196	0.0167	0.0133
$\tau_M(0)$, cm^2	33.0	35.6	43.6
S_M, liter/g	1.17×10^{-4}	1.17×10^{-4}	1.17×10^{-4}
S_{02}, liter/g-cm	1.74×10^{-5}	1.55×10^{-5}	1.37×10^{-5}
A_1, liter/g	-2.71×10^{-5}	-2.35×10^{-5}	-1.45×10^{-5}
A_2, liter/g	-8.38×10^{-5}	-7.60×10^{-5}	-7.92×10^{-5}
a_1, liter/g	0	4.21×10^{-6}	0
a_2, liter/g	9.09×10^{-7}	2.39×10^{-7}	6.88×10^{-7}
c_1, liter/g	0	0	0
c_2, liter/g	1.16×10^{-4}	1.30×10^{-4}	1.46×10^{-4}
c_3, liter/g	-2.67×10^{-8}	-3.67×10^{-8}	-4.51×10^{-8}
	U^{235} Fuel		
A_F, liter/g	-6.05×10^{-4}	-6.28×10^{-4}	-6.95×10^{-4}
B_M, liter/g	1.15×10^{-4}	1.15×10^{-4}	1.15×10^{-4}
Z,* g-cm/liter	655	757	869

*Conversion factor to convert fuel-macroscopic absorption cross section (cm^{-1}) to fuel concentration (g/liter).

transition region which did not drop below those for nonlaminar flow; for other slurries, however, the associated friction factors were significantly below nonlaminar-flow friction factors. For any particular slurry, when this "dip" was obtained from data for one tube, it was also obtained from data for the other tubes; this same correspondence was obtained when the slurry used produced data which, when plotted, gave no "dip."

Figures 9.25 and 9.26 give typical pseudo-shear diagrams obtained with the various tube diameters; they illustrate the close agreement among the data obtained with the three different tubes in the laminar-flow region. Figure 9.25 also indicates that at high shear rates the laminar-flow shear diagram for slurries approaches that for water.

Figures 9.27 and 9.28 illustrate the flow behavior in the transition region in terms of the Fanning friction factor, Reynolds number (based on coefficient of rigidity), and Hedstrom number. The laminar-flow data obtained with the ⅛-in.-dia tube were used as a basis to normalize the data obtained with the other tubes; the resulting calculated curves using the Hedstrom criteria corresponded with the appropriate experimental data. Also, the good agreement among the data taken with the ⅛- to 1-in.-dia

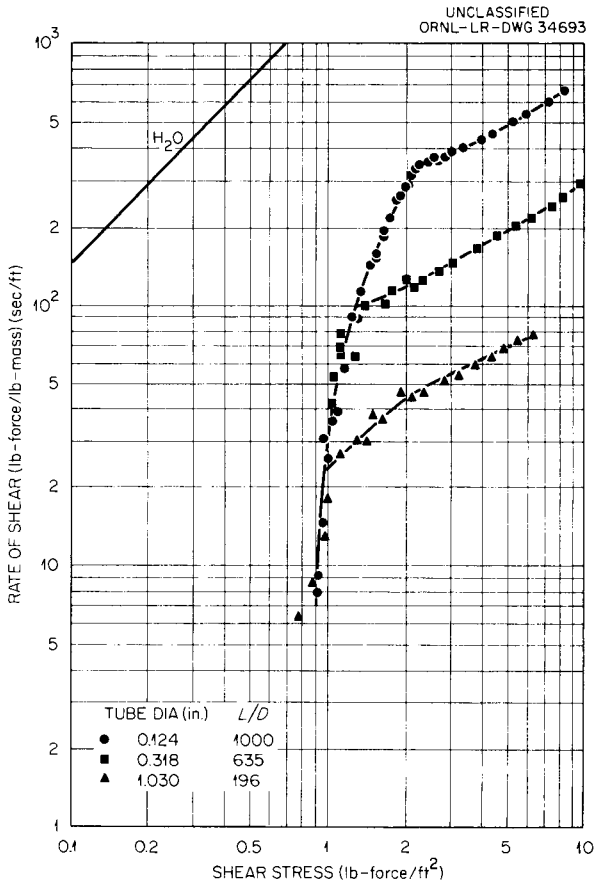

Fig. 9.25. Pseudo-Shear Diagrams for Thoria-Water Slurry Having a Density of 1.90 g/ml, a Coefficient of Rigidity of 5.70 Centipoises, and a Yield Stress of 0.69 lb-force/ft^2.

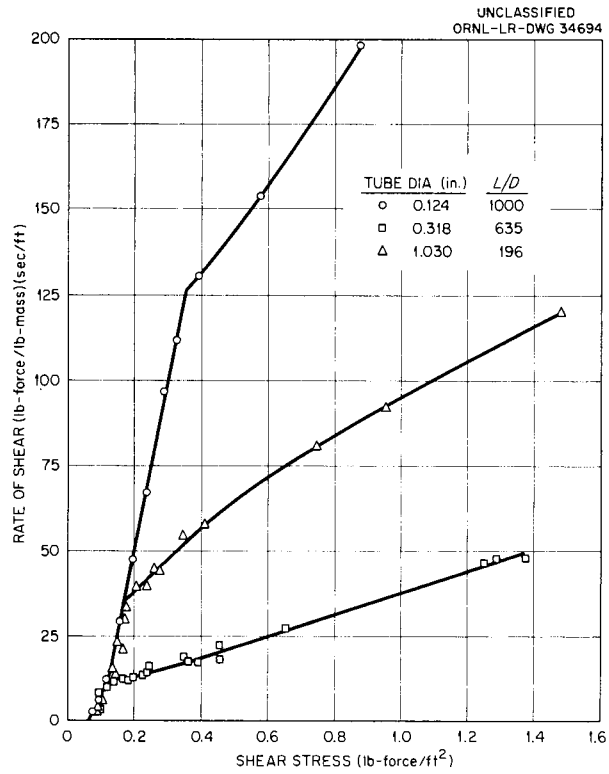

Fig. 9.26. Pseudo-Shear Diagrams for Thoria-Water Slurry Having a Density of 1.67 g/ml, a Coefficient of Rigidity of 2.9 Centipoises, and a Yield Stress of 0.075 lb-force/ft^2.

tubes suggests that nonlaminar friction-factor data obtained using a single tube diameter can be applied to a variety of tube diameters.

In general, it appears that nonlaminar flow data for slurries can be correlated[8] by a Blasius-type relation, namely

$$f = B(N_{Re})^{-b} \quad , \tag{1}$$

where f is the friction factor, N_{Re} is the Reynolds number (based on coefficient of rigidity), and B and b are parameters. The values required of b and B for the various slurries studied are given in Table 9.6. However, the experimental data indicate that neither the coefficient B nor the exponent b are simple functions either of the coefficient of rigidity or of the yield stress. This is illustrated

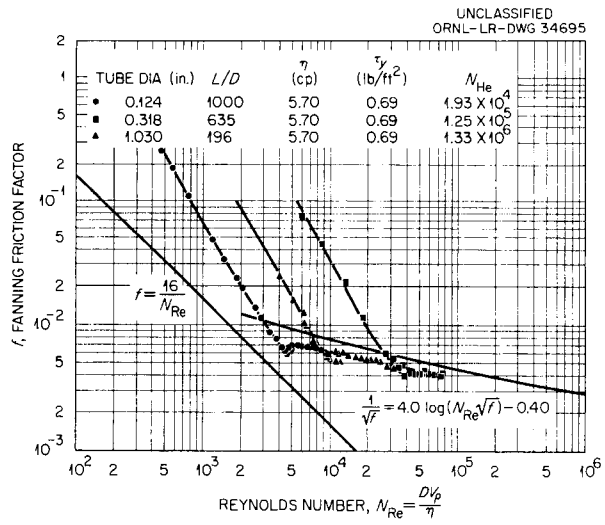

Fig. 9.27. Friction-Factor–Reynolds-Number Plot for Aqueous Thoria Slurries Having a Density of 1.90 g/ml.

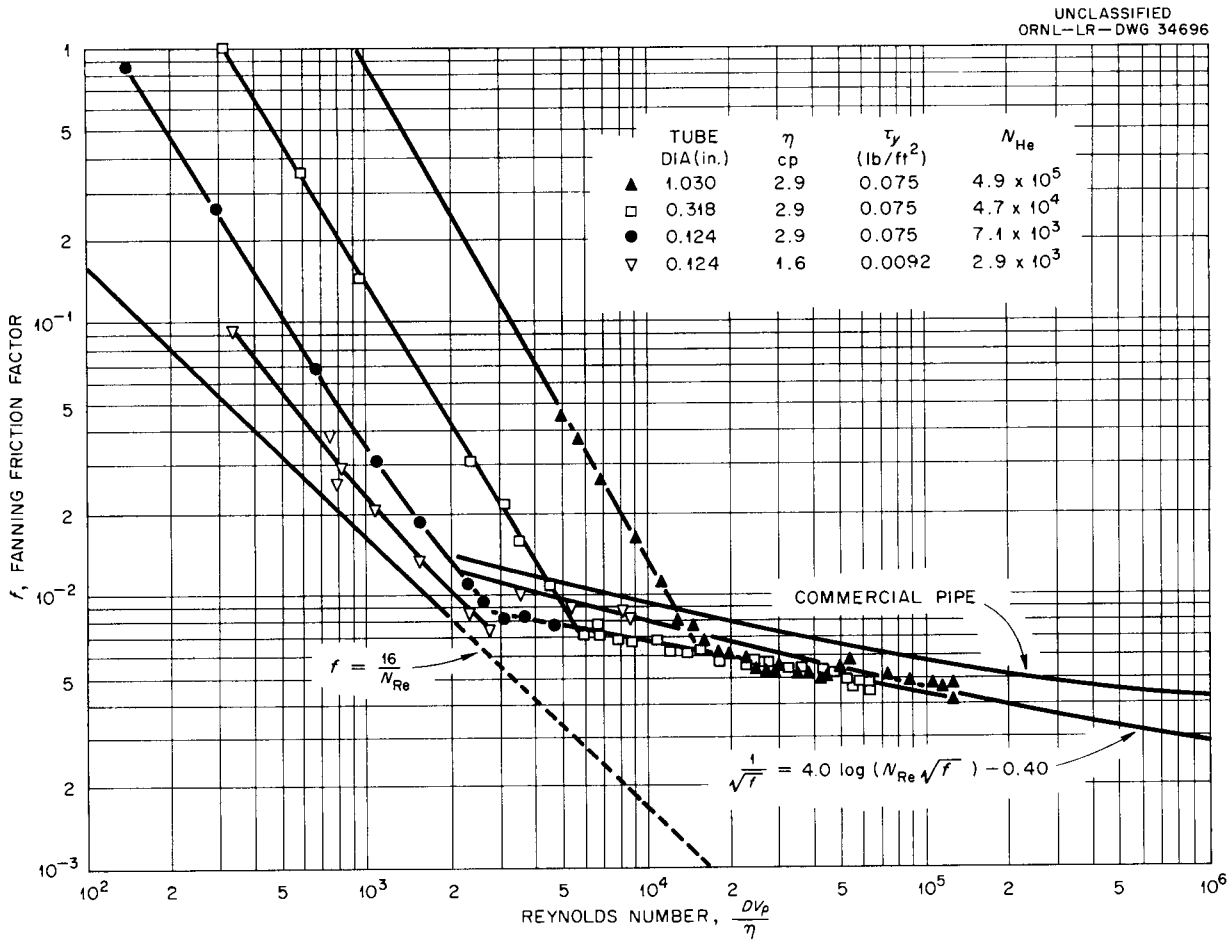

Fig. 9.28. Friction-Factor–Reynolds-Number Plot for Aqueous Thoria Slurries Having a Density of 1.67 g/ml.

in Fig. 9.29, which shows the variation in B and b with yield stress and coefficient of rigidity. The observed variation, in conjunction with dimensional-analysis results, suggests that B and b can be calculated from the functions of the following type:

$$B = 0.079\left[\left(\frac{\mu}{\eta}\right)^{c} + \left(\frac{g_c\rho\tau_y x^2}{\mu^2}\right)^{d}\right], \tag{2}$$

$$b = 0.25\left[\left(\frac{\mu}{\eta}\right)^{c'} + \left(\frac{g_c\rho\tau_y y^2}{\mu^2}\right)^{d'}\right], \tag{3}$$

where c, c', d, d', x, and y are constants to be determined experimentally; μ is the coefficient of viscosity; η is the coefficient of rigidity; ρ is the slurry density; τ_y is the yield stress; and g_c is a dimensional constant. The data given in Table 9.6 are fitted by Eqs. 2 and 3 if $c = 0.55$; $c' = 0.22$; $d = d' = 2$; $x = y = 6.6 \times 10^{-6}$ ft (this value of x and y corresponds very closely to the average particle size of the ThO_2 used in these studies).

Figure 9.30 compares values of B and b calculated from Eqs. 2 and 3 with the experimental values given in Table 9.6. The agreement appears satisfactory but has not been checked at temperatures higher than room temperature.

9.8.1 Critical Reynolds Number

The Reynolds number associated with the transition from laminar flow to nonlaminar flow is termed the critical Reynolds number. This can be determined most reliably by superimposing the nonlaminar friction-factor curve on the laminar-flow curve and

noting the Reynolds number at which the curves intersect. The fluid velocity associated with the critical Reynolds number is termed the "critical velocity."

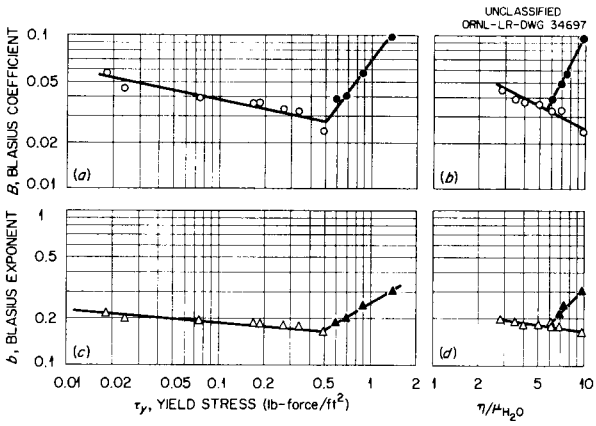

Fig. 9.29. Effect of Yield Stress and Coefficient of Rigidity on B and b for Nonlaminar Flow Conditions. Solid points are used to show correspondence between points in *a* and *b* and in *c* and *d*.

Based on calculations using the Hedstrom plot, the critical velocity is principally dependent upon the value of the yield stress, weakly dependent upon the coefficient of rigidity, and essentially independent of pipe diameter for diameters greater than 1 in.[10] The present data verify the dependence on yield stress and lack of dependence on tube diameter but do not indicate any effect that the coefficient of rigidity might have. The critical velocity for the present data is given by the dimensional equation

$$V_c = \left(\frac{1}{D} + 8.5\right) \tau_y^{0.40} , \tag{4}$$

where

V_c = critical velocity, fps,

[10] D. G. Thomas, "The Relationship of Aqueous ThO_2 Slurry Physical Properties to the Engineering Design of a Reactor System," paper 14-3 presented at the 3rd Annual Meeting of the American Nuclear Society, Pittsburgh, Pa., June 10–12, 1957.

Table 9.6. Nonlaminar-Flow Parameters for Aqueous Thorium Oxide Slurries

Run Series No.	Bingham-Plastic Coefficients: Coefficient of Rigidity, η (centipoises)	Bingham-Plastic Coefficients: Yield Stress, τ_y (lb/ft^2)	Slurry Density, ρ (g/cc)	Nonlaminar Coefficients (Eq. 2): B	Nonlaminar Coefficients (Eq. 2): b
I	2.9	0.075	1.67	0.0398	0.192
II	2.7	0.018	2.08	0.0570	0.220
III	8.2	0.49	2.16	0.0239	0.164
IV	5.2	0.34	1.99	0.0327	0.180
V	5.7	0.27	2.33	0.0333	0.180
VI	5.2	0.59	2.12	0.0391	0.192
IX	6.0	0.89	2.09	0.0575	0.245
X	8.2	1.39	2.17	0.0980	0.305
XI	5.7	0.69	1.90	0.0405	0.205
XII	3.3	0.188	1.66	0.0372	0.185
XIII	4.1	0.170	1.77	0.0365	0.185
XIV	2.3	0.024	1.38	0.0450	0.200

D = tube diameter, in.,

τ_y = yield stress, lb/ft^2 ($\tau_y > 0.01$ lb-force/ft^2).

Equation 4 appears valid for $\tau_y > 0.01$ lb-force/ft^2; it has not been checked at temperatures other than room temperatures.

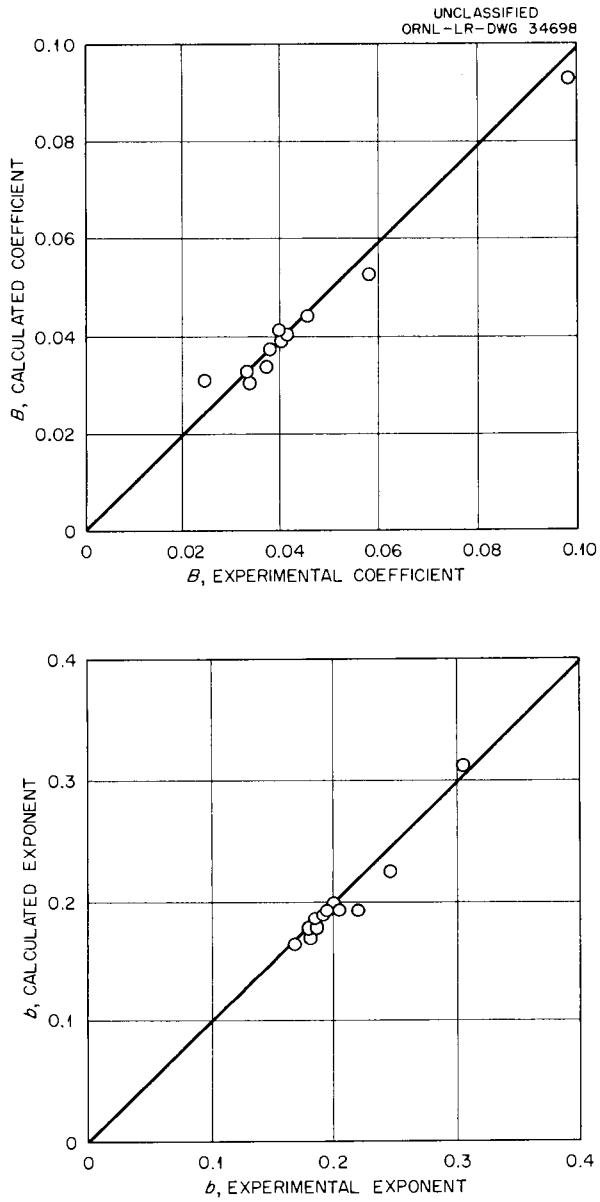

Fig. 9.30. Comparison of Experimental and Calculated Values of B and b for Nonlaminar Flow of Thoria-Water Slurries.

9.9 PHYSICAL PROPERTIES OF THORIA-WATER SLURRIES

9.9.1 Influence of Surface-Active Agents on Slurry Behavior

A qualitative analysis has been made[11] of the influence which surface-active agents might exert upon slurry properties. The addition of such agents appears to result in an electrically charged double layer of ions near or on the thoria surface and a tendency for the slurry to disperse. During reactor operation, however, the ionic strength of the liquid medium will increase with time owing to the buildup of corrosion and fission products; this increase will result in compression of any electrically charged layer on the thoria surface and a lowering of the dispersal power of the originally added surface-active agents. In addition, the effect of these agents will be less at high temperature (280°C) than at room temperatures because of changes in the liquid dielectric constant with temperature.

Similar arguments suggest that coating thoria particles with ceramic or other materials will not strongly influence slurry physical properties after significant reactor operation. Preliminary evidence in out-of-pile studies suggests that electrolyte additives which prevent cake formation in slurries where it otherwise would be expected, influence the rate and nature of primary-particle degradation but do not prevent agglomeration of small particles.

9.9.2 Thoria Caking Studies

The investigation of factors involved in thoria cake formation was continued by circulation of thoria-water slurries in the 30-gpm loop. Thoria from batch LO-20 was circulated after being autoclaved for 36 hr at 300°C in the presence of 800 ppm H_2SO_4 (based on ThO_2 content). As with batch LO-20 autoclaved in the absence of H_2SO_4,[12] circulation of the slurry was accompanied by sphere formation and by the deposit of thick ThO_2 films in the pump impeller region and in the multidiameter sample barrel. Films were deposited in all three

[11] C. S. Morgan, *Influence of Surface Active Agents on ThO_2 Slurries*, ORNL CF-58-7-56 (July 15, 1958).

[12] P. R. Kasten *et al.*, *HRP Prog. Rep. for Quarters Ending April 30 and July 31, 1958*, ORNL-2561, p 87.

sections of the sample barrel (nominal fluid velocities of 5, 10, and 20 fps); film in the 5-fps section was the easiest to remove.

The effect of oxide particle size on ThO_2 cake formation was also examined with thoria from batch LO-20; prior to loop circulation, the average particle size was reduced from 3 μ to 0.9 μ by treatment in a Waring Blendor. Circulation was at 280°C, with a slurry concentration of 480 g of Th per kg of H_2O. No cake deposits were formed and spheres did not develop; this is contrary to results obtained when no pretreatment was performed. A repeat of this run resulted in the same results. The thoria which was treated in the Waring Blendor had a zeta potential of –59 mv (determined by electrophoretic measurements at room temperature); untreated thoria had a zeta potential of –68 mv, indicating that there was little change in particle surface conditions as a result of the Waring Blendor treatment.

Figures 9.31 and 9.32 are electron micrographs of samples taken 2 hr after the start of circulation in the loop; the thoria in Fig. 9.31 was pretreated in the Waring Blendor, and that in Fig. 9.32 was not pretreated. These micrographs show that the ratio of large thoria particles (>0.5-μ diameter) to intermediate-sized thoria particles (0.1- to 0.5-μ diameter) was greater when no pretreatment took place. This suggests that smaller sized thoria particles do not degrade as readily as larger particles into the extremely fine particles thought to be necessary for cake or sphere formation.

Results from a loop run in which thoria from batch LO-44-100 was circulated also support the above conclusion. The LO-44-100 thoria was prepared by filtering the thorium oxalate immediately after precipitation; subsequent firing was at 800°C for 2 hr. The associated cake resuspension index was 7, which is a value associated with cake-forming slurries. Circulation of this slurry in the 30-gpm loop did not produce cake formation. Figure 9.33 is an electron micrograph of the material after 2 hr of loop circulation. The particle distribution shows a lower ratio of large particles to intermediate particles than was present in batch LO-20 thoria after similar treatment. This suggests that failure of LO-44-100 to form cakes and spheres was due to rapid degradation of large particles to intermediate-sized particles.

In another loop run, thoria from batch LO-20 was circulated at an initial concentration of 75 g of Th per kg of H_2O. During the run the circulating concentration steadily declined owing to migration of thoria into the upper part of the pressurizer and into other nonflow regions. However, sphere or cake formation did not occur.

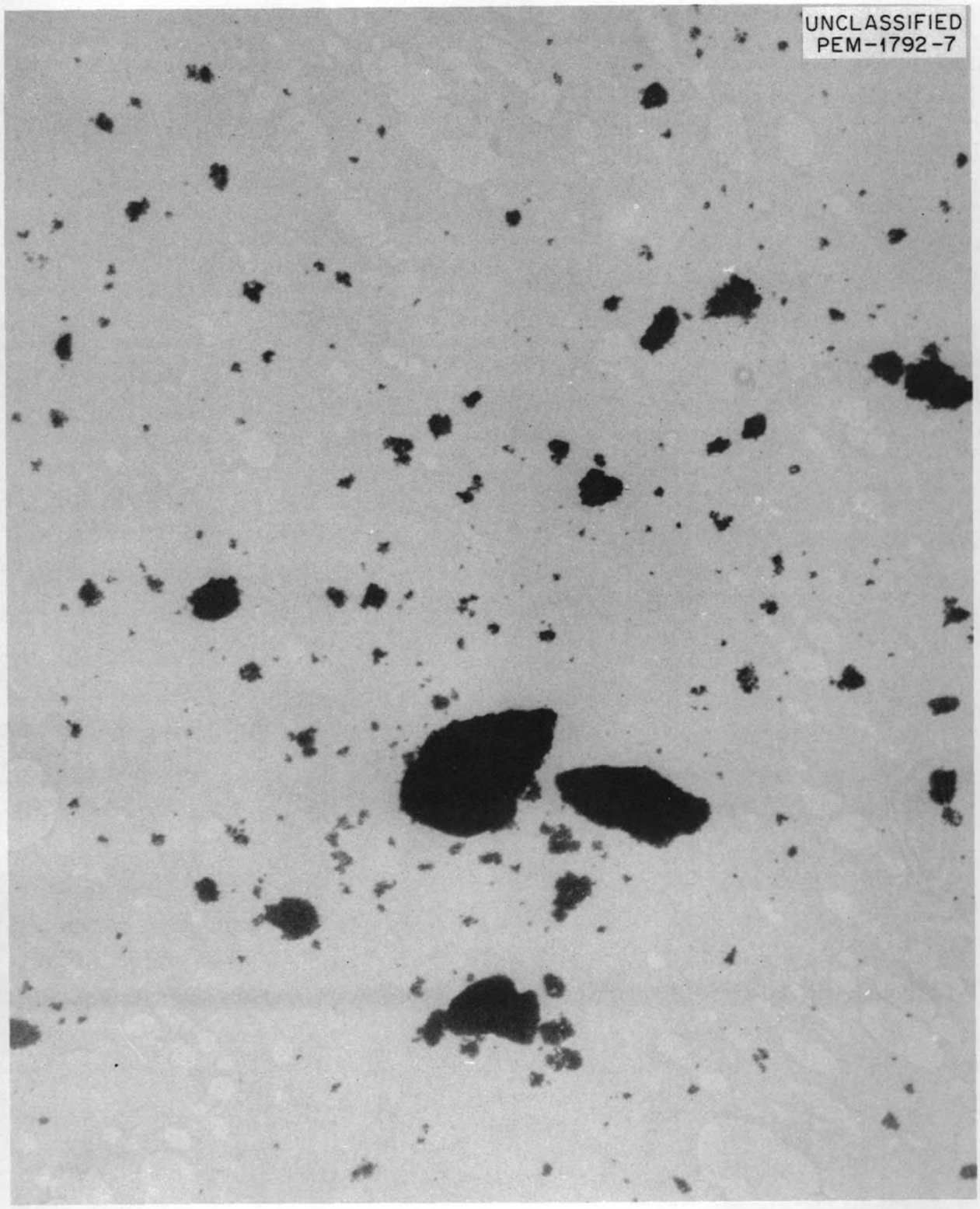

Fig. 9.31. Thoria from Batch LO-20 After 2 hr of Loop Circulation; Before Circulation Thoria Was Treated in Waring Blendor. 20,000X.

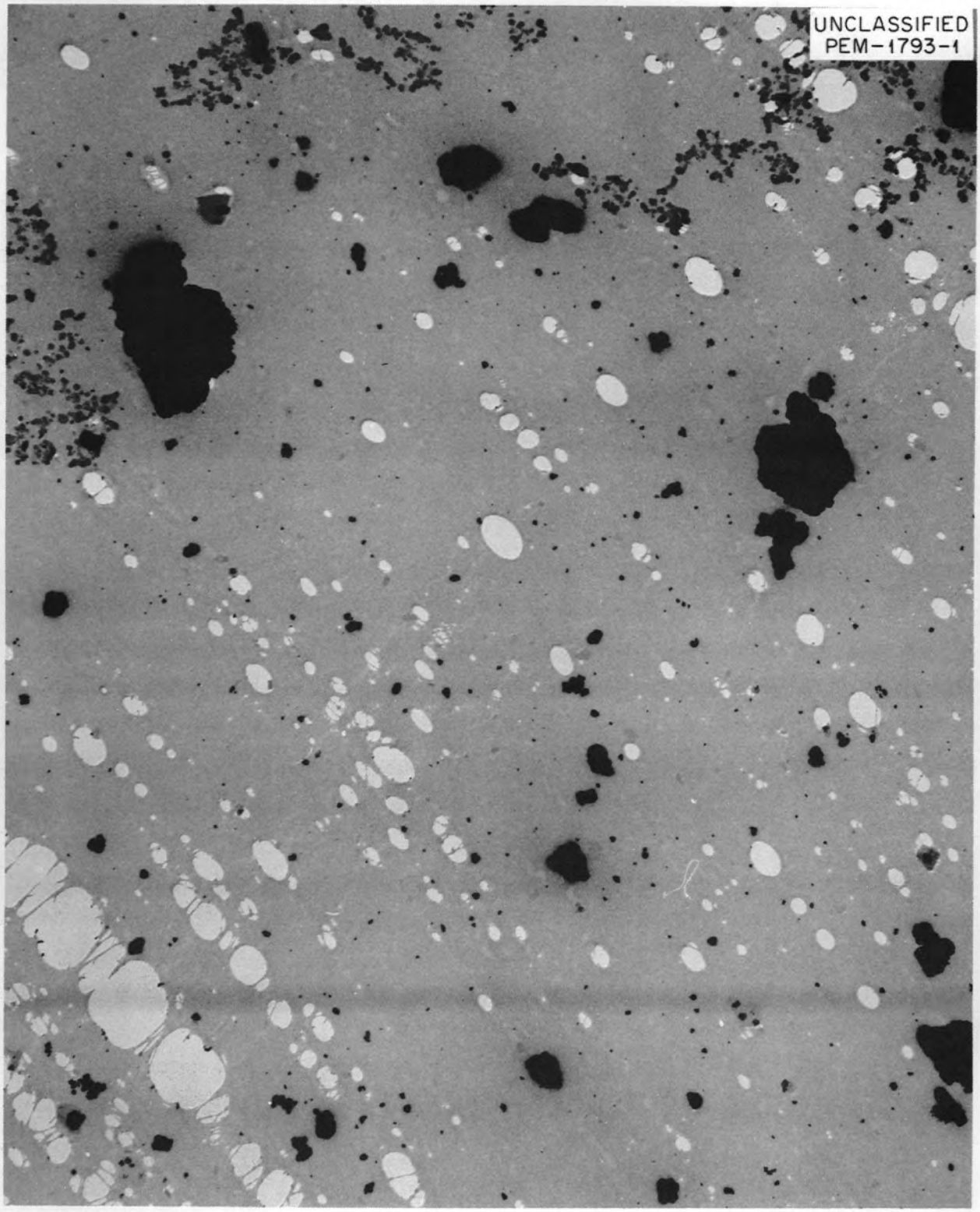

Fig. 9.32. Thoria from Batch LO-20 After 2 hr of Loop Circulation; No Prior Treatment. 20,000X.

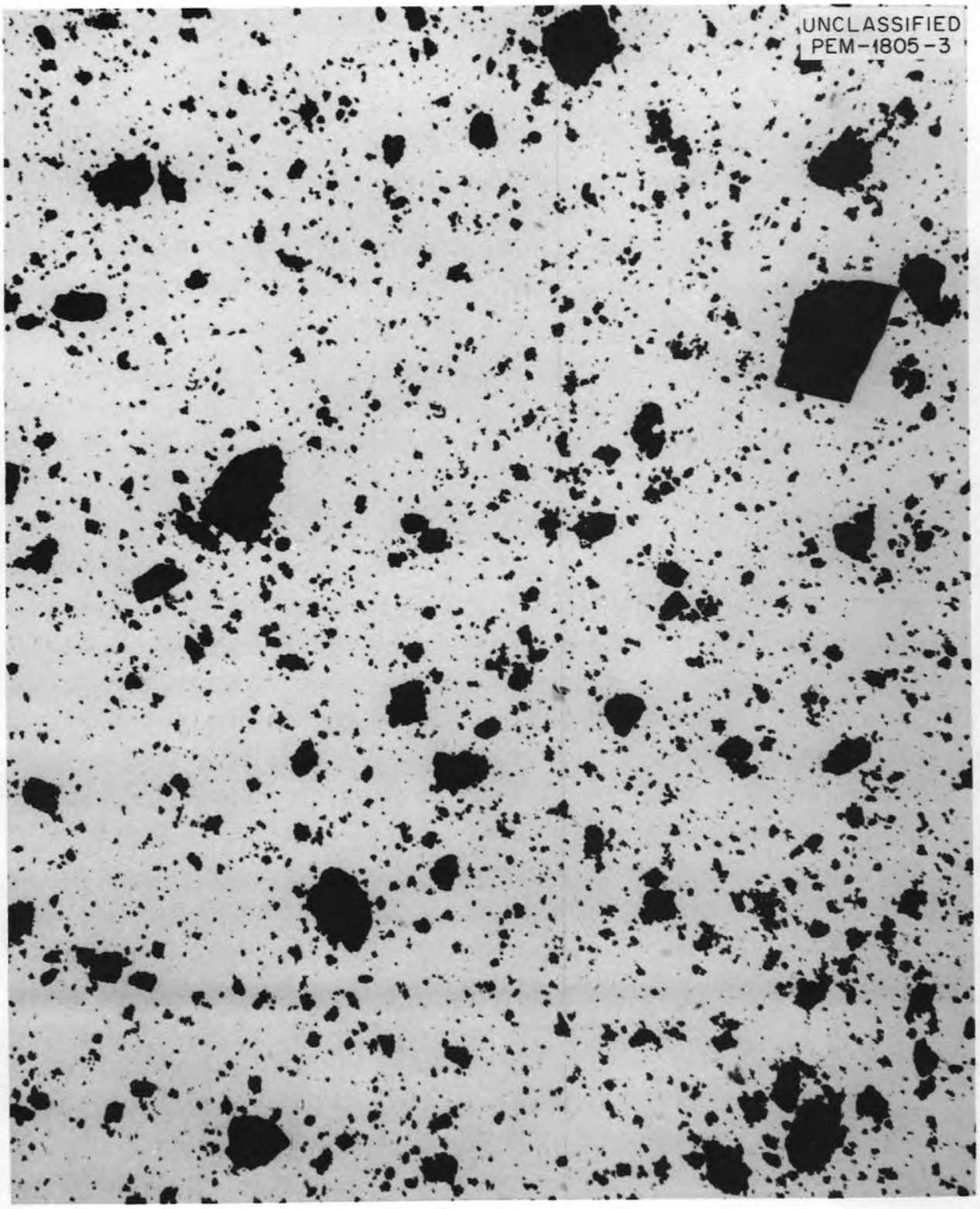

Fig. 9.33. Thoria from Batch LO-44-100 After 2 hr of Loop Circulation; No Prior Treatment. 20,000X.

Part III

ENGINEERING DEVELOPMENT

R. N. Lyon

10. DEVELOPMENT OF FUEL- AND SLURRY-SYSTEM COMPONENTS

I. Spiewak

R. Blumberg
T. G. Chapman
J. S. Culver
D. M. Eissenberg
C. H. Gabbard
B. A. Hannaford
E. C. Hise
C. G. Lawson
J. E. Mott
J. C. Moyers
I. K. Namba
H. R. Payne
D. L. Snyder
R. P. Wichner

10.1 RECOMBINER AND PRESSURIZER DEVELOPMENT

10.1.1 High-Pressure Recombiner Loop

The natural-circulation recombiner was operated for 220 hr in preliminary runs so that its characteristics could be studied. No explosions or corrosion failures were experienced. At stoichiometric gas inputs of 0.75 scfm at 1500 psi pressure, the entire vapor loop was superheated. The system will be operated continuously following the present shakedown runs.

10.1.2 Syracuse Contract

In a long 0.434-in.-dia tube the lower reaction limit of $D_2 + \frac{1}{2}O_2$ in D_2O vapor at 300°C was 29%, as compared with 11% in the hydrogen system. No detonations were experienced in the deuterium system at 300°C; the maximum gas concentration tested was 35%. Experimental work on this subcontract was completed; a final report is being prepared.

10.1.3 Solubility of Oxygen and Hydrogen in Fuel Solution

It was previously reported[1] that the solubility of stoichiometric $H_2 + \frac{1}{2}O_2$ in H_2O at 250°C was about 50% greater than that of oxygen alone. This conclusion was based on comparison of several runs with stoichiometric gas and one with oxygen, made under the same conditions. Solubility determinations which showed no such effect have since been made at 200 and 275°C. In order to verify conclusively the observations at 250°C, work outside the scope of the present program would be required.

[1] I. Spiewak *et al.*, *HRP Prog. Rep. for Quarters Ending April 30 and July 31, 1958*, ORNL-2561, p 98.

10.2 CENTRIFUGAL PUMPS

10.2.1 20-cfm Allis-Chalmers Blower

The 20-cfm canned-motor blower continued circulating a steam-nitrogen mixture at 170°C and 1400 psi (4.8 lb/ft^3 density); the blower has operated for approximately 4800 hr with no difficulty.

10.2.2 Reliance 6000-gpm Pump

The Reliance 6000-gpm pump is being purchased as a prototype for circulating solutions through intermediate-scale reactors. The hydraulic design of the pump is complete except for minor revisions; detailing of the motor end is approximately 50% complete.

The "top maintenance" feature of the pump makes necessary a flexible mechanical joint to prevent leakage at the thermal barrier. Initial tests of a Belleville spring gasket, with stainless-to-stainless sealing surfaces, failed to produce a seal. Tests with aluminum wire inserts (simulating gold sealing surfaces) appeared to be successful. A preliminary test indicated that a seal can be made with a 0.032-in.-dia gold wire insert with a force of 1000 lb per linear inch.

The insulation-test stator being irradiated in the HRT cell to study its radiation resistance has received a dose of 22×10^6 rads to date. Its electrical resistance to ground has decreased considerably, but this is believed to be the result of physical damage to the leads.

A second test stator being irradiated in a Co^{60} source has received about 1.2×10^9 rads to date, which is above the anticipated life. Although there is some indication of deterioration above 2000 v, the insulation seems to be practically unaffected at the operating voltage of 460 v (see Fig. 10.1).

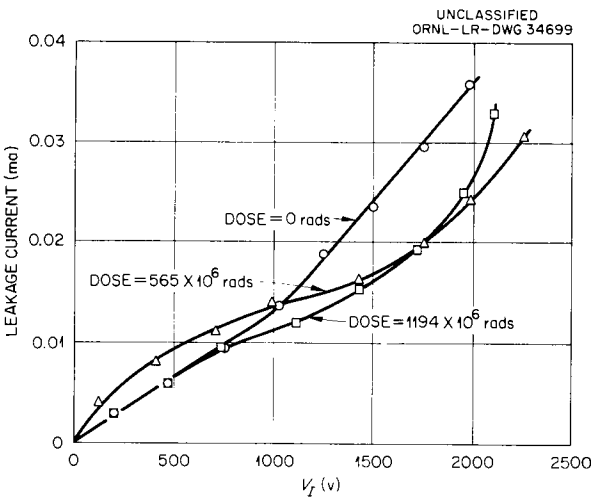

Fig. 10.1. Effect of Irradiation on the Leakage Current of Stator Insulation.

10.2.3 300A Slurry Pump and Loop[1]

The jet eductor used to circulate the steam-gas mixture through the pressurizer and condensate system of the 300A slurry loop was removed owing to the excessive quantities of gas which were entrained in the main loop flow. It was impossible to prevent the entrained gas from collecting in the back of the pump, ultimately causing a bearing failure. The loop was modified for either steam or gas pressurization, with a thermal-convection loop for condensing purge water.

The pump has been equipped with aluminum oxide radial and thrust bearings and with a modified titanium impeller, which will be used to evaluate various vane inlet and exit geometries.

A major leak developed across the gold wire insert in the pump flange and forced termination of the initial run. The seal failure was attributed to a rough sealing face. The sealing face was reconditioned and a larger gold wire insert was installed in preparation for the next run.

10.2.4 200Z Loop and Pump

Conversion of the 400A-2 pump to the 200Z slurry pump was completed; loop construction is approximately 65% complete. The pump will be fitted with aluminum oxide radial bearings and a Stellite-Graphitar thrust bearing for the initial run. Design modifications are in progress which will permit the future installation of a flame-plated aluminum oxide Koppers floating-bushing seal and a thrust bearing employing line-contact leveling linkages.

10.2.5 320A SBM Pump

The pressure drop through an idle pump may be of concern in some dumping applications. Flow vs pressure drop was determined for the 320A SBM pump by forcing flow through the pump with no electrical power applied. With a 15-ft pressure drop and flow in the normal direction, the flow rate was 195 gpm with the rotor locked and 225 gpm with the rotor free. With reversed flow and the same pressure drop, the flow rate was 120 gpm with the rotor locked and 130 gpm with the rotor free.

10.2.6 Slurry-Bearing Test Program

A set of thrust-bearing shoes with aluminum oxide wear-surface inserts was fabricated and installed in the 300A pump. A similar set of shoes was procured from Coors Porcelain Co. for future installation. A complete set of aluminum oxide flame-plated radial and thrust bearings is being purchased from Linde Air Products.

A thrust bearing with a solid shoe (i.e., no leveling linkage) is being designed. If successful in operation, such a bearing will eliminate the linkage wear which has been noted in standard Kingsbury bearings.

Franklin Institute is preparing a revised time schedule and cost estimate for the work to be accomplished under their hydrodynamic slurry-bearing contract.

10.2.7 Shaft Seals

A Koppers floating-bushing rotary seal was tested in the reverse position in the shaft-seal test rig; it allowed a mixing flow of less than 0.06 cc/hr with a purge rate of 9 liters/hr. In order to apply this seal to solution or slurry pumps, it is necessary to find a running material which does not gall or corrode in service. Tungsten carbide, the material used to date, has deteriorated rapidly in low- or high-temperature oxygenated water. Preliminary tests of 322-W (a precipitation-hardened stainless steel) and INOR-8 (a nickel-base alloy) were interrupted by galling. A nitrided titanium assembly is being fabricated. If a material suitable for high-temperature use cannot be found, it is possible to modify the Westinghouse pump design to permit an aluminum oxide seal to operate in a low-temperature region.

10.2.8 Impeller-Velocity Study

A study was completed to determine the magnitude of velocities existing in slurry pumps currently in use and to determine possible methods of reducing the velocities in order to obtain longer life.[2] The maximum velocities in the 100A, 200A, and 300A pumps are between 39 and 54 fps, with the exception of the 100A absolute discharge velocity, which is 80.6 fps. It was suggested that the substitution of pumps that provided the rated head-flow at a lower motor speed would possibly reduce impeller wear.

10.3 OXYGEN COMPRESSORS

The Pressure Products Industries diaphragm-type oxygen compressor, driven by a Scott & Williams P1 purge-pump drive and a water-filled intermediate isolation leg, has performed, without maintenance, for 1725 hr of HRT mockup operation.

The Harwood compressor was reassembled, and, after being test-operated, was placed in standby service by the Systems Development Section.

Performance tests of the three-stage, 2-cfm, remote-drive oxygen compressor are scheduled for the first week of November at the vendor's factory. If these tests are satisfactory, the compressor will be ready for delivery.

10.3.1 Turbine Pump

The Roth single-stage turbine pump operated for 3370 hr, delivering 10 gpm of fuel solution against a 300-psi head before being shut down for replacement of the mechanical shaft seal. There was no change in pump performance over this period. The electrolyzed type 316 stainless steel impeller bore evidence of having rubbed against the wear rings; otherwise, it appeared to be in its original condition. The aluminum oxide wear rings showed slight evidence of having undergone rubbing. The pump was reassembled, with a new seal, and was returned to operation.

10.3.2 Slurry Feed Pumps

The high-pressure slurry feed-pump test loop, a duplex unit consisting of a diaphragm head with remote check valves and a single-contour head with close-coupled check valves (Fig. 10.2), was operated for 1400 hr with average conditions of: flow,

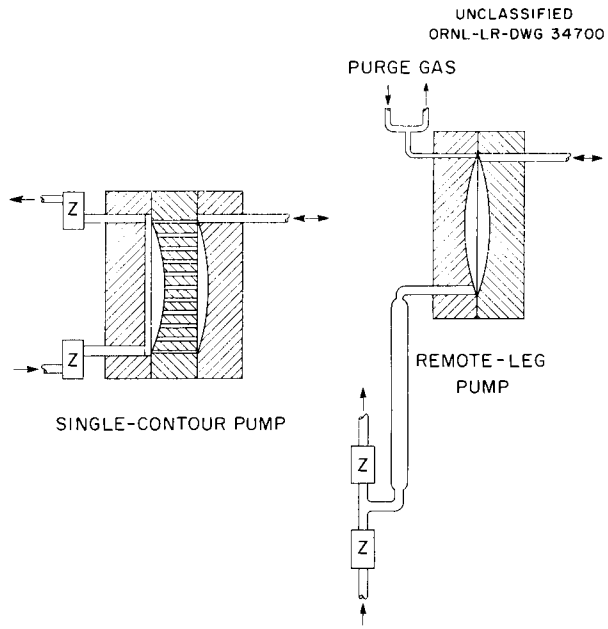

Fig. 10.2. Slurry Diaphragm Feed-Pump Heads.

1 gpm; discharge pressure, 1500 psi; temperature, 100°F; pumped material, 1600°C-fired ThO_2 slurry of specific gravity 1.5.

The remote-leg head, which acts as a gas trap, is continuously vented from the upper fitting of the head through a check valve and a capillary choke which leads to the high-pressure system. This vent system provides a high-resistance path in parallel to the main discharge line and permits a small flow of gas, water, and/or slurry each stroke, thus keeping the head clear of gas. Although a density gradient is maintained, the upward flow permits some slurry to enter the head. Figure 10.3 shows the face of a diaphragm from a remote-leg pump that had pumped slurry for 1800 hr; the surface is etched, but there is no severe damage.

The single-contour pump can be built as a through-flow pump and has no inherent gas-binding problem. However, for a given size head it can pump only half as much as a conventional head, since it is limited to stroking from the intermediate contour to center.

A net positive-suction head of 15 to 20 psi is provided in the test loop by a low-pressure circulating system and pump. A conventional 5-gpm turbine pump suffered complete packing failure in 33 hr. A canned-rotor pump with all-stainless-steel hydrostatic bearings operated fairly satisfactorily for 350

[2] C. H. Gabbard, *Velocity Study of Centrifugal Pump Impellers*, ORNL CF-58-8-84 (Aug. 22, 1958).

UNCLASSIFIED
PHOTO 31322

Fig. 10.3. Slurry Feed-Pump Diaphragm After 1800 hr of Service on Remote-Leg Test Loop. Diaphragm material: type 347 stainless steel, annealed, 0.031 in. thick. Diaphragm protected by 40-μ screens.

hr but suffered rather severe wear. A Vanton Flexiliner pump with a Buna N body and a neoprene Flexiliner has operated for more than 1000 hr with no difficulty at all. This pump requires no maintenance other than lubrication and cannot leak unless the Flexiliner breaks. The use of a positive-suction head has permitted the feed pump to operate at a high volumetric efficiency.

Figure 10.4 shows the damage that occurred to Stellite check-valve trim in approximately 60 hr of service. Figure 10.5 shows the damage to tungsten carbide trim after 1250 hr of service. Pump output had dropped to approximately 65% of the original output just prior to the removal of the tungsten carbide trim. Aluminum oxide trim will be tested during the next quarter.

The loop was charged with 1600°C-fired ThO_2 having an average particle size of 2.5 μ, with 3% less than 1 μ. The particles have now degraded to 51% less than 1 μ and 1% less than 0.1 μ. When charged, the oxide settled rapidly in the dump tank, a sharp slurry-water interface formed just below the return line, and the specific gravity of the circulating stream was 1.5. As the material degraded,

Fig. 10.4. Stellite Check-Valve Trim After 60 hr of Slurry Service, Showing Severe Wear.

Fig. 10.5. Tungsten Carbide Check Valve Trim After 1250 hr of Slurry Service.

the quantity of foam increased, the supernate became cloudier until no interface existed, and the specific gravity of the circulating stream dropped to 1.1, indicating almost complete homogeneity. A small quantity of chromic acid was then added to the slurry, whereupon the slurry returned to its original flocculated behavior.

10.4 VALVE TRIM

10.4.1 Dump-Valve Trim for Solutions

Dump-valve trim of stainless steel type 347 (seat) and 17-4 PH (plug) was tested for 6000 dumps with no apparent change in operating characteristics. After removal it was found to leak 10 cc/min with a 2000-psi ΔP. The plug appeared to be unaffected, but the seat was scored as if from foreign material and was deformed on one side as if from misalignment.

A tantalum plug operating against a type 347 stainless steel seat failed almost immediately. The plug was deeply dented on one side, again as if from misalignment.

The valve test loop has been reworked in an effort to promote circulation of solids. The dumping cycle will be changed to increase the enthalpy of the loop contents at the time that dumping takes place.

Since it appears that the valves must operate with solids present in a reactor and since guiding a plug on the end of the long bellows-sealed stem is difficult, it is planned to test two approaches to overcoming these problems. The present valve design will be fitted with harder trim materials in an attempt to find materials that will resist scoring by solids and will guide themselves to a correct seat. Hardened 17-4 PH stainless steel trim has been installed and is ready for test. Zirconium-niobium alloy trim is being fabricated, and other materials that appear promising will be tested. A new design, utilizing a free ball plug, has been fabricated and will be tested.

10.4.2 Slurry Hand Valves

A station for testing hand valves under severe throttling conditions was installed in the high-pressure system of the slurry feed-pump test loop to evaluate valve trim materials under reasonably reproducible conditions. The test consists in drawing 100-ml samples, with a ΔP across the valve of 1500 psi, until the valve fails to shut off. Type 18-8 and 17-4 stainless steels and Rexalloy trims failed to shut off after the first sample. After 30 samples, tungsten carbide trim still shuts off; valves trimmed with single-crystal Al_2O_3 and Zr-Nb alloys will be tested.

10.4.3 Slurry Letdown Valves

A fixed letdown system consisting of 110 ft of $\frac{1}{4}$-in.-OD, $\frac{1}{8}$-in.-ID tubing was installed in the slurry feed-pump loop and operated satisfactorily for about 400 hr at a stream velocity of 28 fps.

A second fixed-resistance letdown device consisting of 10 ft of 0.063-in.-bore capillary tube, made up in three sections in series, has been in service on the slurry check-valve-material test loop with

average conditions of: pressure, 1300 psi; temperature, 100°F; velocity, 42 fps; and slurry specific gravity, 1.6. Figure 10.6*a* shows a hole that occurred about an inch downstream of the entrance to the first section after 1690 hr of operation. Figure 10.6*b* is of the same relative position in the second section of capillary, which was in service during the same period as the first section plus 1600 additional hours. The severe erosion to the first section was probably the result of mechanical damage during fabrication.

A variable-length capillary valve was operated for 1000 hr at a fluid velocity of 80 fps. The throttling regions of the valve suffered only minor damage, and some variation in flow was obtained. It is possible that by careful design and materials selection this device could be made practical.

UNCLASSIFIED
T-15194

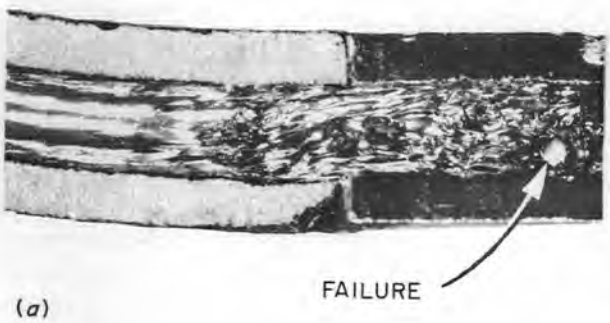

(*a*)

UNCLASSIFIED
T-15881

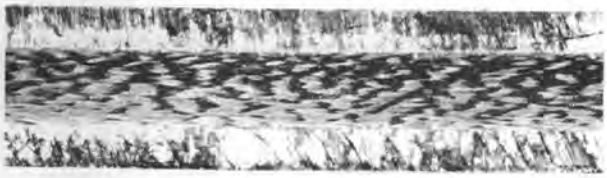

(*b*)

Fig. 10.6. Capillary Tubing Used to Throttle Slurry at 42 fps. (*a*) First section; operating time, 1690 hr. (*b*) Second section; operating time, 3290 hr.

10.5 TITANIUM PROGRAM

A small experimental heat exchanger was designed and fabricated by The Pfaudler Co. in order to demonstrate the feasibility of manufacturing titanium-lined equipment. All surfaces to be contacted by primary fluid were titanium or titanium-lined. Prior to shipment to ORNL, The Pfaudler Co. hydrostatically tested the unit at 3000 psi on the tube side and at 900 psi on the shell side.

A repeat hydrostatic test was attempted at ORNL. At 150 psi a slight leak was detected between the 4-in. 1500-lb flanges. The flanged joint was dismantled for inspection of its sealing surfaces. An examination of the 4-in. 1500-lb cover flange revealed a transverse crack at the titanium-lined inner groove. A dye-penetrant test of the titanium-lined surface revealed additional defects at some of the weld seams; however, the tube-joint welds (24 tubes) appeared sound.

10.6 SLURRY HEAT EXCHANGER FLOW TESTS

A loop was constructed to allow observation of slurry behavior in plastic models of proposed heat exchanger designs. The loop, equipped with a 100-gpm Moyno pump coupled to a variable-speed drive, has adequate head and a wide range of flow rates for room-temperature testing.

For the initial test a 6-ft plastic tube bundle, containing seven Plexiglas tubes ($\frac{1}{2}$-in. OD × 0.049-in. wall thickness), was piped in a horizontal position. Both inlet and outlet headers were designed to resemble an eccentric reducer with a 30-deg slope. The slurry used was an 800°C-fired thoria, with concentrations varying from 200 to 1000 g of ThO_2 per liter of slurry.

Drop-out and settling of slurry in the tubes occurred at velocities of 1.6 to 1.8 fps at concentrations from 200 to 600 g of ThO_2 per liter of slurry. No measurable difference in drop-out velocity was detected as the slurry concentration was changed. The turbulence in the tube-sheet headers was detectable at velocities in excess of 4 fps. At velocities less than 2 fps, preferential flow in the upper row of tubes was observed.

At slurry concentrations of 800 to 1000 g of ThO_2 per liter, the drop-out velocity was difficult to determine. Observations made on several runs indicated that drop-out and plugging of tubes occurred nearly simultaneously at high concentrations. In

general, at velocities less than 1.0 fps, slurry flow gradually ceased and the tubes became plugged. Subsequent runs demonstrated thar plugged tubes can be readily blown out and slurry flow resumed.

10.7 CORE HYDRODYNAMICS

10.7.1 HRE-3 Re-entrant Core Model

Visual and heat transfer observations of the HRE-3 re-entrant core model were made in the region where the inlet jet impinges on the core wall. It was observed, by injecting dye at the wall, that high random velocities were generated immediately adjacent to the wall. Heat transfer coefficients of about 2000 Btu/ft^2·hr·°F at design conditions were indicated at two locations within this region.

Fluid leaving the jet-impingement area was observed to travel very rapidly in a strong boundary layer to the outlet. Measurements with a pitot tube indicated velocities of 8 to 11 fps in this boundary at the rated 6000 gpm. The heat transfer coefficients measured previously in this region correspond to the observed velocities.

The heat transfer data of the HRE-3 model[3] have been generalized in dimensionless form with other re-entrant models as follows:

$$\frac{hR_V}{k} = 1.55 \left(\frac{R_j V_j \rho}{\mu}\right)^{0.6} \theta^{-0.4} \left(\frac{C\mu}{k}\right)^{1/3} ,$$

where

h = local heat transfer coefficient, Btu/hr·ft^2·°F,

R_V = radius of vessel, ft,

k = thermal conductivity, Btu/hr·ft^2(°F/ft),

R_j = radius of inlet nozzles, ft,

V_j = velocity of fluid in inlet nozzles, ft/hr,

ρ = density of fluid, lb/ft^3,

μ = viscosity of fluid, lb/hr·ft,

C = specific heat of fluid, Btu/lb·°F,

θ = angular displacement of position where h is measured from pole opposite inlet, radians.

10.7.2 Single-Region Slurry Core

An MIT Practice School group operated the cone-bottom 30-in. core model with water. Wall shear stress was measured with re-entrant and straight-through flow. The effect of an entrance nozzle plus diffuser was compared with that of an entrance nozzle alone. General conclusions were that the re-entrant system created greater wall shear than the straight-through system and that the diffuser gave a more uniform shear distribution. In particular, the diffuser increased the shear in the conical portion of the vessel, which is subject to slurry sedimentation.

10.8 SLURRY DUMP TANKS AND EVAPORATORS

The feasibility of suspending settled slurry beds by use of an externally heated conical bottom section was demonstrated. Eleven liters of a slurry of 1600°C-fired thoria at a concentration of 800 g of Th per liter of slurry was boiled in a bottom-heated 6-in.-dia dump tank for 100 hr. After cooling and settling for three days, the slurry was resuspended by applying external heating only. The minimum heat rate required to maintain the slurry in suspension was determined to be 0.10 kw/liter, or 5.6 kw/ft^2 based on the projected bottom area of the dump tank.

10.9 PROPERTIES OF SETTLED BEDS

Settled-bed properties of interest in component development are the ultimate settled-bed concentration, the ease of resuspension in a vessel, the pressure drop necessary to institute flow of a settled bed in a pipe, and the effect on these properties of reactor conditions of temperature and electrolyte environment.

The gravity-settled-bed concentration for a pure thoria slurry was found to be largely a function of the average particle size. A relationship was derived, based on a model of a spherical particle surrounded by a diffuse double layer assumed to be 1 μ thick, as follows:

$$S = \left(\frac{0.845D}{1 + D}\right)^3 ,$$

where D is the average particle diameter in microns and S is the fraction of solids in the settled bed. This formula has been applied successfully in the case of regular-shaped glass and thoria particles.

It was found that pure thoria slurry which had settled in ¼-in. glass tubes while being subjected to vibration or 30 g centrifugal fields could be made

[3] I. Spiewak *et al.*, *HRP Prog. Rep. for Quarters Ending April 30 and July 31, 1958*, ORNL-2561, p 105.

to flow with very low pressure differentials. The flow generally was as a plug, which appeared to slip at the wall owing to a thin water layer. This water layer could have the thickness of the lyosphere (assumed 1 μ) based on colloidal theory.[4] The plugs were readily extruded through an orifice.

When the pure slurry was dispersed with nitric acid and permitted to settle for several days, settled beds which formed in $\frac{1}{4}$-in. copper tubing withstood a 1000-psi differential across a column approximately 2 ft long. The same slurry without the dispersant flowed under less than 0.5-psi differential in the same tube.

Addition of the corrosion product, chromic acid, was found to change the settled-bed density of pure thoria slurry. There was an apparent maximum density at low chromate concentrations, and there was a steady increase in density again at high chromate concentrations. The former effect seemed to be related to the electrical surface properties of the slurry (zeta potential). It has been found that chromic acid will flocculate a slurry which has become dispersed as a result of either nitric acid addition or particle degradation.

[4]R. Houwink, *Elasticity, Plasticity, and the Structure of Matter*, 2d ed., p 342, Harren Press, Washington, 1953.

11. DEVELOPMENT OF REACTOR SLURRY SYSTEMS

R. B. Korsmeyer F. N. Peebles
D. G. Davis L. F. Parsly M. Richardson
R. B. Gallaher H. B. Piper A. N. Smith
R. J. Kedl R. Van Winkle

11.1 CIRCULATING-SLURRY BEHAVIOR

Four slurry circulation runs were completed during the past quarter – three in the 200-gpm loop and one in a 100-gpm loop (S-loop). A summary of the runs is given in Table 11.1. A fluidized-bed test was made in another 100-gpm loop (T-loop) with thoria microspheres prepared by the Houdry Corp.

11.1.1 200-gpm Loop Operation

Run 200A-15 was conducted in order to determine the circulation and degradation characteristics of 1600°C-fired thorium oxide. The run was started on February 4 and was terminated on July 28 after 3822 hr of circulation at 300°C and 2000 psig.[1] The loop was initially charged to 1500 g of Th per kg of H_2O and operated at this concentration for 400 hr before the oxide concentration was reduced to 700 g of Th per kg of H_2O to bring down the yield stress to the HRE-3 design value of 0.1 lbf/ft^2. $UO_3 \cdot H_2O$ was added at 1544 hr ($\frac{1}{2}$ wt % of uranium based on the thorium oxide) so that its effect on the slurry yield stress and handling characteristics could be studied; MoO_3 was added at 2419 hr to a concentration of 1.16 mole % MoO_3.

The nitrogen absorption surface area remained constant at 1.5 ± 0.1 m^2/g for the entire run. The average mean particle size decreased from 1.8 ± 0.2 μ to 1.6 ± 0.1 μ at 1350 hr (95% confidence level). After the addition of $\frac{1}{2}$ wt % of uranium at 1544 hr, the average mean particle size decreased to 1.3 ± 0.2 μ. The molybdenum addition at 2419 hr reduced further the average mean particle size to 1.0 ± 0.2 μ. The decreases in apparent particle size occurred within 100 hr of the addition of the uranium and of the molybdenum, thus indicating that a further dispersion of agglomerates had taken place rather than attrition of the individual thoria particles.

The generalized system attack rate, calculated from the iron buildup in the slurry and on the assumption that uniform attack occurred over all the loop area, was 1.5 mpy at a concentration of 1500 g of Th per kg of H_2O and decreased to 0.6 mpy at 700 g of Th per kg of H_2O. After the uranium addition, at a slurry concentration of 650 g of Th per kg of H_2O, the attack rate increased to 0.9 mpy, and after the molybdenum addition, with a slurry concentration of 700 g of Th per kg of H_2O, the attack rate increased to 1.1 mpy for the final 1305 hr of the run.

When the loop was opened for inspection, there was no evidence of film formation or caking. The titanium scroll liner was in excellent condition, showing only a small area of high attack, as can be seen in Fig. 11.1. The type 347 stainless steel $1\frac{1}{8}$-in. orifice (velocity 65 fps) lost 9.96 g; the $1\frac{1}{2}$-in. orifice (velocity 37 fps) lost 2.34 g. The type 347 stainless steel impeller had localized pitting attack at the vane entrance and along the vanes (see Fig. 11.2). A portion of the inside of the shrouds was covered with a protective oxide film and had sustained very little wear, as shown in Fig. 11.3. The impeller lost 108 g (5.4%), or 2.8 g per 100 hr. The thermal barrier had localized pitting in the region opposite the back balance vanes of the impeller (see Fig. 11.4). Attack at this location was not observed in previous runs.

The Stellite-19 overlays on the pump journals were in very good condition. The upper Graphitar bearing had no measurable wear, and the lower Graphitar bearing wore only 0.0045 in. During the run the temperature in the thermal cavity was approximately 138°C, which compares with 190°C for the previous run in which 0.038 in. of wear was found on the lower radial bearing. (The lower part of this bearing is exposed to the thermal cavity.) During cleaning after run 200A-15, the lower $\frac{1}{8}$ in. of the bearing cracked and fell off. The Kingsbury-type thrust bearing was in very good condition. The Graphitar thrust runner wore only 0.004 in., and the Stellite-19 shoes were in

[1] R. B. Korsmeyer *et al.*, *HRP Prog. Rep. for Quarters Ending April 30 and July 31, 1958*, ORNL-2561, p 109.

Table 11.1. High-Temperature Slurry Circulation – Run Summaries

	Run No.			
	200A-15	200A-16	200A-17	S-121
Test dates	2/4 to 7/28	8/15 to 8/18	8/18 to 8/27	7/29 to 8/4
Running time, hr	3822	71	109.3	151
Objective	To determine the circulation and degradation characteristics of 1600°C-Fired ThO_2	To produce thoria spheres	To produce thoria spheres	To observe degradation and caking tendencies of undigested oxide
Charge				
ThO_2, kg	57.7 (LO-36-1600)* 18.6 (LO-39-1600)	23.7 (LO-20-800)	32 (LO-20-800)	3.6 (LO-44-100, undigested)
Water, kg	60	60	60	12
Additives				
Oxygen, liters	75	75	75	25
$UO_3 \cdot H_2O$, g	232			
MoO_3, g	233			
Temperature, °C	300	250	200–150	290
Pressure, psig	2000	1000	1000	1700
Average circulating concentration, g of Th per kg of H_2O	1500 Initial ~700 Final	417	355 Initial 413 Final	350
Reason for termination	Scheduled shutdown	Scheduled shutdown	Scheduled shutdown	Scheduled shutdown
Equilibrium mean particle size, μ	1.0	12.0	20.3	2.6–0.6
Cake location	No cake	No cake	Thin layer on all visible pipe sections	No cake
Fe buildup in slurry, g	166	11.3	5.6	11.8
Ni buildup in slurry, g		1.4	1	1.8
Cr buildup in slurry, g		2.9	2	3.0
Impeller weight loss, g	108	Not determined	No weight loss	8
Orifice-plate weight loss, g				
1 ⅛ in. (velocity 65 fps)	9.96	Not determined	Not determined	0.23**
1 ½ in. (velocity 37 fps)	2.34			

*ThO_2 batch number.

**Weight gain.

good condition; a slight film which covered the shoes was removed with emery cloth.

Uranium added as $UO_3 \cdot H_2O$ was partially dissolved by the water, as evidenced by uranium in the slurry filtrate and accumulation of uranium in the pressurizer liquid. The U/Th ratio decreased from 6.7 to 0.9 mg/g. Likewise, the molybdenum was slightly soluble, with the Mo/Th ratio decreasing from 3.7 to 1.2 mg/g. Figure 11.5 shows the iron/thorium, uranium/thorium, and molybdenum/thorium ratios during the run.

When the impeller was inspected, a 3.9-g piece of black material was found lodged in the entrance to one of the vanes. The material was primarily uranium, molybdenum, and chromium. From the curvature of the surface of the piece, it apparently formed on the pressurizer wall and flaked off near the end of the run. Screening of the slurry and

Fig. 11.1. Titanium Scroll Liner of 200A Pump After Run 200A-15.

UNCLASSIFIED
PHOTO 32021

Fig. 11.2. Stainless Steel Impeller from 200A Pump After Run 200A-15.

close examination of the loop failed to reveal any other large deposits of this material. A water run which followed failed to show any soluble uranium, molybdenum, or chromium, indicating that no similar deposit remained in the loop.

Rheological properties of run 200A-15 slurry were measured with the capillary-tube viscometer-sampler[2] at high temperature and with a vertical-tube viscometer[3] at room temperature. The data are shown in Table 11.2. The addition of uranium and of molybdenum substantially reduced the yield stress (τ_y) and the coefficient of rigidity (η).

Runs 200A-16 and 200A-17 were carried out to produce kilogram quantities of thoria spheres for

[2]R. B. Korsmeyer *et al.*, *HRP Quar. Prog. Rep. July 31, 1957*, ORNL-2379, p 52–54.

[3]R. B. Korsmeyer *et al.*, *HRP Prog. Rep. for Quarters Ending April 30 and July 31, 1958*, ORNL-2561, p 118.

Fig. 11.3. Sections of Impeller from 200A Pump After Run 200A-15.

fluidized-bed studies. Advantage was taken of the well-known sphere-forming properties of LO-20, 800°C-fired thoria. During run 200A-16, at 250°C, 14- to 16-μ spheres were formed after 56 hr of circulation. An attempt was made to increase the sphere size by decreasing the loop flow rate which was accomplished by reducing the frequency of the electrical power to the pump. A slight increase in sphere size was noted during the last 15 hr of operation, at an estimated flow rate of 150 gpm.

In an experiment to observe concentration gradients in horizontal pipes, the flow velocity was reduced by reducing the frequency of the current supplied to the pump motor in decrements of 5 cps from 60 to 15 cps. It was found that significant slurry drop-out occurred at a velocity of 3.8 fps (20 cps). A gamma traverse was used to detect concentration gradients.

Larger spheres were produced in run 200A-17, with an operating temperature of 200°C initially and about 150°C for the last 18 hr. The final maximum sphere size was approximately 25 μ. Fifteen kilograms of thoria spheres was produced from run 200A-16, and 26.4 kg from run 200A-17.

At the beginning of run 200A-17, the circulating pump failed because of a leak in the seal weld of the rotor can. When the loop was opened for pump repair, it was determined that no cake deposition had occurred during the previous run (run 200A-16). After the completion of run 200A-17, however, it was found that there was a uniform deposition of thoria cake on the piping and pump surfaces. The thickness of this cake was estimated to be $\frac{1}{32}$ in. or less.

Modifications to the loop after run 200A-17 included installation of differential-pressure cells for measurement of pump head and pressurizer liquid level. Data from these instruments will permit better estimates of the loop inventory and of the circulating-slurry density during operation.

During the shutdown the venturi meter for measurement of loop flow was recalibrated. No significant changes in the flow characteristics were found (within the limits of accuracy of the calibrations) after more than 11,000 hr of slurry service at elevated temperatures. The throat velocity was about 24 fps for most of the operating period.

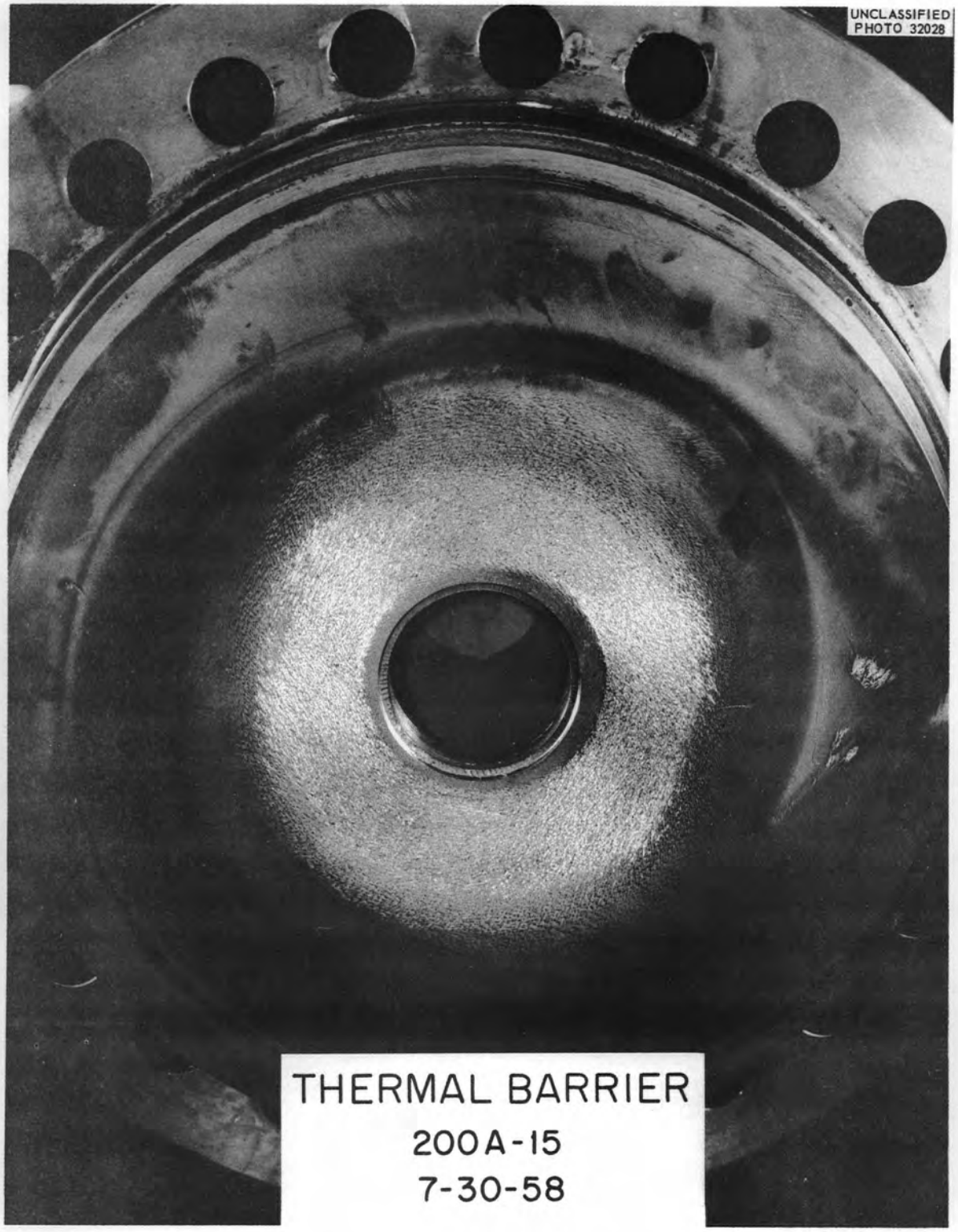

Fig. 11.4. Stainless Steel Thermal Barrier After Run 200A-15.

Table 11.2. Rheologic Properties of Run 200A-15 Slurry

Slurry Additive	Concentration (g of Th per kg of H_2O)	Temperature (°C)	τ_y (lbf/ft^2)	η (centipoises)
None	1550	275	0.65	1.34
None	920	290	0.18	1.16
½ wt % U	670	275	0.005	0.91
½ wt % U, 1.16 mole % Mo	640	275	0.003	0.53
None	1550	23	0.38	4.30
None	920	23	0.06	2.19
None	1090	31	0.30	2.88
½ wt % U, 1.16 mole % Mo	1090	31	0.14	2.54

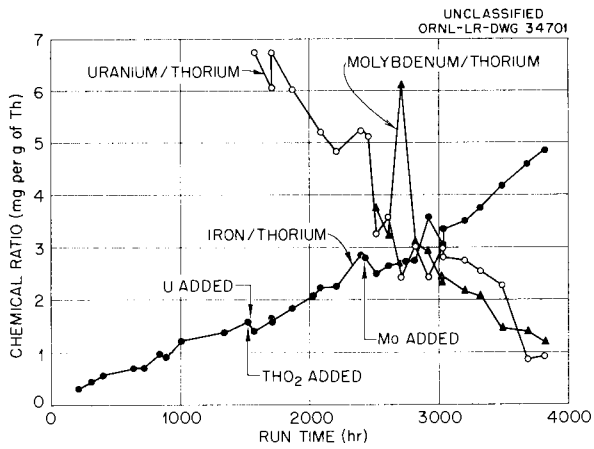

Fig. 11.5. Iron, Uranium, and Molybdenum Contents for Run 200A-15 Slurry.

11.1.2 Circulating Test in S-Loop (100 gpm)

Run S-121, containing 350 g of Th per kg of H_2O (800°C-fired ThO_2, undigested) at 200°C and 1700 psi, was completed after 151 hr of circulation. The run was made for comparison with a run with digested oxide. No cakes or films were observed when the loop was opened for inspection. Spheres formed during the early part of the run, but they disappeared with time. The mean particle size decreased from an original value of 2.6 μ to a final value of 0.6 μ. The over-all attack rate decreased during the run and leveled off at 4 mpy. The system attack rate was slightly lower than that in the run with digested 800°C-fired oxide; however, there was much more degradation of the undigested oxide. As reported for run T-102,[4] the digested oxide degraded to a mean particle size of 1.6 μ.

11.1.3 Fluidized-Bed Test in T-Loop (100 gpm)

A fluidized bed of thoria or thoria-urania particles has attractive features as a reactor blanket or fuel material. Most of the solids can be retained in the reactor vessel, thereby reducing the problems associated with solids circulation through pumps and heat exchange equipment. Preliminary tests have been initiated to determine the behavior of fluidized beds of thoria. The objective of the first series of tests was to determine whether excessive particle attrition would occur in a fluidized bed under out-of-pile conditions at temperatures of interest for homogeneous reactor operations. T-loop was modified for the tests, and a 6-in. sched-160 pipe was used for the fluidization column. Figure 11.6 is a schematic flow diagram of this system.

Concurrently, a 6-in. glass fluidization column was constructed for room-temperature studies of some of the physical characteristics of a fluidized bed. A schematic flow diagram of this system is shown in Fig. 11.7.

Approximately 40 kg of thoria microspheres, manufactured by the Houdry Process Corp., were made available for the study. Properties of the material were as follows: (1) particles very nearly

[4] R. B. Korsmeyer *et al.*, *HRP Prog. Rep. for Quarters Ending April 30 and July 31, 1958*, ORNL-2561, p 112.

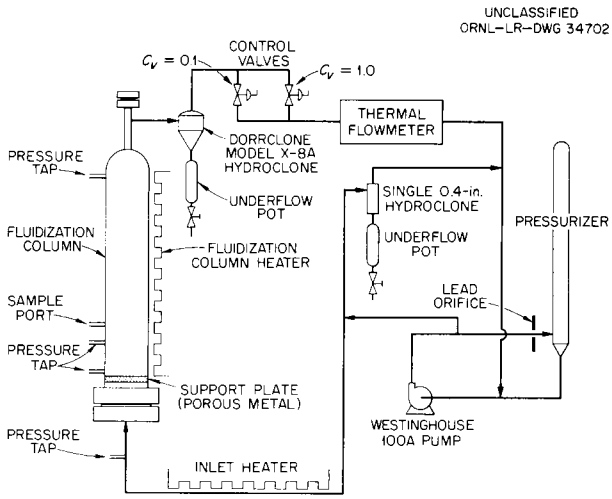

Fig. 11.6. High-Temperature Fluidization Equipment (T-Loop).

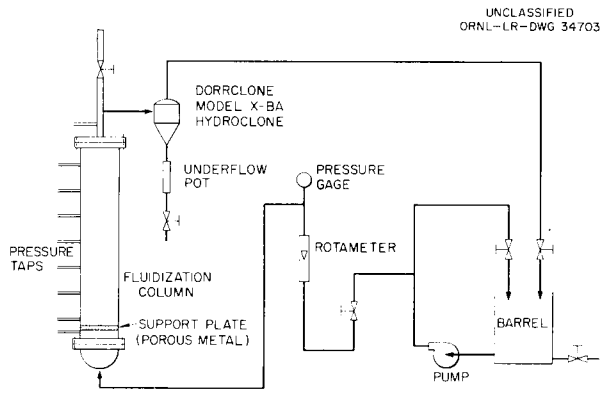

Fig. 11.7. Room-Temperature Fluidization Equipment.

spherical; (2) particle diameter, 10 to 70 μ; (3) particle density, 9.97 g/cc as determined by water displacement; (4) very little, if any, tendency to agglomerate.

The spheres, as received, were placed in the glass column, and the void (liquid) fraction vs the ratio of superficial velocity to settling velocity was measured. These data appear in Fig. 11.8, where V_{sf} = superficial velocity, V_t = Stokes free-settling velocity, and ϵ = void fraction. It is believed that the displacement of the experimental data from the line representing data from the literature is due to the nonuniform particle sizes of the thoria microspheres.

With the bed fluidized to a void fraction of 0.882, pressure-drop measurements were made for various increments of height along the length of the glass column. Since the pressure drops were due principally to the weight of the material being suspended, they can be converted to void fractions of liquid contained in the corresponding increment of column. This plot is shown in Fig. 11.9. The total weight of material in the various sections should equal the total weight of the original charge, and 92.7% of the original charge was accounted for by these measurements. It is believed that the discrepancy is due to incomplete fluidization of some of the largest particles. The density variation in the column was correlated with the mean particle size of samples taken at various levels through the bed.

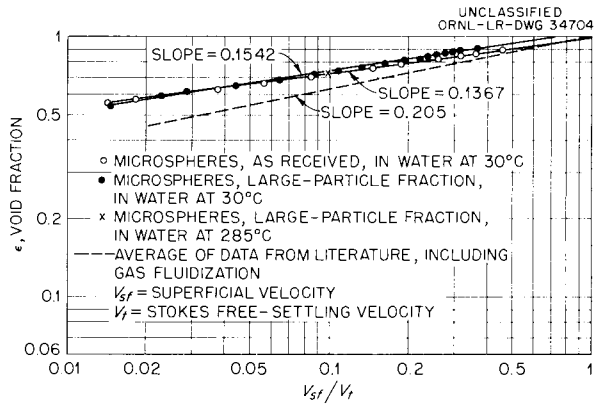

Fig. 11.8. Fluidization Characteristics of Thoria Microspheres.

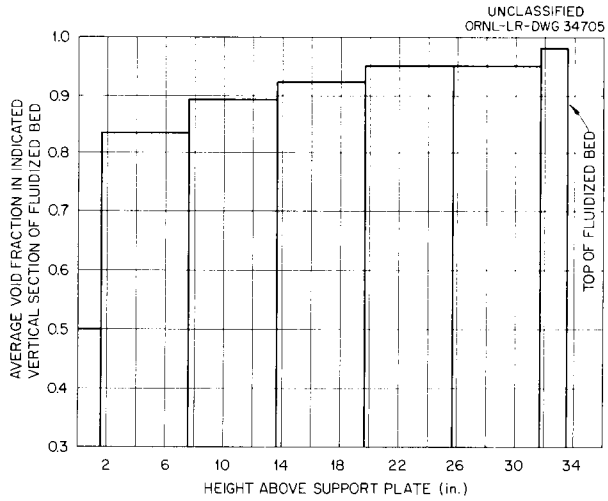

Fig. 11.9. Void-Fraction Distribution in a Fluidized Bed of Thoria Microspheres.

The results are presented in Fig. 11.10, where particle size is plotted against height above the support plate. The length of the vertical line indicates the range of particle sizes found in each sample, and the circle indicates the arithmetic average diameter of 12 randomly chosen particles.

At no time during the low-temperature experiment was there any indication of unstable flow. It was possible to get slugging in the fluidized bed only with radical changes of flow rate.

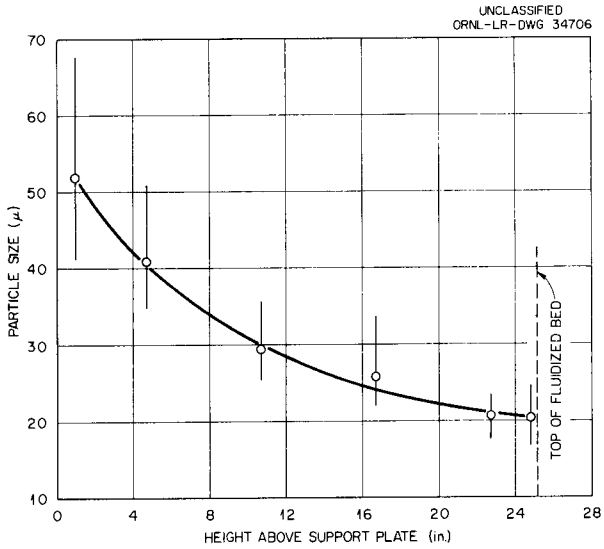

Fig. 11.10. Mean-Particle-Size Distribution in a Fluidized Bed of Thoria Microspheres.

The fluidized bed was used as a particle classifier to divide the original batch of spheres into two fractions, each with particles more uniformly sized than those in the original charge. The two fractions were removed from the column and dried, and representative samples were taken. The portion with the larger spheres was then placed back in the glass column, and void fraction vs superficial velocity data were determined. These data are shown in Fig. 11.8 as the "large particle fraction." The slope of the line was a little greater than the original slope, since the particles were more uniformly sized. This portion of larger particles was used in the high-temperature experiment.

The thoria microspheres were fluidized in the high-temperature system at 285°C for 264 hr. The run was terminated because of failure of the circulating-pump stator, which was not unexpected, as the cumulative operating time with this stator exceeded 10,000 hr. The entire 264-hr run, with the exception of startup and shutdown periods, was carried out with the bed fluidized to a void fraction ranging from 0.70 to 0.72. The void fraction was determined at one superficial velocity at 285°C; the value, plotted in Fig. 11.8, lies near the lines for measurements at 30°C. Measurement of the thoria-water interface with gamma-ray transmission equipment permitted calculation of the void fraction of liquid in the bed.

After the pump failure, all the microspheres were removed from the system for analysis. Figure 11.11 shows the particle-size analysis of the thoria before the run, after the run, and from the hydroclone underflow pot after the run. The measured attrition rate, which was determined from the amount of

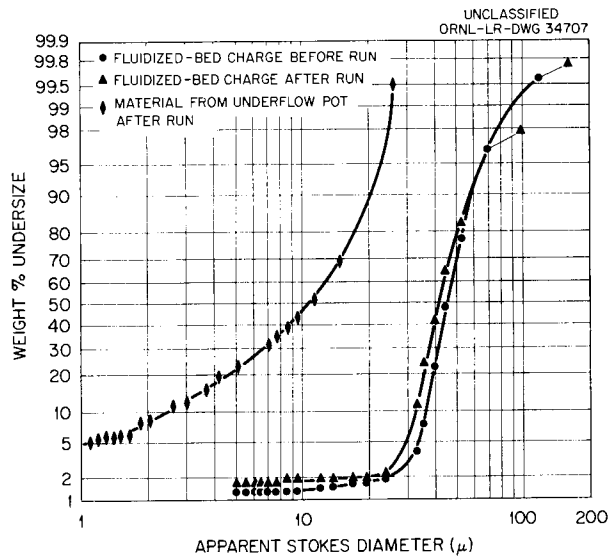

Fig. 11.11. Particle-Size Distribution Data Before and After Fluidization Run.

material collected in the underflow pot, was 0.26 wt % per day. Figure 11.12 shows photomicrographs of samples removed from the hydroclone underflow pot, the fluidized bed after the run, and the original charge to the fluidization column. The material from the underflow pot resembled small thoria spheres rather than fractured particles. It was also noted that little of the material from the fluidization column resembled fractured spheres. Many of the primary spheres of the original charge had one or more very small spheres attached to them. These smaller spheres were

UNCLASSIFIED
PHOTO 45831

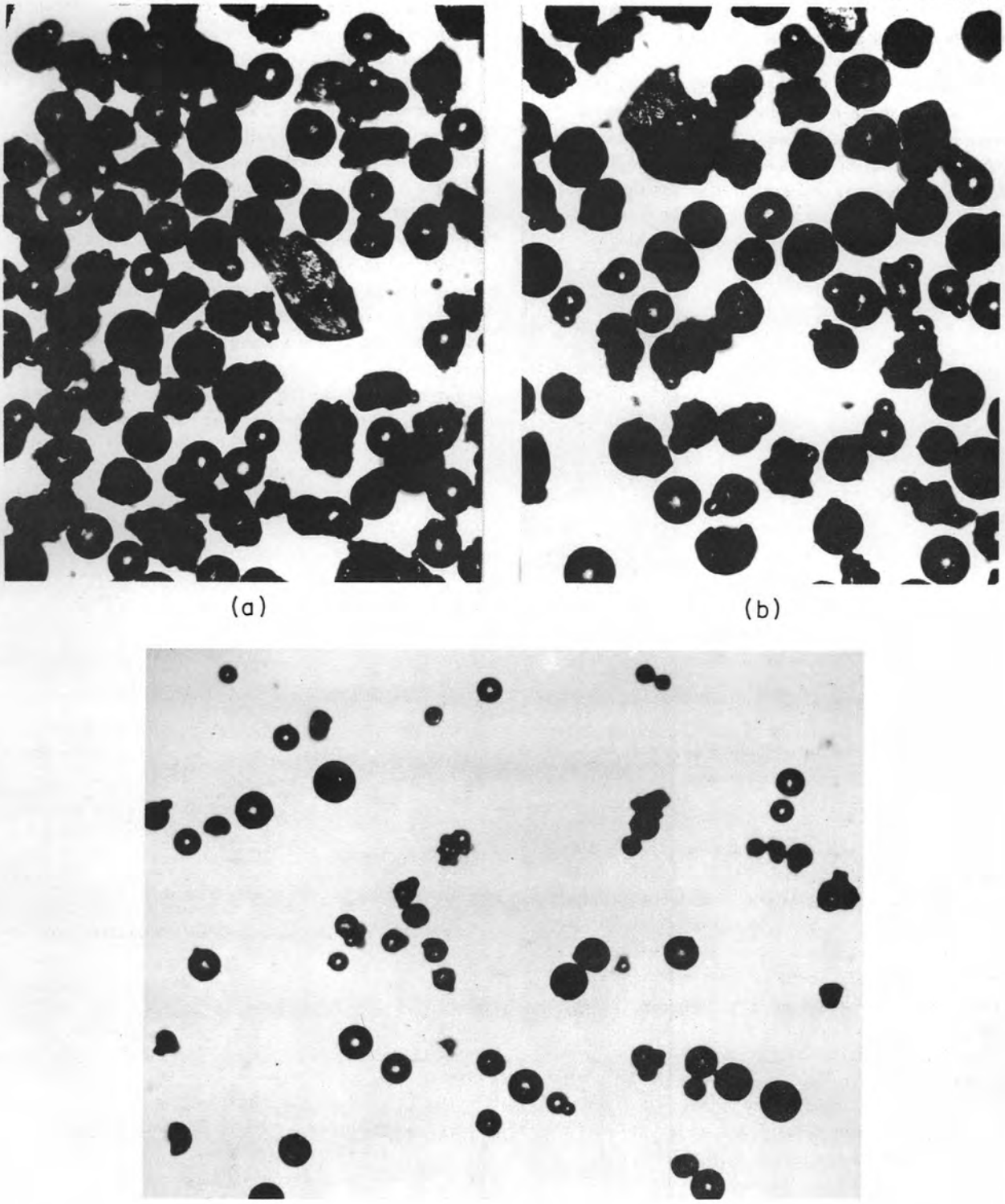

(a) (b) (c)

Fig. 11.12. Thoria Microspheres from Fluidized-Bed Test. 250X.

apparently attached by bonds of strength ranging from the forces involved in particle agglomeration to an actual fusion bond, and were probably a result of the manufacturing process. It is believed that the apparent attrition rate was a measure of the rate at which the more weakly bonded spheres were detached from the primary spheres. It is also believed that the measured attrition rate would be reduced greatly as the more weakly bonded spheres are selectively broken loose and carried from the fluidized bed.

During the run the thoria spheres turned a very light shade of brown because of corrosion products being deposited on the surface of the particles. Chemical analysis after the run showed an increased iron, nickel, and chromium concentration in the thoria.

11.2 BLANKET SYSTEM DEVELOPMENT

11.2.1 System Performance Data

During the report period, effort was concentrated on analysis of the data from the five blanket test runs completed during the past two years. A large mass of system and component performance data has been accumulated, and time has not previously been available to extract all the information of value from these data.

The slurry concentration sampling data accumulated during Run SM-5[5] were submitted to the Data Processing Facility at the Oak Ridge Gaseous Diffusion Plant for an analysis of variance. The data indicated that the circulating concentration was a function of both temperature (settling rate) and flow rate. The blanket data indicated the existence of vertical and radial concentration gradients and a tendency for the 12 locations under investigation to have preferentially high or low concentration.

Corrosion rates for the two stainless steel impellers were 40 mpy for the 4.31-in.-OD impeller used in runs SM-1 and -2[6] and 66 mpy for the 5.00-in.-OD impeller used in run SM-3.[7] These rates are roughly proportional to the flow rates developed by the impellers. The 5.00-in. titanium impeller used in run SM-4[8] had a corrosion rate of 6 mpy, and the Zircaloy impeller used in run SM-5 had a rate of 5 mpy. Severe lower-bearing wear was experienced when operating with the two stainless steel impellers; lower-bearing wear was negligible during the last two runs.

11.2.2 Conversion of 300-SM Loop to High-Pressure Operation

Fabrication of the 30-in.-dia experimental pressure vessel[9] is proceeding on schedule. The dump tank for the revised installation is ready for shipment; most of the other purchased components are on hand. Drawings were completed for the components to be fabricated at Oak Ridge. Piping drawings for the low-pressure system are 90% complete. Tests will be carried out on the dump tank while final installation of the high-pressure system is under way.

Plans to install gamma absorption equipment on the new pressure vessel have been delayed, and distribution of slurry within the pressure vessel will be determined by sampling. A continuous monitoring system is being developed for the various sample lines.

11.2.3 Pressure-Vessel Model Studies

In order to obtain slurry distribution data for establishing scaling relationships, a program of slurry flow and distribution studies in small models of the 30-in. pressure vessel was initiated. A 6-in. Lucite vessel (Fig. 11.13) is being used for initial studies. This model was set up for straight-through flow with a bottom inlet and a top outlet, both 0.305 in. in diameter.

Initially, attempts were made to measure the thorium distribution by use of a Co^{60} source and scintillation detection equipment. However, erratic results were obtained, and a check of the technique with $Th(NO_3)_4$ solution in the vessel showed that the precision of the measurements was unsatisfactory. Therefore the model was revised to provide sampling facilities for measurement of point concentrations. Visual observations during the scouting experiments undertaken

[5] R. B. Korsmeyer *et al.*, *HRP Prog. Rep. for Quarters Ending April 30 and July 31, 1958*, ORNL-2561, p 120.

[6] L. F. Parsly, Jr., H. L. Falkenberry, and I. M. Miller, *Report of Slurry Blanket Test Run SM-2*, ORNL CF-57-4-87 (April 29, 1957).

[7] L. F. Parsly, Jr., *Report of Slurry Blanket Test Run SM-3*, ORNL CF-57-10-2 (Oct. 15, 1957).

[8] R. B. Korsmeyer *et al.*, *HRP Quar. Prog. Rep. Jan. 31, 1958*, ORNL-2493, p 75.

[9] R. B. Korsmeyer *et al.*, *HRP Prog. Rep. for Quarters Ending April 30 and July 31, 1958*, ORNL-2561, p 126–27.

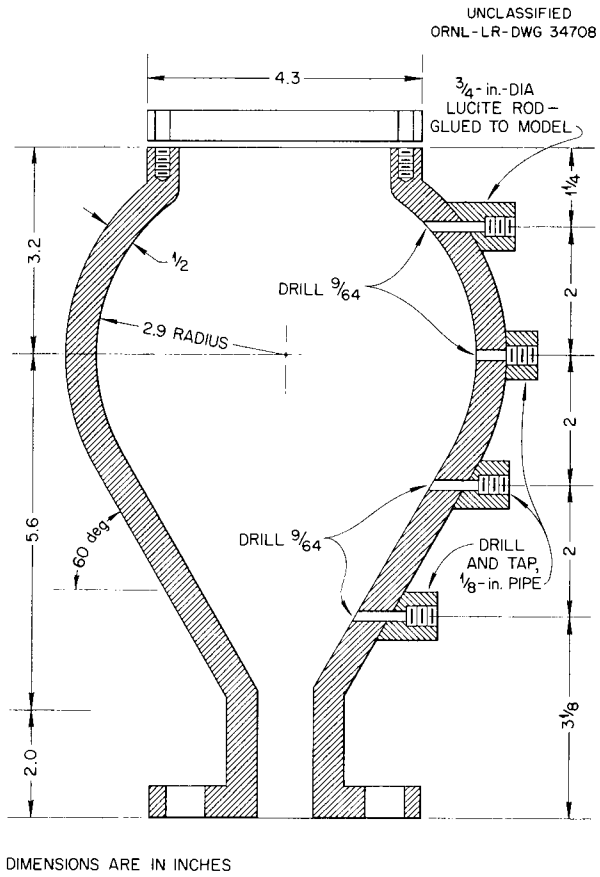

Fig. 11.13. Lucite Model for Slurry Distribution Studies.

so far have indicated a region of high concentration along the vessel wall between the inlet and the equator.

A similar vessel with a 15-in. diameter is being designed. Results on the 6- and 15-in. models at room temperature in conjunction with tests on the 30-in. vessel over the range from room temperature to 300°C should provide the data needed to obtain the desired scaling relationships.

11.2.4 Development of Gamma-Transmission Density Measurements

Experiments were performed on adapting a commercial gamma density meter for use in continuously monitoring slurry samples withdrawn from the 30-in. high-pressure vessel. It was decided rather arbitrarily that no sample should exceed 1 gpm (0.3% of nominal flow). On this basis, the sample tube size was limited to ½ in. in outside diameter in order to maintain a reasonable velocity in the sample tube. The manufacturers of the commercial equipment[10] indicated that satisfactory precision cannot be obtained on pipes smaller than 1-in. IPS, and efforts to make measurements by scanning across small tubes confirmed this information. In order to provide greater sample thickness and thus to increase the change in signal intensity with changing density, the arrangement shown in Fig. 11.14 was investigated. A 6-in. length of ½-in. tubing was

[10] P. E. Ohmart and H. L. Cook, Jr., *Instrument Society of America, First International Congress and Exposition, September 1954*, vol 9, Part 2, paper 54-22-1.

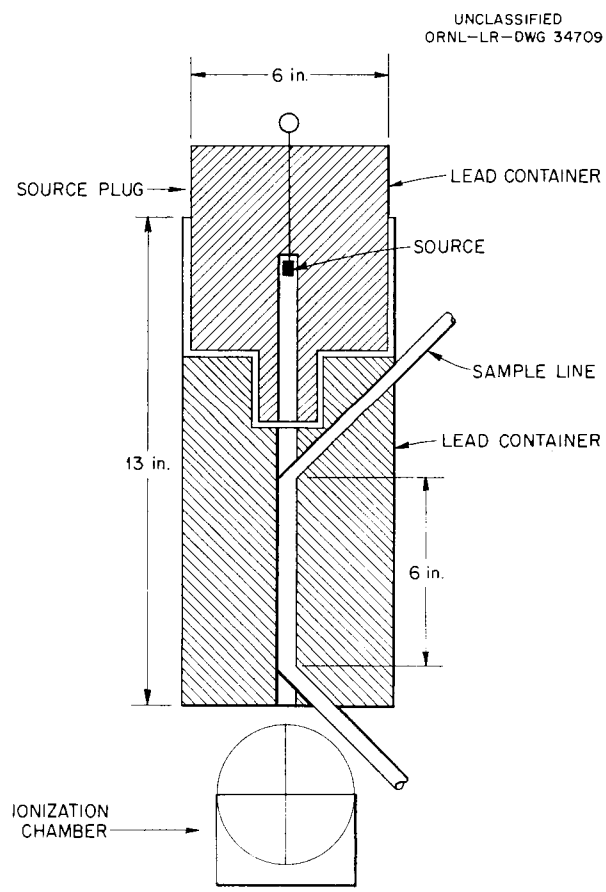

Fig. 11.14. Gamma-Ray Densitometer Equipment.

scanned axially with a 5-curie Cs^{137} source and an ionization chamber coupled to a micromicroammeter as the detector. Zero suppression was supplied by a stable battery. The precision achieved was better than that required for the high-pressure slurry distribution studies. Response to density changes was practically instantaneous, and the instrument signal remained stable over periods of several days.

The possibility of using smaller diameter tubes was investigated, and it was established that the ½-in. size is probably the minimum diameter permissible. With smaller tubes the ion current was reduced to the point where the signal-to-noise ratio became quite low and high precision was not obtainable.

12. INSTRUMENT AND VALVE DEVELOPMENT

D. S. Toomb

A. M. Billings R. L. Moore
E. H. Bell J. L. Redford
H. D. Wills

12.1 INSTRUMENT DEVELOPMENT

12.1.1 Flush-Diaphragm Differential-Pressure Transmitter

To avoid the possible plugging of lines to differential-pressure transmitters connected to HRP slurry systems, a transmitter based on the conceptual design illustrated in a previous report[1] is being constructed by The Foxboro Company on a best-effort basis. The prototype transmitter illustrated in Fig. 12.1 has a diaphragm flush with the slurry-vessel wall to avoid plugging. The diaphragm is mechanically coupled by a rod to range springs and the ferrite core of a differential transformer. The core motion is sensed through a pressure housing to provide a well-sealed design. The back side of the diaphragm will be connected to the vapor space of a reference-pressure system or to a constant gas pressure.

12.1.2 Heated-Thermocouple-Probe Liquid-Level Sensor

A special adapter was designed which allows greater flexibility in the application of the heated-thermocouple-probe liquid-level sensor described earlier.[2] The adapter, which can also be used with sheathed thermocouples, is illustrated in Fig. 12.2. The adapter is designed around high-pressure compression fittings (Autoclave Engineers) and eliminates the difficult weld between the thin-walled probe sheath and the massive vessel wall found in the earlier design. The new design permits easy replacement of a failed unit and facilitates adjustment of the depth of insertion of the probe.

12.1.3 Liquid-Level Alarm Transmitter

The measurement of liquid level in HRP high-pressure systems is necessary to indicate or control the vapor-liquid interface in process vessels. The liquid phase in such a system may be uranyl sulfate, thorium oxide slurry, or water. Instruments now used for this application include differential-pressure transmitters, which lack the desired sensitivity, and displacement-type transmitters, which are undesirably complex.

A commercially available Copes-Vulcan[3] boiler-water-level alarm transmitter was tested to determine its suitability for these measurements.[4] The instrument, illustrated in Fig. 12.3, develops a signal-producing motion from differential expansions caused by the difference in heat loss from the liquid and vapor sections of the measuring tube. Since the part of the tube which contains steam attains saturation temperature while the part of the tube which contains water operates at a lower temperature, a temperature gradient is established which produces sufficient motion when multiplied by a lever mechanism to operate alarm switches for high and low water-level conditions.

Performance tests on the loop pressurizer shown in Fig. 12.4, which also illustrates the alarm transmitter, indicated that the steady-state temperature of the tubes containing steam was within 2°C of the saturation temperature at 1200 psi, while the tubes containing condensate operated at 65 to 95°C above the room ambient temperature of 25°C. The motion produced by the switch arms was approximately 0.050 in., and the time of response to a level change was between 1 and 2 min.

The instrument has the advantages, for HRP applications, of incorporating no thin-walled members and of being completely weld-sealed. It has the disadvantages of slow response, of being difficult to adjust remotely, and of insensitivity when the process vessel is at or near room temperature.

---

[1] D. S. Toomb *et al.*, *HRP Quar. Prog. Rep. Oct. 31, 1957*, ORNL-2432, p 72.

[2] D. S. Toomb *et al.*, *HRP Prog. Rep. for Quarters Ending April 30 and July 31, 1958*, ORNL-2561, p 130.

[3] Copes-Vulcan Division of Blaw-Knox Company, 936 West 26th Street, Erie 4, Pa.

[4] H. D. Wills, *Performance Test of a Boiler Water-Level Alarm*, ORNL CF-58-6-28 (June 10, 1958).

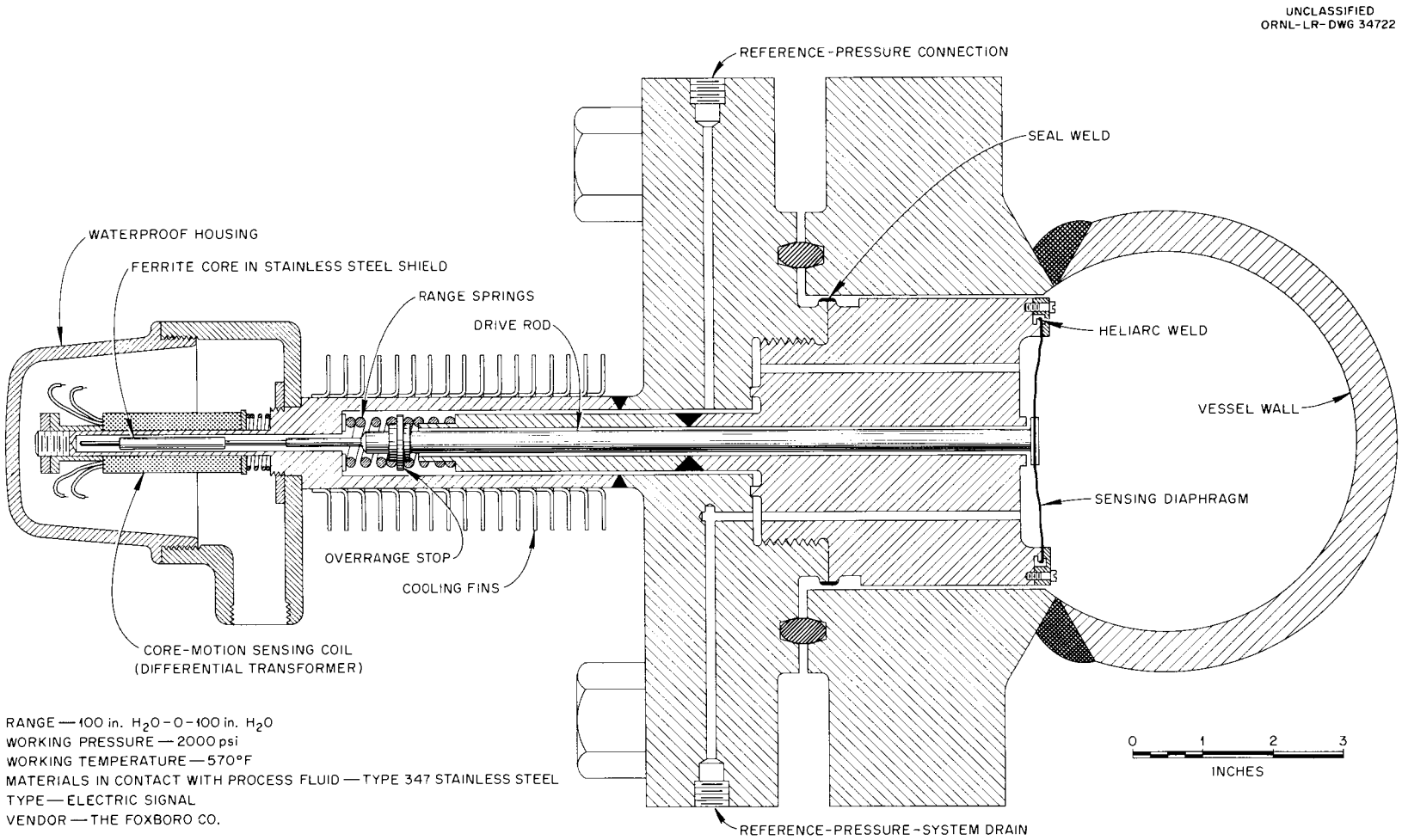

Fig. 12.1. Flush-Diaphragm Differential-Pressure Transmitter.

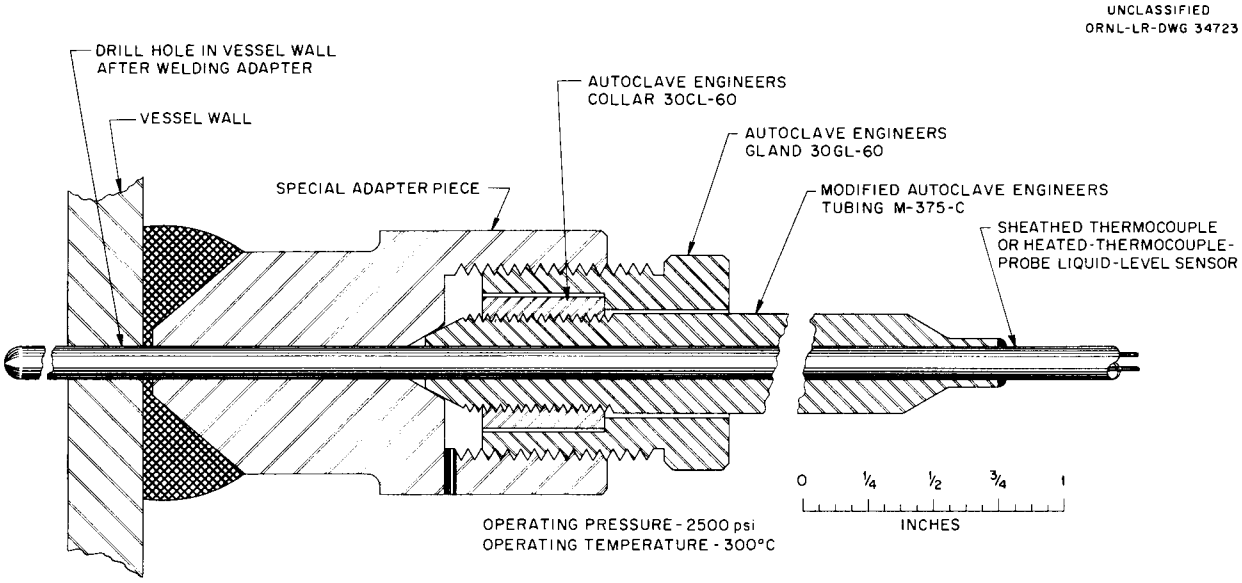

Fig. 12.2. Mounting Adapter for Sheathed Thermocouples or Heated-Thermocouple-Probe Liquid-Level Sensors.

12.1.4 Capacitance-Type Liquid-Level Measuring System

A commercial capacitance-type liquid-level measuring system was tested[5] to determine the suitability of this kind of instrument for HRP liquid-level applications. The sensing element, illustrated in Fig. 12.5, consists of an electrode made of $\frac{3}{8}$-in.-OD stainless steel rod covered with a $\frac{5}{8}$-in.-OD Kel-F insulator and sealed in a 1-in. sched-80 stainless steel pipe by a Nylon-Teflon compression seal. The entire assembly forms a 21-in.-long coaxial condenser whose capacitance varies with the height of the liquid-level column in the annulus between the stainless steel wall and the Kel-F electrode insulator.

The probe forms one leg of a capacitance bridge supplied by a 30-kc/sec oscillator. As the liquid level in the sensing element is changed, the capacitance-bridge circuit is unbalanced; the resultant signal is amplified and rectified and is displayed on a microammeter.

The tests indicate that the measurement is nonlinear for the first 7 in. of the 21-in. range and that there is a short-term hysteresis error of 5% of full scale due to water adhering to the electrodes and insulators. Increasing pressure caused a positive change in output at all levels and resulted in an error of $3\frac{1}{2}$% of full scale at 2000 psi for a liquid level of 20% of full scale. The error increases with decreasing liquid level in the measuring element.

The instrument was also tested on a thorium oxide slurry with a composition of approximately 1000 g of Th per liter. The result was a difference of output signal at full level of 3% from that obtained with water.

12.2 VALVE DEVELOPMENT

12.2.1 Solution Sampling Valve

General-purpose sampling valves for solution service were procured from the Fulton Sylphon Division, Robertshaw-Fulton Controls Company. The valve shown in Fig. 12.6 was designed to ORNL specifications with a replaceable plug and seat. The bellows assembly may be sealed with a full-penetration weld, or with a metal gasket for more flexibility in less critical applications. A variety of plug contours are available to achieve different full-stroke flow rates; the maximum flow is determined by the $\frac{1}{4}$-in.-bore seat. A fluorothene resilient plug-insert is also available for low-temperature applications requiring extremely tight shutoff.

[5] J. L. Redford, *Performance Test of "Jarco" Liquid-Level Indicating System*, ORNL CF-58-5-91 (May 19, 1958).

UNCLASSIFIED
ORNL-LR-DWG 28207

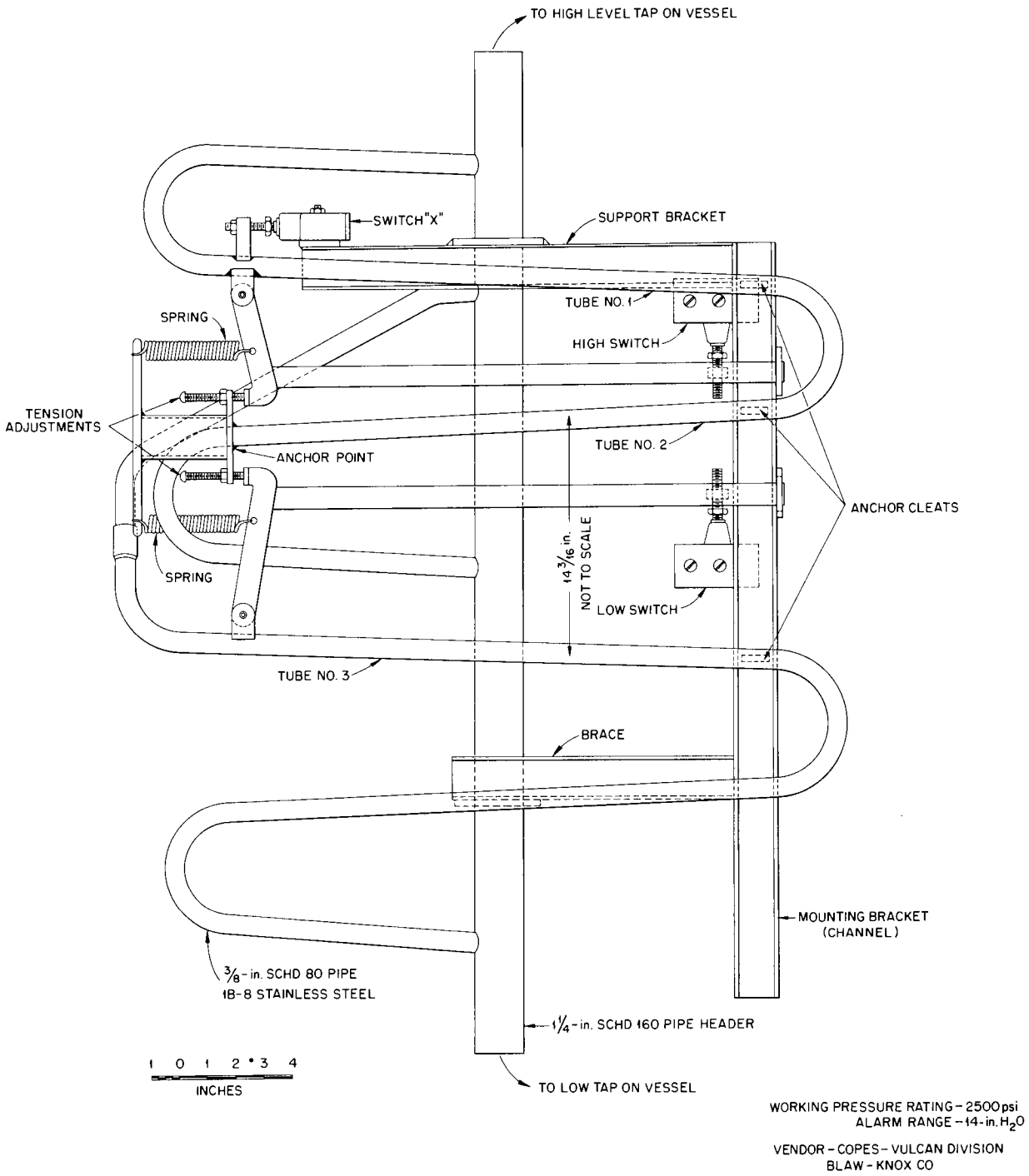

Fig. 12.3. Liquid-Level Alarm Transmitter.

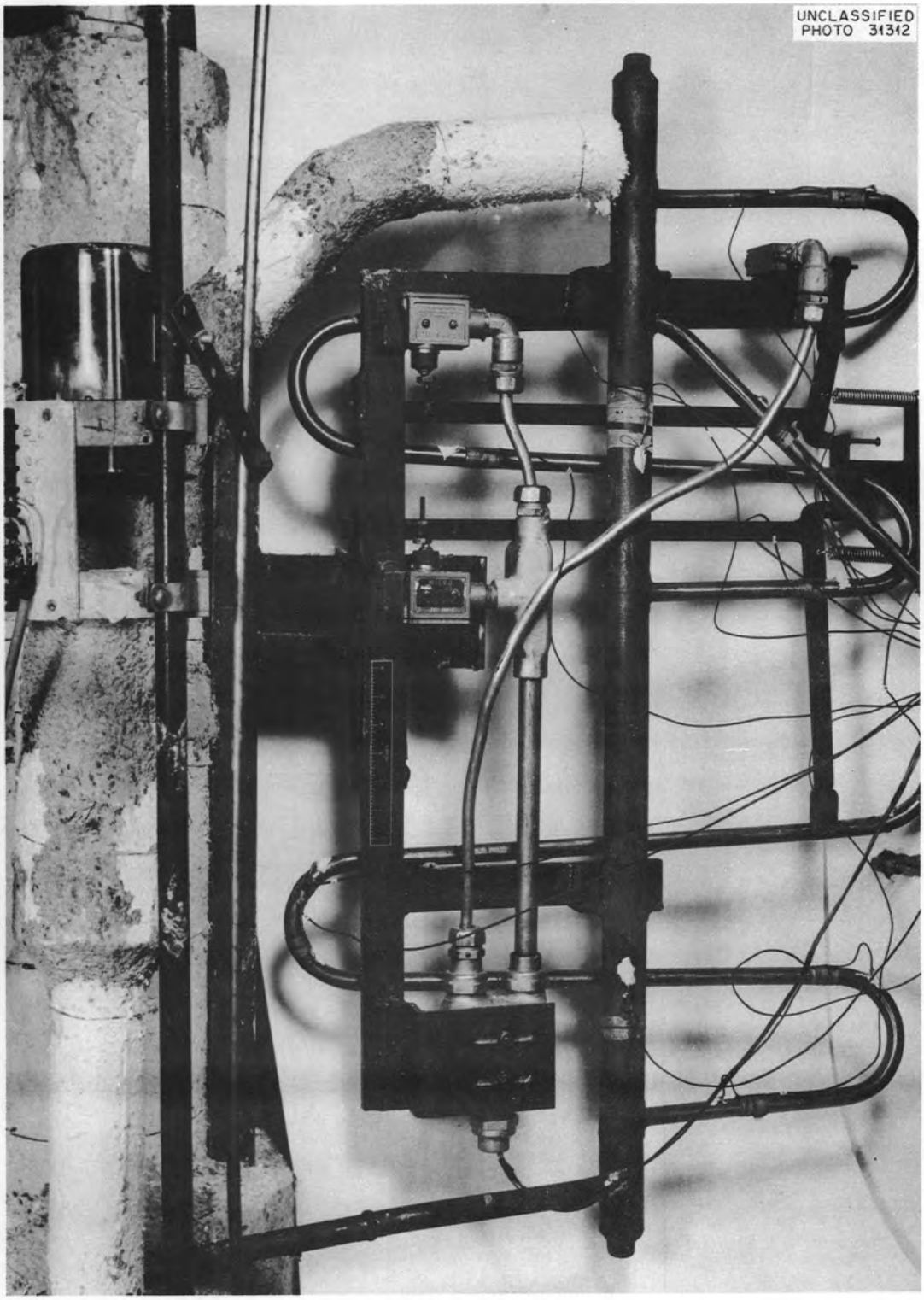

Fig. 12.4. Test Stand for Liquid-Level Alarm Transmitter.

UNCLASSIFIED
ORNL-LR-DWG 30072R

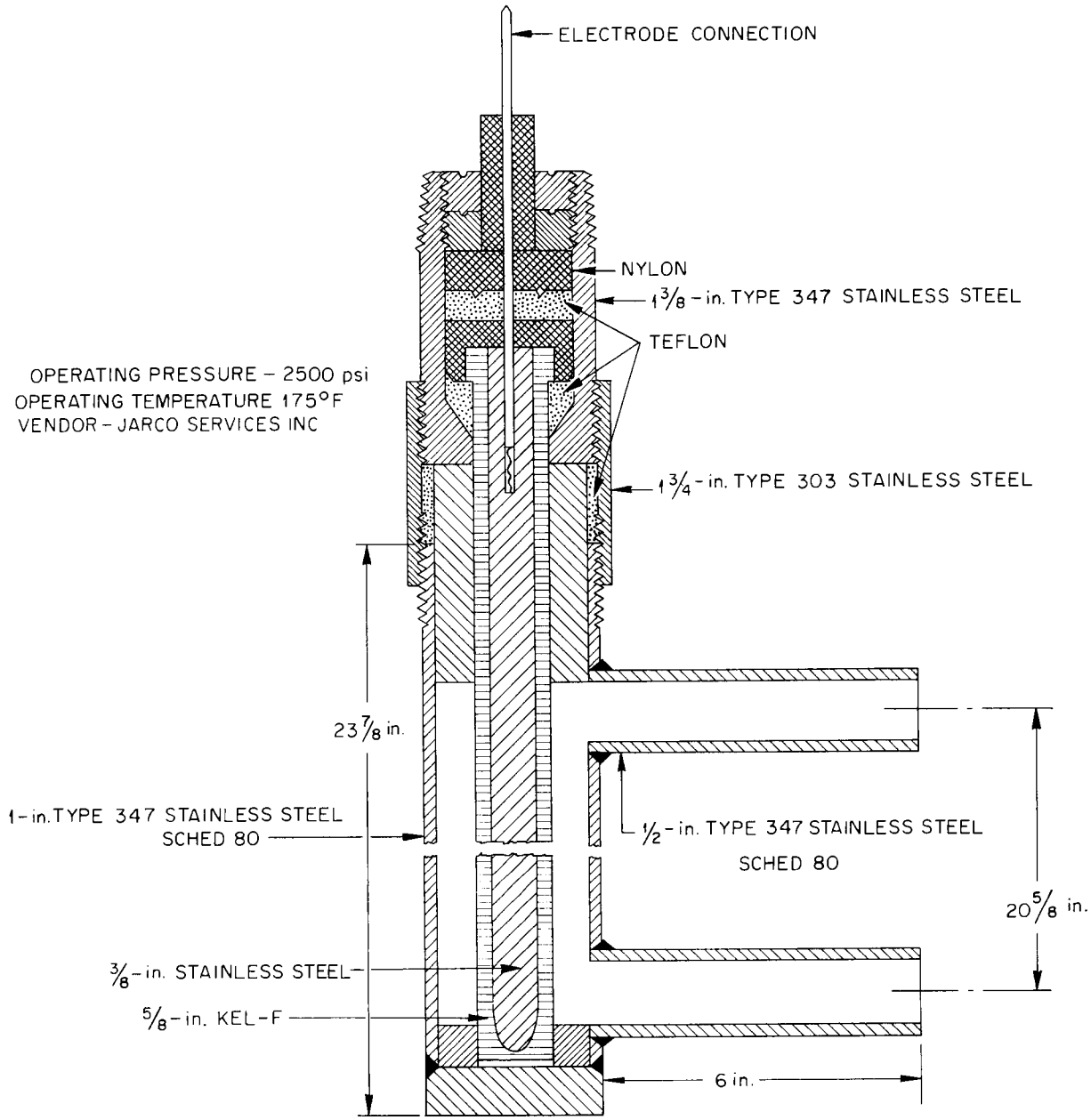

Fig. 12.5. Capacitance-Type Liquid-Level Sensing Element.

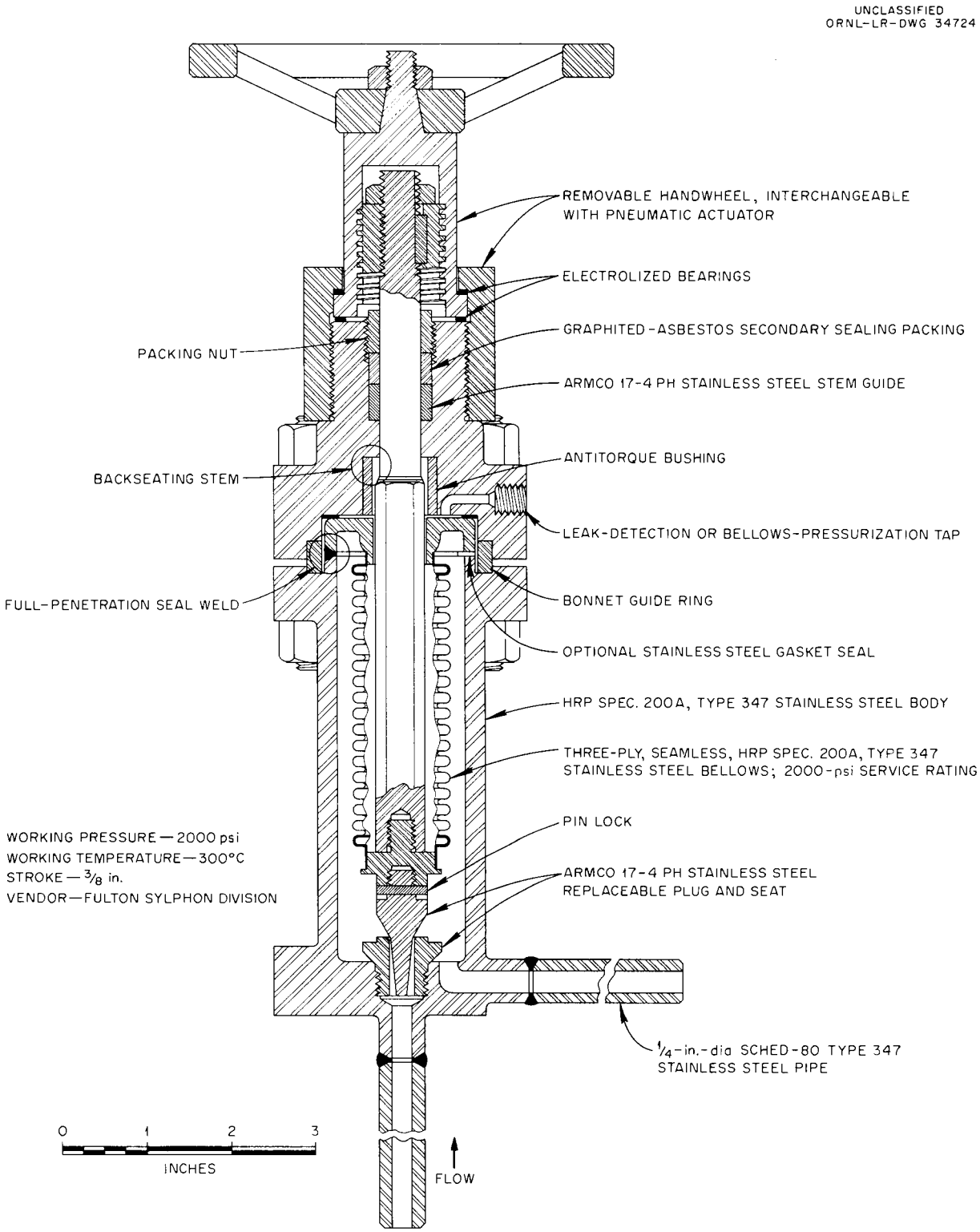

Fig. 12.6. Solution Sampling Valve.

A removable handwheel actuator is provided. However, a pneumatic actuator may be substituted without removing or interchanging any other parts. The all-metal 40-in.^{2} reversible-action actuator described in a previous report[6] is designed for easy mounting on this valve.

12.2.2 Valve Actuators

The control-valve actuating system using 500-psi water as the working fluid failed by a fatigue rupture of the cylinder wall after 86,715 cycles. The 10-in. I-beams used as a cylinder loading spring introduce a side load when sprung, which may have hastened the failure. However, performance of this system was considered to be very good. Figure 12.7 shows the test stand, which includes the cylinder, cylinder loading beams, water pump, hydraulic pilot valve, and electric control for the hydraulic pilot system.

The hydraulic cylinder utilized for shakedown operation is shown in Fig. 12.8. Cylinders with all-metal seals for highly radioactive environments are being developed.

12.2.3 Remotely Actuable Air-Line Disconnect

To facilitate the removal of pneumatically actuated reactor control valves for maintenance, a remotely disconnectable coupling is required for the air supply and exhaust lines. The experimental disconnect illustrated in Fig. 12.9 was designed for this application and is now being fabricated. The clamping air pressure acting on the actuating bellows holds the coupling closed. Release of this pressure causes the coupling to break, and the built-in check valve blocks the supply air line.

[6]D. S. Toomb *et al.*, *HRP Prog. Rep. for Quarters Ending April 30 and July 31, 1958*, ORNL-2561, p 134.

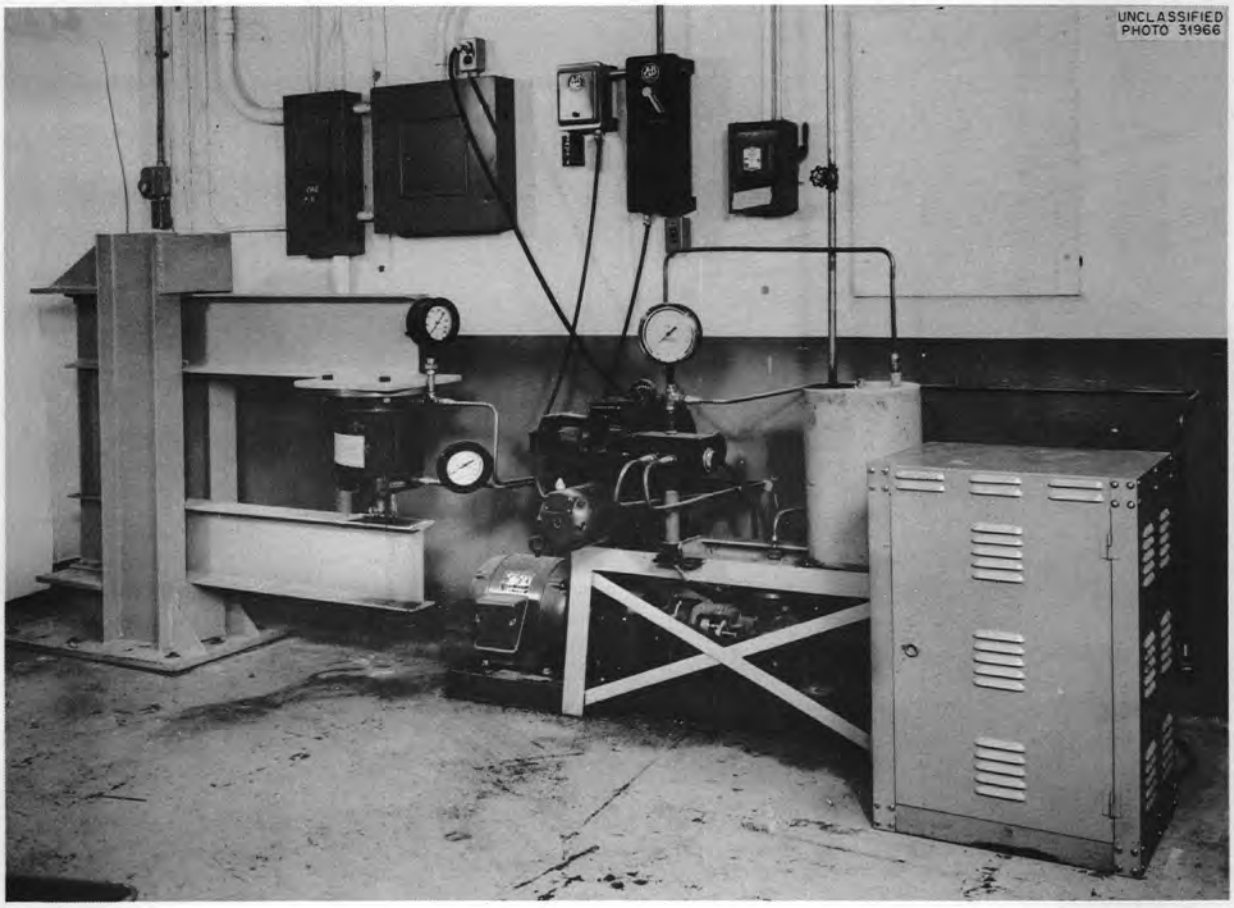

Fig. 12.7. Test Stand for Hydraulic Control-Valve Actuator.

UNCLASSIFIED
ORNL-LR-DWG 34725

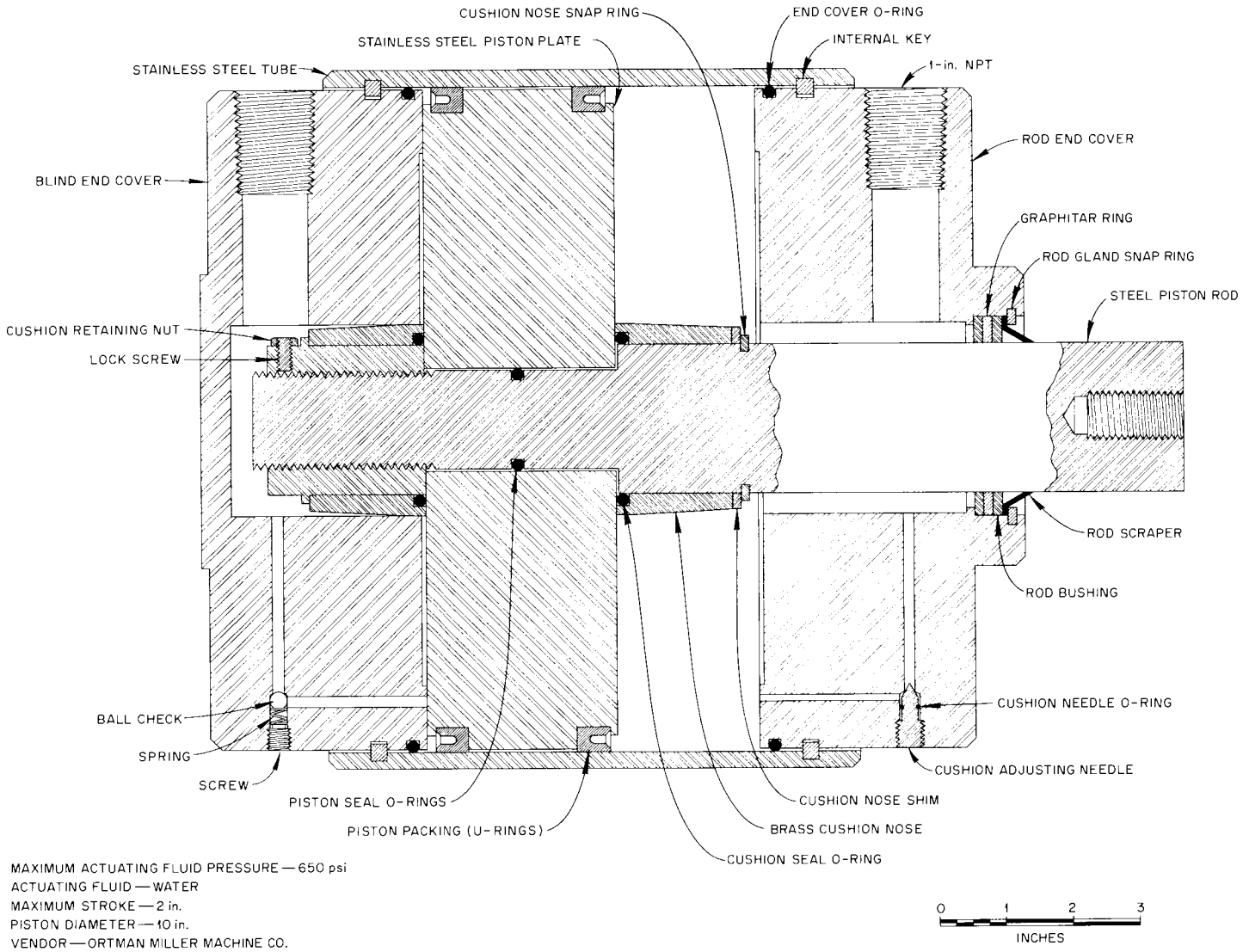

MAXIMUM ACTUATING FLUID PRESSURE — 650 psi
ACTUATING FLUID — WATER
MAXIMUM STROKE — 2 in.
PISTON DIAMETER — 10 in.
VENDOR — ORTMAN MILLER MACHINE CO.

Fig. 12.8. Hydraulic Cylinder for Control-Valve Actuator.

12.2.4 Slurry Service Valves

A chromium carbide valve plug and seat – installed as a replacement for the tungsten carbide trim set which failed earlier in the flow-control valve installed on the 30-gpm slurry test loop[7] – was replaced after 300 hr of operation, because of scale buildup which caused the plug to freeze in its guide. The chrome carbide trim was replaced with a Zircaloy plug and seat, and the tungsten carbide plug guide was replaced with one machined from type 17-4 PH stainless steel. This third trim set is still operating satisfactorily after 800 hr.

[7] *Ibid.*, p 138.

UNCLASSIFIED
ORNL-LR-DWG 34726

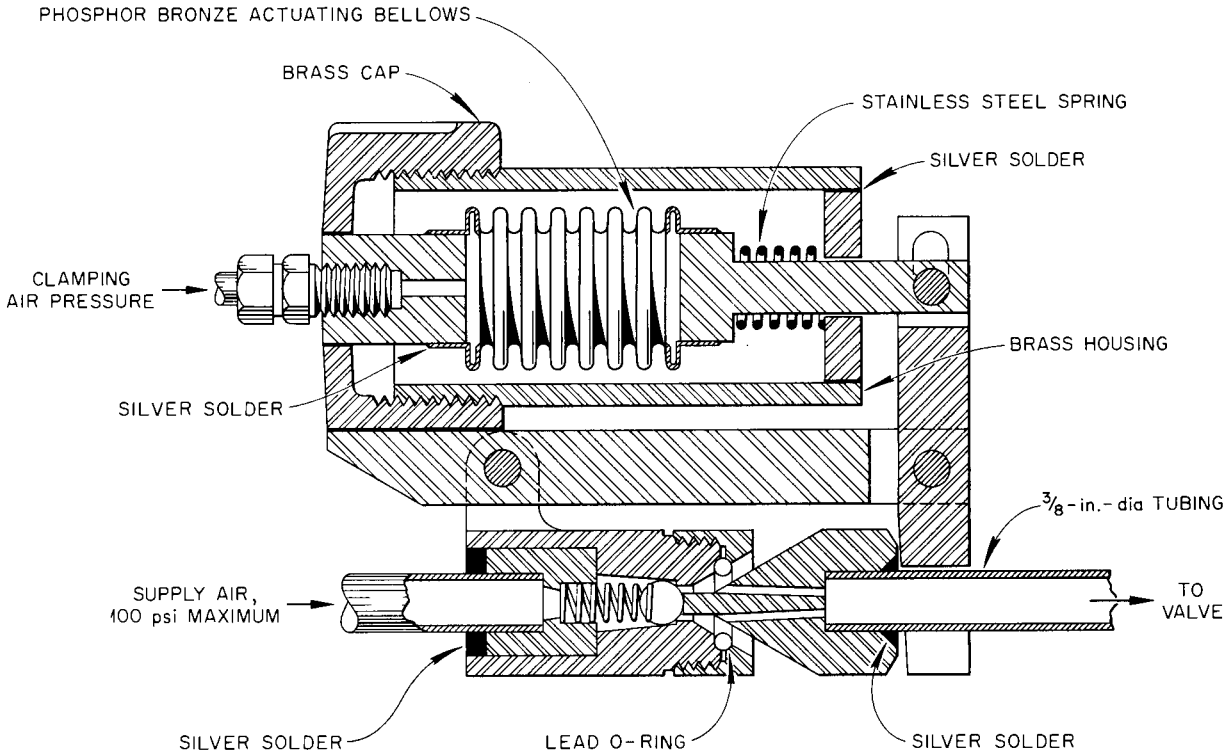

Fig. 12.9. Experimental Remotely Actuable Air-Line Disconnect.

Part IV

REACTOR MATERIALS RESEARCH

E. G. Bohlmann

13. SOLUTION CORROSION[1]

J. C. Griess H. C. Savage
S. E. Bolt D. N. Hess
S. R. Buxton P. D. Neumann
J. L. English E. S. Snavely
R. S. Greeley W. C. Ulrich
N. E. Wisdom[2]

13.1 DYNAMIC SOLUTION CORROSION

13.1.1 Instability of Dilute Uranyl Sulfate Solutions in a Heated Bypass Section

Several experiments have been performed to study the stability of a solution of uranyl sulfate similar to that used in HRT run 17, namely, 0.025 *m* UO_2SO_4, 0.014 *m* D_2SO_4, 0.011 *m* $CuSO_4$, and 0.0036 *m* $NiSO_4$ in heavy water, when circulated in a system having a small heated region. The experimental conditions were chosen to approximate those that existed in the Zircaloy-2 core tank of the HRT during power operation. A titanium loop was used which was equipped with a heated Zircaloy-2 bypass through which flow of solution could be varied by varying the frequency of power supplied to the pump. Heat was supplied to the bypass from five, 1-kw Calrod units equally spaced around the Zircaloy-2 pipe, the assembly being cast in aluminum.

As shown in Fig. 13.1, the solution was stable when circulated in the loop under isothermal conditions at 280°C. With the flow rate through the bypass at 0.2 fps and the system pressurized to 1750 psi with oxygen, application of sufficient heat to the bypass to raise the temperature of the solution emerging from the bypass to 320°C caused an immediate decrease in concentration of all salts in the circulating solution, as shown by samples taken from the main line where a temperature of 280°C prevailed. There was very little change in the acid concentration of the main circulating stream. When about two-thirds of the uranium had been removed from the solution, flow through the bypass was increased to 0.6 fps, and the concentrations of the solution components returned rapidly to normal values.

Similar behavior was observed when the temperature of the solution emerging from the bypass was maintained at 310 and 300°C, although the rate of loss of solution components was somewhat slower at the lower temperature. In all cases, increasing the flow rate through the bypass returned concentrations to normal values. The irregularities in the curves at 300°C (Fig. 13.1) are unexplained.

When the loss of components was at a maximum during the 300°C run, the bypass was isolated by valves at its extremities, and the contained solution was removed and analyzed. The results of the analysis showed that all components lost from the solution were in the bypass section. In addition, the solution removed from the bypass contained a considerable quantity of zirconium dioxide, indicating a higher corrosion rate than had ever been observed out of pile.

Another run was made with a solution of the same composition. In this case the temperature of the solution in the main circulating stream was 250°C, and the temperature of the solution leaving the bypass was 287 to 290°C. The total pressure on the system (oxygen and steam) was 1400 to 1500 psi. Under the above conditions uranium, copper, and nickel sulfates were lost from solution in a manner similar to that shown in Fig. 13.1. A loss of heater power caused the loop and bypass temperature to decrease to 215°C and resulted in the composition of the solution returning to its original value.

A subsequent run showed that the solution used in the above experiments was stable when circulated isothermally at 320°C. Hence the loss of uranyl, copper, and nickel sulfates indicates either that the wall temperature of the heated bypass was above the second-liquid phase temperature, 334 to 336°C for the solution used, or that boiling resulted in crystallization of the salts on the wall. Experiments are in progress to determine which occurred.

---

[1]Reported in greater detail by J. C. Griess *et al.*, *Quarterly Report of the Solution Corrosion Group for the Period Ending October 31, 1958*, ORNL CF-58-10-95 (to be issued).

[2]Summer employee.

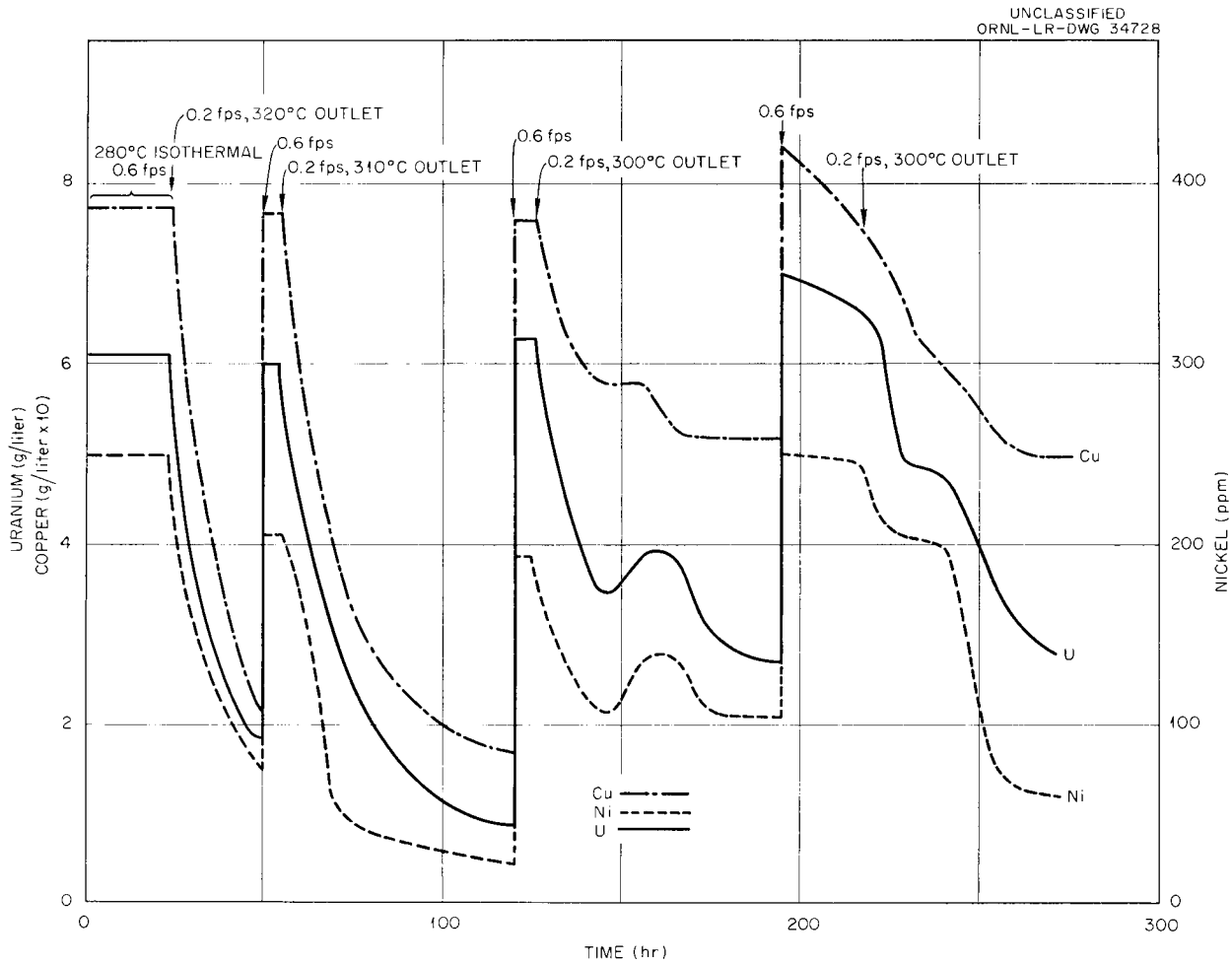

Fig. 13.1. Changes in Concentrations of Various Ions in Solution Circulated in a Titanium Loop with a Heated Zircaloy Bypass.

13.1.2 Stability of Dilute Uranyl Sulfate Solutions Containing Alkali or Alkoline-Earth Sulfates

To complete the survey of effects of alkali and alkaline-earth sulfates on the stability and corrosivity of simulated HRT fuel solutions, two loop runs were made to determine the effects of sodium and potassium sulfate additions. Previous studies in which additions of lithium, rubidium, magnesium, or beryllium sulfates were made have been reported.[3] Either 0.04 *m* Na_2SO_4 or 0.04 *m* K_2SO_4 was added to a solution containing 0.04 *m* UO_2SO_4, 0.025 *m* D_2SO_4, and 0.03 *m* $CuSO_4$ in heavy water, and the resulting solution was circulated at 300°C for 200 hr. The results of the two runs showed that in each case about 30% of the copper was lost from solution during the 200-hr run, but in neither case was a detectable amount of uranium lost from solution. In both cases the corrosion of stainless steel was less than in a similar solution without the added sulfate salts.

The study of the stability and corrosivity of 0.04 *m* UO_2SO_4 solutions containing 0.025 *m* D_2SO_4, 0.03 *m* $CuSO_4$, and 0.04 *m* alkali or alkaline-earth sulfate in heavy water at 300°C was completed. The solutions containing lithium, sodium, potassium, and rubidium sulfates were not stable; in all

[3] J. C. Griess *et al.*, *HRP Prog. Rep. for Quarters Ending April 30 and July 31, 1958*, ORNL-2561, p 148.

cases copper was lost from solution, and on occassion, with some of the sulfate salts, solids which contained small amounts of uranium were found. In all cases, however, the solutions were less corrosive to stainless steel than were similar solutions without the sulfate additions. Solutions containing 0.04 *m* $BeSO_4$ or 0.04 *m* $MgSO_4$ were stable under the conditions of test. The solution containing beryllium was more corrosive than a similar solution without beryllium sulfate. The magnesium-containing solution was less corrosive than a similar solution without magnesium sulfate. Based on the above series of tests, the only solution which was completely stable and which was less corrosive than the simple fuel solution was the one containing magnesium sulfate. Therefore, further tests are being conducted with it.

Undoubtedly, all the other solutions could be stablized by increasing the acid concentration, but a higher acid concentration would increase the out-of-pile corrosivity of the solution to stainless steel. It has been shown, however, that relatively high concentrations of acid and sulfate salts in uranyl sulfate solutions suppress in-pile corrosion of zirconium.[4]

13.1.3 Oxidation of Chromium(III) in Uranyl Sulfate Solutions in the Presence of Ruthenium

It has been reported that the addition of a ruthenium salt to oxygenated uranyl sulfate solutions being circulated at high temperature in stainless steel loops causes an increase in the rate at which chromium(VI) forms.[5]

Several loop runs were carried out to determine the rate at which the oxidation occurs. In each case a 0.04 *m* UO_2SO_4 solution containing 0.025 *m* H_2SO_4 and 0.03 *m* $CuSO_4$ was heated in a stainless steel loop. After the desired temperature was attained, a sufficient quantity of a concentrated solution of chromic sulfate and ruthenium chloride was added to produce a loop concentration of approximately 500 ppm chromium and 25 ppm ruthenium. Samples were then withdrawn and analyzed to determine the rate at which chromium(VI) was being formed.

Figure 13.2 shows the temperatures and oxygen concentrations investigated and the results obtained. Values on the ordinate are plotted as $C_t - C_0$, where C_t is the concentration of chromium(VI) at a given time and C_0 is the concentration of chromium(VI) when the chromic sulfate and ruthenium chloride were added to the loop. Not shown on the graph is the result of a run made at 300°C with 800 ppm oxygen. Under these conditions the rate of oxidation was so fast that by the time the first sample was obtained all the added chromic sulfate had been oxidized to the hexavalent state.

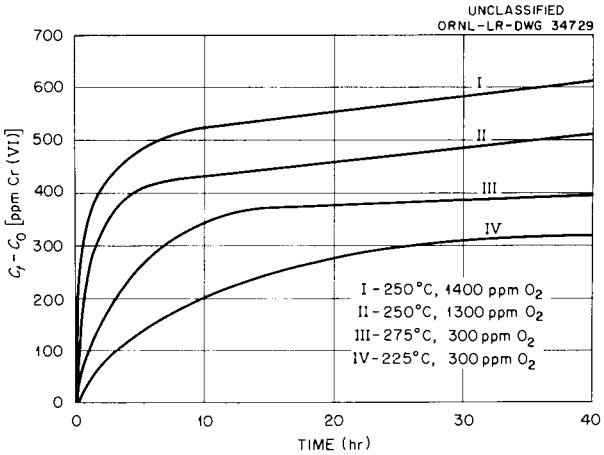

Fig. 13.2. Rate of Oxidation of Cr(III) to Cr(VI) in 0.17 *m* UO_2SO_4 Containing 25 ppm Ruthenium.

The data clearly show that ruthenium catalyzes the formation of chromium(VI), which effectively inhibits corrosion of stainless steel and increases the critical velocity out of pile. Whether or not the addition of ruthenium to in-pile solutions will result in a steady-state chromium(VI) concentration which similarly inhibits corrosion remains to be demonstrated.

13.1.4 Effect of Cold Work and Heat Treatment on the Corrosion of Type 347 Stainless Steel

Several previous investigations of the effect of metallurgical variables on the corrosion of type 347 stainless steel have been made. These showed that an anneal at 1950°F was beneficial but that heat treatment at 2200 to 2300°F was deleterious.[6,7]

[4] G. H. Jenks *et al.*, *HRP Prog. Rep. for Quarters Ending April 30 and July 31, 1958*, ORNL-2561, p 202.

[5] J. C. Griess *et al.*, *HRP Prog. Rep. for Quarters Ending April 30 and July 31, 1958*, ORNL-2561, p 152.

[6] J. C. Griess *et al.*, *Solution Corrosion Group Quarterly Report for the Period Ending April 30, 1956*, ORNL CF-56-4-138, p 25.

[7] J. C. Griess *et al.*, *HRP Quar. Prog. Rep. July 31, 1957*, ORNL-2379, p 73–75.

However, other variables, such as prior cold work, cooling rates, chemical composition, and annealing atmosphere were not completely controlled. Therefore a further investigation was made in which were observed the effects of cold work and subsequent heat treatment on the corrosion behavior of type 347 stainless steel that was otherwise treated identically.

From a single heat of steel, a ½-in.-dia rod was obtained, and pin specimens were prepared from this material after it had been cold-reduced 0, 10, 25, 50, and 75%. Those with no cold reduction served as control specimens and were machined from the ½-in. bar as it was received (hot rolled, annealed, and pickled). One-third of the pins of each degree of cold work were given no heat treatment; one-third were encapsulated in Vycor tubes in a helium atmosphere, heated for 1 hr at 1950°F, and water quenched; and the other third were encapsulated as above, heated for 2½ hr at 2200°F, furnace-cooled to 1950°F, held for 1 hr, and water quenched. All specimens were electropolished prior to exposure in the loop.

The corrosion test consisted in a 200-hr exposure in 0.17 *m* UO_2SO_4 containing about 1000 ppm oxygen at 250°C. Duplicate pins of each degree of cold work and each heat treatment were exposed at 10, 13, and 17 fps. After the exposure the pins were defilmed and weight losses were determined.

The results of the test showed that there was no effect of the degree of cold work regardless of subsequent heat treatment or exposure. Table 13.1 shows the average weight losses of the specimens which received different heat treatments. From the table it is apparent that annealing of type 347 stainless steel at 1950°F improved its corrosion resistance substantially, as observed previously. Heating type 347 stainless steel to 2200°F, however, did not impair its corrosion resistance in uranyl sulfate solution. In fact, a slight improvement occurred. This result is contrary to the previous observation and illustrates that minor differences in chemical composition or heat treatment can cause widely different corrosion rates. A more detailed discussion of the results and photomicrographs showing the microstructure of the metal are reported elsewhere.[8]

13.1.5 Stress-Corrosion Cracking of Stainless Steel in Water at 200°C; Effects of Fluoride and Phosphate Ions

Three loop runs were made to determine the susceptibility of type 347 stainless steel to stress-corrosion cracking in chloride-containing water at 200°C. Each run was of 200-hr duration. In the first run the water contained 50 to 60 ppm chloride as potassium chloride and about 10 ppm oxygen. After 200 hr all the type 347 stainless steel stress specimens, whether coupled to carbon steel or not, contained numerous cracks. Many of the specimens fell apart during handling.

The next two runs differed from the first in that, in addition to the chloride and oxygen, 60 ppm phosphate as trisodium phosphate was present in

[8] J. C. Griess *et al.*, *Quar. Rep. of the Solution Corrosion Group for the Period Ending October 31, 1958*, ORNL CF-58-10-95 (to be issued).

Table 13.1. Average Weight Losses (200-hr Run) of Pin-Type Specimens That Received Different Heat Treatments

Flow Rate (fps)	Average Weight Loss (mg/cm^2)		
	No Heat Treatment	Heated at 1950°F for 1 hr, Water Quenched	Heated at 2200°F for 2½ hr, Furnace Cooled to 1950°F, Held for 1 hr, Water Quenched
10	19.2	6.2	14.3
13	35.0	8.1	26.6
17	40.9	11.8	34.1

one and 190 ppm fluoride as potassium fluoride was present in the other. In the phosphate system, only two small cracks were found, and these cracks did not originate in the region of maximum tensile stress but started at the edge of the drilled bolt holes. All the stress specimens exposed in the solution to which fluoride had been added showed a few small cracks in the region of maximum tensile stress, but in no case did a crack extend through the thickness of the specimen. Two pits were found in the region of the bolt holes, and cracks originated from the base of the pits.

Phosphate ions are normal constituents of boiler water, and this run indicates that they are effective in reducing the susceptibility of austenitic stainless steels to chloride-induced stress-corrosion cracking. Many tests have shown, however, that phosphate ions are only partially effective.

It has been reported by others that fluoride ions are partially effective in reducing cracking,[9] but only autoclave tests had been conducted. Although the data show that cracks were found in all the specimens exposed to the fluoride-containing solution, the frequency and severity of cracks were less than in the same environment in the absence of fluoride ions. However, in view of the cracking that was observed, it is doubtful that the incorporation of fluoride ions in standard boiler water would markedly reduce the probability of cracking in the event the boiler water was contaminated with chloride ions.

[9] E. J. Kreh, Conference Memorandum of Stress-Corrosion Coordination Meeting at Bettis Plant, Oct. 16, 1957.

13.2 LABORATORY CORROSION STUDIES

13.2.1 Stress-Corrosion Cracking in Uranyl Sulfate Solution

Type 347 stainless steel is subject to stress-corrosion cracking in boiling (100°C) 0.04 *m* UO_2SO_4–0.02 *m* H_2SO_4–0.005 *m* $CuSO_4$ solutions containing 25 to 500 ppm of chloride.[10–12] Recently tests have been run to determine whether any of the constituents of the solution enhance the action of chloride ions in producing stress-corrosion cracking. Preliminary results of the tests have been reported.[12]

In the above solution containing 50 ppm of chloride, approximately 50% of a total of 60 U-bend specimens cracked in 500 hr or less in this boiling and aerated environment. Table 13.2 summarizes

[10] J. C. Griess *et al.*, *HRP Quar. Prog. Rep. April 30, 1957*, ORNL-2331, p 90–91.

[11] J. C. Griess *et al.*, *HRP Quar. Prog. Rep. Oct. 31, 1957*, ORNL-2432, p 82–83.

[12] J. C. Griess *et al.*, *HRP Quar. Prog. Rep. Jan. 31, 1958*, ORNL-2493, p 92.

Table 13.2. Effect of HRT Fuel-Solution Components on Stress-Corrosion Cracking Behavior of Type 347 Stainless Steel at Atmospheric Boiling (All Solutions Contained 50 ppm Chloride)

Solution	Number of Specimens	Total Test Time (hr)	Remarks
0.04 *m* UO_2SO_4 0.02 *m* H_2SO_4 0.005 *m* $CuSO_4$	60	2500	29 specimens cracked in 500 hr or less
0.04 *m* UO_2SO_4 0.02 *m* H_2SO_4	8	3000	No cracking
0.04 *m* UO_2SO_4 0.005 *m* $CuSO_4$	9	2500	No cracking
0.04 *m* UO_2SO_4	22	3000	9 specimens cracked in 500 hr or less
0.02 *m* H_2SO_4	14	3000	1 specimen cracked during interval between 200 and 500 hr
0.005 *m* $CuSO_4$	15	2500	No cracking

the cracking behavior of type 347 stainless steel in boiling solutions containing 50 ppm of chloride and, either singly or in combination, the components of the simulated reactor solution. Other than the control solution (the one containing all components), the only environment in which fairly consistent cracking occurred was the chloride-containing 0.04 *m* UO_2SO_4 solution. Why cracking did not occur in the 0.04 *m* UO_2SO_4 solution containing either 0.02 *m* H_2SO_4 or 0.005 *m* $CuSO_4$ is not known. One isolated case of cracking occurred in the 0.02 *m* H_2SO_4 solution. Although all tests were run for at least 2500 hr, all specimens that cracked did so in 500 hr or less.

Since the uranyl ion appeared to be a promoter of stress-corrosion cracking, tests were run in 0.004, 0.04, 0.20, 0.40, 1.33, and 2.26 *m* UO_2SO_4 solutions, each containing 50 ppm of chloride. In 2500-hr tests, cracking occurred only in the 0.04 and 0.20 *m* solutions, during the first 500 hr. Thus it appears that there is an effect of uranium concentration on the incidence of cracking. Additional studies will be conducted to examine this effect.

13.2.2 Stress-Corrosion Cracking in Chloride-Containing Water

(*a*) **Effect of Surface and Heat Treatments.** – A number of tests in which type 347 stainless steel is exposed to distilled water containing 100 ppm of chloride and approximately 10 ppm of oxygen at 300°C are being run to determine the effect of various surface and heat treatments on the stress-corrosion cracking behavior of the alloy. All the control U-bend specimens, which were in the as-received condition (sheared from a 25-mil-thick sheet which had been annealed and pickled), cracked in periods of 500 hr or less. Electropolished specimens exhibited the same degree of susceptibility to cracking, as did specimens annealed (to remove the shearing effects) before forming. The initial water pH for all tests was 2.8.

In other tests in a similar environment, specimens were annealed in air at 1066°C (1950°F) both before and after forming into U-bends. The specimens were not pickled after annealing. Although preliminary data indicated some increased resistance to cracking by the specimens annealed after forming, metallographic examination upon completion of the 2000-hr tests showed all four specimens to be cracked. The time at which cracking occurred was not established since low-magnification examinations during the tests disclosed no evidence of cracking. The four specimens that were annealed before forming exhibited visible cracks after 500 hr or less in test.

Two prefilming treatments were investigated as means of protecting type 347 stainless steel from stress-corrosion cracking. The first treatment consisted in exposing U-bend specimens for 100 hr at 300°C in distilled water containing 500 ppm of chromate as sodium chromate. Upon subsequent exposure in the chloride-containing environment, all four specimens cracked during the first 100 hr of test. The second prefilming treatment consisted in exposing U-bend specimens for 100 hr in a boiling (100°C) 0.04 *m* UO_2SO_4–0.02 *m* H_2SO_4–0.005 *m* $CuSO_4$ solution. Previous work had shown this prefilming treatment to be 100% effective in preventing cracking in a similar boiling solution containing chloride.[13] The prefilmed specimens have been exposed for 200 hr thus far in chloride-containing water at 300°C without signs of cracking. Normally, a fairly large percentage of unfilmed specimens would have cracked during this period.

(*b*) **Behavior of Cast Stainless Steel.** – Standard beam-type specimens of cast type 347 stainless steel were exposed in a number of environments that normally produce cracking of the austenitic stainless steels. The test conditions and results appear in Table 13.3. The specimens were stressed at 20,000 psi in each test.

Although the test program is not complete, it appears that cast type 347 stainless steel is considerably more resistant to chloride-induced stress-corrosion cracking than is the wrought material. No cracking has been observed in any of the tests thus far. Fairly severe subsurface attack was experienced in the magnesium chloride test, as shown in Fig. 13.3. There were no signs of cracks, however. Normally, wrought type 347 stainless steel under a comparable stress undergoes cracking in a matter of several hours in this environment. Similarly, in the chloride-containing water at 300°C, cracking is generally observed on wrought specimens in intervals shorter than those reported in Table 13.3.

[13] J. C. Griess *et al.*, *Quarterly Report of the Solution Corrosion Group for the Period Ending July 31, 1958*, ORNL CF-58-7-132, p 24–26.

Table 13.3. Stress-Corrosion Cracking Behavior of Cast Type 347 Stainless Steel

Environment	Chloride Content (ppm)	Initial Solution pH	Temperature (°C)	Exposure Time (hr)	Remarks
42% $MgCl_2$			154	30	No cracking; subsurface attack
Distilled H_2O*	<0.5	6.5	300	800	No cracking
Distilled H_2O	100	2.8	300	200	No cracking
Distilled H_2O	100	6.5	300	400	No cracking
	100	6.5	300	1000	No cracking
Distilled H_2O	100	10.5	300	200	No cracking

*All tests at 300°C were made with approximately 10 ppm of oxygen.

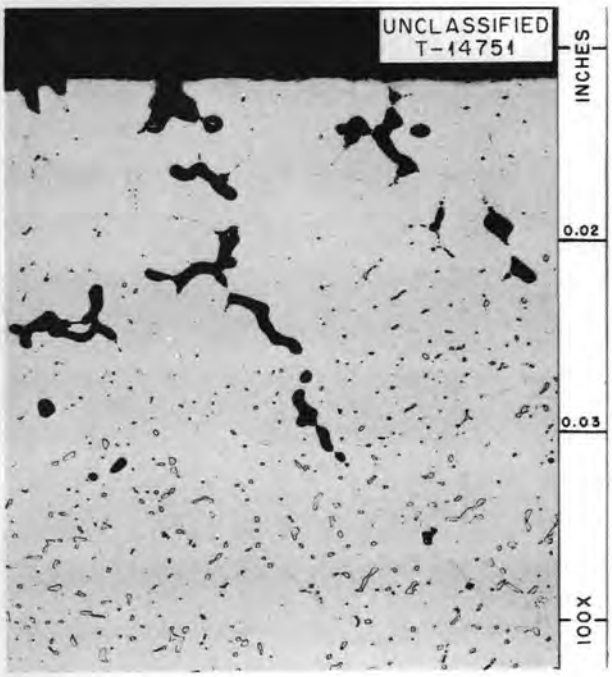

Fig. 13.3. Subsurface Attack on Cast Type 347 Stainless Steel After 30 hr in 42% $MgCl_2$ Solution at 154°C. 100X.

13.2.3 Stress-Corrosion Cracking in Oxygenated Thorium Oxide Slurry

Because chloride ions are possible contaminants of thoria slurries, the stress-corrosion cracking behavior of Zircaloy-2 and type 347 stainless steel is undergoing examination at 300°C in air-saturated thorium oxide slurry with and without an added 100 ppm of chloride (based on the thoria; added as potassium chloride). So that sufficient oxide would be present to completely cover the U-bend specimens in the autoclaves, a slurry was prepared, from LO-37-1400 thorium oxide, which contained 300 g of ThO_2 per 100 g of H_2O.

The stainless steel specimens have been exposed for 600 hr, both in the chloride-free and the chloride-present environments; no cracking has occurred. Similarly, no cracking or other localized attack has been observed on the Zircaloy-2 specimens after a total of 1000 hr in the two environments.

In the tests, which contained initially 100 ppm of chloride, analysis of the supernatant liquid at the end of the first 100 hr showed the chloride contents to be less than 5 ppm.

13.2.4 Chemiluminescent Solution for Detection of HRT Core-Tank Defect

Since it was possible that difficulties might be encountered in locating the defect in the HRT core tank wall by examination with electrical illumination, a method of detection using chemiluminescence as the light source was investigated. If used, the method would have entailed introducing the reagent into the empty core tank and observing from the blanket side the luminescent solution leaking through the defect. The chemiluminescent solution tested was similar to that described by Huntress *et al.*,[14] and consisted of a mixture of Luminol (5-amino-2,3-dihydro-1,4-phthalazinedione), hydrogen peroxide, potassium ferricyanide, and sodium hydroxide. Experiments were performed to

[14] E. Huntress, L. N. Stanley, and A. S. Parker, *J. Chem. Educ.* 11, 142–45 (1934).

establish conditions for producing the brightest and most long-lasting glow by varying the proportions and concentrations of the reagents. The final conditions, with heavy water as the solvent, were as follows: 15 ml of 5% NaOH solution was added to 1 g of Luminol in 1 liter of heavy water. To 750 ml of this solution were added 250 ml of 2.5% $K_3Fe(CN)_6$ and 20 ml of 3% H_2O_2. The resulting solution had considerable brightness for approximately 15 min, had moderate brightness for 30 min, and ceased glowing after more than 1 hr. It was observed that to obtain light-water and heavy-water solutions of approximately equal brightness, the alkali requirement for the heavy-water solutions is about 50% greater.

The defect in the HRT core vessel was located clearly with specially designed remote-viewing equipment, and it was not necessary to resort to the use of the chemiluminescent solution. However, the method may prove useful in some future applications where viewing with electrical illumination is difficult.

13.2.5 Miscellaneous Corrosion Tests

The corrosion behavior of two materials of possible interest to the Homogeneous Reactor Project was examined in several reactor-related environments. The materials were CD4MCu stainless steel and Multimet.

(*a*) **CD4MCu Stainless Steel.** – Tests were run with a new, cast, age-hardenable, nongalling material designated as CD4MCu stainless steel. The nominal chemical composition of the alloy is 25% Cr, 5.5% Ni, 2% Mo, 3% Cu, 0.04% C maximum, and balance iron. The material is reported to have mechanical and physical properties superior to, and corrosion resistance approximately equal to, those of the conventional 18-8 stainless steels.

The alloy was tested in five heat-treated conditions as shown in Table 13.4. The maximum recommended hardness for use is 34 Rockwell C; beyond this value appreciable loss in ductility occurs. Corrosion rates of 0.6 mpy or less were observed on as-cast specimens exposed in boiling (100°C) 5% HNO_3 solution and in 0.04 *m* UO_2SO_4–0.02 *m* H_2SO_4–0.005 *m* $CuSO_4$ solution at atmospheric boiling and at 300°C. A bolt made of the cast material was also resistant to stress-corrosion cracking and showed no tendency toward galling during bolting and unbolting for stressing in a test conducted for 1000 hr at 300°C in oxygenated 0.04 *m* UO_2SO_4–0.025 *m* H_2SO_4–0.01 *m* $CuSO_4$ solution.

Table 13.4. Heat-Treated Conditions for CD4MCu Stainless Steel

Heat Treatment	Hardness (Rockwell C)
1. As-cast	26
2. Cold rolled, aged 3 hr at 900°F	43
3. Hot rolled, annealed 1 hr at 1950°F, water quenched	25
4. Hot rolled, annealed as in (3), aged 4 hr at 850°F, air cooled	33
5. Hot rolled, annealed as in (3), aged 2 hr at 900°F, air cooled	34

The applied stress in the special test assembly was approximately 40,000 psi.

Age-hardened specimens (condition 2 in Table 13.4) were stressed at 60,000 psi and exposed in boiling 42% $MgCl_2$ solution; cracking occurred in 2 hr. Similar specimens were elastically stressed and exposed for 2500 hr at atmospheric boiling in 0.04 *m* UO_2SO_4–0.02 *m* H_2SO_4–0.005 *m* $CuSO_4$ solution containing 50 ppm of chloride. No cracking occurred; observed corrosion rates were 0.1 mpy. Under similar test conditions, 55% of elastically stressed U-bend specimens of type 347 stainless steel cracked.[15] One of the CD4MCu specimens was cathodically defilmed after the cracking test; the other was left in the filmed condition. Both specimens, in a stressed condition, were then placed in boiling 42% $MgCl_2$ solution; both cracked during the first hour.

Annealed and age-hardened specimens (conditions 3, 4, and 5 in Table 13.4) showed nearly the same corrosion resistance to oxygenated 0.04 *m* UO_2SO_4–0.02 *m* H_2SO_4–0.005 *m* $CuSO_4$ at 300°C. Corrosion rates were 0.7 mpy or less, and the attack was uniform. No cracking was observed on elastically stressed age-hardened specimens after 2000 hr at atmospheric boiling in 0.04 *m* UO_2SO_4–0.02 *m* H_2SO_4–0.005 *m* $CuSO_4$ solution, with and without 50 ppm of chloride.

The preliminary corrosion data warrant further examination of CD4MCu stainless steel as a material for reactor application. Its high-strength

[15] J. C. Griess *et al.*, *Quarterly Report of the Solution Corrosion Group for the Period Ending July 31, 1958*, ORNL CF-58-7-132, p 24–26 (July 31, 1958).

mechanical properties in the age-hardened condition and its apparent immunity to stress-corrosion cracking in boiling chloride-containing uranyl sulfate solution make its use especially attractive.

(*b*) **Multimet.** – Because of its excellent high-temperature mechanical properties, Multimet, a product of the Haynes Stellite Company, was considered for use as a possible bolt material. The alloy contains 20–22.5% Cr, 19–21% Ni, 0.08–0.16% C, 2.5–3.5% Mo, 0.75–1.25% Cb plus Ta, 18.5–21% Co, 0.1–0.2% N, and balance iron. A wide range in mechanical properties of the alloy can be developed by various forging techniques. Heat-treating at 1149 to 1260°C (2100 to 2300°F) followed by rapid cooling after hot-working greatly improves ductility and toughness but decreases the strength of the alloy. Specimens annealed at 1204°C (2200°F) were exposed in oxygenated 0.04 *m* UO_2SO_4–0.02 *m* H_2SO_4–0.005 *m* $CuSO_4$ solution at 100, 200, and 300°C for 1000 hr; the average corrosion rates were 0.2, 2, and 3 mpy, respectively. The specimens underwent a pickling type of attack, the intensity of which increased with increasing temperature. An elastically stressed U-bend specimen exposed in a boiling solution of the above composition and also containing 50 ppm of chloride experienced no cracking during a 2500-hr test. A period of 40 hr was required to crack a U-bend specimen in boiling 42% $MgCl_2$ solution. The corrosion resistance of the alloy was excellent in boiling 5% HNO_3 solution; the rate was less than 0.1 mpy.

Although the corrosion attack on Multimet by high-temperature uranyl sulfate solutions is somewhat greater than that on type 347 stainless steel, its adequate corrosion resistance combined with its favorable mechanical properties warrant its consideration for use in certain reactor environments.

14. SLURRY CORROSION

E. L. Compere H. C. Savage

J. M. Baker
S. E. Bolt
V. A. DeCarlo
D. T. Jones
R. A. Lorenz
A. R. Olsen
S. A. Reed
L. Rice
W. C. Ulrich
L. F. Woo

14.1 PUMP LOOPS

14.1.1 Loop Engineering: Hydroclone for Slurry Removal

As reported previously,[1] hydroclones were used successfully to remove thorium oxide slurry from the 100A pump loops. During the past quarter, however, the hydroclones would not remove slurry circulating in runs BS-23 and ES-5.

After 2.6 hr of slurry operation at 280°C during run BS-23, attempts to remove the slurry and concentrate it in an underflow pot were unsuccessful both at 280°C and at room temperature. The slurry was from batch DT-15 fired at 1600°C, at a nominal concentration of 250 g of Th per kg of D_2O, and contained molybdenum trioxide, a proposed recombination catalyst, as an additive. Some difficulty was encountered in maintaining flow through the hydroclone; so it was concluded at this point that insufficient flow through the hydroclone was the cause for malfunction of the unit. Subsequently, the slurry in the loop was drained, and the loop was rinsed to remove residual thorium oxide.

Run BS-24 was started with the same thoria batch as in run BS-23 at a nominal concentration of 500 g of Th per kg of D_2O but without the molybdenum trioxide added. An oxygen overpressure of ~250 psi was maintained at the loop operating temperature of 280°C. Molybdenum trioxide was added to the loop while operating at temperature 195 hr after the thoria addition. After 450 hr of operation at temperature and pressure, an attempt was made to remove the slurry via the hydroclone. Although flow through the hydroclone was easily maintained, very little slurry was transferred to the underflow pot. The loop temperature was again lowered to room temperature with no improvement in the hydroclone performance.

On the basis of a hypothesis that slurry was partially plugging the underflow port of the hydroclone, a line was added to return fluid from the underflow pot to the loop to provide forced underflow as shown in Fig. 14.1. A small fraction of the flow through the hydroclone was diverted through the underflow pot, and no further difficulty has been encountered. With the loop at room temperature the concentration of thorium oxide was reduced from 350 to 58 g of Th per kg of D_2O in 40 min at a flow rate of ~0.7 gpm through the hydroclone. The concentration was not reduced below 58 g/kg with additional operating time through the 0.4-in. hydroclone with the loop at room temperature.

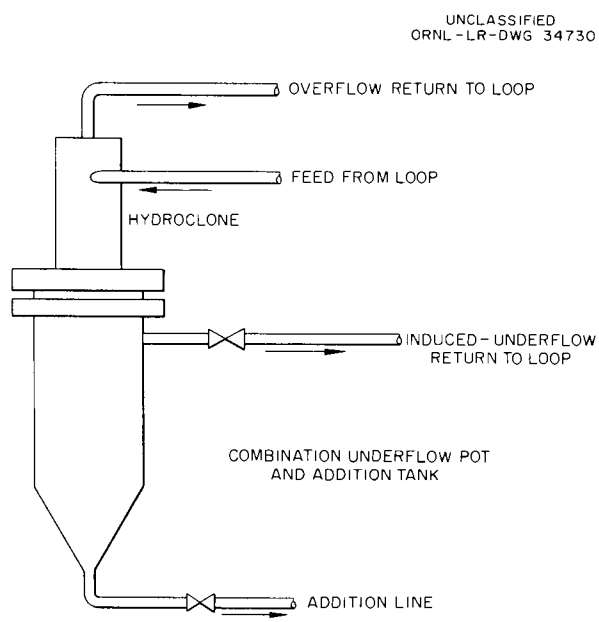

Fig. 14.1. Hydroclone as Connected for Slurry Removal from 100A Pump Loops.

The oxygen was vented from the loop and replaced with 100 psi of deuterium and 125 psi of argon, which were added to the loop at room temperature. After 450 hr of operation at 280°C with the deuterium and argon atmosphere, efforts were made to remove the slurry at 280°C with the hydroclone. In the absence of forced underflow the slurry was not removed, but with forced underflow 8.2 kg of thorium

[1] E. L. Compere *et al.*, *HRP Prog. Rep. for Quarters Ending April 30 and July 31, 1958*, ORNL-2561, p 166.

oxide was transferred to the hydroclone underflow pot in ~45 min with a hydroclone feed rate of ~0.7 gpm. The loop concentration was reduced from ~530 to ~3 g of Th per kg of D_2O.

After similar difficulties were encountered in attempting to remove slurry during runs 4 and 5 in loop ES, the 0.4-in. hydroclone in loop ES was modified to provide induced underflow as in loop BS. During run ES-6, now in progress, three partial removals of the slurry have been made without incident. The slurry removed is replaced with an equivalent amount of new, unpumped slurry. By this procedure an inventory of pumped slurry is being accumulated for future testing.

With the addition of the return line from the hydroclone underflow pot to the loop to induce underflow, the 0.4-in. hydroclones in conjunction with the addition tank[2] are satisfactorily removing slurry from or adding slurry to the 100A pump loops while at operating temperature and pressure.

14.1.2 Introduction to Pump Loop Tests

Two additional tests were made during the quarter with slurries of 1600°C-calcined sized thoria. One circulation test with 2.4-μ thoria was concerned with the corrosion-erosion attack of a ThO_2-D_2O slurry in oxygen and in deuterium atmospheres. The test is still in progress.

The second test, with an oxygenated slurry of 0.9-μ thoria, was made to screen materials of possible interest for various proposed slurry reactors.

14.1.3 Circulation of ThO_2·D_2O Slurry in Oxygen and Deuterium Atmospheres

One loop circulation test, run BS-24, was initiated during the quarter in cooperation with the Chemical Technology Division to evaluate a slurry of thoria prepared for use in the joint ORNL-Westinghouse (PAR) in-pile loop program. The thoria, designated batch DT-15, which was prepared by calcining 10°C-precipitated $Th(C_2O_4)_2$ at 1600°C for 4 hr, was sized by sedimentation classification to provide an average particle size of 2.4 μ (σ = 1.25), with 90% of the material having a diameter between 1 and 5 μ.

The test, which is still in progress, is designed to provide corrosion-erosion data and slurry-property data with a heavy-water slurry of the oxide during circulation at 280°C, at a concentration of 450 g of Th per kg of D_2O with both oxygen and deuterium atmospheres, and with the addition of MoO_3, a proposed recombination catalyst, to the slurry.

Recombination tests are being made in the Chemical Technology Division laboratories to follow the catalytic activity of the slurry as the run progresses (see Sec. 20.2.1).

Circulation periods of 485 hr with an oxygen atmosphere and 478 hr with a deuterium atmosphere have been completed. The final phase of the test, with an oxygen atmosphere, is in progress.

(*a*) **Slurry Loading.** – Initially it was proposed to charge the test loop with slurry containing ~0.025 *m* MoO_3 by injecting a concentrated slurry charge (700 g of Th per kg of D_2O containing 0.032 *m* MoO_3) while the loop was being operated at 280°C with oxygenated D_2O. One half of the required charge, 10.4 kg of ThO_2 and 52 g of MoO_3, was injected into the system without difficulty. However, when the second injection was initiated, the ⅜-in.-OD line between the addition tank and the loop was partially blocked by solids. The blockage originated at the entrance to a needle valve in the line and extended approximately 12 in. upstream of the valve. As a result the valve became inoperative, and the run was stopped.

The blockage appeared to be related to the fact that handling properties of the concentrated slurry charge had been altered considerably by the addition of 0.032 *m* MoO_3. The pH of the slurry was lowered from 5.6 to 2.8, and the settling rate of the thoria was decreased approximately threefold. On settling, the thoria formed a highly compacted bed which was very difficult to resuspend.

Consequently, a second charging was attempted with the same procedure being used but without MoO_3 addition. The slurry was injected into the loop without incident.

(*b*) **Addition of MoO_3.** – After the oxygenated slurry had been circulated for 195 hr, 32 g of MoO_3, dissolved in D_2O, was injected into the loop to provide an 0.008 *m* concentration of MoO_3. The system was sampled immediately after the addition of the molybdenum oxide. By chemical analysis, approximately 75% of the molybdenum was found to be associated with the slurry solids; the remainder was in the supernatant liquid. Gradually the molybdenum was sorbed by the thoria, and after 19 hr it was detected only in the solid phase of the slurry. During the first 195 hr, the pH of the slurry decreased from 5.7 to 4.7, a normal result of chromate buildup. The

[2] E. L. Compere *et al.*, *HRP Quar. Prog. Rep. April 30, 1956*, ORNL-2096, p 87.

pH of the slurry decreased from 4.7 to 2.3 as a result of the MoO_3 addition.

During the following 200 hr of circulation, the molybdenum continued to be associated with the slurry solids and remained essentially constant at 0.008 *m* concentration. At that time additional ThO_2 and MoO_3 were added to the loop, which increased the MoO_3 concentration to 0.012 *m*. It remained at that concentration during the final 71 hr of circulation under oxygen atmosphere.

When the test was resumed under deuterium-argon atmosphere, the molybdenum remained with the slurry solids. After 316 hr of circulation, additional MoO_3 was added to the system to increase the concentration to 0.015 *m*. Approximately 90% of the added MoO_3 was sorbed on the solids within 30 min after the addition; the remainder was contained in the supernatant liquid (at room temperature) as a blue colloidal suspension. By polarographic analyses, the molybdenum in the suspension was determined to be in the pentavalent state (probably Mo_2O_5). All the molybdenum was associated with the slurry solids within 26 hr after the addition.

(c) **Slurry Properties.** – Other than the difficulty encountered in the initial charging operation, which was discussed previously, the handling properties of the slurry have been very satisfactory. Because of frequent sampling, several additions of raw ThO_2 and MoO_3 were required during the course of the test to maintain the circulating concentration near 450 g of Th per kg of D_2O. The average circulating concentration for the 963-hr circulating period was 445 g of Th per kg of D_2O.

No particle degradation was detected by sedimentation particle-size analysis.

At the conclusion of the initial 485-hr circulation period with an oxygen atmosphere, the circulating pump was stopped, and the loop was allowed to cool from 280°C to room temperature. The circulating pump was restarted after the slurry had remained in the system at room temperature for approximately 24 hr. Complete resuspension of the solids was verified by a sample taken 20 min after startup. The thoria was then removed from the system at room temperature by use of a hydroclone. After 478 hr of circulation under a deuterium-argon atmosphere, the solids were removed from the loop with the hydroclone while the system was operated at 280°C and ~1100 psig pressure. Hydroclone performance during these periods is discussed in Sec 14.1.1.

Recombination data for samples withdrawn from the test loop during both phases of operation are presented in Sec 20.2.1.

(*d*) **Corrosion-Erosion.** – Attack rates of the type 347 stainless steel test loop and impeller and of the titanium pump scroll and thermal barrier were computed during the tests from corrosion products detected by chemical analyses in slurry samples withdrawn from system. The mean stainless steel corrosion rate for the 485-hr period with oxygen in the system was 0.9 mpy. The average oxygen concentration was 560 μg/ml. Titanium was not detected in the samples. The addition of MoO_3 to the slurry did not detectably change the attack rate.

The mean stainless steel corrosion rate for the 478-hr circulation period with deuterium-argon atmosphere was 5.6 mpy. The titanium was not detectably attacked. The average deuterium concentration during the period was 103 μg/ml.

During the first phase of the test with oxygen atmosphere, slurry pH values, measured at room temperature, ranged from 5.7 initially to 2.3 after the addition of MoO_3. When circulation was resumed with deuterium in the system, the pH of the slurry gradually increased from 3.6 to a final value of 8.6.

The weighted average corrosion rate for the stainless steel in the system during the first two phases of operation (963 hr) was 3.2 mpy.

At the conclusion of the 485-hr circulation period with oxygen in the system, the pin-type corrosion specimens contained in the main stream of the loop were removed and inspected for evidence of attack. The specimens were not defilmed. Average attack rates, approximated from weight changes were, at 20 and 40 fps, respectively: austenitic stainless steels, 0.3 and 3.8 mpy; Zircaloy-2, 0.0 and 0.4 mpy; CD4MCu cast stainless steel, 0.4 and 5 mpy; Incoloy, 0.8 and 7 mpy; platinum, 0.7 and 11 mpy; Croloys 2¼ and 5, 0.3 and 0.6 mpy; and Inconel, 4 and 11 mpy.

14.1.4 Materials Evaluation Tests

The initial run of a series of screening tests being made to study the corrosion-erosion attack of materials of interest for application in slurry reactors was completed during the quarter. The 223-hr test, run ES-5, was made at 280°C with oxygenated slurry at an average circulating concentration of 277 g of Th per kg of water. The slurry was prepared from batch LO-39 thoria, a 1600°C-calcined 0.9-μ-average-particle-size preparation which had been circulated

previously in an oxygen atmosphere for 719 hr in run ES-4.[3]

Conditions and results of the test are presented in Table 14.1 and Fig. 14.2.

For purposes of comparison, the attack data are divided into two groups. The data presented in Table 14.1 show the relative attack rates of the selected alloys and their dependence on flow velocity.

[3]E. L. Compere *et al.*, *HRP Prog. Rep. for Quarters Ending April 30 and July 31, 1958*, ORNL-2561, p 169–72.

Specimens of austenitic, ferritic, and martensitic stainless steels displayed comparable attack rates over the velocity range 16 to 50 fps. Attack rates of Incoloy and Nionel at 16 and 25 fps closely approximated those of the stainless alloys but were two- to threefold higher at 38 and 50 fps than the stainless alloys. At all velocities attack on Inconel was four to five times higher than on the stainless alloys. Erosion attack was not noted on any of the specimens at 16 or 25 fps but was readily apparent on specimens exposed at 38 and 50 fps. Attack on specimens of Hastelloys B, C, and L was uniform

Table 14.1. Corrosion by Circulating Thorium Oxide Slurry in Loop Test ES-5

Time: 223 hr
Temperature: 280°C
Load concentration: 308 g of Th per kg of H_2O
Average concentration: 277 g of Th per kg of H_2O
Calcination temperature: 1600°C
Thoria batch no.: LO-39 (previously circulated 719 hr)
Atmosphere: O_2 (average 1000 μg/ml)
pH of slurry: 5–6
Average prerun particle size: 0.9 μ
Average postrun particle size: 0.9 μ
Impeller weight loss: none detected
Loop corrosion rate: 0.4 mpy

Material	Velocity, fps (±10%)				
	16	22	25	38	50
Range of Pin Attack Rates, mpy					
Type 347 SS	0–0.2	0.1*	0.2–0.3	0.6–1.5	0.9–1.9
Type 430 SS	0.2		0.2	1.6	1.6
Type 431 SS	0.2	0.1*	0.3	1.4	1.4
Type 440 SS	0.7		1.7	0.8	1.8
Type 446 SS	0.4	0.3*	0.4	1.5	2.2
CD4MCu cast SS		0.1*			
Gold	0.1		0.3	1.9	2.5
Platinum–5% iridium	0.1		0.2	1.1	1.1
Hastelloy B	10		14	32	37
Hastelloy C	18		20	35	37
Hastelloy L	90		116	170	173
Incoloy	0.1		0.5	2.2	3.1
Inconel	3.8		3.3	8.2	10
Nionel	0.4		0.7	3.1	4.1
Zircaloy-2		0.0*			

Average Corrosion Rates of Alloy Steel Coupons at 22 fps (Defilmed)

	Croloy No.								
	½	1	2	3M	5	5 Si	7	9M	ASTM A-7
Corrosion rate, mpy	2.6	2	1.4	1.3	0.5	0.6	0.4	0.2	4.2

*Coupon specimens.

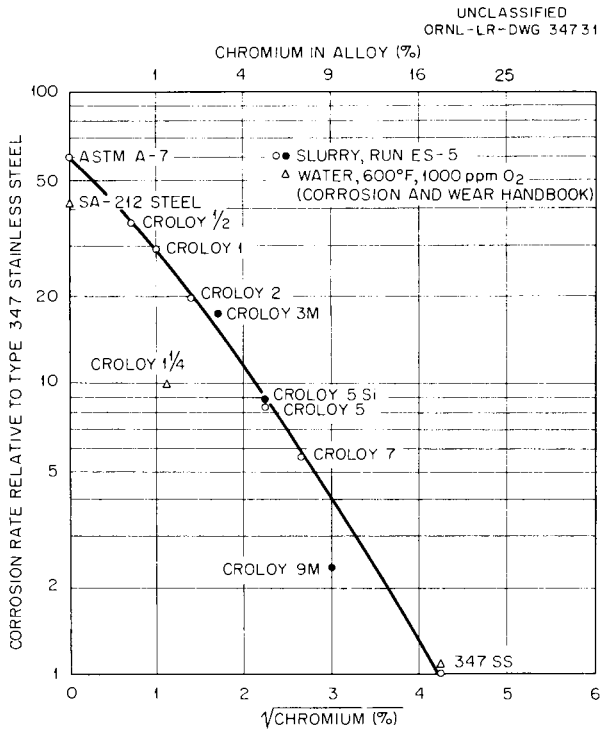

Fig. 14.2. Effect of Chromium Content of Alloy Steels on Attack by Circulating Oxygenated Aqueous Thoria Slurries.

and was mainly due to corrosion rather than abrasion. All specimens of Hastelloy L were generally pitted.

At a flow velocity of 22 fps, coupons of Zircaloy-2 were not detectably attacked; CD4MCu cast stainless steel coupon specimens displayed rates of 0.1 mpy.

The second group of alloys exposed in run ES-5 consisted of a series of coupon specimens of alloy steels containing varying percentages of chromium which were exposed at a constant flow velocity of 22 fps. The alloy compositions ranged from ASTM A-7 carbon steel containing no added chromium to type 347 stainless steel containing approximately 19% chromium. At the test conditions the attack rates were found to be strongly dependent on the chromium content of the alloy. The corrosion rates of the specimens, normalized to the rate of type 347 stainless steel (0.1 mpy), plotted as a function of the chromium content of the alloys are presented in Fig. 14.2. The rates may be generally approximated as a function of chromium content by the expression

$$\text{Log}\,\frac{R}{R_0} = -k\,\text{Cr}^{1/2} \quad .$$

Because no erosion was apparent on the specimens in this series, the attack of the alloys appeared to be due essentially to corrosion. The attack rates would therefore be expected to closely approximate the rates observed with high-temperature oxygenated water alone. For comparison, data taken from the literature[4] for SA-212 carbon steel, Croloy $1\frac{1}{4}$, and type 347 stainless steel, which were exposed in oxygenated water at similar test conditions (600°F, 1000 cc of O_2 per liter, 30 fps, pH 9–11) are also included in Fig. 14.2. Considering the differences in test conditions, the corrosion-rate ratios, relative to stainless steel, of the alloys in oxygenated water are in generally good agreement with those observed in the test with slurry and appear to display a similar dependence on the chromium content of the alloys.

The general attack of the austenitic stainless steel test loop during run ES-5 was 0.4 mpy. The cast Zircaloy-2 impeller and the titanium scroll liner used in the circulating pump were not detectably attacked.

14.2 TOROIDS

14.2.1 Introduction

Toroid tests during the quarter were concerned with pilot tests of thoria prepared by the draft-tube method and of thoria microcubes. Also, a toroid which had been severely attacked in previous tests was examined.

14.2.2 Tests with Slurries of Thoria Prepared by the Draft-Tube Method

In cooperation with the Chemical Technology Division, one series of toroid tests was completed during the quarter to evaluate slurries of thoria which were early preparations by the new draft-tube precipitation method.[5] Oxygenated slurries of four preparations of different particle sizes were circulated in 100-hr tests at 280°C, 26 fps, and concentrations of 1500 g of Th per kg of H_2O.

One preparation, a composite of batches DT-2 and -3, calcined at 1600°C, was classified by sedimentation to a fraction >3 and <7 μ. The apparent mean Stokes' diameter of the classified product was 3.8

[4] D. J. DePaul (ed.), *Corrosion and Wear Handbook for Water Cooled Reactors*, TID-7006, p 104–12 (March 1957).

[5] R. L. Pearson *et al.*, *Preparation of ThO_2 for Homogeneous Reactor Blanket Use*, ORNL-2509, p 17 (May 26, 1958).

μ. Batch DT-4 was calcined at 650°C and classified to a mean particle size of 1.1 μ. Two fractions of batch DT-5, a 1600°C-calcined preparation, were tested; an (original) unclassified portion of 2.1-μ mean particle size and a fraction which, after classification, had an average particle size of 3.1 μ. The latter fraction contained some contaminants as a result of the classification procedure, which were suspected of causing aggregation during the final calcination.

The results of these tests are shown in Table 14.2. The attack data were examined by use of the factor analysis method[6] which permitted the separation of the effect of variables as multiplicative factors. The results of this examination are also included in Table 14.2.

Several generalized effects of the variables may be noted. There was a substantial difference in the response of the various metals, generally consistent with past experience. The difference in rates between type 347 stainless steel pin specimens and the toroid rings can be associated with the flow pattern to which each was subjected.

A significant difference between thoria preparations was noted; batch DT-2-3 showed the most aggressive behavior. An attempt to correlate aggressiveness with original particle size was not conclusive, although the preparation containing batch DT-2-3 had a higher weight per cent of particles above 5 μ than the other preparations. Batch DT-4 (650°C-calcined) showed an increased corrosion of about a factor of 3 over the 1600°C-calcined thoria of batch DT-5. The average diameter of the particles did not decrease during circulation.[7] The high attack by this preparation cannot be readily explained until further tests are conducted.

The thoria prepared by this method exhibited a substantially greater aggressiveness than some preparations previously examined. Thus the normalized rate for type 347 stainless steel at 26 fps, 280°C, O_2, was, at 1500 g of Th per kg of H_2O for the best of the above preparations, 24 mpy (100-hr test). For a number of thoria preparations previously reported,[8] values of this factor ranged from 4 to 12 mpy at concentrations of 1000 g of Th per kg of H_2O (300-hr test). Higher concentration and short duration of the tests on draft-tube preparations could be factors in this difference.

14.2.3 Tests with Slurries of Thoria Microcubes

A second series of toroid tests was completed to study the corrosion-erosion attack and circulation behavior of aqueous slurries of thoria microcubes.[9] Two preparations, with respective apparent average mean Stokes' diameters of 3.3 and 2.1 μ, were tested.

Aqueous slurries of 1600°C-calcined cubes were circulated at concentrations of 250, 1000, and 1500 g of Th per kg of H_2O at 26 fps and 280°C in 100-hr tests. One preparation, LSMC-I (3.3 μ mean particle size), was tested only in an oxygen atmosphere; the other preparation, LSMC-II (2.1 μ mean particle size), was tested in both oxygen and hydrogen atmospheres. The results of the test series are presented in Table 14.3.

From a statistical evaluation of the data, the following generalizations of the major variables may be noted. There was a difference in the response of the various metals which was consistent with general past experience. The relative concentration factors for the 250 and 1000 g of Th per kg of H_2O were consistent with previously reported concentration effects.[10] The lower value of the factor for the concentration of 1500 g of Th per kg of H_2O indicated the possibility of partial noncirculation of this slurry. A difference between thoria preparations may be noted, with the LSMC-I preparation being the more aggressive.

Examination of the hydrogen data for the LSMC-II preparation indicated that attack under hydrogen atmosphere was much more severe than under oxygen atmosphere and that this oxide was generally more aggressive than other 1600°C-calcined oxides in comparable hydrogenated tests.[10]

14.2.4 Examination of a Severe Impingement and Eddy Erosion Attack

Corrosion-erosion attack data previously reported[11] for tests with certain slurries of thoria microspheres

[6] E. L. Compere, *Factor Analysis of Corrosion Data Using Logarithmic Transforms*, ORNL CF-58-9-3 (to be issued).

[7] E. L. Compere *et al.*, *HRP Quar. Prog. Rep. Oct. 31, 1956*, ORNL-2222, p 89.

[8] E. L. Compere *et al.*, *HRP Prog. Rep. for Quarters Ending April 30 and July 31, 1958*, ORNL-2561, p 180–91.

[9] The preparation method for the cubic particles is described in Sec 20.3.2.

[10] E. L. Compere *et al.*, *Dynamic Slurry Corrosion Studies: Quarter Ending January 31, 1956*, ORNL CF-56-1-168, p 25.

[11] E. L. Compere *et al.*, *HRP Prog. Rep. for Quarters Ending April 30 and July 31, 1958*, ORNL-2561, p 189.

Table 14.2. Results of Toroid Tests with Slurries of Thoria Prepared by the Draft-Tube Method

Time: 100 hr
Velocity: 26 fps
Temperature: 280°C
Concentration: 1500 g of Th per kg of H_2O
Atmosphere: Oxygen

Thoria Preparation	Calcination Temperature (°C)	Attack Rate* (mpy)					pH Postrun	Prerun Particle Size	
		Toroid (type 347 SS)	Type 347 SS	Ti-75A	SA-212-B	Zircaloy-2		Average (μ)	Per Cent >5 μ
DT-2-3	1600	29	210	26	130	15	8.5	3.8	25
DT-4	650	4.7	40	19	51	14	5.8	1.1	1
DT-5									
Original	1600	6.9	19	5.6	25	0.6	4.8	2.1	7
Sized	1600	2.9	18	3.1	31	0.2	6.2	3.1	22

Average Effect of Major Variables, Expressed as Multiplicative Factors Obtained by Statistical Analysis (Normalized rate of type 347 stainless steel at 1500 g of Th per kg of H_2O, batch DT-5, sized = 24 mpy)

Effect of Major Variables

Metals	Factor**	Batch		Factor
Toroid (type 347 SS)	0.18	DT-2-3	(1600°C)	12.9
Type 347 SS	1.0	DT-4	(650°C)	4.8
Ti-75A	0.24	DT-5 (original)	(1600°C)	1.6
SA-212-B	1.15	DT-5 (sized)	(1600°C)	1.0
Zircaloy-2	0.06			

*Corrected for slug flow.
**Relative to normalized rate.

Table 14.3. Toroid Tests with Thoria Microcubes

Time: 100 hr
Velocity: 26 fps
Temperature: 280°C
Calcination temperature: 1600°C

Thoria	Concentration (g of Th per kg of H_2O)	Atmosphere	Attack Rate[a] (mpy)					pH Postrun	Average Particle Size (μ)	
			Toroid	Type 347 SS	Ti-75A	SA-212-B	Zircaloy-2		Prerun	Postrun
LSMC-I	1500	Oxygen	0.9	*b*	*b*	*b*	*b*	6.0	3.3	3.3
LSMC-I	250	Oxygen	0.4	1.0	3.0	44	WG	6.1	3.3	2.9
LSMC-I	1000	Oxygen	0.9	11	3.1	40	10	5.2	3.3	3.0
LSMC-I	1500	Oxygen	1.8	14	2.5	79	WG	5.9	3.3	3.2
LSMC-II	250	Oxygen	0.8	3.6	WG	16	WG	4.5	2.1	2.2
LSMC-II	1000	Oxygen	3.3	9.3	2.2	15	0.4	5.7	2.1	1.9
LSMC-II	1500	Oxygen	3.2	13	3.7	14	WG	5.2	2.1	2.7
LSMC-II	1500	Hydrogen	19	270	320	390	33	9.2	2.1	3.6

Average Effect of Major Variables, Expressed as Multiplicative Factors Obtained by Statistical Analysis (Balanced Pattern)
(Normalized rate of type 347 stainless steel, 1000 g of Th per kg of H_2O as LSMC-II oxide = 10 mpy)

Effect of Major Variables

Metals	Factor[c]	Concentration (g of Th per kg of H_2O)	Factor	Oxide	Factor
Toroid	0.2			LSMC-I	1.6
Type 347 SS	1.0	250	0.23	LSMC-II	1.0
Ti-75A	0.3	1000	1.0		
SA-212-B	4.4	1500	0.68		
Zircaloy-2	0.04				

[a]Corrected for slug flow. [b]No specimens exposed. [c]Relative to normalized rate.

were abnormally high for pin specimens and type 347 stainless steel toroid rings. The results for a particular ring will be discussed. In some 3100 hr of prior use in miscellaneous slurry tests, the average corrosion-erosion attack rate on the ring was less than 1 mpy. A series of three 300-hr tests[11] at 280°C were then carried out with thoria microspheres at a concentration of 1500 g of Th per kg of H_2O. In all three tests the nominal thoria particle-size fraction was 3–10 μ, and an oxygen atmosphere was used in each case, although all the oxygen was consumed in the course of the tests with the 1200°C- and 1600°C-calcined thoria. The test conditions and results may be summarized as follows:

Calcination temperature, °C	1000	1200	1600
Circulation velocity, fps	10	26	26
pH, postrun	6	10	10
Toroid corrosion rate, mpy	1	160	100
Type 347 pin corrosion rate, mpy	3	730	>1900

After the first of the tests, which exhibited mild attack, the toroid ring was used in two tests under conditions which led to oxygen depletion; very severe generalized toroid attack rates of 160 and 100 mpy were observed. The severe attack of this toroid and of other toroids in the general series appears to be associated with high final pH, oxygen depletion, and the higher (26 fps) circulation velocity.

The ring was sectioned and examined. All portions of the ring downstream from the corrosion specimens were attacked as shown in Fig. 14.3, with the

UNCLASSIFIED
T-15093

(*a*) IMPINGEMENT ATTACK ON PIN SPECIMEN

UNCLASSIFIED
T-15090

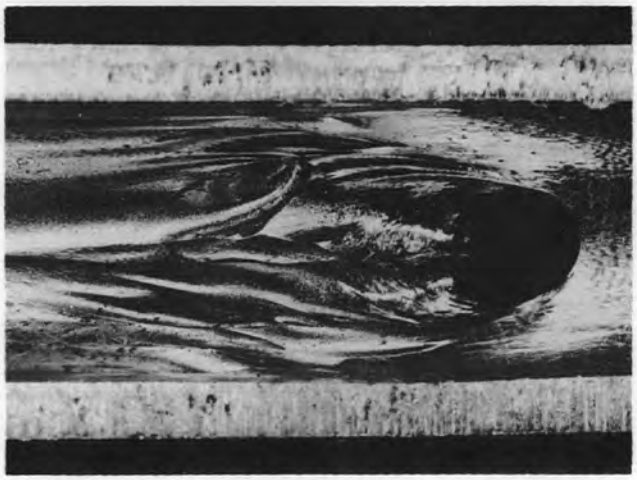

FLOW

(3X)

(*b*) EDDY ATTACK ON TOROID RING

Fig. 14.3. Impingement Attack on Toroid Pin Spucimen (6X) and Eddy Attack on Toroid Ring (3X) by Circulating Thoria Slurries.

heaviest attack being associated with the entrance of the pin through the outer surface of the channel. The attack is considered to be an eddy erosion caused by flow separation around the pin specimens. The wall thickness of the ring was 0.090 in., and penetrations of 0.060 in. or more were measured.

In the second test described above, the impingement of thoria particles on the upstream side of a type 347 stainless steel pin specimen resulted in attack as shown in Fig. 14.3. Only the front surface of the pin was attacked, the cross section of the metal which remained having the approximate appearance of a 90- to 120-deg circular sector, the angle of which pointed upstream.

The severe attack in the second and third tests is not a type that occurs with slurries under ordinary conditions. Instead, it is representative of a typical combination of adverse slurry corrosive factors and conditions leading to strong eddies and impingement of relatively large particles.

14.3 IN-PILE AUTOCLAVE SLURRY CORROSION TESTS

14.3.1 Development, Construction, and Operation

One HB-6 type rocking-autoclave experiment, L6Z-127S, containing a thorium-uranium slurry was assembled and was inserted in beam hole HB-6 of the LITR on October 14. The Zircaloy-2 autoclave contained six pin-type corrosion specimens: three of Zircaloy-2, two of type 347 stainless steel, and one of Inconel.

The autoclave was loaded with dry thorium oxide coprecipitated with 5 wt % enriched uranium, based on thorium, 0.01 *m* molybdenum trioxide catalyst for the recombination of radiolytic gas, and sufficient D_2O dispersant to give a nominal composition of 400 g of Th per kg of D_2O.

The autoclave was operated in the out-of-pile mockup facility for a total of 217 hr at various temperatures and pressures up to 280°C and 2050 psia as a leak test and to activate the molybdenum trioxide catalyst. The catalyst activation as specified by the Chemical Technology Division also involved operation with both oxygen and deuterium gas atmospheres, each gas being used separately. Prior to insertion in the LITR, an oxygen atmosphere of about 400 psi at 25°C was obtained by the addition[12] of gaseous oxygen.

[12] E. L. Compere *et al.*, *HRP Quar. Prog. Rep. Jan. 31, 1958*, ORNL-2493, p 112.

14.3.2 Introduction to Autoclave Experiments

Operating results from an in-pile autoclave slurry corrosion experiment containing an excess deuterium atmosphere[13] and generating a maximum fission power density a factor of 10 higher than in previous experiments are presented below. The experiment, L6Z-126S, utilizing a special thoria-urania preparation which contained 5 wt % enriched uranium, based on thorium, and including added MoO_3, was performed in the HB-6 facility of the LITR at 280°C. Studies of the rates of production of radiolytic gases and the catalytic recombination of these gases were made during in-pile operations. The autoclave was operated out of pile for 144 hr at 280°C and 1120 psia before insertion in the LITR.

14.3.3 Abnormal Pressure Behavior

Figure 14.4 is a graph of net gas pressure observed in experiment L6Z-126S versus time under the different operating conditions. For the first 17 hr in pile, the experiment was operated in the retracted position at 9% full flux – that is, at an estimated fission power density of 0.5 w/ml – to ensure that safe pressure levels were being obtained. Insertion of the autoclave to 30% full flux, which corresponded to an estimated fission power density of 1.8 w/ml, caused no significant change in the total pressure of the autoclave. When the autoclave was inserted fully, thereby generating a fission power density of 6 w/ml, the rate of pressure rise was 70 psi/hr initially and leveled off at 6 psi/hr. This ultimate rate of pressure rise appeared to be the result of an ingrowth of deuterium gas from the corrosion of the autoclave and its metallic contents. From the initial pressure rise and the change in the rate of pressure rise, the G_{D_2} (number of molecules of D_2 formed per 100 ev of fission energy generated) was estimated to be 0.017. This value was in good agreement with the G_{D_2} obtained for the previous experiment in a deuterium atmosphere, L6Z-125S,[14] which had operated at a maximum fission power density of 0.6 w/ml. The catalytic activity in the present experiment at this time was estimated to be 0.12 mole of D_2 per liter per hour at 100 psi D_2.

A retraction of the autoclave to 9% full flux along with a reactor shutdown reduced the pressure in the

[13] E. L. Compere *et al.*, *HRP Prog. Rep. for Quarters Ending April 30 and July 31, 1958*, ORNL-2561, p 191–99.

[14] *Ibid.*, p 195.

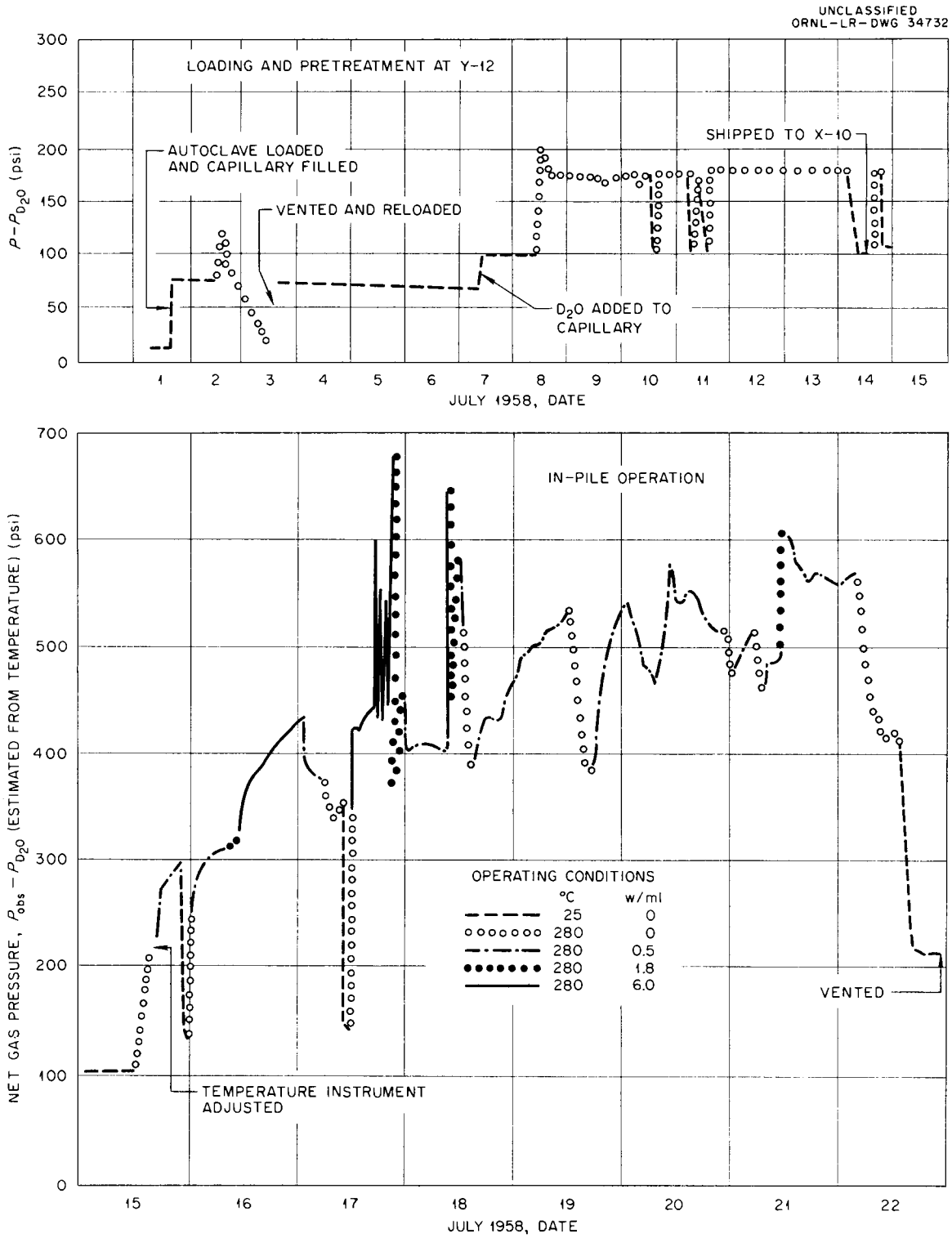

Fig. 14.4. Radiation Corrosion under D_2 Atmosphere, Experiment L6Z-126S, Zircaloy-2 Autoclave.

autoclave because of recombination of radiolytic gases in the absence of fissioning. When the reactor power was brought back up to 3000 kw with the autoclave already inserted, the pressure in the autoclave rose back to the pressure level originally observed at a fission power density of 6 w/ml. The pressure maintained its 6-psi/hr increase for 6 hr; then, unexpectedly, it started to climb at a rate of 250 psi/hr. After an increase of 150 psi the rise halted and the pressure began decreasing at a rate of 730 psi/hr. Four more pressure surges were observed, with rates of pressure increase between 310 and 380 psi/hr and rates of pressure decrease as high as 1000 psi/hr. Assuming no change in the recombination rate at this time, the rate of radiolytic-gas production appeared to be higher by at least a factor of 4. When the autoclave was retracted to 30% full flux on the fifth pressure surge, the pressure dropped 330 psi in 2 min and started to climb back up. The autoclave was then completely retracted to 9% full flux. Eleven hours later, reinsertion of the autoclave to full flux caused the pressure to rise at a rate of 530 psi/hr (an estimated G_{D_2} value of 0.11). When a net gas pressure of 650 psi was reached, the autoclave was retracted to 30% full flux. The pressure immediately dropped 200 psi and then started to climb at a rate of 55 psi/hr. The autoclave was then retracted, and a reactor shutdown followed.

On the next reactor startup, with the autoclave in the retracted position (9% full flux), the pressure increased at an average rate of 5 psi/hr with no signs of leveling-off at a safe operating pressure. In contrast to this pressure phenomenon, the pressure in the initial period of in-pile operation appeared to be leveling-off after an increase of 50 psi with the autoclave retracted at 9% full flux. The reactor was shut down to lower the pressure and in an attempt to repeat the pressure behavior of the initial in-pile operation. On reactor startup the pressure again went up, but this time at a rate of 20 psi/hr. Reaching a net gas pressure of 540 psi, the pressure started down. After a decrease of 80 psi, which included a small pip before the pressure reached its minimum, the pressure again started to rise at 20 psi/hr. A total of four pressure peaks were observed for this retracted period. Two reactor cycles followed, with similar increases in pressures on each reactor startup. An insertion of the autoclave to 30% full flux caused the pressure to climb at a rate of 190 psi/hr, corresponding to a calculated G_{D_2} value of 0.16. The autoclave was retracted after a net gas pressure of 600 psi was reached. On the next reactor shutdown a sluggish pressure response was observed when the temperature in the autoclave was lowered to 25°C, indicating that a partial plug had developed in the capillary line leading from the autoclave to the Baldwin pressure-sensing cell. The autoclave was vented and the experiment was terminated.

14.3.4 Recombination of Radiolytic Gases

Table 14.4 and Fig. 14.5 present the recombination and gas production data from this experiment. By use of the nuclear constants and the experimental techniques described previously,[15] the recombination rate of the catalyst, in terms of moles of D_2 reacted per liter of slurry per hour at 100 psi radiolytic D_2 (or 150 psi radiolytic gas), and the G_{D_2}, the molecules of deuterium produced per 100 ev of fission energy generated, have been calculated. Although catalyst activities are expressed

[15] E. L. Compere *et al.*, *HRP Prog. Rep. for Quarters Ending April 30 and July 31, 1958*, ORNL-2561, p 193–95.

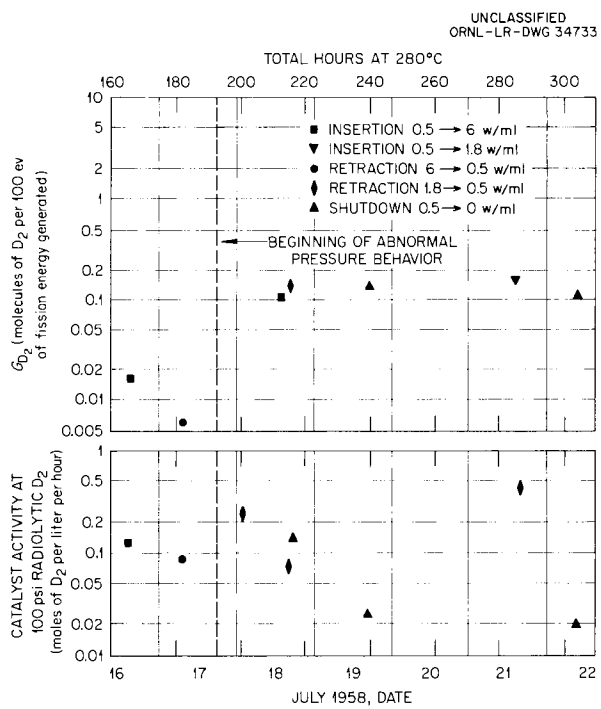

Fig. 14.5. In-Pile Recombination of Radiolytic Gas, Experiment L6Z-126S.

Table 14.4. In-Pile Recombination of Radiolytic Gas in an Excess Deuterium Atmosphere, Experiment L6Z-126S

980 g of Th per kg of D_2O, 5% enriched U based on Th, 0.04 *m* MoO_3
280°C, 200 psi D_2
3000-kw LITR power = 0.5×10^{13} neutrons·cm^{-2}·sec^{-1} (HB-6)

Fission Power (w/ml)	Hours Above 100°C	Radiation Hours	Type of Experiment	Observed Rate[a] (moles of D_2 per liter per hr)	Radiolytic D_2 Equilibrium Pressure (psi)	Calculated Catalyst Activity at 100 psi D_2 (Radiolytic) (moles of D_2 per liter per hr)	Calculated G_{D_2}
6	166	1	I[b]	0.038	31.5	0.122	0.017
6	182	16	R[b]	0.012	14.3	0.087	0.006
1.8	201	26	R	ND[c]	ND[c]	0.251	ND[c]
6	213	27	I	0.246	ND[d]	ND[d]	0.110
1.8	216	28	R	0.099	137	0.072	0.147
0.5	217	28	SD[e]	ND[c]	ND[c]	0.144	ND[c]
0.5	240	30	SD[e]	0.028	103	0.027	0.140
1.8	286	34	I	0.114	ND[d]	ND[d]	0.169
1.8	287	34	R	ND[c]	ND[c]	0.422	ND[c]
0.5	304	35	SD[e]	0.022	107	0.020	0.109

[a]Recombination rate at the equilibrium pressure equals production rate.
[b]I, insertion experiment; R, retraction experiment.
[c]Not determined owing to pressure not being in equilibrium at the beginning of experiment.
[d]Not determined owing to experiment not having progressed sufficiently to obtain a good evaluation.
[e]Reactor shutdown.

relative to 100 psi radiolytic D_2, in order to be consistent with general previous usage, in these experiments such a statement means 150 psi radiolytic gas. The rate appears to be proportional to the first power of radiolytic-gas pressure, and no more detailed inference is drawn here. In the first two recombination experiments, catalytic activities of 0.122 and 0.087 mole of D_2 per liter per hour at 100 psi D_2 were obtained. These values are in good agreement with the catalytic activity estimated from out-of-pile recombination experiments by the Chemical Technology Division with the same MoO_3 to urania-thoria ratio at lower slurry concentrations. Following the first pressure abnormalities observed, which were described above, data for the values of the catalytic activity became considerably more scattered, with a range of 0.02 to 0.42 mole of D_2 per liter per hour at 100 psi D_2. No significant trend in the catalytic activity was noted.

The G_{D_2} values of 0.017 and 0.006, obtained for the first two recombination experiments with run L6Z-126S, are in good agreement with the G_{D_2} values of between 0.010 and 0.027 obtained in experiment L6Z-125S, which also operated in an atmosphere of excess deuterium but at a fission power density of only 0.6 w/ml. Following the wide pressure excursions that were discussed earlier, the level of G_{D_2} values became higher by approximately a factor of 10, with values ranging from 0.11 to 0.17. The reasons for the apparent increase in the G_{D_2} are as yet unexplained.

14.3.5 Effects of Time and Radiation on Generalized Corrosion Rates

In experiment L6Z-126S, generalized corrosion of the autoclave and contents were followed in the usual way[16,17] by observing the temperature and pressure of the autoclave at suitable times, especially at room temperature, during reactor shutdown periods. Since the corrosion of the Zircaloy-2 in a deuterium atmosphere can be assumed to follow the reaction, metal + D_2O → metal oxide + D_2, the corrosion may be followed by measuring the increase in pressure.

Figure 14.6 presents the corrosion results for the experiment as estimated from the D_2 pressure measured at 25°C during reactor shutdown periods. The solid points represent the experimental data. There are too few points to permit the fitting of an individual equation for this experiment. The lines represent the corrosion computed from rates estimated from the equation,

$$\text{mpy} = \frac{20}{\text{hr}} + \frac{340 \times \text{w/ml}}{\text{hr}} ,$$

which was derived from data from experiment L6Z-125S, the previous experiment, in an atmosphere of excess D_2.[18] The equation seems to fit the data of the present experiment reasonably well, but any generalization will require more rigorous testing with experiments of longer duration. The over-all generalized corrosion rate of the autoclave for the in-pile operation was estimated to be 2.1 mpy at an average fission power density of 1.2 w/ml.

In the early portion of the preirradiation period a fairly large decrease in the D_2 pressure was observed instead of an increase as would have been expected in the corrosion process. The sequence of events is shown in Fig. 14.4 for the load and pretreatment period at Y-12. Together with the additional D_2 involved in the initial corrosion shown in Fig. 14.6, which was estimated from the above equation, the total consumption of D_2 was equivalent to a 0.031-mil penetration of metal or 590 micromoles of D_2 gas. It is well at this point to consider a previous experiment.

An autoclave from an earlier duplicate experiment subjecting the uranium-thorium oxide slurry and MoO_3 with a D_2 atmosphere to high temperature was examined, after a leak had been discovered and the experiment discontinued before irradiation. It was discovered that black material was deposited on both ends of the pins and pin rack and on certain areas of the inside surfaces of the autoclave. By electron diffraction the material was found to contain MoO_2. Conventional chemical analysis revealed the presence of molybdenum and uranium in these deposits. Since 150 micromoles of MoO_3 and 830 micromoles of uranium oxide were loaded into the autoclave, a total of 980 micromoles of D_2 could theoretically have been consumed in the reduction of the MoO_3 to MoO_2 and UO_3 to UO_2. This

[16] E. L. Compere *et al.*, *HRP Quar. Prog. Rep. Jan. 31, 1958*, ORNL-2493, p 113.

[17] K. S. Warren and R. J. Davis, *In-Reactor Autoclave Corrosion Studies – LITR. I. Outline of Methods and Procedures*, ORNL CF-57-5-110 (May 22, 1957).

[18] E. L. Compere *et al.*, *HRP Prog. Rep. for Quarters Ending April 30 and July 31, 1958*, ORNL-2561, p 195–98.

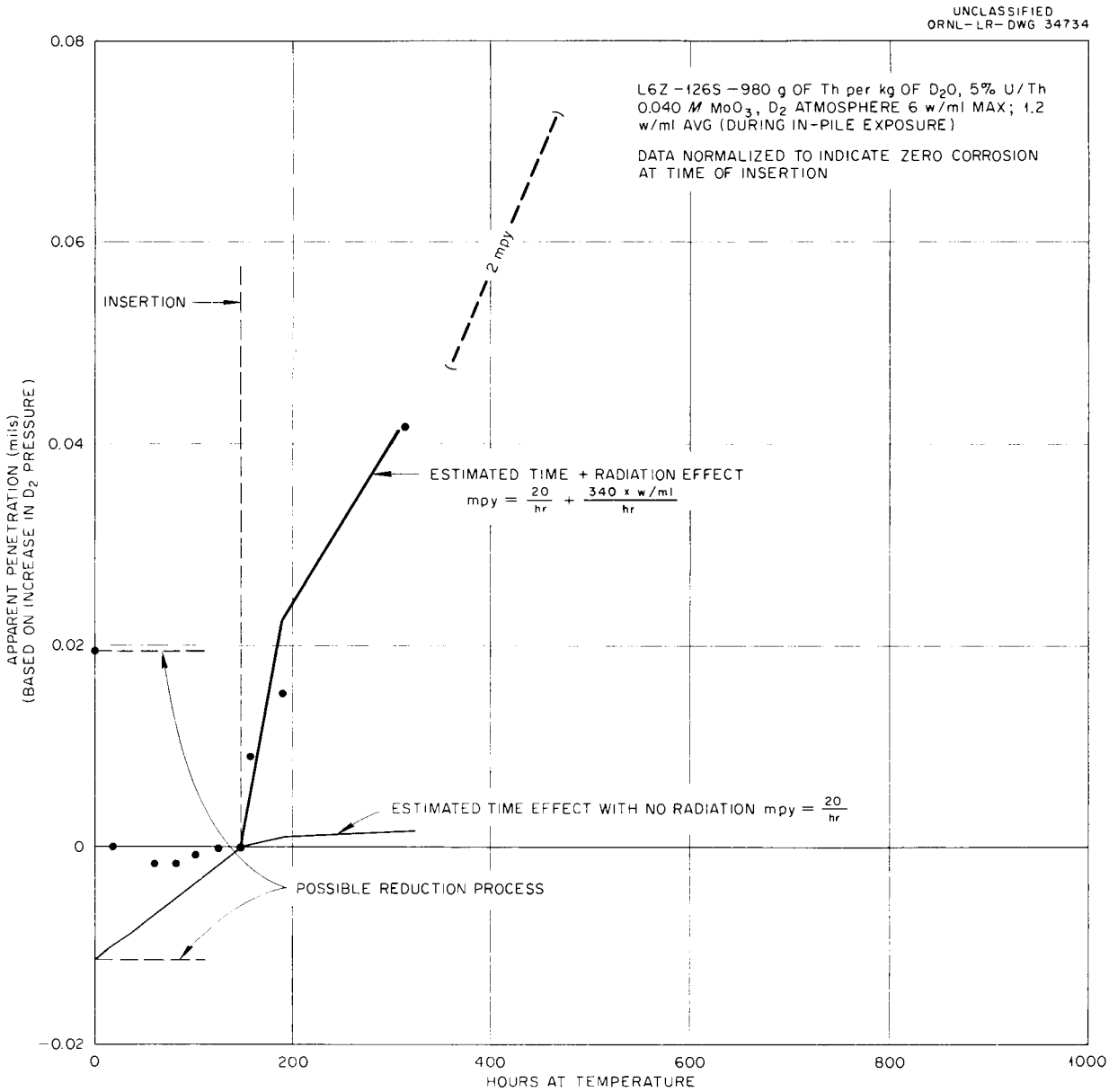

Fig. 14.6. Factors in Zircaloy-2 Corrosion by Slurry under Deuterium Atmosphere.

requires the assumption that, in the calcination step of the preparation of the urania-thoria, all the uranium had been oxidized to UO_3. It was concluded that the consumption of D_2 in the early high-temperature period of the autoclave experiment was the result of a partial reduction of the molybdenum and uranium, with the reduction products being deposited on localized areas of the metal surfaces.

Another observation made with the slurry was the unusually low pH of 2.5 found in the supernatant of a sample made up for control analyses. The addition of the same quantity of MoO_3 to pure D_2O with no urania-thoria gave a pH of 2.3 in a subsequent sample. The low pH in the supernatant of the slurry was attributed to the dissolution of the solid MoO_3 to form soluble molybdic acid. The solubility of the MoO_3 would permit consideration of mechanisms accounting for the observed deposits of reduced materials localized on the metal surfaces.

Thus it appears that the reduction of molybdenum and uranium trioxides could occur, under the pretreatment conditions of the in-pile experiment, in sufficient quantity to account for the observed loss

in deuterium pressure. Since no leaks were observed, it is tentatively concluded that this was the case.

14.3.6 Examination of Irradiated Thoria and Pin Corrosion Specimens

The operating results of experiments L6Z-122S and L6Z-125S were reported previously.[16] During the present quarter the autoclaves were opened, and the examination of the contents was partially completed.

Table 14.5 contains analytical results of experiment L6Z-122S. Analyses of original material prior to any irradiation are listed in the first column. This material was a special urania-thoria preparation by the Chemical Technology Division, made by coprecipitation of 0.5 wt % enriched uranium, based on thorium, with thorium oxalate and fired at 1300°C.

Mechanical difficulties were encountered in opening the autoclave after irradiation, and as a result most of the slurry was lost. Based on the 0.021 g of thorium recovered, the ratio of uranium to thorium did not change significantly during the irradiation. All the molybdenum appeared to have disappeared from the slurry. No analysis of the U^{233} was made because of the high contamination of fission products in the thoria and the insufficient quantity of sample.

Particle-size analysis indicated that in the irradiated material the fraction above 3 μ increased from

Table 14.5. Analysis of Irradiated Thoria from Autoclave Experiment L6Z-122S

	Original Material[a]	Irradiated Material
Volume recovered		~0.2 ml solids, 8 ml rinse[b]
Th recovered, g		0.021[b]
U, mg per g of Th	5.0	5.5
Mo, mg per g of Th	2.1[c]	0
Fe, μg per g of Th	6	NA[d]
Cr, μg per g of Th	6	NA
Ni, μg per g of Th	16	NA
Zr, μg per g of Th	NA	1700
U^{233} counts/min per g of Th		NA
Particle size by sedimentation[e]		
Average diameter, μ	0.8	0.6
Weight per cent		
>3 μ	20	30
1.5–3 μ	0	5
1.0–1.5 μ	16	2
0.5–1.0 μ	43	15
<0.5 μ	21	48

[a]Original material was a special preparation by the Chemical Technology Division and consisted of 0.5 wt % enriched uranium coprecipitated with thorium oxalate and fired at 1300°C.

[b]A large portion of the slurry was lost due to difficulties encountered in opening the autoclave.

[c]The molybdenum concentration was calculated from amounts added when the autoclave was loaded.

[d]NA = no analysis made.

[e]In the original material, determination of large particles was made in 0.005 m $Na_4P_2O_7$ in glycerol-H_2O and of the smaller particles in saturated $Na_4P_2O_7$ in methyl alcohol. In the irradiated material determination was made in 0.005 m $Na_4P_2O_7$.

20% to 30% of the total. The fraction below 0.5 μ increased from 21% to 48%.

Tables 14.6 and 14.7 present the corrosion data on pin specimens for experiments L6Z-122S and L6Z-125S, respectively. All pins showed slight increases in defilmed weights, amounting to a few tenths of a milligram. The corrosion rates were calculated from the weight gains. Considering the small changes in weights involved, all the results fell within a reasonable error range. No significant differences between the corrosion rates of the various alloys were observed. Reasonable agreement with the generalized corrosion rate of the Zircaloy-2 autoclave as estimated from gas-pressure data is indicated.

14.4 IN-PILE SLURRY TOROID

14.4.1 Engineering Development

The status of the temperature control system[19] for the in-pile slurry toroid-rotator model remains unchanged; no further tests of the system were made during the quarter.

The single-arm in-pile toroid rotator previously described[20] was modified by replacing the Oilite sleeve bearing with a Stellite 98M2 journal bushing and Graphitar No. 14 bearing combination with provision for continuous lubrication. After several tests it was found that water was a satisfactory lubricant. A water feed of 40 cc/min is sufficient for this purpose. The single-arm in-pile toroid-rotator model with the Stellite journal bushing and Graphitar bearing was operated continuously for more than 1500 hr at a speed of 1000 rpm in an out-of-pile test at room temperature without difficulty. Bearing wear was negligible. Based on this operating test, the in-pile rotator appears to be mechanically satisfactory for long-term operation. Work on the unit is being suspended, however, as a result of increased effort on other projects.

14.5 IN-PILE SLURRY LOOP

14.5.1 Loop Development

Development work on the experimental in-pile slurry loop, L-4-24S,[21] continued during the quarter.

[19] E. L. Compere *et al.*, *HRP Prog. Rep. for Quarters Ending April 30 and July 31, 1958*, ORNL-2561, p 199.

[20] E. L. Compere *et al.*, *HRP Prog. Rep. Jan. 31, 1958*, ORNL-2493, p 114, text, and Figs. 13.3 and 13.4.

[21] E. L. Compere *et al.*, *HRP Prog. Rep. for Quarters Ending April 30 and July 31, 1958*, ORNL-2561, p 200–201.

Table 14.6. Radiation-Corrosion of Zirconium-Alloy Pin Specimens Under Oxygen Atmosphere, Experiment L6Z-122S

990 g of Th per kg of D_2O, 0.5% U based on Th, 0.02 *m* MoO_3
280°C, Zircaloy-2 autoclave
0.6 w/ml maximum; 0.4 w/ml average
Hours at temperature, 1074
Hours of radiation (LITR at 3000 kw), 681
Autoclave generalized corrosion rate, 0.8 mpy

Pin Material	Pin Corrosion Rate, Based on Weight Gain (mpy)
Zircaloy-2	0.3, 0.4
Zr–15% Nb, 550°C heat-treated for two weeks	0.6
Zr–15% Nb, beta-quenched	*
Zr–15% Nb–2% Pd, beta-quenched	0.4
Zr–15% Nb–5% Mo, beta-quenched	0.8

*Specimen broke during disassembly; no notable attack or brittleness reported.

Table 14.7. Radiation Corrosion of Zirconium-Alloy Pin Specimens Under Deuterium Atmosphere, Experiment L6Z-125S

950 g of Th per kg of D_2O, 0.5% U based on Th, 0.017 *m* MoO_3
280°C, Zircaloy-2 autoclave
0.6 w/ml maximum; 0.4 w/ml average
Hours at temperature, 1232
Hours of radiation (LITR at 3000 kw), 774
Autoclave generalized corrosion rate, 0.4 mpy

Pin Material	Pin Corrosion Rate, Based on Weight Gain (mpy)
Zircaloy-2	0.8
Zr–15% Nb, 550°C heat-treated for two weeks	0.7
Zr–15% Nb, beta-quenched	0.9
Zr–15% Nb–2% Pd, beta-quenched	0.9
Zr–15% Nb–5% Mo, beta-quenched	0.8

Since the slurry of thorium oxide could not be prevented from accumulating in the horizontal pressurizer under operating conditions of temperature and pressure, an investigation of methods of removing the thoria from the feed stream to the pressurizer was initiated.

The possibility of using a hydroclone to remove the thoria from the pressurizer feed stream was investigated briefly. This method consisted in connecting a hydroclone between the loop and pressurizer in such a way that the hydroclone overflow could be routed to the pressurizer with the underflow being returned to the main circulating loop. Tests of 0.16-, 0.40-, and 0.50-in. hydroclones indicated efficiencies,

$$\left(1 - \frac{\text{overflow concentration}}{\text{feed concentration}}\right) \times 100 \ ,$$

of 75 to 90% at room temperature with slurries in the concentration range of 200–300 g of Th per kg of H_2O with a pressure drop of ~40 ft across the hydroclone. The thoria slurries tested were from batch LO-40 and a mixture of batches LO-17 and TO-10. These batches were 1600°C-fired material with a mean particle size of 1.2 μ. The hydroclone efficiencies obtained in these tests were considered unsatisfactory for use in the in-pile slurry loop.

Another method of removing the slurry from the pressurizer feed is by means of a sintered-metal filter. Tests were conducted on a Poroloy sintered-metal filter, 3-μ mean pore size, in the form of a tube 12 in. long and $\frac{5}{8}$ in. in diameter. Tests at room temperature with a 40-ft pressure drop across the filter produced a filtrate virtually free of thorium oxide. There appeared to be no tendency for the filter to plug during several days of operation. Thus the filter unit was installed in a bypass line of loop L-4-24S, with the filtrate routed to the pressurizer, as shown in Fig. 14.7.

Two loop runs, 11 and 12, were made with the filter unit installed. Approximately 300 hr of loop operation were accumulated, with slurry concentrations up to 500 g of Th per kg of H_2O at temperatures up to 250°C. Loop operation was entirely satisfactory, and this initial test indicates that a sintered-metal filter is very effective in preventing slurry accumulation in the horizontal pressurizer. There appeared to be no plugging of the filter as evidenced by the fact that there was no loss of filtrate flow to the pressurizer, even though thorium oxide accumulated in the slurry flow annulus between the filter and its housing. Although the accumulation of slurry around the filter did not hinder the filtration appreciably, it did represent a holdup of a large percentage of the loop inventory. The filter unit, which was on hand and used for expediency to obtain preliminary data, has been modified for full loop flow through the inside of the filter and for filtrate collection in the annulus between the outside of the filter and its housing in an attempt to eliminate slurry holdup in the unit.

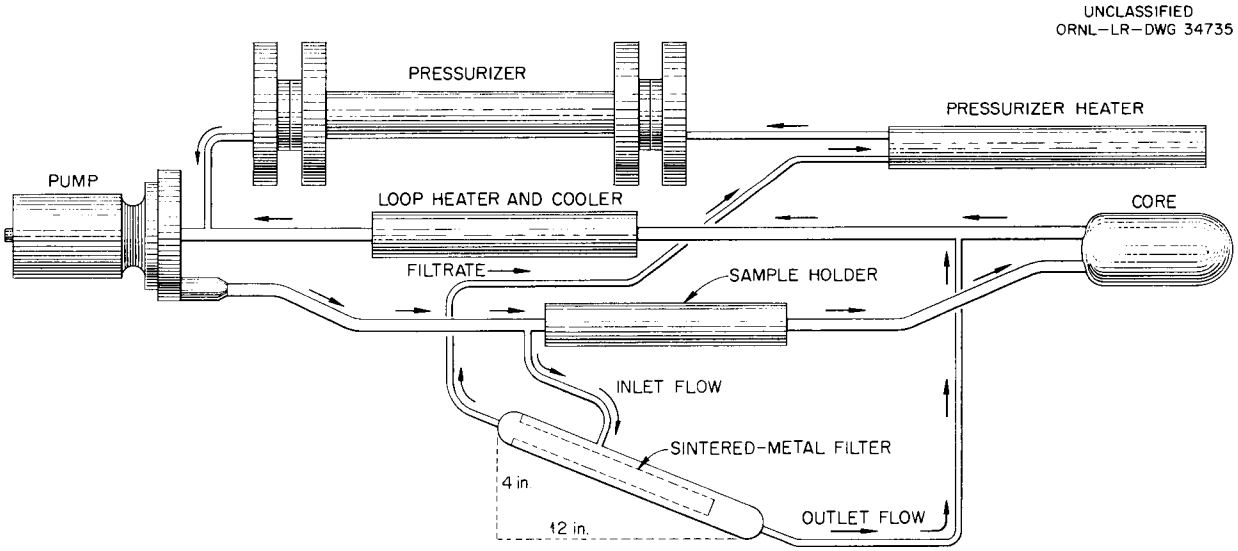

Fig. 14.7. In-Pile Slurry Loop with Sintered Metal Filter.

15. RADIATION CORROSION

G. H. Jenks H. C. Savage

A. L. Bacarella
J. E. Baker
S. J. Ball
J. C. Banter
S. E. Bolt
R. J. Davis
V. A. DeCarlo
B. O. Heston
D. T. Jones
F. A. Knox
R. A. Lorenz
J. R. McWherter
A. R. Olsen
A. J. Shor
M. D. Silverman
W. C. Ulrich
K. S. Warren
S. H. Wheeler
W. C. Yee

15.1 IN-PILE LOOPS

15.1.1 General Description of In-Pile Loop Experiment L-2-21

Stainless steel loop experiment L-2-21 was completed. It was the sixteenth in-pile loop experiment and the sixth to be irradiated in the HB-2 beam hole at the LITR. A solution of 0.17 *M* UO_2SO_4 in D_2O was circulated at 280°C in the main stream and at 296°C in the pressurizer.

The loop was originally constructed for operation in the HB-4 beam hole and was designated as L-4-21. Before being modified and reassembled as L-2-21, the loop circulated natural-uranium UO_2SO_4 solution out-of-pile for 97 hr. At that time two coupons became dislodged from the core tapered-channel holder and were swept into the first stage of the circulating pump. The pump was damaged, and pretreatment operations were terminated. The core channel, core nose, and core annulus sample holders, the pump, and the in-line annulus sample holders were removed and disassembled. The in-line channel coupon array and the stress-specimen assemblies located in the pressurizer were left intact.

The damaged Byron-Jackson 5-gpm fuel-circulating pump was replaced with a 5-gpm ORNL pump of the outboard-bearing design containing Kearfott aluminum oxide bearings and journal bushings. Both front and rear bearings were pinned to the bearing housings to prevent movement. The length of the loop was modified to fit into the HB-2 loop container, and the HB-4 shielding plug was replaced with the HB-2 plug. In addition, this loop was the first to contain a combined loop heater-cooler. (This 20-in.-long unit was constructed in accordance with drawing TD-E-4784.) Previously, separate heater and cooler units were used.

All loop components, fabricated from type 347 stainless steel, were designed for 2000-psi, 300°C operation. Excluding the areas of the stainless steel corrosion specimens and specimen holders and the low-temperature area of the pump, about 30% of the steel contained in L-2-21 was new material that had not previously been used in loop L-4-21. The pressurizer, of the ORR loop pressurizer design, was fabricated from 1½-in. sched-80 pipe instead of the 1¼-in. sched-80 pipe normally used, thereby increasing the volume about 20%.

Many of the specimens in L-2-21 had been exposed to pretreatment solutions in loop L-4-21. The in-line channel coupons and the pressurizer stress-specimens were transferred, intact, to similar locations in loop L-2-21. Other specimens from L-4-21 which were reinstalled in L-2-21 were first scrubbed and reweighed, but they were not defilmed. The L-2-21 arrays did not contain all specimen types or materials originally in L-4-21 so that the reassembled loop contained many new, unexposed, specimens. All annulus type coupons were the modified (scalloped) type, 0.5 × 0.5 × 0.060 in. All annulus specimen holders were fabricated from titanium-75A. Specimen materials and locations are given in Table 15.1. Two 4-in.-long cobalt-wire flux monitors canned in stainless steel were contained in the core annulus region.

Loop L-4-21 was operated for short periods with five different solutions during the out-of-pile tests and pretreatment. A 4.3-hr run with 3% trisodium phosphate solution was made at 90°C in a helium atmosphere, followed by a 24-hr run with a 5% HNO_3 solution in the same atmosphere and at the same temperature. After removal of the acid solution, two charges of water were circulated at 280°C, in oxygen atmospheres, for periods of 3.5 and 27 hr, respectively. A run was started at 280°C with a natural-uranium solution (0.17 *M* UO_2SO_4, 0.045 *M* H_2SO_4, and 0.007 *M* $CuSO_4$) but was terminated after 97 hr when the pump was damaged. The overall corrosion rate observed during this 97-hr period

Table 15.1. Alloy Specimens Contained in Experiment L-2-21

Array	Number of Specimens	Specimen Material	Heat Treatment*	Specimen History**
		Coupons in Core Tapered-Channel Holder		
	8	Type 347 SS		O, 5; N, 3
	9	Zircaloy-2		O, 7; N, 2
	7	Ti-110AT		O
		Coupons in In-Line Tapered-Channel Holder		
	8	Type 347 SS		O
	8	Zircaloy-2		O
	8	Ti-110AT		O
		Coupons in Core Ladder Holders		
TB-6	1	Zircaloy-2	G	N
	2	Zr–15% Nb	A	O
	5	Zr–15% Nb–2% Mo	A, 2; B, 1; C, 2	N
TB-7	2	Zr–25% Nb	A	O
	2	Zr–15% Nb–5% Mo	A	O
	2	Zr–20% Nb–2% Mo	A	O
	2	Zr (sponge)–15% Nb–2% Pd	A	O
TB-8	6	Zircaloy-2	G, 2; H, 2; I, 2	N
	2	Zr–20% Nb	A	O
TB-9	2	Zircaloy-2	G	O
	2	Zr–10% Nb	A	O
	2	Zr–15% Nb–2% Mo	E	N
	2	Zr–20% Nb–2% Pd	A	O
TB-10	2	Zr–5% Pd	A	O
	2	Zr–7.5% Nb	A	O
	2	Zr–15% Nb–5% Pd	A	O
	2	Zr–15% Nb–2% Th	A	O
TB-13	6	Zr–15% Nb–2% Pd	A, 2; C, 2; E, 2	N
	2	Zr–15% Nb–0.5% Cu	A	O
TB-14	4	Zr–15% Pd	J, 2; L, 2	N
	4	Zr–15% Pt	K, 2; M, 2	N
		Coupons in In-Line Ladder Holders		
TB-11	1	Zr–7.5% Nb	A	O
	1	Zr–10% Nb	A	O
	1	Zr–15% Nb	A	O
	3	Zr–15% Nb–2% Pd	A, 1; C, 1; E, 1	N
	1	Zr–15% Nb–5% Pd	A	O
TB-12	3	Zircaloy-2	G, 1; H, 1; I, 1	N
	1	Zr–20% Nb	A	N
	1	Zr–25% Nb	A	O
	1	Zr–15% Nb–5% Mo	A	O
	1	Zr–20% Nb–2% Mo	A	O
	1	Zr–20% Nb–2% Pd	A	O

Table 15.1 (continued)

Array	Number of Specimens	Specimen Material	Heat Treatment*	Specimen History**
		Coupons in In-Line Ladder Holders		
TB-15	1	Zr–5% Pd	A	N
	2	Zr–15% Pd	J, 1; L, 1	N
	2	Zr–15% Pt	K, 1; M, 1	N
	3	Zr–15% Nb–2% Mo	A, 1; C, 1; L, 1	N
		Alloys Contained in Core Nose Holder		
	1	Zircaloy-2		
	1	Type 347 SS		
		Alloys Contained in Stress-Specimen Assemblies in Pressurizer Liquid Phase		
	2	Type 430L SS		O
	2	Ti-110AT		O
		Alloys Contained in Stress-Specimen Assemblies in Pressurizer Vapor Phase		
	2	Type 430L SS		O
	2	Ti-110AT		O

*Heat treatments:

A: Beta quenched (900°C, 3 hr, water quenched)
B: Beta quenched plus 400°C, 2 hr, water quenched
C: Beta quenched plus 400°C, 2 weeks, air cooled
E: Beta quenched plus 500°C, 2 weeks, air cooled
G: Commercially annealed (machined from item 60; material rolled to give minimum preferred orientation
H: 1000°C, 30 min, water quenched in capsule
I: 1000°C, 30 min, furnace cooled in capsule
J: 1000°C, 5 hr, water quenched
K: J plus 500°C, 24 hr, air cooled
L: J plus 600°C, 24 hr, air cooled
M: J plus 700°C, 24 hr, water quenched

The Zr–5% Pd alloy was cold rolled, beta quenched, machined, ground, numbered, and then pickled. All other alloys in the annulus arrays, except Zircaloy-2, Zr–15% Pd, and Zr–15% Pt, were prepared from hot-rolled beta-quenched stock. The Zircaloy-2 specimens were machined from $\frac{1}{8}$-in. rolled and commercially annealed stock, and the Zr–15% Pt and Zr–15% Pd specimens were cut from hot-rolled stock which had not been beta quenched.

The stock material was cut into specimen blanks machined on one edge only. These blanks were numbered and heat treated, where aging was desired, and given the final machining and grinding. After the grinding operation all alloys except the Zr–15% Pd and Zr–15% Pt were pickled to remove cold-worked surface material. The Zr–15% Pd and Zr–15% Pt were left in the as-ground condition. Pickling was done in baths containing HNO_3 and HF ($\sim$10:1), with additions of water, HCl, H_2O_2, or lactic acid as needed. Film, if formed during the pickling, was removed with HNO_3, acetic acid, and HF (25:25:1).

**N: new specimens, not previously contained in L-4-21
O: old specimens, previously contained in L-4-21

was 3.1 mpy based on the amount of nickel in solution and 5.8 mpy based on the amount of oxygen consumed.

The reassembled loop, L-2-21, was operated for short periods with six different solutions during the out-of-pile tests and pretreatment. A 3.9-hr run with 3% trisodium phosphate was made at 93°C in a helium atmosphere, followed by a 24-hr run with a 5% HNO_3 solution in the same atmosphere and at the same temperature. After removal of the acid solution, two charges of water were circulated at 280°C, in oxygen atmospheres, for periods of 2.1 and 26 hr, respectively. Two runs of 103 and 104 hr were made at 280°C in oxygen atmospheres with identical natural-uranium solutions: 0.17 *M* UO_2SO_4, 0.04 *M* H_2SO_4, and 0.022 *M* $CuSO_4$. The over-all loop corrosion rates during the natural-uranium runs were 1.5 and 1.4 mpy, respectively, based on oxygen consumption, and 1.4 and 0.7 mpy, respectively, based on the amount of nickel found in the solutions.

The loop was operated in-pile for three separate periods, with fresh enriched-uranium solution being used in each period. The compositions of the original and make-up solutions for each period are given in Table 15.2.

The main-stream and pressurizer temperatures were held at 280 and 296°C, respectively, except during the second period of in-pile operation when the pressurizer temperature was raised to 302°C for about 35 hr and for the final 21 hr of that period when the main-stream and pressurizer temperatures were lowered to 250 and 265°C, respectively.

Enriched solution was circulated for 67 hr before radiation was initiated, Table 15.3. Samples of solution during the first period of operation indicated that the solution was stable; however, after 705 hr of circulation, the nickel content of the solution had risen to about 700 ppm, whereupon the run was terminated and the solution was drained from the loop.

The second enriched solution was circulated for 19 hr before radiation was initiated. During the next 8 hr with the reactor at the 3-Mw level, followed by 24 hr at zero power, the nickel in solution rose to 266 ppm and the radiolytic-gas pressure to 20–25 psi. An unusually high over-all corrosion rate of 30 mpy, based on oxygen consumption, was observed during this period. Because the copper concentration had been lowered to 0.012 *M* in the second solution, it was considered possible that gas and steam bubbles were forming in the main stream and accelerating the attack. To reduce the possibility of bubble formation, the pressurizer temperature was raised to 302°C from 296°C. The reactor power was then lowered to 1.5 Mw, and operation continued at that level for an additional 8 hr. Based on oxygen consumption, the over-all corrosion rate during this time was about 18 mpy.

In the next operation, the reactor power was lowered to 0.3 Mw and the pressurizer temperature to the original 296°C. During the next 7 hr the O_2 corrosion rate was about 1 mpy. The reactor power was then raised to 0.6 Mw for the next 13 hr, and the O_2 corrosion rate increased to 11 mpy. Because

Table 15.2. Enriched Solutions for In-Pile Operation

	U (*M*)	SO_4 (*M*)	Cu (*M*)	Cr (*M*)	H_2SO_4 (*M*)
First period					
Original solution	0.17	0.24	0.022		0.04
Make-up	0.17	0.28	0.022	0.0021	0.07
Second period					
Original solution	0.17	0.22	0.012	0.0002	0.04
Make-up	0.16	0.25	0.012	0.0021	0.07
Third period					
Original solution	0.17	0.24	0.024		0.04
Make-up	0.17	0.26	0.024	0.0022	0.07

Table 15.3. Summary of General Operating Conditions and Data

Cumulative Time (hr)	LITR Power (Mw)	Accumulated LITR Energy (Mwhr)	Temperature (°C)		Radiolytic-Gas Pressure in Pressurizer (psi)	O_2 Pressure in Pressurizer (psi)	O_2 Incremental Corrosion Rate (mpy)	Nickel (ppm)
			Pressurizer	Main Stream				
				First Period				
0–67	0	0	296	280	0	120–110	1.2	135
67–115	3	106	296	280	33–26	110–60	6.2	64
115–276	3	535	296	280	18–18	145–85	2.0	210–415
276–535	3	1203	296	280	18–18	85–40	1.3	416–452
535–705	3	1611	296	280	18–11	145–95	1.7	506–700
				Second Period				
0–19	0	0	296	280	0	70	0	42
19–27	3	23	296	280	25–20	70–33	30	
27–29	0	23	296	280	0	33–23	20	
29–51	0	23	302	280	0	110–101	0.2	266
51–59	1.5	33	302	280	20–12	101–80	18	
59–64	0	33	302	280	0	81	10.2	
64–88	0	33	296	280	0	81–32–120	0	533
88–95	0.3	48	296	280	3	125–123	1	
95–108	0.6	56	296	280	5	123–109	11	510
108–129	0	56	265	250	0	109–50	7*	537–653
				Third Period				
0–19	0	0	296	280	0	175–145	1	0
19–31	2	23	296	280	13	145–121	12	225
31–45	0.6	26	296	280	4	98–75	14	412
45–50	0	26	296	280	0	63–58	10	344
50–52	3	38	296	280	23	57–47	25–30	
52–53	0	38	296	280	0	47		
53–54	3	42	296	280	18	47–42	25–30	423

*Includes several hours (after reactor shutdown) during which a high corrosion rate was observed.

of the high nickel concentration in solution two-liquid-phase formation was suspected. The mainstream and pressurizer temperatures were lowered to 250 and 265°C, respectively, at zero power, but the solution was drained from the loop when a continued increase in the nickel concentration and high oxygen consumption were observed during the final 21 hr of operation.

Prior to operation with the third enriched solution, heavy water was circulated in the loop for 15 min at 280°C. After removal of the D_2O, the third enriched solution was charged to the loop and circulated for 19 hr before radiation was initiated. During the next 12 hr, with the reactor at a maximum power level of 2 Mw, the nickel concentration in solution rose to 225 ppm. The over-all corrosion rate for this period, based on oxygen consumption, was 12 mpy. The reactor power level was then lowered to 0.6 Mw, but during the next 14 hr the oxygen consumption rate did not change and the nickel in solution increased to 412 ppm. During the final 9 hr of operation the LITR energy level was maintained alternately at 0 and 3 Mw for four short periods. The over-all corrosion rates during these periods, based on oxygen consumption, were observed to be 10 mpy with the reactor at zero power and 25–30 mpy with the reactor at 3 Mw.

No difficulties were encountered with the operation of the circulation pump during this experiment.

The average fission power during operation of the loop with the first enriched solution at 3 Mw was 1490 w, determined from Cs^{137} analyses. The over-all average total fission and gamma heat for the same period, as determined by electric-heater power requirements, was 2404 w. Data obtained from measurements of fission and gamma heat for previous stainless steel loops operated in the HB-2 facility have indicated an average value of about 700 w for the gamma component. The fission heat for this experiment, as determined by electrical power requirements, may therefore be estimated at about 1700 w. If the fission heat calculated on the basis of Cs^{137} analyses is assumed to be correct, then the heat loss from the heater to the cooler section of the combined heater-cooler unit (mentioned above) may be estimated at about 200 w.

Very small amounts of reactor energy were liberated during the second and third periods of loop operation. Consequently, only small amounts of fission heat were produced, and so the power-requirement measurements for these periods are considered unreliable. Fission-power values for the same periods, based on Cs^{137} analyses, are also unreliable since incomplete drainage of the first and second enriched solutions and of the D_2O rinse following the second period resulted in unknown amounts of contamination to the succeeding solutions.

The thermal-neutron fluxes to which core specimens were exposed were determined from induced-activity measurements of representative Zircaloy-2 coupons from the core channel and core annulus arrays. Flux values obtained from the core channel and core annulus coupons were in agreement, showing the usual axial flux gradient and the absence of a radial gradient in the core. The flux values ranged from 1.2×10^{13} neutrons·cm^{-2}·sec^{-1} at the location of the leading core channel coupon to 3.4×10^{12} at the rear coupon. The flux at the core nose, obtained by extrapolation of the coupon data, was 1.5×10^{13}.

Thermal-neutron flux levels in the core were also measured by two cobalt-aluminum flux monitors, located in the core annulus, which were segmented and measured for induced activity. The values 1.2×10^{13} neutrons·cm^{-2}·sec^{-1} at the core nose and 2.6×10^{12} at a position radial to the location of the rear channel coupon, were only 75 to 80% of those obtained from zirconium-specimen analyses. It is interesting to note that in the two previous HB-2 experiments which contained cobalt flux monitors, L-2-17[1] and L-2-19,[2] flux values determined from cobalt were 75 and 87%, respectively, of those obtained from the Zircaloy-2 specimens. In L-4-18,[3] an HB-4 experiment and the only other one to contain a cobalt monitor, flux levels were in agreement with values obtained from the Zircaloy-2 core specimens. Agreement in flux values obtained from analyses of Zircaloy-2 core channel and core annulus coupons indicated that there was no radial flux gradient.

The thermal-flux values determined from Zr^{95}-Nb^{95} measurements were used to calculate fission power densities in solution. The values ranged from 15.5 w/ml for the leading core channel coupon to 4.4 w/ml for the rear coupon. Estimated solution

[1] G. H. Jenks *et al.*, *HRP Quar. Prog. Rep. Jan. 31, 1958*, ORNL-2493, p 120.

[2] G. H. Jenks *et al.*, *HRP Prog. Rep. for Quarters Ending April 30 and July 31, 1958*, ORNL-2561, p 214–26.

[3] G. H. Jenks *et al.*, *HRP Prog. Rep. for Quarters Ending April 30 and July 31, 1958*, ORNL-2561, p 203.

power densities were 19.6 w/ml at the nose of the core and 16.8 w/ml at the Zircaloy-2 and type 347 stainless steel core nose specimens. Power densities associated with the absorption of fast-neutron energy in this experiment are estimated to have been approximately 0.5 w/ml at the location of the leading core channel coupon and 0.1 w/ml at the rear coupon.

15.1.2 Results of Qualitative Inspection and Metallographic Examination of Loop L-2-21

Loop L-2-21 was dismantled without difficulty. The components removed from the loop included the core, the two in-line sample holders, the pressurizer, two sections of the pressurizer heater, four sections of the loop piping (from the pump and core inlets and outlets), a section of the loop heater-cooler, the pump, and one section each from the sampling-line capillary and the two pressurizer gas-addition capillaries.

Specimens from the loop components which were examined metallographically included sections from the core-cap nose, pressurizer body, pressurizer-heater line, loop piping, volute at pump outlet, pump rotor shaft, pump thermal spacer, sample-line capillary tube, oxygen-line capillary tube, and the pressure-line capillary tubing.

Metallographic examination of some representative core and in-line channel coupons and pressurizer stress specimens was also completed.[4] A summary of the metallographic investigation of these corrosion specimens is presented in Table 15.4. Examination of the zirconium-alloy core and in-line annulus coupons has been deferred until surface inspection of these specimens has been completed.

The pump from this loop was completely dismantled and examined. Before dismantling, it was noted that the impeller rotated freely and that there was adequate end-play. After dismantling, examination of the volute showed severe pitting attack on the volute lip at the outlet port. Pits up to 100 mils deep were noted[4] as shown in Fig. 15.1. The bearing surfaces and other portions of the pump, with the exception of the thermal-barrier region, appeared to be in good condition. The nature and location of attacked areas in the thermal-barrier region appear to be about the same as those noted in L-2-19.[5] Corrosive attack on the pump rotor shaft occurred in a very restricted region, approximately 0.15 in. in length. The maximum depth of attack, about 12 mils, occurred abruptly toward the impeller end of the attacked area; the attack decreased to zero within the 0.15-in. length. The inner and outer

[4] A. E. Richt, *Metallographic Examination of Components and Coupons from HRP In-Pile Loop L-2-21 – Part I*, ORNL CF-58-9-15 (Sept. 2, 1958).

[5] G. H. Jenks *et al.*, *HRP Prog. Rep. for Quarters Ending April 30 and July 31, 1958*, ORNL-2561, p 217.

UNCLASSIFIED
RE-148

Fig. 15.1. Pump-Volute Outlet-Port Trailing Edge. 10X.

Table 15.4. Summary of Zircaloy-2, Type 347 Stainless Steel, and Ti-110AT Core Coupon Corrosion Rates and Metallographic Examination of Stress Specimens and Core and In-Line Channel Coupons

Coupon No.	Power Density (w/ml)	Solution Velocity (fps)	Calculated Penetration from Weight Measurements (mils)		Corrosion Rate (mpy)		Metallographic Results			
							Measured Thickness (mils)			Surface Appearance
			Exposed Area	Total Area	Exposed Area	Total Area	End	Center	End	
Type 347 Stainless Steel										
Core nose coupon										
SA-1588	16.8	~1.0	5.15	3.25	78.9*		51.0	51.0	52.0	Severe general corrosion; all exposed surfaces
Core channel coupons										
SA-1578	13.1	11.3	5.22	3.33	80.1*					
SA-1581	12.4	12.4	4.35	2.77	66.6*					
SA-1623	11.1	15.8	4.69	2.98	71.9		46.0	54.0	45.5	Severe general corrosion; particularly at ends
SA-1624	9.6	27.0	5.08	3.28	77.8*					
SA-1625	8.2	37.3	8.41	5.35	128.9		21.0	51.0	0	Severe general corrosion; on one surface only, ends heavily attacked
SA-1626	6.2	18.8	0.15	0.10	2.4*					
SA-1582	5.2	12.4	0.18	0.12	2.8		59.0	58.5	58.5	Scattered pits < $\frac{1}{4}$ mil deep; all surfaces
SA-1583	4.4	9.2	0.05	0.03	0.8*					
Line channel coupons										
SA-1632		15.8	+11 mg/cm^2	+7 mg/cm^2			59.0	59.0	59.0	No attack, nonuniform scale; all surfaces
SA-1634		37.3	+4 mg/cm^2	+3 mg/cm^2			59.0	59.0	59.0	Pitting attack to 3 mils under uniform $\frac{1}{4}$-mil scale
SA-1636		12.4	+9 mg/cm^2	+6 mg/cm^2			59.0	59.0	59.0	Slight pitting attack under heavy 1-mil scale
Zircoloy-2										
Core nose coupon										
ZB-42	16.8	~1.0	5.15	3.25		7.8				
Core channel coupon										
ZB-178	14.6	9.5	0.68	0.43		6.6*				
ZB-179	14.0	10.3	0.67	0.42		6.5				
ZB-180	10.6	18.3	0.48	0.31		4.7*				
ZB-181	9.1	32.1	0.37	0.24		3.6	61.0	60.5	60.5	Smooth, even surface; possible attack at stringers
ZB-182	7.6	41.2	0.31	0.19		3.0				
ZB-183	7.3	37.5	0.28	0.18		2.7*				
ZB-184	5.6	13.9	0.19	0.12		1.8				
ZB-210	4.9	11.0	0.10	0.07		1.0*				
ZB-211	4.7	10.0	0.13	0.09		1.3	61.0	60.5	60.0	Smooth, even surface; possible attack at stringers
Core annulus coupons										
3-2	12.2	~1.0	0.36	0.34		5.1				
4-4	9.7	~1.0	0.25	0.23		3.6*				
3-6	7.9	~1.0	0.19	0.18		2.8*				
10-5	6.3	~1.0	0.15	0.13		2.1				
4-8	6.3	~1.0	0.17	0.16		2.5*				
Line channel coupons										
ZB-189		32.1	+3 mg/cm^2	+2 mg/cm^2			60.0	60.0	60.5	Smooth, even surface; $\frac{1}{2}$-mil scale
ZB-193		10.0	+4 mg/cm^2	+3 mg/cm^2			61.5	61.0	61.0	Smooth, even surface; $\frac{1}{2}$-mil scale

Table 15.4 (continued)

Coupon No.	Power Density (w/ml)	Solution Velocity (fps)	Calculated Penetration from Weight Measurements (mils)		Corrosion Rate (mpy)		Metallographic Results			
							Measured Thickness (mils)			Surface Appearance
			Exposed Area	Total Area	Exposed Area	Total Area	End	Center	End	
Titanium 110AT										
Core channel coupons										
TD-3	15.5	8.8	0.19	0.12	3.0*					
TD-4	11.8	13.9	0.03	0.02	0.5		56.0	55.0	55.0	Smooth, even surface; no scale formation
TD-5	10.0	21.4	0.01	0.01	0.1*					
TD-6	8.5	34.6	0.02	0.02	0.4*					
TD-7	7.3	28.0	0.01	0.01	0.1		55.0	55.0	55.0	Smooth, even surface; no scale formation
TD-8	6.5	22.5	0.04	0.03	0.7					
TD-9	5.8	16.0	0.11	0.07	1.7		54.0	52.5	52.5	Smooth, even surface; ½-mil scale on one surface
Line channel coupons										
TD-31		13.9	+11 mg/cm^2	+7 mg/cm^2			60.0	60.0	59.0	Smooth, even surface; ½-mil scale on both surfaces
TD-15		28.0	+10 mg/cm^2	+6 mg/cm^2			58.0	61.0	64.0	Smooth, even surface; ¼-mil scale on both surfaces
Pressurizer liquid-phase stress specimens										
TD-5		$\ll$1.0	+12 mg/cm^2	+10 mg/cm^2			63.0	62.0	61.0	Smooth, even surface; oxide scale on both surfaces**
TD-10		$\ll$1.0	+6 mg/cm^2	+5 mg/cm^2			60.0	61.0	62.0	Smooth, even surface; oxide scale on both surfaces**
Pressurizer vapor-phase stress specimens										
TD-13		$\ll$1.0	0.04		0.60		60.0	61.0	62.5	Smooth, even surface; no evidence of surface scale
TD-14		$\ll$1.0	+0.04 mg/cm^2	+0.04 mg/cm^2			63.5	63.0	64.0	Smooth, even surface; no evidence of surface scale
Type 430L Stainless Steel										
Pressurizer liquid-phase stress specimens										
SL-17		$\ll$1.0	0.01	0.01	0.2		63.0	62.5	62.5	Smooth, even; no evidence of attack
SL-18		$\ll$1.0	0.02	0.01	0.2		61.5	62.0	62.5	Smooth, even; no evidence of attack
Pressurizer vapor-phase stress specimens										
SL-13		$\ll$1.0	0.08	0.06	1.2		63.0	63.0	63.0	Smooth, even; no evidence of attack
SL-14		$\ll$1.0	0.08	0.06	1.2		61.5	62.5	63.0	Smooth, even; no evidence of attack

*Corrosion rates calculated by using the "as-removed" specimen weight. Specimens were not defilmed but were submitted for gross scale analyses.

**Covered with a heavy 1½-mil oxide scale on tension surfaces, with a light ½-mil oxide scale on compression surfaces.

threaded portions of the thermal spacer were similarly severely corroded, although the depth of attack could not be accurately estimated because of the threads. Sections of the pump inlet and outlet pipes, only slightly corroded, were covered with a ¼-mil oxide scale.

The components outside the core region were generally covered with heavy, flaky, dark-gray scale with an additional heavy dark-reddish-brown, rustlike deposit, particularly in the low-velocity areas and crevices. After transverse sectioning, a large quantity of loose, dark-colored, porous scale fell from the pressurizer. A small sample was analyzed chemically, and the results are reported in Sec 15.1.3. The pressurizer vapor-phase region was relatively free from scale, particularly at the ends, which were bright and shiny. However, the liquid-phase area was uniformly covered with a heavy dark-brown, almost-black, scale. There was no scale accumulation in the interface region. Metallographic examination[4] showed little evidence of corrosive attack, but oxide scales 1 mil and ¼ mil thick were found on the liquid- and vapor-phase sections, respectively. Sections from the pressurizer-heater inlet line, U-bend, and outlet line showed only slight, general surface roughening. The inlet and U-bend specimens were covered with 3-mil duplex scales and the outlet specimens with a ¼-mil oxide scale.

Sections of the oxygen-line and pressure-line capillary tubes showed no evidence of attack or scale formation, but the sampler-line capillary showed heavy corrosive attack along the entire length of the examined section, with a minimum depth of 1 mil. This is in contrast to the appearance of the sampler lines from previous loops which showed only localized attack at the pump-outlet end of the capillary.

The coupons and specimens from the line channel, line annulus and pressurizer region were unusual in appearance. Typical heavy dark-brown, rustlike scale was found principally along the clamped edges. In general, the surfaces were covered with a heavy dark-gray scale, brittle in appearance, which flaked off in some areas. This was most notable on the Zircaloy-2 coupons, which are usually covered with a very adherent film. Two Zr–15% Pd coupons from the line annulus array showed a loose gray-white scale with some spots of overlying brown scale. There was no visual evidence of cracking or localized attack on any of the pressurizer stress specimens. The standard cathodic defilming technique was not entirely effective in removing the scale from the out-of-core coupons and specimens.

The high-flux end of the interior surface of the type 347 stainless steel core body was covered with a film which appeared to be thin and light-brown-to-bronze in color; this film gradually thickened and darkened along the core, and at the rear, it had a heavy, soft, dark-brown, almost-black appearance. Examination of sections of the core-cap nose, core body, and core inlet and outlet pipes showed severe but uniform corrosion with no evidence of localized attack. Macroscopic examination of the weld joining the core body to the core cap indicated the possibility of some knife-line attack adjacent to the weld head. Unfortunately, a section of this area was lost during preparation for metallographic examination and it is not known whether such attack had occurred.

The two "core nose" specimens, originally attached to the forward end of the core spider, were missing when the core specimen assembly was removed. Only the welds remained where the type 347 stainless steel mounting brackets had been attached to the spider. The brackets could not be found, but the nose specimens were lying in the core. The stainless steel "core nose" specimen was heavily corroded in the exposed areas, while the edge positions originally held in the brackets were partially protected. The film on the type 347 stainless steel spiders was similar to that found on the core body in the same flux regions. There was evidence of pitting on the forward spider. The titanium CA coupon holders were generally covered with typical thin bronze-colored films at the high-flux ends. The films gradually thickened and darkened along the holders. At the rear they were dark gray and appeared to be overlaid by black scale. The Zircaloy-2 CC coupon holder was covered with a typical thin gray film at the high-flux end. At the low-flux end the holder was covered with a heavy gray-to-black scale with patches of brown scale. Scale accumulation was heavier on the interior surfaces of the holder.

The titanium-110AT CC coupons were covered with a thin layer of dark-brown-to-gray scale over a typical bronze-colored film. Surfaces of the Zircaloy-2 CC coupons appeared slightly roughened and were covered with a thin layer of dark scale over a typical irridescent gray film. Surfaces of the type 347 stainless steel CC coupons appeared severely corroded and retained some dark scale. The stainless steel CC coupons in the forward portion of the

holder showed evidence of only partial protection in the clamped-end areas. Figure 15.2 is a photograph of the most severely corroded type 347 stainless steel CC coupon, showing the widespread shallow-pit nature of the attack and the inadequate protection in the clamped areas. As shown, one coupon corner stands up in relief, while another is almost completely corroded away.

15.1.3 Analysis of Data from Loop L-2-21

(a) Analyses of Scale from Low-Power-Density Regions. – Chemical analyses for U, Cu, Cr, Ni, Fe, and Zr were made on samples of bulk scale removed from the rear of the core wall, the in-line annulus coupon holder, the pump volute, the liquid- and vapor-phase sections of the pressurizer at the inlet and outlet, and on loose scale found in the pressurizer. In addition, analyses were made on solutions in which the rear and front pump journals were leached. The reported analytical results show wide variation in the composition of the scales taken from different loop locations, a characteristic in common with the results of scale analyses in some previous in-pile loop experiments.[6–9] On the average, excluding the pump-journal sample, the scales on L-2-21 contained 0.09% U, 4.2% Zr, 7.5% Ni, 0.4% Cr, 2.6% Cu, and 53.2% Fe. A material balance of Fe, Ni, Cr, and Zr was attempted as in previous experiments.[6–9] The results, considered of qualitative significance only, exhibited the same features as those from prior experiments. The nickel was almost evenly distributed between the loop solution and the scales, and the total amount indicated was a factor of 1.5 greater than that calculated to have been present as a result of the oxidation of steel based on O_2 data. The results indicate that only a small part of the zirconium that was oxidized in the core is accounted for in the scale contained outside the core, a result in contrast with results from some previous loops where complete transfer of ZrO_2 was indicated.[6,8,9]

(b) Analyses for Uranium on Core and In-Line Coupons and Holders. – (1) *Procedure and Results.* – Correlations between corrosion rates and the amounts of uranium sorbed in scales have indicated a strong effect of sorbed uranium on radiation-corrosion. Therefore a large number of specimens from the core of this loop were submitted for scale analyses. In addition, two type 347 stainless steel LC coupons and the Zircaloy-2 LC coupon holder were also analyzed for surface uranium. Each specimen was treated separately with a concentrated acid solution composed of H_2SO_4, HCl, and HNO_3 in the ratio of 8:2:1, except for the titanium coupons, which were treated with 5 *M* HCl. Visually,

[6] G. H. Jenks *et al.*, *HRP Prog. Rep. for Quarters Ending April 30 and July 31, 1958*, ORNL-2561, p 208–42.

[7] *Ibid.*, p 219–42.

[8] G. H. Jenks *et al.*, *HRP Quar. Prog. Rep. July 31, 1957*, ORNL-2379, p 113.

[9] G. H. Jenks *et al.*, *HRP Quar. Prog. Rep. Jan. 31, 1958*, ORNL-2493, p 124.

UNCLASSIFIED
PHOTO-43244

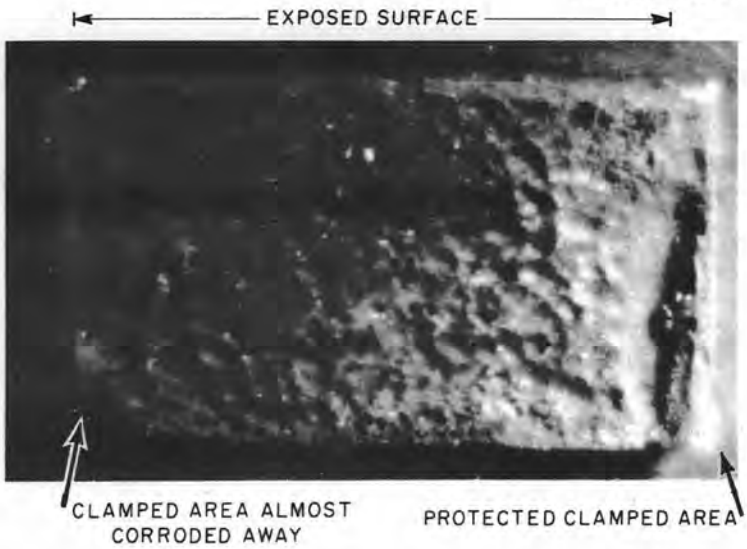

Fig. 15.2. Type 347 Stainless Steel CC Coupon SA-1625. 6.6X.

the specimens appeared clean after these treatments. The solution samples, containing scale and base metal, were analyzed for U, Cu, Cr, Ni, Fe, Zr, Pt, Pd, Ti, Ru^{103}, and Cs^{137}. In Table 15.5, the amount of each constituent is listed as per cent by weight of the amount of material in the sample, with the exception of Ru^{103}, which is reported as disintegrations per minute, and Cs^{137}, reported as total fissions. The weight per cent of each scale sample not represented by the reported analyses is listed under the column "other." The ruthenium and cesium analyses were made 74 days after termination of the experiment. All specimens were analyzed in the as-removed condition except for ten of the core coupons, which were first subjected to the usual defilming procedure.

The total weight of uranium for a given specimen was calculated from the analytical results, and the calculated values are listed in Tables 15.5 and 15.6 as the weight of uranium per unit area of a given specimen. The weight of iron contained in the surface scales was also calculated for each specimen of a material other than stainless steel; these values are in Table 15.6. For these calculations the amount of iron found in each scale sample was corrected by subtracting the weights of the element oxidized from the alloys, assuming the following values for the iron content of the alloys: Zircaloy-2, 0.12%; Zr-Nb alloys, 0.02%; Ti-110AT, 0.05%.

(2) *Discussion of Results.* – No special significance has been noted for the Ru^{103} and Cs^{137} results at this time. The rate of decay of the total quantity of Ru^{103} at the time of counting was 8×10^{12} dis/min; the total quantity of Cs^{137} was equivalent to the amount produced by 8×10^{19} fissions.

The calculated values for surface iron show that many of the specimen films contained transported iron oxide in amounts ranging up to about 1 mg/cm^2. One of the sections of the Zircaloy-2 channel coupon holder exhibited about 3 mg of iron per square centimeter. There is no evidence from the results obtained with the cathodically defilmed specimens that the defilming operation appreciably affected the retained iron oxide. For comparison with previous results, the Zircaloy-2 and crystal-bar-zirconium core specimens from loop L-2-19 (0.17 *m* UO_2SO_4, 0.2 *m* Li_2SO_4, 0.1 *m* H_2SO_4, and 0.02 *m* $CuSO_4$ at 280°C) held a maximum of 31 μg of iron per square centimeter and a negligible amount of uranium.[10]

In L-2-17 (0.04 *m* UO_2SO_4, 0.025 *m* H_2SO_4, 0.005 *m* $CuSO_4$ at 300°C) the two Zircaloy-2 specimens which were examined held, respectively, 27 and 50 μg of iron per square centimeter and 21 and 5.5 μg of uranium per square centimeter. These two specimens from L-2-17 were exposed in a core position where the fission power density was approximately equal to the average power density in the core. Specimens from the rear of the core in L-2-17 for which information was obtained by analyzing the pickling solution showed[11] for iron about 10^4 μg/cm^2 and for uranium about 100 μg/cm^2. In experiment L-2-21 the Zircaloy-2 specimens near the front of the core were free of transported iron, but the Ti-110AT specimen, TD-3, in the high-flux region held 950 μg of iron per square centimeter.

The uranium held on the L-2-21 Zircaloy-2 surfaces which were free of transported iron oxide, or which retained fairly small amounts of iron, is in the range of 0 to 6.4 μg/cm^2, with an average value of 1.6 μg/cm^2. The Zircaloy-2 core specimens with appreciable amounts of transported iron exhibit, in general, greater amounts of retained uranium, and the values for the ratio of U/Fe held by these specimens is fairly constant, as shown in Table 15.6. Thus it appears that uranium is sorbed on the iron oxide and deposited along with it. The U/Fe ratio for the Ti-110AT core specimens is, on the average, a factor of 3 less than the average value of the ratio for Zircaloy-2. The average value of the ratio for the in-line Zircaloy-2 channel holder is a factor of 8 less than the average for the core Zircaloy-2.

The effect on corrosion of the uranium sorbed along with the iron is probably quite small. The average of the ratio of U/Fe for the core Zircaloy-2 specimens which held appreciable iron is 0.055. The weight of transported oxide on a surface may be estimated as twice that of the iron. Hence the uranium probably comprised 2.5 to 3% of the weight of the transported oxide. Consideration of the ranges of fission fragments in iron oxide and in water indicate that the intensity of fission-fragment irradiation of a surface in contact with a ferric oxide film containing 2 to 3% uranium is about the same as that of a surface in contact with a solution 0.17 *m* UO_2SO_4.

[10] G. H. Jenks *et al.*, *HRP Prog. Rep. for Quarters Ending April 30 and July 31, 1958*, ORNL-2561, p 219–26.

[11] G. H. Jenks *et al.*, *HRP Quar. Prog. Rep. Jan. 31, 1958*, ORNL-2493, p 125.

Table 15.5. Analyses for Uranium and Other Elements on Core and In-Line Coupons and Holders in Loop L-2-21

Specimen	Power Density at Specimen (w/ml)	Solution Velocity (fps)	Total Area (cm^2)	Sample Weight (mg)	Amount in Sample (wt %)										Weight Uranium Per Unit Area ($\mu g/cm^2$)	Ru^{103} (dis/min)	Cs^{137} (total fissions)
					U	Cu	Cr	Ni	Fe	Zr	Pd	Pt	Ti	Other			
Zircaloy-2 Core Coupon Holder																	
																$\times 10^8$	$\times 10^{14}$
Front			24	119	0.44	0	2.0	0.30	10.1	64.3				22.9	21.8		
Center front			24	5,910	0	0	0.06	0.08	0.03	83.2				16.6	0		
Center rear			24	6,643	0.0004	0	0.02	0.04	0.005	98.8				1.1	1.11		
Rear			24	10,207	0	0	0.02	0.04	0.005	66.7				33.2	0		
Zircaloy-2 In-Line Coupon Holder																	
Front			24	2,479	0.014	0	0.62	0.18	2.82	73.9				22.5	14.5		
Center front			24	577	0.04	0.04	0.76	0.08	4.2	79.5				15.4	9.6		
Center rear			24	1,067	0.01	0.02	0.42	0	1.38	80.6				17.6	4.4		
Rear			24	165	0.06	0.1	0	0.4	11.0	123				34.6	4.1		
Coupon Specimens																	
Type 347 SS																	
Core channel																	
SA-1578	13.1	11.3	2.2	51	0.05	0	0.3	5.0	60.7	0.8	0***	0***	0	33.2	11.6	1.59	0.25
SA-1581	12.4	12.4	2.2	72	0.01	0	0.1	6.7	58.7	0.7	0	0	0	33.8	3.3	0.55	0.16
SA-1624	9.6	27.0	2.2	70	0.08	0	0.4	6.0	61.6	0.6	0	0	0	31.3	25.5	1.51	1.0
SA-1626	6.2	18.8	2.2	47	0.07	0.04	1.0	7.6	61.8	0.5	0	0	0	28.6	12.7	1.46	2.4
SA-1583	4.4	9.2	2.2	54	0.08	0	0.8	3.6	62.5	0.7	0	0	0	32.3	19.6	1.48	2.2
Line channel																	
SA-1633		27.0	2.2	28	0.30	0	0.9	6.3	57.0	0.7	0	0	0	34.8	38.2	3.58	0.25
SA-1637		9.2	2.2	11	1.00	0	Negligible	2.9	40.8	1.3	0	0	0	54.0	50.0	3.68	0.94
Zircaloy-2																	
Core channel																	
ZB-178	14.6	9.5	2.2	128	0.004	0.06	Negligible	0.2	0.1	78.1	0	0	0	21.5	2.3	0.67	1.43
ZB-179	14.0	10.3	2.2	198*	0	0.03	Negligible	0.1	0.1	97.7	0	0	0	2.1	0*	0.51	1.99
ZB-180	10.6	18.3	2.2	27	0.05	0.24	Negligible	0.6	0.5	61.4	0	0	0	37.2	6.1	0.47	0.77
ZB-182	7.6	41.2	2.2	108*	0.02	0	Negligible	0.1	0.5	83.1	0	0	0	16.3	9.8*	0.23	1.68
ZB-183	7.3	37.5	2.2	59	0.04	0.16	Negligible	2.8	0.8	89.3	0	0	0	6.9	10.7	0.47	0.71
ZB-184	5.6	13.9	2.2	193*	23**	0	Negligible	164**	710**	13,620**	0	0	0		10.5**	0.76	0.91
ZB-210	4.9	11.0	2.2	171	0.03	0	Negligible	0.1	0.8	85.0	0	0	0	14.1	23.3	1.80	2.57
Core annulus																	
10-5	6.3	~1.0	3.4	95*	0.018	0	Negligible	0.1	0.5	95.0	0	0	0	4.4	5.0	0.25	2.10
3-6	7.9	~1.0	3.4	527	0.007	0.03	Negligible	0.03	0.2	87.3	0	0	0	12.4	10.9	0.24	3.00
4-4	9.7	~1.0	3.4	467	0.012	0.03	Negligible	0.03	0.4	79.3	0	0	0	20.2	16.5	0.14	2.88
4-8	6.3	~1.0	3.4	71	0.005	0	Negligible	0.02	0.2	85.3	0	0	0	14.5	1.0	0.87	2.94
Core nose	16.8		2.2	156	0.002	0	Negligible	0.1	0.06	76.3	0	0	0	23.5	1.4	0.25	2.40

Table 15.5 (continued)

Specimen	Power Density at Specimen (w/ml)	Solution Velocity (fps)	Total Area (cm^2)	Sample Weight (mg)	Amount in Sample (wt %)										Weight Uranium Per Unit Area ($\mu g/cm^2$)	Ru^{103} (dis/min)	Cs^{137} (total fissions)
					U	Cu	Cr	Ni	Fe	Zr	Pd	Pt	Ti	Other			
Coupon Specimens																	
Ti-110AT																	
Core channel																	
TD-3	15.5	8.8	2.2	27	0.20	0	0.04	0.3	7.8	0.7	0	0	71.2	19.8	24.5	3.0	9.52
TD-5	10.0	21.4	2.2	29	0.01	0	Negligible	0.2	1.0	0.6	0	0	89.8	8.4	1.3	0.89	6.40
TD-6	8.5	34.6	2.2	28	0.04	0.4	Negligible	0.2	1.4	0.8	0	0	95.0	2.2	5.1	1.11	3.52
TD-8	6.5	22.5	2.2	33*	0	0.3	Negligible	0.3	1.0	0.7	0	0	83.3	14.4	0	0.34	2.80
Zr–15% Nb																	
Core annulus																	
1-1	13.3	~1.0	3.4	481	0.006	0	Negligible	0.02	0.3	85.2	0	0	0	14.5	8.5	1.09	3.60
1-5	9.7	~1.0	3.4	656*	0.011	0	Negligible	0.02	0.3	83.1	0	0	0	16.6	21.2	0.98	3.13
Zr–7.5% Nb																	
Core annulus																	
5-1	13.3	~1.0	3.4	105*	0.008	0	Negligible	0.12	0.12	83.7	0	0	0	16.1	2.5	0.53	2.42
Zr–15% Nb–2% Pd																	
Core annulus																	
2-2	12.2	~1.0	3.4	35*	0.025	0	Negligible	0.48	0.07	49.6	2.3	0	0	47.5	2.6	0.70	4.64
2-6	17.9	~1.0	3.4	157*	0.005	0	Negligible	0.39	0.08	76.3	0.48	0	0	22.7	2.3	0.34	2.42
Zr–15% Nb–2% Mo																	
Core annulus																	
8-7	7.0	~1.0	3.4	145*	0.025	0	Negligible	0.08	0.10	75.9	0	0	0	23.9	10.7	0.25	5.46

*Specimens defilmed by usual procedure before treatment and analyses.

**Portion of sample solution lost; results reported in total micrograms.

***Pt and Pd values of zero indicate analysis showed less than detectable limits of 500 μg total Pd and 1500 μg total Pt.

Table 15.6. Iron and Uranium on Various Surfaces in L-2-21

Specimen	Total Iron Reported ($\mu g/cm^2$)	Amount of Iron from Base Metal ($\mu g/cm^2$)	Transported Iron ($\mu g/cm^2$)	Uranium ($\mu g/cm^2$)	Uranium/Transported Iron
Scale Specimens Containing Negligible or No Transported Iron					
Zircaloy-2					
Core channel coupon holder					
Center front	74	296	0	0	
Center rear	14	332	0	1.1	
Rear	22	510	0	0	
Core channel coupons					
ZB-178	58	70	0	2.3	
ZB-179*	89	108	0	0	
ZB-180	62	14	48	6.4	
Core nose coupon					
ZB-42	42	187	0	1.4	
Core annulus coupon					
4-8	41	26	15	1.3	
Zirconium alloys					
Core annulus coupons					
Zr–7.5% Nb: 5-1*	38	6	32	2.5	
Zr–15% Nb–2% Pd: 2-2*	8	2	6	2.6	
2-6*	37	9	28	2.3	
Zr–15% Nb–2% Mo: 8-7*	43	9	34	10.7	
Scale Specimens Containing Transported Iron					
					$\times 10^3$
Zircaloy-2					
Core channel coupon holder					
Front	501	6.0	495	21.8	44
In-line channel coupon holder					
Front	2913	124	2789	14.4	5.2
Center front	1002	29	973	9.6	9.9
Center rear	613	53	560	4.5	8.0
Rear	756	8	732	4.1	5.6
Core channel coupons					
ZB-182*	241	60	181	9.8	54
ZB-183	210	33	177	10.7	60
ZB-184*	317**	107**	210**	10.4**	50**
ZB-210	610	98	513	23.5	46
Core annulus coupons					
10-5*	139	32	107	5.0	47
4-4	541	163	378	16.4	43
3-6	301	183	118	10.9	94

Table 15.6 (continued)

Specimen	Total Iron Reported ($\mu g/cm^2$)	Amount of Iron from Base Metal ($\mu g/cm^2$)	Transported Iron ($\mu g/cm^2$)	Uranium ($\mu g/cm^2$)	Uranium/Transported Iron
	Scale Specimens Containing Transported Iron				
					$\times 10^3$
Zr–15% Nb					
Core annulus coupons					
1-1	424	29	395	8.5	22
1-5*	579	38	541	21.2	39
Titanium 110AT					
Core channel coupons					
TD-3	957	6	951	24.5	26
TD-5	132	7	125	1.3	10
TD-6	178	6	172	5.1	30
TD-8*	150	8	142	0	0

*Specimens defilmed by usual procedure before treatment and analyses.

**Portion of sample lost; results reported in total micrograms.

The average amount of uranium, 1.6 $\mu g/cm^2$, found on Zircaloy-2 surfaces which held small amounts of iron or no iron is less than would be expected from the results of previous experiments, L-2-15 (0.17 *m* UO_2SO_4, 0.03 *m* H_2SO_4, 0.015 *m* $CuSO_4$ in H_2O at 280°C) and L-4-16 (0.19 *m* UO_2SO_4, 0.025 *m* H_2SO_4, 0.015 *m* $CuSO_4$ in H_2O at 280°C). Analyses for surface uranium were not made in these previous experiments, but the correlation which has been made between surface uranium and corrosion rate at a given solution power density had led to the conclusion that the uranium sorption on the core channel specimens in L-2-15 and L-4-16 was approximately 9 $\mu g/cm^2$ and on the core annulus specimens was more than 15 $\mu g/cm^2$. As will be discussed later, the corrosion rate of Zircaloy-2 at a given solution power density in the L-2-21 experiment is less than that in the L-4-16 and L-2-15 experiments, and there is no reason to suspect the validity of the above-mentioned correlation. However, the explanation for the lower uranium absorption in L-2-21 is unknown.

(c) Results of Specimen Weight Measurements and Discussion. – (1) *General.* – All corrosion-rate values reported below were calculated from weight-loss data with the specimen area and total radiation time (equivalent to 570 hr of LITR operation at 3 Mw) used as the bases for the calculations. The weight loss for each defilmed coupon, including the coupons which were exposed to pretreatment solutions in loop L-4-21 and then scrubbed and remounted in L-2-21, was assumed to be the difference between the original and defilmed weights. The weight loss for coupons submitted for gross-scale analyses without defilming was assumed to be the difference between the original and as-removed weight. Average solution velocities across the coupons contained in the tapered-channel holders were 8.8 to 41.2 fps. Solution velocity across the annulus coupon arrays was estimated at about 1 fps. Power-density values for the core specimens are based on flux values determined from the induced activity in zirconium. Unless otherwise stated, the power-density values do not include the estimated fast-neutron contribution at the specimen positions. The core channel and core annulus specimens are designated as CC and CA, respectively, and the corresponding in-line specimens as LC and LA. Stress specimens located in the liquid or vapor regions of the pressurizer are designated PL and PV.

(2) *Zircaloy-2.* – Core specimens. – Corrosion rates derived from weight measurements are listed in Table 15.4 for the core channel and nose coupons and for the five annulus coupons which were prepared from commercially annealed material. The

channel coupons were also of commercially annealed stock but were not pickled prior to insertion; the core annulus coupons were pickled. A summary of the results of metallographic examination of several Zircaloy-2 coupons is included in Table 15.4. The corrosion data are plotted vs fission power density in Fig. 15.3. For comparison, results from L-2-15, L-4-16, L-2-14, L-2-19, and L-2-17 specimens are also shown.

Corrosion data for other core annulus specimens, which were prepared from specially heat treated material, are listed in Table 15.7.

In-Line Specimens. – All specimens from the LC and LA positions, after being defilmed by the usual

UNCLASSIFIED
ORNL-LR-DWG 34736

EXP. NO.	CC	CA	CORE NOSE	SOLUTION COMPOSITION (*M*) UO_2SO_4	$CuSO_4$	H_2SO_4	OTHER	TEMPERATURE (°C)
L-2-15	▲	△		0.17	0.015	0.03		280
L-4-16	■	□		0.17	0.015	0.025		280
L-2-21	●	○	◒	0.17	0.012–0.024	0.04		280
L-2-14	▼	▽		0.17	0.015	0.42		280
L-2-19	⧫	◊		0.17	0.02	0.10	0.2 Li_2SO_4	280
L-2-17	◪			0.04	0.005	0.025		300

NOTES: 1. CORROSION RATES FOR COUPONS MARKED "X" CALCULATED FROM UNDEFILMED COUPON WEIGHT.
2. RATES BASED ON TOTAL AREA AND RADIATION TIME
3. FAST-NEUTRON CONTRIBUTION NOT INCLUDED IN POWER DENSITY

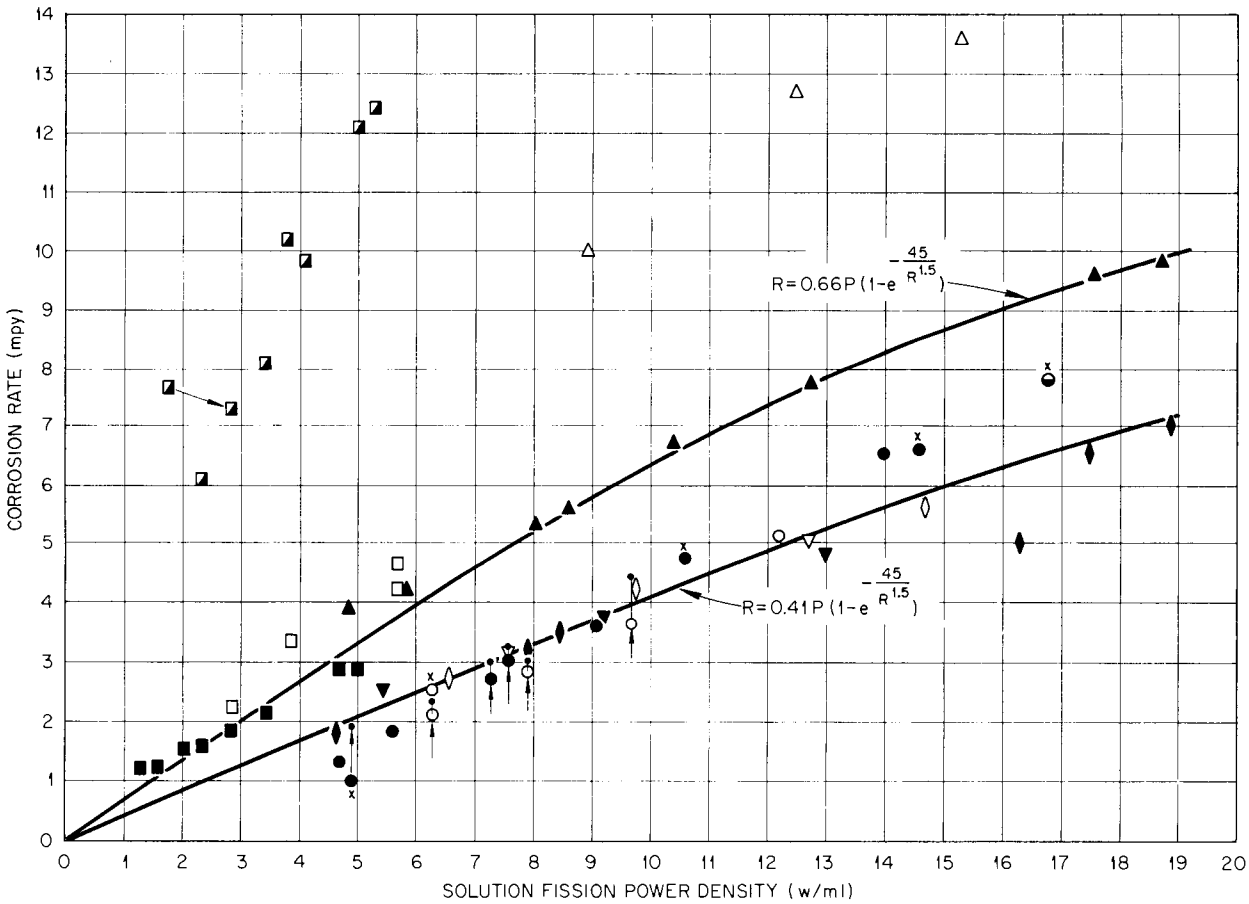

Fig. 15.3. Zircaloy-2 Corrosion Rates vs Fission Power Density.

Table 15.7. Relative Corrosion Rates of L-2-21 Zirconium-Alloy Core Annulus Coupons

Alloy	Power Density[a] (w/ml)	Relative Corrosion Rate[b] for Various Heat Treatments[c]									
		A	B	E	C	M	L	K	J	H	I
Zircaloy-2	6.3										1.04
	7.0									1.12	
	9.7										1.00
	10.9									1.07	
Zr–7.5% Nb	8.8	3.29									
	13.3	1.81									
Zr–10% Nb	8.8	1.74									
	13.3	1.27									
Zr–15% Nb	9.7	0.33									
	13.3	0.37									
Zr–20% Nb	8.8	0.31									
	13.3	0.36									
Zr–25% Nb	8.8	0.60									
	13.3	0.54									
Zr–5% Pd	7.0	0.88									
	10.9	0.96									
Zr–15% Pd	7.0						8.65				
	8.8								6.23		
	10.9						5.28				
	13.3								2.44		
Zr–15% Pt	6.3					1.05					
	7.9							0.60			
	9.7					1.18					
	12.2							0.60			
Zr–15% Nb–2% Mo	7.0			7.81	1.81						
	7.9		0.83								
	8.8	0.57									
	10.9			5.09	1.35						
	12.2	0.55									
Zr–20% Nb–2% Mo	6.3	0.27									
	9.7	0.53									
Zr–15% Nb–5% Mo	7.0	1.42									
	10.9	0.81									
Zr–15% Nb–2% Pd	7.0				2.27						
	7.9	0.77[d]		5.5							
	8.8	0.20									
	10.9				1.61						
	12.2	0.55[d]		3.7							
	13.3	0.36									

Table 15.7 (continued)

Alloy	Power Density[a] (w/ml)	Relative Corrosion Rate[b] for Various Heat Treatments[c]									
		A	B	E	C	M	L	K	J	H	I
Zr–15% Nb–5% Pd	7.9	0.53									
	12.2	0.43									
Zr–20% Nb–2% Pd	7.9	0.50									
	12.2	0.55									
Zr–15% Nb–2% Th	6.3	1.00									
	9.7	0.65									
Zr–15% Nb–0.5% Cu	9.7	0.38									

[a]Power density does not include contribution from fast neutrons (>1.0 Mev).

[b]Ratio of corrosion rate to that of commercially annealed Zircaloy-2 core coupons at similar power densities; rates based on total coupon area and radiation time.

[c]Heat treatments:

A: Beta quenched (900°C for 3 hr, water quenched)
B: Beta quenched plus 400°C for 2 hr, water quenched
C: Beta quenched plus 400°C 2 weeks, air cooled
E: Beta quenched plus 500°C for 2 weeks, air cooled
M: 1000°C for 5 hr, water quenched; 700°C for 24 hr, water quenched
L: 1000°C for 5 hr, water quenched; 600°C for 24 hr, air cooled
K: 1000°C for 5 hr, water quenched; 500°C for 24 hr, air cooled
J: 1000°C for 5 hr, water quenched
H: 1000°C for 30 min, water quenched in capsule
I: 1000°C for 30 min; furnace cooled in capsule

[d]Sponge zirconium base.

technique, exhibited weight gains. The eight LC coupons showed weight increases which varied from 0.5 to 5.1 mg/cm^2 (based on total coupon area of 2.2 cm^2) and averaged 2.0 mg/cm^2. The single LA coupon showed a weight increase of 1.9 mg/cm^2.

Discussion of Results. – As illustrated in Fig. 15.3, the results for the core channel and nose specimens fall near the line represented by the equation:

$$R = 0.41P\left(1 - e^{-45/R^{1.5}}\right), \quad (1)$$

where R is the corrosion rate, mpy, and P is the fission power density, w/ml. This equation expresses the L-2-19 and L-2-14 corrosion data shown in Fig. 15.3 and is considered the probable relationship between corrosion rate and fission power density in solution in the absence of any contribution to fission power at the Zircaloy-2 surface from uranium sorbed on the surface. The L-2-21 data for the channel specimens at the higher power densities fall above the line, as does the point for the high-power-density core nose specimen. As discussed in Sec 15.1.3(*b*), these specimens were nearly free of transported iron oxide, but they exhibited an average of 1.6 μg of uranium per square centimeter on their surfaces. The effect of this surface uranium on the corrosion rate may be compared in the following manner with that in a previous experiment, L-2-17, in which core specimens retained appreciable quantities of uranium. As stated above, the relationship between corrosion rate and fission power density given by Eq. 1 is assumed for systems which are free of any contributions of surface

uranium to power density.[12] The postulated effect of surface uranium is expressed by the equation:

$$P_c = P_s + K^0 U_w f \ , \tag{2}$$

where P_c is the corrected power density at the wall, w/ml; P_s is the power density in solution, w/ml; U_w is the uranium held on the wall, $\mu g/cm^2$; f is the thermal-neutron flux; and K^0 is a constant. Since P_s is determined by the flux and the uranium concentration in solution, Eq. 2 may be written:

$$P_c = P_s \left(1 + K \frac{U_w}{U_s} \right) , \tag{3}$$

where U_s is the uranium concentration in solution (g/liter) at the exposure temperature, and K is a constant. If the assumption is made that the deviation of the results of L-2-17 annulus specimens from the relationship shown by Eq. 1 was due to the absorption of 21 μg of uranium per square centimeter, the amount found on the one specimen examined, the calculated value of K in Eq. 3 is 2.1. With this value for the constant, the corrected power density, P_c, for those L-2-21 specimens which retained 1.6 μg of uranium per square centimeter is 1.11 times the solution power density. As can be seen by reference to Fig. 15.3, increasing the power-density values by 11% brings the high-power-density points near to the line.

The data for L-2-21 core channel specimens at low power densities fall below the line, but, as discussed in Sec 15.1.3(*b*), these specimens retained appreciable amounts of transported iron oxides when weighed. .A correction to the weight-loss value has been made for each specimen for which transported-scale data are available by assuming that the weight of retained oxide is twice the weight of retained iron. Corrected data points are shown in Fig. 15.3, identified by arrows. The corrected points fall, as expected, nearer the line than do the uncorrected points.

The results for the annulus specimens of pickled Zircaloy-2 are in near agreement with those of the as-machined channel specimens, both when compared before correction for retained iron oxide and after correction for retained iron oxide. The results of previous experiments have indicated corrosion rates for pickled specimens which are about 10% lower than those for as-machined specimens.[13] At the low rates observed in this experiment, a difference of 10% is well within the spread of the data.

The annulus specimens of Zircaloy-2 which were subjected to special heat treatments (Table 15.1) exhibited rates that are in near agreement with those for the specimens prepared from the commercially annealed material.

(3) *Other Zirconium Alloys.* – Weight data for all core specimens are listed in Table 15.7 as ratios of the observed corrosion rates to the rates exhibited by the commercially annealed Zircaloy-2 coupons at similar power densities.

All combinations of alloys and heat treatments represented in the CA coupon arrays were also represented by the LA coupons, except for two ternary zirconium alloys and one heat treatment. All LA coupons, after being defilmed by the usual technique, exhibited weight gains, except for the two Zr–15% Pd LA coupons. Weight losses for the two exceptions, which had been subjected to heat treatments J and L, are expressed as total-area corrosion rates, 10.2 and 39.9 mpy.

No discussion of these results will be attempted in this report except to note the high weight losses of the Zr–15% Pd alloys, both in the core annulus and in the in-line positions. The total weight loss from the several specimens of this alloy was 650 mg. Of this amount, 15%, or about 100 mg, was palladium which was carried away in some form from the specimens. This large amount of palladium in solution may have had some bearing on the high steel corrosion rates in L-2-21, although no consideration is given to this possibility in the discussion of steel corrosion in the following section.

(4) *Stainless Steel.* – Results. – The results for the CC and core nose specimens of type 347 stainless steel are listed in Table 15.4, together with a summary of the results of the metallographic examinations. Six of the eight type 347 stainless steel LC coupons exhibited weight increases, based on exposed area, of 4.2 to 11.3 mg/cm^2, after being defilmed by the usual technique. The remaining two coupons, submitted for gross-scale analysis without having been defilmed, exhibited weight increases, in the as-removed condition, of 11 and 11.3 mg/cm^2. The data for the LC specimens which were examined

[12] G. H. Jenks *et al.*, *HRP Prog. Rep. for Quarters Ending April 30 and July 31, 1958*, ORNL-2561, p 220–21.

[13] G. H. Jenks *et al.*, *HRP Quar. Prog. Rep. Oct. 31, 1956*, ORNL-2222, p 109.

metallographically are included in Table 15.4. It is noteworthy that the metallographic examination revealed pitting under a uniform scale on two of the three specimens examined.

The results of the metallographic and visual examinations of components of the loop other than the specimens are described in Sec 15.1.2. The operating history of the loop and the corrosion data based on oxygen consumption are summarized in Table 15.3.

The results obtained with the four stress specimens of type 430L stainless steel, which were exposed in the pressurizer, are given in Table 15.4. These specimens exhibited low corrosion rates and bore no evidence of localized attack.

Discussion of Results. – The corrosion of type 347 stainless steel in the L-2-21 experiment, as indicated by oxygen and nickel data, was more severe than that observed in other 280°C loop experiments. As will be discussed below, it appears that a large portion of the total corrosion was in the loop core. Localized corrosion was detected in several locations in the in-line regions, and there was probably more localized attack in-line in L-2-21 than in previous 280°C experiments. The complete explanation for these differences in behavior is unknown. However, it appears likely that the concentration of excess H_2SO_4 was one of the major factors influencing the behavior.

Experiment L-2-21 was the first 280°C experiment in a steel loop with 0.17 *M* UO_2SO_4 in which the initial concentration of excess H_2SO_4 was 0.04 *M*. All other 280 or 300°C experiments, except L-2-19,[14] an Li_2SO_4 additive experiment, contained 0.02–0.03 *M* excess H_2SO_4.[15–18] In contrast, a majority of the 250°C loop experiments employed 0.04 *M* excess H_2SO_4 with 0.17 *M* UO_2SO_4 dissolved in H_2O;[19–23] that is, except for the solvent, the majority of 250°C experiments employed solutions comparable to those in L-2-21. All the 250°C experiments were carried out in the LITR HB-4 facility; hence the maximum and average fission power densities in the 250°C experiments were a factor of 3 to 4 less than those in L-2-21. Each of the 250°C experiments in steel loops which employed 0.04 *M* excess H_2SO_4 in the charge solution exhibited a rapid over-all rate, from 7 to 11 mpy, following the initiation of exposure.[24–28] These initial rates persisted, usually, for more than 100 hr of circulation, during which time an over-all steel corrosion penetration of from 0.1 to 0.15 mil took place. In one 250°C experiment in an all-steel loop, the initial solution was replaced with a second charge after the initial high rate had leveled off to some extent. The initial rate with the second charge of solution was 8 mpy, and this rate persisted for 120 hr of circulation. In all cases a lower rate followed the initial periods of high rate.

The L-2-21 behavior during operation with charge No. 1 appeared to be qualitatively the same as that of the 250°C experiments, and the initial rate of 6 mpy is not appreciably different from that observed with some of the 250°C experiments. However, the corrosion in L-2-21 with the second and third solution charges was greater than with the first charge and did not level off. The LITR was operated at several levels of power during operation with charges No. 2 and 3, and the over-all rate generally decreased as the reactor power decreased. The duration of exposure in L-2-21 was fairly short with both charges 2 and 3 (as shown in Table 15.3), and, on the basis of experience with the 250°C loop experiments, no decrease in rate would necessarily be

[14] G. H. Jenks *et al.*, *HRP Prog. Rep for Quarters Ending April 30 and July 31, 1958*, ORNL-2561, p 214–16.

[15] G. H. Jenks *et al.*, *HRP Quar. Prog. Rep. Jan. 31, 1957*, ORNL-2272, p 104.

[16] G. H. Jenks *et al.*, *HRP Quar. Prog. Rep. July 31, 1957*, ORNL-2379, p 101.

[17] G. H. Jenks *et al.*, *HRP Quar. Prog. Rep. July 31, 1957*, ORNL-2379, p 112.

[18] G. H. Jenks *et al.*, *HRP Quar. Prog. Rep. Jan. 31, 1958*, ORNL-2493, p 119.

[19] G. H. Jenks *et al.*, *HRP Quar. Prog. Rep. April 30, 1955*, ORNL-1895, p 99.

[20] G. H. Jenks *et al.*, *HRP Quar. Prog. Rep. July 31, 1955*, ORNL-1943, p 109.

[21] J. E. Baker *et al.*, *HRP Radiation Corrosion Studies: In-Pile Loop L-4-8*, ORNL-2042, p 3 (Aug. 8, 1956).

[22] J. R. McWherter and J. E. Baker, *HRP Radiation Corrosion Studies: In-Pile Loop L-4-11*, ORNL-2152, p 5 (June 11, 1958).

[23] G. H. Jenks *et al.*, *HRP Quar. Prog. Rep. Oct. 31, 1956*, ORNL-2222, p 102.

[24] G. H. Jenks *et al.*, *HRP Quar. Prog. Rep. April 30, 1955*, ORNL-1895, p 108.

[25] G. H. Jenks *et al.*, *HRP Quar. Prog. Rep. July 31, 1955*, ORNL-1943, p 119.

[26] J. E. Baker *et al.*, *HRP Radiation Corrosion Studies: In-Pile Loop L-4-8*, ORNL-2042, p 17 (Aug. 8, 1956).

[27] J. R. McWherter and J. E. Baker, *HRP Radiation Corrosion Studies: In-Pile Loop L-4-11*, ORNL-2152, p 18 (June 11, 1958).

[28] J. R. McWherter and J. E. Baker, *HRP Radiation Corrosion Studies: In-Pile Loop L-4-12*, ORNL-2163 (in press).

expected during these short periods. The over-all rates observed during operation with charges No. 1 and 2 are in fair agreement, at comparable power densities, with the initial rates observed in the 250°C experiments as shown in Fig. 15.4, where over-all rate data from L-2-21 are plotted and the range of rates observed in the initial operating periods with various 250°C experiments are indicated. The manner of plotting the data in Fig. 15.4 is that suggested by previous correlations of corrosion rate data obtained with core specimens in previous 280°C loop experiments.[29] Although there is appreciable scattering, the data obtained with charges No. 2 and 3 in L-2-21 group around the line which is drawn through the charge No. 2 data. To locate, on the graph, the range of data from the 250°C experiments, it is assumed that the radiation intensity in the core of the HB-4 loops when the LITR was at 3 Mw, was equivalent to the radiation intensity in the L-2-21 core when the LITR power was in the range of 0.85 to 1 Mw.

As discussed in a previous report,[30] for the 250°C experiments it is likely that most of the corrosion indicated by oxygen data during the initial periods of high rate took place in the loop core. The same likelihood exists also for L-2-21. Severe corrosion was exhibited by the steel specimens located in the forward portion of the core channel and for the core nose specimen. The 10-mil-thick holder for the nose specimen was dissolved. Metallographic examination indicated severe corrosion of the core cap and of the inlet and outlet lines. Localized attack was observed outside the core at several locations: the pump shaft and thermal spacer, the pump volute, the loop drain line, and the two line channel specimens which were at relatively high velocities. However, an estimate of the total amount of metal which was dissolved in these out-of-core locations indicates that this amount is less than 20% of the total amount of steel which was oxidized during the in-pile operations. If it is true that a majority of the corrosion indicated by the oxygen data was localized in the core, it is likely that the steel at the forward portion of the core was corroding at rates of 500 mpy or more when the over-all oxygen rate was 30 mpy.

As may be noted in Table 15.4, the weight loss of steel specimens located in the forward portion of the core of L-2-21 did not decrease appreciably as the fission power density at the specimen decreased. In fact, the specimen at the mid-point of the core channel holder lost more weight than any of the other specimens. These relative rate data are considered to have no particular bearing on the interpretation of the power-density effect on steel corrosion in this experiment. The results of the metallographic examinations showed that the clamped portions of the specimens located in the forward portion of the core channel were heavily attacked and that this attack became more pronounced as the velocity at the specimen increased. The specimens in this group which were exposed to the lowest power densities were exposed to the highest velocities. Thus it appears that there was a decrease in radiation-induced corrosion as the power density decreased, but this wos masked by an increased fretting attack.

To summarize, it is possible that the corrosion behavior of steel in L-2-21 is a manifestation of a pronounced adverse effect on radiation corrosion of H_2SO_4 concentrations in excess of some critical value in 0.17 *M* UO_2SO_4 solution. A critical value of 0.03 *M* excess H_2SO_4 is indicated by the results to date. Little is known about any critical acid concentration in solutions of uranium concentration

[29] G. H. Jenks *et al.*, *HRP Prog. Rep. for Quarters Ending April 30 and July 31, 1958*, ORNL-2561, p 212–13.

[30] G. H. Jenks *et al.*, *HRP Quar. Prog. Rep. Oct. 31, 1956*, ORNL-2222, p 105.

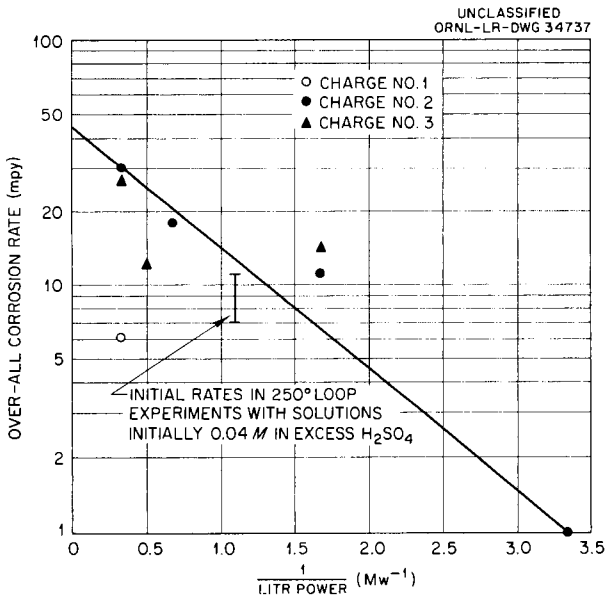

Fig. 15.4. Over-All Corrosion Rates in L-2-21, Oxygen Data.

other than 0.17 *M*. It may be noted, however, that steel corrosion in experiment L-2-17, which employed 0.025 *M* excess H_2SO_4 in a 0.04 *M* UO_2SO_4 solution at 300°C, was not considered excessive in comparison with that in the usual 280°C experiments.[31]

(5) *Titanium 110AT*. – The results for the CC coupons of titanium 110AT are listed in Table 15.4, together with a summary of the results of metallographic examination. The specimen exposed at the highest power density exhibited a rate of 3 mpy; the one at the lowest power density corroded at a rate of 1.7 mpy. The rates for the other CC coupons were less than 1 mpy.

All LC coupons exhibited weight gains as measured after the defilming operation. The weight gains, based on exposed coupon area, ranged from 7.0 to 10.8 mg/cm^2 and averaged 9.5 mg/cm^2. The results for the two LC specimens which were examined metallographically are included in Table 15.4.

Results for the four stress specimens exposed in the pressurizer are also included in Table 15.4. Two of these were in the vapor and two in the liquid. The specimens were stressed beyond their yield point by hand before being placed in the holder. Metallographic examination revealed no evidence of attack. Based on exposed specimen area, weight increases, after the defilming operation, were 6.1 and 12.2 mg/cm^2 for the liquid-phase specimens and 0.05 mg/cm^2 for one vapor-phase specimen. The other vapor-phase specimen exhibited a weight loss which corresponds to a corrosion rate of 0.6 mpy.

15.1.4 Development and Construction

(*a*) **HB-2 Loop Package.** – Out-of-pile tests of loop L-2-22 were completed satisfactorily, and the loop was installed in beam hole HB-2 of the LITR on July 28, 1958. The loop solution is 0.04 *M* UO_2SO_4, 0.2 *M* Li_2SO_4, 0.1 *M* H_2SO_4, and 0.0025 *M* $CuSO_4$ in D_2O at 280°C. As of October 15, the loop had operated for 1900 hr circulation time and 4800 Mwhr LITR operation. No difficulties have been encountered during operation of the loop. The over-all corrosion rate has been approximately 0.5 mpy, based on oxygen consumption.

A change in plans for loop L-2-23, which necessitates some changes in the loop construction, has delayed completion of the loop.

(*b*) **ORR Loop Package.** – Following completion of the ORR loop mockup facility and the assembly of the first test loop, designated O-1-20, tests were undertaken to determine the operational and control characteristics of the system. An uninterrupted 700-hr run at 280°C was made with an HRT-type solution of 0.04 *M* UO_2SO_4, 0.025 *M* D_2SO_4, and 0.01 *M* $CuSO_4$ in D_2O. Operation was excellent except for several minor instrument problems. The stainless steel corrosion rate, based on nickel found in solution and oxygen consumption, was less than 0.5 mpy.

A number of heating and cooling tests were completed on the loop mockup. In order to simulate the fission and gamma heating of the loop during in-pile operation, four heaters, in addition to the units used for loop temperature control, were incorporated in the loop. A reactor scram or setback was simulated by a rapid decrease of power to the auxiliary heaters. The control system was able to maintain loop temperature within 5°C of the 280°C control temperature when as much as 14 kw of heat was removed in a manner simulating a reactor scram or setback.

Other tests were made to calibrate the heating and cooling capacities of the loop heater-coolers, the loop core cooler, and to determine the pump purge rate.[32] Test results indicated that the operation of these components met the design requirements.

ORR loop O-1-25 is being assembled. The layout of the loop is similar to the present loops being operated in the LITR and has been described previously.[33] The core section includes two tapered-channel corrosion-specimen holders instead of the single holder used in the LITR loop. This change results in an increased fluid velocity in the annular space, which is considered necessary for adequate removal of heat from the specimens and holders. The core section of the loop and the tapered-channel specimen holders are shown in Fig. 15.5. The tapered channel of the specimen holder gives a velocity gradient across the test specimens of 11 to

[31] G. H. Jenks *et al.*, *HRP Quar. Prog. Rep. Jan. 31, 1958*, ORNL-2493, p 132.

[32] H. C. Savage *et al.*, *HRP Prog. Rep. for Quarters Ending April 30 and July 31, 1958*, ORNL-2561, p 202.

[33] G. H. Jenks *et al.*, *HRP Quar. Prog. Rep. April 30, 1957*, ORNL-2331, p 113.

UNCLASSIFIED
ORNL-LR-DWG 34738

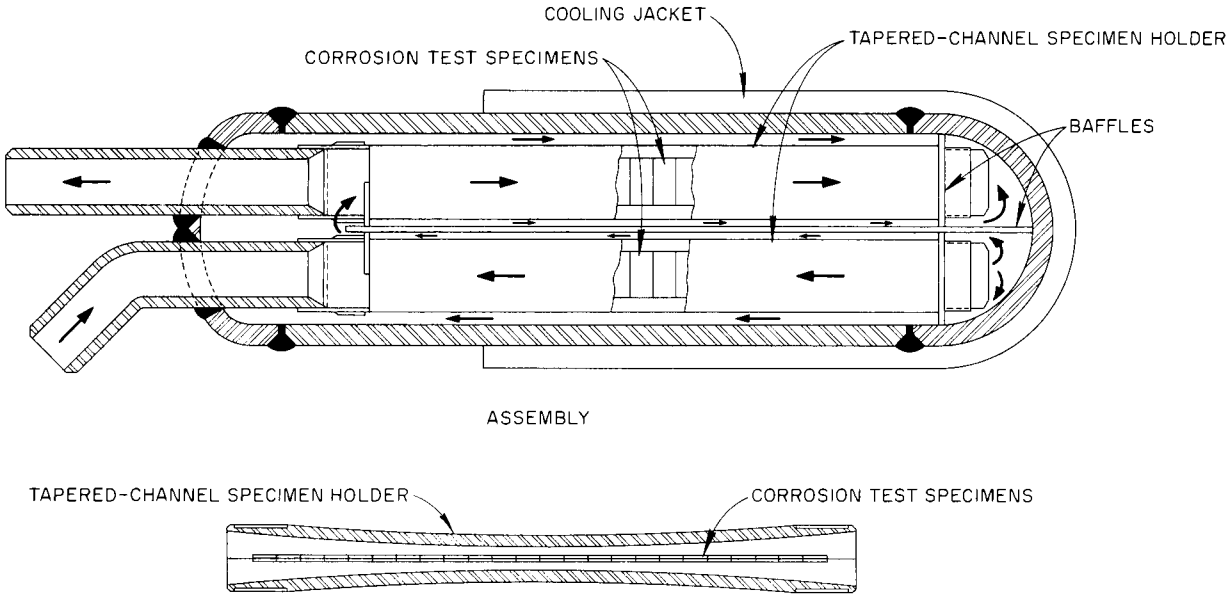

Fig. 15.5. Core and Specimen Holder, ORR In-Pile Loop.

23 fps, symmetrical about the mid-point, at the nominal loop flow rate of 5 gpm.

The circulating pump is of the ORNL 5-gpm type[34,35] with sintered aluminum oxide bearings and journal bushings.[36] This pump has given very satisfactory service in the LITR in-pile loops.

Temperature control of the loop, designed for operation at 300°C and 2000 psia, is by means of two heater-cooler units[37] with a combined heating capacity of 8 kw and a cooling capacity equivalent to 16 kw. A mixture of air and water is used as the cooling medium. These units are considered sufficient to maintain and control the loop temperature with the fission and gamma heat loads expected during in-pile operation. An additional cooler, installed on the outside wall of the loop core section to remove the gamma heating in the core walls, has been described previously.[38]

Supplementary equipment installed at the HN-1 beam hole of the ORR includes the beam-hole extension sleeve, liner, dummy plug, and both the small and large equipment chambers in which valves and tanks are mounted.

The stems and bodies for valves to be used in the equipment chambers of the ORR in-pile loop have been selected. These valves are ¼-in. size rated at 30,000 psi, with type 304 stainless steel bodies and seats. Valve stems are of a nonrotating type and are made of 17-4 PH stainless steel fully hardened (H-900 heat-treated condition). Valve-stem packing material is Teflon reinforced with Fiberglas. These valve components, under test, appear to be superior to the valves presently used in the LITR in-pile loop system. The LITR loop valves are

[34] H. C. Savage *et al.*, *HRP Quar. Prog. Rep. July 31, 1957*, ORNL-2379, p 104, Fig. 14.4.

[35] A. Weitzberg and H. C. Savage, *Performance Test of 220-v Three-Phase Stator for Use with 5-gpm In-Pile Loop Pump*, ORNL CF-57-10-24 (Oct. 4, 1957).

[36] H. C. Savage, *Sintered Alumina as a Pump Bearing and Journal Material*, ORNL CF-57-11-122 (Nov. 26, 1957).

[37] T. H. Mauney and H. C. Savage, *Test Results on a Heater-Cooler Unit for the ORR In-Pile Loop*, ORNL CF-57-6-66 (June 28, 1957).

[38] R. A. Lorenz and D. T. Jones, *Laboratory Test of a Core Cooler for ORR Loop HN-1*, ORNL CF-56-12-65 (Dec. 18, 1956).

identical in size but contain a rotating stem of type 420 stainless steel with type 316 stainless steel bodies and seats. In service these valves are exposed to various types of gas as well as water and uranyl sulfate solutions (at temperatures usually less than 100°C).

15.2 IN-PILE ROCKING-AUTOCLAVE TESTS – LITR

15.2.1 Development, Construction, and Operation

(*a*) **HB-5.** – The assembly and operation of HB-5 rocking autoclaves for solution radiation-corrosion studies in beam hole HB-5 of the LITR continued. Four experiments – L51Z-134, L53Z-135, L52Z-136, and L51Z-137 – were assembled and were operated in the reactor.

Autoclave L51Z-134 developed a leak at the closure fitting when heated to 280°C after being inserted into the reactor and had to be withdrawn before corrosion data were obtained. Autoclave L53Z-135 was exposed to reactor radiation for only 1 hr as an experiment to obtain information on the mechanism of the corrosion of Zircaloy-2 exposed to fuel solution under reactor conditions. Experiments L52Z-136 and L51Z-137 were operated in the reactor for 259 and 372 hr, respectively, without incident.

(*b*) **HB-6.** – One solution autoclave, L6Z-142, was assembled and was operated for 138 hr at 280°C in beam hole HB-6 of the LITR during the quarter. No operating difficulties were encountered.

15.2.2 Results and Discussion

(*a*) **Introduction.** – Postexposure measurements are incomplete for the four HB-5 experiments and the one HB-6 experiment exposed during the quarter. However, one of the HB-5 experiments, in which exposure temperatures were above the two-liquid phase separation temperature, is essentially complete and will be discussed. An HB-6 experiment in which type 347 stainless steel coupons were exposed in a Zircaloy-2 bomb will also be discussed and compared with the results of previous, similar experiments.

(*b*) **Zircaloy-2 Autoclave L52Z-136, Exposed at a Temperature Above the Two-Liquid-Phase Separation Temperature.** – Possible abnormal reactor operation might lead to regions of sufficiently high temperature to yield a separation of two liquid phases. Rapid corrosion of Zircaloy-2 might occur in the heavy, very concentrated liquid phase. Autoclave L52Z-136 was exposed in the LITR HB-5 facility at temperatures above the two-liquid-phase separation temperature in a scouting-type experiment to test for corrosion and other effects resulting from the phase separation. A summary of pertinent data from this experiment is given in Table 15.8.

The solution employed was 0.17 *M* UO_2SO_4 and 0.04 *M* $CuSO_4$ in D_2O. The two-liquid-phase separation temperature out-of-radiation was determined by heating the solution in quartz tubes. The composition of two liquid phases at 307°C in a solution similar to that in L52Z-136 but containing 0.01 *M* rather than 0.04 *M* $CuSO_4$ was also estimated from the results of quartz-tube tests. A series of small liquid samples in quartz tubes were heated to 307°C and quickly frozen. The two phases were then separated and were analyzed for uranium and copper.

The lowest temperature at which two liquid phases were observed in the L52Z-136 solution was 285°C. The results of the measurements of phase composition at 307°C in the similar solution are shown in Table 15.9, together with quantities estimated for the in-pile experiment from the results. It appears that about half the uranium and copper entered the heavy phase and about half remained in the light phase. The volume of the heavy phase was about 2% of the total volume. These results, though probably not very accurate, are considered as indications of the phase-separation behavior at 307°C. If it is assumed that these same relationships prevailed in the in-pile autoclave at 307°C, the volume of the heavy phase was 0.17 ml and the volume of the light phase was 8.8 ml.

The L52Z-136 autoclave system was similar to other recent HB-5 experiments[39] except that a $\frac{1}{16}$-in.-dia, 2-in.-long pin was included and laid loosely on the bottom of the autoclave. The usual coupon rack with six scalloped-edge coupons suspended along the center line of the autoclave was also included. At any position of the bomb in its rocking cycle, the coupons on the rack would not contact a 0.2-ml droplet of heavy solution lying on the bottom of the bomb. The purpose of the loose pin was to ensure that one specimen contacted the heavy liquid phase. It is important to remember that the rocking of the HB-5 autoclave is about the long axis and might better be described as a gentle oscillating rolling action, 70 deg each side of the normal. The gentle mechanical action would not break up any accumulation of heavy phase and keep it suspended.

[39] G. H. Jenks *et al.*, *HRP Quar. Prog. Rep. Jan. 31, 1957*, ORNL-2272, p 112.

Table 15.8. In-Pile Autoclave Corrosion Data

Designation, Facility, Design Type	Dates In and Out	Solution Composition Before and After Exposure				pH	Pretreatment		Temperature (°C)	Radiation Time	Total Time at Elevated Temperature In-Pile (hr)	Average Power Density (w/ml)	Average Power Density Corrected for Scale Uranium (w/ml)	Average Radiolytic-Gas Pressure (psi)	Oxygen Pressure, Initial and Final (psi)	Average Corrosion Rate (mpy)		Average Corrosion Penetration (mils)	
		UO_2SO_4 (molar STP)	Enrichment (% U^{235})	$CuSO_4$ (molar STP)	H_2SO_4 (molar STP)		Time Exposed to Water; to Solution (hr)	Temperature (°C)								O_2 Consumed	Specimen Weight Losses	O_2 Consumed	Specimen Weight Losses
L52Z-136,[a] HB-5	9/16/58	0.170	93.2	0.040		3.05[b]	7	310	270	40.5	240	16.0	28.2	c	1295[d]	12.2		0.381	0.417
	9/20/58	0.158		0.046		1.75[b]	118	270	300	90.9		15.1	26.7		127[d]	17.7			0.354[e]
									310	29.7		14.7	26.0			19.0			
									320	8.9		14.4	25.5			18.8			
									270	13.1		16.0	28.2			2.0			
									270	18.9		16.0	28.2			10.5			
									320	0.6		14.4	25.5						
L6Z-133,[f] HB-6	6/4/58	0.172	93.2	0.002	0.030	1.55	7	310	280	172.0	300	12.1	12.4	653	1095	12.4[g]	h	0.250[g]	
	6/17/58	0.150		0.001		1.85	20	250							147		15.2[i]		0.298[i]
																	13.8[j]		0.271[j]

[a] D_2O solvent; 2.86% U in coupon scale; 1.07% U in pin scale.

[b] Glass-electrode readings in D_2O solution plus 0.25.

[c] Varied; see experiment description.

[d] Pressures at 270°C.

[e] Loose pin specimen.

[f] 0.1% U in Zircaloy-2 scale; 0.09% U in type 347 SS scale.

[g] Average corrosion estimated for Zircaloy-2 autoclave and specimens.

[h] As-machined Zircaloy-2 pins broke on disassembly.

[i] Sand-blasted Zircaloy-2 pin.

[j] Type 347 SS pins.

The preirradiation treatment of L52Z-136 included the usual hydrostatic pressure test with water at 305°C for 7 hr and a 118-hr run with the test solution at 270°C. The in-pile exposure was performed at 270, 300, 310, 320, 270, and finally 320°C. From time to time during the in-pile exposure, the temperature was varied over a range of values as part of a study of the behavior of radiolytic gas in the system. The length of each exposure period and the lengths of the short periods devoted to incremental changes in temperature to make radiolytic-gas pressure observations are listed in Table 15.10.

Radiolytic gas pressure-temperature data were obtained over the range 250 to 320°C. Similar pressure-temperature observations were made during reactor shutdowns or during periods when the experiment was retracted out of the high flux, to establish periodically a pressure-temperature base line from which radiolytic-gas pressures could be estimated. The radiolytic-gas pressure data are reported in Fig. 15.6 as a plot of the logarithm of the estimated radiolytic-gas pressure vs the reciprocal of the absolute temperature. Data are categorized according to the total amount of exposure accumulated on the experiment at the time of each group of measurements, to determine whether any time-dependent changes occurred during exposure. The chronological sequence of observations of data points within each group of data is noted in order to show a possible effect depending on whether observations were made on an ascending or descending temperature cycle. Data points which were taken at a particular temperature after several hours of operation at that temperature are noted to show whether long equilibration times under irradiation gave values different from those obtained in the rather short

Table 15.10. Autoclave L52-Z136 Exposure Schedule

Temperature (°C)	Radiation Time		Duration of Period (hr)
	Start (hr)	End (hr)	
270	0	39.3	39.3
P-T data	39.3	40.5	1.2
300	40.5	66.4	25.9
P-T data	66.4	67.9	1.5
300	67.9	131.4	63.5
P-T data	131.4	132.2	0.8
310	132.2	138.8	6.6
P-T data	138.8	143.8	5.0
310	143.8	161.1	17.3
320	161.1	170.0	8.9
270	170.0	183.1	13.1
P-T data	183.1	185.1	2.0
270	185.1	202.0	16.9
320	202.0	202.6	0.6

Table 15.9. Results of Quartz-Tube Determinations of Phase Composition and Derived Values for In-Pile Experiment

Constituents	Concentrations		
	Single Phase	Two Phase	
		Heavy	Light
UO_2SO_4, molar, STP	0.17	3.8	0.08
$CuSO_4$, molar, STP	0.011	0.16	0.011
Copper/uranium	0.065	0.041	0.138
Volume, arbitrary units		1	50
Predicted volume of phase in autoclave at 307°C with 6.7 ml (STP) charged to autoclave, ml		0.17	8.8
Predicted weight of uranium in phase at 307°C, mg		120	120

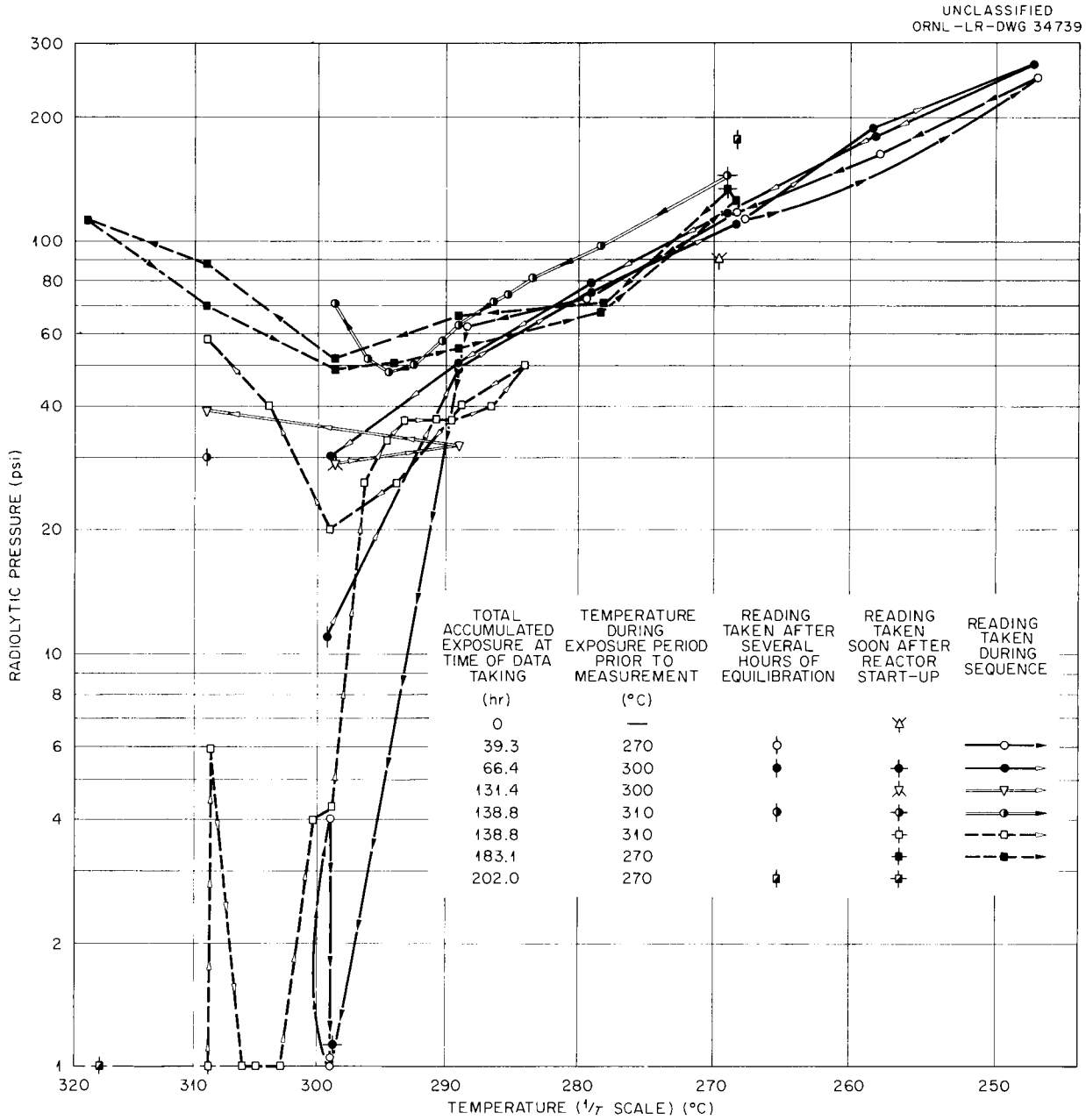

Fig. 15.6. Estimated Radiolytic-Gas Pressure in L52Z-136 as a Function of Temperature and Exposure History.

equilibration period which transpired between data points in the sequences of data shown. Finally, data points taken at a particular temperature soon after a reactor startup or after insertion of the experiment while the experiment was held at that temperature are particularly noted. It was thought that the radiolytic-gas pressure at temperatures above the phase separation might depend on whether or not the heavy phase was present when the irradiation began.

After completion of the exposure, the autoclave was dismantled and the solution was removed for analysis. The specimens, including the six coupons and the loose pin, were removed and carefully examined for evidence of localized attack. The interior walls of the autoclave were also visually in-

spected for localized attack after the autoclave had been sectioned in such a manner that the bottommost and topmost surfaces were untouched by the cutting operation. Four of the six coupon specimens were defilmed and weighed. The forward and rear coupons were not cathodically defilmed but were reserved for determinations of surface uranium. The second and fourth coupons and the pin specimen which were cathodically defilmed were also submitted for determination of surface uranium. A sample of loose scale recovered from coupon surfaces and a second sample from the pin were also analyzed.

In considering the significance of the radiolytic-gas pressure measurements plotted in Fig. 15.6, it must be recalled that, in HB-5, there is a flux gradient along the length of the autoclave during exposure, and hence a temperature gradient in the rates of radiolytic-gas generation and recombination also. The temperature gradient and the gentle mixing within the autoclave can establish an over-all condition in which gas stratification can occur to varying degrees, so a given radiolytic-gas pressure reading may or may not be representative of the highest rate of gas generation in the system. The estimates of the radiolytic-gas pressure are questionable; however, the reproducibility in radiolytic-gas pressure values within a given sequence of measurements is generally quite good. The two 270°C values taken after 39.3 hr of exposure, pairs of values at 260, 270, 280, and 290°C (but not 300°C) taken after 66.4 hr of exposure, values in the range 285 to about 295°C (but not 295 to 310°C) in the second sequence of data taken after 138.3 hr, and pairs of values at 280, 290, 300, and 310°C taken after 183 hr of exposure all show good agreement. All the data points below about 290°C agree reasonably well, with a probable chronological increase in pressure values during the course of the exposure. This continual increase with exposure time (a factor of about 2 between initial and final reading) may have resulted from a continual loss of copper during the run, although the final solution analysis for copper does not verify this idea.

The good reproducibility observed makes a careful look at these gas data worth while. The data for the temperature range 300°C and above in Fig. 15.6 may be interpreted in terms of two classes of data: those above 10 psi and those below 10 psi. The radiolytic-gas pressure values higher than 10 psi show a deviation at about 300°C from the linear relationship observed below 300°C and also show a continuing increase in pressure with increase of temperature from 300 to 320°C. The deviation from the linear relation at about 300°C may result from the occurrence of two liquid phases and the accompanying distribution of uranium and copper between the two phases. The continuing increase in radiolytic pressure on heating from 300 to 320°C implies that the distribution of copper and uranium changes continuously with temperature in this range or that the uranium and, hence, the gas generation were becoming more localized.

With the exception of a series of observations made at 300°C after 39 hr of exposure, the below 10 psi values were all observed soon after a reactor startup with the experiment already separated into two phases. The series of data taken after 139 hr of exposure particularly exemplify the difference in results obtained with a difference in heating schedule. In this case the experiment was at about 310°C when the irradiation started, and a series of observations of radiolytic pressures were made following incremental decreases in temperature to about 285°C, followed by incremental temperature increases back to 310°C. During the descending-temperature schedule, the radiolytic pressure remained less than 10 psi to about 300°C. On further cooling, the radiolytic pressure increased from 26 psi at about 298°C to 50 psi at about 285°C. These latter values are generally in agreement with other data in this temperature range. On reversing the temperature schedule and heating back to 310°C, reasonable agreement with the earlier values was obtained until 300°C was reached. On further heating to 305 and 310°C, the radiolytic-gas pressure increased to about 40 and 60 psi, respectively, in agreement with the other cases where a sequence of increasing temperatures was employed but in disagreement with the values observed soon after irradiating the system while it was in the two-phase region. The data points indicating 1 psi or less radiolytic pressure are consistent with the postulate that exposure to irradiation of a system already in the two-liquid-phase region yields (at least temporarily) a distribution of uranium and/or copper which is different from that obtained by approaching the same conditions by first irradiating and then heating to the two-phase region.

The progress of corrosion during exposure as measured by oxygen consumption is shown in Fig. 15.7. The temperatures of operation are indicated, but the least-squares lines are drawn through the

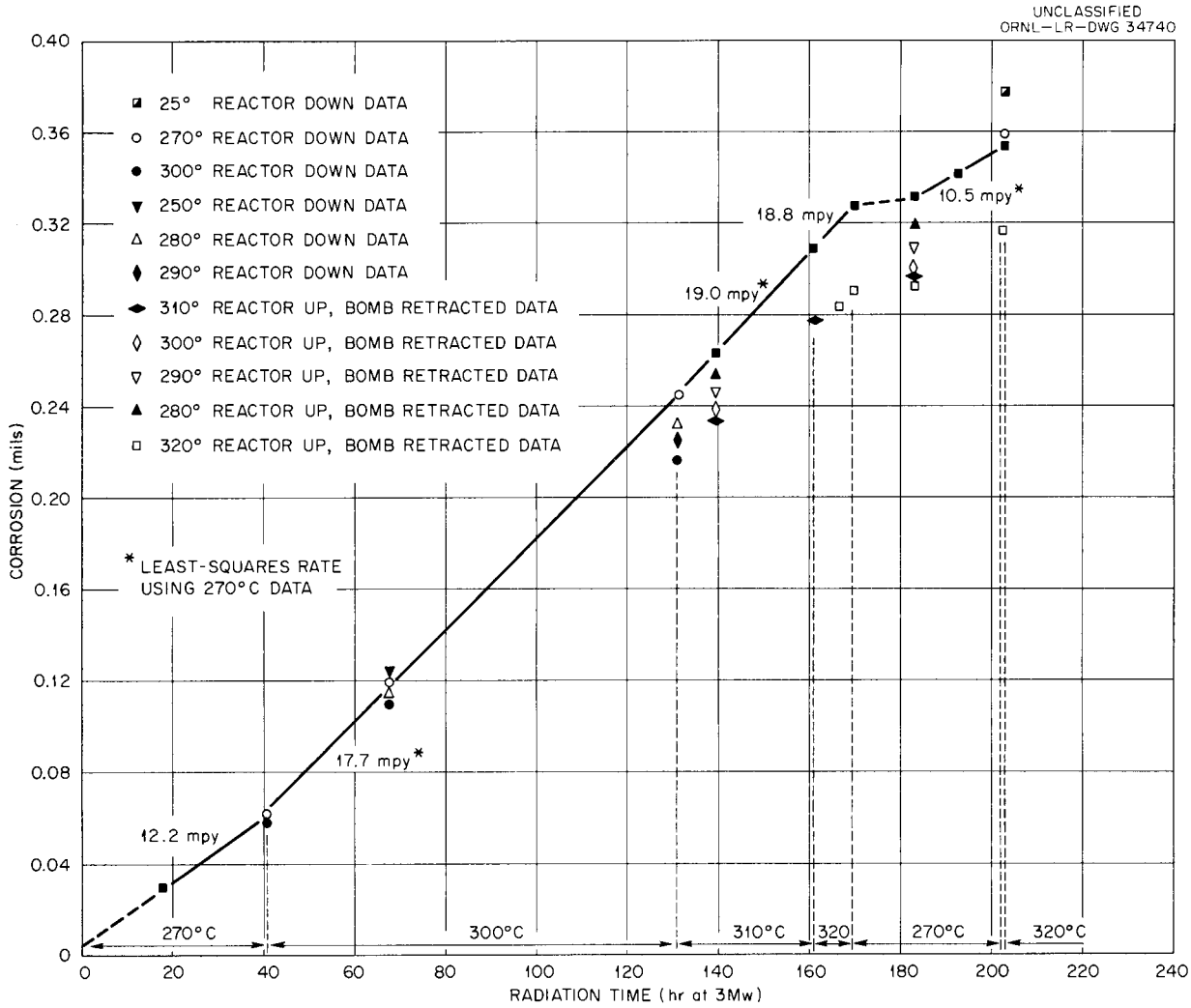

Fig. 15.7. Corrosion Measured in Experiment L52Z-136 by Oxygen Consumption.

penetration points calculated from pressures observed at 270° C. The oxygen-pressure values determined from the 270° C measurements were employed to improve the reliability of the relative rate values calculated from the oxygen data. In addition, the absolute values determined from the 270° C data were expected to be more nearly accurate than those determined from the measurements made at the higher temperature. The final 270° C point is in fair agreement with the final point obtained at room temperature, and this room-temperature result is considered the most nearly accurate measure of the over-all oxygen loss during exposure. One point of interest in these data is that for 13 hr at 270° C, after an exposure at 320° C, an abnormally low rate of about 2 mpy was observed. The rate subsequently rose to a more nearly normal 10.5 mpy. These results indicate that the high-temperature operation inhibited corrosion for a time at the lower temperature. Such an inhibition has not been recognized in previous autoclave data, although, as discussed below, a similar inhibition may have occurred in the Z-27 experiment[40] in which a 300° C exposure followed a 330° C exposure.

The average corrosion penetrations determined from weight measurements for each of the four coupons which were cathodically defilmed are shown in Fig. 15.8. Also shown is the average penetration

[40] G. H. Jenks *et al.*, *HRP Quar. Prog. Rep. Jan. 31, 1957*, ORNL-2272, p 110–15.

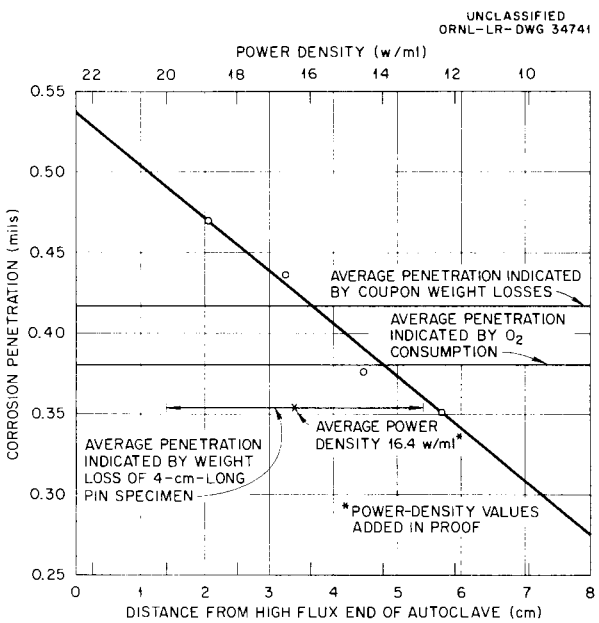

Fig. 15.8. Penetration vs Coupon Position and Power Density in Autoclave Experiment L52Z-136.

value for the Zircaloy-2 in the autoclave, which is obtained by assuming that the penetration suffered by Zircaloy-2 at a given axial position is represented by a straight line drawn through the four coupon points. The average corrosion penetration for the single loose pin specimen is shown in Fig. 15.8, calculated in the same manner, but with the added assumption that the opposite ends of the pin were equidistant from the front and rear of the autoclave. The value for the average penetration determined from the oxygen data is also shown in Fig. 15.8. The averages determined from the oxygen and from the coupon data differ by about 10%, with the oxygen value being the lower. This difference is within the estimated uncertainty of the calculated averages. The pin result is still lower than the oxygen, but the axial position of the pin is uncertain. If the pin was closer to the rear than to the front of the autoclave, it was in a region of lower-than-average solution power density.

Values for the thermal-neutron flux during exposure are such that the fission power density in a 0.17 *M* UO_2SO_4 solution would have been about 22 w/ml in the front of the autoclave and 10 w/ml in the rear. Analyses for uranium in the recovered scales and on specimen surfaces are not complete, but the preliminary information indicates that the scale uranium is no greater or a little less than would be expected in a solution of comparable composition in H_2O rather than D_2O and operated at 280° C.

The question as to whether the relative corrosion rates observed at the different temperatures in L52-Z136 are similar to or different from those which would have been expected in the absence of a two-phase separation cannot be satisfactorily resolved by recourse to a simple comparison with corrosion rates observed in other single-phase experiments. The parameters involved (temperature and power density) do not independently affect the corrosion rate. For example, in the fairly well established curves of corrosion rate vs power density for experiments at 250 and 280° C,[41] the temperature dependence of corrosion varies decidedly with power density. However, a comparison of the L52-Z136 results, on the basis of logarithm of corrosion rate vs reciprocal absolute temperature, with other experiments at about the same power density should reveal any gross differences in regard to the corrosion rates.

Corrosion data from four experiments[40,42–44] which operated at two or more temperatures and at estimated effective power densities (power-density values corrected for scale uranium) of about the same magnitude as estimated for L52-Z136 are listed in Table 15.11. These data are plotted as logarithm of corrosion rate vs reciprocal absolute temperatures in Fig. 15.9. A nearly linear relation between logarithm of corrosion rate and reciprocal absolute temperature was obtained in past experiments which operated at temperatures from 225 to about 300° C. Z-27 is the only earlier test which operated above 300° C, and the corrosion rate during the final 300° C period in Z-27 appeared to be anomalously low in comparison with the rates observed at other temperatures. A similar circumstance occurred in L52Z-136; following operation at 320°C, a period of 13 hr at 270° C elapsed during which corrosion was nearly stifled. Thus a possible interpretation of the Z-27 result is that operation at 330° C

[41] G. H. Jenks, *Effect of Radiation on the Corrosion of Zircaloy-2*, ORNL CF-57-9-11, p 21 (Sept. 30, 1957).

[42] G. H. Jenks *et al.*, *HRP Quar. Prog. Rep. July 31, 1955*, ORNL-1943, p 127–29.

[43] G. H. Jenks *et al.*, *HRP Quar. Prog. Rep. April 30, 1956*, ORNL-2096, p 93–94.

[44] G. H. Jenks *et al.*, *HRP Quar. Prog. Rep. July 31, 1956*, ORNL-2148, p 98–104.

Table 15.11. Comparison of Corrosion Rates Obtained From Experiments Which Were Operated at Two or More Temperatures

Experiment	Temperature (°C)	Solution Power Density (w/ml)	Power Density Corrected for Scale Uranium (w/ml)	Observed Corrosion Rate (mpy)
Z-10	225	5.0	13.0	3.1
	250	4.8	12.8	5.7
	280	4.5	12.4	10.1
	290	4.4	12.3	12.2
Z-11	250	9.8	21.0	7.6
	280	9.2	20.3	16.1
	232	10.2	21.4	5.6
Z-19	280	17.1	22.3	24.2
	300	16.4	21.6	32.8
Z-27	250	4.5	18.6	8.5
	280	4.3	18.6	16.2
	330	3.7	18.1	21.5
	300	4.1	18.5	12.8
L52Z-136	270	16.0	28.2	12.2
	300	15.1	26.7	17.7
	310	14.7	26.0	19.0
	320	14.4	25.5	18.8
	270	16.0	28.2	2.0
	270	16.0	28.2	10.5

partially inhibited corrosion during the subsequent 300° C operation. If this anomalous 300° C result in Z-27 is neglected, the L52Z-136 data in Fig. 15.9, with the exception of the 2 mpy at 270° C, very closely parallel previous results, particularly the Z-27 results at temperatures above 300° C. It appears that the temperature dependence of the corrosion rate in L52Z-136 was very much the same as would have been expected in the absence of the two-phase separation.

As mentioned, the weight loss of the pin specimen which was located so as to have a high probability of contacting an accumulation of heavy phase, indicated no greater (indeed somewhat less) corrosive attack than the coupons. Visual inspection of specimens and of the autoclave interior revealed no evidence of localized attack. The radiolytic-gas pressure-temperature relationship in this experiment indicates that some change took place in the autoclave at temperatures of 290° C and above, and these data are considered as evidence that a two-liquid phase separation of some type occurred as expected from the out-of-pile observations of the solution. The continual increase in radiolytic pressure with an increase in temperature (under some conditions) from 300 to 320°C indicates a significant temperature dependence of the relative distribution of uranium and/or copper in the two phases. The occurrence of a different value (essentially zero) for radiolytic-gas pressure in the several instances where the irradiation began after the system was already in the two-liquid phase region implies that irradiating a system which has separated into two phases may give (at least temporarily) a different situation than separating into two phases a system which is already being irradiated.

(c) Corrosion of Steel Exposed in Zircaloy-2 Autoclaves, Experiment L6Z-133. – In several previous experiments type 347 stainless steel samples were exposed in a Zircaloy-2 autoclave at 280° C in order to minimize the rate of buildup of stainless steel corrosion products in solution. The corrosion attack on the steel specimens in these experiments

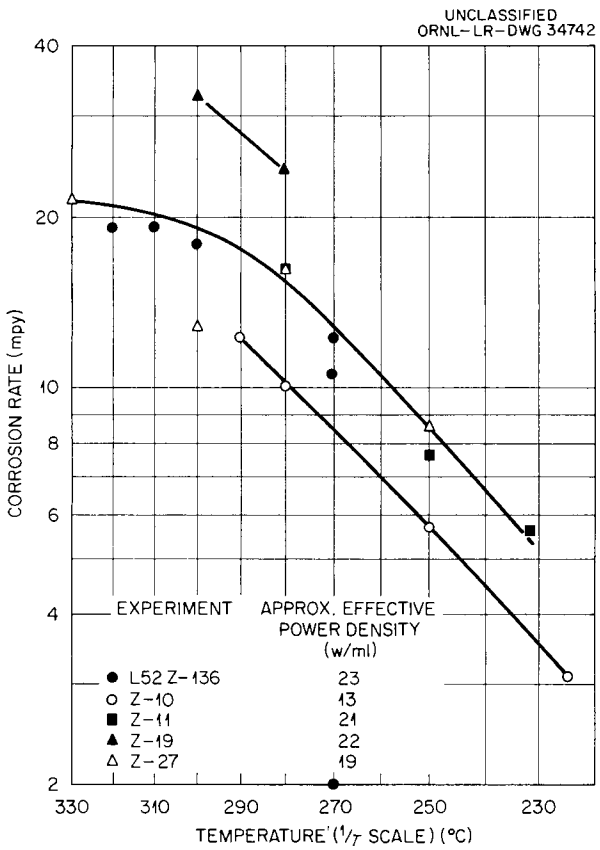

Fig. 15.9. Temperature Dependence of Zircaloy-2 Corrosion in L52Z-136 and Other Experiments.

was greater than expected from results of prior experiments at 250°C in which all-steel systems were employed and in which the radiolytic-gas pressures were greater than in the 280°C experiments. A correlation has been noted between the steel corrosion rates in the core of 280°C in-pile loops and estimated concentrations of radiolytic gas in solution.[45] The rate at a given power density decreases with increasing gas concentration. In view of these loop results it was considered possible that the high steel rates in the 280°C autoclaves resulted from low radiolytic-gas pressure. To test this hypothesis, experiment L6Z-133 was carried out with type 347 stainless steel specimens in a Zircaloy-2 autoclave as before but with a solution containing 15 times less copper than the solutions previously employed. The steady-state pressure of radiolytic gas was thus many times greater in this experiment than in the previous cases. An experiment was operated out-of-pile as a control. Solution and other data for experiment L6Z-133 are given in Table 15.8.

The in-pile pressure behavior of experiment L6Z-133 (Fig. 15.10) was notable in that a pressure anomaly occurred that was similar in some respects to the anomaly discussed by Day.[46] This is the

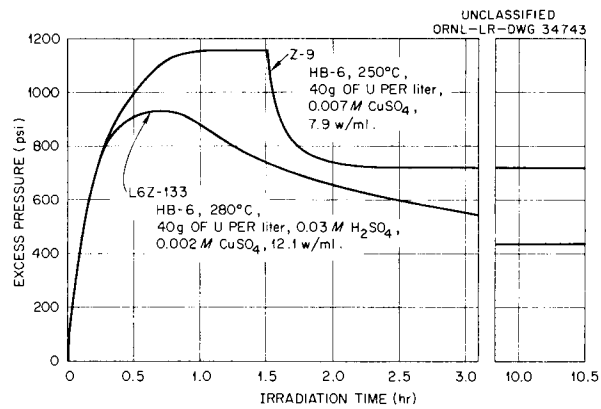

Fig. 15.10. Initial Pressure Maxima Noted in Rocking-Autoclave Experiments.

first time that an effect of this type has been observed in an autoclave experiment at 280°C with a uranium concentration of 0.17 *M* or less in solution. The effect was observed at 280°C in experiment Z-23,[47] which employed a 1.3 *M* UO_2SO_4 solution. Pressure data from a previous experiment, Z-9,[48] are included in Fig. 15.10 for comparison. The anomaly described by Day is well illustrated by the Z-9 data. Following the initiation of irradiation, the apparent radiolytic-gas pressure in L6Z-133 increased to a maximum of 940 psi in a period of about 45 min. It then passed through this pressure maximum and decreased very gradually (8 to 10 hr) to a steady-state pressure of 440 psi. Upon continuing the exposure, the average radiolytic-gas pressure gradually and continually increased from 440 to about 960 psi, with an average value of 653 psi.

[45] G. H. Jenks *et al.*, *HRP Quar. Prog. Rep. Jan. 31, 1958*, ORNL-2493, p 128–32.

[46] H. O. Day, *The Anomalous Decrease of Radiolytic Gas Pressure in In-Pile Corrosion Studies. The Possible Importance to the Homogeneous Reactor Project*, ORNL CF-56-9-26 (Sept. 11, 1956).

[47] G. H. Jenks *et al.*, *HRP Quar. Prog. Rep. April 30, 1957*, ORNL-2331, p 120–23.

[48] G. H. Jenks *et al.*, *HRP Quar. Prog. Rep. July 31, 1955*, ORNL-1943, p 127.

This later increase, however, is believed to be related to a continuing loss of copper during the run (note in Table 15.8 that the final $CuSO_4$ concentration was half the original) and not related to the pressure anomaly at the outset. The large pressure maximum observed in L6Z-133 resembles the phenomenon described by Day in that it happened only once and at the beginning of the run. A pressure plateau following the achievement of the maximum pressure and a sharp break in pressure at the end of the plateau, illustrated by the Z-9 data, are two typical features which the L6Z-133 curve lacks.

The corrosion results obtained with stainless steel specimens in L6Z-133 will be compared and discussed together with those of the previous similar experiments and those of the out-of-pile control experiment. The solution composition employed with each of these experiments is given in Table 15.12 together with the approximate value of the radiolytic-gas pressure which prevailed during the experiment, the fission power density in solution, exposure temperatures, and exposure times. Corrosion results obtained with the steel specimens are also included in Table 15.12. The penetration during the 310°C water treatment was estimated to be 0.01 mil in each case. The corrosion during pretreatment, at 250°C in each case, was estimated from the total oxygen consumption during the pretreatment minus the oxygen required for Zircaloy-2 corrosion as estimated from available out-of-pile data. The final penetrations were calculated from specimen weight losses. An estimate of the total penetration of stainless steel in the case of the out-of-pile control experiment was also made from the total oxygen consumed minus an estimate of that required for the Zircaloy-2 corrosion. The values for the corrosion penetration during the in-pile exposure were taken as the difference between the total corrosion values and the estimated corrosion during pretreatment. The corrosion which occurred in the control experiment during the 280°C exposure was estimated in a like manner.

The results of the in-pile experiments are plotted in Fig. 15.11 as the logarithm of the observed average value of the corrosion rate vs the reciprocal of the fission power density. Plots of this type have been used in the correlation of stainless steel data obtained in loop experiments,[45] and plotted in Fig. 15.11 for comparison is a line which represents the loop L-2-15 results[49] (0.17 *M* UO_2SO_4, 0.015 *M* $CuSO_4$, 0.03 *M* H_2SO_4 in H_2O at 280°C and with

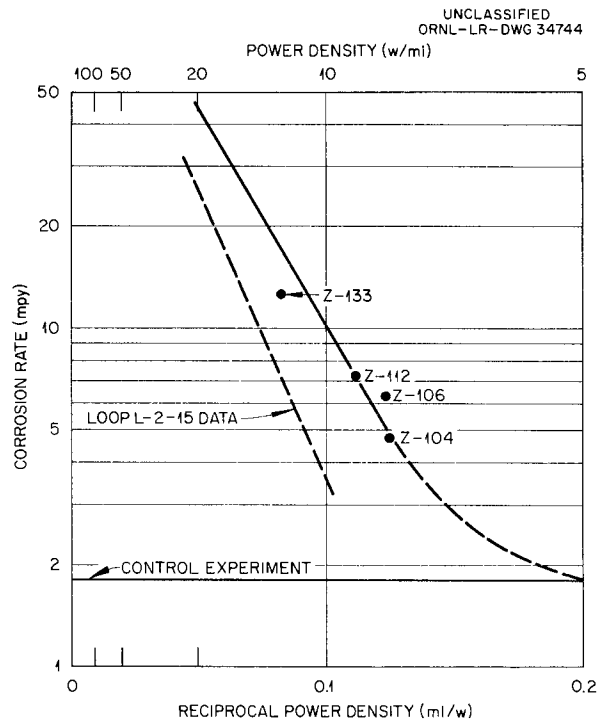

Fig. 15.11. Type 347 Stainless Steel Corrosion in Zircaloy-2 Autoclaves.

~80 psi radiolytic gas). In the out-of-pile control experiment the oxygen data demonstrated that the rate of attack of the steel was not constant during the exposure at 280°C; the attack was initially rapid and became increasingly less rapid as the exposure continued. The average rate of attack for the control during the 280°C exposure is shown in Fig. 15.11 as a horizontal line.

The average rate of attack of stainless steel in the Zircaloy-2 autoclaves was greater during in-pile exposure than during the out-of-pile exposure, the rate increasing with increasing fission power density. The form of the relationship between fission power density and average corrosion rate is the same as that observed at 280°C in-pile loop experiments. There was no evidence in these experiments of any difference in radiation corrosion between solutions with an initial H_2SO_4 concentration of 0.03 *M* and those with 0.06 *M*. Changing the radiolytic gas pressure from the neighborhood of 50 psi to 500–1000 psi did not appear to affect the corrosion.

[49] G. H. Jenks *et al.*, *HRP Quar. Prog. Rep. July 31, 1957*, ORNL-2379, p 101–10.

Table 15.12. Compilation of Data Pertaining to the Radiation Exposure of Type 347 Stainless Steel Corrosion Specimens in Zircaloy-2 Autoclaves

Experiment No.	Solution Composition (M)			Oxygen Pressure, Initial and Final (psi)	Average Radiolytic-Gas Pressure (psi)	Solution Power Density (w/ml)	Reciprocal Power Density (ml/w)	Pressure Tests with 310°C Water		Pretreatment, at 250°C		Total Time in Reactor at Temperature (hr)	Time in Reactor Exposed to Irradiation (hr)	Over-all Penetration from Specimen Weight Losses and Oxygen Consumed (mils)				Penetration[c] During In-Pile Run (mils)	Average In-Pile Corrosion Rate[d] (mpy)
	UO_2SO_4	H_2SO_4	$CuSO_4$					Time (hr)	Penetration[a] (mils)	Time (hr)	Penetration[b] (mils)			Specimen 1	Specimen 2	O_2 Consumed	Average Value		
L6Z-104	0.17	0.03	0.03	1158 97	61	8.0	0.125	8	0.01	19	0.07	308[e]	276.8[e]	0.206	0.247		0.227	0.15	4.8
L6Z-106	0.17	0.03	0.06	1073 404	38	8.1	0.123	6.5	0.01	19	0.02	263	180.5	0.200	0.119		0.160	0.13	6.3
L6Z-112	0.17	0.03	0.06	869 82	70	8.9	0.112	6.5	0.01	22	0.04	405	279.4	0.244	0.323		0.284	0.23	7.2
L6Z-133	0.17	0.03	0.002	1095 147	653	12.1	0.083	7	0.01	20	0.04	300	172.0	0.289	0.289		0.289	0.25	12.7
Control	0.17	0.03	0.03		0	0	0	6.5	0.01	22	0.01	288	0	0.123	0.056	0.061	0.080	0.06[f]	1.8[f]

[a] Penetration during 310°C water treatment estimated from other data.
[b] Penetration during 250°C pretreatment estimated from oxygen consumed and available Zircaloy-2 data.
[c] Penetration during in-pile period estimated by difference from measured total and estimated preirradiation corrosion.
[d] Corrosion rate during in-pile run calculated in terms of penetration during in-pile exposure and exposure time.
[e] L6Z-104 operated 23 hr (20.5 exposure hr) at 250°C and then 285 hr (256.3 exposure hr) at 280°C.
[f] These values pertain to the 280°C portion of the out-of-pile control experiment.

15.3 CORROSION SPECIMEN EXPOSED IN HRT BLANKET REGION DURING RUNS 13 AND 14

Specimens exposed in the blanket region of the HRT during runs 13 and 14 were examined and weighed in the as-removed condition. A portion of one specimen each of Zircaloy-2 core-tank material, type 347 stainless steel, and Ti-A40 were submitted to the Analytical Group for scale analyses. The results of these examinations and measurements are reported elsewhere;[50] a summary of the findings is given in this report.

[50] A. R. Olsen, *HRE-2 Corrosion Specimens – Blanket Region of Pressure Vessel (Loading No. 1) – Weight Data and Scale Analysis*, ORNL CF-58-10-83 (Oct. 31, 1958).

The specimen assembly, designated blanket loading No. 1, was installed in the reactor on December 30, 1957, and was removed on April 8, 1958, after reactor runs 13 and 14 had been completed. Heavy water with no added oxygen was the fluid in the blanket during most of the exposure period, although for a short time at the end of run 14 the blanket fluid contained some core solution which entered through the hole in the core-tank wall. The reactor generated 375 Mwhr during the exposure. The total time at temperatures greater than 250°C was 752 hr; the additional time at temperatures between 100 and 250°C was 227 hr.

The results of weight measurements of the various specimens are summarized in Table 15.13. All the specimens except one were covered with a very

Table 15.13. Weight Changes Observed for Corrosion Specimens Exposed in the HRT Blanket Region During Runs 13 and 14

Material	Station and Position	Weight Change Per Unit Area Measured As-Removed (mg/cm^2)
Zircaloy-2 core-tank material	J-2	+0.28
	K-2	+0.36
	L-2	+0.28
	M-2	+0.18
Zircaloy-2, Allegheny Ludlum	K-6	+0.14
	M-6	+0.17
Type 347 stainless steel	J-4	+0.17
	K-4	+0.13
	L-4	+0.08
	M-4	+0.12
Zircaloy-2 weld specimens	L-1	−0.76*
	J-1	+0.21
	M-1	+0.12
Zirconium sponge–15% niobium	J-5	+4.55**
	L-5	+0.08
	K-1	+0.26
	K-5	+0.24
Ti-A40	J-3	+0.19
	K-3	+0.27
	L-3	+0.28
	M-3	+0.15
	J-6	+0.13
	L-6	+0.18
Ti-110AT	M-5	+0.29

*This sample has white corrosion-product accumulations on both ends.

**There is no visual evidence for this high weight increase. The original weight may be in error.

thin, dark, adherent film and exhibited weight gains in the as-removed condition. The exception, a Zircaloy-2 weld specimen (station and position, L-1), showed a weight loss of 0.8 mg/cm^2 averaged over the total specimen area. Copious amounts of white oxide were found at each end of the specimen. During the out-of-pile pretreatment, some white corrosion product developed in the same sections on this specimen.[51]

The primary purpose of the scale analyses was to determine the amount of uranium on the specimens, although analyses were made for other possible constituents to determine whether transported oxides comprised part of the scales. Uranium was not detected on either the steel or the Zircaloy-2 specimens, but an amount equivalent to 2 μg/cm^2 was reported for the Ti-A40 specimen surface. Transported zirconium oxide was present in the scale on both the titanium and steel specimens, and transported iron and nickel oxides comprised part of the scale on the Zircaloy-2 and Ti-A40 specimens.

The results indicate that the attack on the specimens was in no case appreciably different from that which would have occurred in the absence of radiation.

15.4 EXAMINATION OF CORE ACCESS FLANGE, ATTACHED SPECIMEN, AND SCALES REMOVED FROM THE HRT AFTER RUN 16

The type 347 stainless steel core access flange with an attached type 347 stainless steel specimen was removed from the HRT after run 16 and transferred to the Materials Section for examination. The results of this examination are reported elsewhere;[52] a summary is given in this report.

A new, freshly machined, type 347 stainless steel flange with an attached type 347 stainless steel specimen was installed in the reactor following run 14. The specimen, attached to the flange with Ti-6Al-4V spacers and bolts as previously described,[53] had been pretreated in oxygenated water prior to installation. During the exposure, the reactor generated 1655 Mwhr. The total time at temperatures above 250°C was 664 hr; the time below 250°C but above 100°C was 352 hr.

As received from the reactor, the assembly exhibited an unusual appearance. All the visible surfaces, including the recessed portion of the flange, the stainless steel specimen, and the titanium cap screws, were uniformly covered with an off-white-colored scale. When the array was dismantled, it was apparent that all surfaces that had been exposed to solution were covered with a similar scale. This off-white scale was easily dislodged, and when it was flaked off, a rust-red deposit was revealed next to the metal. This two-layer scale construction prevailed also for the Ti-6Al-4V, although the amount of rust-red deposit was judged to be less on the titanium alloy.

The total weight of scale on the stainless steel specimen and titanium spacers was determined by complete defilming. The scale weight lost by the stainless steel specimen corresponds to an average weight of 6.0 mg/cm^2. The scale weight determined for the three titanium spacers ranged from 2.1 to 5.9 mg/cm^2, the highest value being considered the most reliable. The difference between the initial and final weights for the stainless steel specimen corresponds to an average metal weight loss of 0.32 mg/cm^2 or a penetration of 0.016 mil. Thus the steel corrosion did not contribute appreciably to the total weight of scale on the specimen.

Samples of scale for chemical analyses were obtained by scraping the stainless steel sample, the flange, and two of the titanium spacers. Samples of the defilming solutions mentioned above were also submitted for chemical analyses. The results of these analyses indicate that the major part of each scale was comprised of the oxides of stainless steel constituents; the remainder was largely zirconium. Values for zirconium ranged from 5 to 20 wt %, with an average value of about 10 wt %. The scales also reportedly contained amounts of uranium in the range 0.3 to 5 wt %. The off-white appearance of the outer layer suggests that it is richer in ZrO_2 than the rust-red-colored inner scale. However, no significant difference is noted between the results for iron and zirconium in the samples of scraped scale, which were probably rich in the off-white material, and the scale from combined scraped and unscraped areas represented in the defilming solutions. Uranium found in the scraped scale was a factor of ten less than that in the total scale.

---

[51] R. M. Warner, D. T. Jones, and W. J. Leonard, *HRT Corrosion Specimens and Holder-Blanket Region of Pressure Vessel (Loading No. 1)*, ORNL CF-58-4-38, p 26 (April 8, 1958).

[52] A. R. Olsen, *Examination of Core Access Flange Specimen and Scales Removed from HRE-2 After Run 16*, ORNL CF-58-10-84 (to be issued).

[53] G. H. Jenks, A. R. Olsen, and W. C. Yee, *Examination of Specimens and Scales Taken from the HRT Following Runs 13 and 14*, ORNL CF-58-9-37 (Sept. 11, 1958).

The amount of scale found on the various surfaces in the core-access-flange assembly indicates that appreciable quantities of oxide were transported by the solution during run 16 and deposited on surfaces outside the core. Based on observations from in-pile loop experiments, this transfer behavior would be expected for ZrO_2 formed by corrosion in the core.[54] It is also considered likely from loop experience that other oxides such as Fe_2O_3, which may have been present in the core at the start of the run, would be carried out of the core and deposited elsewhere. In this connection, visual inspections of the core indicated less scale accumulation after run 16 than after run 14.[55,56]

The amount of scale on the surfaces of the core-access-flange assembly and the fraction of zirconium in the scale may be used as a basis for speculation as to the amount of zirconium which was oxidized during run 16. If it is assumed that the average amount of zirconium deposited on the flange-specimen assembly is representative of the average amount deposited on other surfaces in the core circulation system but external to the core, then the total amount deposited during run 16 was about 250 g. If it is further assumed that all the ZrO_2 formed within the core circulation system was deposited on the surfaces within the high-pressure core circulation system external to the core, an average weight loss of 6.4 mg/cm^2 is obtained for the 3.9×10^4 cm^2 of Zircaloy-2 surface area inside the core. This weight loss corresponds to an average penetration of 0.4 mil, which is on the low side of the range of average penetration values expected from in-pile loop experience. However, it is known that all the ZrO_2 formed during run 16 did not deposit on the walls of the core system; the chemical plant, which was operating part of the time, separated 27 g of zirconium.[57] In addition, it is possible that ZrO_2 collected in other areas such as the dump tanks, but sufficient information is not available for judging this possibility.

[54] G. H. Jenks *et al.*, *HRP Quar. Prog. Rep. Jan. 31, 1958*, ORNL-2493, p 120–22.

[55] A. R. Olsen, "Visual Observations on the HRE No. 2 Core Interior," HRP-58-378, July 22, 1958.

[56] R. B. Briggs, oral communication.

[57] O. O. Yarbro, *HRT-Chemical Plant Run 16 Summary*, ORNL CF-58-10-111 (Oct. 9, 1958).

15.5 SUPPORTING RADIATION-CORROSION STUDIES

Several series of batch adsorption experiments were carried out in a study of the adsorption of uranium from UO_2SO_4 solution on hydrous zirconium oxide at elevated temperature. The experiments and results are reported in detail elsewhere.[58] The hydrous oxide was prepared from available zirconium hydroxide. The zirconium hydroxide was evaporated with concentrated nitric acid to oxidize organic impurities. The last of the nitric acid was removed by repeated evaporation with sulfuric acid. Addition of excess 1 *M* NH_4OH to the acidic sulfate solution precipitated a hydrous oxide. This material was washed repeatedly by decantation until the precipitate began to peptize. It was then filtered, and the filter cake was dried at 100–110°C overnight. Samples of one batch of material prepared in this way lost 18.7 wt % on ignition, corresponding to very slightly less than 2 moles of water per mole of ZrO_2.

The adsorption tests were carried out in ampoules made of 9-mm-ID Pyrex tubes, enclosed in small stainless steel autoclaves. A small amount of water was placed outside the ampoule to provide an external pressure and prevent breakage. In two series of tests the solutions studied were nominally 40, 20, 10, 5, 2.5, and 1.25 g of depleted uranium per liter, and all contained 0.02 *M* added H_2SO_4. In a third series nominal uranium concentrations of 40, 20, 10, 5, and 2.5 g/liter were employed, with 0.1 *M* excess H_2SO_4 and with and without 0.2 *M* Li_2SO_4. About 0.1 g of the $ZrO_2 \cdot xH_2O$ was placed in each ampoule, and 1 ml of the appropriate solution was added. After the ampoules were sealed, one set of solutions was allowed to stand at room temperature for 24 hr, one set was heated to 150°C for 1 hr, and the third set was heated to 250°C for 1 hr. No room-temperature tests were made with solutions containing 0.1 *M* excess acid and Li_2SO_4. At the end of the heating period, the samples were cooled quickly, centrifuged immediately, and opened for sampling; the supernatant liquid was then analyzed. Initial and final values for the uranium in the solution were used in calculating the amount of uranium adsorbed. Results for the second series of tests (1.25–40 g of uranium per liter as UO_2SO_4 and 0.02 *M* H_2SO_4) are given in Table 15.14. The data from Table 15.14

[58] B. O. Heston, *Adsorption of Uranium on Hydrous Zirconium Oxide*, ORNL CF-58-11-39 (in press).

Table 15.14. Data Obtained with Second Series of Batch Adsorption Measurements

Sample No.	Weight ZrO_2 (g)	Equilibrium Concentration (mg/ml)	Uranium Adsorbed in Experiment (mg)	Milligrams of Uranium Adsorbed per gram of Loaded ZrO_2
43*		40.55		
44*		20.54		
45*		10.32		
46*		5.16		
47*		2.40		
48*		1.24		
49		11.93 (remainder of sample No. 3)		
50		10.35 (same as No. 45)		
		Room-Temperature Adsorption		
27	0.0981	38.24	2.15	22
30	0.1110	17.5	3.04	27.4
33	0.0954	8.06	2.26	23.7
36	0.1099	2.40	2.76	25
39	0.0998	1.08	1.32	13.3
42	0.0957	0.42	0.82	8.5
		150°C Adsorption		
25	0.1049	32.89	7.66	72.7
28	0.0927	13.96	6.58	71.2
31	0.1093	3.52	6.80	62
34	0.1036	0.61	4.55	44
37	0.0953	0.20	2.20	23.1
40	0.0941	0.04	1.20	12.8
		250°C Adsorption		
26	0.0938	35.20	5.35	57
29	0.0973	15.77	4.77	49
32	0.1058	6.86	3.47	33
35	0.0943	2.54	2.62	27.8
38	0.0972	1.22	1.18	12
41	0.0958	0.34	0.90	9.3
		100°C Adsorption		
76	0.0996	33.29	7.26	73
77	0.1064	14.64	5.90	55

*Samples 43–48 were stock solutions prepared by dilution and used as starting solutions in all series 2 experiments.

are plotted in Fig. 15.12 to show the amount of uranium adsorbed as a function of solution concentration at different temperatures. Results for the solutions containing additives are listed in Table 15.15 and plotted in Fig. 15.13.

It has been pointed out that the hydrous oxide, as prepared at 100–110°C, loses about 20 wt % on ignition. Further experiments, in which some of this oxide was sealed in an ampoule with water and heated for 1 hr at 150 and 250°C, shows that the material is partially dehydrated in the high-temperature water. Oxide that has been heated with water to 150°C and then dried at 100–110°C loses only 15% on ignition; the material treated at 250°C loses only 5% on ignition. Either of these preparations is more readily settled by centrifugation than is the original preparation. It is concluded that a physical change in the state of the oxide may be one factor influencing the amount of uranium adsorbed. To determine the effect of heating in water on the areas of the powdered adsorbent, several samples were submitted for area determination by the BET method. The reported areas were 221.8 and 218 m^2/g for two samples of the as-prepared material, 256 m^2/g for material heated to 150°C, and 76.1 m^2/g for material heated to 250°C. There are some reasons for believing that the value obtained for the 150°C material is too high, but this high value may have resulted from a variation in the preparation of the material. In any case, if the uranium sorption data from Table 15.14 are expressed in weight of uranium per unit area of adsorbent, the order of the adsorption isotherms is changed, and it is found that the adsorption increases regularly with increasing temperature. Figure 15.14 shows the logarithm of the

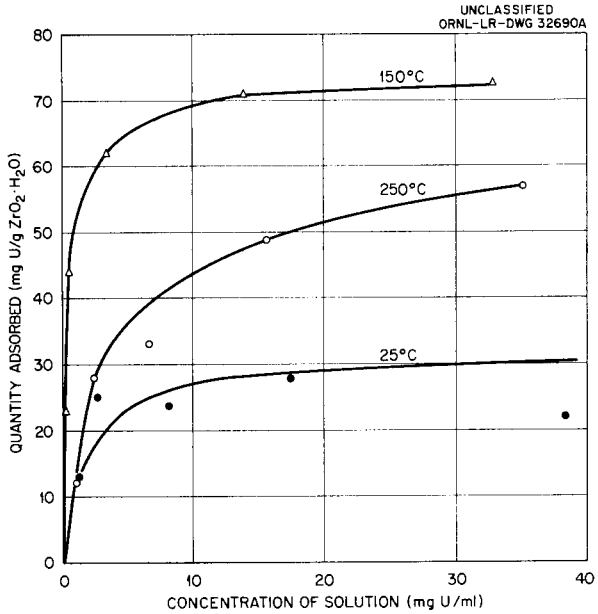

Fig. 15.12. Adsorption of Uranium on Hydrous Zirconium Oxide.

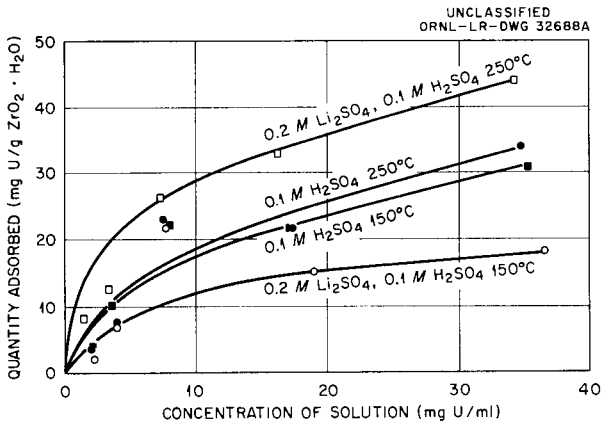

Fig. 15.13. Adsorption Isotherms with Added Sulfates.

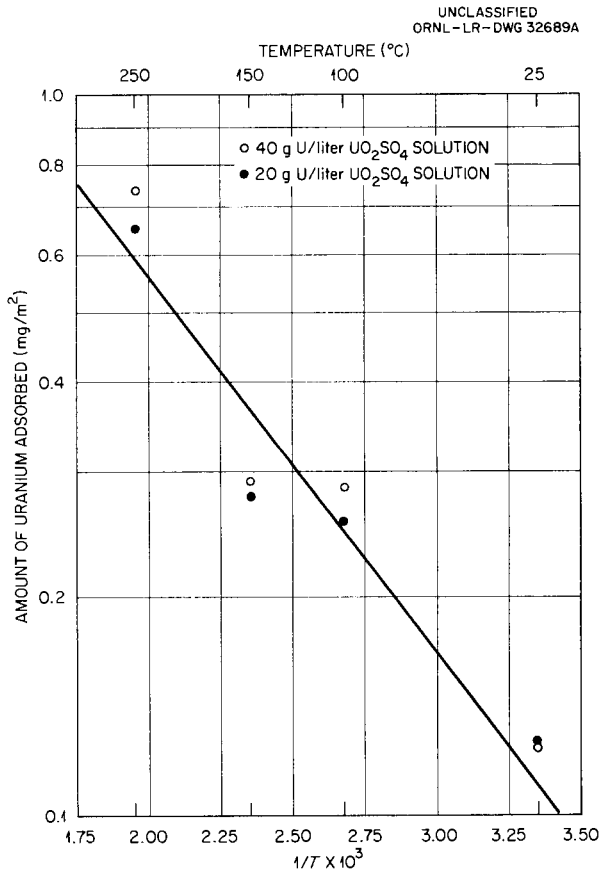

Fig. 15.14. Temperature Dependence of Uranium Adsorption on Hydrous Zirconium Oxide per Unit Area of Oxide Surface.

Table 15.15. Data from Batch Adsorption Studies with Solutions Containing Added Sulfate

Sample No.	Weight ZrO_2 (g)	Equilibrium Concentration (mg/ml)	Uranium Adsorbed in Experiment (mg)	Milligrams of Uranium Adsorbed per gram of Loaded ZrO_2
71*		38.44		
72*		19.41		
73*		9.86		
74*		4.60		
75*		2.36		
		150°C with 0.2 *M* Li_2SO_4 and 0.1 *M* added H_2SO_4		
51	0.1034	36.58	1.86	18
52	0.0965	17.95	1.46	15.1
53	0.1001	7.70	2.16	21.6
54	0.1065	3.90	0.70	6.65
55	0.0987	2.16	0.20	2.0
		150°C with 0.1 *M* added H_2SO_4		
56	0.1039	35.25	3.19	30.7
57	0.0967	17.32	2.09	21.6
58	0.0935	7.80	2.06	22
59	0.0938	3.65	0.95	10.1
60	0.0937	2.00	0.36	3.84
		250°C with 0.2 *M* Li_2SO_4 and 0.1 *M* added H_2SO_4		
61	0.0954	34.25	4.19	44
62	0.0978	16.20	3.21	32.7
63	0.1018	7.20	2.66	26.2
64	0.0990	3.35	1.25	12.6
65	0.0949	1.60	0.76	8.0
		250°C with 0.1 *M* added H_2SO_4		
66	0.1079	34.78	3.66	33.9
67	0.0973	17.32	2.09	21.4
68	0.1004	7.55	2.31	23.1
69	0.1051	3.80	0.80	7.6
70	0.0988	2.00	0.36	3.64

*Samples 71–75 were dilution standards and stock solutions for these determinations. All contained 0.1 *M* added H_2SO_4, and Nos. 71, 73, and 75 contained 0.2 *M* added Li_2SO_4.

quantity of uranium adsorbed per unit area vs the reciprocal of absolute temperature for the 40- and 20-g/liter UO_2SO_4 solutions. Note on Fig. 15.14 that the 150°C point ($1/T \sim 2.4$) falls below a straight line through the rest of the data. These apparently low data points probably resulted from the high value for the area previously mentioned.

The data presented here are results of exploratory experiments and could be misleading because the solutions remained in contact with the oxide during the time required to cool the autoclave system, open it, and remove the solution. In addition, effects of possible reaction between the solutions and the glass container have not been investigated.

A high-pressure all-metal chromatographic column has been designed and constructed which allows separation of solution from adsorbent at temperature. The column can operate up to about 300°C and 2000 psi. This equipment will be used in a continuation of the adsorption studies.

16. METALLURGY

G. M. Adamson

R. G. Berggren
E. S. Bomar
F. W. Cooke
C. E. Curtis
T. M. Kegley
W. J. Leonard
S. G. Nelson
M. L. Picklesimer
J. J. Prislinger
P. L. Rittenhouse
R. L. Stephenson
J. K. White
J. C. Wilson
C. H. Wodtke

16.1 PHYSICAL METALLURGY

16.1.1 Zircaloy-2 Fabrication Study

Zircaloy-2 produced by the normal commercial practice of rolling from 1550°F contains intermetallic and gas stringers and an undesirable amount of preferred orientation, with the accompanying anisotropy of mechanical properties.[1] A fabrication schedule which eliminates the intermetallic stringers and decreases considerably the preferred orientation has been developed for HRP use.[1] However, the developed schedule has not been shown to produce optimum properties with minimum preferred orientation. A detailed fabrication study involving all the fabrication variables, including cross-rolling,[2] has therefore been started.

Zircaloy-2 specimen material has been fabricated to ten experimental schedules and two commercial fabrication schedules, one in which the cross-rolling was carried out in the ingot breakdown and the other with only straight-rolling. Tensile specimens from each of these schedules have been broken. Stress-strain curves were determined for specimens at room temperature and 300°C for all schedules and at 150°C for some schedules, and for specimens from longitudinal and transverse orientations for all schedules, and 22.5, 45, and 67.5 deg from the rolling direction for some schedules.

Typical tensile-property data and the cross-section measurements of the fracture areas of specimens broken at room temperature, from two plate orientations, for the 12 fabrication schedules are presented in Table 16.1. All these values are averages of two individual tests. Comparison of the tensile data for the different schedules does not provide a reasonable measure of the effects of rolling temperatures, intermediate annealing temperatures, or reductions per anneal. In general, only small changes were noted in tensile strength and per cent extension, with slightly larger changes in yield strength and reduction in area. In all cases, changes in both directions may be noted. A determination of the ratio of the major axis to the minor axis of the fracture, also presented in Table 16.1 for each schedule and test direction, does not completely separate the fabrication variables; the ratio values for schedule 4 are near 1.0, indicating almost circular cross sections although the elongations and reductions of area are low, while those for schedule 9 indicate large ellipticity although the reductions of area and elongations are high. The actual linear reductions in the different directions can be determined by subtracting the fracture dimensions from 0.125, the original gage diameter of the specimens. Then it can be seen that for the majority of specimens the reduction in the normal direction to the sheet has been comparatively small, indicating that an anisotropy does exist which is difficult to detect in the usual tensile-property data.

The ellipticity measurements have been extended by making optical comparator examinations of the cross sections of fractured specimens from the fracture to the shoulder. It has been shown that an analysis based on data from these cross sections, relating ellipticity and reduction in area, permits the desired separation of the effects. This study has shown that the sections are true ellipses whose major axes are within 3 deg of the normal to the rolling plane (except for schedule J, Table 16.1) and that the eccentricity of the elliptical cross section varies with the degree of plastic strain, orientation of the specimen relative to the rolling direction, and the fabrication schedule. Such measurements have been completed on specimens from three schedules; partial measurements have been made on specimens from the other schedules.

Impact specimens have been rough-machined from material from all of the 12 fabrication schedules and

[1] M. L. Picklesimer and G. M. Adamson, *Development of a Fabrication Procedure for Zircaloy-2*, ORNL CF-56-11-115 (Nov. 21, 1956).

[2] G. M. Adamson *et al.*, *HRP Prog. Rep. for Quarters Ending April 30 and July 31, 1958*, ORNL-2561, p 245–46.

Table 16.1. Zircaloy-2 Room-Temperature Tensile Properties[a]

Schedule	Tensile Strength (psi)			Yield Strength (psi)			Extension in 1 in. (%)			Reduction in Area (%)			Fracture Diameter (in.)					
													Transverse Direction			Rolling Direction		
	Transverse Direction	Rolling Direction	Difference	Transverse Direction	Rolling Direction	Difference	Transverse Direction	Rolling Direction	Difference	Transverse Direction	Rolling Direction	Difference	Major	Minor	Major/Minor	Major	Minor	Major/Minor
1	73,200	77,800	+4600	62,700	58,000	−4,700	22.0	24.8	+2.8	52.6	48.5	−4.1	0.1058	0.0700	1.51	0.0904	0.0876	1.03
2	77,100	76,200	−900	69,000	56,300	−12,700	22.5	23.0	+0.5	53.0	48.0	−5.0	0.0976	0.0752	1.30	0.0977	0.0832	1.17
3	79,600	79,400	−200	70,200	65,100	−5,100	20.0	21.8	+1.8	48.5	44.0	−4.5	0.1036	0.0790	1.31	0.1042	0.0839	1.24
4	74,200	73,600	−600	61,400	52,200	−9,200	17.5	17.2	−0.3	39.0	18.7	−20.3	0.1085	0.0892	1.19	0.1158	0.1096	1.06
5	79,400	80,200	+800	72,900	62,400	−10,500	18.2	19.2	+1.0	45.5	40.9	−4.6	0.1081	0.0788	1.37	0.1059	0.0871	1.22
6	70,200	72,900	+2700	62,600	55,800	−6,800	22.0	21.3	−0.7	54.2	48.2	−6.0	0.1086	0.0699	1.62	0.1064	0.0760	1.40
7	78,700	82,100	+3400	68,300	56,000	−12,300	11.2	20.0	+8.8	36.2	33.1	−3.1	0.1131	0.0881	1.29	0.1095	0.0955	1.15
8	68,100	67,800	−300	58,300	54,900	−3,400	19.5	24.3	+4.8	46.2	46.3	+0.1	0.1158	0.0726	1.60	0.1161	0.0723	1.61
9	67,000	68,300	+1300	55,700	53,200	−2,500	21.5	22.5	+1.0	46.9	50.5	+3.6	0.1166	0.0712	1.64	0.1134	0.0683	1.66
10	73,500	75,000	+1500	66,600	57,000	−9,600	21.6	22.5	+0.9	54.9	49.7	−5.2	0.1018	0.0682	1.49	0.0998	0.0787	1.27
62	74,200	75,800	+1600	63,200	55,800	−7,400	21.8	22.5	+0.7	46.2	46.5	+0.3	0.1037	0.0810	1.28	0.0965	0.0867	1.11
J	78,100	74,900	−3200	70,000	52,000	−18,000	22.0	21.5	−0.5	46.8	29.2	−17.6	0.0952	0.0873	1.09	0.1147[b]	0.0965	1.19

Description of Fabrication Schedules

1	Beta-worked stock;[c] 1832°F, 30 min, air cool; 1000°F roll to 0.50 in.; 1832°F, 30 min, air cool; 1000°F roll to 0.35 in.; 1832°F, 30 min, air cool; 1000°F roll to 0.25 in.; annealed at 1425°F for 30–45 min
2	Beta-worked stock;[c] 1832°F, 30 min, water quench; 1000°F roll to 0.50 in.; 1832°F, 30 min, water quench; 1000°F roll to 0.35 in.; 1832°F, 30 min, water quench; 1000°F roll to 0.25 in.; annealed at 1425°F for 30–45 min
3	Beta-worked stock;[c] 1832°F, 30 min, air cool; 1000°F roll to 0.35 in.; 1832°F, 30 min, air cool; 1000°F roll to 0.25 in.; annealed at 1425°F for 30–45 min
4	Alpha-worked stock;[d] 1832°F, 30 min, air cool; 1832°F roll to 0.35 in.; 1832°F, 30 min, air cool; 1000°F roll to 0.25 in.; annealed at 1425°F for 30–45 min
5	Beta-worked stock;[c] 1832°F roll to 0.50 in.; 1832°F, 30 min, air cool; 1000°F roll to 0.25 in.; annealed at 1425°F for 30–45 min
6	Beta-worked stock;[c] 1832°F, 30 min, air cool; 1000°F roll to 0.25 in.; annealed at 1425°F for 30–45 min
7	Beta-worked stock;[c] 1832°F, 30 min, air cool; 1472°F roll to 0.25 in.; annealed at 1425°F for 30–45 min
8	Alpha-worked stock;[d] 1472°F, 30 min, air cool; 1000°F roll to 0.25 in.; annealed at 1425°F for 30–45 min
9	Alpha-worked stock;[d] 1472°F roll to 0.50 in.; 1472°F, 30 min, air cool; 1000°F roll to 0.25 in.; annealed at 1425°F for 30–45 min
10	Alpha-worked stock;[d] 1832°F, 30 min, water quench; 1382°F roll to 0.45 in.; 1832°F, 30 min, water quench; 1000°F cross-roll to 0.25 in.; annealed at 1425°F for 30–45 min
J	Rolled to 0.75-in. plate at 1900°F (included cross-rolling to spread ingot) from 12-in.-dia ingot; 1440°F roll to 0.44 in.; 1830°F, 30 min, spray quench; 1000°F roll to 0.31 in.; 30-min anneal at 1425–1450°F
62	Same as schedule J except that no cross-rolling was done

[a]Tensile specimens: 1-in. gage length, 0.125 ± 0.001 in. diameter in gage section; round specimens machined from plate.
[b]Major axis in plane of plate; major axis for all other specimens 90 deg from plane of plate (parallel to normal direction).
[c]Forged from 4-in.-dia ingot to 1-in. plate at 1950°F.
[d]Forged from 4-in.-dia ingot to $1\frac{3}{4}$-in. plate at 1950°F; forged to 1-in. plate at 1475°F.

are being finish-machined. They will be broken within the coming quarter.

The data analyzed so far indicate (1) that no schedule yet studied will produce material sufficiently superior to material produced by the presently used HRP schedule to justify the added complications and (2) that cross-rolling in the early stages of the presently used fabrication schedule has little effect on the final anisotropy while cross-rolling in the final reductions after the last beta quench produces considerable anisotropy.

16.1.2 Morphology of Zircaloy-2

A resistometric transformation apparatus designed for determining the transformation kinetics of various zirconium-base alloys during isothermal and beta-quench and reheat transformations by changes in resistance at temperature was used to determine the alpha/alpha-plus-beta and beta/alpha-plus-beta temperatures for Zircaloy-2. The resistance-temperature curves for Zircaloy-2 were determined by holding the specimen at the desired temperature points for 20 to 30 min. Zircaloy-2 containing the normal commercial amount of 40 to 50 ppm hydrogen had an alpha/alpha-plus-beta temperature of 815 ± 1°C. When vacuum annealed to a content of less than 5 ppm hydrogen, the transformation temperature was increased to 832 ± 1°C.

Typical resistance-temperature curves for Zircaloy-2 for the two hydrogen contents are shown in Fig. 16.1. Successive determinations of the

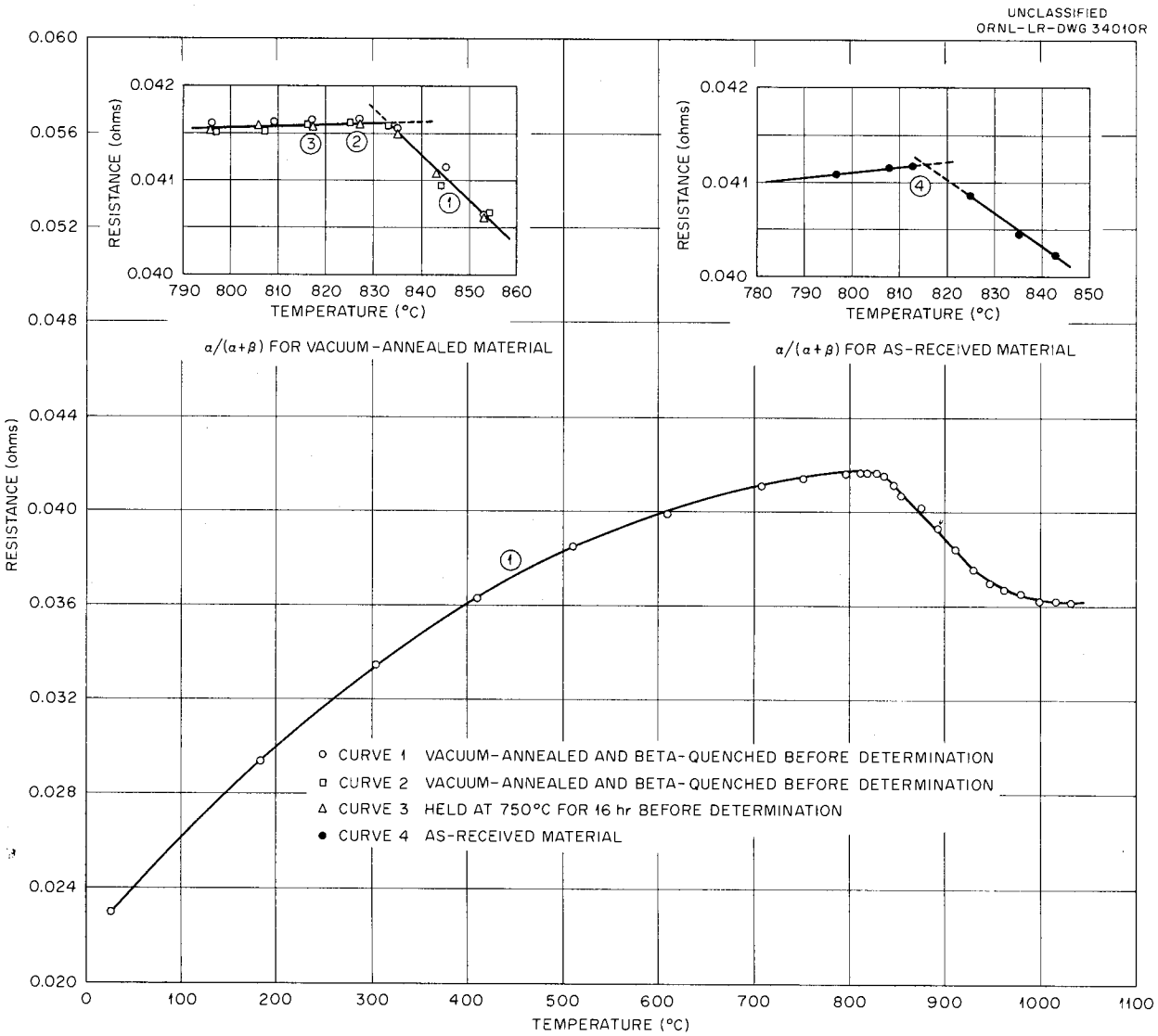

Fig. 16.1. Resistance-Temperature Curves for Zircaloy-2.

alpha/alpha-plus-beta temperature after vacuum annealing and helium quenching indicate the reproducibility of the method. The resistance-temperature curves also show that the resistance of Zircaloy-2 specimens (and therefore the resistivity for the material) approximately doubles in heating from room temperature to about 700°C, increases only a small amount in heating from 700 to 815–832°C, decreases rapidly as small amounts of beta phase are formed, and remains almost constant with increasing temperature from 975 to 1040°C (the highest temperature examined).

16.1.3 Chemical Machining and Pickling Study of Zirconium-Base Alloys

Recent data from in-pile autoclave studies[3,4] have shown that a sand-blasted surface on Zircaloy-2 apparently decreases the corrosion resistance of the material to uranyl sulfate. Other observations, metallographic procedures, and decisions on standard specimen preparation for in-pile corrosion specimens have pointed out the need for a study of chemical machining and pickling of zirconium-base alloys to determine the effects of bath compositions, temperatures, and rinse and drying procedures on the rates of metal removal and on the smoothing of surfaces of machined, ground, abraded, or sand-blasted specimens.

In the first portions of the study, the bath has been maintained at room temperature and the amounts of HNO_3 and HF have been varied. Specimens of three surface conditions – sand-blasted, hand-abraded, and chemically polished – have shown that (1) aqueous solutions containing only HF from 1 to 3 vol % attack very rapidly and pit severely, (2) additions of HNO_3 to a 2% HF solution decrease the rate of attack, with an apparent minimum rate of attack occurring at 5% HNO_3, (3) HNO_3 contents of approximately 5% and of more than 10% are required, respectively, to prevent pitting and to produce smoothing of a machined surface, (4) for an HNO_3 content of 20%, the rate of attack is a function of the HF content, the rate doubling for each 1% HF addition, from 1 to 3%, and (5) increasing the HNO_3 content of a 2% HF solution from 20 to 30% did not affect the rate of attack. Some of these solutions are capable of yielding metallographic polishes from ground surfaces.

[3] R. J. Davis, private communication.

[4] V. A. DeCarlo, *Operation of HRP In-Pile Autoclave Corrosion Test L53Z-135*, ORNL CF-58-10-11 (Oct. 7, 1958).

16.1.4 Electroless Nickel Plating on Zirconium Alloys and Oxide

One of the most difficult problems in the microstructural examination of corroded zirconium-base alloys has been the protection of the surface edge of mounted cross sections of specimens to permit the microexamination of the surface layers and oxides. The deposition of a hard layer of metal, such as Electroless nickel, presents the possibility of preventing edge-rounding of the polished specimen. Adherent coatings of Kanigen nickel[5] have been successfully deposited on unoxidized and on anodized Zircaloy-2 specimens to a thickness of 0.0025 in.

In order to produce adherent coatings, the use of a boiling ½% HF aqueous solution for pretreatment is necessary for proper preparation of the surface. A chemical displacement bath to produce a thin "flash" coating of nickel must also be used as a pretreatment for the anodized specimens, a slow rate of deposition of the Kanigen nickel from the bath being necessary for the production of adherent coatings and thick layers.

No technique yet tried will produce adherent coatings of nickel on air-oxidized specimens. Specimens having a water-corrosion oxide film have not yet been studied.

16.1.5 Zirconium-Hydrogen Study

The presence of amounts of hydrogen greater than 100 ppm is known to embrittle Zircaloy-2 at room temperature. The absorption of considerable amounts of hydrogen during water corrosion in autoclaves has been shown by several studies. Despite several determinations, hydrogen pickup during in-pile loop testing of Zircaloy-2 in oxygen-containing uranyl sulfate fuel solutions has been neither conclusively demonstrated nor disproved. Recently obtained impact specimens exposed in uranyl sulfate solution in D_2O in in-pile loop L-4-13 and others exposed to D_2O in the HRT blanket region, during run 14, have been sectioned and analyzed for hydrogen content and the ratio of hydrogen to deuterium. The data are reported in Table 16.2. Since all deuterium present must have been picked up during the exposure, while the hydrogen was either picked up in handling or was present in the as-received material, these data show that Zircaloy-2 and experimental alloy Zr-20Nb did

[5] A. Brenner and G. Riddell, *J. Research Natl. Bur. Standards* 39, 385 (1947).

Table 16.2. Deuterium Contents of Irradiated Zirconium-Alloy Specimens

Specimen No.	Position	Material	Total H_2 (ppm)	D/H+D	Amount D_2 (ppm)	Remarks
			In-Pile Loop L-4-13			
864	Core	Zr-20Nb	190	0.00159	0.303	
867	Core	Zr-20Nb	150	0.00220	0.330	
874	Core	Zr-3a	34	0.0	0	Not detectable at this level
873	Core	Zr-3a	32	0.0	0	
868	Line	Zr-20Nb	130	0.0376	4.89	
876	Line	Zr-3a	53	0.0682	3.61	
877	Line	Zr-3a	42	0.1068	4.49	
866	Control	Zr-20Nb	180	0.0318	5.73	Specimen never in D_2O; error
			HRT Blanket			
P-1157-1*	Control	Zr-2	19	0.0	0	
-2	Control	Zr-2	24	0.0	0	
-3	Control	Zr-2	20	0.0	0	
-4	Control	Zr-2	17	0.0	0	
-5	Blanket	Zr-2	26	0.00696	0.181	
-6	Blanket	Zr-2	30	0.00279	0.084	
-7	Blanket	Zr-2	23	0.00302	0.069	
-8	Blanket	Zr-2	16	0.003761	0.060	

*H_2 analytical specimens cut from grip and gage sections of Zircaloy-2 HRT blanket A-3-d and its control. The material is core-tank Zircaloy-2.

not pick up deuterium during corrosion in these exposures to D_2O or the deuterium-containing uranyl sulfate fuel solution. The core specimens show less than 1 ppm D although they had shown definite weight losses after loop testing. The line specimens show from 3 to 6 ppm D although they all showed weight gains after test. It is believed that the D contents observed are due to either D, D_2, or D_2O incorporated or absorbed in the oxide corrosion film rather than in the metal itself.

16.1.6 Zirconium-Alloy Development

Zr-Nb-*X*, Zr-Pd, and Zr-Pt alloys have shown promise of possessing an in-pile corrosion resistance to uranyl sulfate solution superior to that of Zircaloy-2. They are also being considered for valve trim and similar special applications in slurry systems. Considerable data on the physical metallurgy and transformation kinetics of these alloys have been reported.[6–11]

Long-time aging of twenty Zr-Nb-*X* alloys at 350, 450, and 550°C was completed during the report period. This completes the aging heat treatments

[6] G. M. Adamson *et al.*, *HRP Quar. Prog. Rep. Oct. 31, 1956*, ORNL-2222, p 114.

[7] G. M. Adamson *et al.*, *HRP Quar. Prog. Rep. April 30, 1957*, ORNL-2331, p 124.

[8] G. M. Adamson *et al.*, *HRP Quar. Prog. Rep. July 31, 1957*, ORNL-2379, p 122.

[9] G. M. Adamson *et al.*, *HRP Quar. Prog. Rep. Oct. 31, 1957*, ORNL-2432, p 131.

[10] G. M. Adamson *et al.*, *HRP Quar. Prog. Rep. Jan. 31, 1958*, ORNL-2493, p 141.

[11] G. M. Adamson *et al.*, *HRP Prog. Rep. for Quarters Ending April 30 and July 31, 1958*, ORNL-2561, p 245 ff.

of this series of alloys. The specimens, now being mounted, await metallographic examination and hardness measurements.

16.2 WELDING DEVELOPMENT

16.2.1 Titanium

The inner weld reinforcement in small pipe and tubing is often required to be flush, or nearly so, with the inner pipe surface in order to prevent any flow constriction in service. The use of a preplaced root insert for the first weld pass usually makes it easier to meet close tolerances. Round, elliptical, and EB-type (Electric Boat, a proprietary type) inserts have been investigated previously in titanium air-welding studies. Welds made with the round insert were most satisfactory, providing very little root reinforcement, and with a single exception these welds were equivalent in all properties to hand-fed wire root passes. Some nitrogen and oxygen pickup was indicated for the insert root passes, which had average hardnesses in the range of 220 to 230 DPH; hardnesses of the hand-fed root passes ranged from 180 to 190 DPH.

Several welds have now been made in which conditions were varied by decreasing welding heat input, changing joint design, varying insert wire diameter, increasing torch gas coverage, and varying internal purging conditions. The best results were from the use of a J-type bevel with $\frac{1}{16}$-in.-dia round insert and argon backup gas. Welds were obtained with an average hardness of 200 to 215 DPH; although the hardness values are still higher than those of hand-fed wire, the welds are not considered seriously contaminated and are acceptable for use. Figure 16.2 is a photograph of the root face of this type of weld.

A square type of insert was also investigated; it produced welds of desirable configuration and with average hardnesses in the range of 190 to 200 DPH, indicating very little contamination of the weld metal. However, these welds contained a large amount of porosity, which made them unfit for use. A higher welding heat input with this type of insert eliminated most of the porosity, but the average hardness increased to 220 to 230 DPH and the weld-metal fluidity resulted in an undesirable concave root surface.

16.2.2 Zircaloy-2

Various welding wires used in titanium and zirconium welding have sparked during welding, an indication of impurities within the metal. A microscopic examination of such wires showed inclusions and porosity through the entire cross section. Wires that sparked usually produced welds having porosity and contamination.

UNCLASSIFIED
T-15946

PREPLACED ROUND WIRE INSERT ROOT PASS RC-A40 IN $\frac{1}{16}$-in. RC-A40 SHEET

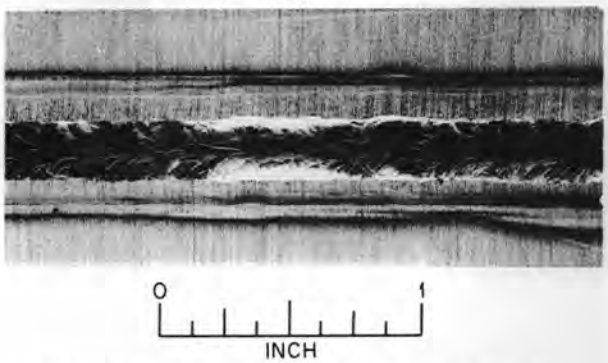

Fig. 16.2. Root Face of Titanium Weld With Root Insert.

In an attempt to establish a quality standard for Zircaloy-2 welding wire, wire of known performance was sectioned and examined microscopically. Figure 16.3*a* is a macrograph of 0.092-in. diameter wire used in welding the HRT core tank. Figure 16.3*b* is a macrograph of wire (0.093-in. diameter) recently fabricated by a commercial vendor. Although each wire contained center porosity, both wires produced satisfactory weld metal. A second commercial batch of wire showed no porosity as-polished, but after being etched center porosity could be detected, possibly indicative of healing of a void previously present during some phase of fabrication. It was concluded that although a small longitudinal void is present at some position in most drawn and swaged Zircaloy-2 wire, such a void does not necessarily result in poor welding quality.

Several test welds were made in $\frac{5}{16}$-in.-dia $\frac{1}{16}$-in.-wall Zircaloy-2 tubing and $\frac{3}{8}$-in. sched-40 pipe, duplicating the possible sample probe design for the HRT. Welds were made in air, with a small enclosed box containing inert gas surrounding the joint. All welds had a weld-metal hardness in the same range as dry-box welds (180–190 DPH) and appeared to be entirely satisfactory by other inspection methods.

Corrosion tests of many Zircaloy-2 air welds in 650°F water resulted in formation of a white, powdery

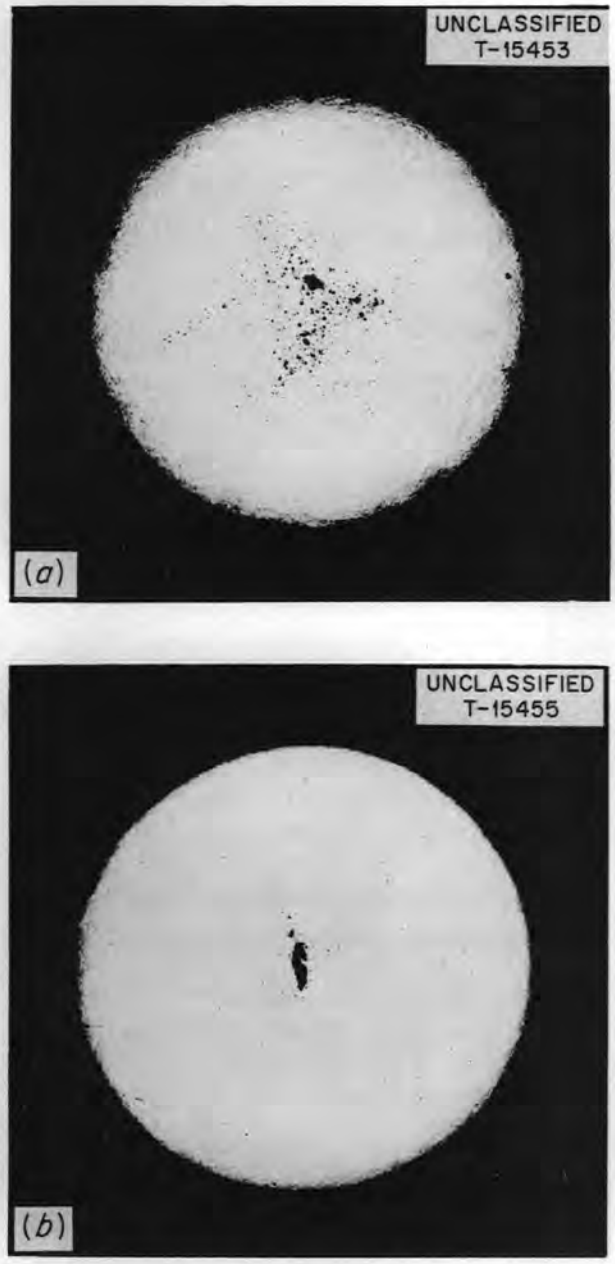

Fig. 16.3. Voids in Zircaloy-2 Weld Wire. (*a*) Wire used in welding the HRT core tank; (*b*) wire recently fabricated by a commercial vendor.

oxide film on the surface of the weld and the heat-affected zone of the base metal, which supposedly indicated a material with undesirable corrosion resistance. A glossy black surface film formed on trailer and dry-box weldments in this test. This variation in corrosion is thought to be due to a difference in the amount of oxygen and nitrogen pickup on the surface as a result of welding heat. When the air welds were retested after approximately 0.005 in. of surface metal had been removed by chemical polishing of specimens, hot-water corrosion tests duplicated results obtained on dry-box welds. It appears that nitrogen and oxygen diffusion into the surface of a properly shielded air weld is very shallow.

A zirconium–15% niobium alloy is being developed and proposed as a high-strength heat-treatable zirconium alloy for reactor use. Two single-pass butt welds were made with this material in 0.062-in. sheet. This material appeared amenable to air-welding, with Zircaloy-2 welding techniques being used. The alloy was in the beta-quenched condition, which permits an age-hardening embrittlement when held in the temperature range of 300–475°C for short times. Hardness traverses of the welds showed no appreciable hardening in the weld metal or heat-affected base-metal zone. A multipass weld in $\frac{1}{4}$-in. plate with $\frac{3}{32}$-in. filler wire gave essentially the same results. Examination of the microstructure and hardness data gave no definite indication of appreciable amounts of the age-hardening transformation.

16.3 NONDESTRUCTIVE TESTING DEVELOPMENT

16.3.1 Ultrasonic Attenuation

Early work[10] has shown that some metals attenuate ultrasonic energy so rapidly that a satisfactory inspection is difficult. A technique has been devised[12] to measure attenuation and thus to expand our knowledge of the phenomenon. A number of different stainless steel weld compositions were investigated to determine whether one composition might have outstanding transmission characteristics which would permit a thorough ultrasonic inspection. The results of this investigation of stainless steel welds are shown in Fig. 16.4, along with the frequency-attenuation characteristics of a carbon-steel weld and a stainless steel base metal. None of the stainless steel welds tested compared with the carbon-steel weld in ability to transmit ultrasonic energy. Although the stainless steel welds varied in composition from fully austenitic to over 10% ferritic, none of them were clearly less attenuating than the others.

[12] J. K. White, R. W. McClung, and J. W. Allen, "Implications of Ultrasonic Attenuation to Nondestructive Testing," to be published in *J. Soc. Non-Destructive Testing.*

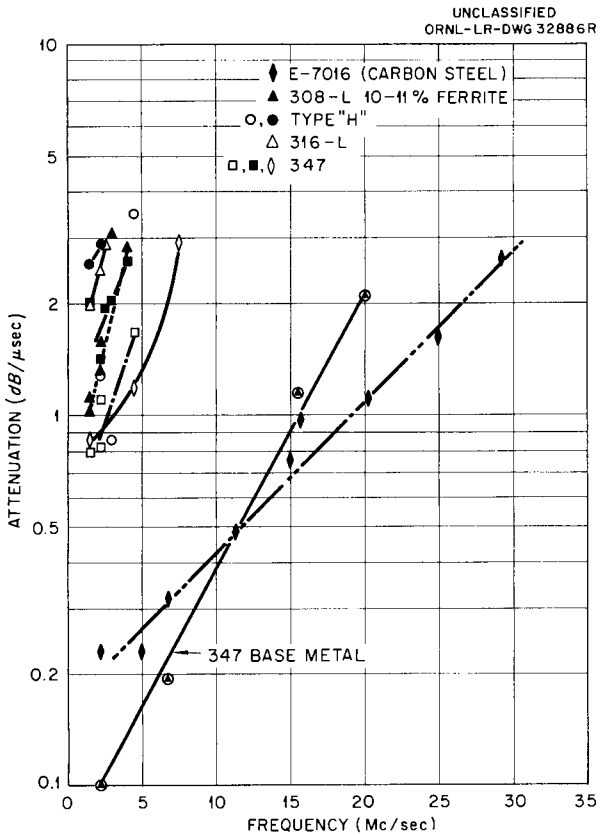

Fig. 16.4. Ultrasonic Attenuation vs Frequency in Several Welds.

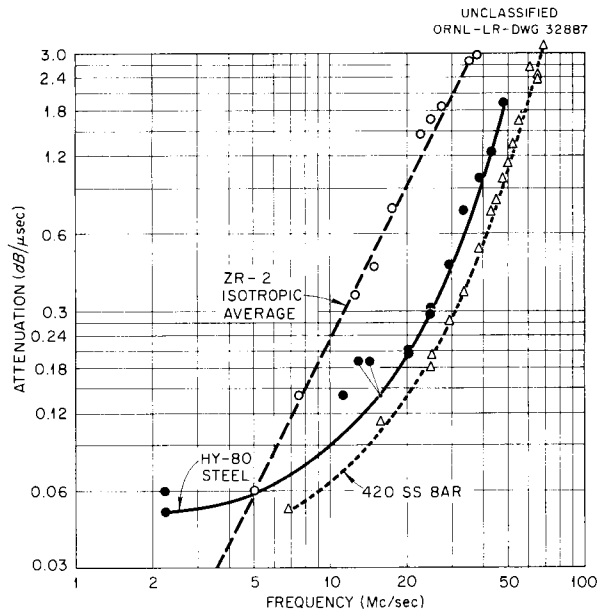

Fig. 16.5. Ultrasonic Attenuation vs Frequency in Various Metals.

The attenuation of ultrasonic energy in Zircaloy-2 was studied. Over the low-megacycle region the attenuation of longitudinal ultrasound in Zircaloy-2 varies as the fourth power of the frequency. This relationship is characteristic of a particulate type of scattering and indicates that the only major cause of attenuation in Zircaloy-2 is Rayleigh scattering. Figure 16.5 compares the attenuation of a carbon steel and a stainless steel with that of Zircaloy-2. In these steels some other factor is involved which causes a more rapid increase in attenuation as the frequency is increased. Both these and all other steels with attenuation low enough to be measured over a broad frequency range showed a similar relation of attenuation to frequency.

16.3.2 Resonance Measurements of the Zircaloy-2 Core Shell

In order to monitor corrosion of the HRT core vessel, ultrasonic resonance measurements of the vessel thickness have been carried out over the course of its use. Previous measurements, including one after run 14, had ranged upward a few thousandths of an inch from 0.315 in. After run 17 a measurement was made which indicated a thickness of 0.278 in. This unexpectedly large change has prompted a desire to make a series of such measurements at various locations on the core to provide a more definite picture of the general attack, rather than the single measurement which has heretofore been the practice. This multiple measurement is planned for the next shutdown period.

Tests with the lead zirconate-titanate transducer presently in use indicate no perceptible resonance shift or loss of polarization of the transducer under a gamma field of approximately 50,000 r, which is comparable to that inside the reactor.

16.3.3 Combustion of Titanium and Zirconium

During the report period the combustion studies being conducted under a subcontract at Stanford Research Institute were concerned primarily with ignition of Zircaloy-2. The most striking feature of this work has been the complete lack of reproducibility in the data. In static tensile tests Zircaloy-2 rods have been broken at room temperature under oxygen pressures varying from 650 to 1500 psi. At every pressure some samples ignited while others did not.

No ignition was found in single tests at 500, 550, and 600 psi. With 20-mil tensile strips a reaction occurred in one out of three tests at 750 psi, but none occurred in two tests at 500 psi and one at 600 psi.

In dynamic gas-flow tests in which 20-mil sheets were ruptured by a plunger after which gas flowed through the opening, a similar scatter was found in the data. Ignition took place with oxygen pressures as low as 50 psi; however, some samples did not react at 200, 300, and 500 psi, while others did. As yet no satisfactory explanation has been offered for these wide variations.

16.4 EFFECTS OF RADIATION ON STRUCTURAL METALS AND ALLOYS[13]

16.4.1 Equipment and Facilities

In the HB-3 facility of the LITR, steel tensile specimens and Charpy V-notch impact specimens were irradiated at 575 and 140°F. In a separate experiment steel tensile, Charpy, and subsize Izod impact specimens were irradiated at 140°F.

Installation of instruments and other equipment for irradiations in the ORR is in progress, and the first irradiation of structural metals will begin during the next quarter. The "hydrostatic canning" method[12] successfully used to can Charpy and Izod specimens is being extended to the canning of tensile specimens.

Accessory equipment that will allow operation of the full-size Charpy machine in the hot cell is almost completed. Previously, Charpy tests could be conducted on only mildly radioactive specimens with temporary shielding around the testing machine.

16.4.2 Impact Tests

Subsize Izod impact tests were conducted on high-purity iron and an iron-carbon alloy (0.1% carbon). The results[14] indicate much less radiation-induced transition-temperature shift than has been commonly observed in carbon steels exposed to the same neutron dose. Contrary to the usual observations, a fine-grained iron showed a higher initial transition temperature and a greater radiation-induced shift of transition temperature than did a coarse-grained iron. The reasons for these peculiarities are, at present, unknown. These results suggest that the large radiation-induced transition-temperature shifts in steel are not an inherent property of the body-centered cubic structure.

Transition-temperature increases in irradiated subsize Izod impact specimens from ¾-in.-thick plates of ASTM A-212B, A-285A (in both hot-rolled and normalized conditions), and A-301B steels at fast-neutron doses of 2×10^{19} to 12×10^{19} neutrons/cm^2 were all similar in magnitude to results obtained on the 4-in.-thick plate of ASTM A-212B steel reported previously.[12] The Charpy V-notch transition-temperature shifts determined at a dose of 5×10^{18} neutrons/cm^2 for these same steels (at two irradiation temperatures) showed larger differences between the steels than the subsize Izod test data at integrated fluxes above 2×10^{19} neutrons/cm^2. The transition-temperature shifts observed in these steels and in normalized, coarse-, and fine-grained ASTM A-106 steel, were approximately 300°F after irradiation at 175°F to doses of 10^{20} *nvt* (>1 Mev). Similar tests on an ASTM A-302B steel, irradiated at 175°F, gave transition-temperature shifts of 150°F at a dose of 5×10^{18} *nvt* (>1 Mev) to 350°F at a dose of 2×10^{20} *nvt* (>1 Mev).

The effect of irradiation temperature on the notch impact strength of class HY-80 steel[15] was investigated. Irradiation at 175°F resulted in a transition-temperature shift of about 350°F at 10^{20} *nvt* (>1 Mev), but irradiation to the same neutron dose at temperatures of 540 to 600°F resulted in a shift of only 100 to 150°F (Fig. 16.6). In general, this range of irradiation temperatures is more effective in reducing the transition-temperature shift in this alloy than in any steel yet tested.

The results of subsize Izod impact tests conducted on Zircaloy-2 weld metal, irradiated at temperatures of 440 to 600°F and doses of 1.6 to 12×10^{19} *nvt* (>1 Mev), are shown in Fig. 16.7. No significant radiation-induced change in impact properties was observed, and the test results were almost in the center of the scatter band for results previously obtained for wrought Zircaloy-2.

16.4.3 Tensile Tests

A carbon-steel tensile specimen[12] that failed without localized deformation (necking) after a few

[13] This work was conducted in the Solid State Division.

[14] J. C. Wilson *et al.*, *Solid State Ann. Prog. Rep. Aug. 31, 1958*, ORNL-2614, p 98 ff.

[15] Navy Department designation for nickel-chromium-molybdenum alloy steel of 80,000 psi minimum yield strength and containing 0.22% maximum carbon; 0.45 to 0.60% molybdenum, 2.75 to 3.25% nickel, and 1.25 to 1.85% chromium.

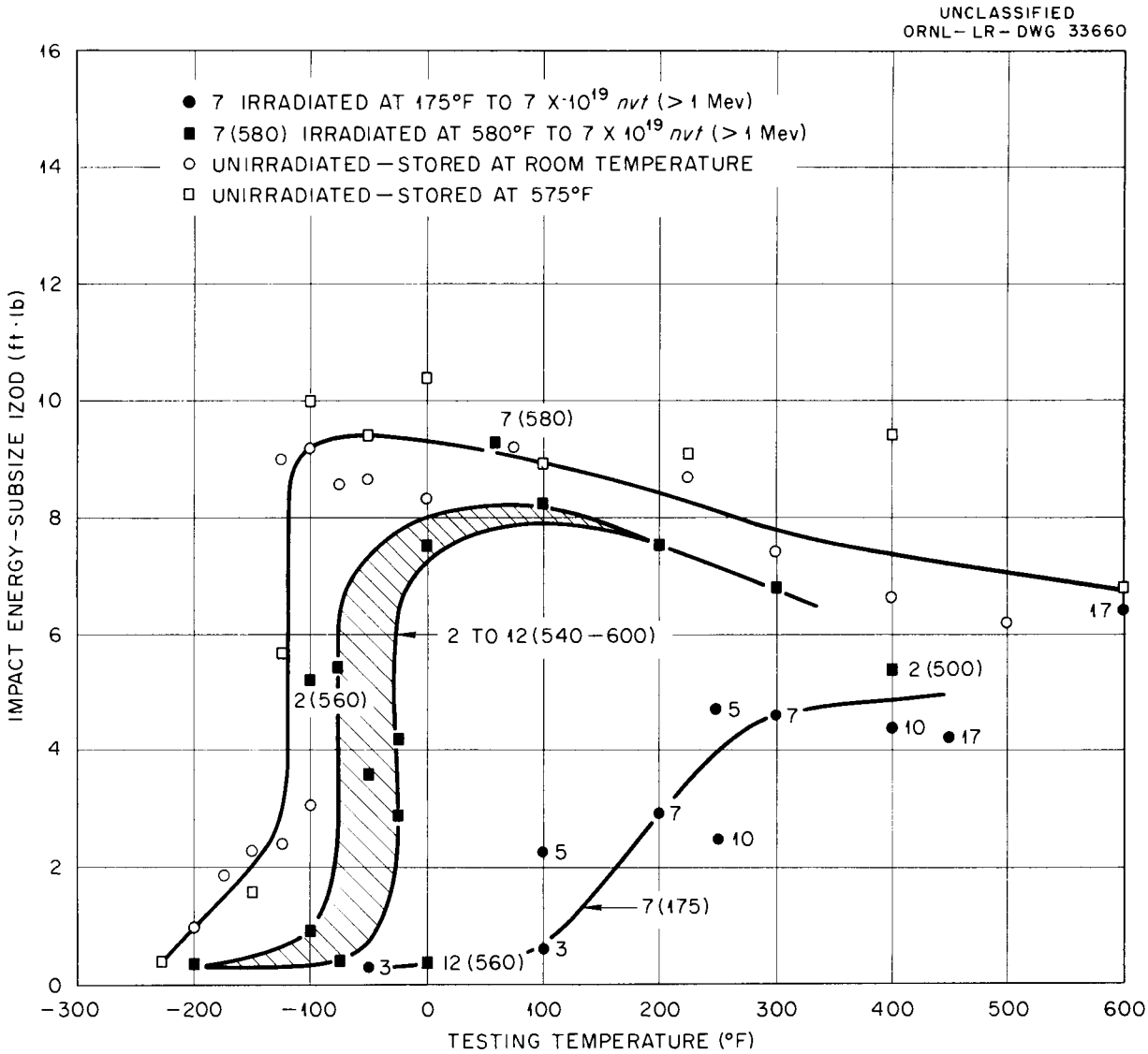

Fig. 16.6. Subsize Notch-Impact Results for Irradiated HY-80 Steel.

per cent uniform elongation following irradiation at 580°F to a dose of 8×10^{19} *nvt* (>1 Mev) was sectioned, and the fracture was examined metallographically. A mixture of transgranular (cleavage) fractures and intergranular fractures was found, with an insignificant amount of shear failure. Macroexamination of the notch impact specimens showed cleavage to be the predominant mode of fracture. The reason for this embrittlement is not known, but radiation-induced temper embrittlement at higher irradiation temperatures is suggested.

The stress-strain curves of high-purity iron and iron-carbon alloys of high purity have been found to be strongly dependent on microstructure. In high-purity iron, high neutron doses eliminate the ability of the metal to work-harden. The presence of iron-carbide lamellae in the carbon-containing alloys apparently permits even the highly irradiated metal to work-harden to some extent. Whether this phenomenon is connected with brittle-fracture behavior is not yet known, but the data do show that the ductile behavior of irradiated iron alloys and steels depends strongly upon microstructure.

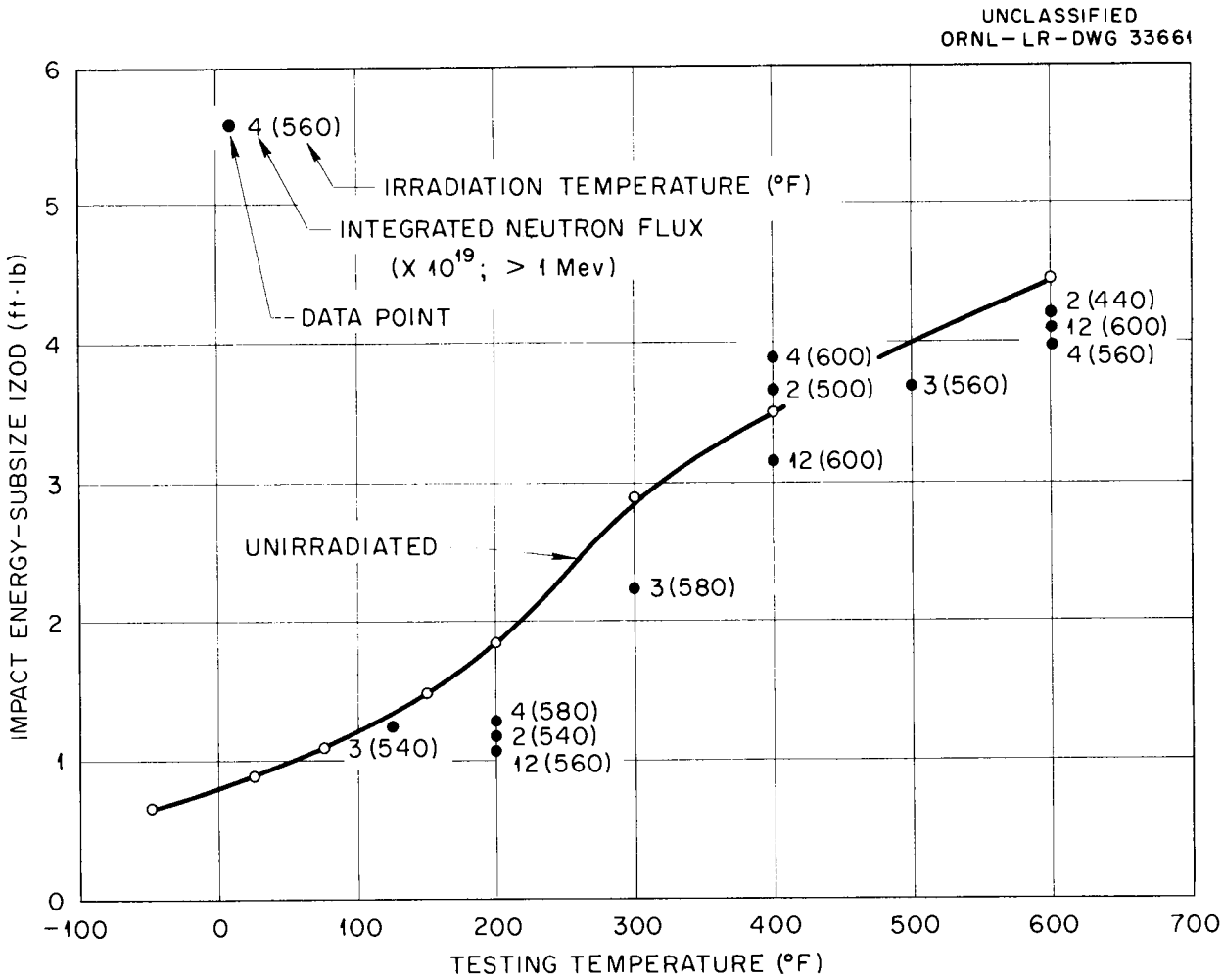

Fig. 16.7. Subsize Notch-Impact Results for Irradiated Zircaloy-2 Weld Metal.

Part V

CHEMICAL ENGINEERING DEVELOPMENT

D. E. Ferguson

17. URANYL SULFATE FUEL PROCESSING

R. A. McNees

P. A. Haas S. Peterson D. J. Price

17.1 IODINE CHEMISTRY

17.1.1 Laboratory Experiments

Further tests of the effect of Co^{60} radiation on the valence behavior of iodine in simulated fuel solutions at 250–300°C have shown that the equilibrium distribution between elemental and iodate valence states is not affected by radiation at intensities up to 23 w per kg of H_2O. When a stainless steel pressure vessel and a titanium sample line were used and a prescribed sampling technique was rigidly followed, 20% of the iodine present in solution was in the iodate form. This was the case whether oxygen at 100, 200, or 400 psi was added to the pressure vessel at room temperature, whether the solution (0.04 *m* UO_2SO_4, 0.02 *m* H_2SO_4, 10^{-5} *m* HIO_3) was 0.005 or 0.03 *m* in $CuSO_4$, and whether the temperature was 250 or 300°C. These results differ somewhat from those which were previously reported[1] and which were obtained with a slightly different piece of experimental apparatus.

At 270°C in simulated HRT fuel solution, corrosion-product solids which had been obtained from high-pressure loops removed about 50% of the iodine initially present in solution (10^{-5} *m* HIO_3). Whether such removal is by reaction, adsorption, or absorption, exchange of the iodine so held with iodine in solution is sufficiently rapid to establish equilibrium in less than 5 min at 270°C.

17.1.2 HRT Operating Experience

Samples taken from the HRT during run 17 and analyzed for total iodine content and I^{133}/I^{131} activity ratio have produced essentially the same values previously reported[1] for run 16. Iodine activity in run 17 samples, as in previous runs, was low and erratic, indicating rapid removal of iodine from the reactor system, while the age of the iodine found, as measured by I^{133}/I^{131} activity ratios, indicated a much slower removal rate.

Laboratory experiments have shown that loss of iodine from simulated HRT fuel solutions to either the glass walls of the HRT sample container or the rubber closures does occur when such solutions contain only small (10^{-5} *m*) concentrations of iodine. Losses to the rubber closures are increased by Co^{60} radiation. After 20–24 hr of irradiation at 2–23 w/liter, 30 to 85% of the iodine initially present was transferred to the rubber closure. However, since more than 95% of the iodine would have to be lost from the HRT samples to account for the discrepancy, this observed loss does not provide an adequate explanation for the discrepancy. Addition of small amounts of hydrogen peroxide (final solution 0.01 *m* H_2O_2) to similar solutions resulted in comparable iodine losses to the rubber closures in the absence of radiation. So far, no material has been found which could be added to the HRT sample containers to prevent such iodine losses.

In an attempt to explain these anomalous observations, two theories of iodine behavior in the HRT have been considered. One possibility is that only a fraction of the iodine entering the dump tanks is volatilized and held by the silver adsorber, while the remainder is returned to the high-pressure system. This theory is consistent with the isotope ratios observed in run 14, assuming that 10–20% of the iodine in the dump tanks evaporated and was held by the iodine trap. However, the amount of iodine found in the samples does not agree with this possibility by at least a factor of 10.

The second theory assumes that about 10% of the iodine in the high-pressure system is in solution and circulating, while the remainder is held by solids in the high-pressure system. Only the iodine in solution is free to be transferred from core to blanket or let down to the low-pressure system with its attendant removal by the iodine trap. Exchange of iodine fresh from the fissioning process with aged iodine held by reactor solids would give iodine activity ratios consistent with those observed. In substantiation of this second possibility, the results of laboratory experiments cited in the previous section show that there is significant adsorption of iodine on insoluble corrosion products under simulated HRT conditions.

---

[1] R. A. McNees *et al.*, *HRP Prog. Rep. for Quarters Ending April 30 and July 31, 1958*, ORNL-2561, p 267.

17.2 SOLIDS BEHAVIOR

The corrosion loop at Y-12 on which a hydroclone has been operating to remove corrosion-product solids under conditions simulating those of the HRT was modified by inserting several carbon-steel test pins into the loop. The purpose was to provide larger amounts of solids over shorter periods of time and thus allow for more rapid evaluation of the effects of configuration changes in the system. In the first test with the hydroclone feed take-off point at right angles to a straight section of pipe, only 4 g of solids were collected out of an estimated 42 g produced. The feed point for the hydroclone has now been moved to the right-angle bend beneath the pressurizer, and tests with this configuration are being made. A hydroclone large enough to handle 30–40 gpm has been designed, is being constructed, and will be inserted in loop to test the effect of increased processing rates at somewhat lowered efficiencies.

17.3 ALTERNATE CORE PROCESSING DEVELOPMENT

The rapid corrosion rate experienced during the early stages of HRT power operation indicated the possible need for developing a simple method for removing nickel from HRT fuel solutions. Various precipitation and ion exchange methods were attempted with no success.

Attempts to precipitate nickel, while leaving uranium in solution, were made by pressurizing simulated HRT fuel solutions containing 300 ppm nickel to either 5000 psi with CO_2 or 300 psi with H_2S after the solutions had been neutralized to the point of incipient uranium precipitation. No nickel removal by either method was observed. Various ion exchange methods using organic resins and silica gels which had been treated for surface-charge reversal were tried without success.

18. GASEOUS FISSION-PRODUCT DISPOSAL

R. D. Ackley R. E. Adams W. E. Browning

18.1 ABNORMAL BEHAVIOR OF HRT CHARCOAL BEDS DURING RUN 17

Studies of the behavior of fission gases during the past three months were concerned with providing a satisfactory explanation for the abnormal behavior of the HRT charcoal beds described in Sec. 3.2.2. Attention was given to the effect of carbon dioxide on krypton holdup by charcoal, identification of the products of combustion of charcoal by oxygen under simulated HRT conditions, and the effectiveness of the charcoal as a catalyst for recombining hydrogen and oxygen. Results of the ignition studies and the observed deleterious effects of carbon dioxide on krypton holdup by charcoal explain the breakthrough of rare-gas activity during run 17 startup. However, determination of the factors responsible for ignition of the charcoal requires further investigation.

The combustion of charcoal by oxygen in a 0.66-in.-ID stainless steel pipe was studied, with particular emphasis being given to the products of the reaction under various conditions of oxygen flow and temperature. In the course of the investigation, the minimum flows of oxygen required to sustain combustion were determined roughly for two cases external water cooling and no water cooling. In terms of superficial linear velocity, the values obtained were 2.2 and 0.9 ft/min, respectively. The exit gases from the combustion of Columbia G charcoal in flowing oxygen under three different sets of conditions were analyzed for oxygen, carbon dioxide, and carbon monoxide; the results are summarized in Table 18.1. Each concentration represents the average of four values. As would be anticipated, the ratio of the concentration of carbon dioxide to that of carbon monoxide increases as the linear velocity of the oxygen decreases, or, in effect, as the reaction temperature decreases.

Table 18.1. Analysis of Exit Gases from Combustion of Charcoal in Oxygen

Oxygen Linear Velocity (ft/min)	External Water Cooling	Concentration in Exit Gas (vol %)			
		O_2	CO_2	CO	Residual
1.5	No	1	94	0	5
2.9	Yes	4	83	13	1
21.6	Yes	1	26	66	7

The effect of adsorbed carbon dioxide on the krypton holdup performance of charcoal is shown in Fig. 18.1, where the dynamic adsorption coefficient k is plotted versus the concentration of carbon dioxide in the sweep gas which is in equilibrium with the charcoal surface. As may be seen, holdup of krypton is considerably reduced by appreciable concentrations of carbon dioxide.

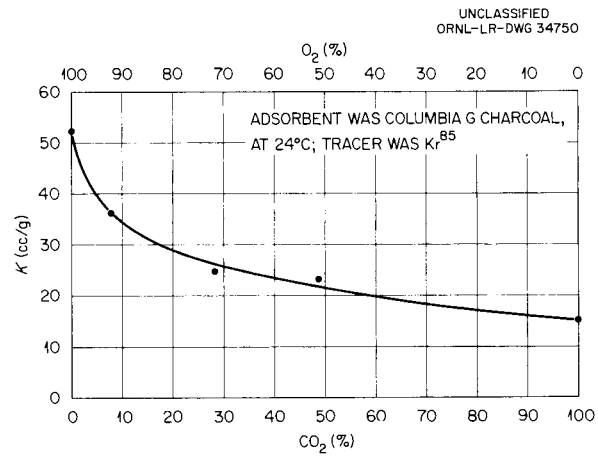

Fig. 18.1. Effect of CO_2 in the Sweep Gas on the Dynamic Adsorption Coefficient k.

In studying the recombination of hydrogen and oxygen on activated charcoal, a stoichiometric mixture of the gases was allowed to flow through heated tubes containing Columbia G charcoal. The water contents of the exit gases were then determined periodically by means of a dew-point meter. Four sets of experimental conditions were employed, each of which may be characterized by the temperature and the space velocity (the volume flow rate divided by the volume of the charcoal bed): (1) 120°C and 4 min^{-1}, (2) 140°C and 4 min^{-1}, (3) 140°C and 0.7 min^{-1}, and (4) 200°C and 0.30 min^{-1}. No appreciable recombination was indicated in these experiments; the observed dewpoints did not appear to be significantly higher than those obtained when oxygen alone was passed through the charcoal. It does not appear that the beds were

ignited by recombination of the gases on the charcoal unless radiation has an important effect.

The holdup performance of another adsorbent, Corning porous glass No. 7930, was evaluated in the usual manner[1] with Kr^{85} as the tracer and oxygen as the sweep gas. This material gave very low values for the dynamic adsorption coefficient k, 0.9 cc/g at 24°C and 0.8 cc/g at 150°C. These values are about 2% of the values for activated charcoal.

[1]W. E. Browning and C. C. Bolta, *Measurement and Analysis of the Holdup of Gas Mixtures by Charcoal Adsorption Traps*, ORNL-2116 (July 27, 1956).

19. EQUIPMENT DECONTAMINATION

R. E. Leuze A. B. Meservey

19.1 HRT DECONTAMINATION STUDIES

Methods are being developed for the production of chromous sulfate solution on a scale suitable for the descaling and decontamination of the HRT. The reduction of chromic to chromous sulfate, by chromium and zinc metals, and electrolytic reduction are being studied. The decontamination of hot HRT components, such as flanges and valves, will be attempted as demonstrations prior to HRT decontamination.

The use of other reagents for the HRT decontamination is also being studied. Among these reagents are those of Turco Products, Inc. Preliminary laboratory tests at ORNL have shown excellent removal of thin oxide coatings on stainless steels without corrosion, and good decontamination from niobium in some cases. The Thorex pilot plant was decontaminated in October 1958 by the use of the Turco 4501 process, with very substantial savings in time and cost over previously used methods. The Turco reagents will be tested on HRT reactor components as soon as practicable.

20. THORIUM OXIDE SLURRY DEVELOPMENT

J. P. McBride P. A. Haas W. H. Lewis

C. V. Ellison K. H. McCorkle J. C. Suddath
C. C. Haws L. E. Morse W. J. Watt
K. O. Johnsson R. L. Pearson W. M. Woods
N. A. Krohn C. E. Schilling E. L. Youngblood

20.1 SLURRY IRRADIATION STUDIES

20.1.1 Slurry Irradiations in the LITR

Two short-term slurry irradiations (LITR-48 and -49) were carried out in the C-44 vertical tube facility. Both slurries contained 250 g of Th per kg of D_2O as a 1000°C-fired thorium–5% natural-uranium oxide prepared from the coprecipitated oxalates. One slurry was irradiated under 1 atmosphere of air and the other under a pressure of 200 psi of D_2 gas (measured at room temperature). The respective irradiation times at 300°C were 310 and 354 hr. No radiolytic-gas pressure was observed at 300°C in either experiment, although a residual gas pressure of 200 psi was found at 33°C at the end of the experiment with an air atmosphere. A slow leak developed in the pressure-capillary connection of the D_2 atmosphere experiment after two weeks of operation and prevented the measurement of residual gas pressure at the end of the experiment.

20.1.2 Postirradiation Examinations

Three previously irradiated slurries of 1000°C-fired ThO_2–5% natural-uranium (LITR-44, -46, and -47) were recovered as black slurries and analyzed. The high uranium content had little effect on the fission-product distribution, as compared with the distribution in previous irradiations of pure ThO_2 or ThO_2–0.5% U slurries, although iodine seemed less strongly adsorbed (Table 20.1). The material showed a corrosion rate, both in and out of pile (Table 20.2), much higher than the rate for previous slurries, which probably indicates more abrasive particles. An increase in corrosion-product pickup over that observed with ThO_2 slurries had also been obtained with a ThO_2–0.5% U slurry in the dash-pot bomb, and jet abrasion tests showed a similar result.

The sample of 1600°C-fired pilot-plant ThO_2 which was irradiated for 3235 hr in the LITR as a settled slurry was recovered. The autoclave, because of the addition of cooling fins, could not be

Table 20.1. Distribution of Fission Products in Irradiated Slurries

1000°C-fired ThO_2–5% natural U in D_2O

Component	Per Cent of Component in Supernatant		
	LITR-44,* 750 g of Th per kg of D_2O	LITR-46, 500 g of Th per kg of D_2O	LITR-47, 250 g of Th per kg of D_2O
Gross β	0.9	0.02	0.10
Gross γ	0.8	0.02	0.12
Sr	10.5	0.2	0.3
Zr	2.9	24.9	7.5
Cs	23.7	37.1	43.0
Ru	6.2	0.5	1.3
Total rare earths	3.7	0.04	0.1
I	10.8	18.8	20.0
Pa	0.9	0.02	0.1

*Lost D_2O during irradiation; reslurried in light water after opening.

given the usual shaking before it was opened. When the autoclave was opened, a loose agglomerate of thoria which broke up into dark grainy particles was found in the bottom. A sample of the dried slurry was refluxed for 30 min in 4 *N* HNO_3; the solids were separated and were refluxed for 30 min in 4 *N* HNO_3 containing 1.5% H_2O_2. One and a half milliliters of 30% H_2O_2 was then added, the suspension was refluxed for an additional 30 min, and the solids were again recovered. The two acid solutions and the residual solids were then analyzed for various radioactive components and corrosion products (Table 20.3).

Thirty-six per cent of the U^{233}, 40% of the Pa, and only 0.2% of the Th were dissolved in the first nitric acid leach. The nitric acid–peroxide leach dissolved an addition of 52, 25, and 36% of the U^{233}, Pa, and Th, respectively. Sixty-five per cent of the gross gamma and beta activities were removed from the solids in the two acid leaches. Seventy to eighty per cent of the Sr, Zr, Cs, and Fe were dissolved in the two leaching solutions, along with lower percentages of Ru, Nb, Ni, and Cr. An unexpectedly high fraction of the Cs (31%) stayed on the residual solids. The Ru was particularly resistant to leaching, only 3% being dissolved by the two processes.

Table 20.2. Corrosion in Dash-Pot Bomb

ThO_2–5% natural U in D_2O
Temperature: 300°C

Concentration (g/kg)	Time (hr)		Corrosion Products (g per kg of Th)		
	Stirred	Irradiated	Fe	Ni	Cr
250	350	0	88	76	11
250	450	354	268	31	9
500	405	361	84	20	16
750	80	49	16	2	0.6

20.1.3 In-Pile Gas Production and Recombination Studies

Two irradiation experiments in the ORNL Graphite Reactor were made for the purpose of

Table 20.3. Nitric Acid Leaching of Irradiated Slurry

1600°C-fired ThO_2
3235-hr irradiation

Component	Per Cent of Component		
	In 4 *N* HNO_3 After 30-min Reflux	In 4 *N* HNO_3–1.5% H_2O_2 After 1-hr Reflux	Remaining in Solid Phase
Th	0.2	36.1	63.7
U	36.2	51.5	12.3
Pa	39.7	25.0	35.3
Gross γ	38.9	25.0	36.1
Gross β	40.9	25.0	34.1
Sr	64.5	9.8	25.7
Zr	34.5	40.1	25.4
Ru	1.3	2.0	97.1
Cs	60.6	8.3	31.1
Nb	32.1	15.2	52.7
Fe	70.2	13.7	16.1
Ni	10.7	14.2	75.1
Cr	0	58.2	41.8

measuring radiolytic-gas production and recombination rates in slurries. The slurries contained 500 g of Th per kg of D_2O as thorium oxide containing 2.8% enriched uranium prepared by calcining coprecipitated thorium-uranous oxalate at 650°C in the first test and at 1000°C in the second. The initial production of gas at 200°C was measured in both cases, the values being 4.8×10^{-4} mole of D_2 per hour for the 650°C-fired oxide and 4.9×10^{-4} mole of D_2 per hour for the 1000°C-fired oxide, as compared with values of 3.3×10^{-4} mole of H_2 per hour previously observed for light-water systems. Assuming that the flux was the same, the G value for D_2 production was therefore almost one and one-half times that for H_2, or approximately 1.2 molecules of D_2 produced for every 100 ev of energy absorbed. Observed equilibrium pressures at temperatures from 200 to 280°C with 650°C-calcined oxide in D_2O did not differ significantly from those obtained previously in a light-water test for 900°C-calcined oxide (Fig. 20.1). The slurry of 1000°C-fired oxide showed some anomalies: initial radiolytic-gas pressures were much higher, with a steeper temperature dependence; as the experiment progressed radiolytic-gas pressures became lower and

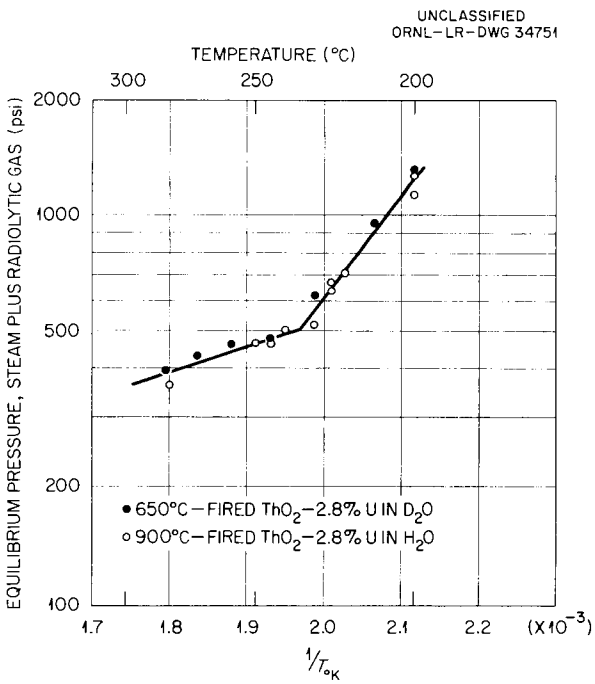

Fig. 20.1. In-Pile Radiolytic-Gas Pressures Over Slurries of Thorium-Uranium Oxide Containing 500 g of Th per kg of H_2O; Flux, $\sim 4.2 \times 10^{11}$ Neutrons·cm^{-2}·sec^{-1}.

the temperature dependence became much smaller. Details of the experimental procedure are being studied to resolve the discrepancy.

20.1.4 Equipment Development

Preliminary results of tests on cooling the dash-pot bomb with water flowing in a 40-mil-ID capillary coil wrapped around the bomb indicate that more than 1 kw of heat can be removed with an 80-ml/min water flow rate and a maximum bomb temperature of 300°C. A Hills-McCanna McCannameter pump operating at ~2000 psi was used. Pressures greater than 1500 psi are required to keep the water at 300°C from flashing to vapor in the capillary. Vapor binding appears to cut down on the rate of heat transfer by about 25% at 300°C. This system of cooling may be considered as an alternative to modifying the configuration of the C-43 facility for more efficient cooling.

20.2 GAS RECOMBINATION STUDIES

Experiments were continued on the use of MoO_3 and PdO catalysts in thorium and thorium-uranium oxide slurries for the catalytic recombination of radiolytic gas. Effort was concentrated on (1) the effect of pumping in a high-temperature loop on the catalytic activity of a slurry of 1600°C-fired oxide containing MoO_3 and (2) the development of a catalyst for use in thorium-uranium oxide slurries containing U/Th $\geqq$ 0.05. The high-temperature loop experiment is being carried out as part of an overall program of out-of-pile testing of slurries projected for use in the in-pile slurry loop program.

20.2.1 High-Temperature Loop Experiments

A high-temperature loop test (BS-24) is being carried out at 280°C and under both O_2 and D_2 atmospheres to determine the effect of loop conditions on both slurry handling characteristics and catalytic activity (see Sec. 14.1.3). The high-fired oxide (DT-15 and -16) was specially prepared for in-pile loop use. The slurry at a concentration of 450 g of Th per kg of D_2O was loaded into the loop and pumped for 197 hr under an O_2 atmosphere before the addition of the MoO_3 in aqueous solution-suspension to give a concentration of 0.008 m MoO_3. Samples of the slurry were withdrawn from time to time and used for gas recombination experiments in small stainless steel autoclaves. The principal effect noted was the development of an "induction period" before maximum catalytic activity was

achieved. The length of the induction period increased with increased pumping time under O_2 (Table 20.4), the slurry apparently becoming deactivated under oxygen and reactivated when placed in a D_2 and O_2 atmosphere ($D_2 + \frac{1}{2} O_2$) in the recombination tests. Substitution of a D_2 atmosphere for the O_2 atmosphere in the loop eliminated the induction period.

Recombination experiments were performed in groups of three; D_2 and O_2 were added at room temperature for each experiment, the reaction autoclave was brought to temperature, and the recombination was followed by the decrease in total pressure. At the end of three experiments the autoclave was opened, excess D_2O was removed, and the autoclave was resealed for another series of experiments. The results of the third experiments shown in Table 20.4 showed little change in catalytic activity up to 168 hr pumping time in the O_2 atmosphere at 280°C. The results of the first experiments, up to 168 hr pumping time, showed a relatively slow reaction rate, the rate decreasing with increasing pumping time. After 168 hr of operation with O_2 and 0.008 *m* MoO_3, fresh ThO_2 and MoO_3 were added to the loop to replace slurry removed as samples, and the run was continued under O_2 for an additional 120 hr, when a D_2 atmosphere was substituted for the O_2.

The sample taken 3 hr after the addition of D_2 showed an initial high reaction rate for the first recombination experiment; in the sixth experiment the rate decreased to a value equal to that obtained in the sixth experiment with the last slurry sample from the oxygen system (see Table 20.4). A similar phenomenon has been observed in laboratory experiments after treatment of slurries containing MoO_3 with H_2 or D_2 at 270°C for 2 hr. The slurry loop samples changed from a light gray to a light tan during the gas recombination tests.

20.2.2 Catalysis in Thorium-Uranium Oxide Slurries

Reaction rates of stoichiometric H_2 and O_2 mixtures in thorium-uranium oxide slurries (250 g of Th per kg of H_2O) containing a uranium-to-thorium ratio of 0.05 were determined with MoO_3,

Table 20.4. The Effect of Circulation Time and Conditions on the Reaction Rate of Stoichiometric D_2-O_2 Mixtures in ThO_2-D_2O Slurries Containing MoO_3

REED Slurry Corrosion Group run BS-24
450 g of Th per kg of D_2O, 1600°C-calcined ThO_2 (DT-15 and 16)
0.008 *m* MoO_3
Circulation temperature, 280°C

Loop Circulation Time* (hr)	Gaseous Atmosphere	Reaction Rate, 280°C, P_{D_2} = 100 psi (moles of D_2 per hour per liter)	
		First Experiment	Third Experiment
18	O_2	2.9**	3.5
66	O_2	1.4	3.7
168	O_2	0.13	3.0
(After 168 hr, approximately half the loop charge was replaced with fresh ThO_2 and MoO_3)			
		First Experiment	Sixth Experiment
289.5	O_2	0.31	4.6
292.8	D_2	8.85 (250°C)	4.6

*Time after addition of MoO_3; for total circulation time add 197 hr.
**This rate obtained after a 15-min "induction" period.

PdO, and Fe_2O_3 as catalysts (Table 20.5). Two thorium-uranium oxide preparations were studied: one prepared by calcining the coprecipitated oxalates for 24 hr at 1000°C and the other by autoclaving a simple oxide mixture (650°C-fired ThO_2 + $UO_3 \cdot H_2O$) at 300°C for 24 hr and calcining the recovered solids at 1000°C for 24 hr. Both MoO_3 (0.03 *m*) and PdO (1000 ppm Pd, based on thorium) gave acceptable recombination rates in slurries of mixed oxide prepared from the coprecipitated oxalates. The MoO_3, however, was not an effective catalyst in a similar slurry prepared from the simple oxide mixtures. A slurry of the mixed oxide prepared from the coprecipitated oxalates containing Fe_2O_3 (2080 ppm Fe) did not give satisfactory recombination activity.

The MoO_3 and $PdO \cdot H_2O$ catalysts were added as dry powders and mixed with uranium-bearing ThO_2 by tumbling for 1 hr. The Fe_2O_3 was added to the slurry as a sol prepared by oxidizing $Fe(CO)_5$ in H_2O_2 in water. All slurries were heated at 280°C for 3 hr in an O_2 atmosphere (300 psi at 25°C) before the reaction rates were measured.

(a) MoO_3 Catalysis. – A slurry of thorium-uranium oxide, prepared from the coprecipitated oxalates, containing 1000 g of Th per kg of D_2O and 0.032 *m* MoO_3 (activated by preheating for 2 hr at 270°C in a D_2 atmosphere) gave a recombination rate estimated to be 10 moles of D_2 per hour per liter at 280°C and 100 psi D_2 partial pressure. The rate was calculated by extrapolating data obtained at 240–250°C.

Reaction rates in a slurry of the "autoclaved-reburned" thorium-uranium oxide at 250 g of Th per kg of H_2O concentration and containing 0.03 *m* MoO_3 were less than 1 mole of H_2 per hour per liter at 250°C and P_{H_2} = 100 psi both for the slurry as prepared and after heating with an H_2 atmosphere. Reaction rates in the slurry without added catalyst were much lower. Treatment of the slurry (without MoO_3) with H_2 gave a high but temporary catalytic

Table 20.5. Reaction Rate of H_2:½ O_2 and D_2:½ O_2 Mixtures in Thorium-Uranium Oxide Slurries (U/Th = 0.05)

Oxide Preparation	Slurry Concentration (g of Th per kg of H_2O, D_2O)	Catalyst Concentration	Reaction Temperature (°C)	Reaction Rate, P_{H_2} = 100 psi (moles of H_2 per hour per liter of slurry)	
				Slurry as Prepared	H_2-Treated Slurry
Coprecipitated oxalates, fired 1000°C, 24 hr	1000	0.032 *m* MoO_3	280		10.1*
	250	1000 ppm Pd (based on thorium) added as $PdO \cdot H_2O$	194	11.5	
			241	5.9**	
			240	3.5***	
			181	9.7	
		2080 ppm Fe added as Fe_2O_3 sol	280	<0.1	0.60
Simple mixture, wet-autoclaved at 300°C, 24 hr; fired 1000°C, 24 hr	250		280	0.01	0.27
		0.03 *m* MoO_3	280	<0.1	0.53

*D_2-D_2O system; value extrapolated from results at 240-250°C.

**Rate after heating slurry at 280°C for 60 hr in O_2 (300 psi, 25°C).

***Rate after heating slurry again at 280°C for 60 hr in O_2 (300 psi, 25°C).

activity which was lost when the reaction temperature reached 280°C. This phenomenon may have resulted from the production of reduced uranium species which became oxidized in the presence of the stoichiometric hydrogen and oxygen mixtures used in the recombination experiments.

The results indicate that MoO_3 may not be a suitable catalyst with this mixed oxide or, very likely, with any mixed oxide prepared with uranium in the U^{6+} valence state. There appear to be important differences in the properties of the thorium-uranium oxides prepared from simple mixtures and those obtained from the coprecipitated oxalates. Apparently the uranium in the simple mixed-oxide system is free to react with the MoO_3 to form catalytically inactive species.

(b) PdO Catalysis. – The reaction rate for H_2-O_2 mixtures in a slurry of thorium-uranium oxide (250 g of Th per kg of H_2O, U/Th = 0.05) prepared from the coprecipitated oxalates and containing 1000 ppm Pd (based on thorium), added as $PdO{\cdot}H_2O$, was 11.5 moles of H_2 per hour per liter at 194°C and 100 psi H_2 partial pressure. Heating this slurry at 280°C for 60 hr in an O_2 atmosphere caused a temporary decrease in reaction rate, but the catalyst recovered activity in subsequent experiments. The time for recovery of catalytic activity decreased with increasing reaction temperature. The results reported in Table 20.5 appear to imply that maximum catalytic activity occurs in the region of 190°C; however, there is not sufficient information available to justify this conclusion, and further studies of the variation of catalytic activity with temperature are in progress. Owing to extremely rapid reaction of the stoichiometric gas mixture at high pressure in the presence of palladium, the data used to calculate the reaction rates above 180°C were obtained with total reactant gas pressure of less than 200 psi in excess of steam. Improvements in the apparatus are being made so that the precision of the pressure and temperature measurements can be increased.

(c) Fe_2O_3 Catalysis. – The reaction rate in slurries prepared with thorium-uranium oxide (U/Th = 0.05) obtained from the coprecipitated oxalates and with Fe_2O_3 as a catalyst (2080 ppm Fe, based on total oxide) was 0.6 mole of H_2 reacted per hour per liter of slurry at 280°C and a partial pressure of 100 psi H_2, after the slurry was heated with H_2 (500 psi at 25°C) for 2 hr at 270°C. Stoichiometric H_2-O_2 reaction rates in the slurry as prepared were very low.

20.3 THORIUM OXIDE PREPARATION DEVELOPMENT

20.3.1 Thorium Oxalate Precipitation

Some properties of ThO_2 slurries appear to depend partly on the preparative conditions of the thorium oxalate precursor.[1] In order to determine the factors influencing this dependence, an investigation was made of the changes occurring in the thorium oxalate and its oxide product as a function of the oxalate digestion time and temperature. Properties investigated were particle size, chemical nature of the surface, x-ray crystallite size, surface area, and caking tendencies of the oxide slurries.

Digestion seemed to reduce the number of large particles in the fired oxide even though the average particle size remained the same. Electron micrographs of the oxalate crystals showed no significant changes in particle characteristics as digestion proceeded. There was no change in the crystallite size of the oxalate or the oxide prepared from it as a result of digestion of the oxalate up to 48 hr at 75°C. Crystallite sizes of the oxalate hexahydrate and dihydrate and the 800°C-fired oxide were 750, 300, and 150 Å, respectively. Caking of the oxide product, as indicated by the cake resuspension index,[1] was eliminated by digestion (6 hr, 75°C; >24 hr, 28°C) of the oxalate precipitate. The surface areas of the oxides prepared from digested oxalates were in general about twice as large as those of oxides prepared from the undigested materials. There was no consistent effect of digestion time on water content of the oxalate, determined thermogravimetrically, or nitrate and water content, determined by infrared adsorption.

20.3.2 Preparation of Cubic Particles

The addition of certain bi- and polydentate organic compounds, principally amines, to the oxalate precipitate system caused the freshly precipitated thorium oxalate to grow on digestion into square-faced, more or less cubic, particles (Fig. 20.2, Table 20.6) whose characteristics are essentially retained in the oxide product. Important variables were thorium concentration, ratio of oxalic acid to thorium, ratio of complexing agent to thorium, nitric acid concentration, and strength of

[1] C. S. Morgan, *Status Report on ThO_2 Caking Studies*, ORNL CF-57-9-102 (Sept. 26, 1957).

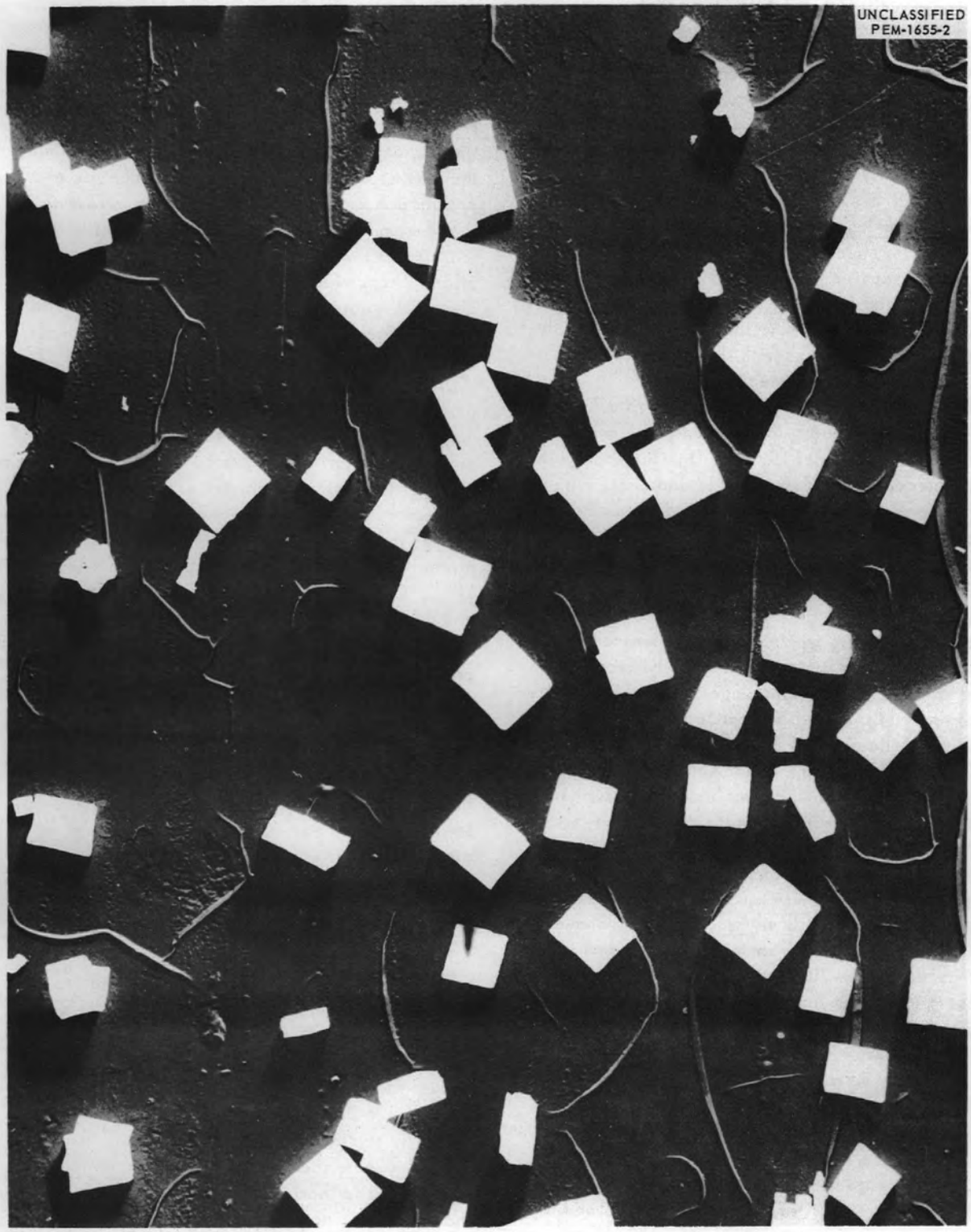

Fig. 20.2. Cubic Thorium Oxide Particles: 1.8 μ Average Size.

Table 20.6. Preparation of Cubic Thorium Oxalate Particles

Conditions: Room temperature
Vigorous agitation
24-hr digestion

Complexing Agent	Molar Concentrations*			Thickness-to-Edge Ratio
	Thorium Nitrate	Complexing Agent	Oxalic Acid	
Urea	0.05	0.05	0.5	0.5–0.7
Urea	0.05	0.05	0.1	Platelets
EDA	0.05	0.025	0.5	~1
TEA	0.05	0.0026	0.5	~1.0

*In precipitating media assuming no reaction.

the complexing agent. Particles with an average diameter of from <1 to >20 μ were made.

The ratio of thickness to a side of the square face varied from about 0.2 to 1.0, being larger at lower thorium concentrations, higher ratios of oxalate to thorium, higher ratios of complexing agent to thorium, and greater strength of the complexing agent. The effect of nitric acid depended on the nature of the complexing agent. A final concentration of 1.0 to 2.0 M HNO_3 was necessary to produce any effect with urea, ethylenediamine, and propylenediamine, while triethanolamine affected the precipitation to about the same extent whether nitric acid was added or not and citric acid showed less effect with added nitric acid and an enhanced effect with added ammonia.

The velocity of the recrystallization in general was increased by the conditions which increased the thickness-to-edge ratio. The velocity of recrystallization, however, also depended on the time of complete mixing. Propylenediamine-containing solutions crystallized much more slowly than the effectiveness of the reagent for producing cubes would indicate.

The complexing agents can be arranged in order of effectiveness approximately as follows: urea $\leqq$ guanidine < pentaerythritol < citric acid < ethylenediamine $\leqq$ propylenediamine < triethanolamine < versene. This order corresponds more or less with the strength of the ligand-cation bonds measured with cations other than thorium.

The thoria prepared from the oxalates that had been precipitated from solutions containing complexing agents showed the following characteristics:

1. Yield stress was not greatly affected, if at all, by the change in shape.
2. Erosiveness of the larger sized particles was less than for the standard oxide.
3. Stable particles seem to be prepared at lower firing temperatures than is the case with normal production oxide.
4. Aggregates were not so readily formed during firing as in the case of the normal production oxide.

20.3.3 Flame Denitration Studies

Mixed thorium-uranium oxides were prepared by direct denitration of methanol solutions of thorium nitrate and uranyl nitrate in reflected flames. The initial product particle size (see Figs. 20.3 and 20.4) and the surface area and chemical composition (see Table 20.7) were within the range considered of interest for mixed slurries. Figure 20.4 also shows a ThO_2 flame-calcined product, prepared by use of a ZrO_2 reflector, for comparison. A mixed thorium-aluminum oxide was prepared by a similar procedure.

Flashbacks and damage to the fuel-gas system limited flame denitration to short periods with the burner previously used for ThO_2 slurry calcinations. All of several arrangements using premixing of the methanol nitrate salt solution with oxygen-acetylene fuel gas were undependable. A crude test involving separate injection of the alcohol-nitrate and the fuel gases was successful; therefore a torch was built incorporating this feature. Reflector temperatures above 1600°C were easily obtained with this improved design. These temperature levels

Table 20.7. Flame Denitration Tests

Feed Solutions: Hydrated nitrate salts dissolved in CH_3OH, 15 to 25 ml solution per minute

O_2 as from cylinders (~100%)

Run No.	Conditions		Estimated Wall Temperature (°C)	Feed Solution		Product						
	Fuel Gas	Reflector		Thorium Nitrate (g/liter)	Uranyl Nitrate (g/liter)	Quantity (g)	d_{50} (microns)	Surface Area (m^2/g)	Yield Stress (lb/ft^2)	Th (%)	U (%)	NO_3^- (ppm)
28	C_2H_2	ZrO_2	>1773	79	6	37	2.0	4.6		80.2	7.5	<10
29	C_2H_2	ZrO_2	>1773	79*	*	54	3.4	2.2		85.9*		<10
35	C_2H_2	Graphite	1400	79	6	127	1.1	5.8				
36	C_2H_2	Graphite	1300	79	6	255						
37	C_2H_2	MgO	1450	79	6	53		4.8				
38	C_2H_2	MgO	1600	158	6	270	1.2	4.9		82.6	4.4**	
39	C_2H_2	MgO	1550	158	12	350	2.0	5.9	0.275			
40	C_2H_2	MgO	1550	158	12	406	13.5***	7.8				
41	C_3H_8	MgO	1550	158	12	27.5						
42	C_3H_8	MgO	1500	158	12	190						
Pilot-plant product			1600				1.6	2.2	0.20			~0

*27 g/liter of $Al(NO_3)_3$ to give 1.18% Al in product.

**U(IV) < 1000 ppm.

***Modified torch to give low-velocity solution feed.

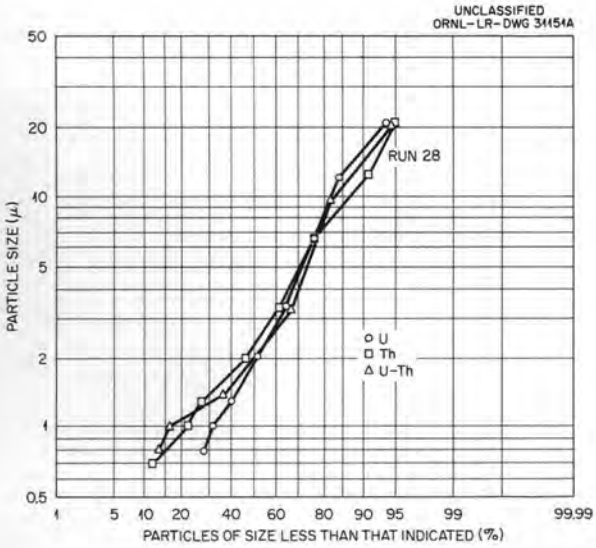

Fig. 20.3. Flame-Calcination Experiments – Particle-Size Distribution for a Firing of Mixed Nitrates (TNT-UNH).

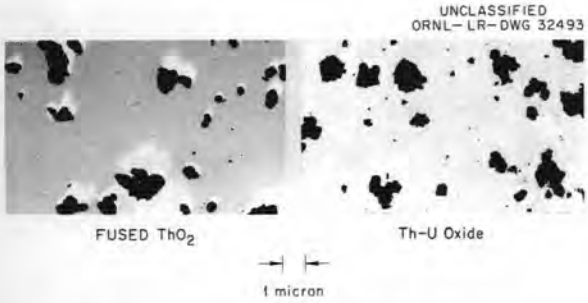

Fig. 20.4. Flame-Calcined Products.

are believed adequate for complete flame denitration. An improved size distribution of 1.5 μ mean diameter and 85 wt % below 5 μ was obtained in three subsequent firings with the new torch (Table 20.7). For reference, previous firings produced an average particle size of 2 μ, with 80% of the particles being less than 10 μ. The three firings provided approximately 1 lb of product, from which a classified (<5-μ) sample was submitted for toroid testing. Surface area of the later material, however, is 5.8 m^2/g vs 4.6 m^2/g for the first product.

The initial flame denitrations were with oxyacetylene flames and ZrO_2 reflectors at about 2000°C. Product has been prepared at 1600, 1400, and 1000°C to investigate the use of simpler equipment and procedures at lower temperatures. For temperatures above 2000°C the C_2H_2-O_2 flame and the ZrO_2 reflectors are probably necessary. Reflectors of MgO have been used for up to 1600°C. A propane-oxygen flame easily gives 1600°C with the methanol solution feed and may be usable up to 2000°C. Propane-air-methanol gives only 1000°C with the present system, although industrial furnaces fired with propane-air are used up to 1600°C.

20.3.4 Fluidized-Bed Denitration Studies

Installation and preliminary testing of a system to study fluidized-bed denitration of $Th(NO_3)_4$ or mixed thorium-uranium nitrates were completed. This program is intended to produce 50- to 500-μ thorium or thorium-uranium oxides for fluidized-bed reactor fuels or blankets. Operation with a ThO_2 bed and a pure water feed was smooth and trouble-free. Continuous operation with aqueous $Th(NO_3)_4$ solution feed has not been achieved because of caking and feed-nozzle problems. Operating changes and equipment alterations aimed at achieving continuous operation without bed caking are being tested.

20.4 THORIUM-URANIUM OXIDE

Two methods of adding uranium to the thorium oxide in the production of engineering quantities of mixed oxide for fuel slurry studies are under consideration.[2] One involves the coprecipitation of the thorium-uranous oxalates and their subsequent decomposition. Uranous oxalate complexed with ammonium oxalate is added to the oxalic acid solution used in the precipitation step. The method appears limited to the production of mixed oxides containing U/Th ratios <0.05; it has been used to produce in the pilot plant about 300 lb of simulated blanket oxide containing U/Th = 0.005 and fired at 1225°C. The second method involves precipitation of the uranium onto a 650°C-fired thorium oxide from ammonium uranyl carbonate solution and subsequent firing to incorporate the uranium in the solid. The final mixed oxide has the particulate properties of the thorium oxide used (Table 20.8); hence the particle size and shape can be controlled in the thorium oxide preparation step. The method can be used to produce mixed oxides containing U/Th >0.05, and about 40 lb of an 8%-uranium-containing oxide fired at 1050°C has been prepared for engineering study. The rate of diffusion

[2] J. P. McBride *et al.*, *HRP Prog. Rep. for Quarters Ending April 30 and July 31, 1958*, ORNL-2561, p 281.

Table 20.8. Effect of Firing Temperature on Thorium-Uranium Oxide Properties: Adsorption Preparation Method

U/Th = 0.1

Oxide Designation	Average Size (μ)	Oversize Particles, > 10 μ (%)	U Solubilized in 8 N HNO_3 (%)	Surface Area (m^2/g)
DT-4-650°C	1.06	0.90 ± 0.04		
-800°C	0.93	1.04 ± 0.6	43	15.6
-900°C	1.01	1.51 ± 0.3	13	6.1
-1000°C	1.10	1.06 ± 0.2	4.7	4.0
-1100°C	1.13	3.6 ± 2.3	2.1	1.0
-1200°C	1.13		1.6	0.8

of the uranium is not known, but preliminary results indicate a 4-hr firing at 1000°C incorporates the bulk of the uranium in the solid. The upper firing-temperature limit is determined by the effect of uranium in lowering the sintering temperature. Selection of the final firing temperature for the mixed oxides will be based on results of slurry engineering tests.

20.4.1 Coprecipitation

Control of particle size has been achieved in the production of thorium-uranium oxide prepared from coprecipitated thorium-uranous oxalates containing 0.5 g of U per 100 g of Th. The two most important variables upon which control of the particle size depends were found to be the temperature and concentration of the reagents during coprecipitation (Table 20.9). Data from three pilot-plant-scale preparations have confirmed the laboratory experience (Fig. 20.5).

Two series of laboratory preparations were made at various temperatures in the range 30–50°C, one at 0.5 M and the second at 0.7 M. The method of preparation, described previously,[3] consisted in adding to a stirred, thermostated thorium nitrate solution a uranium-spiked solution of oxalic acid of equal molarity.

The laboratory draft-tube equipment of 4-liter capacity was used to simulate pilot-plant conditions. In all cases 50% recirculation was used. The addition time varied from 45 to 65 min. A 60-min digestion time was allowed, during which the temperature was allowed to drift downward, in general less than 10°C. The particle-size data reported here were obtained for the 800°C-fired oxide by the activation-sedimentation method.

The reagents used in each series are summarized below:

	Series I	Series II
Thorium reagent		
Thorium nitrate	0.5 M; 1050 ml	0.7 M; 1050 ml
Hydrazine	85%; 2.70 ml	42%; 7.7 ml
Nitric acid (conc.)	16.4 ml	23 ml
Oxalate reagent		
Oxalic acid	0.5 M; 2285 ml	0.7 M; 2285 ml
Uranous ammonium oxalate solution	34.8 g of U^{4+} per liter; 8.0 ml	34.8 g of U^{4+} per liter; 24.6 ml

Figure 20.5 and Table 20.9 show that the particle size of the oxides fired at 800°C increased linearly with oxalate precipitation temperature. The slope of these plots was found to increase markedly with a decrease in reagent concentration. Fixing the concentration of both reagents at 0.7 M gave a particle-size range of 1.1 to 2.0 μ in the temperature range 30–50°C. For the same temperature

[3] D. E. Ferguson *et al.*, *HRP Quar. Prog. Rep. Jan. 31, 1956*, ORNL-2057, p 112.

Table 20.9. Coprecipitation of Uranium and Thorium Oxolates: Effect of Temperature and Reagent Concentration on Oxide Particle Size

Preparation No.	Reagent Concentration (Same for Oxalic Acid and Thorium Nitrate) (M)	Precipitation Temperature (°C)	Oxide Particle Size, d_g (μ)	Geometric Mean Deviation (σ)
28	0.5	30	1.6	1.3
31	0.5	37	2.3	1.2
27	0.5	50	4.2	1.3
22	0.7	30	1.1	1.4
23	0.7	40	1.7	1.2
24	0.7	50	2.0	1.3
DT-10*	0.7	8–15	0.57	1.3
DT-18*	0.7	41–43	1.72	1.35
DT-22*	0.7	(40)–45	1.68	1.38

*Pilot-plant preparations.

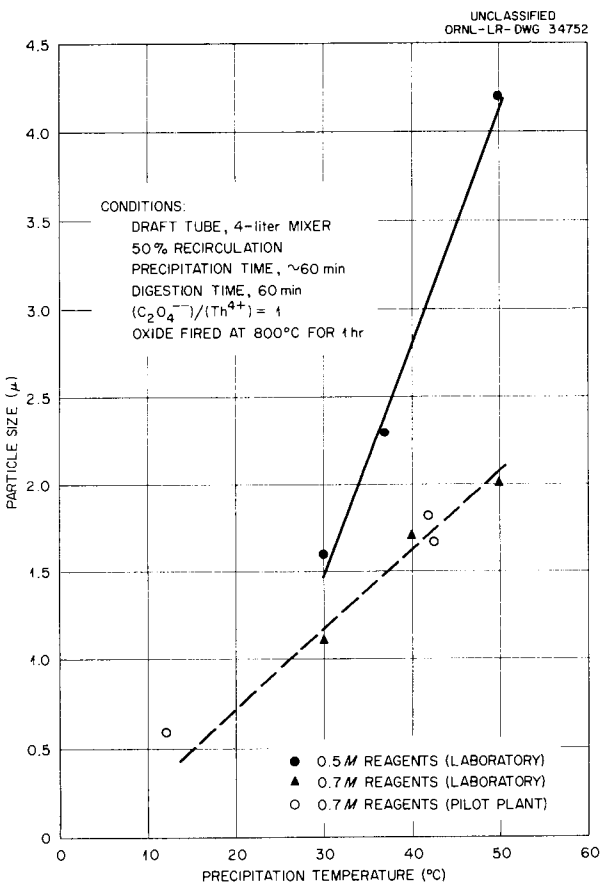

Fig. 20.5. Oxide Particle Size as a Function of Coprecipitation Temperature for 0.5% U in Thorium Oxalate.

range with 0.5 M solutions the particle-size range was 1.6 to 4.2 μ.

These data can be summarized in the following equations:

$$D_{g(0.5)} = 0.132t - 2.475 \text{ (applicability 30–50°C)} ,$$

$$D_{g(0.7)} = 0.0468t - 0.265 \text{ (applicability 10–50°C)} ,$$

where $D_{g(0.5)}$ = the mean particle size with 0.5 M reagents and t = coprecipitation temperature in degrees Centigrade.

20.4.2 Adsorption

Thorium-uranium oxides containing U/Th ratios from 0.04 to 0.33 were prepared for laboratory evaluation and toroid tests (kilogram quantities). In a typical preparation 650°C-fired thorium oxide was slurried in ammonium uranyl carbonate solution (solubility ~0.15 m), and the solution was boiled until all the uranium had deposited on the thoria. The solids were filtered and washed and were then refired at various temperatures.

Particle-size data on one of the products containing a U/Th ratio of 0.1 (Table 20.8) showed essentially no change in the particulate properties of the thorium-uranium oxide up to 1000°C firing temperature when compared with the pure oxide from which the mixed oxide was prepared. The same mixed-oxide products were refluxed for 1 hr

with 8 N HNO_3. The fraction of uranium solubilized decreased with firing temperature from 43% for the 800°C firing to 1.61% for the 1200°C firing (Table 20.10). In addition, the 1000°C-fired sample was autoclaved at 300°C for 24 hr as an aqueous slurry with an O_2 overpressure. The recovered supernatant contained only 0.2% of the total uranium, and refluxing the solids for 1 hr with 8 N HNO_3 removed only an additional 0.07%. Hence it would appear that a firing temperature of 1000°C is sufficient to incorporate the bulk of the uranium in the mixed-oxide solid.

A study was also carried out with the 1000°C-fired material to determine the uniformity of distribution of the uranium in the solid. The solids were subjected to successive refluxing with 8 N HNO_3, 4 N HNO_3 containing 5% H_2O_2, and 4 N HNO_3 containing 10% H_2O_2. The per cents thorium dissolved in the successive leaches were 0, 25, and 40, respectively; the U/Th ratios in the acid leaches and final solids were 0.1, 0.13, 0.12, and 0.09, respectively, indicating a fairly homogeneous distribution of uranium.

The properties of the 650°C-fired mixed oxides and their aqueous slurries prepared in kilogram quantities for toroid tests are shown in Table 20.10. The most striking difference in the properties of the mixed oxide when compared with the pure oxide is a marked lowering of the yield stress for the mixed oxide containing a U/Th ratio of 0.05.

20.5 THORIUM OXIDE PRODUCTION

Eighteen 30°C thorium oxalate precipitations (DT-18 through -36) were made to prepare 2895 lb of thorium oxide. Approximately 1130 lb of ThO_2 was calcined at 1600°C and classified to 95% less than 5 μ. The equivalent of 1765 lb of ThO_2 as the 30°C-precipitated thorium oxalate was digested at 85°C for 48 hr and calcined at 800°C. The 800°C-calcined oxide had an average particle size of 2–3 μ and required no classification. The important factor in controlling particle size was the addition rate of the oxalic acid to the thorium solution in the precipitator: addition rates of 3.5 to 4.0 gpm produced thorium oxide with an average particle size of about 2.5 μ. The total quantity of thorium oxide product delivered for slurry engineering study was 1607 lb.

Table 20.10. Effect of U/Th Ratio on the Physical Properties of Thorium-Uranium Oxide (650°C): Adsorption Preparation Method

U/Th Ratio	Average Particle Size (μ)	X-ray Crystallite Size (Å)	Surface Area (m^2/g)	Yield Stress, $P = 2$ (lb/ft^2)	Modulus of Rigidity, $P = 2$ (centipoises)
0*	1.35	106	26.5	0.47	3.54
0.05	1.3	113	23.4	0.16	2.89
0.09	1.4	107	23.8	0.18	2.84
0.12	1.3	113	18.3	0.36	2.40
0.33	1.7	104	17.0	0.64	3.93

*ThO_2 used in preparation of the mixed oxides.

21. IN-PILE SLURRY LOOP

W. E. Unger

T. A. Arehart
J. W. Brown, Jr.
P. A. Haas
L. J. King
B. B. Klima
W. F. Schaffer, Jr.
L. B. Shappert
J. W. Snider
W. M. Woods

21.1 WESTINGHOUSE STATUS

In October a run was started in the Westinghouse mockup loop on high-fired thorium oxide slurry in order to determine the suitability of the slurry for use in the present loop system. It was intended that the run would continue for 1000 hr and that it would be followed by a 500-hr demonstration run on slurry with the in-pile loop package connected to the loop auxiliaries at Westinghouse. However, equipment failure forced early termination of the test.

Shortly after the run started, power pips were observed on the wattmeter monitoring the power to the pump; the pips continued for about 24 hr and then disappeared. The loop, after approximately three days of operation, was shut down owing to the rupture of a bellows on one of the two air-operated sample valves (Little Richard, Aminco).

The Westinghouse model A-13 C1 pump, which is designed for in-pile service, was used in the run. Bearing failure in the model A-30 pump had been responsible for two previous loop shutdowns. Examination of the bearings in the model A-13 C1 pump showed severe wear of the thrust-bearing face, approximately $\frac{1}{4}$ in., precluding the use of Graphitar bearings for slurry operation. An unbalanced condition of the impeller, caused by plugging of the balancing ports, may have been responsible for the bearing failure.

On ORNL recommendation the pump is to be fitted with aluminum oxide bearings and journals, which have operated successfully in a slurry environment. The pump will be modified by ORNL personnel, who are familiar with the modification and have the equipment and the bearing and journal blanks required. Westinghouse will equip the impeller with balancing vanes instead of balancing holes. The revisions are expected to require at least six weeks.

After a short run with slurry, equipment chambers B and C and the panel board will be tested, and these auxiliaries will be shipped to Oak Ridge so that the ORNL installation can continue with only minor delay. The final demonstration of the loop package will be made with the auxiliaries at the mockup loop at Westinghouse. A tentative schedule indicates that the loop may be ready for this slurry demonstration run by January 1, 1959.

21.2 ORNL STATUS

The construction of the ORNL facilities at the ORR are nearing completion and await the receipt of equipment from Westinghouse. The installation of the slurry-removal and cleanup system will begin about November 1, upon completion of the basement modifications being handled on outside contract, and is scheduled for completion in April. The schedule allows for a demonstration of the package unit prior to installation in chamber D. The system employs auxiliary pumps and a hydroclone in connection with the main loop circulating pump to remove slurry from the system. Failure of the loop pump in the current loop design will preclude effective loop cleanup, and subsequent cleaning will be required in the segmenting facility. A tank will be provided, with a carrier, to retain the slurry from each in-pile run. The tanks, designed to be removable from the carrier, will be kept in a storage canal until the slurry is required for evaluation tests.

Auxiliaries, including the instrument panel, can be installed at ORNL by March 1. The in-pile loop checkout tests will start at that time. This schedule is now compatible with that of the segmenting facility, which should be available for operation in May.

Equipment chamber A is shown in Fig. 21.1 in the last phases of construction; all the lines have been installed in the chamber. The utilities and process-piping manifold west of equipment chamber C is shown in Fig. 21.2 in the last phase of its installation. The auxiliary area and booster pumps, together with the frame for the lead shield around the booster pumps, are shown essentially complete in Fig. 21.3. The carriers are shown in Fig. 21.4 mounted on trailers as they were received from Paducah.

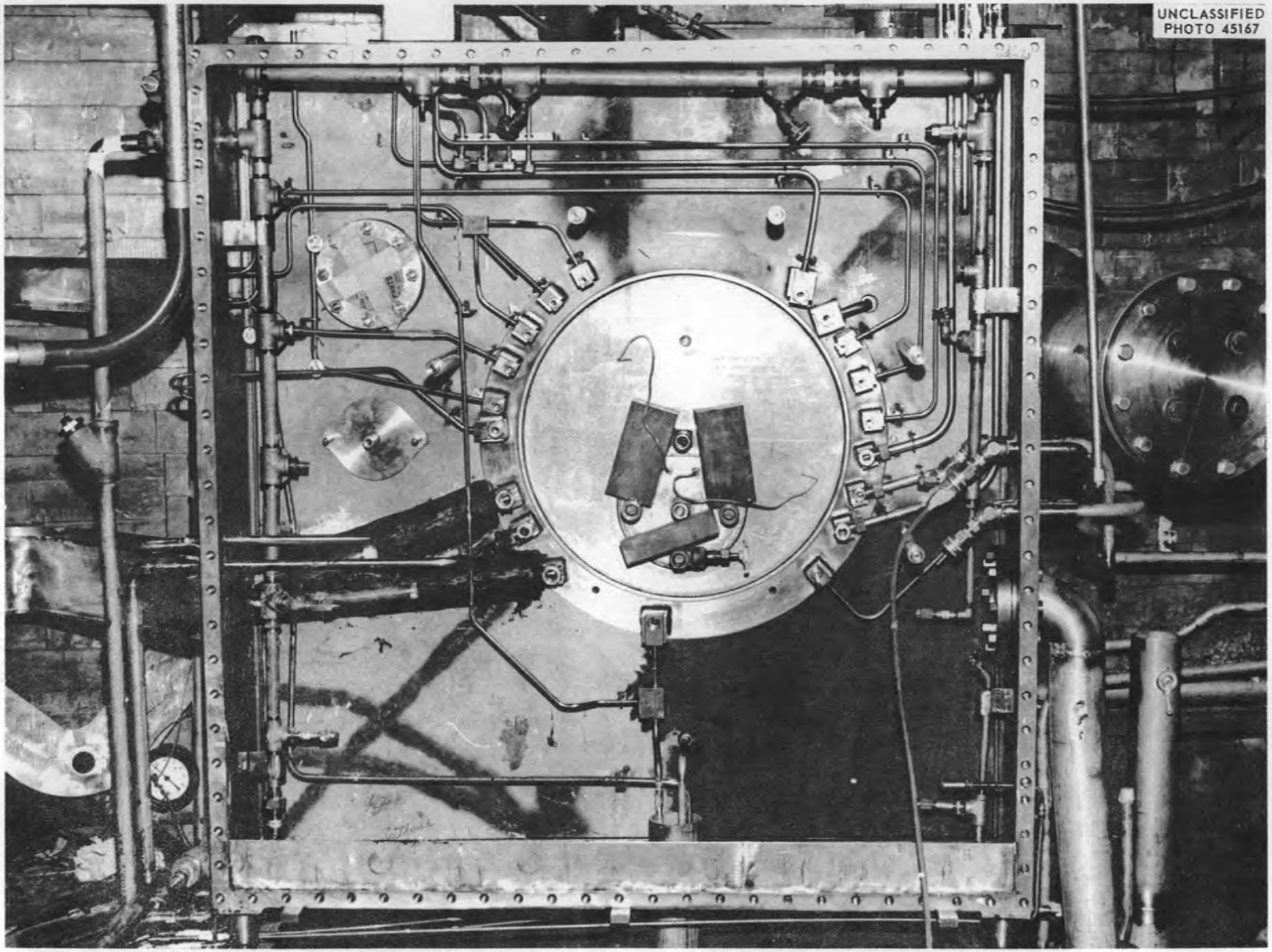

Fig. 21.1. PAR Loop Installation; Equipment Chamber A – Essentially Complete Showing Insulated High-Temperature Cooling-Water Lines (October 10, 1958).

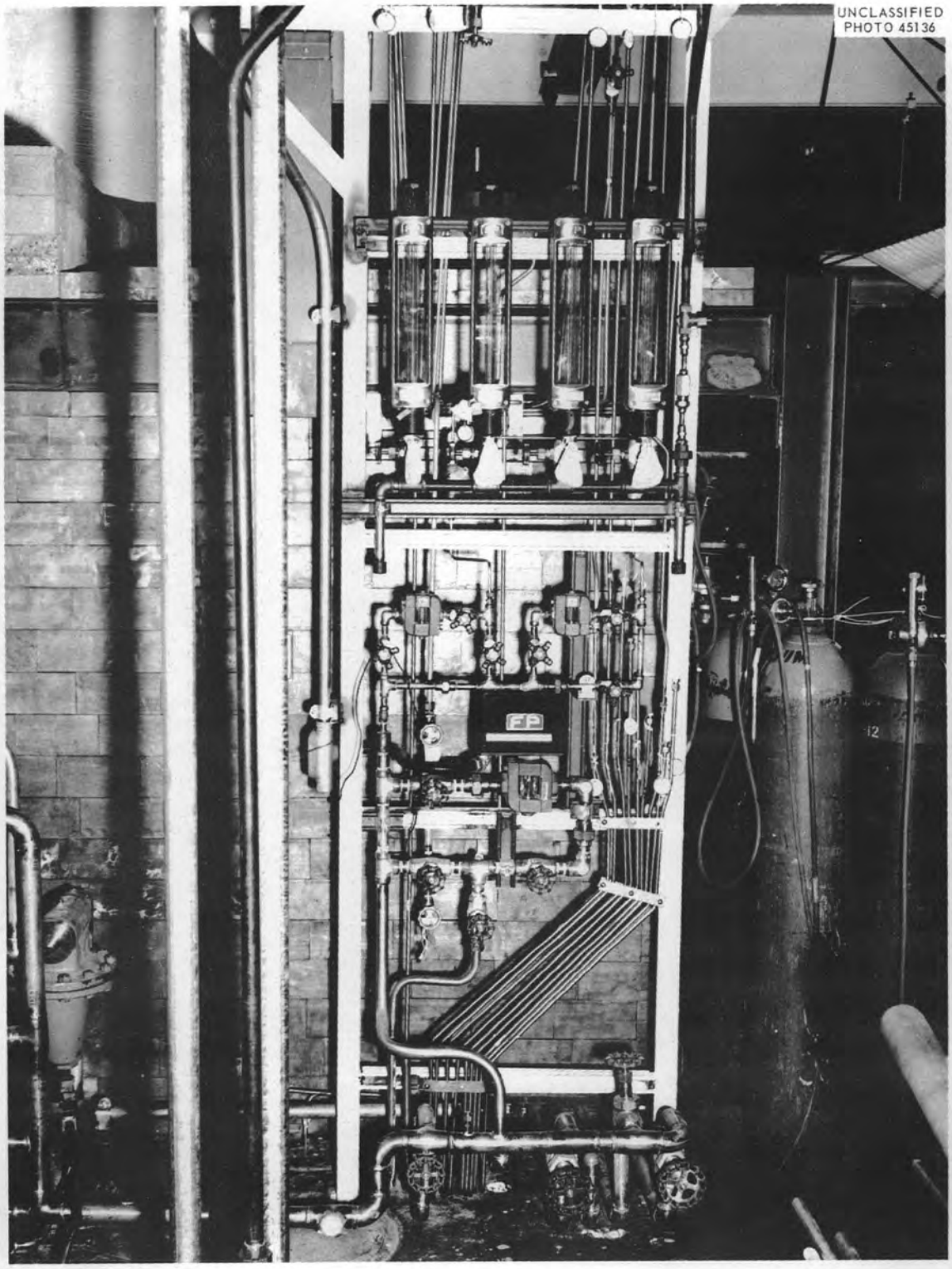

Fig. 21.2. PAR Loop Installation; Over-All View of Piping Manifold West of Chamber C (October 3, 1958).

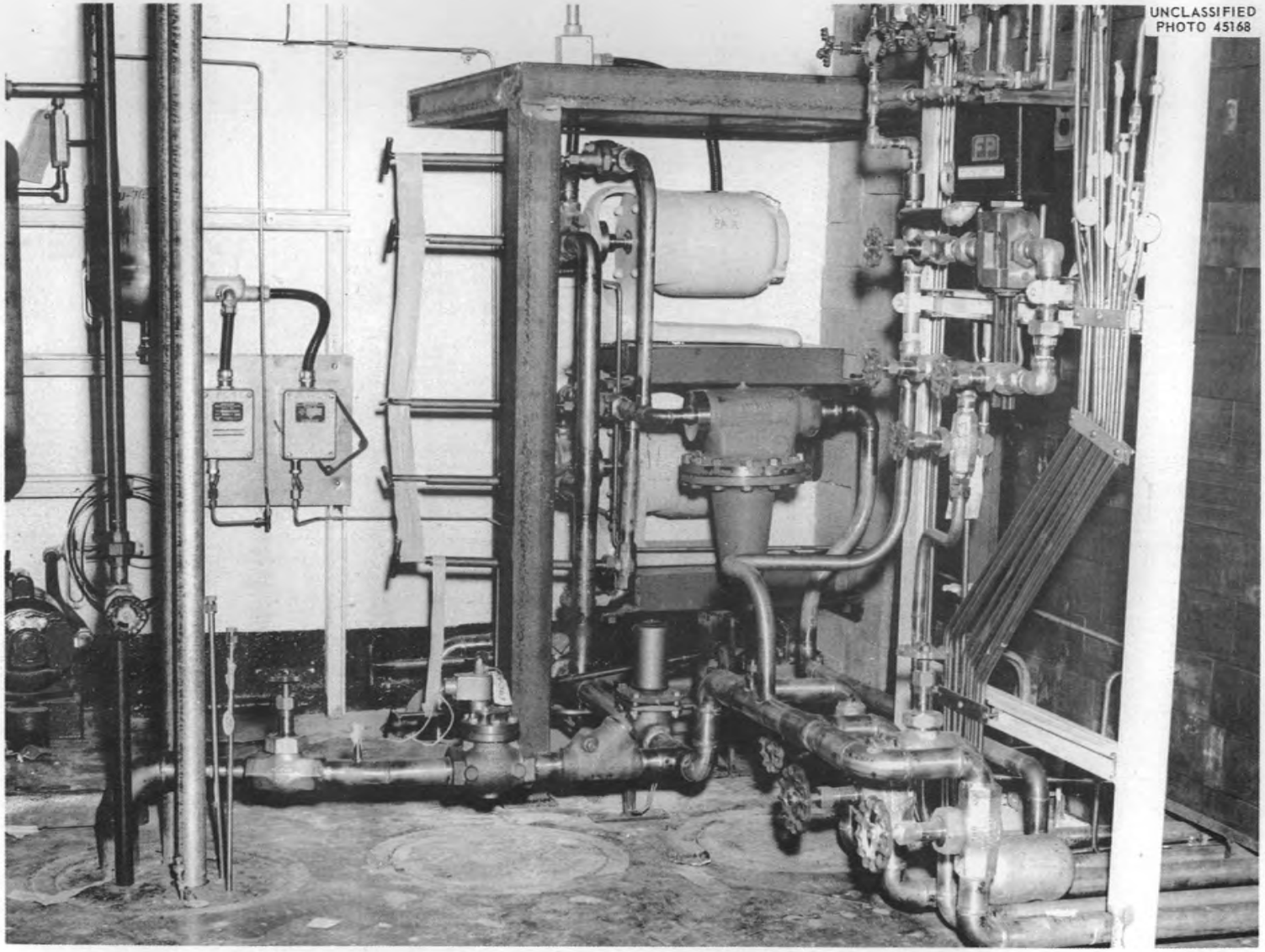

Fig. 21.3. PAR Loop Installation; Auxiliary Area Showing Lead Shield Frame Around Booster Pumps and Water Supply Line.

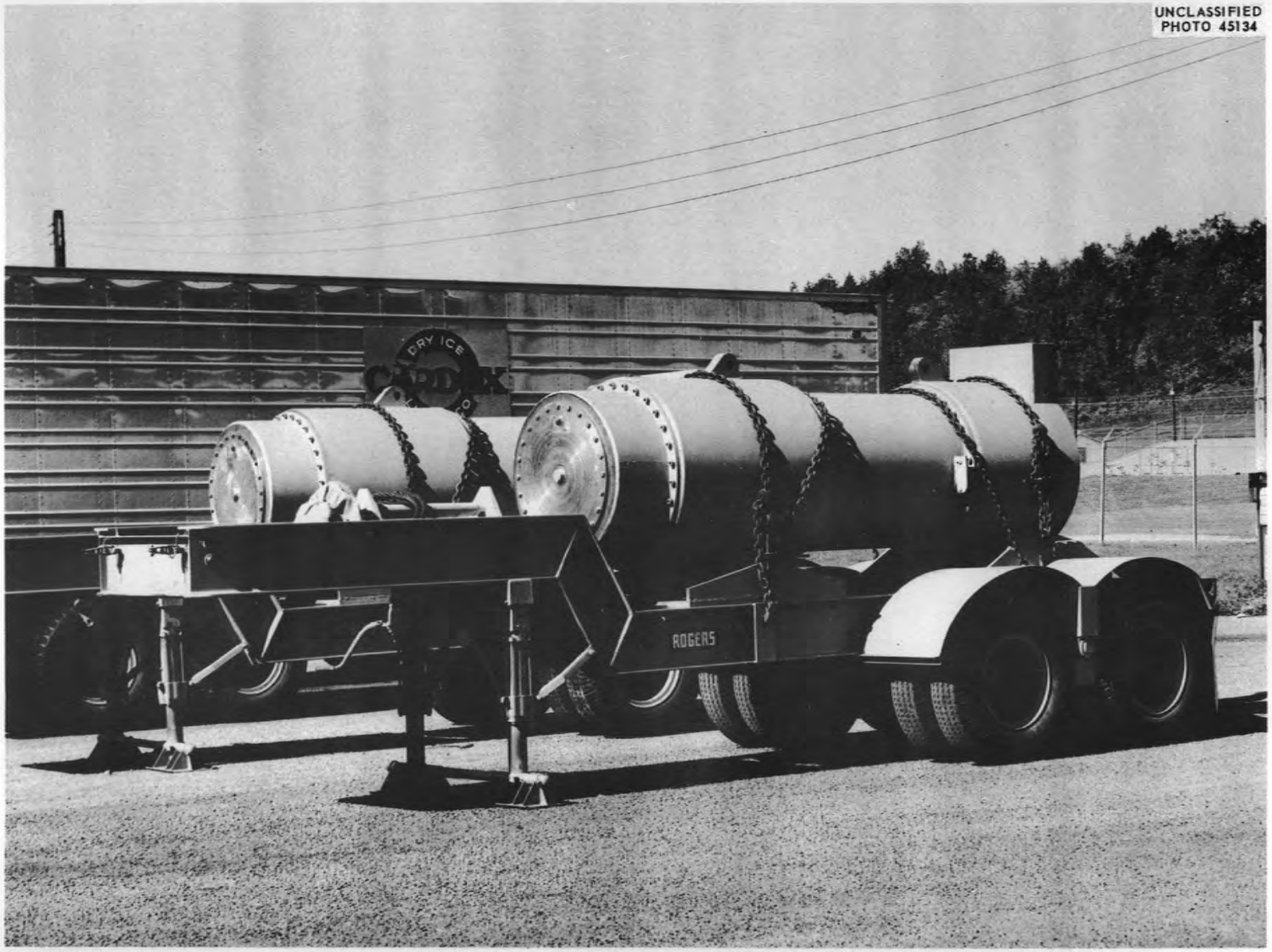

Fig. 21.4. PAR Loop Carriers; View Showing Carriers Mounted on Trailers (October 6, 1958).

21.3 EQUIPMENT DEVELOPMENT

21.3.1 Hydroclone Collection of ThO_2 Slurry

The collection of ThO_2 slurry by cylindrical hydroclones with induced-underflow receivers was compared with collection in conventional conical hydroclones (Fig. 21.5). Although the efficiency is slightly reduced (Fig. 21.6), the cylindrical design should eliminate plugging of the underflow pot during operation with slurries that

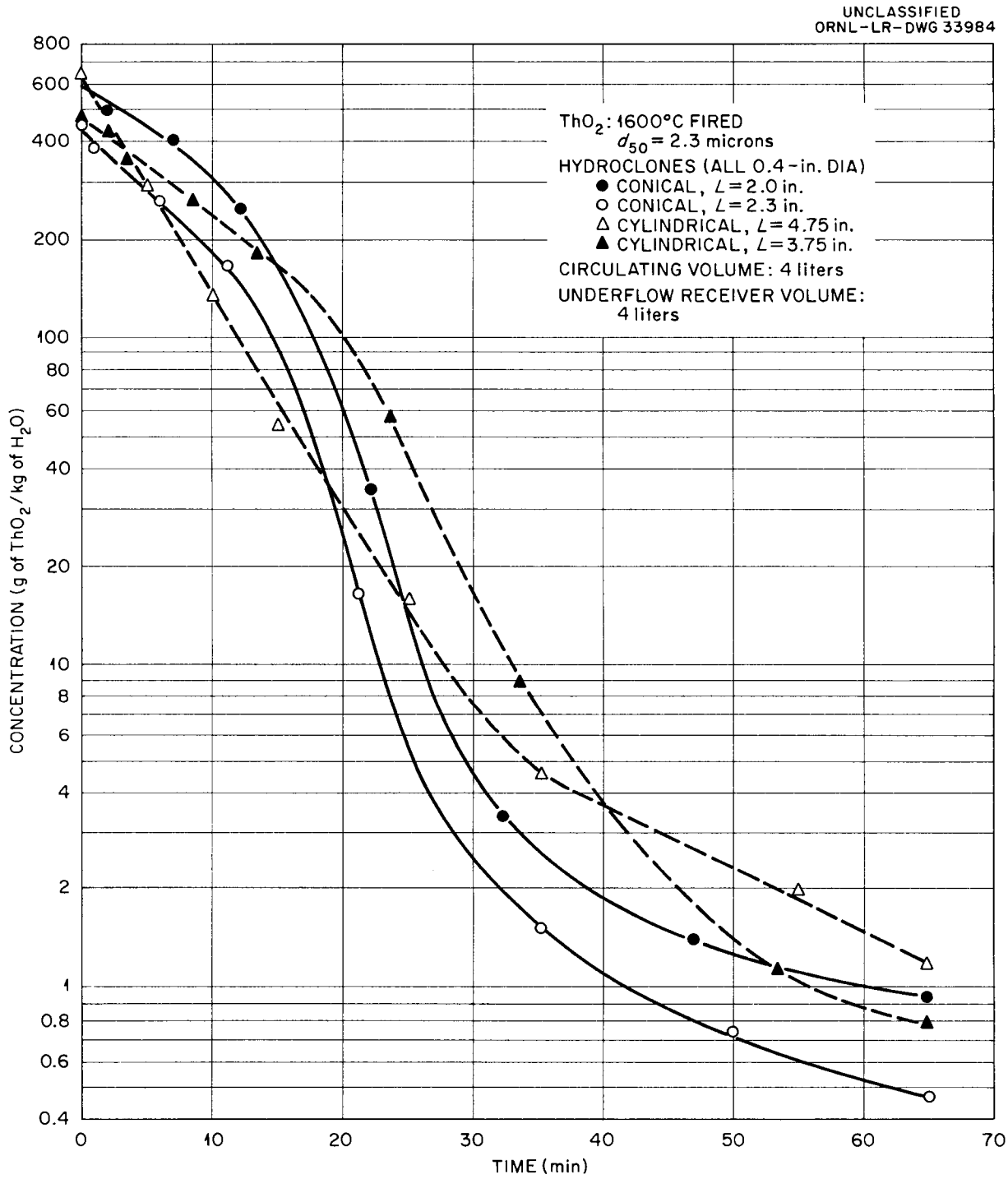

Fig. 21.5. Hydroclone Collection of ThO_2 into an Induced-Underflow Receiver.

tend to cake. The concentration-time curve (Fig. 21.5) applies only to the ratio of loop volume to hydroclone feed rate for which it was obtained. The apparent-efficiency–concentration curve (Fig. 21.7) is independent of this ratio and could be used with a graphical or numerical integration to obtain a concentration-time curve for some other system.

The apparent efficiency is less than the hydroclone efficiency calculated from correlations for dilute slurries.[1] For the high ThO_2 concentrations at the start of the tests, the apparent efficiency is limited by the concentration which the induced underflow stream can attain, that is, by the rate at which ThO_2 can be transferred into the underflow receiver. During operation with dilute slurry at the end of the tests, the apparent efficiency is limited by the recycle of ThO_2 from the induced-underflow receiver back into the hydroclone. Therefore a maximum in apparent efficiency occurs at an intermediate concentration.

21.3.2 Hydroclone Purge-Water Preparation

A two-stage cascade of a 0.4- and a 0.25-in.-dia hydroclone was tested for clarifying slurries of 240–400 g of ThO_2 per kg of H_2O. The concentration ratios (feed to last-stage overflow) were between 6 and 61 (Table 21.1). These values are larger than the ratios between 1.3 and 18, obtained under similar conditions except with a three-stage

[1] P. A. Haas, *Hydraulic Cyclones for Application to Homogeneous Reactor Chemical Processing*, ORNL-2301 (Nov. 29, 1957).

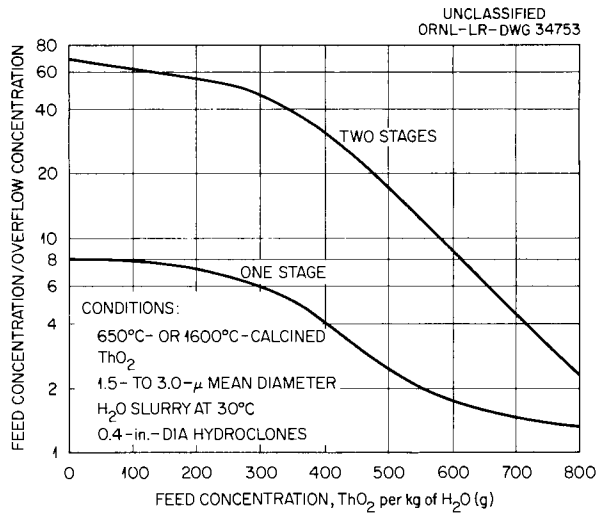

Fig. 21.7. Hydroclone Clarification of ThO_2 Slurries.

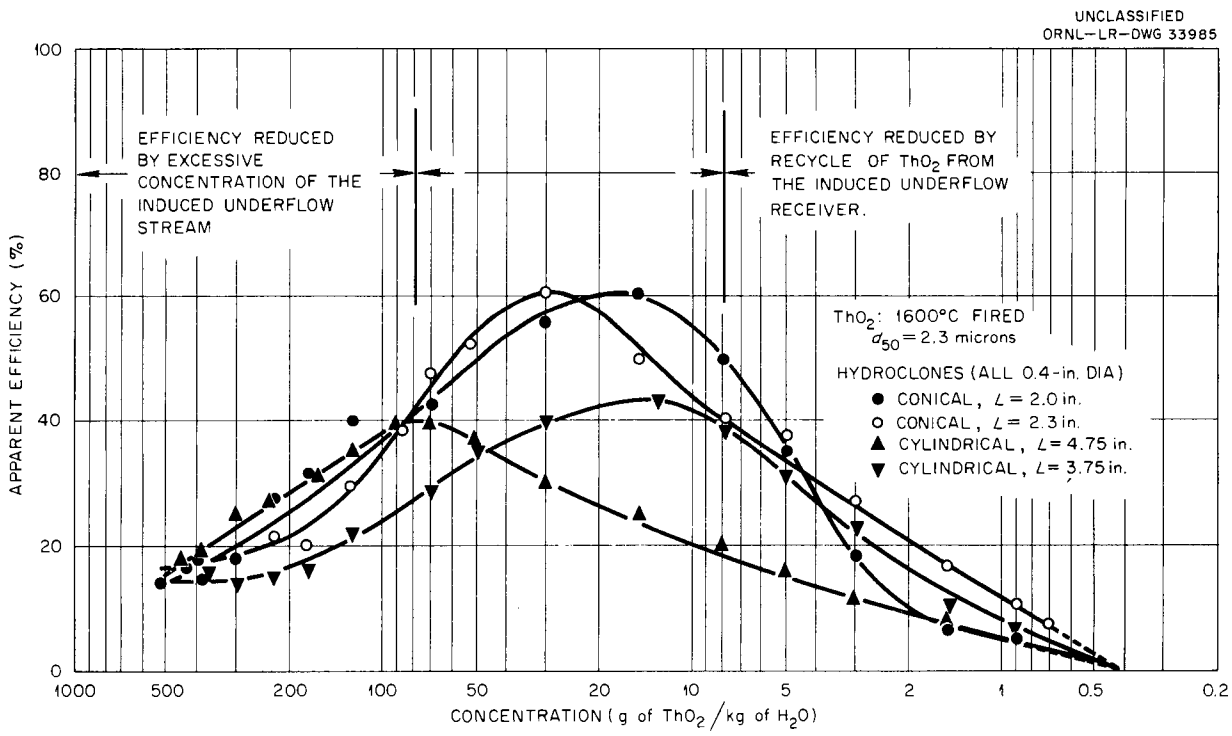

Fig. 21.6. Apparent Hydroclone Efficiencies for Batch Collection of ThO_2.

cascade of a 0.8-, a 0.4-, and a 0.25-in.-dia hydroclone. This indicates either that the 0.8-in.-dia hydroclone is not an effective initial stage or that dividing 65 to 75 ft of pressure drop between three hydroclones is less effective than dividing it between two hydroclones.

Results typical of the 0.4-in.-dia hydroclones were obtained in tests with slurries of 650°C- and 1600°C-calcined ThO_2 of 1.5 to 3.0 μ mean diameter (Fig. 21.7). The concentration ratios (feed to second-stage overflow) decreased from values of more than 60 for low concentrations to values of approximately 2 for 800 g of ThO_2 per kg of H_2O.

Table 21.1. Preparation of Purge Water Two-Hydroclone Cascade Test

ThO_2: 650°C-calcined (DT-7) with indicated 2.3-μ mean diameter
Conditions: 65–70 ft fluid pressure drop, room temperature

ThO_2/H_2O, Feed Sample (g/kg)	First (0.4-in.) Hydroclone			Second (0.25-in.) Hydroclone				$\frac{C_{feed}}{C_{product}}$
	ΔP (ft)	Bottoms-to-Feed Ratio, B/F	ThO_2/H_2O, Underflow (g/kg)	ΔP (ft)	Bottoms-to-Feed Ratio, B/F	ThO_2/H_2O, Underflow (g/kg)	ThO_2/H_2O, Overflow (g/kg)	
239	35	0.41	515	30	0.48	101	3.9	61
320	35	0.60	529	30	0.69	64	6.9	46
393	35	0.58	608	30	0.077	426	65.3	6
355	60	0.72	465	6	0.52	128	7.3	49
342	60	0.73	445	6	0.17	320	15.9	22
346	60	0.70	452	6	0.76	86	9.1	38
286*	40	0.47	506	9	0.38	226	14.8	19*
341	20	0.33	731	50	0.54	271	13.8	25
362	20	0.34	758	50	0.79	197	13.9	26

*Total pressure drop was 40 + 9 = 49 ft.

Part VI

SUPPORTING CHEMICAL RESEARCH

H. F. McDuffie

22. REACTIONS IN AQUEOUS SOLUTIONS

H. F. McDuffie

L. O. Gilpatrick H. H. Stone

22.1 HOMOGENEOUS CATALYSIS OF THE HYDROGEN-OXYGEN REACTION IN AQUEOUS SOLUTIONS

During the past several quarters, studies have been carried forward in which simultaneous estimation has been attempted of the catalytic activity, k_{sol}, of a copper-containing solution and the hydrogen distribution coefficient, $1/\alpha$, between that solution and the vapor phase. Preliminary studies had already indicated interesting effects on these two parameters when temperature, acidity, and copper concentration were varied.[1] The presently reported work is an extension and revision of that work in the sulfate system ($CuSO_4$-H_2SO_4-H_2O).

Two improvements have been made in the interpretation and execution of the experiments. The interpretation had been based on the determination of the slope and intercept of the linear relationship between V_g/V_l, the gas-to-liquid ratio used in the experiment, and $1/k_\pi$, the observed time constant for pressure decrease. The actual equation used was

$$\frac{1}{k_\pi} = \frac{\alpha}{RTk_{sol}} \cdot \frac{V_g}{V_l} + \frac{1}{k_{sol}} . \tag{1}$$

Since the magnitude of $1/k_\pi$ changed from values which were as small as 1 hr to values which were as large as 40 hr, with experimental errors which were correspondingly smaller or larger, it was difficult to weight the experimental observations properly for purposes of using a least-squares correlation of the data. However, the stratagem of interchanging the slope and intercept, by casting the equation into the form,

$$\frac{1}{k_\pi} \cdot \frac{V_l}{V_g} = \frac{1}{k_{sol}} \cdot \frac{V_l}{V_g} + \frac{\alpha}{RTk_{sol}} , \tag{2}$$

permitted the use of the least-squares correlation with equal weighting of all the data, since the previous intercept, now the slope, was usually less than 1.0.

An indication of the importance of temperature control, for a reaction with a 24-kcal activation energy, is given by the hypothetical data presented in Fig. 22.1. The solid line represents an assumed relationship following Eq. 2. The plotted points represent hypothetical results which were obtained by assuming that there was a random variation of temperature with a standard deviation of 1°C, normally distributed about the solid line. Points were obtained for the indicated values of V_l/V_g at intervals of 0.1. A correction of 5.5% in the rate was required for a 1.0°C error in temperature. The dashed lines indicate limits of ±1.0°C (one standard deviation). The imprecision inevitably associated with the least-squares determination of the slope and intercept from such data is obvious. Since the temperature controller used in previous work had, for reasons of flexibility, been furnished with a 0–500°C range covering a 6-in. chart, the mechanical difficulties alone of reproducing the position of the pointer along the control slide-wire

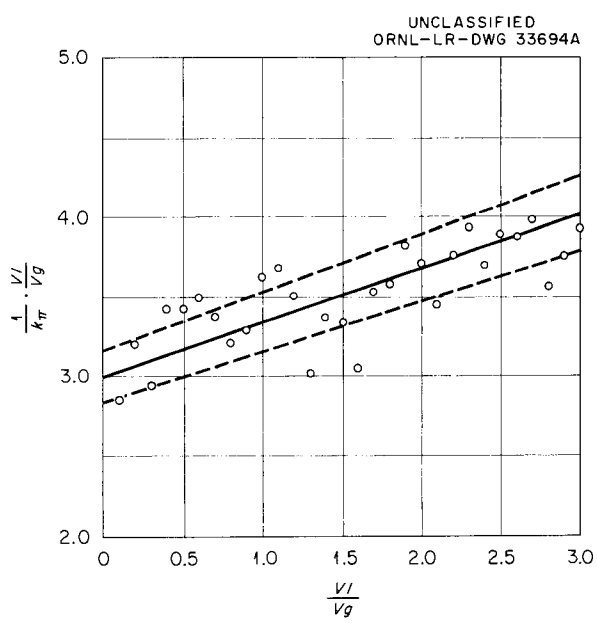

Fig. 22.1. Hypothetical Recombination Data for 1°C Standard Distribution.

[1] C. H. Secoy *et al.*, *HRP Quar. Prog. Rep. April 30, 1957*, ORNL-2331, p 173; *HRP Quar. Prog. Rep. July 31, 1957*, ORNL-2379, p 161.

probably prevented temperature control better than to within 1°C. A new controller was obtained which made use of an external suppression potentiometer and a control slide-wire registering 0.0 ± 0.5 mv. The desired electromotive force was supplied by the suppression potentiometer, and control was achieved when this was exactly balanced by the potential of the thermocouple in the apparatus. The span on a 10-in. chart was now only 18°C. This increase in sensitivity made possible a much more effective use of the controller, and, at present, the temperature control is believed to be well within a distribution with 0.2°C standard deviation. The thermocouples used in previous work were calibrated by the Instrumentation and Controls Division, and previous results were adjusted for this calibration so that their average is correct although their spread may be too large.

An indication of the data being obtained with the improved temperature control and the calibrated thermocouples is given by the results in Table 22.1. These results were correlated by Fr. H. R. Jolley, S.J., a summer employee of the Chemistry Division from Loyola University, with the assistance of M. H. Lietzke of the Chemistry Division, by use of an Oracle code developed by Lietzke.

Examination of the results thus far correlated indicates that increasing acidity is associated with a decrease in k_{sol} and a decrease in the combination parameter, k_{sol}/α; it is clear that for a given hydrogen pressure the over-all rate of reaction decreases with increasing acidity, but it is not yet clear whether the hydrogen distribution coefficient is substantially and significantly affected. Extension of these data to additional combinations of temperature, copper concentration, and acidity will provide the necessary broader basis for drawing valid conclusions.

Hydrogen-oxygen recombination studies were performed at 200°C, and the results were compared with those of similar studies in which the oxygen gas was replaced by CrO_3 dissolved in the solution. The observed rate constants for the decrease in hydrogen pressure were indistinguishable from those for the decrease in hydrogen-oxygen pressure. Thus the presence of oxygen gas does not invalidate the interpretation of the results of laboratory experiments that has previously been used in the study of homogeneous catalysis.

22.2 CHEMICAL STUDIES RELATING TO HRT RUN 17-A

A number of miscellaneous experiments were performed in connection with various possibilities examined as potential explanations of the chemical behavior of the HRT during run 17-A and previous runs.[2]

[2]H. F. McDuffie, *Chemical Indications of HRT Misbehavior in Run 17-A*, ORNL CF-58-9-41 (Sept. 18, 1958).

Table 22.1. Homogeneous Catalysis in Sulfate System

Temperature (°C)	$CuSO_4$ (M)*	H_2SO_4 (M)*	Number of Experiments	Intercept, α/RTk_{sol}		Slope, $1/k_{sol}$		Standard Error of Fit	k_{sol} (hr^{-1})	$10^4/\alpha$ ($M \cdot psi^{-1} \cdot 10^{-4}$)
				Value	Standard Error	Value	Standard Error			
175	0.04	0.025	47	2.034	0.040	0.3672	0.0232	0.1369	2.72	3.34
	0.08	0.025	43	1.102	0.047	0.245	0.020	0.149	4.08	4.12
	0.08	0.075	48	1.678	0.036	0.321	0.020	0.118	3.12	3.54
200	0.01	0.025	33	2.399	0.142	0.161	0.086	0.534	6.21	1.18
	0.01	0.050	31	3.284	0.122	0.299	0.064	0.370	3.34	1.60
	0.01	0.075	37	4.172	0.189	0.660	0.105	0.634	1.52	2.78
	0.01	0.100	43	4.818	0.144	0.848	0.073	0.555	1.18	3.09
	0.02	0.075	33	1.711	0.047	0.250	0.025	0.156	4.0	2.56

*Measured at room temperature.

Hydrogen peroxide was added quickly to a simulated HRT fuel solution at 90°C in an amount sufficient to precipitate part of the uranium. The mixture was immediately filtered and the precipitate analyzed. No copper was found in the precipitate. From this result it was concluded that it is unlikely that peroxide precipitation was involved in the uranium disappearance during HRT run 17-A, since, in that run, substantial amounts of copper disappeared from solution along with the uranium. However, the large difference in temperature between the run and the experiment makes it impossible to eliminate this possibility completely.

A recombination experiment at 250°C, in which a partial reduction of the solution was permitted by using excess hydrogen, gave a final solution which was substantially depleted with respect to hexavalent uranium but contained the original concentration of copper and no detectable amounts of tetravalent uranium. The missing uranium was recovered by washing the walls of the autoclave with nitric acid. It thus appears that simultaneous disappearance of uranium and copper from solution in HRT run 17-A was probably not caused by a partial reduction of the solution.

Examination of the results of chemical analyses of samples of the HRT fuel solution taken during run 17-A revealed significant changes in solution composition which could be correlated with changes in the power level of the reactor. The electrical neutrality ratio, an indication of the self-consistency of the over-all analytical results, did not show any significant relationship to the reactor power level but was strongly correlated with the serial sampling order. This effect appeared to be due largely, but not entirely, to cyclical variations in the analytical free-acid determinations. Planned controls should eliminate this source of variation. The over-all conclusion from the results is that a rise in reactor power level causes the deposition of uranium, copper, and probably nickel, in some hydrolytic process within the core circulation system in a region which is at a position between zero and average nuclear importance. This deposition requires from several minutes to several hours and is relatively easily reversible when the power is lowered.

The cyclical variations in the free-acid results in HRT run 17-A prompted consideration of possible causes. In the analytical procedure the solution sample is mixed with an excess of saturated potassium oxalate solution and ethanol to give about 60% alcohol by volume. The mixture (liquid plus precipitated uranium oxalate) is cooled to a thick slurry in an ice bath and titrated with 0.1 *N* standard sodium hydroxide. The recorded pH, from conventional one-drop electrodes, is used to determine the end point of the titration. Since the solution is kept in an ice bath, although it might be intensely radioactive, the procedure is not conducive to the decomposition of any peroxide initially present or formed during the test. Since the solution is ultimately made neutral (and even basic) by the titration, it appeared necessary to consider the effect of the neutralization upon the equilibrium between uranium and peroxide. This equilibrium is commonly expressed as:

$$UO_2^{++} + H_2O_2 = UO_4 + 2H^+ \qquad (3)$$

Obviously, neutralization of the acid would tend to shift the reaction to completion. The complexing of uranium by potassium oxalate solution does not appear to be dependent upon the pH. Therefore, even with the uranium strongly complexed initially with oxalate and precipitated, the presence of peroxide should cause a complete shift of the equilibrium as the point of neutrality is reached. A shift of five pH units, for example, implies a shift of 10^{10} in the equilibrium ratio of UO_4:H_2O_2, since the hydrogen ion concentration appears as the square. It was not clear, however, whether the rates of resolubilization of once-precipitated uranium oxalate complex would be sufficiently fast to allow peroxide to interfere with the results of the determination. Tests made with simulated HRT fuel solution to which had been added amounts of peroxide up to four times the amount of the initial free acid showed that the apparent free acid was always increased by the peroxide, up to 53% of the true value, but the increase was not quantitative. It does not appear that the presence of the small amounts of peroxide which could be tolerated by the solution sample without precipitation, or which might be developed in the solution during a short period at ice-bath temperature, would cause errors in the determination of free acid which would be large compared with the total free acid or as large as the variations reported in HRT run 17-A. During the testing, however, it was found that the apparent pH, above about 7.5, was very sensitive to the rate of addition of base; when the base was added very slowly with good stirring and up to 5 min time delay between small additions, the pH curve was very erratic and the first derivative of the curve failed to give a satisfactory indication of an end point. These results were made available to the Analytical Chemistry Division for their consideration in connection with possible improvements in the procedure.

Part VII

ANALYTICAL CHEMISTRY

M. T. Kelley

23. ANALYTICAL CHEMISTRY

O. Menis

R. G. Ball
H. P. House
D. L. Manning
T. C. Rains

23.1 DETERMINATION OF URANIUM IN TIN

In connection with a study of the solubility of UO_2 in molten tin, it was necessary to devise a method for the determination of uranium in low concentrations of tin. The tin is dissolved in concentrated HCl and the solution is evaporated to near dryness, following which the tin and uranium are oxidized by the addition of a small amount of nitric acid. Over 99% of the tin is then separated from the uranium by volatilizing it as $SnCl_4$. This is accomplished by repeated additions of concentrated HCl and evaporating to a small volume. The uranium is then determined by derivative polarography in 1 *M* HCl, utilizing the U(VI) $\longrightarrow$ U(V) reduction wave at −0.22 v versus the SCE. The small quantity of residual tin does not interfere. Uranium in tin ranging from 0.5 to 2 wt % was evaluated by this method with a coefficient of variation of about 3%.

23.2 DETERMINATION OF CHLORIDE IN URANYL SULFATE SOLUTIONS

The coulometric stripping technique which was introduced by Zittel *et al.*[1] was further investigated as a means of determining microgram quantities of chloride in solutions of uranyl sulfate. For this application, an ORNL high-sensitivity polarograph was substituted for the electronic coulometric stripper[1] previously utilized by Zittel (circuitry described in ORNL-LR-DWG 24166). When the microelectrode, which consists of a drop of mercury contained in a J-shaped capillary tube, is made the anode, any chloride in the solution is deposited on the surface of the anode as insoluble mercurous chloride. The mercurous chloride is then redissolved by scanning the potential in the negative direction. The current which flows during the dissolution period (stripping cycle) is a measure of the chloride and is proportional to the peak height of the recorded current-voltage curve.[2] A 0.1 *M* KNO_3, 0.1 *M* citric acid solution is used for the supporting electrolyte. In this medium, up to 110 mg of uranium does not interfere. By increasing the citric acid concentration to 0.5 *M*, as much as 600 mg of uranium can be tolerated. Minor components such as iron, nickel, chromium, copper, and molybdenum in concentrations normally encountered in solutions of uranyl sulfate do not interfere. From 1 to 10 μg of chloride in a final volume of 10 ml can be measured by this method with a coefficient of variation of about 15%.

23.3 DETERMINATION OF IRON IN URANYL SULFATE AND OTHER SOLUTIONS

A rapid, sensitive method was developed for the extraction and subsequent flame-photometric determination of microgram quantities of iron in uranyl sulfate solutions containing copper. The method is also applicable for the determination of iron in 0.5 *M* $CuSO_4$, 1 *M* H_3PO_4, 1 *M* H_2SO_4, or 1 *M* HF solutions. Of the flame-photometric methods in the literature for iron, only one by Dean and Lady[3] makes use of a prior extraction procedure. They use acetylacetone in selectively extracting iron at pH 0. Several extractions are required since a single extraction removes only 50% of the iron. In the method developed by this laboratory, microgram quantities of iron are quantitatively extracted from a 6 *M* HCl solution with 4-methyl-2-pentanone (hexone).[4] Equilibrium is reached in a period of 30 sec; the HCl concentration of the aqueous phase may be from 4 to 8 *M*. After extraction, the organic phase is used for the emissivity measurement which is made at a wave length of 372 mμ.

The emissivity is greatly enhanced, at least tenfold, by introducing the iron into the flame in an organic rather than an aqueous medium. Furthermore, by this procedure the removal of copper, an interference, by electrodeposition is avoided. For iron, in the range of 2 to 10 μg/ml in uranyl sulfate and other solutions, the coefficient of variation is 2%.

---

[1] H. E. Zittel *et al.*, *Anal. Chem. Ann. Prog. Rep. Dec. 31, 1957*, ORNL-2453, p 16.

[2] J. G. Nikelly and W. D. Cooke, *Anal. Chem.* **29**, 933 (1957).

[3] J. A. Dean and J. H. Lady, *Anal. Chem.* **27**, 1533–36 (1955).

[4] H. Specker and W. Doll, *Z. anal. Chem.* **152**, 178–84 (1956).

OAK RIDGE NATIONAL LABORATORY
HOMOGENEOUS REACTOR PROJECT

NOVEMBER 1, 1958

PROJECT DIRECTOR
R. B. BRIGGS — D

ASSOCIATE PROJECT DIRECTOR
C. E. WINTERS** — D
A. L. GUNNELS, SEC. — REF

TECHNICAL ASSISTANT
F. KERTESZ — REE

PROJECT EDITOR
W. D. REEL — TI

DESIGN AND ENGINEERING
R. N. LYON, ASSISTANT DIRECTOR — REE
T. S. CARLSMITH,* SEC. — REE

DESIGN
W. R. GALL, SECTION CHIEF — REE
M. I. LUNDIN, ASSISTANT SECTION CHIEF — REE

SPECIAL PROBLEMS
C. L. SEGASER — REE

MECHANICAL DESIGN, SPECIFICATIONS AND DRAFTING
F. C. ZAPP, GROUP LEADER — REE
C. A. BURCHSTED — REE
C. W. COLLINS — REE
J. E. JONES — REE
W. ROBINSON — REE
H. H. BRADFORD — REE
R. L. CAUBLE — REE
C. W. DAY — REE
J. P. DILORENZO — REE
F. GUINESS — REE
T. E. HAYNES — REE
A. R. KERR — REE
W. B. KRICK — REE
A. S. LUDLOW — REE
C. A. ROBERTS — REE
R. D. SATTERFIELD — REE
R. H. SIGLER — REE
W. G. STERLING — REE

SITE AND STRUCTURES
J. N. ROBINSON — REE

COMPONENT DEVELOPMENT
I. SPIEWAK, SECTION CHIEF — REE

HEAT EXCHANGERS AND MECHANICAL ENGINEERING PROBLEMS
J. S. CULVER, GROUP LEADER — REE
R. BLUMBERG — REE
B. D. DRAPER — TVA
P. P. HOLZ — REE
I. K. NAMBA — REE
T. L. CASTILE — REE
C. JONES — REE

CIRCULATING PUMPS
C. H. GABBARD, GROUP LEADER — REE
T. G. CHAPMAN — REE
J. C. MOYERS — REE
H. P. PAYNE — REE
C. C. HURTT — REE
R. J. LOCKETT — REE

FEED PUMPS AND VALVES
E. C. HISE, GROUP LEADER — REE
H. C. ROLLER — REE
J. P. HURST — REE
G. A. WINDLE — REE

CORE AND BLANKET AND CHEMICAL ENGINEERING PROBLEMS
C. G. LAWSON, GROUP LEADER — REE
D. M. EISSENBERG — REE
B. A. HANNAFORD — REE
J. E. MOTT — REE
D. L. SNYDER — REE
R. P. WICHNER — REE
R. GOODWIN — REE
S. R. WEST — REE
B. J. YOUNG — REE

RESEARCH AND ANALYSIS
P. R. KASTEN, SECTION CHIEF — REE

REACTOR ANALYSIS
M. R. ROSENTHAL, GROUP LEADER — REE
S. JAYE — REE
B. E. PRINCE — PEE

REACTOR PHYSICS
M. TOBIAS, GROUP LEADER — REE
R. CHALKLEY — REE
C. W. NESTOR, JR. — REE

PROGRAMING
T. B. FOWLER — REE
M. P. LIETZKE — REE

TRANSPORT PROPERTIES OF SLURRIES
D. G. THOMAS, GROUP LEADER — REE
P. H. HAYES — REE
R. M. SUMMERS — REE

PHYSICAL CHEMISTRY OF SLURRIES
C. S. MORGAN, GROUP LEADER — REE
B. G. SUTTON — REE

FLUID FLOW AND HEAT TRANSFER
H. C. CLAIBORNE, GROUP LEADER — REE
H. A. MACCOLL — REE

STRESS ANALYSIS AND CLOSURE RESEARCH
R. D. CHEVERTON, GROUP LEADER — REE
T. H. MAUNEY — REE

SYSTEMS DEVELOPMENT
R. B. KORSMEYER, SECTION CHIEF — REE
F. N. PEEBLES, ASSISTANT SECTION CHIEF — REE

SLURRY SYSTEMS DEVELOPMENT I
R. VAN WINKLE, GROUP LEADER — REE
H. B. PIPER — REE
C. A. MCLAUGHLIN — REE

SLURRY SYSTEMS DEVELOPMENT II
L. F. PARSLY, JR., GROUP LEADER — REE
R. J. KEDL — REE
M. RICHARDSON — REE
R. E. CARNES — REE

HRT CORE MOCKUP
P. H. HARLEY, GROUP LEADER — REE
L. E. PENTON — REE
T. R. WILSON — REE

OPERATIONS
A. N. SMITH, GROUP LEADER — REE
T. L. BOSWELL — REE
B. R. CHILCOAT — REE
J. T. DICKIE — REE
C. A. CIFFORD — REE
H. G. MOORE — REE
D. H. WALLACE — REE

INSTRUMENTATION AND CONTROLS
D. S. TOOMB, SECTION CHIEF — I&C

REACTOR I&C SYSTEM DESIGN
J. R. BROWN, GROUP LEADER — I&C
J. A. RUSSELL — I&C
R. W. BORGERS — I&C

HRP SUPPORTING SERVICES
D. G. DAVIS, GROUP LEADER — I&C
S. J. BALL — I&C
P. G. HERNDON — I&C
H. D. MILLS — I&C
R. M. BURNETT — I&C
M. A. MEACHAM — I&C
P. E. SMITH — I&C

VALVES AND ACTUATORS
A. M. BILLINGS, GROUP LEADER — I&C
E. H. BELL — I&C
B. J. JONES — I&C

INSTRUMENT DEVELOPMENT
R. L. MOORE, GROUP LEADER — I&C
J. L. REDFORD — I&C
T. M. CATE — I&C

REACTOR MATERIALS RESEARCH
E. G. BOHLMANN, ASSISTANT DIRECTOR — REE
T. S. CARLSMITH,* SEC. — REE
R. MOWELL, SEC. — REE
R. E. WACKER, RECORDS — REE

SOLUTIONS
J. C. GRIESS, ASSISTANT SECTION CHIEF — REE

LOOPS
R. S. GREELEY, GROUP LEADER — REE
E. S. SNAVELY — REE
W. H. HINDS — REE

LABORATORY STUDIES
J. L. ENGLISH, GROUP LEADER — REE
D. N. HESS — REE
P. D. NEUMANN — REE
L. L. FAIRCHILD — REE
H. L. BARKER — REE
J. E. JACKSON — REE
B. L. JOHNSON — REE
H. R. TINCH — REE
J. L. UNDERWOOD — REE

SLURRIES
E. L. COMPERE, ASSISTANT SECTION CHIEF — REE

LOOPS
S. A. REED,* GROUP LEADER — REE

OUT-OF-PILE STUDIES

R. B. GALLAHER — REE
F. E. MCDANIEL — REE
H. F. HENDERSON — REE

TOROIDS
S. A. REED,* GROUP LEADER — REE

OUT-OF-PILE STUDIES

L. RICE — REE
R. F. BENSON — REE
B. H. PARKS — REE
G. G. WARNER — REE

IN-PILE BOMBS
L. F. WOO — REE

ENGINEERING
H. C. SAVAGE, ASSISTANT SECTION CHIEF — REE

SOLUTIONS
S. E. BOLT, GROUP LEADER — REE
A. J. SHOR — REE
W. C. ULRICH — REE

IN-PILE MOCKUPS
J. R. HART, LEADER — REE
C. H. BURRAGE — REE
D. G. GATES — REE
J. W. MOSIER — REE
R. W. RAY — REE
D. M. SMITH — REE

100A LOOP OPERATIONS
J. F. WINESETTE* — REE
C. M. BURCHELL — REE
C. L. FRANCIS — REE
J. B. FRENCH — REE
J. W. GOOCH — REE

SLURRIES
D. T. JONES, GROUP LEADER — REE
J. M. BAKER — REE

100A LOOP OPERATIONS
J. F. WINESETTE* — REE
L. L. ALLEN — REE
C. R. BENSON — REE
V. R. BULLINGTON — REE
G. A. MOORE — REE
L. G. PHELPS — REE
A. E. PUGH — REE

IN-PILE OPERATIONS
R. A. LORENZ, GROUP LEADER — REE
V. A. DECARLO — REE
J. W. MYERS, LEADER — REE
C. E. ROBERTS — REE
A. L. SUTTON — REE
W. E. TEICHERT, A SHIFT LEADER — REE
T. R. RAYBURN — REE
E. H. GUNN, B SHIFT LEADER — REE
J. P. GORDON — REE
R. M. WALLER, C SHIFT LEADER — REE
R. A. JONES — REE
R. G. ROSS, D SHIFT LEADER — REE
D. G. PEACH — REE

RADIATION
G. H. JENKS, SECTION CHIEF — REE

IN-PILE LOOPS
M. D. SILVERMAN, GROUP LEADER — C
J. E. BAKER — REE
S. H. WHEELER — REE

IN-PILE BOMBS
R. J. DAVIS, GROUP LEADER — C
K. S. WARREN — C
J. L. RUTHERFORD — REE

SUPPORTING RESEARCH
A. L. BACARELLA — C
J. C. BAKER — REE
W. C. YEE — C

REMOTE EVALUATION
A. R. OLSEN — REE
B. W. MCCOLLUM, SHIFT LEADER — REE
C. M. FITZPATRICK — REE
W. J. SCHILL — REE
W. H. SMITH, JR. — REE

METALLURGY
G. M. ADAMSON, SECTION CHIEF — M

METALLURGICAL RESEARCH
M. L. PICKLESIMER, LEADER — M
S. G. NELSON — M
P. L. RITTENHOUSE — M
R. L. STEPHENSON — M
P. J. JONES — M
G. C. NELSON — M
J. J. WOODHOUSE — M

METALLURGICAL ENGINEERING
E. S. BOMAR, LEADER — M
F. W. COOKE — M
W. J. LEONARD — M
J. J. PRISLINGER — M
J. K. WHITE — M
C. H. WOOTKE — M
C. M. SMITH — M
M. A. WHEELER — M

METALLOGRAPHY
R. S. CROUSE,** LEADER — M
T. M. KEGLEY, JR. — M
E. R. BOYD — M
B. F. DAY** — M
R. L. FITZGERALD — M
T. J. HENSON** — M
L. G. SHRADER** — M
C. E. ZACHARY — M

RADIATION DAMAGE
R. G. BERGGREN — SS
J. C. WILSON** — SS
F. B. GRIZZEL — SS

INDUSTRIAL PARTICIPATION

JAPANESE ATOMIC ENERGY RESEARCH INSTITUTE
TENNESSEE VALLEY AUTHORITY

SUBCONTRACTS

FRANKLIN INSTITUTE
RICE INSTITUTE
STANFORD RESEARCH INSTITUTE
TITANIUM FABRICATORS, INC.
UNIVERSITY OF UTAH

AC — ANALYTICAL CHEMISTRY DIVISION
C — CHEMISTRY DIVISION
CT — CHEMICAL TECHNOLOGY DIVISION
D — DIRECTOR'S DIVISION
E&M — ENGINEERING AND MECHANICAL DIVISION
I&C — INSTRUMENTATION AND CONTROLS DIVISION
M — METALLURGY DIVISION
RC — REACTOR CHEMISTRY DIVISION
REE — REACTOR EXPERIMENTAL ENGINEERING DIVISION
SS — SOLID STATE DIVISION
TI — TECHNICAL INFORMATION DIVISION
* — DUAL CAPACITY
** — PART TIME ON PROJECT
† — ATTENDING ORSORT

CHEMICAL TECHNOLOGY
D. E. FERGUSON,* PROGRAM LEADER — CT
I. LOOPE, SEC. — CT

CHEMICAL DEVELOPMENT
D. E. FERGUSON,* SECTION CHIEF — CT

FUEL PROCESSING
R. A. MCNEES, GROUP LEADER — CT
M. H. LLOYD — CT
S. PETERSON — CT
W. B. HOWERTON — CT

THORIUM BLANKET STUDIES
J. P. MCBRIDE, GROUP LEADER — CT
R. L. PEARSON, PROBLEM LEADER — CT

OXIDE PREPARATION

A. T. KLEINSTEUBER — CT
C. E. SCHILLING — CT
C. W. GREENE — CT
N. A. KROHN, PROBLEM LEADER — CT

IRRADIATION STUDIES

K. H. MCCORKLE — CT
L. E. MORSE — CT
P. P. HAYDON — CT
W. L. PATTISON — CT
H. F. SOARD — CT

SURFACE CHEMISTRY
C. H. SECOY, GROUP LEADER — CT
H. F. HOLMES — CT
F. H. SWEETON — CT

DESIGN
W. E. UNGER, ASSISTANT SECTION CHIEF — CT

TiO_2 DEVELOPMENT DESIGN
J. C. SUDDATH — CT

HRT CP DESIGN SUPPORT
H. O. WEBBEN — CT
F. C. MCCULLOUGH — CT

LOOP FACILITIES DESIGN
T. A. AREHART — CT
W. F. SCHAFFER — CT

INSTRUMENTATION
C. S. LISSER — I&C

ENGINEERING AND DRAFTING
B. F. BOTTNFIELD** — CT
B. B. KLIMA — CT
G. B. BERRY** — E&M
E. E. BRIDGES** — E&M
J. D. CUPP — E&M
J. W. DAY — E&M
H. W. FALLON** — E&M
L. C. HUBBARD — E&M
J. H. MANNEY** — E&M
J. D. PHILLIPS** — E&M
F. L. PEISHEL** — E&M
J. H. THOMPSON — E&M
J. N. WHEELER** — E&M

PILOT PLANT
R. B. LINDAUER,** SECTION CHIEF — CT

IN-PILE LOOP OPERATIONS
W. D. BURCH,* GROUP LEADER — CT
L. J. KING, PROBLEM LEADER — CT
J. W. BROWN — CT
R. B. KEELY — CT
L. B. SHAPPERT — CT
E. L. YOUNGBLOOD — CT

SLURRY PREPARATION
W. H. LEWIS, GROUP LEADER — CT
C. V. ELLISON, PROBLEM LEADER — CT
K. O. JOHNSSON — CT

UNIT OPERATIONS
P. A. HAAS, GROUP LEADER — CT

SLURRY PREPARATION DEVELOPMENT
S. D. CLINTON — CT
C. C. HAWS, JR. — CT
R. D. ARTHUR — CT
V. L. FOWLER — CT

ENGINEERING ASSISTANCE STUDIES
W. M. WOODS — CT
J. W. SNIDER — CT
F. N. MCLAIN — CT
D. A. MCWHIRTER — CT

CHEMICAL RESEARCH
H. F. MCDUFFIE,* ASSISTANT DIRECTOR — RC
I. W. HODGE, SEC. — RC

SOLUBILITY EQUILIBRIA IN AQUEOUS SYSTEMS
W. L. MARSHALL, GROUP LEADER — RC
J. S. GILL — RC
G. M. HEBERT — RC
R. SLUSHER — RC

REACTIONS IN AQUEOUS SOLUTIONS
H. F. MCDUFFIE,* GROUP LEADER — RC
L. O. GILPATRICK — RC
H. H. STONE — RC

ANALYTICAL CHEMISTRY
MYRON T. KELLEY,** DIRECTOR
C. D. SUSANO,** ASSOCIATE DIRECTOR
K. A. ODOM, SEC. — AC

CORROSION ANALYTICAL LABORATORY
O. MENIS,* SECTION CHIEF — AC
H. P. HOUSE, ASSISTANT SECTION CHIEF — AC

RESEARCH
O. MENIS,* GROUP LEADER — AC
C. M. BOYD — AC
D. L. MANNING, GROUP LEADER — AC
R. G. BALL — AC
G. GOLDSTEIN — AC
T. C. RAINS, GROUP LEADER — AC
I. B. RUBIN — AC

SERVICE
C. K. TALBOTT, GROUP LEADER — AC
D. E. CARPENTER — AC
N. M. FERGUSON — AC
F. L. LAYTON — AC
T. P. BACON — AC
W. D. CLAPP, JR. — AC
C. A. CLARK — AC
P. S. GOODWIN — AC
B. D. HICKS — AC
A. H. MATTHEWS — AC
T. G. MILLER — AC
V. S. NORMAN — AC
E. ONKST — AC
C. M. WILSON — AC

HRT AND IN-PILE LOOP ANALYSES
U. KOSKELA, SUPERVISOR — AC
L. G. FARRAR, ASSISTANT SUPERVISOR — AC
J. E. ATTRILL — AC
C. P. BAKER — AC
R. E. CORCORAN — AC
S. R. DINSMORE — AC
J. L. MOTTERN — AC
G. M. CAMPBELL — AC
G. I. GAULT — AC
F. K. HEACKER — AC
M. H. MCCORQUODALE — AC
J. L. SHARP — AC
J. SLESSINGER — AC
W. R. WARREN — AC
H. L. WEBB — AC
H. L. WHITTINGTON — AC

RADIOCHEMICAL ANALYSES
E. I. WYATT** — AC

HRT DEVELOPMENT
P. F. THOMASON,** GROUP LEADER — AC
R. E. BIGGERS** — AC
F. J. MILLER** — AC
S. A. REYNOLDS,** GROUP LEADER — AC
J. S. ELDRIDGE** — AC
T. H. HANDLEY** — AC

HIGH RADIATION LABORATORY
J. E. MORTON** — AC

HOMOGENEOUS REACTOR TEST
S. E. BEALL, PROJECT ENGINEER — REE
B. EUBANK, SEC. — REE
M. SWANK, SEC. — CT
P. S. WARD, STENO. — REE

REACTOR PLANNING
S. I. KAPLAN,† GROUP LEADER — REE
J. R. BUCHANAN — CT

PLANT OPERATIONS
J. W. HILL, JR., CHIEF — REE
J. D. FLYNN — REE
R. H. GUYMON — CT
J. HIROTA — JAPANESE ATOMIC ENERGY RESEARCH INSTITUTE
D. SCOTT, JR. — REE
O. W. LEIGH — REE

R. J. HARVEY, SHIFT SUPERVISOR — REE
R. SMITH, JR., CONTROL ROOM SUPERVISOR — REE
D. T. GODWIN — REE
A. L. JOHNSON — REE
L. P. PUGH — REE
W. H. WAGNER — REE
H. F. BAUMAN, SHIFT SUPERVISOR — CT
E. W. BROWN, CONTROL ROOM SUPERVISOR — CT
J. D. BARNES — REE
E. D. BOLLING — REE
W. T. BOSTIC — CT
T. G. HILL — REE
D. F. FRECH, SHIFT SUPERVISOR — REE
R. J. SHANNON, CONTROL ROOM SUPERVISOR — CT
P. D. DAVIS — REE
J. E. EVE — REE
L. J. SHERSKY — CT
J. E. WOLFE — REE
N. C. BRADLEY, SHIFT SUPERVISOR — CT
J. L. STEPP, CONTROL ROOM SUPERVISOR — REE
H. D. CURTIS — REE
H. L. BROWN — REE
T. W. HODGE — REE
F. L. ROUSER — REE

REACTOR MATERIALS AND CHEMISTRY
D. M. RICHARDSON, GROUP LEADER — REE
J. E. SUTHERLAND — REE
J. D. JONES — REE

CHEMICAL PLANT
W. D. BURCH,* GROUP LEADER — CT
R. H. WINGET — CT
O. O. YARBRO — CT
W. A. LINDSEY — CT

REACTOR ANALYSIS
P. N. HAUBENREICH, GROUP LEADER — REE
S. R. BUXTON — REE
J. R. ENGEL — CT
J. O. KOLB — REE
J. A. WATTS — REE

MAINTENANCE PLANNING
W. TERRY, SUPERVISOR — REE
O. H. JOHNSTONE — REE

INSTRUMENTATION
K. W. WEST, GROUP LEADER — I&C
J. A. RUSSELL — I&C

PERSONNEL SUMMARY

	FULL TIME	PART TIME	INDUSTRIAL PARTICIPATION	TOTAL
ADMINISTRATION	8	3		11
ANALYTICAL CHEMISTRY	38	8		46
CHEMICAL RESEARCH	6			6
CHEMICAL TECHNOLOGY	48	9		57
DESIGN AND ENGINEERING	113		1	114
HOMOGENEOUS REACTOR TEST	45		1	46
REACTOR MATERIALS RESEARCH	96	5		101
TOTAL	354	25	2	381

INTERNAL DISTRIBUTION

1. C. E. Center
2. Biology Library
3. Health Physics Library
4. Metallurgy Library
5-6. Reactor Experimental Engineering Library
7-9. Central Research Library
10-14. Laboratory Records Department
15. Laboratory Records, ORNL R.C.
16. G. M. Adamson
17. T. A. Arehart
18. A. L. Bacarella
19. J. E. Baker
20. R. G. Ball
21. S. J. Ball
22. R. D. Baybarz
23. S. E. Beall
24. L. L. Bennett
25. R. G. Berggren
26. G. B. Berry
27. R. E. Biggers
28. A. M. Billings
29. D. S. Billington
30. E. P. Blizard
31. R. Blumberg
32. E. G. Bohlmann
33. S. E. Bolt
34. C. J. Borkowski
35. B. F. Bottenfield
36. G. E. Boyd
37. J. C. Bresee
38. N. A. Brown
39. F. R. Bruce
40. J. R. Buchanan
41. W. D. Burch
42. C. A. Burchsted
43. S. R. Buxton
44. A. D. Callihan
45. T. A. Carlson
46. W. L. Carter
47. G. H. Cartledge
48. R. H. Chapman
49. R. A. Charpie
50. R. D. Cheverton
51. J. M. Chilton
52. C. J. Claffey
53. H. C. Claiborne
54. W. E. Clark
55. S. D. Clinton
56. T. E. Cole
57. C. W. Collins
58. E. L. Compere
59. R. S. Crouse
60. F. L. Culler
61. J. S. Culver
62. D. G. Davis
63. R. J. Davis
64. V. A. DeCarlo
65. B. D. Draper
66. J. S. Drury
67. W. K. Eister
68. L. B. Emlet (K-25)
69. J. L. English
70. D. E. Ferguson
71. J. D. Flynn
72. D. F. Frech
73. J. H. Frye, Jr.
74. C. H. Gabbard
75. J. L. Gabbard
76. W. R. Gall
77. R. B. Gallaher
78. C. H. Gibson
79. E. H. Gift
80. H. E. Goeller
81. R. S. Greeley
82. A. T. Gresky
83. J. C. Griess
84. W. R. Grimes
85. E. Guth
86. R. H. Guymon
87. L. A. Haack
88. P. A. Haas
89. J. Halperin
90. B. A. Hannaford
91. P. H. Harley
92. R. J. Harvey
93. P. N. Haubenreich
94. D. N. Hess
95. J. W. Hill
96. E. C. Hise
97. A. Hollaender
98. P. P. Holz
99. H. P. House
100. A. S. Householder

101. S. Jaye
102. G. H. Jenks
103. D. T. Jones
104. E. V. Jones
105. K. O. Johnsson
106. W. H. Jordan
107. S. I. Kaplan
108. P. R. Kasten
109. C. P. Keim
110. M. T. Kelley
111. F. Kertesz
112. S. S. Kirslis
113. J. O. Kolb
114. R. B. Korsmeyer
115. U. Koskela
116. K. A. Kraus
117. N. A. Krohn
118. J. A. Lane
119. C. G. Lawson
120. R. E. Leuze
121. S. C. Lind
122. R. B. Lindauer
123. C. S. Lisser
124. R. S. Livingston
125. M. H. Lloyd
126. R. A. Lorenz
127. M. I. Lundin
128. R. N. Lyon
129. J. L. Marsh (C&CC, South Charleston)
130. W. L. Marshall
131. J. P. McBride
132. F. C. McCullough
133. H. F. McDuffie
134. H. A. McLain
135. R. A. McNees
136. J. R. McWherter
137. O. Menis
138. E. C. Miller
139. C. S. Morgan
140. K. Z. Morgan
141. L. E. Morse
142. J. P. Murray (Y-12)
143. I. K. Namba
144. M. L. Nelson
145. P. D. Neumann
146. R. H. Nimmo
147. A. R. Olsen
148. L. F. Parsly
149. R. L. Pearson
150. F. N. Peebles
151. Sigfred Peterson
152. H. O. Phillips
153. M. L. Picklesimer
154. R. M. Pierce
155. R. H. Powell
156. B. E. Prince
157. J. J. Prislinger
158. L. R. Quarles
159. S. A. Reed
160. W. D. Reel
161. P. M. Reyling
162. S. A. Reynolds
163. L. Rice
164. D. M. Richardson
165. A. E. Richt
166. G. W. Rivenbark
167. R. C. Robertson
168. W. Robinson
169. H. C. Roller
170. A. M. Rom
171. M. W. Rosenthal
172. H. C. Savage
173. W. F. Schaeffer
174. C. E. Schilling
175. H. E. Seagren
176. H. K. Search
177. C. H. Secoy
178. C. L. Segaser
179. E. M. Shank
180. E. D. Shipley
181. M. D. Silverman
182. M. J. Skinner
183. A. N. Smith
184. E. S. Snavely, Jr.
185. A. H. Snell
186. J. W. Snider
187. D. L. Snyder
188. I. Spiewak
189. H. H. Stone
190. R. W. Stoughton
191. C. D. Susano
192. J. E. Sutherland
193. J. A. Swartout
194. E. H. Taylor
195. W. Terry
196. D. G. Thomas
197. P. F. Thomason
198. M. Tobias
199. D. S. Toomb
200. W. E. Unger
201. W. C. Ulrich
202. R. Van Winkle
203. D. W. Vroom
204. R. E. Wacker

205. F. J. Walter
206. K. S. Warren
207. B. Weaver
208. H. O. Weeren
209. A. M. Weinberg
210. S. H. Wheeler
211. J. K. White
212. E. P. Wigner (consultant)
213. H. D. Wills
214. G. C. Williams
215. J. C. Wilson
216. R. H. Winget
217. C. E. Winters
218. L. F. Woo
219. W. C. Yee
220. F. C. Zapp
221. ORNL – Y-12 Technical Library Document Reference Section
222. HRP Director's Office, Y-12

EXTERNAL DISTRIBUTION

223. E. B. Christiansen, Department of Chemical Engineering, University of Utah
224. D. H. Groelseman, AEC, Washington
225. W. E. Johnson, Westinghouse Electric Corporation
226. Houdry Corporation (Attn: G. A. Mills)
227. Division of Research and Development, AEC, ORO
228-809. Given distribution as shown in TID-4500 (14th ed.) under Reactors-Power category (75 copies – OTS)

Reports previously issued in this series are as follows:

ORNL-527	Date Issued, December 28, 1949
ORNL-630	Period Ending February 28, 1950
ORNL-730	Feasibility Report – Date Issued, July 6, 1950
ORNL-826	Period Ending August 31, 1950
ORNL-925	Period Ending November 30, 1950
ORNL-990	Period Ending February 28, 1951
ORNL-1057	Period Ending May 15, 1951
ORNL-1121	Period Ending August 15, 1951
ORNL-1221	Period Ending November 15, 1951
ORNL-1280	Period Ending March 15, 1952
ORNL-1318	Period Ending July 1, 1952
ORNL-1424	Period Ending October 1, 1952
ORNL-1478	Period Ending January 1, 1953
ORNL-1554	Period Ending March 31, 1953
ORNL-1605	Period Ending July 31, 1953
ORNL-1658	Period Ending October 31, 1953
ORNL-1678	Period Ending January 31, 1954
ORNL-1753	Period Ending April 30, 1954
ORNL-1772	Period Ending July 31, 1954
ORNL-1813	Period Ending October 31, 1954
ORNL-1853	Period Ending January 31, 1955
ORNL-1895	Period Ending April 30, 1955
ORNL-1943	Period Ending July 31, 1955
ORNL-2004	Period Ending October 31, 1955
ORNL-2057	Period Ending January 31, 1956
ORNL-2096	Period Ending April 30, 1956
ORNL-2148	Period Ending July 31, 1956
ORNL-2222	Period Ending October 31, 1956
ORNL-2272	Period Ending January 31, 1957
ORNL-2331	Period Ending April 30, 1957
ORNL-2379	Period Ending July 31, 1957
ORNL-2432	Period Ending October 31, 1957
ORNL-2493	Period Ending January 31, 1958
ORNL-2561	Periods Ending April 30 and July 31, 1958